

Copyright

by

Dustin Roni Klein

2019

**The Dissertation Committee for Dustin Roni Klein Certifies that this is the
approved version of the following dissertation:**

**Structural Characterization of Lipids Using 193 nm Ultraviolet
Photodissociation Mass Spectrometry**

Committee:

Jennifer S. Brodbelt, Supervisor

Eric V. Anslyn

Bryan W. Davies

Livia Schiavinato Eberlin

Lauren J. Webb

**Structural Characterization of Lipids Using 193 nm Ultraviolet
Photodissociation Mass Spectrometry**

by

Dustin Roni Klein

Dissertation

Presented to the Faculty of the Graduate School of

The University of Texas at Austin

in Partial Fulfillment

of the Requirements

for the Degree of

Doctor of Philosophy

The University of Texas at Austin

May 2019

Dedication

For my parents, Mark and Cheryl

Acknowledgements

I would like to first acknowledge my graduate advisor, Jennifer Brodbelt, for giving me the opportunity to earn my degree in her lab and for supporting me during the course of my graduate career. Her tireless efforts to establish meaningful collaborations and procure state-of-the-art instrumentation have enriched my experience and opened up a world of research possibilities.

During the course of my graduate work I have had the privilege of working and collaborating with many talented scientists. I would like to thank Franklin Leach and Jon Amster at the University of Georgia for their expertise in mass spectrometry of glycosaminoglycans, and Stephen Trent and Matthew Powers, also at the University of Georgia, for providing interesting lipooligosaccharides samples. I would also like to thank Livia Eberlin, Clara Feider, Kyana Garza and Jon Lin for all of their efforts with the DESI work.

I am forever indebted to my undergraduate research advisor, Melissa Schultz, for inspiring me to pursue the field of analytical chemistry, and convincing me that graduate school was where I belonged. Her mentorship and friendship have had an immeasurable impact on me.

I would like to thank Brodbelt group members, past and present, for their patience, constructive feedback, and for always lending an ear. Additionally, I am fortunate for my network of friends who have kept me smiling and been a source of comic relief.

Lastly, I would like to thank my family. Adina, Ari, Jonah, Max, Dahlia and Robin have, through their own accomplishments, motivated me to aim high, and been a

reminder of what is possible with hard work and determination. I am especially grateful to my compassionate and selfless parents, Mark and Cheryl, for their constant support, advice, and love. They have taught to pursue all facets of my life with passion and tenacity, and have kept me grounded during this process. I undoubtedly would not have accomplished this feat without them.

Structural Characterization of Lipids Using 193 nm Ultraviolet Photodissociation Mass Spectrometry

Dustin Roni Klein, Ph.D.

The University of Texas at Austin, 2019

Supervisor: Jennifer S. Brodbelt

As their diversity of structures suggests, lipids have a wide range of functions from storing energy to participant signal transduction. Over the last decade, mass spectrometry has emerged as a powerful analytical tool for identification and quantitation of lipids. While tandem mass spectrometry affords a higher level of structural characterization than intact mass measurements alone, conventional ion activation methods often fail to elucidate subtle yet critical structural features. The research presented in this dissertation explores the utility of 193 nm ultraviolet photodissociation (UVPD), a fast and high-energy alternative ion activation method, for structural characterization of phosphatidylcholines and lipooligosaccharides.

Phosphatidylcholines are the most abundant glycerophospholipid in mammalian cell membranes and therefore represent an important analytical target. Low-energy collision-based activation methods generate head group and acyl chain fragment ions that permit determination of the lipid class and acyl chain composition, respectively. Photodissociation at 193 nm UVPD similarly produced head group and acyl chain fragment ions, in addition to diagnostic pairs of fragment ions that afforded localization of double bonds within acyl chains. Implementation of UVPD in a shotgun lipidomic

workflow enabled identification of double bond positional isomers in complex glycerophospholipid extracts that otherwise would have gone undetected with low-energy collision-based activation methods. Coupling of the UVPD method to a mass spectrometry imaging workflow further facilitated detection of double bond positional isomers *in situ*. Changes in the relative abundances of double bond positional isomers were correlated to specific tissue features.

Lipooligosaccharides (LOS) are saccharolipids that are the main component of the outer membrane of Gram-negative bacteria. Determination of unknown lipooligosaccharides structures and modifications is crucial considering the relationship between LOS structures and the development of antibiotic resistance. A mass spectrometry method utilizing the MSⁿ capabilities of linear ion trap mass analyzer, 193 nm UVPD, and high resolution scanning in the Orbitrap mass analyzer facilitated detailed structural characterization of intact LOS structures in both shotgun and chromatographic workflows. The methods permitted both localization of non-stoichiometric modification and determination of unknown core oligosaccharide structures.

Table of Contents

Chapter 1: Introduction	1
1.1 Introduction.....	1
1.2 Mass Spectrometry-Based Lipidomics	1
1.3 Glycerophospholipids	4
1.4 Tandem Mass Spectrometry of Glycerophospholipids.....	6
1.4.1 Low-Energy Collisional-Induced Dissociation (CID) and Infrared Multiphoton Dissociation (IRMPD)	6
1.4.2 High-Energy CID.....	8
1.4.3 Ozone-Induced Dissociation (OzID)	9
1.4.4 Electron-Based Activation Methods	11
1.4.5 He-Metastable Atom-Activated Dissociation (He-MAD) and Charge-Transfer Dissociation (CTD)	12
1.4.6 Radical-Directed Dissociation (RDD) and Ultraviolet Photodissociation (UVPD)	13
1.5 Lipopolysaccharides/Lipooligosaccharides	14
1.6 Mass Spectrometry of LPS/LOS.....	16
1.6 Overview of Chapters	18
1.7 References.....	20
Chapter 2: Experimental Methods	33
2.1 Ionization	33
2.1.1 Electrospray Ionization	33
2.1.2 Desorption Electrospray Ionization	34
2.2 Liquid Chromatography.....	34

2.3 Mass Spectrometry	34
2.3 Ion Activation	35
2.3.1 Collisional Activation	35
2.3.2 193 nm Ultraviolet Photodissociation.....	36
2.4 References.....	36
Chapter 3: Structural Characterization of Phosphatidylcholines Using 193 nm Ultraviolet Photodissociation Mass Spectrometry	38
3.1 Overview.....	38
3.2 Introduction.....	39
3.3 Experimental.....	42
3.4 Results and Discussion	45
3.5 Conclusion	67
3.6 Supporting Information.....	69
3.7 References.....	79
Chapter 4: Desorption Electrospray Ionization Couple with Ultraviolet Photodissociation for Characterization of Phospholipids Isomers in Tissue Sections	84
4.1 Overview.....	84
4.2 Introduction.....	85
4.3 Experimental.....	87
4.3.1 Materials	87
4.3.2 Tissue Samples	87
4.3.3 DESI-MS and DESI-UVPD Profiling and Imaging	87
4.3.4 2D Imaging Data Analysis.....	89
4.3.5 Lipid Notation.....	89

4.4 Results and Discussion	90
4.5 Conclusions.....	111
4.6 References.....	112
Chapter 5: Shotgun Analysis of Rough-Type Lipopolysaccharides Using Ultraviolet Photodissociation	116
5.1 Overview.....	116
5.2 Introduction.....	117
5.3 Experimental.....	119
5.4 Results and Discussion	122
5.5 Conclusion	139
5.6 Supporting Information.....	140
5.7 References.....	143
Chapter 6: Top-Down Characterization of Lipooligosaccharides from Antibiotic- Resistance Bacteria	147
6.1 Overview.....	147
6.2 Introduction.....	148
6.3 Experimental.....	151
6.3.1 Materials and Reagents.....	151
6.3.2 LOS Isolation.....	152
6.3.3 Liquid Chromatography and Mass Spectrometry	153
6.3.4 Data Analysis	154
6.4 Results and Discussion	155
6.5 Conclusion	174
6.6 Supporting Information.....	176

6.6 References.....	194
Chapter 7: Structural Characterization of Glycosaminoglycan Carbohydrates Using Ultraviolet Photodissociation.....	200
7.1 Overview.....	200
7.2 Introduction.....	201
7.3 Experimental.....	204
7.3.1 Materials and Reagents.....	204
7.3.2 Mass Spectrometry	205
7.4 Results and Discussion	207
7.5 Conclusion	225
7.6 Supporting Information.....	227
7.7 References.....	242
Chapter 8: Conclusions	248
8.1 Summary of Chapters	248
8.2 Future Directions	249
8.2.1 Glycerophospholipids	249
8.2.2 LPS/LOS	251
8.3 References.....	252
References	254

Chapter 1: Introduction

1.1 INTRODUCTION

Identification and quantitation of lipids, a subset of metabolites, is essential to achieve a full understanding of complex biological networks. Lipids not only provide insight in to changes in metabolic processes that can result from environmental stimuli, but can be used as biomarkers to identify disease states. While studies during the end of the 20th century and beginning of the 21st century focused largely on DNA and proteins, advances in mass spectrometry technology have greatly advanced our ability to obtain lipidomic data that is complementary to genomic and proteomic data.¹ However, further developments are required to address challenges associated with lipid structural characterization. Alternative ion activation methods, including ultraviolet photodissociation, have proven to be particularly useful for obtaining additional structural information not obtained with low-energy collision-based activation methods. The work presented herein focuses on structural characterization of phosphatidylcholines and lipooligosaccharides, subclasses of glycerophospholipids and saccharolipids, respectively, with an emphasis on coupling novel tandem mass spectrometry methods to shotgun, chromatographic and imaging workflows.

1.2 MASS SPECTROMETRY-BASED LIPIDOMICS

Lipids are a structurally diverse class of biomolecules that influence cell membrane structure, act as energy storage reservoirs, and participate in signal transduction.² Lipids are divided in to eight categories: fatty acyls, glycerolipids, glycerophospholipids, sphingolipids, sterol lipids, prenol lipids and saccharolipids (**Figure 1.1**).

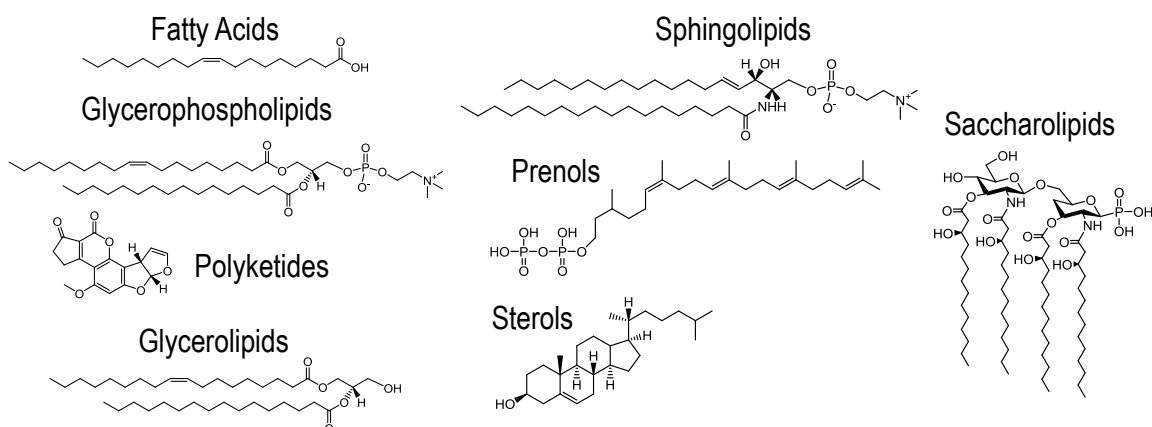


Figure 1.1 Representative structures from each of the eight categories of the lipids

The spatial distributions of lipids in cells is tightly regulated yet highly dynamic, with differences in lipid composition occurring not only across different types of cells, but also between the leaflets of lipid bilayers and laterally across membranes.^{2–7} Alterations in lipid composition have pronounced biological effects in both eukaryotic and prokaryotic cells. While controlled changes permit cells to respond to environmental stimuli, unregulated alterations can result in pathological states. For example, lipid modification in Gram-negative bacteria can provide resistance to antibiotics, whereas aberrant lipid metabolism in eukaryotic cells has been linked to diseases including cancer, diabetes, and Alzheimer's.^{8,9} Lipid characterization is therefore critical for a full understanding of biological processes and provides a measure of phenotypic status of a system. Lipidomics, the field of study that aims to profile and structurally characterize all the lipids within a biological system, has largely been driven by advances in mass spectrometry technology including the development of soft ionization techniques and new mass analyzers.^{1,10–16} Various sample preparation and mass spectrometric approaches have been developed to acquire specific types of information and to address the challenges associated with identification, characterization, and quantitation of each

category of lipids.^{17,18} Direct infusion of lipids, a strategy termed “shotgun lipidomics”, provides a molecular fingerprint and permits a rapid assessment of complex mixtures.^{19–23} However, simultaneous introduction of all lipids without separation can result in signal suppression of lower abundance lipids owing to division of signal across all the components of the mixture. Online chromatographic workflows can be used to alleviate signal suppression associated with shotgun methods.^{24,25} Neither shotgun nor chromatographic workflows provide any information regarding the spatial distribution of lipids in a sample. Mass spectrometry imaging, a technique that samples directly from surfaces, provides lipid spatial information by performing a shotgun-style experiment *in situ* at each point on a sample surface. Two-dimensional plots of m/z intensities provide images that display the relative abundances of ions in space. The most commonly used ionization techniques for MSI are desorption electrospray ionization (DESI) and matrix-assisted laser desorption ionization (MALDI).²⁶ Ion mobility spectrometry, a gas-phase electrophoretic technique that separates ions based on their charge, shape and size, can also be coupled to shotgun, chromatographic and imaging workflows to provide another dimension of separation.²⁷ Considering complexity of spectra generated during shotgun and imaging experiments have benefitted considerably from integration with ion mobility.²⁸

With shotgun, chromatographic, and imaging workflows, differing levels of lipid structural detail can be obtained depending on the type of mass spectra collected.^{20,29} MS¹ spectra provide an intact mass measurement of detected lipids. For methods that rely on intact mass measurements from MS¹ spectra the most informative experiments are ones performed on high resolving power mass spectrometers that can, in some cases, enable molecular formula determination. High resolving power mass spectrometers also permit isobar differentiation, which is particularly beneficial for shotgun and imaging workflows

that often generate complex spectra.³⁰ For a higher level of characterization, methods utilizing tandem mass spectrometry, are employed. Tandem mass spectrometry (MS/MS or MSⁿ) entails gas-phase fragmentation of a mass selected ions. The resulting fragment ions provide a higher level of structural characterization and can therefore provide more detail regarding the overall lipidomic profile.

1.3 GLYCEROPHOSPHOLIPIDS

Glycerophospholipids, the main component of cell membranes, are composed of a glycerol backbone with acyl/alkyl chains at the *sn*-1 and *sn*-2 positions, and a phosphate-linked polar head group at the *sn*-3 position (**Figure 1.2**).³¹

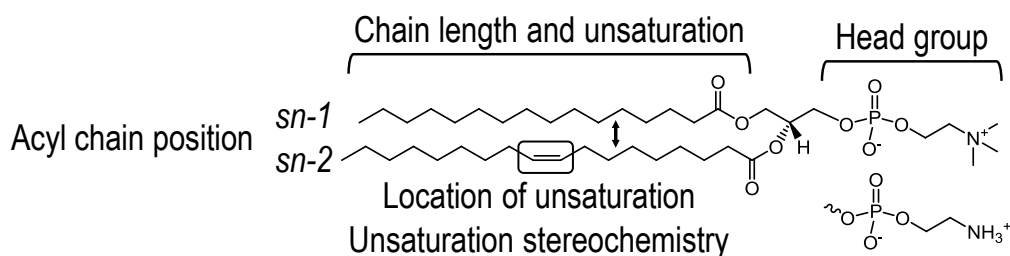


Figure 1.2 General structure of a glycerophospholipid

Combinations of structural features (head group, acyl chain length and unsaturation, *sn*-stereochemistry, unsaturation position, and unsaturation stereochemistry) lead to hundreds of thousands of possible glycerophospholipid structures, with subtle alterations in structure having large biological implications.^{1,6,29,32–34} For example, changes in the positions of double bonds have been shown to influence membrane fluidity.³³ Glycerophospholipid headgroups generally dictate the polarity (negative versus positive ionization modes) in which mass spectrometry experiments are performed, with phosphatidylcholines (PC) and phosphatidylethanolamines (PE) analyzed in positive

mode and phosphatidic acids (PA), phosphatidylserines (PS) and phosphatidylinositols (PI) analyzed in negative mode.³¹ Various complexation and derivatization methods have been devised to influence the ionization preference and increase sensitivity for glycerophospholipids.³⁵ For example, McLuckey and coworker have used gas-phase ion-ion reactions between a dianionic reagent and lipid cations to achieve high signal intensities in negative ion mode for glycerophospholipids that preferentially ionize in positive mode.^{36–38}

Depending on the mass spectrometric workflow, varying levels of structural characterization can be attained. Top-down high-resolution accurate-mass (HRAM) experiments enable determination of the “sum composition” level of structural characterization, as defined by Ekroos), with just an intact mass measurement; this level of characterization includes the head group, total number of carbons in the acyl/alkyl chains, and the number of unsaturations.^{30,39–41} For additional structural information, tandem mass spectrometry is required. Early lipidomics studies performed on ion trap and triple quadrupole instruments utilized tandem mass spectrometry and were critical for establishing the field of lipidomics.³⁹ While the most common low-energy collision-based ion activation methods provide more information than an intact mass measurement alone, they often fail at elucidating some of the more subtle structural features. Various methods, novel ion activation methods, have been investigated in an attempt to provide complete structural characterization.⁴²

1.4 TANDEM MASS SPECTROMETRY OF GLYCEROPHOSPHOLIPIDS

1.4.1 Low-Energy Collisional-Induced Dissociation (CID) and Infrared Multiphoton Dissociation (IRMPD)

Low-energy collision-induced dissociation (CID) is the most commonly used ion activation method for fragmentation of glycerophospholipids and has been characterized in detail.^{31,43,44} Low-energy CID causes fragmentation via conversion of kinetic energy of an ion to internal energy through low-energy collisions with an inert gas, typically helium or nitrogen. Ions with low kinetic energies (<100 eV) require multiple collisions to induce fragmentation and result in cleavage of the most labile bonds. Low-energy CID has been incorporated into modern mass spectrometers either through resonant-excitation of ions in ion traps by application of an auxiliary waveform at the ion secular frequency, or beam-type activation through acceleration of ions into a collision cell. Beam-type activation is the cornerstone of tandem mass spectrometry on triple-quadrupole mass spectrometers with the second quadrupole (Q2) functioning as a collision cell. [Note: Beam-type activation has been termed higher-energy collision-dissociation (HCD) on Thermo Orbitrap platforms where collisional activation occurs in a dedicated collisional cell, and should not be confused with true high-energy keV CID.)] In positive mode, low-energy CID of glycerophospholipids results in abundant product ion or neutral loss fragments corresponding to head group loss, in addition to very low abundance neutral loss ions corresponding to loss of acyl chains either as fatty acids or ketenes.⁴³ Both charge-driven and charge remote processes play a role in the observed fragmentation.⁴³ Activation of glycerophospholipids cations by infrared multiphoton dissociation (IRMPD), an activation method that uses infrared photons from a CO₂ laser to vibrationally excite ions, produces similar fragmentation patterns to low-energy CID.⁴⁵ In negative mode, low-energy CID results in abundant fatty acid product ions and lower

abundance neutral loss ions also corresponding to loss of acyl chains as fatty acids or ketenes. The fragment ions generated by low-energy CID can therefore confirm the glycerophospholipid subclass and acyl chain composition. In addition, the relative abundances of product and neutral loss ions originating from cleavage of acyl chains have previously been correlated to *sn*-position.⁴³ However, even with calibration using isomerically pure standards, caution must be exercised when relying on fragment ion abundances to determine *sn*-position, as the type of mass analyzer, collision energy and glycerophospholipid structure can all influence the relative abundances of fragment ions; to unequivocally determine acyl chain *sn*-position, fragment ions unique to each *sn*-position are necessary.³¹ Predictable head group and acyl chain fragment ions have led to the implementation of low-energy CID in both shotgun^{44,46–48} and LC-based lipidomic workflows. For example, a multidimensional mass spectrometry shotgun method for glycerophospholipid analysis that utilizes the different scanning modes of triple-quadrupole mass spectrometers enables rapid characterization of many glycerophospholipid species present in a complex sample.⁴⁸ Considering the structural information obtained from each polarity, charge-inversion methods have been developed to ensure that the glycerophospholipid precursor ion charge matches the desired analysis polarity.^{36,49,50} For instance, to obtain acyl chain information from fatty acid fragment anions for PCs that preferentially ionize in positive mode, PC cations were converted to anions through gas-phase charge-inversion via complexation with a dianion. Low-energy CID of the resulting electrostatic complex yielded characteristic fatty acid anions.

Low-energy CID is by far the most utilized ion activation technique, yet critical structural features, including double bond position within acyl chains, remain unresolved. Numerous strategies have employed metal complexation^{50–52} or derivatization^{53–67} to alter the observed fragmentation to address the shortcomings of low-energy CID. Using

lithium adduction in combination with MSⁿ activation in an ion trap, Hsu *et al.* were able to determine double bond positions within acyl chains through fragment ions generated by charge-remote fragmentation.⁵¹ While this method is also capable of determining acyl chain *sn*-position, it again relies on ion abundances rather than unique fragment ions. Derivatization methods used to localize unsaturations in acyl chains include, but are not limited to, Paternò-Büchi reactions^{53–59}, epoxidation reactions^{60–62}, and oxidation reactions^{63–65}. In general, derivatization methods chemically modify unsaturations such that they produce diagnostic pairs or sets of fragment ions upon low-energy CID. For example, collisional activation of Paternò-Büchi reaction products form diagnostic pairs of ions separated by 26 Da that enable localization of unsaturations within acyl chains. Workflows utilizing Paternò-Büchi reactions have revealed detectable differences in the relative abundances of double bond positional isomers between tissue and plasma of various pathological states.⁵⁹

While complexation and derivatization strategies enable manipulation of low-energy CID fragmentation patterns, alternative ion activation methods are another means by which to obtain additional structural information. These included high-energy CID, ozone-induced dissociation (OzID), electron-based activation methods, charge-transfer dissociation (CTD), helium metastable atom-activated dissociation (He-MAD), radical-directed dissociation (RDD) and ultraviolet photo dissociation (UVPD). These methods have also been used in conjunction with metal complexation and derivatization, and in tandem with low-energy CID.

1.4.2 High-Energy CID

High-energy CID, similar to low-energy CID, relies on conversion of kinetic energy to internal energy via collisions. However, in high-energy CID, ions are

accelerated to kinetic energies in the keV range.^{68,69} Upon collision with an inert gas, ions can be electronically excited and decompose via charge-remote fragmentation. High-energy CID was traditionally performed on tandem sector mass spectrometers that could accelerate ions to high translational energies. On such instruments, fragmentation along the length of C-C bonds of acyl chains could be used to localize double bonds.⁷⁰ With the decline in popularity of sector instruments, high-energy CID became a less widely used activation method. In recent years, implementation of high-energy CID on MALDI-TOF-TOF instruments has led to resurgence of interest in its application to biomolecule characterization owing to the informative spectra that are generated.⁷¹⁻⁷⁵ In the context of glycerophospholipids, high-energy CID appears to be most successful for salt-adducted species.⁷⁴ Activation of the $[M+K]^+$ ion of PC 16:0_18:1 at m/z 798 resulted in fragment ions typically observed for low-energy CID, including head group and acyl chain neutral losses, in addition to a series of ions above m/z 500 corresponding to C-C bond cleavages, that enable localization of double bonds.⁷⁵ Similarly informative spectra were also obtained for lipid anions. Unlike the spectra for low-energy CID of derivatized lipids, high-energy CID spectra do not contain a distinct set or pair of diagnostic ions, rather cleavage occurs along the entirety of each acyl chain. Therefore, spectra are often congested and can be challenging to interpret. Despite the additional structural information that can be obtained with high-energy CID, the short interaction time between ions and inert gas also results in low fragmentation efficiency and low sensitivity.

1.4.3 Ozone-Induced Dissociation (OzID)

Pioneered by Blanksby and coworkers, ozone-induced dissociation (OzID) is a gas-phase fragmentation technique in which ozone is reacted with ions under vacuum,

primarily at the locations of unsaturations.⁷⁶ In glycerophospholipids, OzID can be used to localize double bonds in acyl chains by forming a primary ozonide ring at the location of unsaturation which subsequently fragments to form diagnostic aldehyde and Criegee ions spaced 16 Da apart. In its first iteration, OzID was implemented on a linear ion trap mass spectrometer where ion-molecule reactions and ion detection occurred in the same region of the instrument. The limited allowable pressure of ozone that could be used without negatively impacting spectral resolution resulted in long activation times (~10 s) and low-intensity informative fragment ions.⁷⁶ In its second iteration, a hybrid triple quadrupole-linear ion trap mass spectrometer was outfitted with OzID, where ion-molecule reactions occurred in Q2 and mass analysis occurred in the linear ion trap (Q3).⁷⁷ Increased ozone pressure was attained in Q2 without negatively affecting the spectral quality; separation of the reaction and analysis regions significantly diminished reaction times (~1s) and increased sensitivity. On both platforms, MSⁿ capabilities allowed OzID to be performed in tandem with low-energy CID. Activation of sodium-adducted glycerophospholipids followed by OzID of the dioxolane-type fragment ion, generated fragments ions diagnostic of acyl chain *sn*-position.⁷⁸ This tandem mass spectrometry method was the first to use unique ions to determine *sn*-position rather than rely on ion abundances as previous methods have done. Double bond positions with acyl chains could additionally be determined by a subsequent OzID activation step [CID/(OzID)²], enabling near complete characterization. Despite relatively long activation times (~1-10s), OzID and CID/OzID were successfully incorporated in to chromatographic and imaging workflows, yet coupling of OzID to UPLC separations, where chromatographic peak widths are narrow, required further reduction in ion-molecule reaction times were required.⁷⁹⁻⁸² As such, a hybrid quadrupole-TOF mass spectrometer with ion mobility separation capabilities was modified to utilize the ion

mobility cell as a high pressure OzID reaction chamber.⁸³ The dramatic increase in allowable ozone pressure in the ion mobility cell further reduced reaction times to 20-200 ms and enabled identification of UPLC-separated PC double-bond positional isomers. Use of the ion mobility cell as a high pressure reaction chamber precluded its use for gas-phase ion mobility separations and inspired implementation of OzID on a quadrupole-TOF mass spectrometer with ion mobility separation capabilities and a separate high pressure trapping ion funnel where ion-molecule reactions took place.⁸⁴ While much progress has been made to increase OzID reaction efficiency, to date, OzID on all platforms occurs along the main ion path. Exposure of all ions to ozone currently limits the utility of OzID to workflows to those that do not require acquisition of MS¹ and tandem mass spectra, i.e., data-dependent acquisition, in sequence. Incorporation of a dedicated reaction chamber orthogonal to the main ion path could further increase the utility of OzID.

1.4.4 Electron-Based Activation Methods

Electron-based activation methods promote fragmentation via gas-phase interaction of ions with either electrons, or radical anions or cations. The fundamental differences between the variety of electron-based activation methods lie in the electron energy and ion polarity. Electron capture dissociation (ECD) and electron transfer dissociation (ETD) induce fragmentation of cations by addition/transfer of electrons to cations via low-energy electrons (~0.1 eV) and radical anions, respectively. ECD and ETD have had much success in the realm of protein analysis, however these methods effectively neutralized singly charged lipid cations and are therefore of little utility for lipid analysis. While ETD and ECD were effectively performed on multiply charged metal-glycerophospholipid complexes, the observed fragmentation patterns yielded

comparable or less structural information than low-energy CID.^{85,86} Methods termed electron-induced dissociation (EID) or electron impact excitation of ions from organics (EIEIO), where ions are irradiated with a beam of higher energy electrons (>9 eV), have been shown to provide informative fragmentation spectra for glycerophospholipid cations.⁸⁷⁻⁹⁰ Higher energy electrons induced charge-remote fragmentation that provided cleavage of C-C bonds along the acyl chains acyl that enabled double bond localization. Fragment ion intensities were additionally used to determine *sn*-position. In general, fragment ion intensities for EID/EIEIO are low and cleavage is not specific, resulting in complex spectra. To date, no negative mode electron-based activation methods have been used to analyze glycerophospholipids.

1.4.5 He-Metastable Atom-Activated Dissociation (He-MAD) and Charge-Transfer Dissociation (CTD)

Helium metastable atom-activated dissociation (He-MAD) and charge transfer dissociation (CTD) are fragmentation techniques in which a beam of high energy metastable helium atoms or helium cations, respectively, are directed at trapped ions.⁹¹⁻⁹³ The fragmentation patterns produced by He-MAD and CTD of phosphatidylcholine cations ions are very similar to each other and to other electron-based activation methods; spectra contain a series of fragment ions corresponding to cleavage of C-C bonds along the entire length of the acyl chains. He-MAD and CTD therefore also permit localization of double bonds within acyl chains. Unique to He-MAD and CTD are product ions with an increased charge state resulting from electron detachment. Also similar to electron-based activation methods, He-MAD and CTD spectra are complex as a result of non-specific cleavage.

1.4.6 Radical-Directed Dissociation (RDD) and Ultraviolet Photodissociation (UVPD)

Activation of ions with UV photons is another means by which to access excited electronic states that can lead to fragmentation patterns that are complementary to those generated by low-energy CID.⁹⁴ Ion-photon reactions are most common performed by directing the beam of a UV laser through an optical window in line with the ion-trapping region of a mass spectrometer. The observed product ions are dependent on the laser wavelength and the photon absorption properties of precursor ions. Radical-directed dissociation (RDD), which utilizes 266 nm photons generated by the fourth harmonic of a neodymium-doped yttrium aluminum garnet (Nd:YAG) laser, is a clever means by which to initiate radical fragmentation for singly charged glycerophospholipids ions.^{95–97} RDD requires two stages of activation: (1) photoactivation of isolated singly-charged ions covalently-modified or non-covalently complexed with molecules containing a “photocaged” radical and (2) low-energy CID of the resulting “uncaged” radical product ion. RDD spectra contain a series of product ions corresponding to cleavage along the acyl/alkyl chain with ions spaced 12 Da apart indicating the locations of unsaturations. Heiles and coworkers also coupled ultraviolet photodissociation (UVPD) at 266 nm with Paternò-Büchi reactions for localization of double bonds within acyl chains and further used the fourth fifth harmonic of a Nd:YAG laser at 213 nm for differentiation of *sn*-position isomers.^{98,99}

Excimer lasers at 193 nm have recently gained popularity for biomolecule fragmentation as innate structural features absorb at this wavelength.⁹⁴ UVPD at 193 nm has been previously used for lipid structural characterization and has recently been utilized to localize double bonds within acyl chains of phosphatidylcholines without derivatization, as is detailed in Chapters 3 and 4.^{100–104} Fragmentation is mediated by

absorption of 193 nm photons at unsaturations, with the number of unsaturations influencing both the fragmentation efficiency and the production of even- and odd-electron fragment ions. UVPD at 193 nm was further extended to determine both double bond positions and acyl chain *sn*-positions using an MS³ method analogous to an MS³ OzID method in which an OzID is performed on a dioxolane-type fragment ion.^{78,105}

1.5 LIPOPOLYSACCHARIDES/LIPOOLIGOSACCHARIDES

Lipopolysaccharides (LPS) are structurally complex saccharolipids that occur exclusively in the outer leaflet of the outer membrane of Gram-negative bacteria (**Figure 1.3a**).¹⁰⁶ LPS is composed of three distinct regions: lipid A, core oligosaccharide and O-antigen.

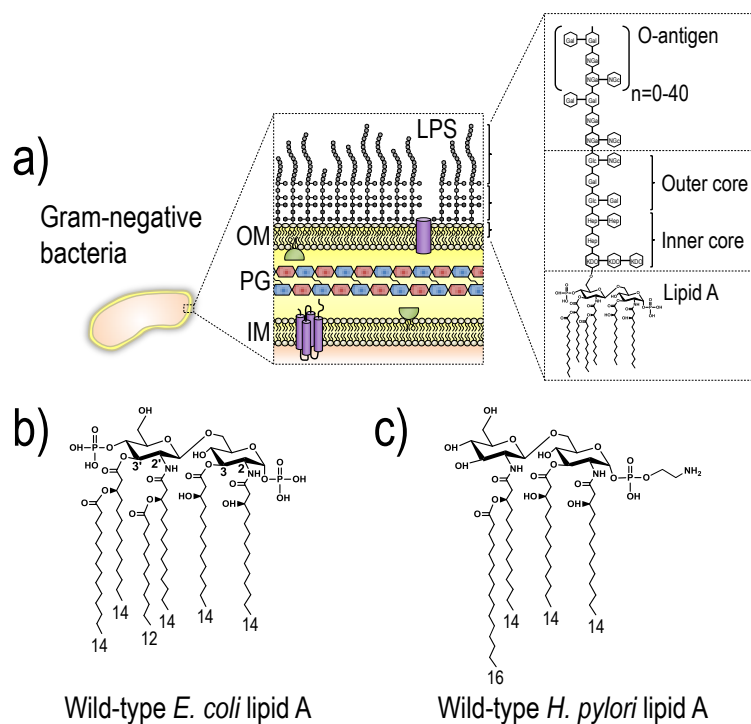


Figure 1.3 a) Schematic of lipopolysaccharides on the surface of Gram-negative bacteria. The outer membrane, peptidoglycan, and inner membrane are labeled OM, PG, and IM, respectively. b) Structure of *E. coli* lipid A with labeled acyl chain positions. c) Structure of *H. pylori* lipid A.

Lipid A is the hydrophobic membrane anchor consisting of a β (1-6)-linked diglucosamine backbone that is variably acylated and phosphorylated at the 2, 3, 2' and 3' positions, and 1 and 4' positions, respectively. Lipid A of LPS is a pathogen-associated molecular pattern (PAMP) recognized by the mammalian innate immune system via the Toll-like receptor 4 (TLR4)/myeloid differentiation factor 2 (MD2) complex.¹⁰⁷⁻¹¹⁰ While recognition of lipid A by the TLR4/MD2 complex is essential for infection clearance, over-stimulation can result in potentially fatal septic shock.¹¹⁰ Bis-phosphorylated, hexa-acylated lipid A elicits the maximum stimulatory effect of the TLR4/MD2 complex (**Figure 1.3b**). Alterations in lipid A structure not only influence immune system recognition and potency of response, but also modulate bacterial susceptibility to antibiotics.¹¹¹ For example, *Helicobacter pylori*, a Gram-negative bacteria that colonizes the gastrointestinal tract, produces a tetra-acylated lipid A with a single phosphoethanolamine modification at the 1 position of the proximal glucosamine (**Figure 1.3c**).¹¹¹⁻¹¹³ The acyl chain composition and phosphate arrangement of *H. pylori* cause a weak response that enable innate immune system evasion. In addition, removal or modification of phosphate groups effectively neutralizes the anionic surface charge of the Gram-negative outer membrane and make cationic antimicrobial peptides (CAMPs) no longer effective. Lipid A modification is one mechanism by which Gram-negative bacteria have developed antibiotic resistance.

The core oligosaccharide is composed of a series of saccharides glycosidically linked to lipid A through 3-deoxy-D-mano-oct-2-ulosonic acid (Kdo). (Kdo)₂-lipid A is the minimal LPS structure required for viable Gram-negative bacteria. The core oligosaccharide can be divided in to an inner core and outer core (**Figure 1.3a**). The inner core is highly conserved among a species and, similar to lipid A, can be non-stoichiometrically modified to further decrease membrane permeability and stabilize the

bacterial membrane.^{114–116} The outer core is generally much more variability in its saccharide structure.

Connected to the core oligosaccharide is the hydrophilic O-antigen, a variably repeating saccharide unit composed of two to eight saccharides.¹¹⁷ Not all bacterial species produce LPS with O-antigen. Those that do have the appearance of smooth colonies on agar plates and are therefore called smooth-type LOS (S-LPS), while those that do not have the appearance of rough colonies on agar plates and are therefore called rough-type LPS (R-LPS) or lipooligosaccharides (LOS).¹¹⁸ O-antigen can also be non-stoichiometrically modified, making it the most variable and structurally complex region of LPS.¹¹⁹ Another mechanism by which Gram-negative bacteria can evade the immune system is to produce O-antigen structures that mimic of host surface antigens. For example, *H. pylori* presents an O-antigen with characteristics that mimic Lewis antigens present on the surface of red blood cells.¹²⁰

Structural characterization of the features of LPS/LOS that confer antibiotic resistance and prevent immune system detection are necessary to further our understanding of bacterial modification systems and provide a guide for novel antibiotic development.

1.6 MASS SPECTROMETRY OF LPS/LOS

Determination of structural features of LPS/LOS by mass spectrometry is most commonly done by decomposing LPS/LOS and performing analysis on its constituent lipid A and polysaccharide portions, often with separation by liquid chromatography (LC) or capillary electrophoresis (CE).^{100,121–130} Of the lipid A characterization methods that employ online separations, the highest quality separations to date have used trimethylamine (TEA) as a mobile phase additive, which is known to cause signal

suppression.^{123–125,131} Other lipid A and oligosaccharide online separation techniques have generally produce modest results. Tandem mass spectrometry has been used heavily for structural characterization of the lipid A moiety. Low-energy CID, IRMPD, UVPD, and activated-electron photodetachment (a-EPD) have all been used to obtained detailed structural characterization of lipid A.^{100,121,127,128,132,133} Low-energy CID cleaves the most labile bonds in lipid A structures, which results in abundant fragments corresponding to acyl chain neutral losses from the 3 and 3' positions, fatty acid anions and small molecule neutral losses, i.e. H₂O, H₃PO₄. While IRMPD produces similar fragmentation patterns to CID, comparison of CID and IRMPD spectra allow rapid identification of phosphate containing fragment ions owing to the fact that P-O bonds are strong IR chromophores, resulting in rapid and preferential annihilation of phosphorylated products.¹⁰⁰ In particular, Madsen *et al.* used CID and IRMPD to confirm phospho-containing product ions of lipid A.¹⁰⁰ Both UVPD and a-EPD cleave C-O and C-N bonds in addition to cross-ring cleavages that assist with localization of acyl chains on the glucosamine ring structures, and therefore produce more structurally informative spectra.^{100,127} A number of lipid A characterization methods have utilized the sequential MSⁿ capabilities of ion traps to assign structures.^{128,134,135} Owing to the amphipathic nature of intact LPS/LOS and the heterogeneity of native LPS/LOS samples, far fewer analytical methods have been developed for intact species, many of them shotgun methods.^{136–140} A number of methods have used collisional activation to bisect the lipid A and saccharide portions in the gas phase, some of which have utilized ion mobility spectrometry to further identify lipid A and oligosaccharide portions.^{139,140} Of the methods that have incorporated online separations of intact LPS/LOS, most experienced either reduced sensitivities or overall modest separation efficiency.^{121,141,142}

1.6 OVERVIEW OF CHAPTERS

Considering the complexity and variety of lipid structures, analytical methods are generally tailored to the specific challenges associated with each lipid category. The research presented in this dissertation aims to improve structural characterization of phosphatidylcholines and lipopolysaccharides/lipooligosaccharides, through the use of UVPD at 193 nm, within the context of the shotgun, chromatographic and imaging workflows.

In Chapter 3, 193 nm UVPD was evaluated as an ion activation method for structural characterization of phosphatidylcholines. Photoirradiation resulted in diagnostic pairs of fragment ions with a 24 Da difference that facilitated localization of double bonds within acyl chains. To assess the influence of specific structural features on the observed fragmentation patterns, UVPD spectra were collected for a series of phosphatidylcholine standards with varying structural features, including double bond positions, acyl chain *sn*-positions, and number of double bonds. The developed UVPD method was then applied to a shotgun infusion experiment whereby double bond positional isomers were identified in a complex lipid extract.

In Chapter 4, the UVPD method developed in Chapter 3, was applied to direct analysis of tissue sections using desorption electrospray ionization (DESI). In all experiments, UVPD was performed on surface-desorbed ions isolated in the mass spectrometer. DESI profiling experiments confirmed successful coupling to UVPD and verified changes in the relative abundances of double bond isomers across tissue types. DESI-UVPD imaging experiments enabled correlation of changes in the spatial distribution of phosphatidylcholine double bond isomers to specific tissue features.

Saccharolipids represent one of the more structurally complex categories of lipids. Traditional workflows to structurally characterize LPS/LOS rely on chemical

decomposition to constituent lipid A and core oligosaccharide components. However, decomposition has the potential to remove biologically relevant labile modifications and precludes determination of combinations of lipid A and oligosaccharide structures present. In Chapter 5, an MS³ method was developed to structurally characterize the lipid A and core oligosaccharide components of intact lipooligosaccharides. Low-energy CID of intact lipooligosaccharides resulted cleavage of the glycosidic bond between the lipid A and core oligosaccharides portions. Subsequent activation of the lipid A and core oligosaccharide fragment ions by UVPD enabled a high level of characterization, including localization of phosphate and pyrophorylethanolamine modifications, and differentiation of lipooligosaccharides isomers.

The data presented in Chapter 5 make obvious the heterogeneity of lipooligosaccharides samples and reveals the pitfalls of relying on direct shotgun analysis. In Chapter 6, the MS³ method developed in Chapter 5 is coupled to online chromatographic separations with MS³ analysis performed in a targeted manner. After assessing separation characteristics of the LC method and the capabilities of UVPD on a standard mutant *E. coli* sample, unknown LOS structures from clinically relevant strains of *Acinetobacter baumannii* were determined.

In Chapter 7, 193 nm UVPD was evaluated for structural characterization of glycosaminoglycan (GAG) saccharides. GAGs are highly acidic, variably sulfated linear polysaccharides whose modifications and structural variants modulate specific interactions with proteins. Low-energy collisional activation of heavily sulfated native GAGs results predominantly in sulfate decomposition which prevents acquisition of saccharide sequence information and sulfate localization. 193 nm UVPD enabled both saccharide sequencing and sulfate localization with results similar to NETD and electron-detachment dissociation (EDD).

1.7 REFERENCES

- (1) Dennis, E. A. Lipidomics Joins the Omics Evolution. *Proc. Natl. Acad. Sci.* **2009**, *106*, 2089–2090.
- (2) van Meer, G.; Voelker, D. R.; Feigenson, G. W. Membrane Lipids: Where They Are and How They Behave. *Nat. Rev. Mol. Cell Biol.* **2008**, *9*, 112–124.
- (3) Holthuis, J. C. M.; Levine, T. P. Lipid Traffic: Floppy Drives and a Superhighway. *Nat. Rev. Mol. Cell Biol.* **2005**, *6*, 209–220.
- (4) Sezgin, E.; Levental, I.; Mayor, S.; Eggeling, C. The Mystery of Membrane Organization: Composition, Regulation and Roles of Lipid Rafts. *Nat. Rev. Mol. Cell Biol.* **2017**, *18*, 361–374.
- (5) Janmey, P. A.; Kinnunen, P. K. J. Biophysical Properties of Lipids and Dynamic Membranes. *Trends Cell Biol.* **2006**, *16*, 538–546.
- (6) Zhang, Y.-M.; Rock, C. O. Membrane Lipid Homeostasis in Bacteria. *Nat. Rev. Microbiol.* **2008**, *6*, 222–233.
- (7) Raetz, C. R. H.; Reynolds, C. M.; Trent, M. S.; Bishop, R. E. Lipid A Modification Systems in Gram-Negative Bacteria. *Annu. Rev. Biochem.* **2007**, *76*, 295–329.
- (8) Harayama, T.; Riezman, H. Understanding the Diversity of Membrane Lipid Composition. *Nat. Rev. Mol. Cell Biol.* **2018**, 1–16.
- (9) Wenk, M. R. The Emerging Field of Lipidomics. *Nat. Rev. Drug Discov.* **2005**, *4*, 594–610.
- (10) Shevchenko, A.; Simons, K. Lipidomics: Coming to Grips with Lipid Diversity. *Nat. Rev. Mol. Cell Biol.* **2010**, *11*, 593–598.
- (11) Hu, T.; Zhang, J.-L. Mass-Spectrometry-Based Lipidomics. *J. Sep. Sci.* **2018**, *41*, 351–372.
- (12) Han, X. Lipidomics for Studying Metabolism. *Nat. Rev. Endocrinol.* **2016**, *12*, 668–679.
- (13) Gross, R. W. The Evolution of Lipidomics through Space and Time. *Biochim. Biophys. Acta BBA - Mol. Cell Biol. Lipids* **2017**, *1862*, 731–739.
- (14) Köfeler, H. C.; Fauland, A.; Rechberger, G. N.; Trötz Müller, M. Mass Spectrometry Based Lipidomics: An Overview of Technological Platforms. *Metabolites* **2012**, *2*, 19–38.
- (15) Rolim, A. E. H.; Henrique-Araújo, R.; Ferraz, E. G.; de Araújo Alves Dultra, F. K.; Fernandez, L. G. Lipidomics in the Study of Lipid Metabolism: Current Perspectives in the Omic Sciences. *Gene* **2015**, *554*, 131–139.

- (16) Harkewicz, R.; Dennis, E. A. Applications of Mass Spectrometry to Lipids and Membranes. *Annu. Rev. Biochem.* **2011**, *80*, 301–325.
- (17) Wenk, M. R. Lipidomics: New Tools and Applications. *Cell* **2010**, *143*, 888–895.
- (18) Holčapek, M.; Liebisch, G.; Ekroos, K. Lipidomic Analysis. *Anal. Chem.* **2018**, *90*, 4249–4257.
- (19) Hsu, F.-F. Mass Spectrometry-Based Shotgun Lipidomics – a Critical Review from the Technical Point of View. *Anal. Bioanal. Chem.* **2018**, *410*, 6387–6409.
- (20) Rustam, Y. H.; Reid, G. E. Analytical Challenges and Recent Advances in Mass Spectrometry Based Lipidomics. *Anal. Chem.* **2018**, *90*, 374–397.
- (21) Han, X.; Gross, R. W. Shotgun Lipidomics: Electrospray Ionization Mass Spectrometric Analysis and Quantitation of Cellular Lipidomes Directly from Crude Extracts of Biological Samples. *Mass Spectrom. Rev.* **2005**, *24*, 367–412.
- (22) Yang, K.; Han, X. Lipidomics: Techniques, Applications, and Outcomes Related to Biomedical Sciences. *Trends Biochem. Sci.* **2016**, *41*, 954–969.
- (23) Wang, M.; Wang, C.; Han, R. H.; Han, X. Novel Advances in Shotgun Lipidomics for Biology and Medicine. *Prog. Lipid Res.* **2016**, *61*, 83–108.
- (24) Damen, C. W. N.; Isaac, G.; Langridge, J.; Hankemeier, T.; Vreeken, R. J. Enhanced Lipid Isomer Separation in Human Plasma Using Reversed-Phase UPLC with Ion-Mobility/High-Resolution MS Detection. *J. Lipid Res.* **2014**, *55*, 1772–1783.
- (25) Cajka, T.; Fiehn, O. Comprehensive Analysis of Lipids in Biological Systems by Liquid Chromatography-Mass Spectrometry. *TrAC Trends Anal. Chem.* **2014**, *61*, 192–206.
- (26) Gode, D.; A. Volmer, D. Lipid Imaging by Mass Spectrometry – a Review. *Analyst* **2013**, *138*, 1289–1315.
- (27) Paglia, G.; Kliman, M.; Claude, E.; Geromanos, S.; Astarita, G. Applications of Ion-Mobility Mass Spectrometry for Lipid Analysis. *Anal. Bioanal. Chem.* **2015**, *407*, 4995–5007.
- (28) Sans, M.; Feider, C. L.; Eberlin, L. S. Advances in Mass Spectrometry Imaging Coupled to Ion Mobility Spectrometry for Enhanced Imaging of Biological Tissues. *Curr. Opin. Chem. Biol.* **2018**, *42*, 138–146.
- (29) Brown, S. H. J.; Mitchell, T. W.; Oakley, A. J.; Pham, H. T.; Blanksby, S. J. Time to Face the Fats: What Can Mass Spectrometry Reveal about the Structure of Lipids and Their Interactions with Proteins? *J. Am. Soc. Mass Spectrom.* **2012**, *23*, 1441–1449.

- (30) Schwudke, D.; Schuhmann, K.; Herzog, R.; Bornstein, S. R.; Shevchenko, A. Shotgun Lipidomics on High Resolution Mass Spectrometers. *Cold Spring Harb. Perspect. Biol.* **2011**, 3, a004614.
- (31) Pulfer, M.; Murphy, R. C. Electrospray Mass Spectrometry of Phospholipids. *Mass Spectrom. Rev.* **2003**, 22, 332–364.
- (32) Antonny, B.; Vanni, S.; Shindou, H.; Ferreira, T. From Zero to Six Double Bonds: Phospholipid Unsaturation and Organelle Function. *Trends Cell Biol.* **2015**, 25, 427–436.
- (33) Martinez-Seara, H.; Róg, T.; Pasenkiewicz-Gierula, M.; Vattulainen, I.; Karttunen, M.; Reigada, R. Interplay of Unsaturated Phospholipids and Cholesterol in Membranes: Effect of the Double-Bond Position. *Biophys. J.* **2008**, 95, 3295–3305.
- (34) Hishikawa, D.; Hashidate, T.; Shimizu, T.; Shindou, H. Diversity and Function of Membrane Glycerophospholipids Generated by the Remodeling Pathway in Mammalian Cells. *J. Lipid Res.* **2014**, 55, 799–807.
- (35) Canez, C. R.; Shields, S. W. J.; Bugno, M.; Wasslen, K. V.; Weinert, H. P.; Willmore, W. G.; Manthorpe, J. M.; Smith, J. C. Trimethylation Enhancement Using ¹³C-Diazomethane (¹³C-TrEnDi): Increased Sensitivity and Selectivity of Phosphatidylethanolamine, Phosphatidylcholine, and Phosphatidylserine Lipids Derived from Complex Biological Samples. *Anal. Chem.* **2016**, 88, 6996–7004.
- (36) Stutzman, J. R.; Blanksby, S. J.; McLuckey, S. A. Gas-Phase Transformation of Phosphatidylcholine Cations to Structurally Informative Anions via Ion/Ion Chemistry. *Anal. Chem.* **2013**, 85, 3752–3757.
- (37) Rojas-Betancourt, S.; Stutzman, J. R.; Londry, F. A.; Blanksby, S. J.; McLuckey, S. A. Gas-Phase Chemical Separation of Phosphatidylcholine and Phosphatidylethanolamine Cations via Charge Inversion Ion/Ion Chemistry. *Anal. Chem.* **2015**, 87, 11255–11262.
- (38) Betancourt, S. K.; Canez, C. R.; Shields, S. W. J.; Manthorpe, J. M.; Smith, J. C.; McLuckey, S. A. Trimethylation Enhancement Using ¹³C-Diazomethane: Gas-Phase Charge Inversion of Modified Phospholipid Cations for Enhanced Structural Characterization. *Anal. Chem.* **2017**, 89, 9452–9458.
- (39) Junot, C.; Fenaille, F.; Colsch, B.; Bécher, F. High Resolution Mass Spectrometry Based Techniques at the Crossroads of Metabolic Pathways. *Mass Spectrom. Rev.* **2014**, 33, 471–500.
- (40) Ghaste, M.; Mistrik, R.; Shulaev, V. Applications of Fourier Transform Ion Cyclotron Resonance (FT-ICR) and Orbitrap Based High Resolution Mass Spectrometry in Metabolomics and Lipidomics. *Int. J. Mol. Sci.* **2016**, 17, 816.

- (41) *Lipidomics: Technologies and Applications*; Ekroos, K., Ed.; Wiley-VCH: Weinheim, Germany, 2012.
- (42) Zheng, X.; Smith, R. D.; Baker, E. S. Recent Advances in Lipid Separations and Structural Elucidation Using Mass Spectrometry Combined with Ion Mobility Spectrometry, Ion-Molecule Reactions and Fragmentation Approaches. *Curr. Opin. Chem. Biol.* **2018**, *42*, 111–118.
- (43) Hsu, F.-F.; Turk, J. Electrospray Ionization with Low-Energy Collisionally Activated Dissociation Tandem Mass Spectrometry of Glycerophospholipids: Mechanisms of Fragmentation and Structural Characterization. *J. Chromatogr. B* **2009**, *877*, 2673–2695.
- (44) Blanksby, S. J.; Mitchell, T. W. Advances in Mass Spectrometry for Lipidomics. *Annu. Rev. Anal. Chem.* **2010**, *3*, 433–465.
- (45) Yoo, H. J.; Håkansson, K. Determination of Phospholipid Regiochemistry by Ag(I) Adduction and Tandem Mass Spectrometry. *Anal. Chem.* **2011**, *83*, 1275–1283.
- (46) Yang, K.; Cheng, H.; Gross, R. W.; Han, X. Automated Lipid Identification and Quantification by Multidimensional Mass Spectrometry-Based Shotgun Lipidomics. *Anal. Chem.* **2009**, *81*, 4356–4368.
- (47) Schuhmann, K.; Herzog, R.; Schwudke, D.; Metelmann-Strupat, W.; Bornstein, S. R.; Shevchenko, A. Bottom-Up Shotgun Lipidomics by Higher Energy Collisional Dissociation on LTQ Orbitrap Mass Spectrometers. *Anal. Chem.* **2011**, *83*, 5480–5487.
- (48) Han, X.; Yang, K.; Gross, R. W. Multi-Dimensional Mass Spectrometry-Based Shotgun Lipidomics and Novel Strategies for Lipidomic Analyses. *Mass Spectrom. Rev.* **2012**, *31*, 134–178.
- (49) Svane, S.; Gorshkov, V.; Kjeldsen, F. Charge Inversion of Phospholipids by Dimetal Complexes for Positive Ion-Mode Electrospray Ionization Mass Spectrometry Analysis. *Anal. Chem.* **2015**, *87*, 8732–8739.
- (50) Hsu, F.-F.; Bohrer, A.; Turk, J. Formation of Lithiated Adducts of Glycerophosphocholine Lipids Facilitates Their Identification by Electrospray Ionization Tandem Mass Spectrometry. *J. Am. Soc. Mass Spectrom.* **1998**, *9*, 516–526.
- (51) Hsu, F.-F.; Turk, J. Structural Characterization of Unsaturated Glycerophospholipids by Multiple-Stage Linear Ion-Trap Mass Spectrometry with Electrospray Ionization. *J. Am. Soc. Mass Spectrom.* **2008**, *19*, 1681–1691.
- (52) Ho, Y.-P.; Huang, P.-C.; Deng, K.-H. Metal Ion Complexes in the Structural Analysis of Phospholipids by Electrospray Ionization Tandem Mass Spectrometry. *Rapid Commun. Mass Spectrom.* **2003**, *17*, 114–121.

- (53) Ma, X.; Chong, L.; Tian, R.; Shi, R.; Hu, T. Y.; Ouyang, Z.; Xia, Y. Identification and Quantitation of Lipid C=C Location Isomers: A Shotgun Lipidomics Approach Enabled by Photochemical Reaction. *Proc. Natl. Acad. Sci.* **2016**, *113*, 2573–2578.
- (54) Ma, X.; Xia, Y. Pinpointing Double Bonds in Lipids by Paternò-Büchi Reactions and Mass Spectrometry. *Angew. Chem.* **2014**, *126*, 2630–2634.
- (55) Stinson, C. A.; Xia, Y. A Method of Coupling the Paternò-Büchi Reaction with Direct Infusion ESI-MS/MS for Locating the C=C Bond in Glycerophospholipids. *Analyst* **2016**, 3696–3704.
- (56) Tang, F.; Guo, C.; Ma, X.; Zhang, J.; Su, Y.; Tian, R.; Shi, R.; Xia, Y.; Wang, X.; Ouyang, Z. Rapid In Situ Profiling of Lipid C=C Location Isomers in Tissue Using Ambient Mass Spectrometry with Photochemical Reactions. *Anal. Chem.* **2018**, *90*, 5612–5619.
- (57) Wäldchen, F.; Becher, S.; Esch, P.; Kompauer, M.; Heiles, S. Selective Phosphatidylcholine Double Bond Fragmentation and Localisation Using Paternò-Büchi Reactions and Ultraviolet Photodissociation. *Analyst* **2017**, *142*, 4744–4755.
- (58) Jeck, V.; Korf, A.; Vosse, C.; Hayen, H. Localization of double-bond positions in lipids by tandem mass spectrometry succeeding high-performance liquid chromatography with post-column derivatization. *Rapid Commun. Mass Spectrom.* **2018**, 1–9.
- (59) Zhang, W.; Zhang, D.; Chen, Q.; Wu, J.; Ouyang, Z.; Xia, Y. Online Photochemical Derivatization Enables Comprehensive Mass Spectrometric Analysis of Unsaturated Phospholipid Isomers. *Nat. Commun.* **2019**, *10*, 79.
- (60) Zhao, Y.; Zhao, H.; Zhao, X.; Jia, J.; Ma, Q.; Zhang, S.; Zhang, X.; Chiba, H.; Hui, S.-P.; Ma, X. Identification and Quantitation of C=C Location Isomers of Unsaturated Fatty Acids by Epoxidation Reaction and Tandem Mass Spectrometry. *Anal. Chem.* **2017**, *89*, 10270–10278.
- (61) Cao, W.; Ma, X.; Li, Z.; Zhou, X.; Ouyang, Z. Locating Carbon–Carbon Double Bonds in Unsaturated Phospholipids by Epoxidation Reaction and Tandem Mass Spectrometry. *Anal. Chem.* **2018**, *90*, 10286–10292.
- (62) Feng, Y.; Chen, B.; Yu, Q.; Li, L. Identification of Double Bond Position Isomers in Unsaturated Lipids by M-CPBA Epoxidation and Mass Spectrometry Fragmentation. *Anal. Chem.* **2019**.
- (63) Moe, M. K.; Strøm, M. B.; Jensen, E.; Claeys, M. Negative Electrospray Ionization Low-Energy Tandem Mass Spectrometry of Hydroxylated Fatty Acids: A Mechanistic Study. *Rapid Commun. Mass Spectrom.* **2004**, *18*, 1731–1740.

- (64) Stinson, C. A.; Zhang, W.; Xia, Y. UV Lamp as a Facile Ozone Source for Structural Analysis of Unsaturated Lipids Via Electrospray Ionization-Mass Spectrometry. *J. Am. Soc. Mass Spectrom.* **2017**, 1–9.
- (65) Harris, R. A.; May, J. C.; Stinson, C. A.; Xia, Y.; McLean, J. A. Determining Double Bond Position in Lipids Using Online Ozonolysis Coupled to Liquid Chromatography and Ion Mobility-Mass Spectrometry. *Anal. Chem.* **2018**, 90, 1915–1924.
- (66) Yang, K.; Diltthey, B. G.; Gross, R. W. Identification and Quantitation of Fatty Acid Double Bond Positional Isomers: A Shotgun Lipidomics Approach Using Charge-Switch Derivatization. *Anal. Chem.* **2013**, 85, 9742–9750.
- (67) Xu, Y.; Brenna, J. T. Atmospheric Pressure Covalent Adduct Chemical Ionization Tandem Mass Spectrometry for Double Bond Localization in Monoene- and Diene-Containing Triacylglycerols. *Anal. Chem.* **2007**, 79, 2525–2536.
- (68) Stroobant, Vincent; de Hoffmann, E. *Mass Spectrometry: Principles and Applications*, 3rd ed.; Jon Wiley & Sons, Ltd: Hoboken, NJ, 2007.
- (69) Sleno, L.; Volmer, D. A. Ion Activation Methods for Tandem Mass Spectrometry. *J. Mass Spectrom.* **2004**, 39, 1091–1112.
- (70) Brouwers, J. F. H. M.; Versluis, C.; Golde, L. M. G. van; Tielens, A. G. M. 5-Octadecenoic Acid: Evidence for a Novel Type of Fatty Acid Modification in Schistosomes. *Biochem. J.* **1998**, 334, 315–319.
- (71) Vestal, M. L.; Campbell, J. M. Tandem Time-of-Flight Mass Spectrometry. In *Methods in Enzymology*; Biological Mass Spectrometry; Academic Press, 2005; Vol. 402, pp 79–108.
- (72) Pittenauer, E.; Allmaier, G. High-Energy Collision Induced Dissociation of Biomolecules: MALDITOF/ RTOF Mass Spectrometry in Comparison to Tandem Sector Mass Spectrometry. *Comb. Chem. High Throughput Screen.* **2009**, 12, 137–155.
- (73) Pittenauer, E.; Allmaier, G. The Renaissance of High-Energy CID for Structural Elucidation of Complex Lipids: MALDI-TOF/RTOF-MS of Alkali Cationized Triacylglycerols. *J. Am. Soc. Mass Spectrom.* **2009**, 20, 1037–1047.
- (74) Pittenauer, E.; Allmaier, G. A Universal Product Ion Nomenclature for $[M-H]^-$, $[M+H]^+$ and $[M+nNa-(N-1)H]^+$ ($N=1-3$) Glycerophospholipid Precursor Ions Based on High-Energy CID by MALDI-TOF/RTOF Mass Spectrometry. *Int. J. Mass Spectrom.* **2011**, 301, 90–101.
- (75) Shimma, S.; Kubo, A.; Satoh, T.; Toyoda, M. Detailed Structural Analysis of Lipids Directly on Tissue Specimens Using a MALDI-SpiralTOF-Reflectron TOF Mass Spectrometer. *PLOS ONE* **2012**, 7, e37107.

- (76) Thomas, M. C.; Mitchell, T. W.; Harman, D. G.; Deeley, J. M.; Nealon, J. R.; Blanksby, S. J. Ozone-Induced Dissociation: Elucidation of Double Bond Position within Mass-Selected Lipid Ions. *Anal. Chem.* **2008**, *80*, 303–311.
- (77) Poad, B. L. J.; Pham, H. T.; Thomas, M. C.; Nealon, J. R.; Campbell, J. L.; Mitchell, T. W.; Blanksby, S. J. Ozone-Induced Dissociation on a Modified Tandem Linear Ion-Trap: Observations of Different Reactivity for Isomeric Lipids. *J. Am. Soc. Mass Spectrom.* **2010**, *21*, 1989–1999.
- (78) Pham, H. T.; Maccarone, A. T.; Thomas, M. C.; Campbell, J. L.; Mitchell, T. W.; Blanksby, S. J. Structural Characterization of Glycerophospholipids by Combinations of Ozone- and Collision-Induced Dissociation Mass Spectrometry: The next Step towards “Top-down” Lipidomics. *Analyst* **2014**, *139*, 204–214.
- (79) Kozłowski, R.; Mitchell, T.; Blanksby, S. Separation and Identification of Phosphatidylcholine Regioisomers by Combining Liquid Chromatography with a Fusion of Collision-and Ozone-Induced Dissociation. *Eur. J. Mass Spectrom.* **2015**, *21*, 191–200.
- (80) Kozłowski, R. L.; Mitchell, T. W.; Blanksby, S. J. A Rapid Ambient Ionization-Mass Spectrometry Approach to Monitoring the Relative Abundance of Isomeric Glycerophospholipids. *Sci. Rep.* **2015**, *5*, 9243.
- (81) Kozłowski, R. L.; Campbell, J. L.; Mitchell, T. W.; Blanksby, S. J. Combining Liquid Chromatography with Ozone-Induced Dissociation for the Separation and Identification of Phosphatidylcholine Double Bond Isomers. *Anal. Bioanal. Chem.* **2015**, *407*, 5053–5064.
- (82) Paine, M. R. L.; Poad, B. L. J.; Eijkel, G. B.; Marshall, D. L.; Blanksby, S. J.; Heeren, R. M. A.; Ellis, S. R. Mass Spectrometry Imaging with Isomeric Resolution Enabled by Ozone-Induced Dissociation. *Angew. Chem.* **2018**, *130*, 10690–10694.
- (83) Poad, B. L. J.; Green, M. R.; Kirk, J. M.; Tomczyk, N.; Mitchell, T. W.; Blanksby, S. J. High-Pressure Ozone-Induced Dissociation for Lipid Structure Elucidation on Fast Chromatographic Timescales. *Anal. Chem.* **2017**, *89*, 4223–4229.
- (84) Poad, B. L. J.; Zheng, X.; Mitchell, T. W.; Smith, R. D.; Baker, E. S.; Blanksby, S. J. Online Ozonolysis Combined with Ion Mobility-Mass Spectrometry Provides a New Platform for Lipid Isomer Analyses. *Anal. Chem.* **2018**, *90*, 1292–1300.
- (85) Liang, X.; Liu, J.; LeBlanc, Y.; Covey, T.; Ptak, A. C.; Brenna, J. T.; McLuckey, S. A. Electron Transfer Dissociation of Doubly Sodiated Glycerophosphocholine Lipids. *J. Am. Soc. Mass Spectrom.* **2007**, *18*, 1783–1788.
- (86) James, P. F.; Perugini, M. A.; O’Hair, R. A. J. Electron Capture Dissociation of Complexes of Diacylglycerophosphocholine and Divalent Metal Ions:

- Competition between Charge Reduction and Radical Induced Phospholipid Fragmentation. *J. Am. Soc. Mass Spectrom.* **2008**, *19*, 978–986.
- (87) Jones, J. W.; Thompson, C. J.; Carter, C. L.; Kane, M. A. Electron-Induced Dissociation (EID) for Structure Characterization of Glycerophosphatidylcholine: Determination of Double-Bond Positions and Localization of Acyl Chains. *J. Mass Spectrom.* **2015**, *50*, 1327–1339.
 - (88) Campbell, J. L.; Baba, T. Near-Complete Structural Characterization of Phosphatidylcholines Using Electron Impact Excitation of Ions from Organics. *Anal. Chem.* **2015**, *87*, 5837–5845.
 - (89) Baba, T.; Campbell, J. L.; Blanc, J. C. Y. L.; Baker, P. R. S.; Ikeda, K. Quantitative Structural Multi-Class Lipidomics Using Differential Mobility-Electron Impact Excitation of Ions from Organics (EIEIO) Mass Spectrometry. *J. Lipid Res.* **2018**, jlr.D083261.
 - (90) Baba, T.; Campbell, J. L.; Le Blanc, J. C. Y.; Baker, P. R. S. Distinguishing Cis and Trans Isomers in Intact Complex Lipids Using Electron Impact Excitation of Ions from Organics Mass Spectrometry. *Anal. Chem.* **2017**, *89*, 7307–7315.
 - (91) Li, P.; Jackson, G. P. Charge Transfer Dissociation of Phosphocholines: Gas-Phase Ion/Ion Reactions between Helium Cations and Phospholipid Cations. *J. Mass Spectrom.* **2017**, *52*, 271–282.
 - (92) Deimler, R. E.; Sander, M.; Jackson, G. P. Radical-Induced Fragmentation of Phospholipid Cations Using Metastable Atom-Activated Dissociation Mass Spectrometry (MAD-MS). *Int. J. Mass Spectrom.* **2015**, *390*, 178–186.
 - (93) Li, P.; Hoffmann, W. D.; Jackson, G. P. Multistage Mass Spectrometry of Phospholipids Using Collision-Induced Dissociation (CID) and Metastable Atom-Activated Dissociation (MAD). *Int. J. Mass Spectrom.* **2016**, *403*, 1–7.
 - (94) Brodbelt, J. S. Photodissociation Mass Spectrometry: New Tools for Characterization of Biological Molecules. *Chem. Soc. Rev.* **2014**, *43*, 2757–2783.
 - (95) Pham, H. T.; Julian, R. R. Re-Print of “Radical Delivery and Fragmentation for Structural Analysis of Glycerophospholipids.” *Int. J. Mass Spectrom.* **2015**, *378*, 225–231.
 - (96) Pham, H. T.; Ly, T.; Trevitt, A. J.; Mitchell, T. W.; Blanksby, S. J. Differentiation of Complex Lipid Isomers by Radical-Directed Dissociation Mass Spectrometry. *Anal. Chem.* **2012**, *84*, 7525–7532.
 - (97) Pham, H. T.; Trevitt, A. J.; Mitchell, T. W.; Blanksby, S. J. Rapid Differentiation of Isomeric Lipids by Photodissociation Mass Spectrometry of Fatty Acid Derivatives. *Rapid Commun. Mass Spectrom.* **2013**, *27*, 805–815.
 - (98) Becher, S.; Spengler, B.; Heiles, S. Effects of Wavelength, Fluence, and Dose on Fragmentation Pathways and Photoproduct Ion Yield in 213 Nm and 266 Nm

- Ultraviolet Photodissociation Experiments. *Eur. J. Mass Spectrom.* **2018**, *24*, 54–65.
- (99) Becher, S.; Esch, P.; Heiles, S. Relative Quantification of Phosphatidylcholine Sn-Isomers Using Positive Doubly Charged Lipid–Metal Ion Complexes. *Anal. Chem.* **2018**, *90*, 11486–11494.
 - (100) Madsen, J. A.; Cullen, T. W.; Trent, M. S.; Brodbelt, J. S. IR and UV Photodissociation as Analytical Tools for Characterizing Lipid A Structures. *Anal. Chem.* **2011**, *83*, 5107–5113.
 - (101) O’Brien, J. P.; Brodbelt, J. S. Structural Characterization of Gangliosides and Glycolipids via Ultraviolet Photodissociation Mass Spectrometry. *Anal. Chem.* **2013**, *85*, 10399–10407.
 - (102) Klein, D. R.; Brodbelt, J. S. Structural Characterization of Phosphatidylcholines Using 193 nm Ultraviolet Photodissociation Mass Spectrometry. *Anal. Chem.* **2017**, *89*, 1516–1522.
 - (103) Klein, D. R.; Feider, C. L.; Garza, K. Y.; Lin, J. Q.; Eberlin, L. S.; Brodbelt, J. S. Desorption Electrospray Ionization Coupled with Ultraviolet Photodissociation for Characterization of Phospholipid Isomers in Tissue Sections. *Anal. Chem.* **2018**, *90*, 10100–10104.
 - (104) Ryan, E.; Nguyen, C. Q. N.; Shiea, C.; Reid, G. E. Detailed Structural Characterization of Sphingolipids via 193 nm Ultraviolet Photodissociation and Ultra High Resolution Tandem Mass Spectrometry. *J. Am. Soc. Mass Spectrom.* **2017**, *28*, 1406–1419.
 - (105) Williams, P. E.; Klein, D. R.; Greer, S. M.; Brodbelt, J. S. Pinpointing Double Bond and Sn-Positions in Glycerophospholipids via Hybrid 193 nm Ultraviolet Photodissociation (UVPD) Mass Spectrometry. *J. Am. Chem. Soc.* **2017**, *139*, 15681–15690.
 - (106) Raetz, C. R. H.; Whitfield, C. Lipopolysaccharide Endotoxins. *Annu. Rev. Biochem.* **2002**, *71*, 635–700.
 - (107) Kawai, T.; Akira, S. The Role of Pattern-Recognition Receptors in Innate Immunity: Update on Toll-like Receptors. *Nat. Immunol.* **2010**, *11*, 373–384.
 - (108) Park, B. S.; Song, D. H.; Kim, H. M.; Choi, B.-S.; Lee, H.; Lee, J.-O. The Structural Basis of Lipopolysaccharide Recognition by the TLR4–MD-2 Complex. *Nature* **2009**, *458*, 1191–1195.
 - (109) Park, B. S.; Lee, J.-O. Recognition of Lipopolysaccharide Pattern by TLR4 Complexes. *Exp. Mol. Med.* **2013**, *45*, e66.
 - (110) Molinaro, A.; Holst, O.; Di Lorenzo, F.; Callaghan, M.; Nurisso, A.; D’Errico, G.; Zamyatina, A.; Peri, F.; Berisio, R.; Jerala, R.; Jiménez-Barbero, J.; Silipo, A.;

- Martín-Santamaría, S. Chemistry of Lipid A: At the Heart of Innate Immunity. *Chem. – Eur. J.* **2015**, *21*, 500–519.
- (111) Needham, B. D.; Trent, M. S. Fortifying the Barrier: The Impact of Lipid A Remodelling on Bacterial Pathogenesis. *Nat. Rev. Microbiol.* **2013**, *11*, 467–481.
 - (112) Cullen, T. W.; Giles, D. K.; Wolf, L. N.; Ecobichon, C.; Boneca, I. G.; Trent, M. S. Helicobacter Pylori versus the Host: Remodeling of the Bacterial Outer Membrane Is Required for Survival in the Gastric Mucosa. *PLOS Pathog.* **2011**, *7*, e1002454.
 - (113) Suarez, G.; Peek, R. M. Helicobacter Pylori: Expect the Unexpected. *Mol. Microbiol.* **2014**, *91*, 858–861.
 - (114) Silipo, A.; Molinaro, A. The Diversity of the Core Oligosaccharide in Lipopolysaccharides. In *Endotoxins: Structure, Function and Recognition*; Wang, X., Quinn, P. J., Eds.; Subcellular Biochemistry; Springer Netherlands, 2010; pp 69–99.
 - (115) Fridrich, E.; Whitfield, C. Lipopolysaccharide Inner Core Oligosaccharide Structure and Outer Membrane Stability in Human Pathogens Belonging to the Enterobacteriaceae. *J. Endotoxin Res.* **2005**, *11*, 133–144.
 - (116) Agrawal, A.; Weisshaar, J. C. Effects of Alterations of the E. Coli Lipopolysaccharide Layer on Membrane Permeabilization Events Induced by Cecropin A. *Biochim. Biophys. Acta BBA - Biomembr.* **2018**, *1860*, 1470–1479.
 - (117) Wang, L.; Wang, Q.; Reeves, P. R. The Variation of O Antigens in Gram-Negative Bacteria. In *Endotoxins: Structure, Function and Recognition*; Wang, X., Quinn, P. J., Eds.; Subcellular Biochemistry; Springer Netherlands, 2010; pp 123–152.
 - (118) Preston, Andrew; Mandrell, Robert E.; Gibson, Bradford W.; Apicella, Michael A. The Lipooligosaccharides of Pathogenic Gram-Negative Bacteria. *Crit. Rev. Microbiol.* **1996**, *22*, 139–180.
 - (119) Lerouge, I.; Vanderleyden, J. O-Antigen Structural Variation: Mechanisms and Possible Roles in Animal/Plant–Microbe Interactions. *FEMS Microbiol. Rev.* **2002**, *26*, 17–47.
 - (120) Li, H.; Liao, T.; Debowski, A. W.; Tang, H.; Nilsson, H.-O.; Stubbs, K. A.; Marshall, B. J.; Benghezal, M. Lipopolysaccharide Structure and Biosynthesis in Helicobacter Pylori. *Helicobacter* **2016**, *21*, 445–461.
 - (121) Kilár, A.; Dörnyei, Á.; Kocsis, B. Structural Characterization of Bacterial Lipopolysaccharides with Mass Spectrometry and On- and off-Line Separation Techniques. *Mass Spectrom. Rev.* **2013**, *32*, 90–117.

- (122) Banoub, J. H.; Aneed, A. E.; Cohen, A. M.; Joly, N. Structural Investigation of Bacterial Lipopolysaccharides by Mass Spectrometry and Tandem Mass Spectrometry. *Mass Spectrom. Rev.* **2010**, *29*, 606–650.
- (123) Sándor, V.; Dörnyei, Á.; Makszin, L.; Kilár, F.; Péterfi, Z.; Kocsis, B.; Kilár, A. Characterization of Complex, Heterogeneous Lipid A Samples Using HPLC–MS/MS Technique I. Overall Analysis with Respect to Acylation, Phosphorylation and Isobaric Distribution. *J. Mass Spectrom.* **2016**, *51*, 1043–1063.
- (124) Sándor, V.; Kilár, A.; Kilár, F.; Kocsis, B.; Dörnyei, Á. Characterization of Complex, Heterogeneous Lipid A Samples Using HPLC–MS/MS Technique II. Structural Elucidation of Non-Phosphorylated Lipid A by Negative-Ion Mode Tandem Mass Spectrometry. *J. Mass Spectrom.* *51*, 615–628.
- (125) Sándor, V.; Kilár, A.; Kilár, F.; Kocsis, B.; Dörnyei, Á. Characterization of Complex, Heterogeneous Lipid A Samples Using HPLC–MS/MS Technique III. Positive-Ion Mode Tandem Mass Spectrometry to Reveal Phosphorylation and Acylation Patterns of Lipid A. *J. Mass Spectrom.* **2018**, *53*, 146–161.
- (126) Kondakov, A.; Lindner, B. Structural Characterization of Complex Bacterial Glycolipids by Fourier Transform Mass Spectrometry. *Eur. J. Mass Spectrom.* **2005**, *11*, 535–546.
- (127) O’Brien, J. P.; Needham, B. D.; Henderson, J. C.; Nowicki, E. M.; Trent, M. S.; Brodbelt, J. S. 193 nm Ultraviolet Photodissociation Mass Spectrometry for the Structural Elucidation of Lipid A Compounds in Complex Mixtures. *Anal. Chem.* **2014**, *86*, 2138–2145.
- (128) Morrison, L. J.; Parker, W. R.; Holden, D. D.; Henderson, J. C.; Boll, J. M.; Trent, M. S.; Brodbelt, J. S. UVliPiD: A UVPD-Based Hierarchical Approach for De Novo Characterization of Lipid A Structures. *Anal. Chem.* **2016**, *88*, 1812–1820.
- (129) Li, J.; Purves, R. W.; Richards, J. C. Coupling Capillary Electrophoresis and High-Field Asymmetric Waveform Ion Mobility Spectrometry Mass Spectrometry for the Analysis of Complex Lipopolysaccharides. *Anal. Chem.* **2004**, *76*, 4676–4683.
- (130) Leung, L. M.; Fondrie, W. E.; Doi, Y.; Johnson, J. K.; Strickland, D. K.; Ernst, R. K.; Goodlett, D. R. Identification of the ESKAPE Pathogens by Mass Spectrometric Analysis of Microbial Membrane Glycolipids. *Sci. Rep.* **2017**, *7*, 6403.
- (131) Rütters, H.; Möhring, T.; Rullkötter, J.; Griep-Raming, J.; Metzger, J. O. The Persistent Memory Effect of Triethylamine in the Analysis of Phospholipids by Liquid Chromatography/Mass Spectrometry. *Rapid Commun. Mass Spectrom.* *14*, 122–123.

- (132) Jones, J. W.; Shaffer, S. A.; Ernst, R. K.; Goodlett, D. R.; Tureček, F. Determination of Pyrophosphorylated Forms of Lipid A in Gram-Negative Bacteria Using a Multivaried Mass Spectrometric Approach. *Proc. Natl. Acad. Sci.* **2008**, *105*, 12742–12747.
- (133) M. Crittenden, C.; M. Herrera, C.; E. Williams, P.; P. Ricci, D.; R. Swem, L.; Stephen Trent, M.; S. Brodbelt, J. Mapping Phosphate Modifications of Substituted Lipid A via a Targeted MS 3 CID/UVPD Strategy. *Analyst* **2018**, *143*, 3091–3099.
- (134) Madalinski, G.; Fournier, F.; Wind, F.-L.; Afonso, C.; Tabet, J.-C. Gram-Negative Bacterial Lipid A Analysis by Negative Electrospray Ion Trap Mass Spectrometry: Stepwise Dissociations of Deprotonated Species under Low Energy CID Conditions. *Int. J. Mass Spectrom.* **2006**, *249–250*, 77–92.
- (135) Ting, Y. S.; Shaffer, S. A.; Jones, J. W.; Ng, W. V.; Ernst, R. K.; Goodlett, D. R. Automated Lipid A Structure Assignment from Hierarchical Tandem Mass Spectrometry Data. *J. Am. Soc. Mass Spectrom.* **2011**, *22*, 856–866.
- (136) Sturiale, L.; Garozzo, D.; Silipo, A.; Lanzetta, R.; Parrilli, M.; Molinaro, A. New Conditions for Matrix-Assisted Laser Desorption/Ionization Mass Spectrometry of Native Bacterial R-Type Lipopolysaccharides. *Rapid Commun. Mass Spectrom.* **2005**, *19*, 1829–1834.
- (137) Sturiale, L.; Palmigiano, A.; Silipo, A.; Knirel, Y. A.; Anisimov, A. P.; Lanzetta, R.; Parrilli, M.; Molinaro, A.; Garozzo, D. Reflectron MALDI TOF and MALDI TOF/TOF Mass Spectrometry Reveal Novel Structural Details of Native Lipooligosaccharides. *J. Mass Spectrom.* **2011**, *46*, 1135–1142.
- (138) Kanie, Y.; Yamaguchi, Y.; Hayashi, A.; Uzawa, J.; Hatakeyama, M.; Hidaka, Y.; Toda, N.; Nakamura, S.; Kanie, O. Structural Analysis of a Novel Lipooligosaccharide (LOS) from *Rhodobacter Azotoformans*. *Carbohydr. Res.* **2019**, *473*, 104–114.
- (139) Phillips, N. J.; John, C. M.; Jarvis, G. A. Analysis of Bacterial Lipooligosaccharides by MALDI-TOF MS with Traveling Wave Ion Mobility. *J. Am. Soc. Mass Spectrom.* **2016**, *27*, 1263–1276.
- (140) Oyler, B. L.; Khan, M. M.; Smith, D. F.; Harberts, E. M.; Kilgour, D. P. A.; Ernst, R. K.; Cross, A. S.; Goodlett, D. R. Top Down Tandem Mass Spectrometric Analysis of a Chemically Modified Rough-Type Lipopolysaccharide Vaccine Candidate. *J. Am. Soc. Mass Spectrom.* **2018**, 1–9.
- (141) O'Brien, J. P.; Needham, B. D.; Brown, D. B.; Trent, M. S.; Brodbelt, J. S. Top-down Strategies for the Structural Elucidation of Intact Gram-Negative Bacterial Endotoxins. *Chem. Sci.* **2014**, *5*, 4291–4301.

- (142) Hübner, G.; Lindner, B. Separation of R-Form Lipopolysaccharide and Lipid A by CE–Fourier-Transform Ion Cyclotron Resonance MS. *Electrophoresis* **2009**, *30*, 1808–1816.

Chapter 2: Experimental Methods

2.1 IONIZATION

2.1.1 Electrospray Ionization

Critical to mass spectrometry is the production of gas-phase ions. Early ionization techniques produce spectra containing abundant molecular ion decomposition products. The invention of electrospray ionization (ESI) in 1989 revolutionized the field of mass spectrometry by enabling facile production of gas-phase molecular ions from solution under ambient conditions.¹ During ESI, a high voltage (± 2.5 -6 kV) is applied to stream of solution flowing through a capillary or emitter to generate a plume of charged droplets. As solvent evaporates, droplet charge density increases until charge repulsion overcomes the droplet surface tension, i. e. the Rayleigh stability limit, and desolvated ions are expelled from droplets.² The process of droplet charge accumulation and solvent evaporation continues until completely desolvated ions enter the mass spectrometer inlet. Nebulizing gas can be used to further facilitate the desolvation process. NanoESI is another iteration of ESI whereby a lower voltage (0.5-2 kV) is applied to a capillary or emitter with a significantly smaller orifice (1-3 μm).³ A smaller initial droplet size permits tolerance of high salt concentration and increased analyte sensitivity.

For the work presented in this dissertation, all LC-MS experiments were performed with an ESI source and all shotgun infusion experiments were performed using a static nanoESI source where the applied voltage drove solution through the pulled capillary. NanoESI required no nebulizing gas.

2.1.2 Desorption Electrospray Ionization

Invented in 2004, desorption electrospray ionization (DESI) is a surface sampling technique in which an electrospray plume is directed at a surface, and desorbed ions are detected by a mass spectrometer.⁴ DESI requires little sample preparation and has been used to obtain chemical profiles directly from tissue surfaces and tissue sections.⁵ DESI has therefore contributed significantly to field of mass spectrometry imaging (MSI). During DESI-MSI experiments, an electrospray plume is rastered over a tissue section in the x and y directions, and the abundances of specific m/z values are mapped in two dimensions to permit visualization of the spatial distribution of biochemicals. DESI-MSI enables differentiation of normal and diseased regions of tissue based on distinct chemical profiles.

2.2 LIQUID CHROMATOGRAPHY

For separations of lipids, various types of liquid chromatography are employed to influence lipid elution order. All of the chromatographic separations performed in this work were reversed-phase. Therefore, all lipids were eluted based on hydrophobicity. A Dionex Ultimate 3000 microflow liquid chromatography system (Sunnyvale, CA) was used for all chromatographic separations performed in this work.

2.3 MASS SPECTROMETRY

All experiments were performed on hybrid quadrupole-Orbitrap-linear ion trap mass spectrometer (Thermo Fisher Orbitrap Fusion or Orbitrap Fusion Lumos; San Jose, CA). A quadrupole mass filter is composed of two pairs of cylindrical or hydrobolic electrodes that are radially-equidistant with one pair orthogonal to the other. A radio frequency (RF) voltage is applied to all electrodes with pairs of electrodes 180 degrees out of phase. A quadrupole can function as a RF only ion guide during MS¹ analysis or an

m/z filter with narrow isolation widths depending on the application of appropriate DC offset voltages to each pair of electrodes. The linear ion trap functions as both an ion activation region and a low resolution mass analyzer. A linear ion trap is also composed of two pairs of orthogonal, radially-equidistant hyperbolic electrodes with RF voltage applied to all electrodes; again, the voltage each pair of electrodes 180 degrees out of phase. Each electrode is segmented into three sections with DC offset voltage applied to the front and back sections to permit ion trapping in the center section.⁶ An RF voltage amplitude ramp allows ions to be mass-selectively ejected from the ion trap through slits in the center electrodes. Collisional activation and ion detection occur in the high and low pressure regions of the dual linear ion trap, respectively. High resolution and high mass accuracy detection occurs in the Orbitrap mass analyzer. Ions injected into the Orbitrap simultaneously orbit radially and oscillate axially around an inner spindle-shaped electrode at high voltage while image current is detected by two outer electrically grounded barrel-shaped electrodes.⁷ The combination of the quadrupole mass filter, the linear ion trap mass analyzer and the Orbitrap mass analyzer allows sophisticated ion manipulations and confident assignment of both precursor and fragment ions.

2.3 ION ACTIVATION

2.3.1 Collisional Activation

On the Orbitrap Fusion and Orbitrap Fusion Lumos platforms, low-energy collision-induced dissociation (CID), where ions are accelerated at m/z specific secular frequencies and undergo collisions with helium, occurs in the high-pressure trap of the dual linear ion trap. During higher-energy collisional dissociation (HCD), ions are accelerated into the ion routing multipole (IRM) region of the instrument which is pressurized with 2-8 mTorr nitrogen. HCD is a non-resonant beam-type collisional

activation method and is therefore more likely to produce fragment ions that are the result of secondary fragmentation.

2.3.2 193 nm Ultraviolet Photodissociation

On the Orbitrap Fusion and Orbitrap Fusion Lumos platforms, the dual linear ion trap is an ideal region to perform photodissociation. The beam of a Coherent Excistar excimer laser at 193 nm was directed through a fused silica optical window in the back panel of the vacuum chamber using a set of optical mirrors. The excimer laser, with a repetition rate of 500 Hz and 5 ns pulse width, can be pulsed every 2 ms. Photodissociation can be performed in either the high-pressure or low-pressure traps of the dual linear ion trap. In the present work, photodissociation was performed in either the low-pressure or high pressure trap with ion activation periods of 10 to 40 ms (corresponding to 5 to 20 pulses and total irradiation times of 25 to 100 nsec).

2.4 REFERENCES

- (1) Fenn, J. B.; Mann, M.; Meng, C. K.; Wong, S. F.; Whitehouse, C. M. Electrospray Ionization for Mass Spectrometry of Large Biomolecules. *Science* **1989**, *246*, 64–71.
- (2) Konermann, L.; Ahadi, E.; Rodriguez, A. D.; Vahidi, S. Unraveling the Mechanism of Electrospray Ionization. *Anal. Chem.* **2013**, *85*, 2–9.
- (3) Wilm, M. S.; Mann, M. Electrospray and Taylor-Cone Theory, Dole's Beam of Macromolecules at Last? *Int. J. Mass Spectrom. Ion Process.* **1994**, *136*, 167–180.
- (4) Takáts, Z.; Wiseman, J. M.; Gologan, B.; Cooks, R. G. Mass Spectrometry Sampling Under Ambient Conditions with Desorption Electrospray Ionization. *Science* **2004**, *306*, 471–473.
- (5) Eberlin, L. S.; Ferreira, C. R.; Dill, A. L.; Ifa, D. R.; Cooks, R. G. Desorption Electrospray Ionization Mass Spectrometry for Lipid Characterization and Biological Tissue Imaging. *Biochim. Biophys. Acta BBA - Mol. Cell Biol. Lipids* **2011**, *1811*, 946–960.
- (6) Schwartz, J. C.; Senko, M. W.; Syka, J. E. P. A Two-Dimensional Quadrupole Ion Trap Mass Spectrometer. *J. Am. Soc. Mass Spectrom.* **2002**, *13*, 659–669.

- (7) Hu, Q.; Noll, R. J.; Li, H.; Makarov, A.; Hardman, M.; Cooks, R. G. The Orbitrap: A New Mass Spectrometer. *J. Mass Spectrom.* **2005**, *40*, 430–443.

Chapter 3: Structural Characterization of Phosphatidylcholines Using 193 nm Ultraviolet Photodissociation Mass Spectrometry*

3.1 OVERVIEW

Advances in mass spectrometry have made it a preferred tool for structural characterization of glycerophospholipids. Collisional activation methods commonly implemented on commercial instruments do not provide fragmentation patterns that allow elucidation of certain structural features, including acyl chain positions on the glycerol backbone and double bond positions within acyl chains. In the present work, 193 nm ultraviolet photodissociation (UVPD) implemented on an Orbitrap mass spectrometer is used to localize double bond positions within phosphatidylcholine (PC) acyl chains. Cleavage of the carbon-carbon bonds adjacent to the double bond provides a diagnostic mass difference of 24 Da and enables differentiation of double-bond positional isomers. The UVPD method was extended to the characterization of PCs in a bovine liver extract via a shotgun strategy. Positive mode higher-energy collisional dissociation (HCD) and UVPD, and negative mode HCD were undertaken in a complementary manner to identify species as PCs and to localize double bonds, respectively.

*Klein, D. R.; Brodbelt, J. S. Structural Characterization of Phosphatidylcholine Using 193 nm Ultraviolet Photodissociation Mass Spectrometry. *Anal. Chem.* **2017**, 89, 1516-1522.

JSB provided mentorship and reviewed the manuscript prior to publication.

3.2 INTRODUCTION

Glycerophospholipids, a diverse subclass of lipids and the main component of cell membranes, have been the focus of many targeted lipidomics studies. In addition to heavily influencing cell membrane dynamics, they also participate in cellular signaling and can influence the organization and structure of proteins within the membrane.¹⁻⁵ Despite their relatively low molecular weights compared to other biomolecules, glycerophospholipids are highly complex as a result of the various combinations of substituents that can occur at each of the three positions of the glycerol backbone.⁶⁻⁸ Consequently, glycerophospholipid isomers are commonplace, with subtle differences potentially having large implications for biological function.^{1,3,9-12} Considering the impact of specific structural features on membrane dynamics, a detailed characterization of glycerophospholipids is necessary to achieve a full understanding of cellular behavior. Two general *ex vivo* mass spectrometric approaches to analyze lipids have been developed: one employing separations with either liquid chromatographic (LC) mass spectrometry¹³ or ion mobility methods¹⁴⁻¹⁶, and the other based on direct infusion of lipids extracts, the latter termed “shotgun lipidomics”.¹⁷⁻²³ With each of these approaches, various levels of structural characterization can be obtained depending on the type of mass spectrometric data collected.^{1,23} High resolution MS¹ data can be used to accurately determine lipid molecular formulas, yet MS/MS spectra are required to identify a specific lipid or class of lipids.

Collection of MS¹ spectra alone for glycerophospholipid analysis, using either LC or a shotgun approach, is high throughput, gives a global profile of lipid composition, and can differentiate isobars at high resolution, yet it provides no structural information and therefore does not permit differentiation of isomers.²² Advances in tandem mass spectrometry have allowed significant inroads into the structural analysis of

glycerophospholipids. The most commonly employed and well-studied method of fragmentation for bottom-up lipid analysis is low-energy collision induced dissociation (CID). Fragmentation patterns in positive and negative mode produce predominant fragments corresponding to the head group and acyl chains, respectively.^{17,24} The different ionization efficiencies of glycerophospholipid subspecies can often dictate the mode of analysis. In an attempt to improve ionization efficiencies, methods involving chemical modification of glycerophospholipid head groups have been developed. Specifically, Wasslen *et al.* and Canez *et al.* trimethylated the glycerophospholipid amino groups to improve ionization in positive mode.^{25,26} Methods that utilize polarity switching have also been developed.²² However, the mode in which ionization is optimal may not produce MS/MS spectra containing the desired structural information. Ion-ion reactions and ion adduction have thus been used to overcome these obstacles.²⁷⁻²⁹ Stutzman *et al.* reacted phosphatidylcholine cations with doubly deprotonated 1,4-phenylenedipropionic acid in the gas phase to produce phosphatidylcholine anions that, upon CID fragmentation, produced informative fragmentation patterns with enhanced signal-to-noise.²⁷ In addition, Ho *et al.* found that CID of glycerophospholipid-metal cation complexes gave more informative spectra.²⁹

Conventional CID methods provide structural information regarding the acyl chain lengths, number of unsaturated C-C bonds, and head groups; however, often CID does not reveal some of the more subtle structural characteristics of glycerophospholipids, including acyl chain position and double bond position. Therefore, the development of new analytical tools to completely characterize glycerophospholipid structures and quantify their abundances remains an active area of interest. For example, Hsu and Turk used lithium adduction and an MSⁿ approach to determine double bond position.³⁰ Xia and coworkers recently reported a selective reaction/CID strategy to

elucidate the position of double bonds in the acyl chains and quantify the relative abundances of mixtures of double bond isomers.^{31–33} The key step exploited the well-known Paternò-Büchi reaction which causes photochemical formation of an oxetane ring from a ketone/aldehyde and double bonds within the acyl chains.^{31–33} Yang *et al.* employed a strategy in which the variation in abundances of neutral loss products were monitored as a function of double bond position to both identify both the double bond position and quantify relative amounts of fatty acid isomers.³⁴ Additional methods have focused on novel ion activation techniques including radical-directed dissociation (RDD) via 266 nm photodissociation followed by CID^{35–37}, ozone-induced dissociation (OzID)^{38–40}, electronic impact excitation of ions from organics (EIEIO)⁴¹, metastable atom-activated dissociation (MAD)^{42,43} and electron-transfer dissociation (ETD)⁴⁴. In parallel studies Pham *et al.* explored non-covalent complexation of 4-iodobenzoic acid or 4-iodoaniline to glycerophospholipids and reactions of 4-iodobenzyl alcohol with fatty acids.^{35,36} Irradiation with 266 nm photons resulted in radical species that allowed assignment of double bond position upon CID. OzID involves the gas-phase reaction of isolated glycerophospholipid cations with ozone in an ion trap^{39,40}; CID subsequently provided information regarding double bond positions and *sn*-position. While EIEIO, MAD and ETD are each initiated by reactions of ions with electrons, metastable helium or argon atoms, or radical anions, respectively, these methods appear to induce similar radical-based fragmentation pathways.

Another ion activation method that produces rich fragmentation spectra for various biomolecules, including lipids, is 193 nm ultraviolet photodissociation (UVPD).^{45–51} Absorption of a 193 nm photon results in deposition of ~6.4 eV of internal energy, and the photoactivation process occurs in a 5 nsec laser pulse period. This high energy excitation affords access to fragmentation pathways not observed by collision

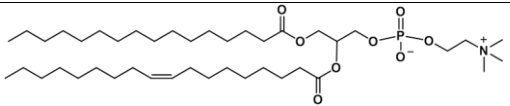
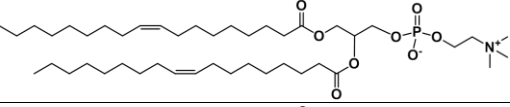
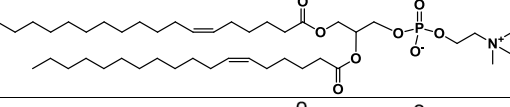
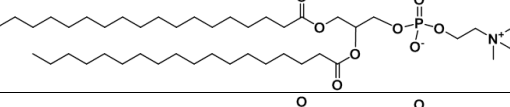
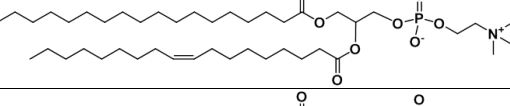
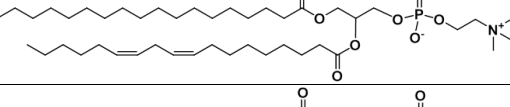
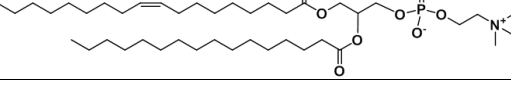
based methods, ultimately providing richer fragmentation patterns that have been useful for characterizing lipooligosaccharides^{49,52} and gangliosides,⁴⁷ as well as other types of biological molecules.⁴⁵ In the present study, 193 nm UVPD is shown to produce fragmentation patterns that allow double-bond isomer differentiation and is used for detailed structural characterization of mixtures of phosphatidylcholines (PC), a subclass of glycerophospholipids highly abundant in mammalian cells.⁵

3.3 EXPERIMENTAL

All PC samples as well as the polar bovine liver extract were purchased from Avanti Polar Lipids (Alabaster, Alabama) and were used without further purification. The structures and molecular weights of all PCs included in the study are shown in **Table 3.1**. Lipid shorthand notation used is in accordance with previously established notation.⁵³ In brief, acyl chain compositions are indicated by the number of carbons atoms in the acyl chain followed by a colon and the number double bonds. For PCs with known acyl chain orientation, the acyl chain compositions of *sn*-1 and *sn*-2 are separated by “/” with *sn*-1 followed by *sn*-2. For unknown acyl chain orientation, acyl chain compositions are separated by “_”. For known double bond positions, positions are indicated in parenthesis after the acyl chain composition by the carbon number and Z, E or Δ to indicate the bond orientation as *cis*, *trans* or unknown, respectively. For example, PC 16:0/18:1(9Z) represents a phosphatidylcholine with palmitate (16 carbon chain) at the *sn*-1 position and oleate (18 carbon chain with 1 unsaturation) at the *sn*-2 position with a *cis* double bond at carbon number 9. Methanol (MeOH), acetonitrile (ACN, and water (H₂O) were purchased from EMD Millipore (Billerica, MA); HPLC grade chloroform (CHCl₃) and LC-MS grade ammonium formate were purchased from Sigma Aldrich (St. Louis, MO). All samples were diluted in 50:50 ACN:H₂O with 30 mM

ammonium formate to 10 μ M for PC standards and 10 μ g/mL for polar bovine liver extract.

Table 3.1 Names, structures and molecular weights of all standard PCs

Lipid Name	Structure	Molecular mass (Da)
1-palmitoyl-2-oleoyl- <i>sn</i> -glycero-3-phosphocholine [PC 16:0/18:1(9Z)]		759.58
1,2-dioleoyl- <i>sn</i> -glycero-3-phosphocholine [PC 18:1(9Z)/18:1(9Z)]		785.59
1,2-dipetroselenoyl- <i>sn</i> -glycero-3-phosphocholine [PC 18:1(6Z)/18:1(6Z)]		785.59
1,2-distearoyl- <i>sn</i> -glycero-3-phosphocholine [PC 18:0/18:0]		789.62
1-stearoyl-2-oleoyl- <i>sn</i> -glycero-3-phosphocholine [PC 18:0/18:1(9Z)]		787.61
1-stearoyl-2-linoleoyl- <i>sn</i> -glycero-3-phosphocholine [PC 18:0/18:2(9Z,12Z)]		785.59
1-palmitoyl-2-stearoyl- <i>sn</i> -glycero-3-phosphocholine [PC 18:1(9Z)/16:0]		759.58

Approximately 10 μ L of sample were loaded into a silver-coated pulled tip glass capillary (1.2 mm OD) and sprayed using a Proxeon offline nano-electrospray set-up (Thermo Scientific, San Jose, CA). The spray voltage was set to 1.1 kV. All positive mode spectra were collected on either a Thermo Scientific Orbitrap Fusion Lumos mass spectrometer or (San Jose, CA) or an Orbitrap Elite mass spectrometer (Bremen, Germany) each modified with a 193 nm Coherent Existar excimer laser (Santa Cruz, CA) to perform UVPD as previously described.^{51,52} On the Orbitrap Elite mass spectrometer, UVPD was performed in the HCD cell with 8 laser pulses at 5 mJ per pulse, and on the Orbitrap

Fusion Lumos mass spectrometer, UVPD was performed in the low pressure trap of the dual linear ion trap by applying 10 laser pulses at 6 mJ per pulse. In each case, the laser was operated at 500 Hz, resulting in an activation period of 16 to 20 ms per scan. For UVPD/CID MS³ spectra collected on the Orbitrap Fusion Lumos mass spectrometer, UVPD activation was first performed in the high pressure trap of the dual linear ion trap with 10 laser pulses at 6 mJ per pulse followed by CID with a normalized collision energy (NCE) of 30. All negative ion mode spectra were collected on the Thermo Scientific Orbitrap Fusion Lumos mass spectrometer. Data were collected with an AGC target between 5×10^4 and 1×10^5 at a resolution of 60,000. To maximize the quality of the benchmark MS/MS spectra, 100 scans were averaged with 2 μ scans per scan, corresponding to approximately one minute per spectrum. MS/MS spectra could be collected with as few as one scan per spectrum, as shown in **Figure 3.1**. All HCD data were collected with an NCE of 25. On the Orbitrap Fusion Lumos mass spectrometer an isolation width of 1 Da was used and on the Orbitrap Elite mass spectrometer an isolation width of 2 was used. Default activation times were used for HCD. All data were analyzed in XCalibur Qual Browser and manually interpreted.

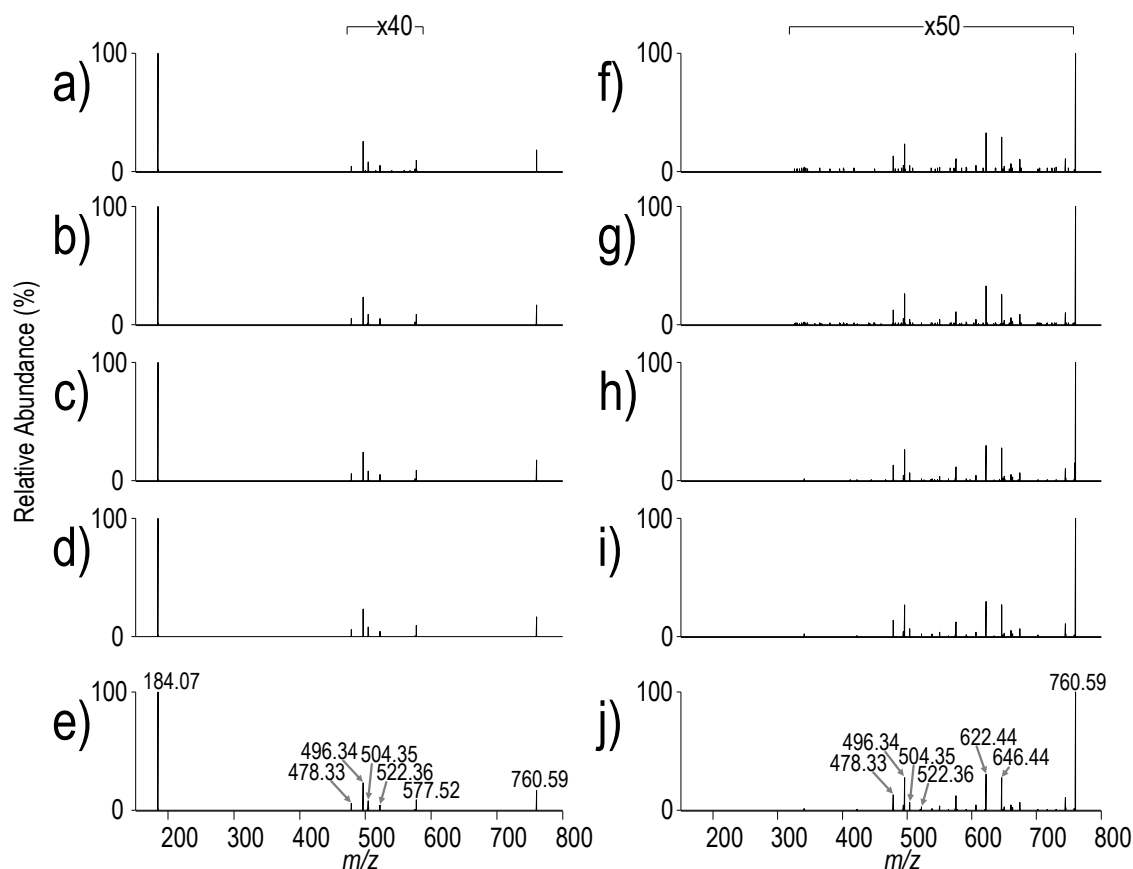


Figure 3.1 HCD mass spectra acquired for the ion of m/z 760.58 from polar bovine liver extract with a) 1, b) 2, c) 5, d) 10 and e) 20 scans averaged. UVPD spectra acquired for the ion of m/z 760.58 from polar bovine liver extract with f) 1, g) 2, h) 5, i) 10 and j) 20 scans averaged. Each scan contains 2 μ scans.

3.4 RESULTS AND DISCUSSION

For this study, a series of PCs were characterized by HCD and UVPD in order to compare the types of fragment ions produced by each activation and evaluate the capability for localization of double bonds and isomer/isobar differentiation. Infusion of each PC in positive mode yielded abundant protonated ($[M+H]^+$) and less abundant sodium cationized ($[M+Na]^+$) ions (**Figure 3.2**).

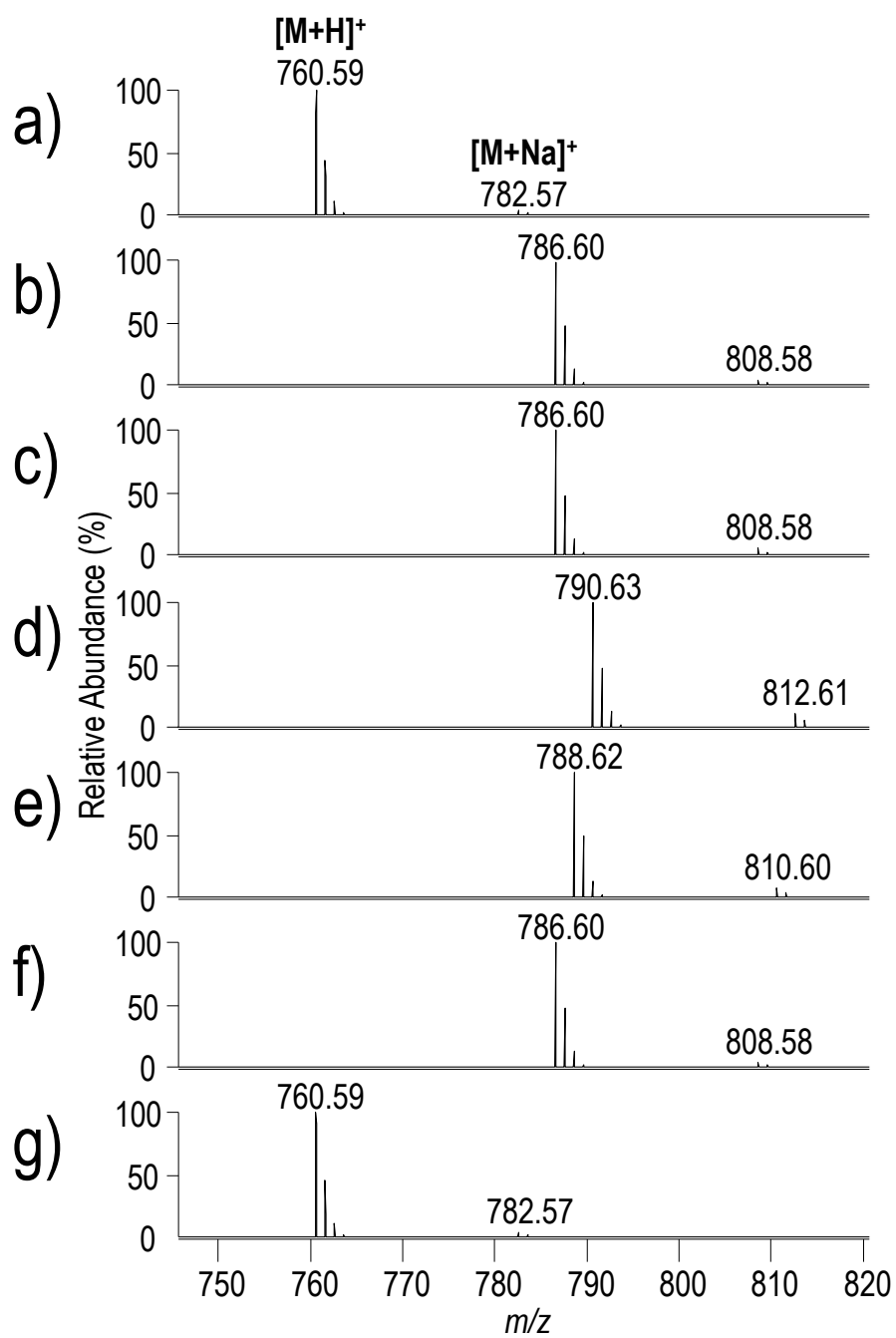


Figure 3.2 MS¹ spectra of a) PC 16:0/18:1(9Z), b) PC 18:1(9Z)/18:1(9Z), c) PC 18:1(6Z)/18:1(6Z), d) PC 18:0/18:0, e) PC 18:0/18:1(9Z), f) PC 18:0/18:2(9Z,12Z), and g) PC 18:1(9Z)/16:0.

Examples of the HCD and UVPD mass spectra are shown in **Figures 3.3** and **3.4**. As an example, HCD of protonated PC 16:0/18:1(9Z) produced an abundant product ion of m/z 184.07, corresponding to the phosphocholine head group, and less abundant ions of m/z 478.33, 496.34, 504.35 and 522.35 corresponding to acyl chain neutral losses (**Figure 3.3a**). All ions observed upon HCD are consistent with results previously reported for collisional activation of PCs.⁵⁴

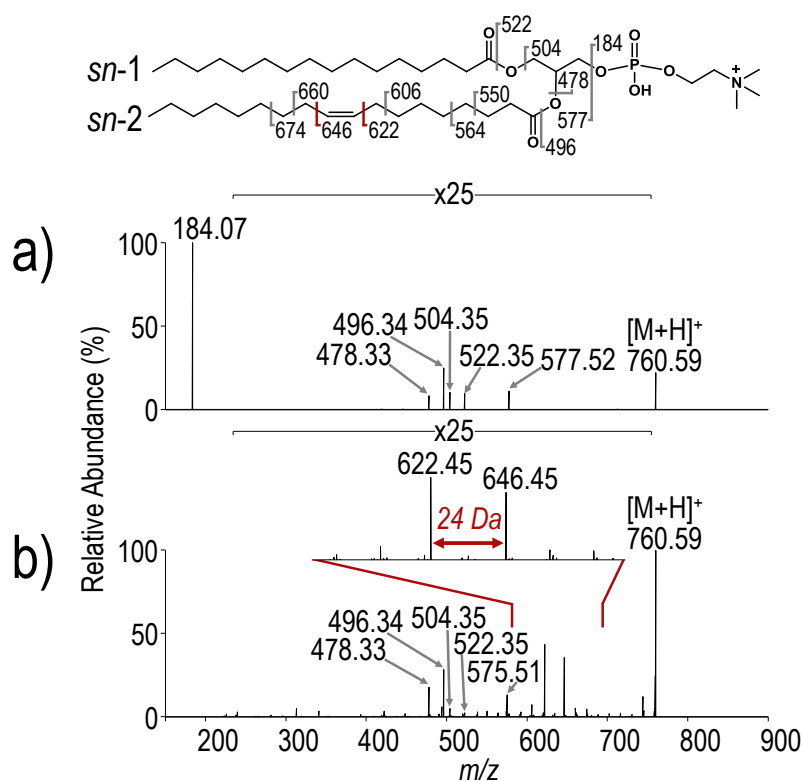


Figure 3.3 a) HCD (NCE 25) and b) UVPD (10 pulses, 6 mJ) spectra of protonated PC 16:0/18:1(9Z) ($[M+H]^+$, m/z 760.59).

UVPD produced the same acyl chain neutral loss ions as well as highly informative ions corresponding to C-C cleavages along the acyl chain (**Figure 3.3b**). The UVPD mass spectrum lacks the predominant head group ion of m/z 184.07 as a result of the default

ion trap q-value when performing UVPD on the Orbitrap Fusion Lumos mass spectrometer; with the current software, the ion trap q-value cannot be decreased below a default value of 0.25. To confirm that the head group ion is in fact generated upon UVPD, HCD and UVPD spectra were collected on an Orbitrap Elite mass spectrometer also equipped with a 193 nm excimer laser, with UVPD performed in the HCD cell (**Figure 3.5**). The UVPD mass spectrum collected on the Orbitrap Elite mass spectrometer confirms that the head group ion of m/z 184.07 is generated.

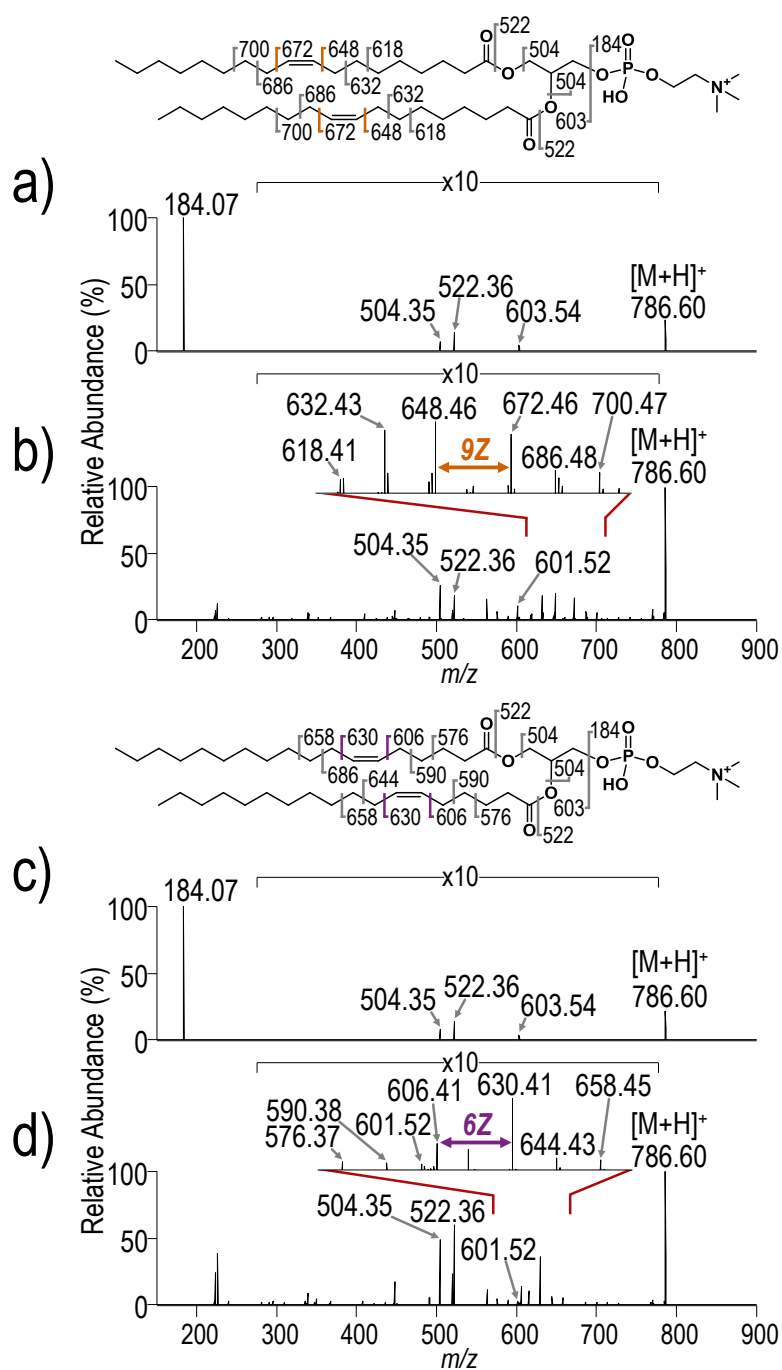


Figure 3.4 a) HCD (NCE 25) and b) UVPD (10 pulses, 6 mJ) spectra of protonated PC 18:1(9Z)/18:1(9Z) ($[M+H]^+$, m/z 786.60). c) HCD (NCE 25) and UVPD (10 pulses, 6 mJ) spectra of protonated PC 18:1(6Z)/18:1(6Z) ($[M+H]^+$, m/z 786.60).

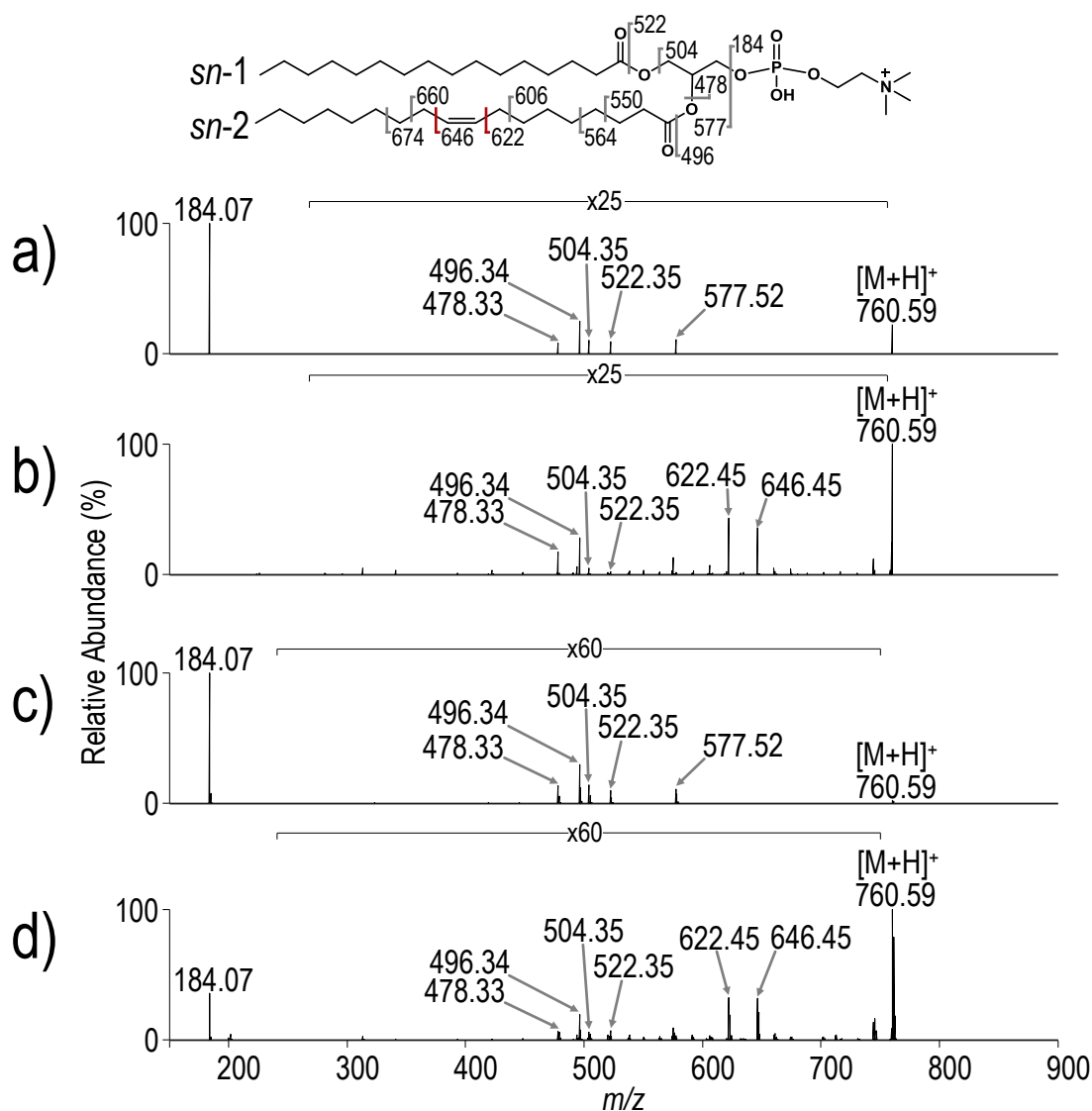


Figure 3.5 a) HCD (NCE 25) and b) UVPD (10 pulses, 6 mJ) of PC 16:0/18:1(9Z) ([M+H]⁺, m/z 760.59) collected on the Orbitrap Fusion Lumos mass spectrometer. c) HCD (NCE 25) and b) UVPD (8 pulses, 5 mJ) of PC 16:0/18:1(9Z) collected on the Orbitrap Elite mass spectrometer. (Data presented in parts a) and b) is the same as data in Figure 3.3)

The most abundant of the C-C acyl chain cleavage products (m/z 622.45 and m/z 646.45) in the spectrum in **Figure 3.3b** correspond to cleavage of either one of the carbon-carbon bonds adjacent to the double bond. The 24 Da mass difference allows facile recognition

of this diagnostic pair of ions. Putative structures of the two marker ions are shown in **Figure 3.6**.

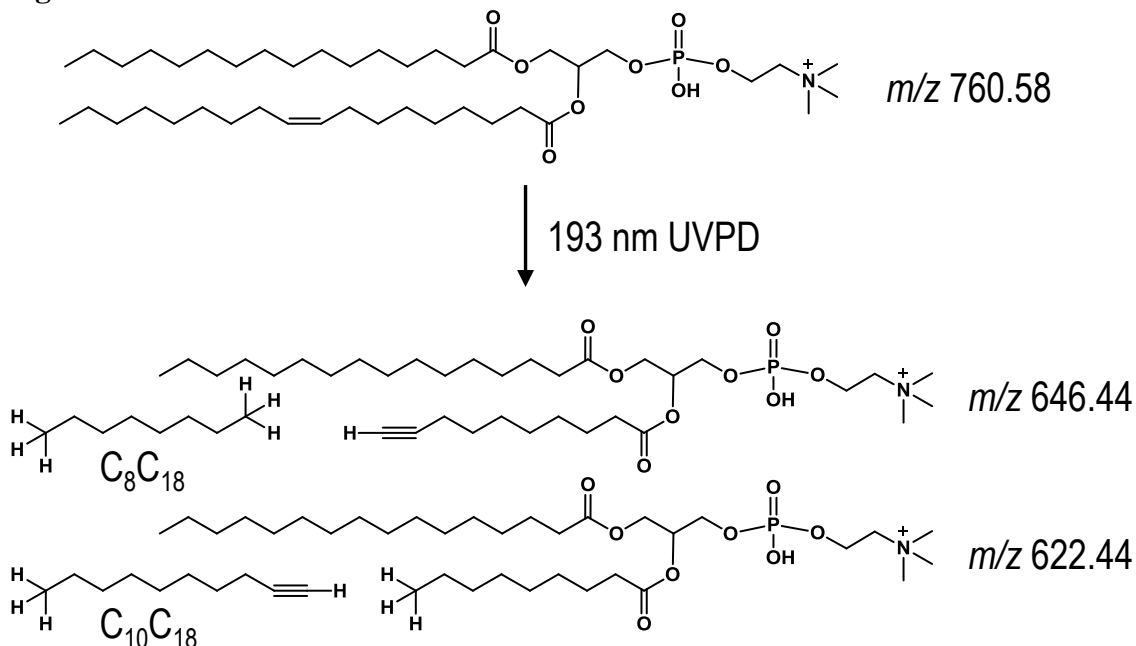


Figure 3.6 Putative structures of the two diagnostic ions (m/z 622.44 and 646.44) generated from UVPD of PC 16:0/18:1(9Z) ($[M+H]^+$, m/z 760.59)

This pair of key diagnostic ions is also generated upon UVPD of the corresponding sodium-cationized PC, as illustrated in **Figure 3.7**. HCD of sodium-cationized PC 16:0/18:1(9Z) results predominantly in neutral losses of choline and phosphocholine (yielding the products of m/z 723.49 and m/z 599.50, respectively), again providing characteristic head group information. Additionally, acyl chain neutral losses consistent with retention or loss of sodium are also observed. In the corresponding UVPD mass spectrum, fragment ions produced by cleavage of the C-C bond on either side of the double bond are again observed (m/z 644.43 and 668.43). Both of these ions retain sodium and confirm that UVPD of sodium-adducted species provides the same type of

double bond positional information as noted for the protonated PC. For the remainder of the study, the analysis will focus on the protonated PCs.

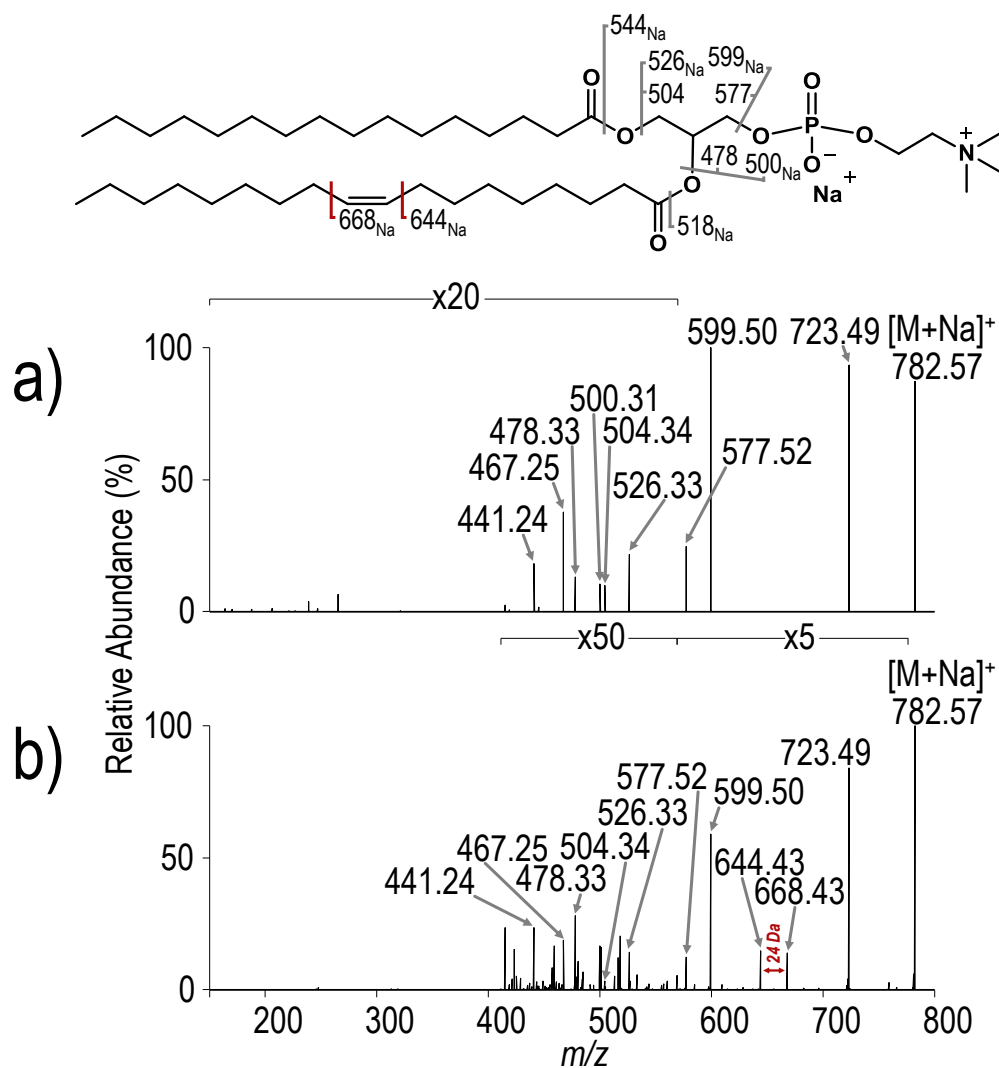


Figure 3.7 a) HCD (NCE 25) and b) UVPD (10 pulses, 6 mJ) of sodium adducted PC 16:0/18:1(9Z) ($[M+Na]^+$, m/z 782.57). The subscript “Na” in the labels of the fragment ion map indicates ions that retain the sodium adduct.

HCD and UVPD spectra of the isomeric lipids PC 18:1(9Z)/18:1(9Z) and PC 18:1(6Z)/18:1(6Z) are shown in **Figure 3.4**. The HCD spectra display informative head

group (m/z 184.07) and diagnostic acyl chain (m/z 504.34 and 522.36) ions, but the HCD spectra for these isomeric PCs are indistinguishable. In contrast, the fragmentation patterns generated by UVPD exhibit ions that allow differentiation of the double bond positional isomers based on the unique C-C cleavage products that differ by 24 Da. The most abundant C-C cleavage fragments for PC 18:1(9Z)/18:1(9Z) are m/z 648.46 and 672.46, and for PC 18:1(6Z)/18:1(6Z) they are m/z 606.41 and 630.41. In addition, the UVPD spectra of PC 16:0/18:1(9Z), PC 18:1(9Z):18:1(9Z), PC 18:1(6Z)/18:1(6Z) and all other PCs with double bonds exhibit the loss of a hydrogen atom from the precursor, resulting in products of m/z 759.57, m/z 785.57 and m/z 785.57, respectively, and also display other odd-electron fragment ions that are suggestive of radical-directed fragmentation processes. The hydrogen atom losses from the precursor ions upon UVPD are shown for a series of PCs in **Figure 3.8**.

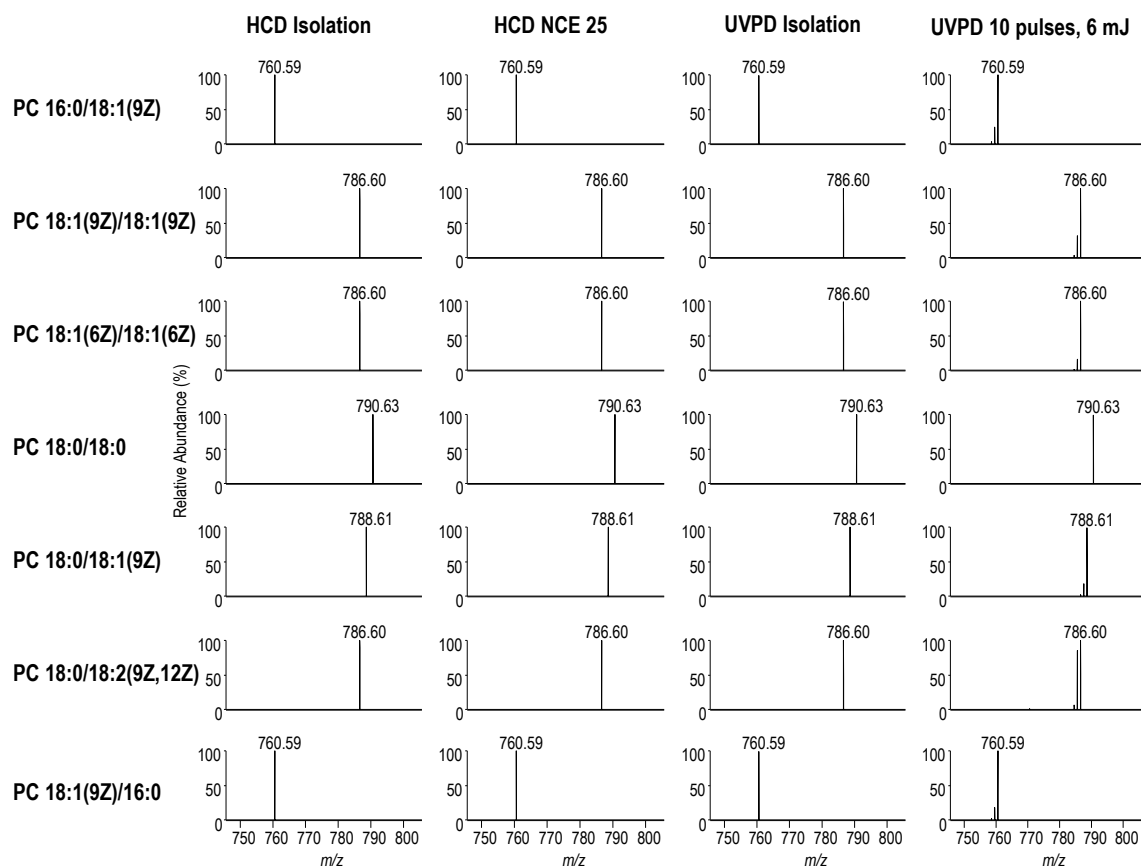


Figure 3.8 Fragmentation spectra expanded on precursor ions during HCD isolation, HCD (NCE 25), UVPD isolation and UVPD (10 pulses, 6 mJ) for PC 16:0/18:1(9Z), PC 18:1(9Z)/18:1(9Z), PC 18:1(6Z)/18:1(6Z), PC 18:0/18:0, PC 18:0/18:1(9Z), PC 18:0/18:2(9Z,12Z) and PC18:1(9Z)/16:0.

To further investigate the nature of the hydrogen atom loss product, UVPD/CID of m/z 759.57 for PC 16:0/18:1(9Z) was performed (**Figure 3.9**).

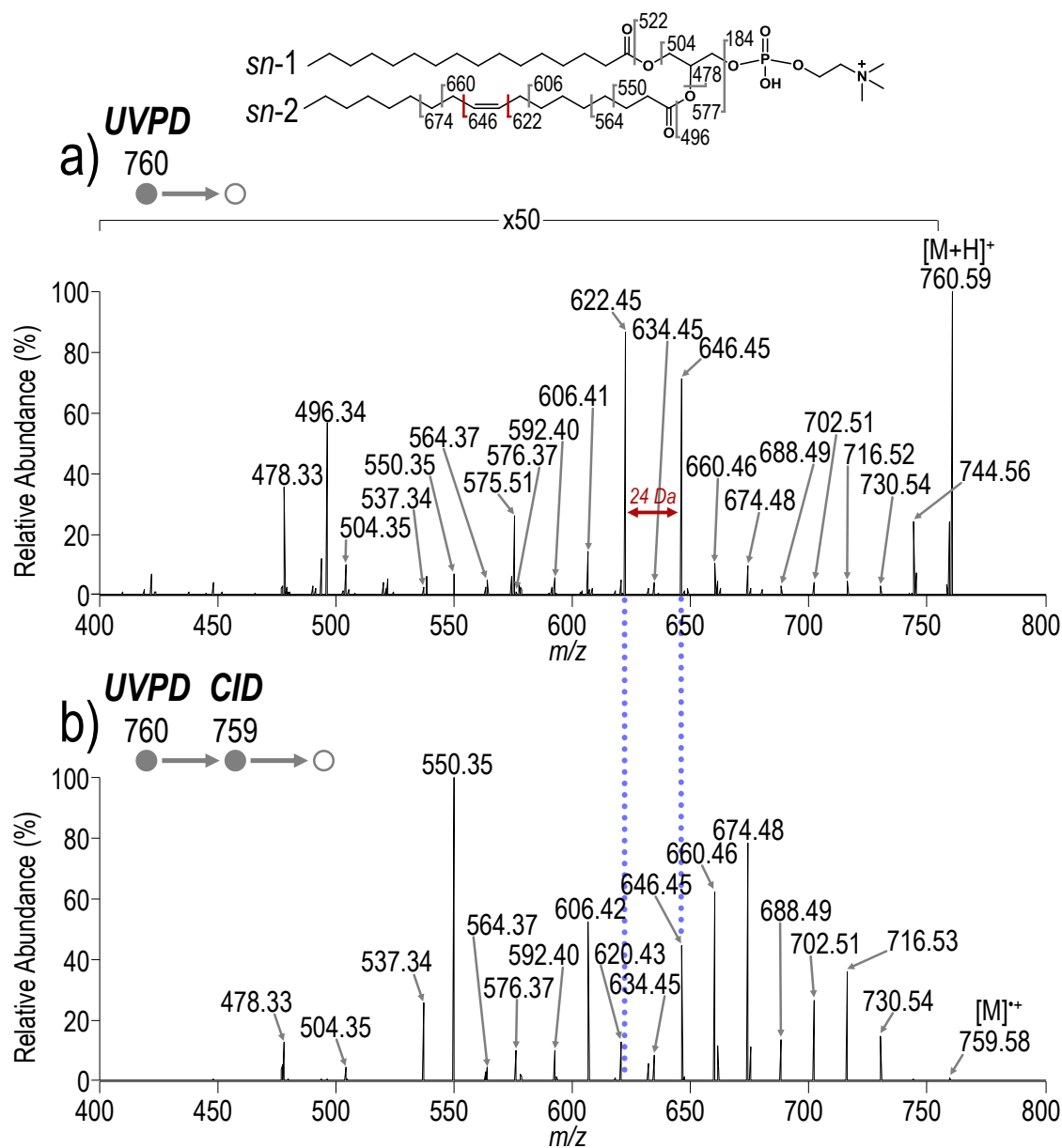


Figure 3.9 a) UVPD (10 pulses, 6 mJ) of PC 16:0/18:1(9Z) and b) UVPD/CID (10 pulses, 6 mJ/NCE 30) of PC 16:0/18:1(9Z). UVPD/CID is an MS³ event where UVPD is first performed on *m/z* 760.59 and then CID is subsequently performed on the atomic hydrogen loss species at *m/z* 759.58.

UVPD was used to generate the hydrogen loss product (*m/z* 759.57) which was subsequently isolated and subjected to CID. While there are obvious differences in

fragment ion abundances between the UVPD and UVPD/CID spectra (**Figure 3.9a** versus **3.9b**), in general, many of the ions present in the UVPD spectrum are also present in the UVPD/CID spectrum. However, there exist fragment ions unique to UVPD, namely the product ion of m/z 622.45 which is one of the key diagnostic fragment ions used to determine double bond position. In the UVPD/CID, there is an alternate product ion of m/z 620.43 which is 26 Da lower in mass, not 24 Da lower in mass, than the companion ion of m/z 646.45.

The production of diagnostic product ions that differ by 24 Da upon UVPD is consistent for a number of PCs containing acyl chains with a single unsaturation, and interestingly it is 2 Da less than the difference between allylic cleavages observed by Pham *et al.* for a radical-directed dissociation (RDD) process³⁵ and for the products in the UVPD/CID spectra (**Figure 3.9**). Beyond the presence of diagnostic C-C cleavage products in the spectra of PC 18:1(9Z)/18:1(9Z) and PC 18:1(6Z)/18:1(6Z), there are differences in the abundances of these ions for each of the two isomers (**Figure 3.4b** and **3.4d**) suggesting that the specific double bond position influences the fragmentation processes.

To further probe the influence of specific structural features on the observed UVPD spectra, HCD and UVPD spectra for a series of PCs were compared. **Figure 3.10** shows the UVPD spectra for PC 18:0/18:0, PC 18:0/18:1(9Z) and PC 18:0/18:2(9Z, 12Z); the only variable feature is the number of double bonds. **Figure 3.11** shows the corresponding HCD mass spectra. The UVPD spectrum for PC 18:0/18:1(9Z) (**Figure 3.10b**), as expected, contains a diagnostic ion pair of m/z 650.47 and m/z 674.47. The UVPD spectrum for PC 18:0/18:2 (9Z, 12Z) (**Figure 3.10c**) contains two sets of diagnostic ions of m/z 650.47 and m/z 674.47, and m/z 690.50 and m/z 714.50, indicating that the positions of multiple unsaturations within an acyl chain can be localized.

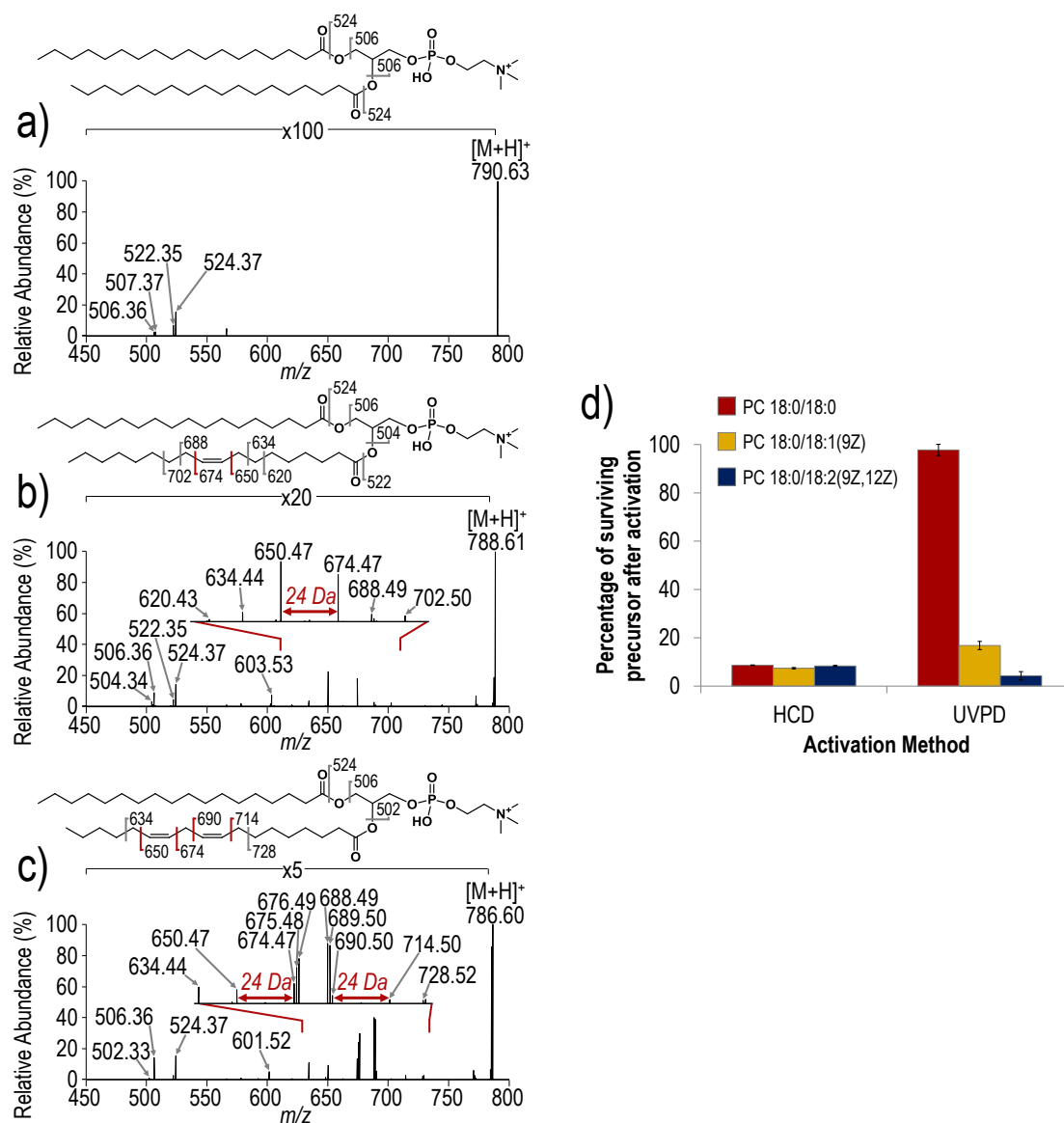


Figure 3.10 UVPD spectra (10 pulses, 6 mJ) of a) PC 18:0/18:0 ($[M+H]^+$, m/z 790.63), b) PC 18:0/18:1(9Z) ($[M+H]^+$, m/z 788.61), and PC 18:0/18:2(9Z,12Z) ($[M+H]^+$, m/z 786.60). d) Bar graph comparing the impact of the number of double bonds on HCD and UVPD as a function of precursor depletion measured as the percentage of surviving precursor after activation.

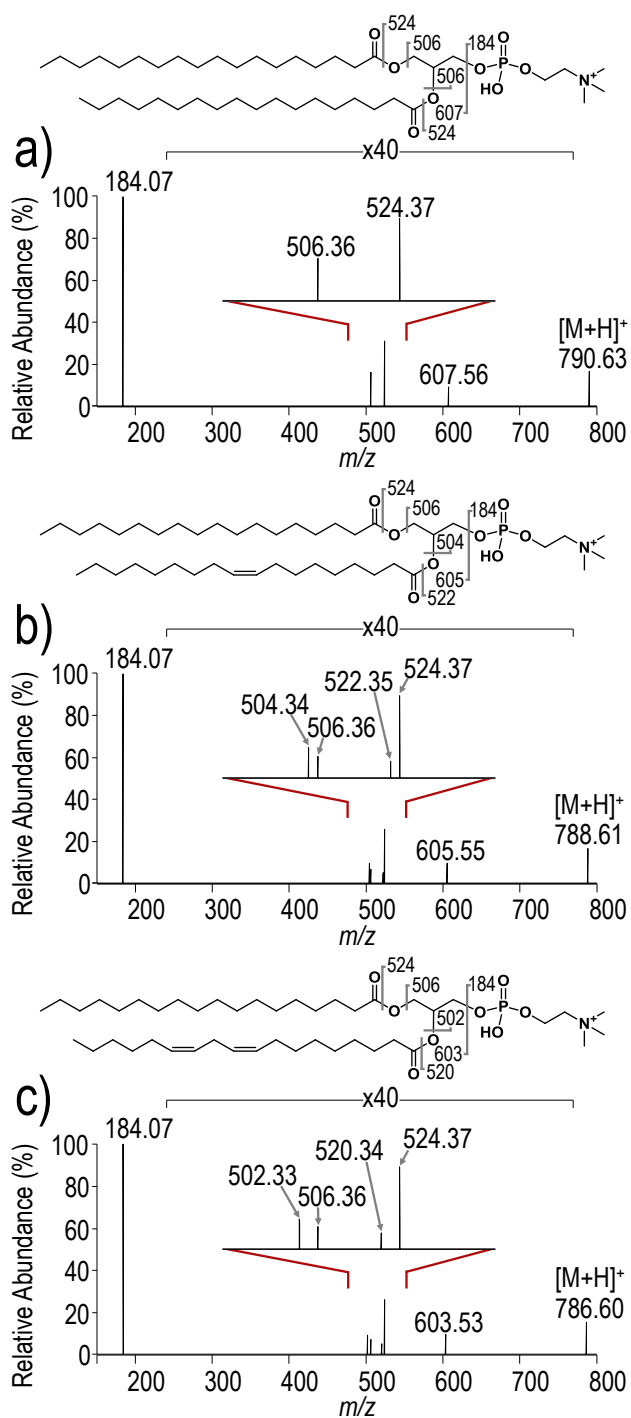


Figure 3.11 HCD (NCE 25) spectra of a) PC 18:0/18:0 ([M+H]⁺, *m/z* 790.63), b) PC 18:0/18:1(9Z) ([M+H]⁺, *m/z* 788.61), c) PC 18:0/18:2(9Z,12Z) ([M+H]⁺, *m/z* 786.60).

However, in contrast to UVPD spectra of PCs with a single unsaturation in an acyl chain, the UVPD spectrum for PC 18:0/18:2(9Z,12Z) contains additional ions of m/z 675.47, m/z 676.48, m/z 688.49 and m/z 689.50, shown in the inset of **Figure 3.10c**. These fragments appear to correspond to odd electron fragments originating from homolytic cleavage of C-C bonds (m/z 675.48 and m/z 689.50) or fragments derived from radical-directed processes (m/z 676.49 and m/z 688.49). The expanded regions of the UVPD mass spectra in **Figure 3.8** confirm an increased abundance of the hydrogen atom loss product for PC 18:0/18:2(9Z,12Z) (see m/z 785.59) compared to isomeric PC 18:1(9Z)/18:1(9Z) and PC 18:1(6Z)/18:1(6Z). **Figure 3.10d** additionally shows how the number of double bonds influences HCD and UVPD efficiency as a function of precursor depletion. Precursor depletion is calculated as percentage of the surviving precursor ion after activation by HCD (NCE 25) or UVPD (10 pulses, 6 mJ). In general, the number of double bonds has little influence on the precursor depletion during HCD, whereas the number of double bonds significantly increases the depletion of the precursor upon UVPD. Increased precursor depletion may be related to an increase in UV photoabsorption cross-section and possibly more facile radical-mediated processes, both which scale with the number of double bonds.

For the acyl chain positional isomers PC 16:0/18:1(9Z) and PC 18:1(9Z)/16:0, HCD leads to preferential loss of acyl chains at the *sn*-2 position as ketenes (**Figure 3.12**). This preferential loss results in the product ions of m/z 496.34 for PC 16:0/18:1(9Z) and m/z 522.36 for PC 18:1(9Z)/16:0. Although the abundances of acyl chain neutral loss ions may be skewed by the presence of contaminating isomers inherent to the sample, as has been previously reported,^{15,41} the same overall trend holds between the positional isomers.

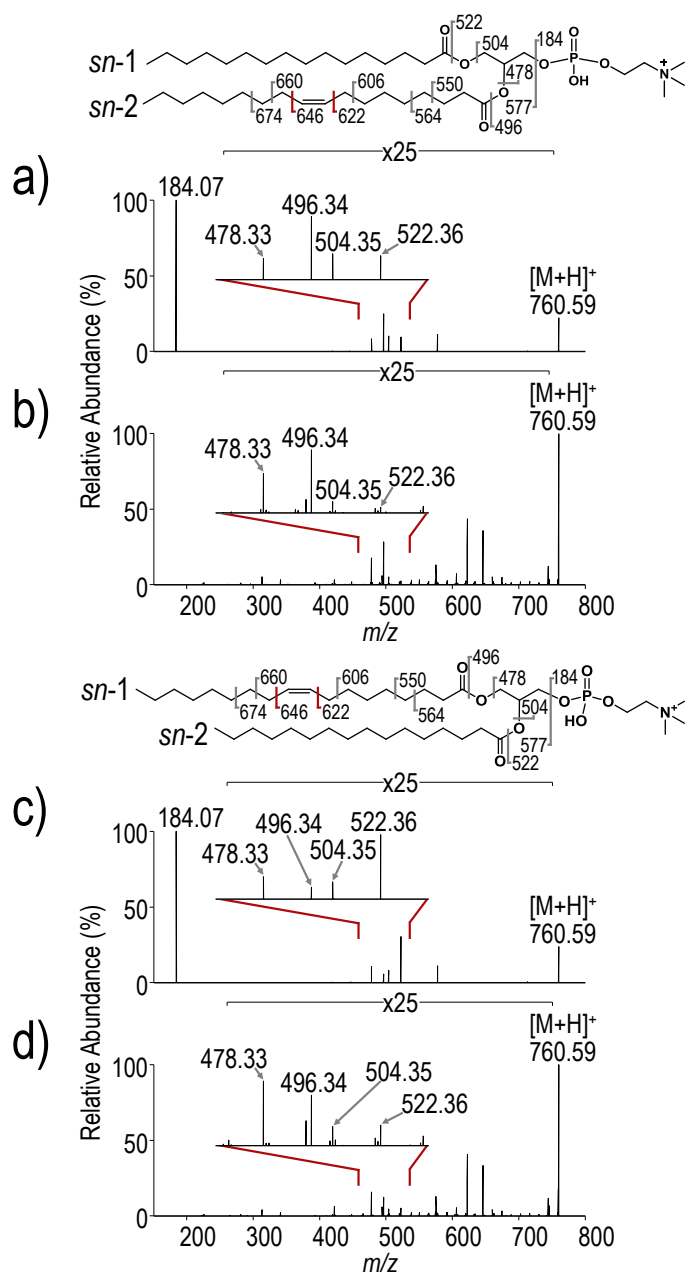


Figure 3.12 a) HCD (NCE 25) and b) UVPD (10 pulses, 6 mJ) of PC 16:0/18:1(9Z) ($[M+H]^+$, m/z 760.58). c) HCD (NCE 25) and d) UVPD (10 pulses, 6 mJ) of PC 18:1(9Z)/16:0 ($[M+H]^+$, m/z 760.58).

In the UVPD spectra of the positional isomers, there appears to be preferential losses of the unsaturated acyl chains leading to more abundant ions at m/z 478.33 and m/z

496.34. Again, this preference suggests that fragmentation is modulated by the presence of the double bond. However, there is no significant difference in the abundances of the fragment ions corresponding to cleavage of either carbon-carbon bond adjacent to the double bond. While it is difficult to determine whether specific fragments are generated via a charge-driven or charge-remote processes without performing experiments with specific deuterium-labeled PCs, it is likely that multiple fragmentation mechanisms contribute to the observed UVPD mass spectra. Moreover, the double bond positions, number of double bonds and acyl chain position may influence which fragmentation pathways are preferentially accessed.

While complete structural characterization of lipids is challenging, detection and differentiation of isomeric lipids in complex biological extracts is crucial for correlation of molecular structure with biological function. For analysis of PCs in biological samples, application of the developed UVPD method is well suited for a shotgun approach for two reasons: 1) as UVPD of PCs suffers from rather low fragmentation efficiency, a shotgun approach offers the ability to average multiple spectra for optimal signal to noise, and 2) while co-isolation and fragmentation of isobaric and isomeric lipids can create convoluted MS/MS spectra that can be challenging to interpret, the high resolution capabilities of the Orbitrap mass spectrometer enable identification of fragment ions with high confidence despite the presence of convoluting species. To demonstrate the UVPD strategy, a bovine liver extract was analyzed owing to its high PC content. **Figure 3.13** shows the positive mode and negative mode shotgun MS¹ mass spectra. The positive mode mass spectrum contains both protonated species and salt adducts for many phospholipids.

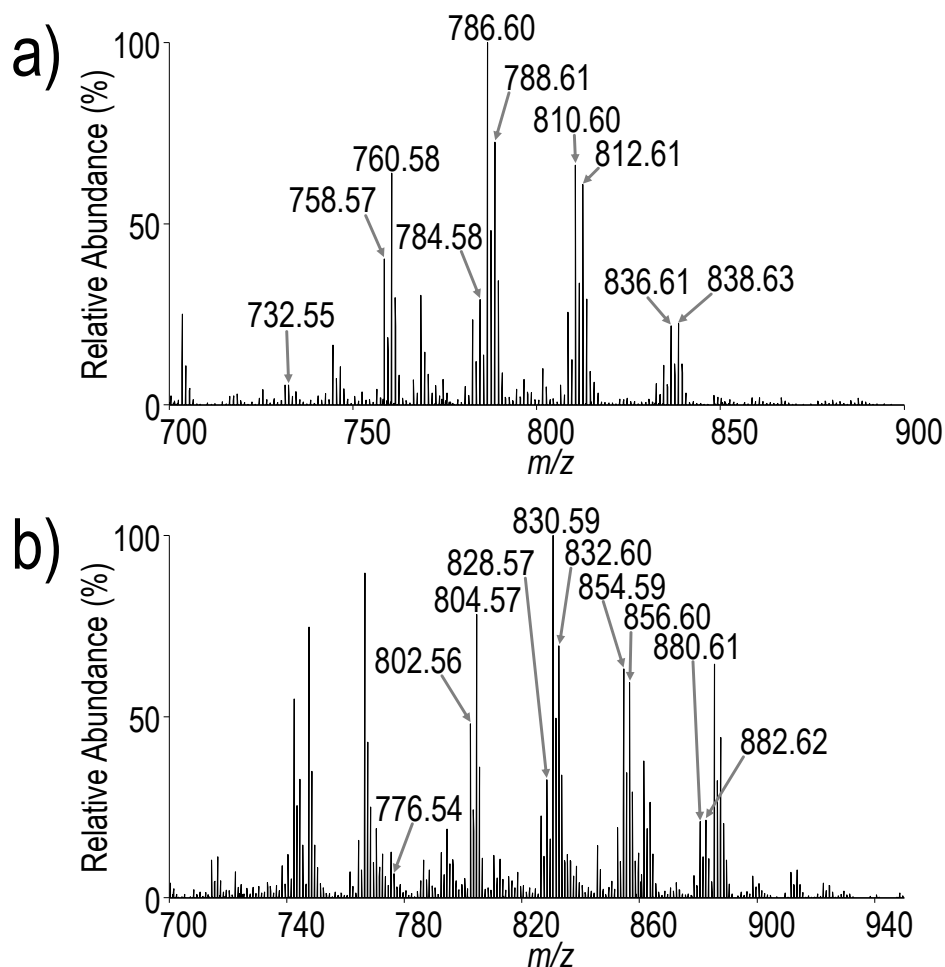


Figure 3.13 a) Positive mode and b) negative mode MS¹ spectra of 10 µg/mL bovine liver extract in 50:50 ACN:H₂O with 30 mM ammonium formate.

High resolution and high mass accuracy allow empirical formulae to be determined from the MS¹ spectra. For structural characterization of PC, ions throughout the mass spectrum were manually selected for subsequent MS/MS analysis. HCD was first performed to identify an ion as a PC species using the characteristic head group product ion of m/z 184.07. Negative mode HCD spectra of the formate adduct ($[M+COOH]^-$) were also collected to verify the acyl chain composition. If a precursor ion was identified as a PC, then the same precursor was subsequently isolated and subjected to UVPD in the positive

mode. For example, HCD was performed on the ion of m/z 760.58 (observed in **Figure 3.14a**). The resulting HCD spectrum displayed an abundant fragment of m/z 184.07 indicative of a PC (**Figure 3.14b**). UVPD was then performed on the ion of m/z 760.58, and fragment ions with a difference of 24 Da were used to determine double bond positions (**Figure 3.14c**).

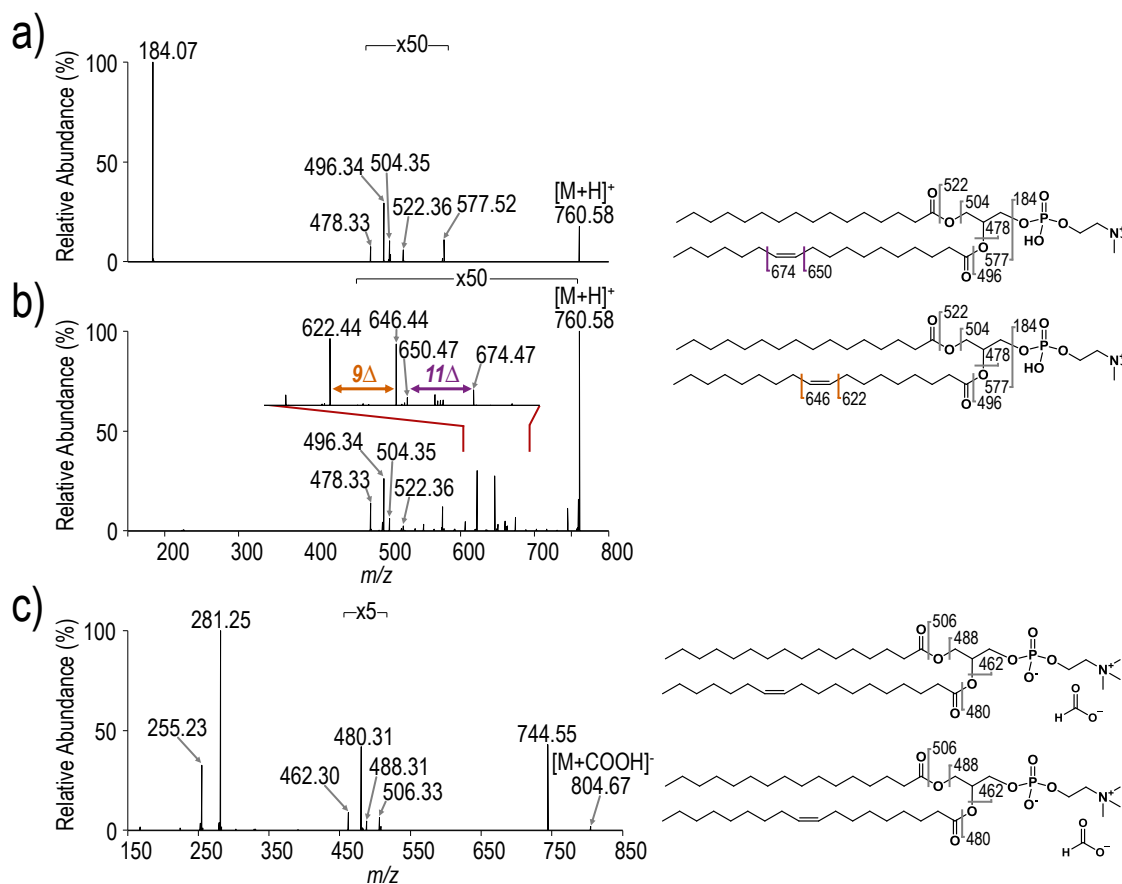


Figure 3.14 Positive mode a) HCD (NCE 25) and b) UVPD spectra (10 pulses, 6 mJ) of m/z 760.58, $[M+H]^+$ and c) negative mode HCD spectrum of m/z 804.67, $[M+COOH]^-$ with corresponding fragment ion maps.

Two sets of ions with a difference of 24 Da were observed in the UVPD spectrum: m/z 622.44 and 646.44 corresponding to PC 16:0_18:1(9Δ) and m/z 650.47 and 674.47 corresponding to PC 16:0_18:1(11Δ). HCD was performed on the formate-adducted

species in negative mode (m/z 804.57, seen in **Figure 3.13**) to further confirm the acyl chain composition. Ions at m/z 255.23 and m/z 281.25 confirm palmitate (16 carbon chain) and oleate (18 carbon chain with 1 unsaturation) acyl chains. This strategy allows differentiation of isomeric PCs in biological samples. **Table 3.2** contains a list of seventeen PCs identified in the bovine liver extract with localized double bonds and the corresponding diagnostics ions. **Figures 3.18-3.27** show the corresponding positive mode HCD and UVPD spectra and negative mode HCD spectra for the identified PCs (Chapter 3, Supporting Information).

Table 3.2 List of identified PCs from polar liver extract

Identified unsaturated PCs	Precursor $[M+H]^+$ (m/z)	Diagnostic ions for double bond position (m/z)		Precursor $[M+COOH]^-$ (m/z)	Acyl chain fragment ions (m/z)	Figure
	+ ion mode	+ ion mode		- ion mode	- ion mode	
PC 14:0_18:1(9 Δ)	732.55	594.41, 618.41		776.54	227.20, 281.25	3.18
PC 16:0_16:1(9 Δ)	732.55	622.44, 646.44		776.54	253.22, 255.23	3.18
PC 16:0_18:1(9 Δ)	760.58	622.44, 646.44		804.57	255.23, 281.25	3.19
PC 16:0_18:1(11 Δ)	760.58	674.47, 650.47		804.56	255.23, 281.25	3.19
PC 16:0_18:2(9 Δ ,12 Δ)	758.57	622.44, 646.44, 662.47, 686.47		802.56	255.23, 279.23	3.20
PC 16:0_20:3(8 Δ ,11 Δ ,14 Δ)	784.58	608.43, 632.43, 648.46, 672.46, 688.49		828.57	255.23, 305.23	3.23
PC 16:0_22:4(7 Δ ,10 Δ ,13 Δ ,16 Δ)	810.60	594.41, 618.41, 634.33, 658.44, 698.47, 714.50		854.59	255.23, 331.26	3.25
PC 18:0_18:1(9 Δ)	788.61	650.47, 674.47		832.60	281.25, 283.25	3.21
PC 18:0_18:1(11 Δ)	788.61	678.50, 702.51		832.60	281.25, 283.25	3.21
PC 18:0_18:2(9 Δ ,12 Δ)	786.60	650.47, 674.47, 690.50, 714.51		830.59	279.23, 283.26	3.22
PC 18:0_18:3(6 Δ ,9 Δ ,12 Δ)	784.58	608.43, 632.43, 648.46, 672.46, 688.49		828.57	277.22, 283.26	3.23
PC 18:0_20:3(8 Δ ,11 Δ ,14 Δ)	812.61	636.46, 660.46, 676.49, 700.49		856.60	283.26, 305.25	3.24
PC 18:0_20:4(5 Δ ,8 Δ ,11 Δ ,14 Δ)	810.60	594.41, 618.41, 634.33, 658.44, 698.47, 714.50		854.59	283.26, 303.23	3.25
PC 18:0_22:4(7 Δ ,10 Δ ,13 Δ ,16 Δ)	838.63	622.44, 646.44, 662.47, 686.47, 702.50, 726.51, 742.53		882.62	283.26, 331.26	3.26
PC 18:0_22:5(7 Δ ,10 Δ ,13 Δ ,16 Δ ,19 Δ)	836.61	622.44, 646.44, 662.47, 686.47, 726.50, 766.54		880.61	283.26, 329.25	3.27
PC 18:1(10 Δ)_18:1(10 Δ)	786.60	662.47, 686.48		830.59	281.25	3.22
PC 18:1(9 Δ)_18:2(9 Δ ,12 Δ)	784.58	646.43, 670.43, 648.46, 672.46, 688.49		828.57	279.23, 281.25	3.23

*All negative mode neutral loss fragments have also lost a head group methyl

Substantial differences in the relative abundances of the diagnostic ions in the UVPD spectrum are apparent in **Figure 3.14b**. Comparison of the variations in relative abundances of diagnostics ions between samples affords insight into changes in the isomer profiles. In fact, changes in the relative abundances of isomeric lipids have previously been correlated to disease states.³³ To assess the ability of the shotgun UVPD method to decipher changes in the relative isomer composition, mixtures containing

various molar ratios of the isomers PC 18:1(6Z)/18:1(6Z) and PC 18:1(9Z)/18:1(9Z) (with a fixed total concentration of 10 μ M) were analyzed (**Figure 3.15, 3.16**).

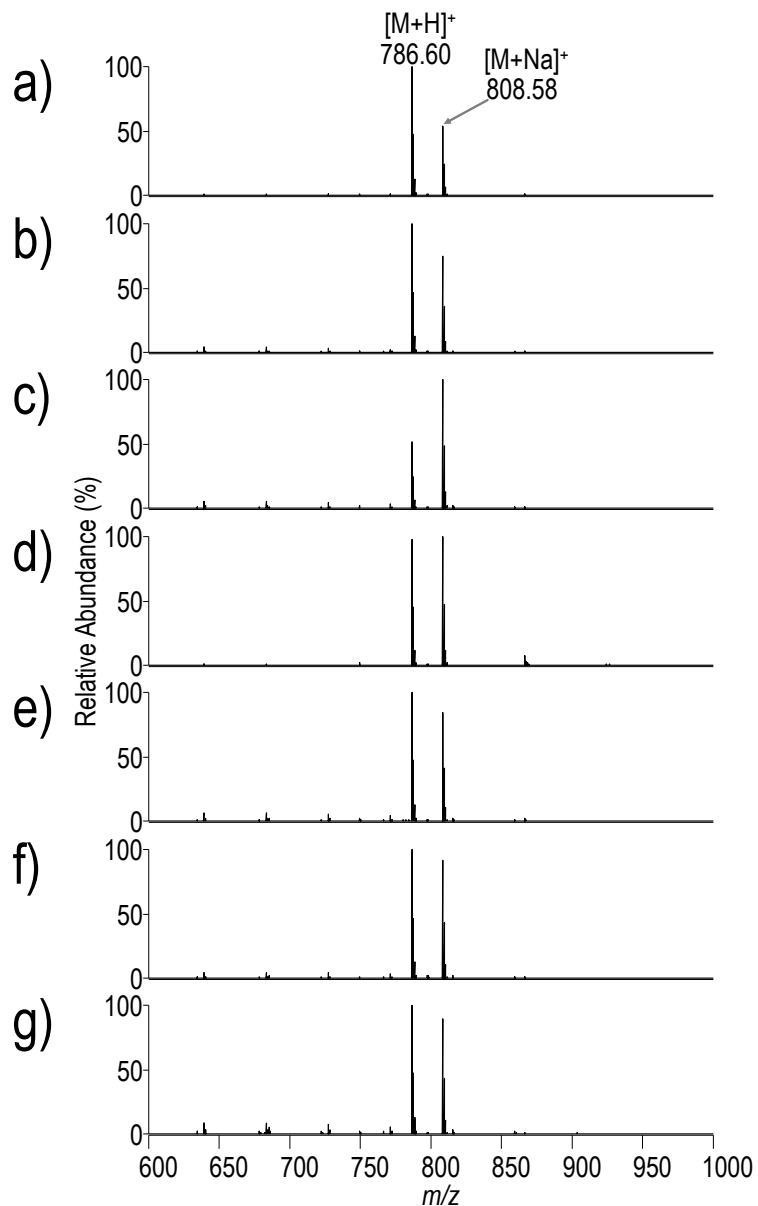


Figure 3.15 MS¹ spectra of solutions containing different molar ratios of PC 18:1(9Z)/18:1(9Z) ([M+H]⁺, m/z 786.60) and PC 18:1(6Z)/18:1(6Z) ([M+H]⁺, m/z 786.60). a) 9:1, b) 7:3, c) 6:4, d) 5:5, e) 4:6, f) 3:7, g) 1:9. The total PC concentration for each solution is 10 μ M. These samples were constituted in 50:50 MeOH:CHCl₃.

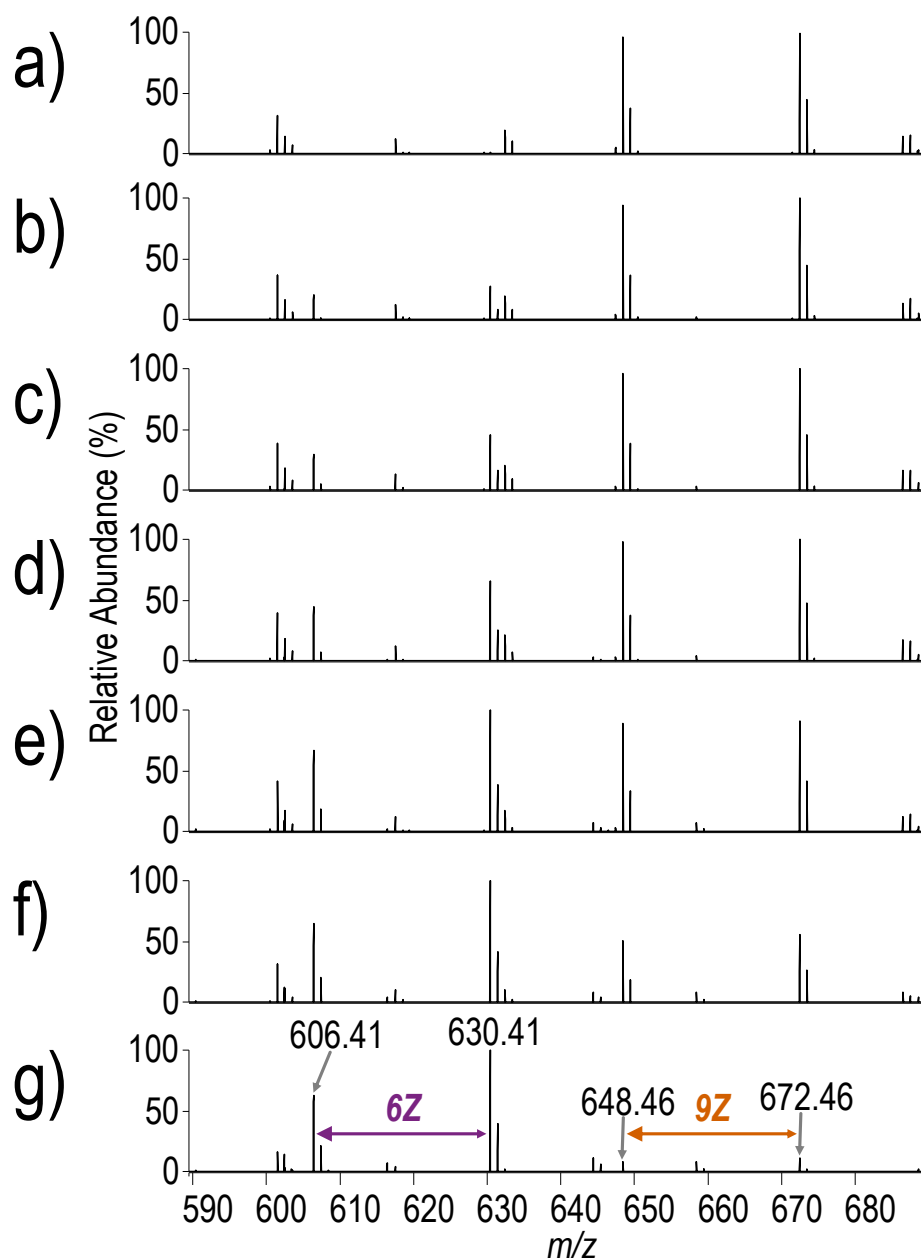


Figure 3.16 Expanded regions of the UVPD spectra for solutions containing various molar ratios of PC 18:1(9Z)/18:1(9Z) and PC 18:1(6Z)/18:1(6Z). Mass spectra correspond to the following ratios of PC 18:1(9Z)/18:1(9Z) to PC 18:1(6Z)/18:1(6Z): a) 9:1, b) 7:3, c) 3:2, d) 1:1, e) 2:3, f) 3:7 and g) 1:9.

UVPD mass spectra were collected, and the abundances of the pair of diagnostic ions for PC 18:1(6Z)/18:1(6Z) were used to calculate the percentage of ion current attributed to PC 18:1(6Z)/18:1(6Z) relative to PC 18:1(9Z)/18:1(9Z)). **Figure 3.17** confirms there is a linear relationship in the percent abundance of diagnostic ions that correlates with the concentration of PC 18:1(6Z)/18:1(6Z), thus providing a means to evaluate the composition of mixtures.

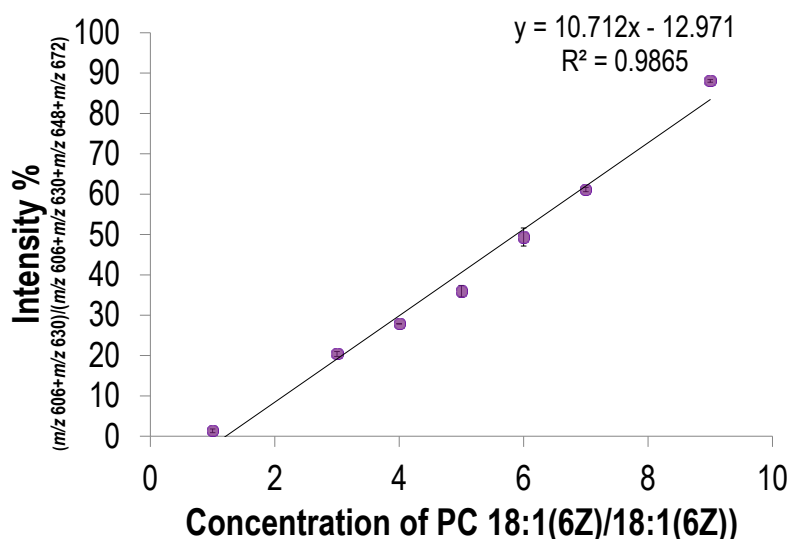


Figure 3.17 Plot confirming the linear relationship between the concentration of PC 18:1(6Z)/18:1(6Z) (x-axis) and intensity percent of the summed diagnostics ions for PC 18:1(6Z)/18:1(6Z) (m/z 606 + m/z 630) relative to the total summed intensity for all diagnostic ions (m/z 606 + m/z 630 + m/z 648 + m/z 672) (y-axis).

3.5 CONCLUSION

Although collisional activation of phospholipids provides head group and acyl chain information, isobaric/isomeric structures resulting from variations in double-bond position and acyl chain position often go undetermined. The presented results confirm that 193 nm UVPD allows PC double bond positional isomers to be discerned.

Comparison of the fragmentation patterns of a series of PCs gave insight into the underlying pathways promoted by UVPD. The series of collected spectra suggest that both the number of double bonds and their relative positions influence photoactivation and fragmentation. A shotgun method utilizing HCD and UVPD in conjunction with the high resolution capabilities of the Orbitrap mass analyzer affords the ability to analyze complex mixtures of phospholipids. From a bovine polar liver extract seventeen PCs were identified, all with double bonds localized. Additionally, preliminary quantitative studies indicate that relative changes in isomer composition can be detected in biological samples. We are currently extending the UVPD method to other subclasses of phospholipids to gain a more detailed global profile of the phospholipids present in biological samples. Despite the advantages of the developed strategy, it is currently not a high throughput method. While automated peak selection and acquisition of MS² spectra could easily be implemented into this method, identification of lipids from UVPD spectra remains a bioinformatics challenge. Most existing lipid identification software that use MS² spectra for identification cater to collision-based fragmentation methods and do not assign peaks originating from cleavage of C-C bonds. Thus, the development of more sophisticated lipid analysis software is essential. In addition, while shotgun spectra are inherently complex, shotgun UVPD spectra are more so, which poses challenges for spectra interpretation and identification of lower abundance species. Coupling of a gas-phase separation method, like differential mobility spectrometry, could allow for spectral simplification while still permitting analysis to be performed in a shotgun fashion.¹⁶

3.6 SUPPORTING INFORMATION

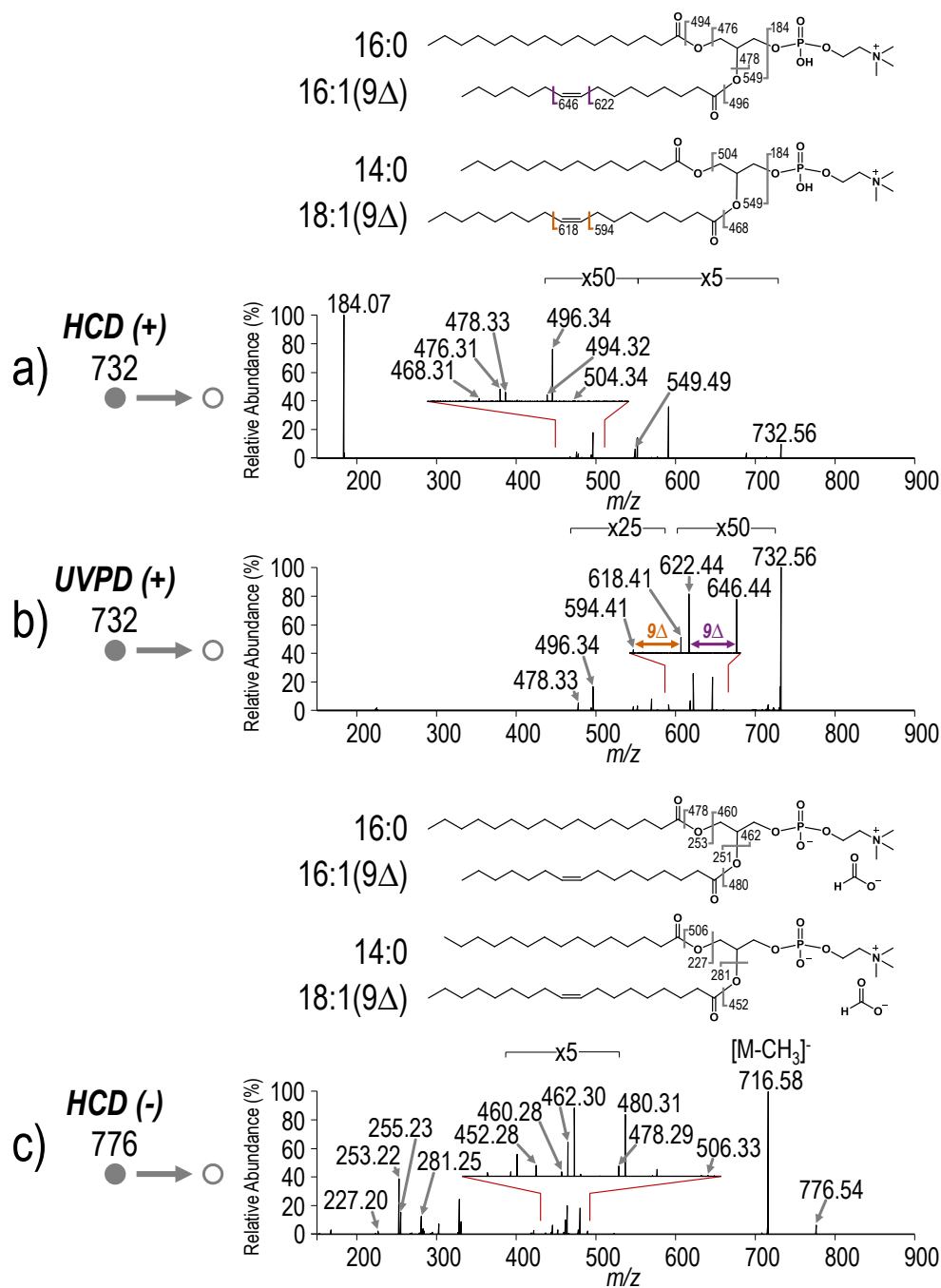


Figure 3.18 a) HCD and b) UVPD spectra of m/z 732.56 ($[M+H]^+$) and c) HCD spectrum of m/z 776.54 ($[M+COOH]^-$).

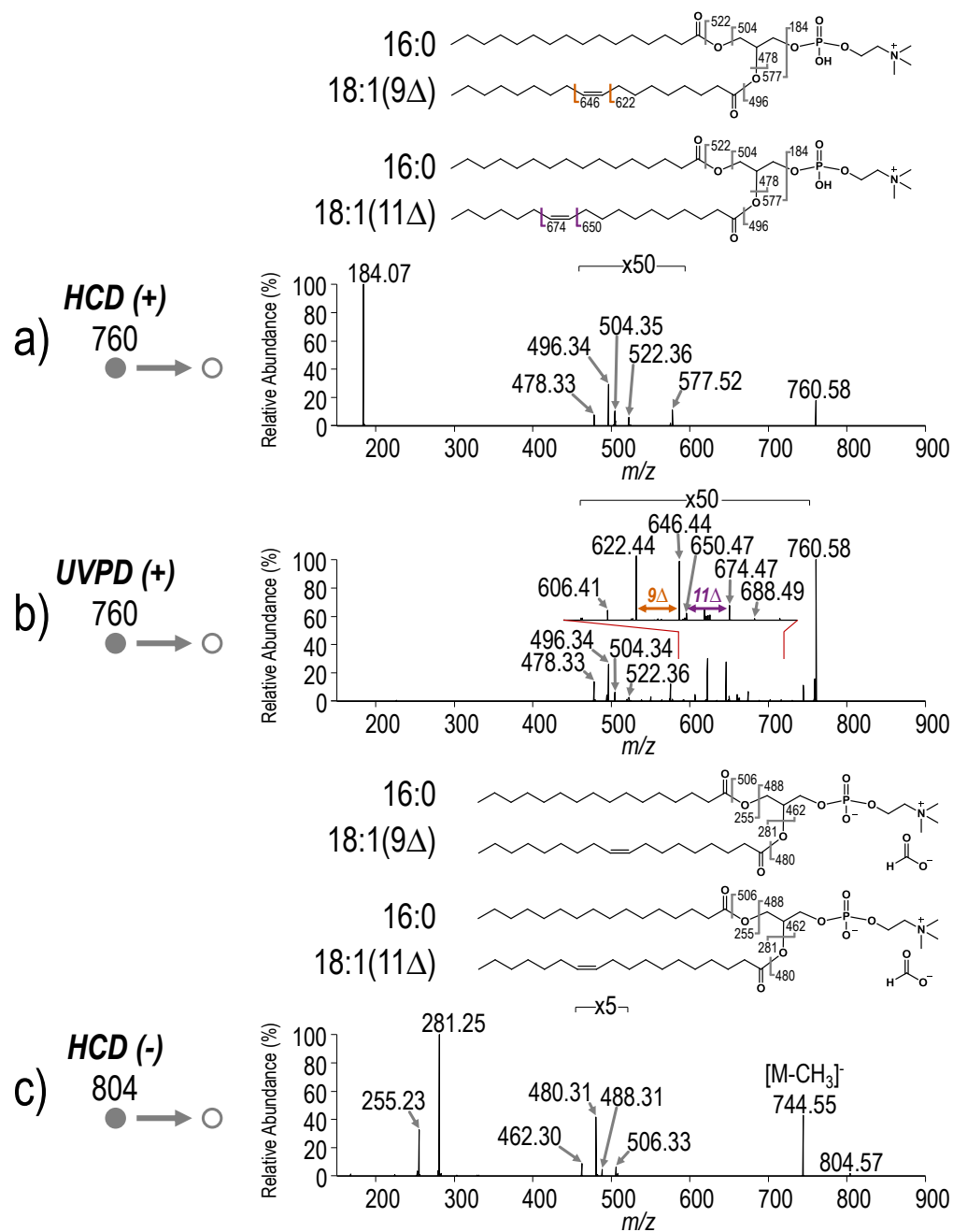


Figure 3.19 a) HCD and b) UVPD spectra of m/z 760.58 ($[M+H]^+$) and c) HCD spectrum of m/z 804.57 ($[M+COOH]^+$)

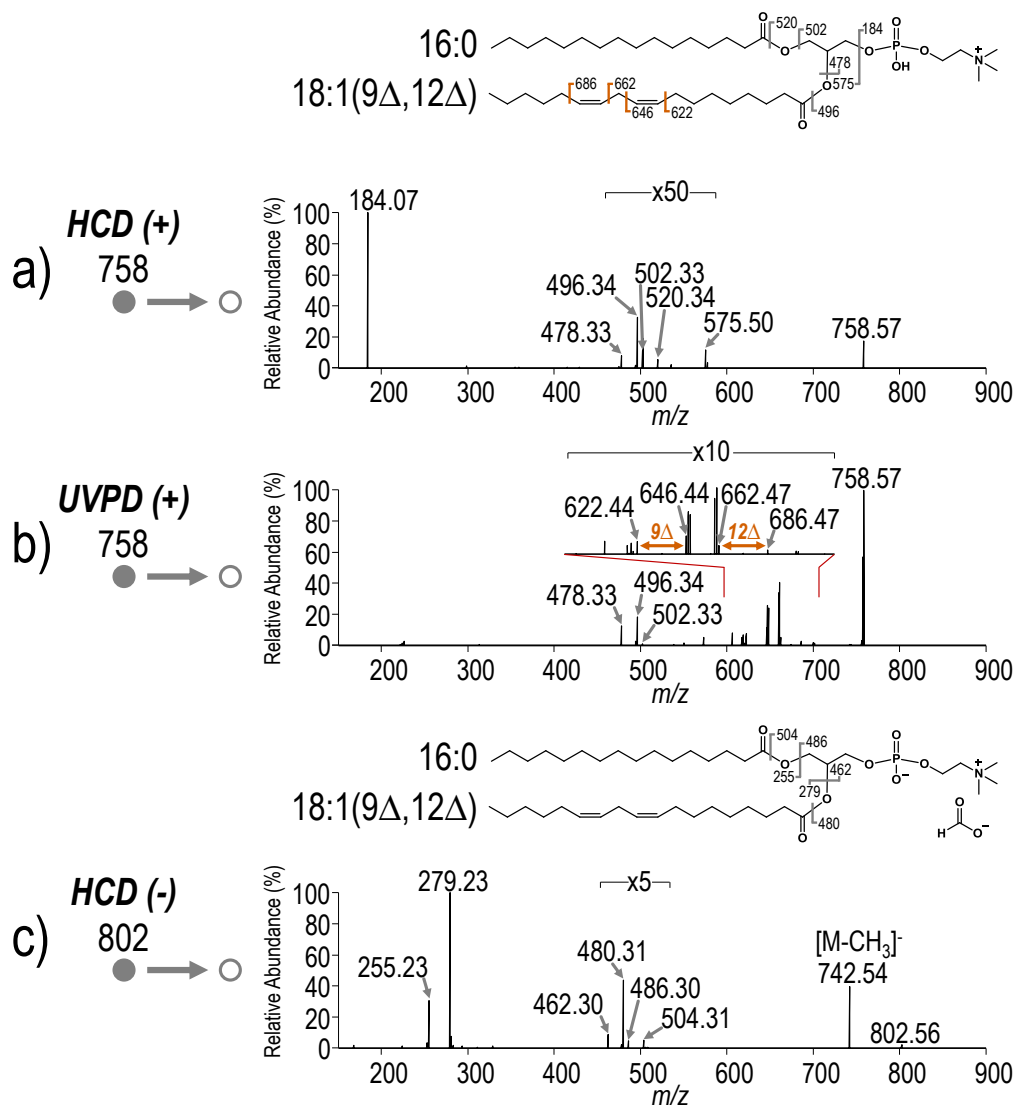


Figure 3.20 a) HCD and b) UVPD spectra of m/z 758.57 ($[M+H]^+$) and c) HCD spectrum of m/z 802.56 ($[M+COOH]^-$)

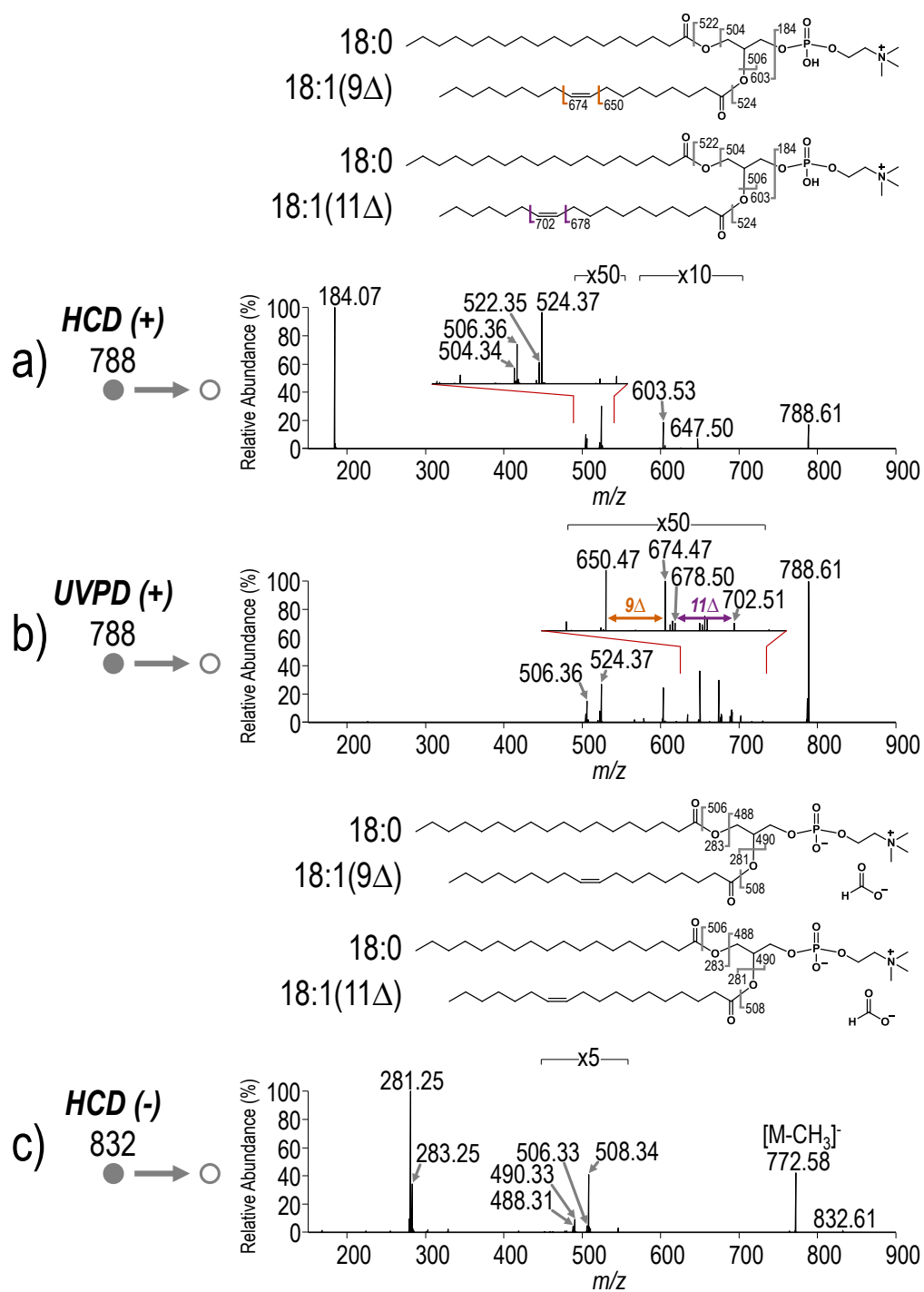


Figure 3.21 a) HCD and b) UVPD spectra of m/z 788.61 ($[M+H]^+$) and c) HCD spectrum of m/z 832.60 ($[M+COOH]^-$)

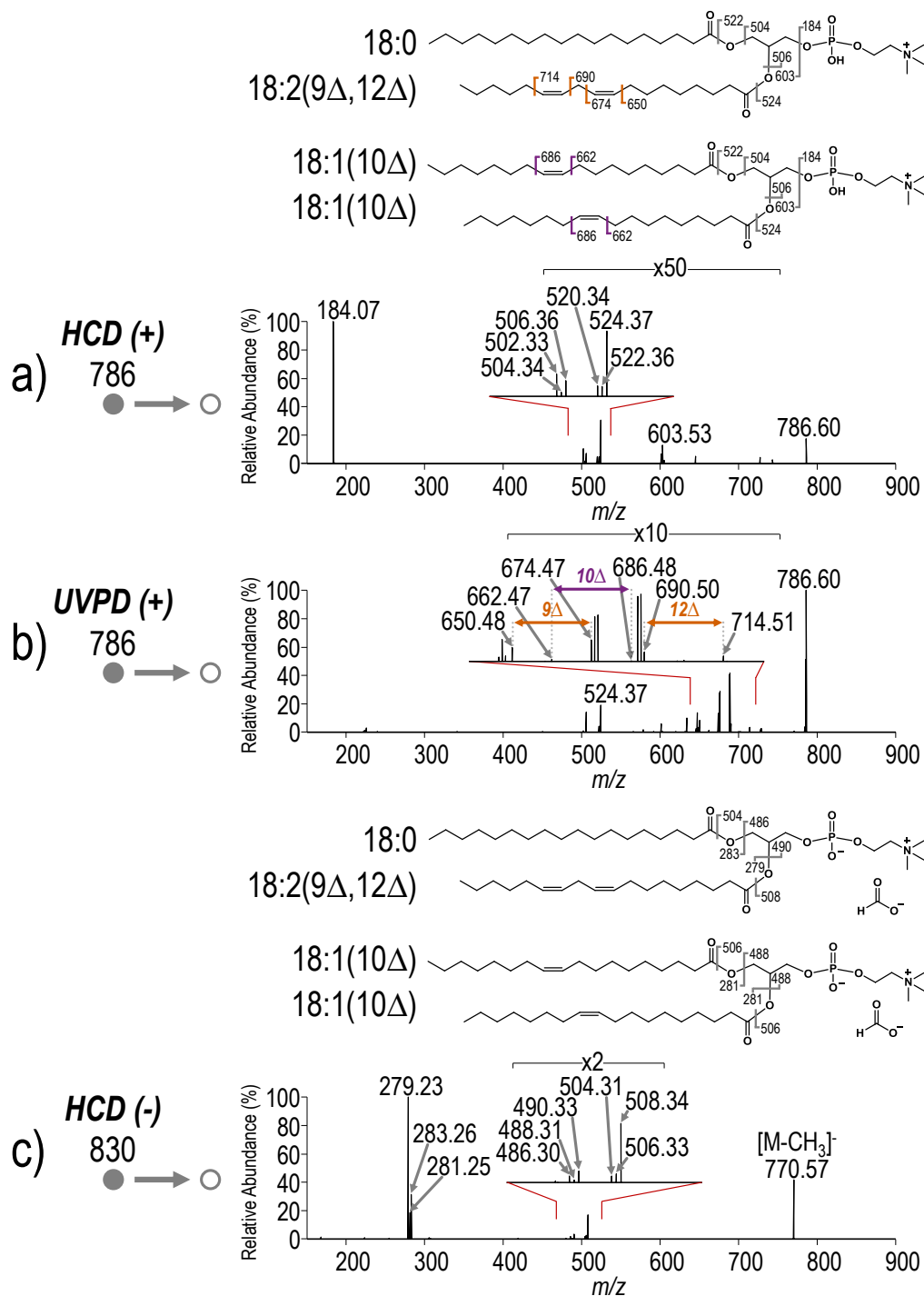


Figure 3.22 a) HCD and b) UVPD spectra of m/z 786.60 ($[M+H]^+$) and c) HCD spectrum of m/z 830.59 ($[M+COOH]^-$)

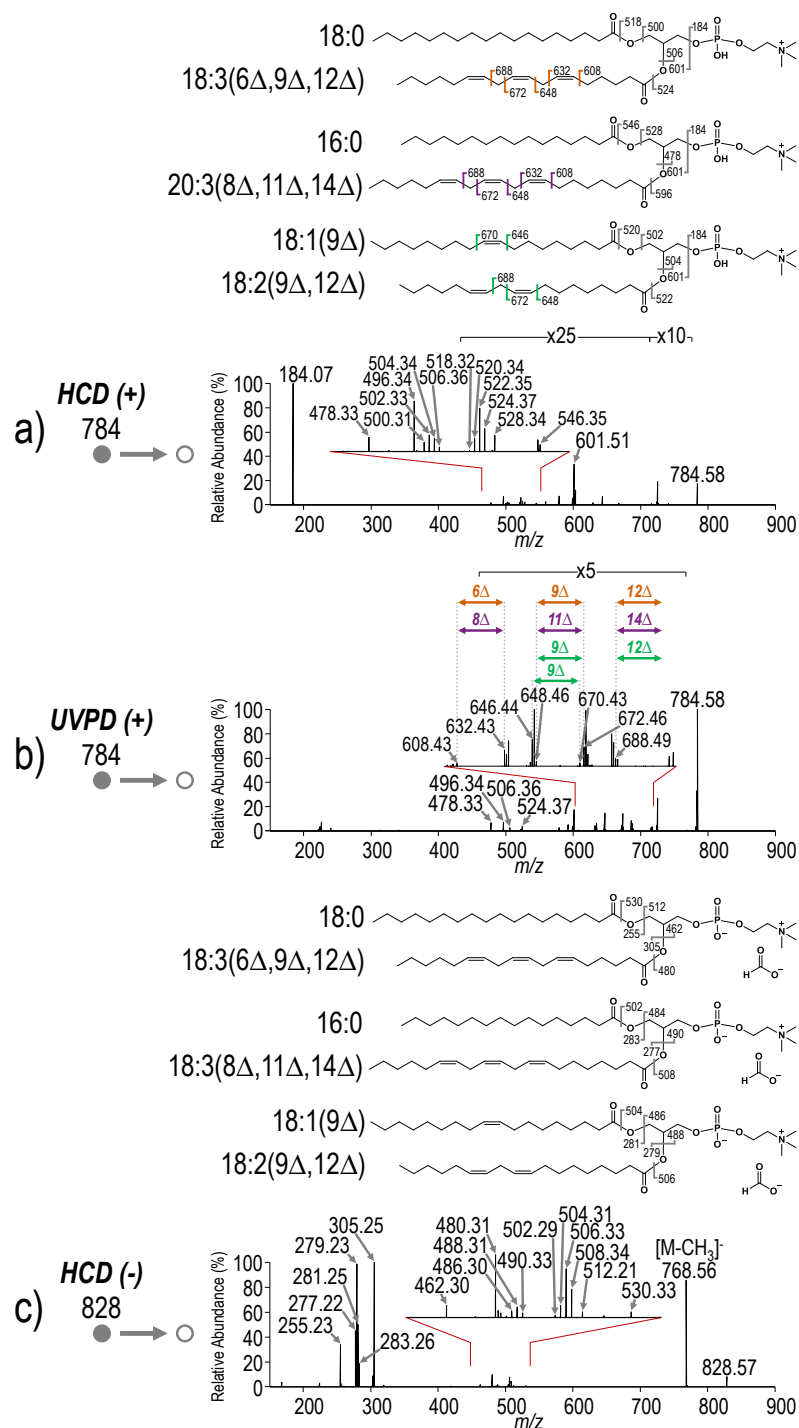


Figure 3.23 a) HCD and b) UVPD spectra of m/z 784.58 ($[M+H]^+$) and c) HCD spectrum of m/z 828.57 ($[M+COOH]^-$)

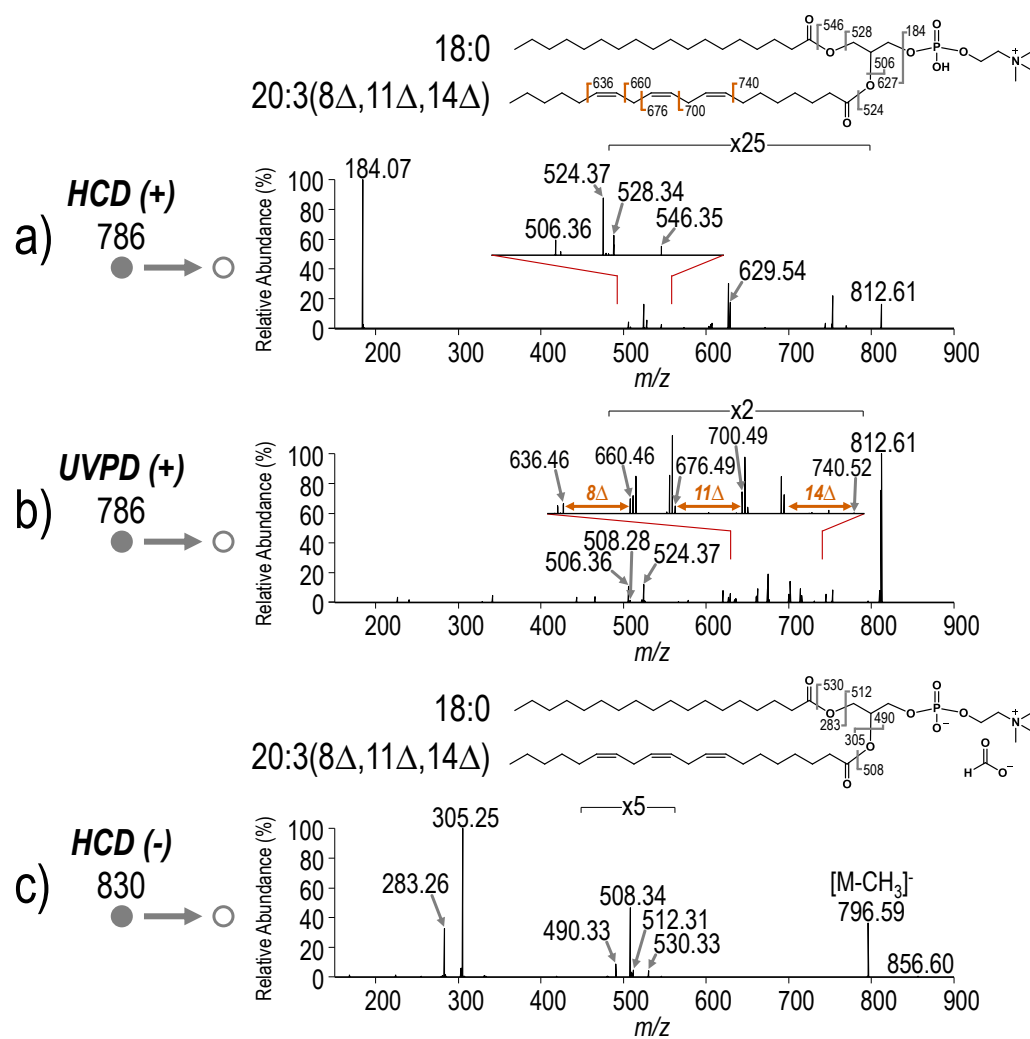


Figure 3.24 a) HCD and b) UVPD spectra of m/z 812.61 ($[M+H]^+$) and c) HCD spectrum of m/z 856.60 ($[M+COOH]^-$)

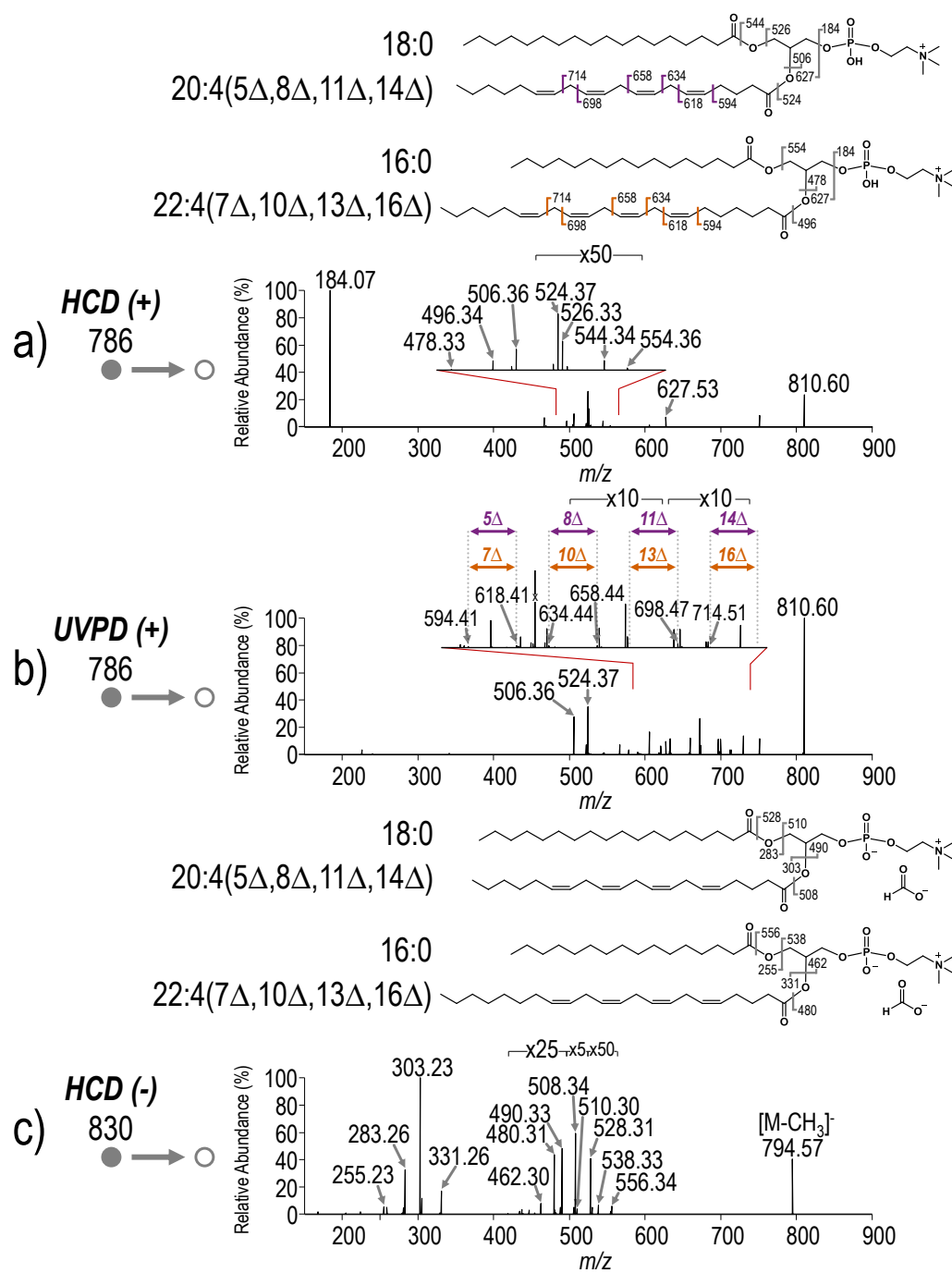


Figure 3.25 a) HCD and b) UVPD spectra of m/z 810.60 ($[M+H]^+$) and c) HCD spectrum of m/z 854.59 ($[M+COOH]^-$)

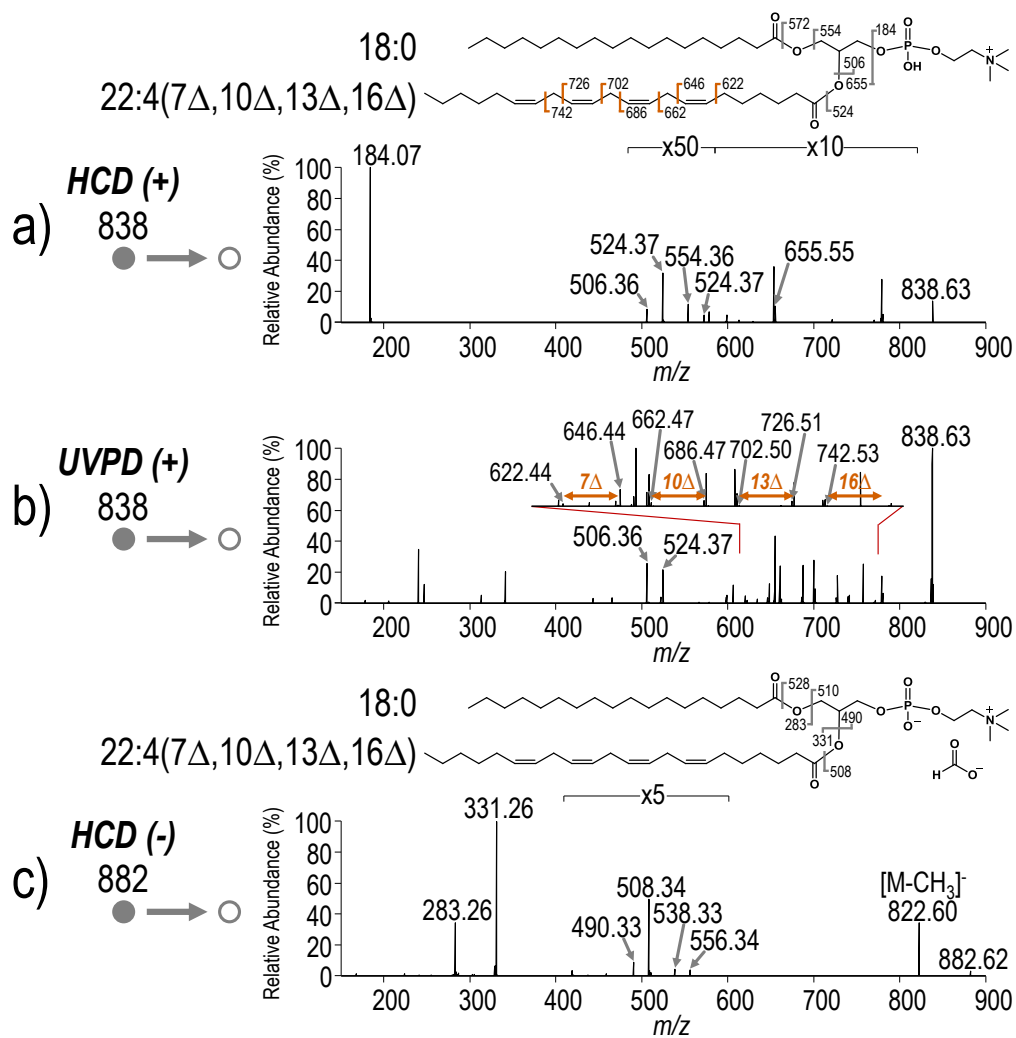


Figure 3.26 a) HCD and b) UVPD spectra of m/z 838.63 ($[M+H]^+$) and c) HCD spectrum of m/z 882.62 ($[M+COOH]^-$)

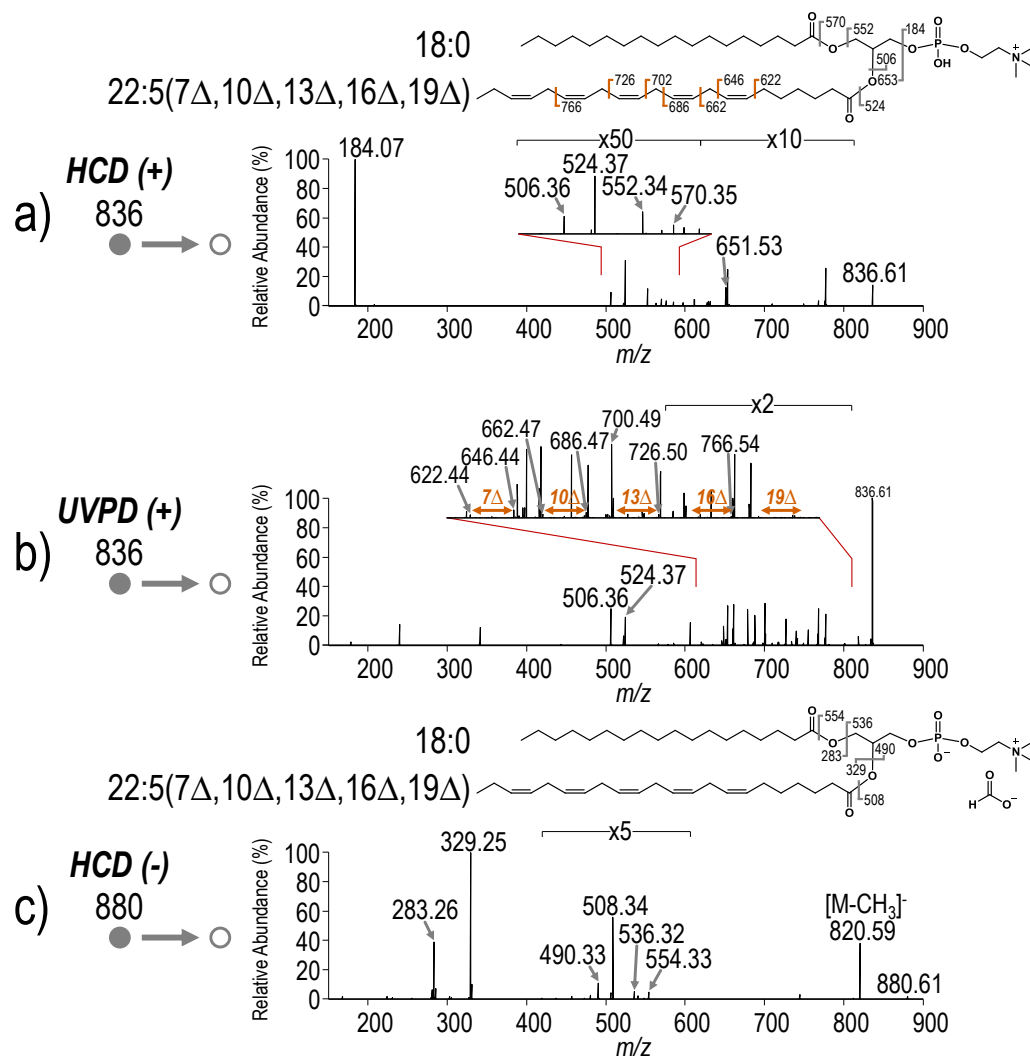


Figure 3.27 a) HCD and b) UVPD spectra of m/z 836.61 ($[M+H]^+$) and c) HCD spectrum of m/z 880.61 ($[M+COOH]^-$)

3.7 REFERENCES

- (1) Brown, S. H. J.; Mitchell, T. W.; Oakley, A. J.; Pham, H. T.; Blanksby, S. J. Time to Face the Fats: What Can Mass Spectrometry Reveal about the Structure of Lipids and Their Interactions with Proteins? *J. Am. Soc. Mass Spectrom.* **2012**, *23*, 1441–1449.
- (2) *Bacterial Membranes: Structural and Molecular Biology*; Remaut, H., Fronzes, R., Eds.; Horizon Scientific Press, 2014.
- (3) Zhang, Y.-M.; Rock, C. O. Membrane Lipid Homeostasis in Bacteria. *Nat. Rev. Microbiol.* **2008**, *6*, 222–233.
- (4) Hussain, N. F.; Siegel, A. P.; Ge, Y.; Jordan, R.; Naumann, C. A. Bilayer Asymmetry Influences Integrin Sequestering in Raft-Mimicking Lipid Mixtures. *Biophys. J.* **2013**, *104*, 2212–2221.
- (5) van Meer, G.; Voelker, D. R.; Feigenson, G. W. Membrane Lipids: Where They Are and How They Behave. *Nat. Rev. Mol. Cell Biol.* **2008**, *9*, 112–124.
- (6) Shevchenko, A.; Simons, K. Lipidomics: Coming to Grips with Lipid Diversity. *Nat. Rev. Mol. Cell Biol.* **2010**, *11*, 593–598.
- (7) Blanksby, S. J.; Mitchell, T. W. Advances in Mass Spectrometry for Lipidomics. *Annu. Rev. Anal. Chem.* **2010**, *3*, 433–465.
- (8) Wenk, M. R. The Emerging Field of Lipidomics. *Nat. Rev. Drug Discov.* **2005**, *4*, 594–610.
- (9) Janmey, P. A.; Kinnunen, P. K. J. Biophysical Properties of Lipids and Dynamic Membranes. *Trends Cell Biol.* **2006**, *16*, 538–546.
- (10) Sandra, K.; Sandra, P. Lipidomics from an Analytical Perspective. *Curr. Opin. Chem. Biol.* **2013**, *17*, 847–853.
- (11) Holthuis, J. C. M.; Levine, T. P. Lipid Traffic: Floppy Drives and a Superhighway. *Nat. Rev. Mol. Cell Biol.* **2005**, *6*, 209–220.
- (12) Martinez-Seara, H.; Róg, T.; Pasenkiewicz-Gierula, M.; Vattulainen, I.; Karttunen, M.; Reigada, R. Interplay of Unsaturated Phospholipids and Cholesterol in Membranes: Effect of the Double-Bond Position. *Biophys. J.* **2008**, *95*, 3295–3305.
- (13) Brouwers, J. F. Liquid Chromatographic–Mass Spectrometric Analysis of Phospholipids. Chromatography, Ionization and Quantification. *Biochim Biophys Acta Mol Cell Biol Lipids* **2011**, *1811*, 763–775.
- (14) Damen, C. W. N.; Isaac, G.; Langridge, J.; Hankemeier, T.; Vreeken, R. J. Enhanced Lipid Isomer Separation in Human Plasma Using Reversed-Phase UPLC with Ion-Mobility/High-Resolution MS Detection. *J. Lipid Res.* **2014**, *55*, 1772–1783.

- (15) Maccarone, A. T.; Duldig, J.; Mitchell, T. W.; Blanksby, S. J.; Duchoslav, E.; Campbell, J. L. Characterization of Acyl Chain Position in Unsaturated Phosphatidylcholines Using Differential Mobility-Mass Spectrometry. *J. Lipid Res.* **2014**, *55*, 1668–1677.
- (16) Lintonen, T. P. I.; Baker, P. R. S.; Suoniemi, M.; Ubhi, B. K.; Koistinen, K. M.; Duchoslav, E.; Campbell, J. L.; Ekroos, K. Differential Mobility Spectrometry-Driven Shotgun Lipidomics. *Anal. Chem.* **2014**, *86*, 9662–9669.
- (17) Pulfer, M.; Murphy, R. C. Electrospray Mass Spectrometry of Phospholipids. *Mass Spectrom. Rev.* **2003**, *22*, 332–364.
- (18) Wenk, M. R. Lipidomics: New Tools and Applications. *Cell* **2010**, *143*, 888–895.
- (19) Brügger, B. Lipidomics: Analysis of the Lipid Composition of Cells and Subcellular Organelles by Electrospray Ionization Mass Spectrometry. *Annu. Rev. Biochem.* **2014**, *83*, 79–98.
- (20) Han, X.; Yang, K.; Gross, R. W. Multi-Dimensional Mass Spectrometry-Based Shotgun Lipidomics and Novel Strategies for Lipidomic Analyses. *Mass Spectrom. Rev.* **2012**, *31*, 134–178.
- (21) Han, X.; Gross, R. W. Shotgun Lipidomics: Electrospray Ionization Mass Spectrometric Analysis and Quantitation of Cellular Lipidomes Directly from Crude Extracts of Biological Samples. *Mass Spectrom. Rev.* **2005**, *24*, 367–412.
- (22) Schuhmann, K.; Almeida, R.; Baumert, M.; Herzog, R.; Bornstein, S. R.; Shevchenko, A. Shotgun Lipidomics on a LTQ Orbitrap Mass Spectrometer by Successive Switching between Acquisition Polarity Modes. *J. Mass Spectrom.* **2012**, *47*, 96–104.
- (23) Schuhmann, K.; Herzog, R.; Schwudke, D.; Metelmann-Strupat, W.; Bornstein, S. R.; Shevchenko, A. Bottom-Up Shotgun Lipidomics by Higher Energy Collisional Dissociation on LTQ Orbitrap Mass Spectrometers. *Anal. Chem.* **2011**, *83*, 5480–5487.
- (24) Hsu, F.-F.; Turk, J. Electrospray Ionization with Low-Energy Collisionally Activated Dissociation Tandem Mass Spectrometry of Glycerophospholipids: Mechanisms of Fragmentation and Structural Characterization. *J. Chromatogr. B* **2009**, *877*, 2673–2695.
- (25) Wasslen, K. V.; Canez, C. R.; Lee, H.; Manthorpe, J. M.; Smith, J. C. Trimethylation Enhancement Using Diazomethane (TrEnDi) II: Rapid In-Solution Concomitant Quaternization of Glycerophospholipid Amino Groups and Methylation of Phosphate Groups via Reaction with Diazomethane Significantly Enhances Sensitivity in Mass Spectrometry Analyses via a Fixed, Permanent Positive Charge. *Anal. Chem.* **2014**, *86*, 9523–9532.

- (26) Canez, C. R.; Shields, S. W. J.; Bugno, M.; Wasslen, K. V.; Weinert, H. P.; Willmore, W. G.; Manthorpe, J. M.; Smith, J. C. Trimethylation Enhancement Using ^{13}C -Diazomethane (^{13}C -TrEnDi): Increased Sensitivity and Selectivity of Phosphatidylethanolamine, Phosphatidylcholine, and Phosphatidylserine Lipids Derived from Complex Biological Samples. *Anal. Chem.* **2016**, *88*, 6996–7004.
- (27) Stutzman, J. R.; Blanksby, S. J.; McLuckey, S. A. Gas-Phase Transformation of Phosphatidylcholine Cations to Structurally Informative Anions via Ion/Ion Chemistry. *Anal. Chem.* **2013**, *85*, 3752–3757.
- (28) Rojas-Betancourt, S.; Stutzman, J. R.; Londry, F. A.; Blanksby, S. J.; McLuckey, S. A. Gas-Phase Chemical Separation of Phosphatidylcholine and Phosphatidylethanolamine Cations via Charge Inversion Ion/Ion Chemistry. *Anal. Chem.* **2015**, *87*, 11255–11262.
- (29) Ho, Y.-P.; Huang, P.-C.; Deng, K.-H. Metal Ion Complexes in the Structural Analysis of Phospholipids by Electrospray Ionization Tandem Mass Spectrometry. *Rapid Commun. Mass Spectrom.* **2003**, *17*, 114–121.
- (30) Hsu, F.-F.; Turk, J. Structural Characterization of Unsaturated Glycerophospholipids by Multiple-Stage Linear Ion-Trap Mass Spectrometry with Electrospray Ionization. *J. Am. Soc. Mass Spectrom.* **2008**, *19*, 1681–1691.
- (31) Ma, X.; Xia, Y. Pinpointing Double Bonds in Lipids by Paternò-Büchi Reactions and Mass Spectrometry. *Angew. Chem.* **2014**, *126*, 2630–2634.
- (32) Stinson, C. A.; Xia, Y. A Method of Coupling the Paternò-Büchi Reaction with Direct Infusion ESI-MS/MS for Locating the C=C Bond in Glycerophospholipids. *Analyst* **2016**, 3696–3704.
- (33) Ma, X.; Chong, L.; Tian, R.; Shi, R.; Hu, T. Y.; Ouyang, Z.; Xia, Y. Identification and Quantitation of Lipid C=C Location Isomers: A Shotgun Lipidomics Approach Enabled by Photochemical Reaction. *Proc. Natl. Acad. Sci.* **2016**, *113*, 2573–2578.
- (34) Yang, K.; Zhao, Z.; Gross, R. W.; Han, X. Identification and Quantitation of Unsaturated Fatty Acid Isomers by Electrospray Ionization Tandem Mass Spectrometry: A Shotgun Lipidomics Approach. *Anal. Chem.* **2011**, *83*, 4243–4250.
- (35) Pham, H. T.; Ly, T.; Trevitt, A. J.; Mitchell, T. W.; Blanksby, S. J. Differentiation of Complex Lipid Isomers by Radical-Directed Dissociation Mass Spectrometry. *Anal. Chem.* **2012**, *84*, 7525–7532.
- (36) Pham, H. T.; Trevitt, A. J.; Mitchell, T. W.; Blanksby, S. J. Rapid Differentiation of Isomeric Lipids by Photodissociation Mass Spectrometry of Fatty Acid Derivatives. *Rapid Commun. Mass Spectrom.* **2013**, *27*, 805–815.

- (37) Pham, H. T.; Julian, R. R. Re-Print of “Radical Delivery and Fragmentation for Structural Analysis of Glycerophospholipids.” *Int. J. Mass Spectrom.* **2015**, 378, 225–231.
- (38) Kozlowski, R.; Mitchell, T.; Blanksby, S. Separation and Identification of Phosphatidylcholine Regioisomers by Combining Liquid Chromatography with a Fusion of Collision-and Ozone-Induced Dissociation. *Eur. J. Mass Spectrom.* **2015**, 21, 191–200.
- (39) Brown, S. H. J.; Mitchell, T. W.; Blanksby, S. J. Analysis of Unsaturated Lipids by Ozone-Induced Dissociation. *Biochim. Biophys. Acta BBA - Mol. Cell Biol. Lipids* **2011**, 1811, 807–817.
- (40) Pham, H. T.; Maccarone, A. T.; Thomas, M. C.; Campbell, J. L.; Mitchell, T. W.; Blanksby, S. J. Structural Characterization of Glycerophospholipids by Combinations of Ozone- and Collision-Induced Dissociation Mass Spectrometry: The next Step towards “Top-down” Lipidomics. *Analyst* **2014**, 139, 204–214.
- (41) Campbell, J. L.; Baba, T. Near-Complete Structural Characterization of Phosphatidylcholines Using Electron Impact Excitation of Ions from Organics. *Anal. Chem.* **2015**, 87, 5837–5845.
- (42) Deimler, R. E.; Sander, M.; Jackson, G. P. Radical-Induced Fragmentation of Phospholipid Cations Using Metastable Atom-Activated Dissociation Mass Spectrometry (MAD-MS). *Int. J. Mass Spectrom.* **2015**, 390, 178–186.
- (43) Li, P.; Hoffmann, W. D.; Jackson, G. P. Multistage Mass Spectrometry of Phospholipids Using Collision-Induced Dissociation (CID) and Metastable Atom-Activated Dissociation (MAD). *Int. J. Mass Spectrom.* **2016**, 403, 1–7.
- (44) Liang, X.; Liu, J.; LeBlanc, Y.; Covey, T.; Ptak, A. C.; Brenna, J. T.; McLuckey, S. A. Electron Transfer Dissociation of Doubly Sodiated Glycerophosphocholine Lipids. *J. Am. Soc. Mass Spectrom.* **2007**, 18, 1783–1788.
- (45) Brodbelt, J. S. Photodissociation Mass Spectrometry: New Tools for Characterization of Biological Molecules. *Chem. Soc. Rev.* **2014**, 43, 2757–2783.
- (46) Madsen, J. A.; Cullen, T. W.; Trent, M. S.; Brodbelt, J. S. IR and UV Photodissociation as Analytical Tools for Characterizing Lipid A Structures. *Anal. Chem.* **2011**, 83, 5107–5113.
- (47) O’Brien, J. P.; Brodbelt, J. S. Structural Characterization of Gangliosides and Glycolipids via Ultraviolet Photodissociation Mass Spectrometry. *Anal. Chem.* **2013**, 85, 10399–10407.
- (48) O’Brien, J. P.; Needham, B. D.; Henderson, J. C.; Nowicki, E. M.; Trent, M. S.; Brodbelt, J. S. 193 nm Ultraviolet Photodissociation Mass Spectrometry for the Structural Elucidation of Lipid A Compounds in Complex Mixtures. *Anal. Chem.* **2014**, 86, 2138–2145.

- (49) O'Brien, J. P.; Needham, B. D.; Brown, D. B.; Trent, M. S.; Brodbelt, J. S. Top-down Strategies for the Structural Elucidation of Intact Gram-Negative Bacterial Endotoxins. *Chem. Sci.* **2014**, *5*, 4291–4301.
- (50) Hankins, J. V.; Madsen, J. A.; Giles, D. K.; Brodbelt, J. S.; Trent, M. S. Amino Acid Addition to *Vibrio Cholerae* LPS Establishes a Link between Surface Remodeling in Gram-Positive and Gram-Negative Bacteria. *Proc. Natl. Acad. Sci.* **2012**, *109*, 8722–8727.
- (51) Shaw, J. B.; Li, W.; Holden, D. D.; Zhang, Y.; Griep-Raming, J.; Fellers, R. T.; Early, B. P.; Thomas, P. M.; Kelleher, N. L.; Brodbelt, J. S. Complete Protein Characterization Using Top-Down Mass Spectrometry and Ultraviolet Photodissociation. *J. Am. Chem. Soc.* **2013**, *135*, 12646–12651.
- (52) Klein, D. R.; Holden, D. D.; Brodbelt, J. S. Shotgun Analysis of Rough-Type Lipopolysaccharides Using Ultraviolet Photodissociation Mass Spectrometry. *Anal. Chem.* **2016**, *88*, 1044–1051.
- (53) Liebisch, G.; Vizcaíno, J. A.; Köfeler, H.; Trötz Müller, M.; Griffiths, W. J.; Schmitz, G.; Spener, F.; Wakelam, M. J. O. Shorthand Notation for Lipid Structures Derived from Mass Spectrometry. *J. Lipid Res.* **2013**, *54*, 1523–1530.

Chapter 4: Desorption Electrospray Ionization Couple with Ultraviolet Photodissociation for Characterization of Phospholipids Isomers in Tissue Sections*

4.1 OVERVIEW

Desorption electrospray ionization (DESI) mass spectrometry imaging has become a powerful strategy for analysis of tissue sections, enabling differentiation of normal and diseased tissue based on changes in the lipid profiles. The most common DESI workflow involves collection of MS¹ spectra as the DESI spray is rastered over a tissue section. Relying on MS¹ spectra inherently limits the ability to differentiate isobaric and isomeric species or evaluate variations in the relative abundances of key isomeric lipids, such as double-bond positional isomers which may distinguish normal and diseased tissues. Here 193 nm ultraviolet photodissociation (UVPD), a technique capable of differentiating double-bond positional isomers, is coupled with DESI to map differences in the double-bond isomer composition in tissue sections in a fast, high throughput manner compatible with imaging applications.

*Klein, D. R.; Feider, C. L.; Garza, K. Y.; Lin, J. Q.; Eberlin, L. S.; Brodbelt, J. S. Desorption Electrospray Ionization Coupled with Ultraviolet Photodissociation for Characterization of Phospholipid Isomers in Tissue Sections. *Anal. Chem.* **2018**, *90*, 10100-10104.

CLF assisted with implementation of DESI on the Orbitrap Fusion Lumos. CLF and KYG participated in data collection, made DESI images and reviewed the manuscript prior to publication. CLF and KYG overall contributed equally. JQL wrote code to enable visualization of DESI-UVPD ratio images. JSB and LSE provided mentorship and reviewed the manuscript prior to publication.

4.2 INTRODUCTION

Mass spectrometry imaging (MSI) has emerged as a formidable tool to obtain spatially-resolved chemical profiles from tissue sections, thus enhancing the diagnosis and prognosis of diseases like cancer.¹⁻⁴ The most widely used ionization techniques for MSI include matrix-assisted laser desorption ionization (MALDI)^{5,6} and desorption electrospray ionization (DESI).⁷⁻⁹ MSI experiments are most commonly performed by collecting MS¹ spectra as the ionization source is rastered over the tissue section with ion intensities subsequently plotted in two-dimensions. Direct sampling of tissue produces complex mass spectra with isobaric species often overlapping or interfering with the analytes of interest. Implementation of MSI on high performance mass spectrometers has alleviated the problem of isobaric interferences and exposed the complexity of biomolecular profiles within tissue sections.¹⁰⁻¹³ While high mass resolution and accuracy measurements facilitate analysis of congested spectra, collection of MS¹ data provides little structural information on the detected species. Consequently, isomeric species remain indistinguishable by MS¹ alone; however, structural characterization via tandem mass spectrometry (MS/MS) provides one approach for deciphering isomers and increasing analyte specificity.^{14,15}

Collisionally activated dissociation (CAD) is the most common MS/MS method used for structural characterization, particularly for lipids.¹⁶ However, a number of subtle features with significant biological implications, including double bond position, acyl chain *sn*-position and double bond stereochemistry, are frequently not confirmed by CAD.¹⁷ Differences in the spatial distribution of isomers arising from these features therefore go unresolved. In particular, double bond positions have been shown to greatly influence lipid membrane thickness and ordering,¹⁸ and play a substantial role in protein-lipid binding.¹⁹ In addition, changes in the relative abundances of double-bond positional

isomers have shown promise for differentiation of normal and diseased tissues.²⁰ Advances in ion mobility spectrometry have enabled fast separation of lipid isomers in the gas phase,^{21,22} and tandem mass spectrometry is crucial for identification of the separated lipids. In-spray Paternò-Büchi reactions with subsequent collisional activation of reaction products have demonstrated success as a means to determine double bond positions.^{21,22} Alternatively, novel ion activation methods are another strategy to elucidate double bond positions. These include high-energy CID^{23,24}, radical-directed dissociation^{25,26}, electron-induced dissociation^{27,28}, electron impact excitation of ions from organics^{29,30}, ozone-induced dissociation (OzID)³¹⁻³⁵, and metastable atom-activated dissociation^{36,37}. Ultraviolet photodissociation (UVPD) at 193 nm has also proven to be a compelling ion activation method for lipid characterization.³⁸⁻⁴¹ For phosphatidylcholines (PC) and sphingolipids, UVPD generates sets of ions that are diagnostic for determining double bond position.³⁹⁻⁴¹

Of the aforementioned methods, only a few have been used for profiling double bond positional isomers *in situ*.^{22,23,32,35} High-energy CID performed on a MALDI-TOF instrument allowed the detailed structural characterization of glycerophospholipids in mouse brain tissue.²³ OzID has been integrated with a DESI platform for the detection of lipid *sn*-positional isomers in tissue sections³² and more recently to a MALDI-Orbitrap for MSI of lipid isomer spatial distribution³⁵. Paternò-Büchi reactions have been coupled with a liquid microjunction surface sampling probe system for profiling and quantitation of double bond positional isomers *in situ*.²² In the present study, DESI is performed on an Orbitrap mass spectrometer equipped with 193 nm UVPD to map spatial distributions of double-bond isomers *in situ*. Our findings reveal that there are changes in the relative abundances of lipid isomers localized to specific tissue features, demonstrating for the

first time that ambient MSI integrated with UVPD-MS allows direct characterization of double bond isomers in tissue.

4.3 EXPERIMENTAL

4.3.1 Materials

Acetonitrile (ACN) was purchased from EMD Millipore (Billerica, MA, USA). PC 18:1(9Z)/18:1(9Z) and PC 18:1(6Z)/18:1(6Z) standards were purchased from Avanti Polar Lipids (Alabaster, AB, USA). Hematoxylin stain was purchased from Ricca Chemical (Arlington, TX, USA) and eosin stain was purchased from Fisher Scientific (Waltham, MA, USA). Glass microscope slides and multi-spot glass microscope slides were purchased from Fisher Scientific (Waltham, MA, USA).

4.3.2 Tissue Samples

Mouse brain and kidney tissue samples were purchased from BioIVT (Hicksville, NY, USA). Pancreas, kidney, lung, fallopian and human tissues were acquired from Cooperative Human Tissue Network (CHTN). Ovarian tissue was acquired from MD Anderson Cancer Center Tissue Bank (Houston, TX, USA). Endometrial tissue was provided by Seton Medical Center (Austin, TX, USA). All tissues were analyzed in accordance with IRB and IBC protocols. Tissues were sectioned on a Cryostar NX50 cryostat (Thermo Scientific, San Jose, CA, USA) at 16 μ m each and stored at -80°C prior to analysis.

4.3.3 DESI-MS and DESI-UVPD Profiling and Imaging

All experiments were performed in positive ion mode on an Thermo Scientific Orbitrap Fusion Lumos mass spectrometer (San Jose, CA, USA) modified with a 193 nm Coherent Excistar excimer laser (Santa Clara, CA, USA) to perform UVPD as previously

described.⁴² All spectra were collected with the instrument operating in full profile mode. DESI was performed using a 2D Omnispray DESI stage and ion source adapter (Prosolia, Inc., Indianapolis, IN, USA) with a custom manufactured extended ion transfer tube for coupling to the Fusion Lumos interface (**Figure 4.1**).

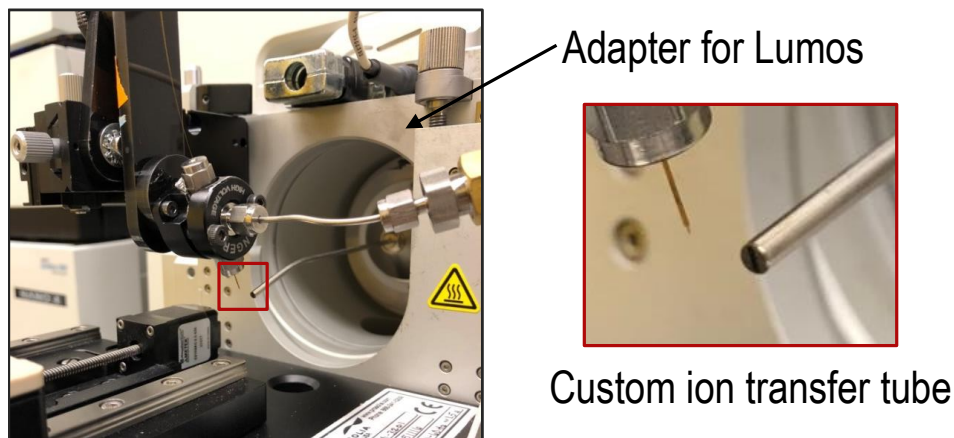


Figure 4.1 Picture of DESI stage set-up on an Orbitrap Fusion Lumos mass spectrometer with custom manufactured extended ion transfer tube.

ACN was sprayed at rate of 5-8 $\mu\text{L}/\text{min}$ through a lab built sprayer using a nitrogen pressure of 180 psi and a spray voltage of 5kV. Higher-energy collisional dissociation (HCD) spectra were collected at a normalized collision energy (NCE) of 30 and UVPD spectra were collected at 20 pulses with 6 mJ per pulse. UVPD was performed in the high pressure trap of the dual linear ion trap with the q-value set to 0.1. For DESI profiling experiments, MS^1 , HCD and UVPD spectra were collected with a maximum ion injection time of 500-1000 ms and an AGC target of $1\text{E}5$ - $1\text{E}6$. MS^1 profiling spectra were collected with a mass range of m/z 300-1600 and are presented with a mass range of m/z 700-1000. HCD and UVPD profiling spectra were collected with a mass range of m/z 100-1000. All representative profiling spectra are a composite of 15 consecutive averaged spectra and all representative spectra from imaging data are a composite of 3 consecutive

averaged spectra. DESI-MS images were collected at an instrument resolving power of 240,000 at m/z 200 with the maximum ion injection time set to 50 ms and an ACG target of 1E6-2E6 to ensure consistent instrument scan times. DESI-UPVD images were collected by continuously activating the isolated m/z value of interest with the instrument operating at a resolving power of 120,000 at m/z 200, the maximum ion injection time set to 1400 ms, the ACG target set to 1E6-2E6 and a mass range of m/z 500-800. Mouse brain tissue section and human lymph node were imaged at a pixel size of 250 μm and human brain was imaged at a pixel size of 175 μm , respectively.

4.3.4 2D Imaging Data Analysis

Thermo RAW files were converted to mzml files using msConvert (ProteoWizard).⁴³ Mzml files were subsequently imported into R using the mzR package from the Bioconductor repository. The peak intensity of an ion within a m/z window of .04 to .12 was taken. Ion intensities or ion ratio values were plotted as a heat map in R.

4.3.5 Lipid Notation

Lipid shorthand notation used is consistent with the notation previously described by Liebisch et al.⁴⁴ In brief, a “/” is used between acyl chains of known orientation with sn-1 followed by sn-2, and “_” is used between acyl chains of unknown orientation. Double bond positions are indicated in parenthesis after the acyl chain composition as carbon number counted down the acyl chain starting at the carbonyl carbon followed by Z, E or Δ to indicate cis, trans or unknown double bond stereochemistry.

4.4 RESULTS AND DISCUSSION

DESI was implemented on an Orbitrap Fusion Lumos mass spectrometer (**Figure 4.1**). The lipid profile observed in the positive ion mode MS¹ spectra of a mouse brain tissue section was consistent with previous reports (**Figure 4.2**).⁴⁵

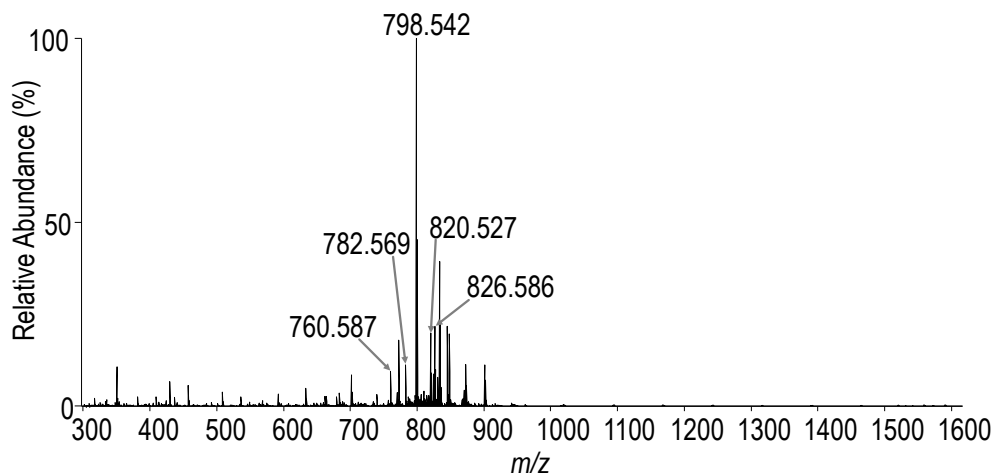


Figure 4.2 The observed positive ion mode MS¹ spectrum of a mouse brain tissue section. HCD and UVPD mass spectra for the prominent ion of m/z 798 with corresponding fragment ion maps are shown in **Figure 4.3**. Product and neutral loss ions in the HCD spectrum confirm the identity of this species as potassium-adducted phosphatidylcholine PC 16:0_18:1. The UVPD mass spectrum provides greater structural detail, confirming the occurrence of a least two double bond positional isomers, namely PC 16:0_18:1(9 Δ) and PC 16:0_18:1(11 Δ), through sets of diagnostic ions spaced apart by 24 Da. These pairs of fragment ions separated by 24 Da are signatures generated uniquely by UVPD and are highly characteristic of double-bond position, as reported previously.^{39–41}

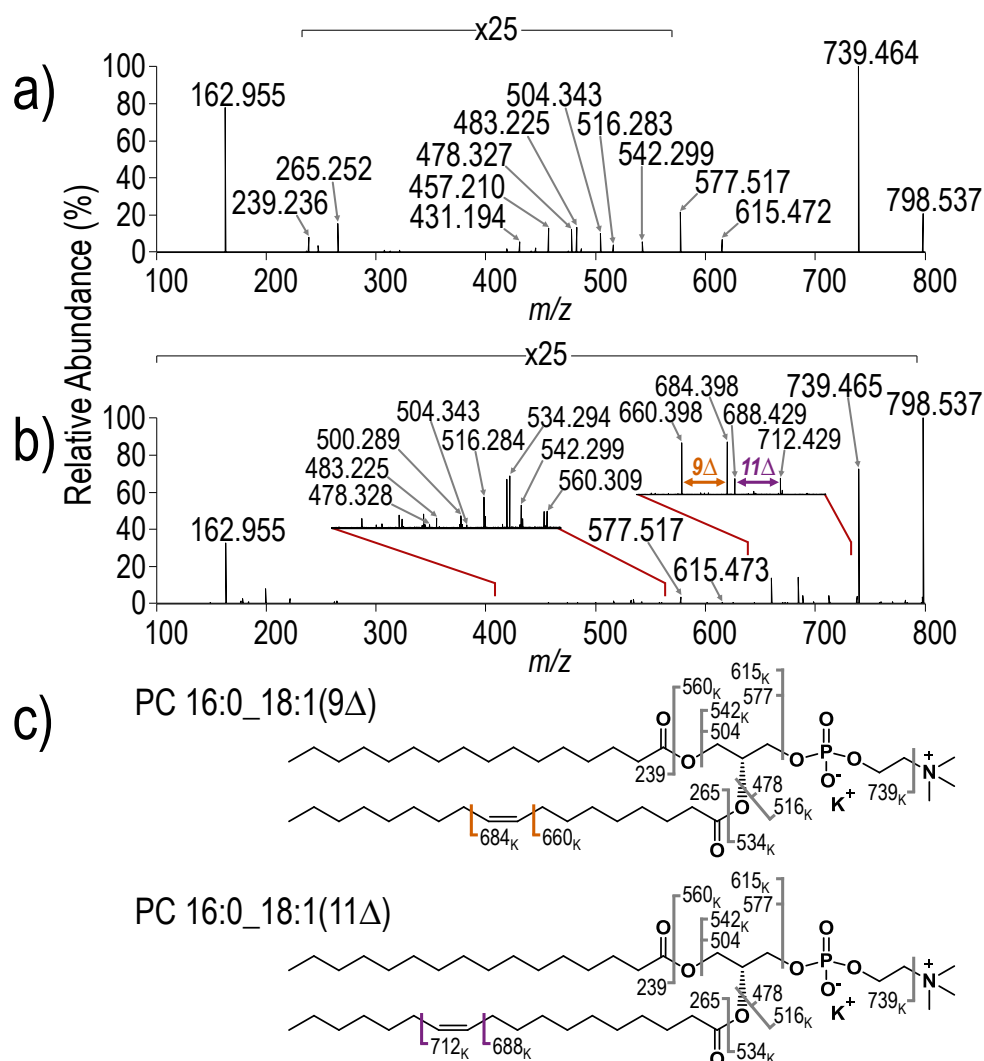


Figure 4.3 a) HCD (NCE 30) and b) UVPD (20 pulses, 6 mJ) mass spectra of the ion of m/z 798 obtained from DESI profiling of a mouse brain tissue section with c) corresponding fragment ion maps for detected isomers [PC 16:0_18:1(9 Δ), PC 16:0_18:1(11 Δ)]. The subscript “K” in the labels of the fragment ion maps indicates ions that retain the potassium adduct. The prominent fragment ion at m/z 162 is characteristic of potassium-adducted PC corresponding to phosphate containing a potassium-adduct.

HCD and UVPD mass spectra for the sodium-adducted and protonated species of PC 16:0_18:1 provide comparable information to the potassium-adducted ion, indicating that acyl chain composition and double bond information can be obtained regardless of adduction status (**Figure 4.4-4.6**). Despite the magnification of the key fragment ion region in some of the MS/MS spectra, S/N ratios of >100 were routinely obtained owing to the high sensitivity of the Orbitrap analyzer.

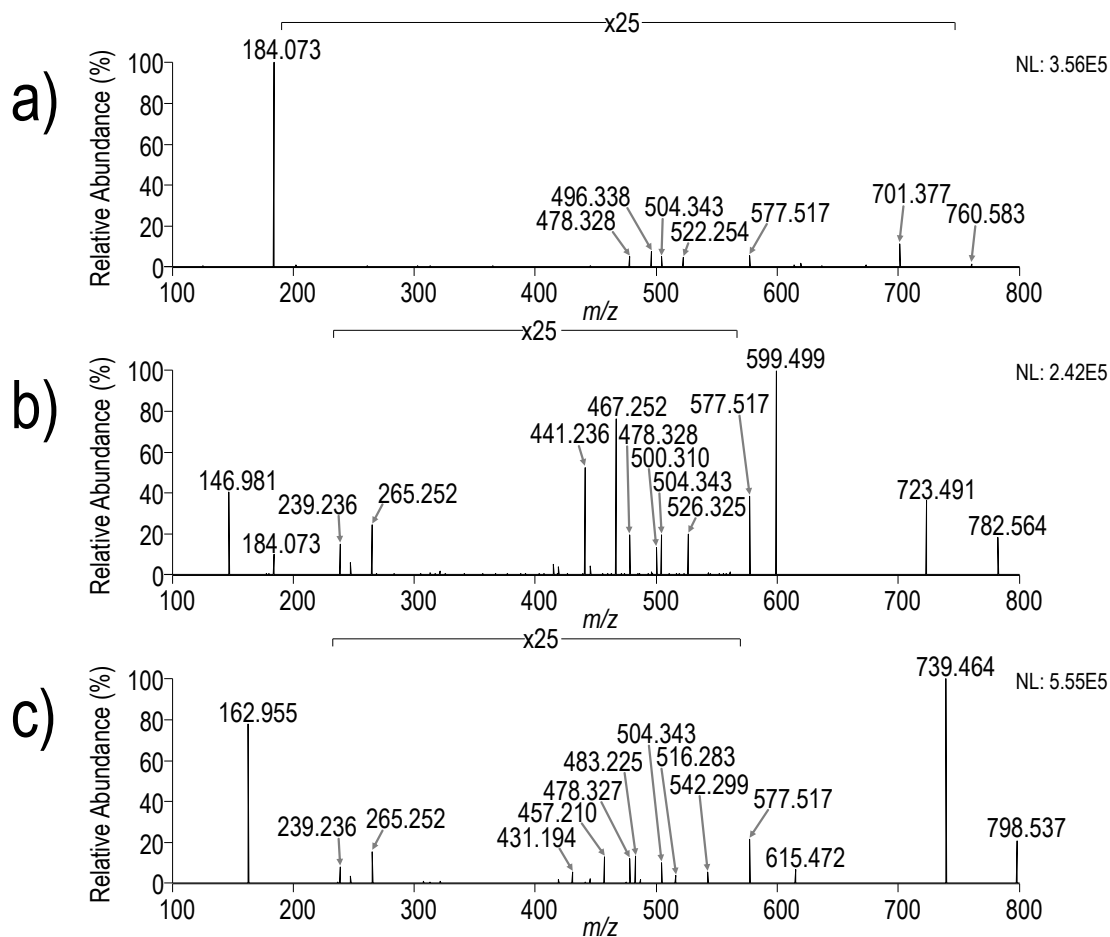


Figure 4.4 HCD (NCE 30) mass spectra of ions of: a) m/z 760, b) m/z 782 and c) m/z 798 from DESI profiling corresponding to the molecular ion, sodium-adducted ion, and potassium-adducted ion for PC 16:0_18:1, respectively. Fragment ion maps are shown in **Figure 4.6**.

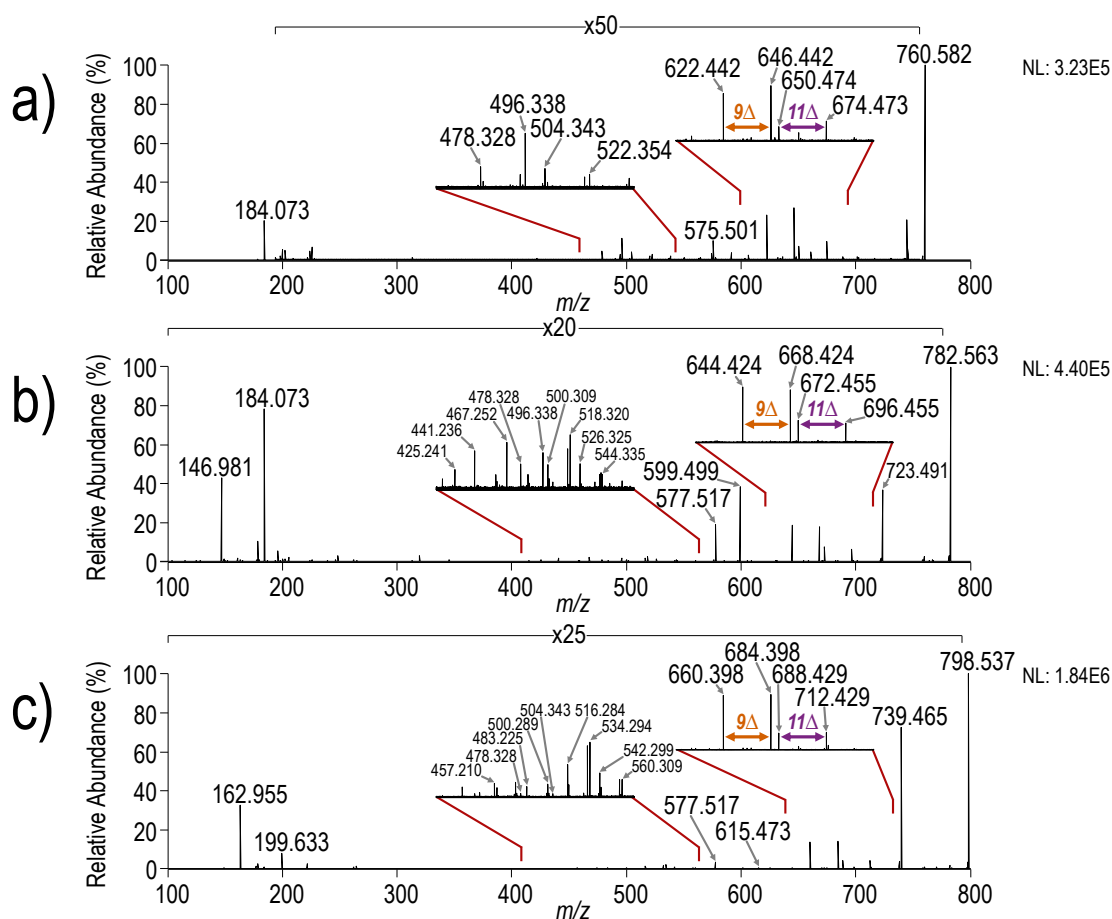


Figure 4.5 UVPD (20 pulses, 6 mJ) mass spectra of ions of: a) m/z 760, b) m/z 782 and c) m/z 798 from DESI profiling corresponding to the molecular ion, sodium-adducted ion, and potassium-adducted ion or PC 16:0_18:1, respectively. Fragment ion maps are shown in **Figure 4.6**.

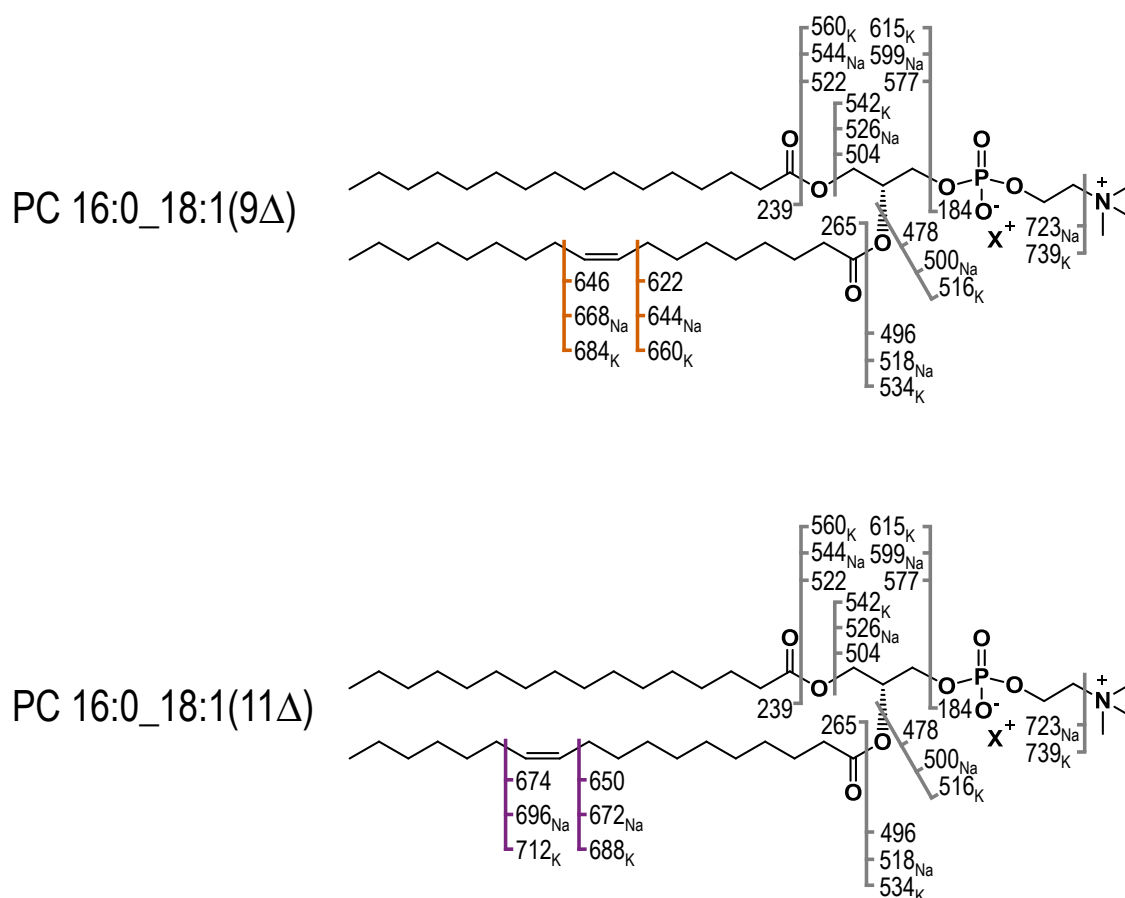


Figure 4.6 Fragment ion map for mass spectra in Supporting Information Figure 2 and Figure 3. Subscripts indicate the presence of a sodium (Na) or potassium (K) adduct. “X” represents either a proton, sodium cation or potassium cation.

HCD and UVPD mass spectra were also collected for other ions of m/z 826 and m/z 820 of high abundance in the lipid profile spectrum (**Figure 4.7-4.8**). The UVPD mass spectra for these other lipids reveal that they are each composed of at least two double bond positional isomers, PC 18:0_18:1(9 Δ) and PC 18:0_18:1(11 Δ) for m/z 826, and PC 16:0_20:4(5 Δ ,8 Δ ,11 Δ ,14 Δ) for m/z 820, based on the presence of paired fragment ions separated by 24 Da. This evidence confirms that UVPD is capable of localizing the positions of multiple double bonds within a single acyl chain for lipids desorbed from tissue.

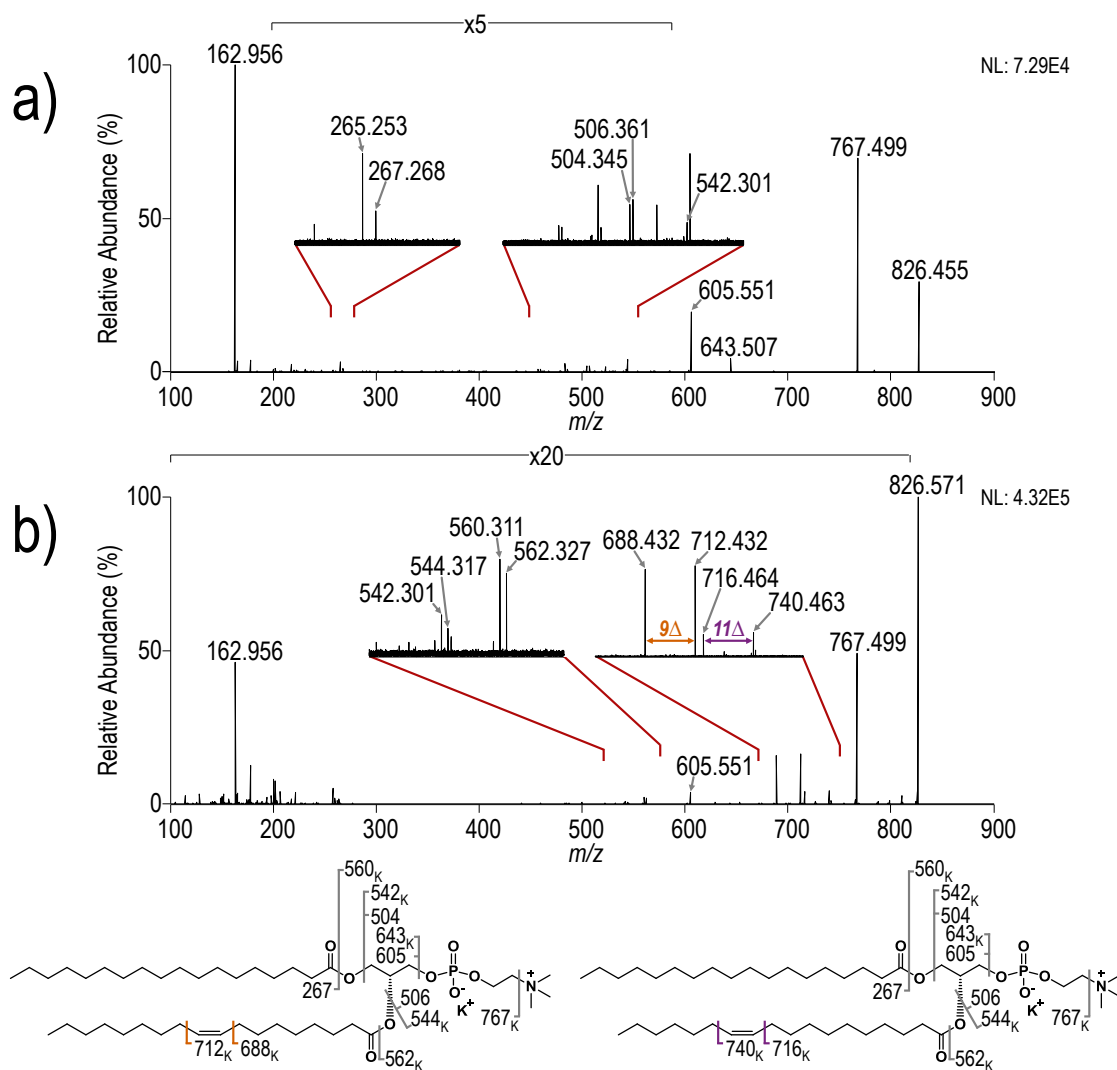


Figure 4.7 a) HCD (NCE 30) and b) UVPD (20 pulses, 6 mJ) mass spectra of the ion of m/z 826 obtained from DESI profiling of a mouse brain tissue section with corresponding fragment ion maps for detected isomers [PC 18:0_18:1(9 Δ), PC 18:0_18:1(11 Δ)]. Subscripts indicate the presence of a potassium (K) adduct.

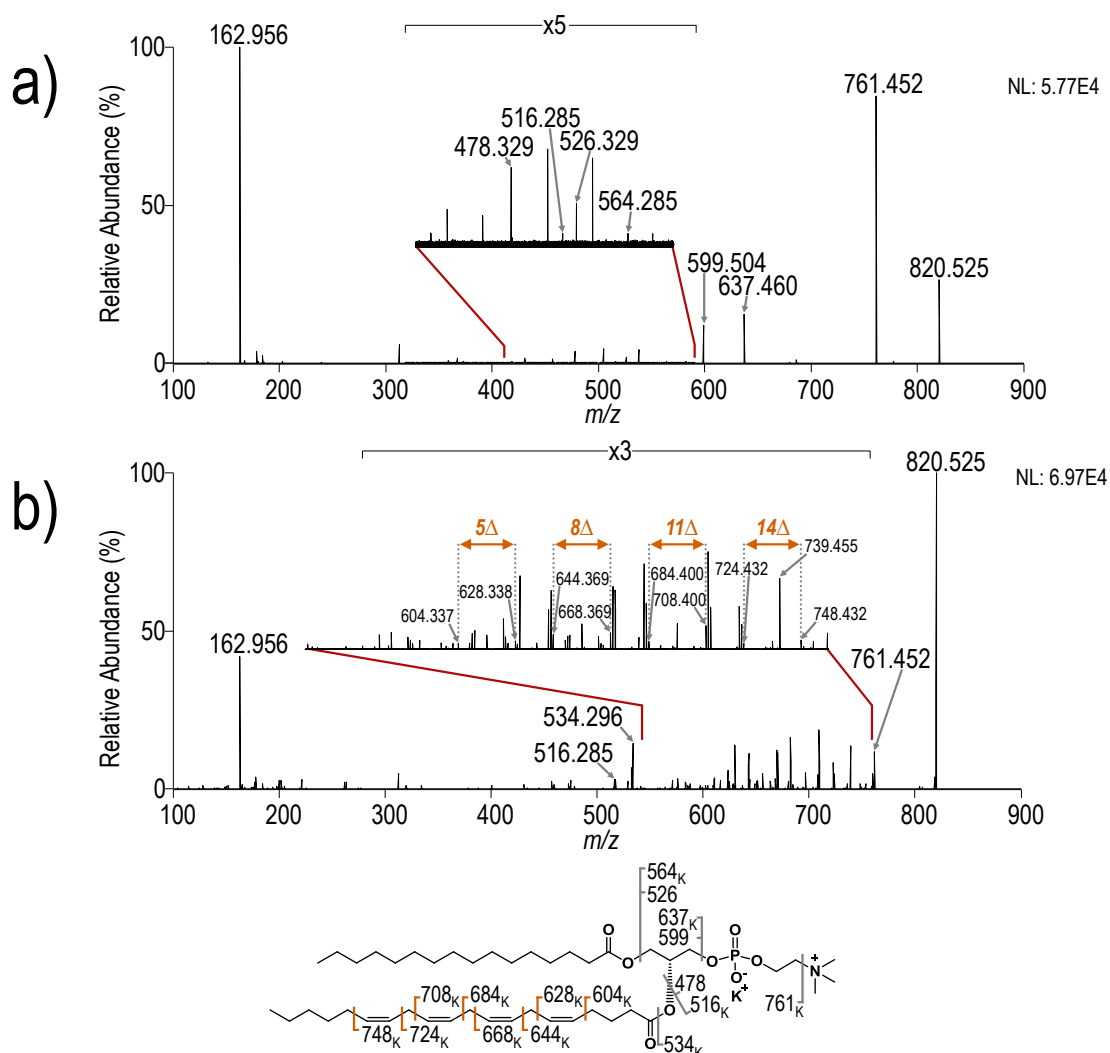


Figure 4.8 a) HCD (NCE 30) and b) UVPD (20 pulses, 6 mJ) mass spectra of the ion of m/z 820 obtained from DESI profiling of a mouse brain tissue section with corresponding fragment ion map. Subscripts indicate the presence of a potassium (K) adduct.

DESI profiling experiments were performed on a number of human tissue types, including endometrial, kidney, lymph node, ovarian, pancreas and brain (**Figure 4.9-4.12**).

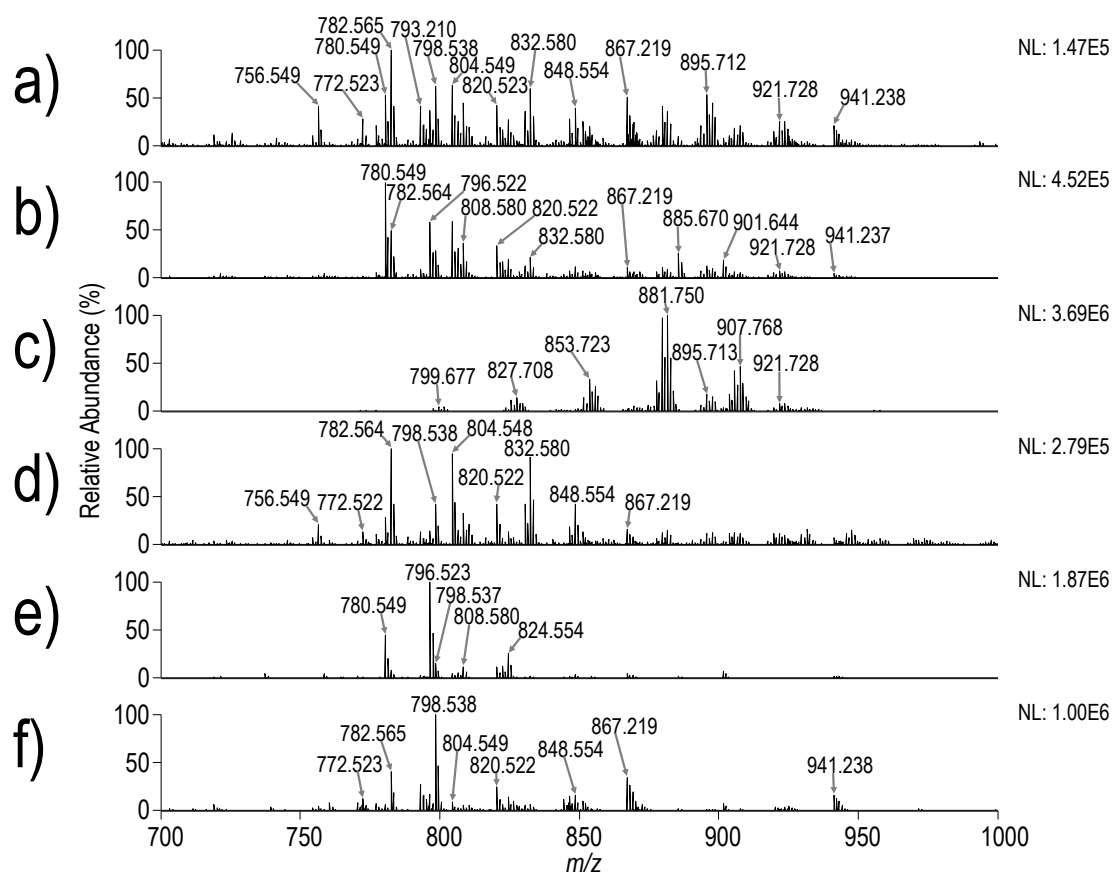


Figure 4.9 MS¹ spectra from DESI profiling of a) endometrial tissue, b) kidney tissue, c) lymph node tissue, d) ovarian tissue, e) pancreas tissue, and f) brain tissue. All tissues were human.

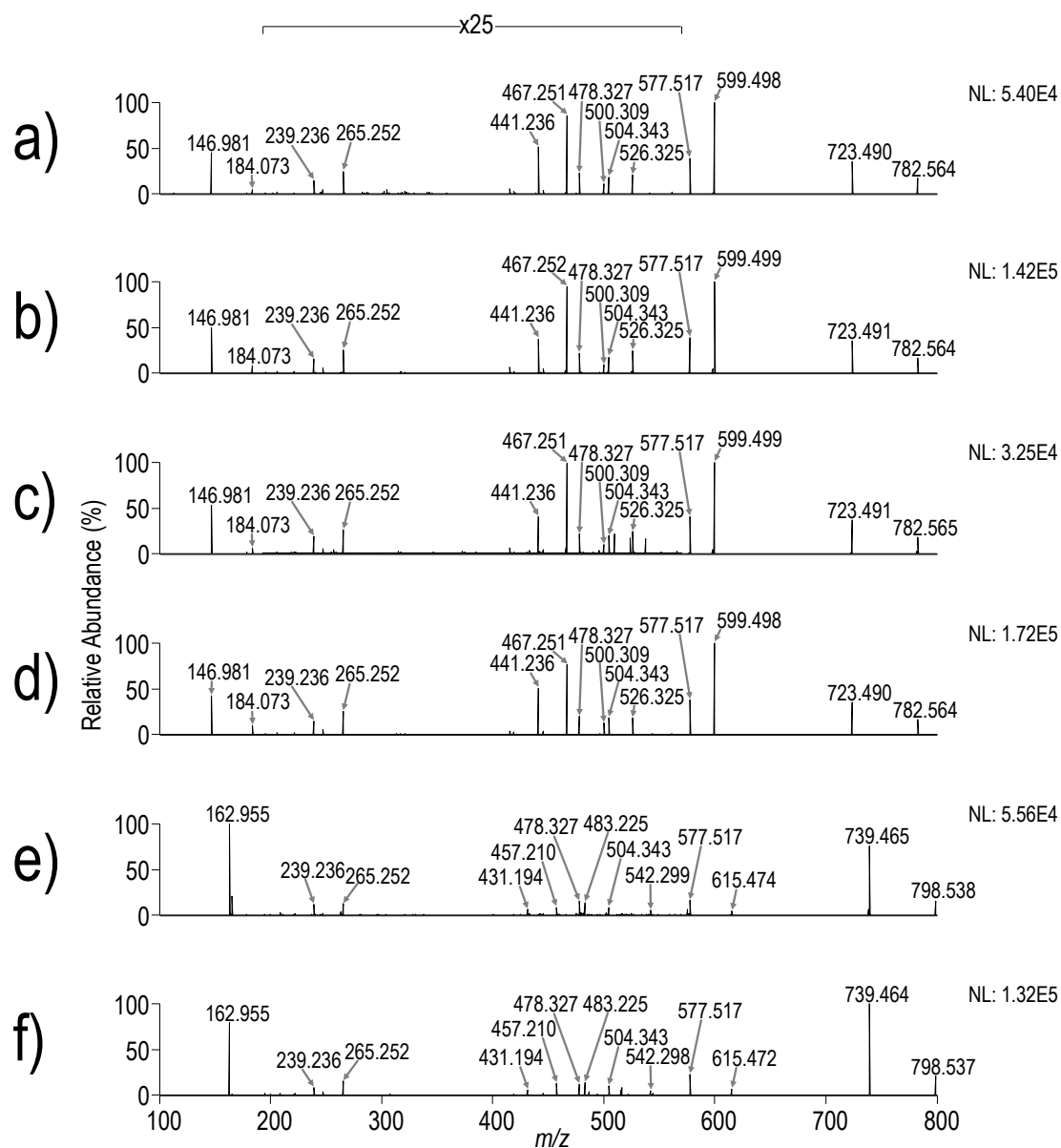


Figure 4.10 HCD (NCE 30) mass spectra from DESI profiling of a) endometrial tissue (m/z 782), b) kidney tissue (m/z 782), c) lymph node tissue (m/z 782), d) ovarian tissue (m/z 782), e) pancreas tissue (m/z 798), and f) brain tissue. All tissues were human. Magnification indicated at the top of the spectra applies to all spectra.

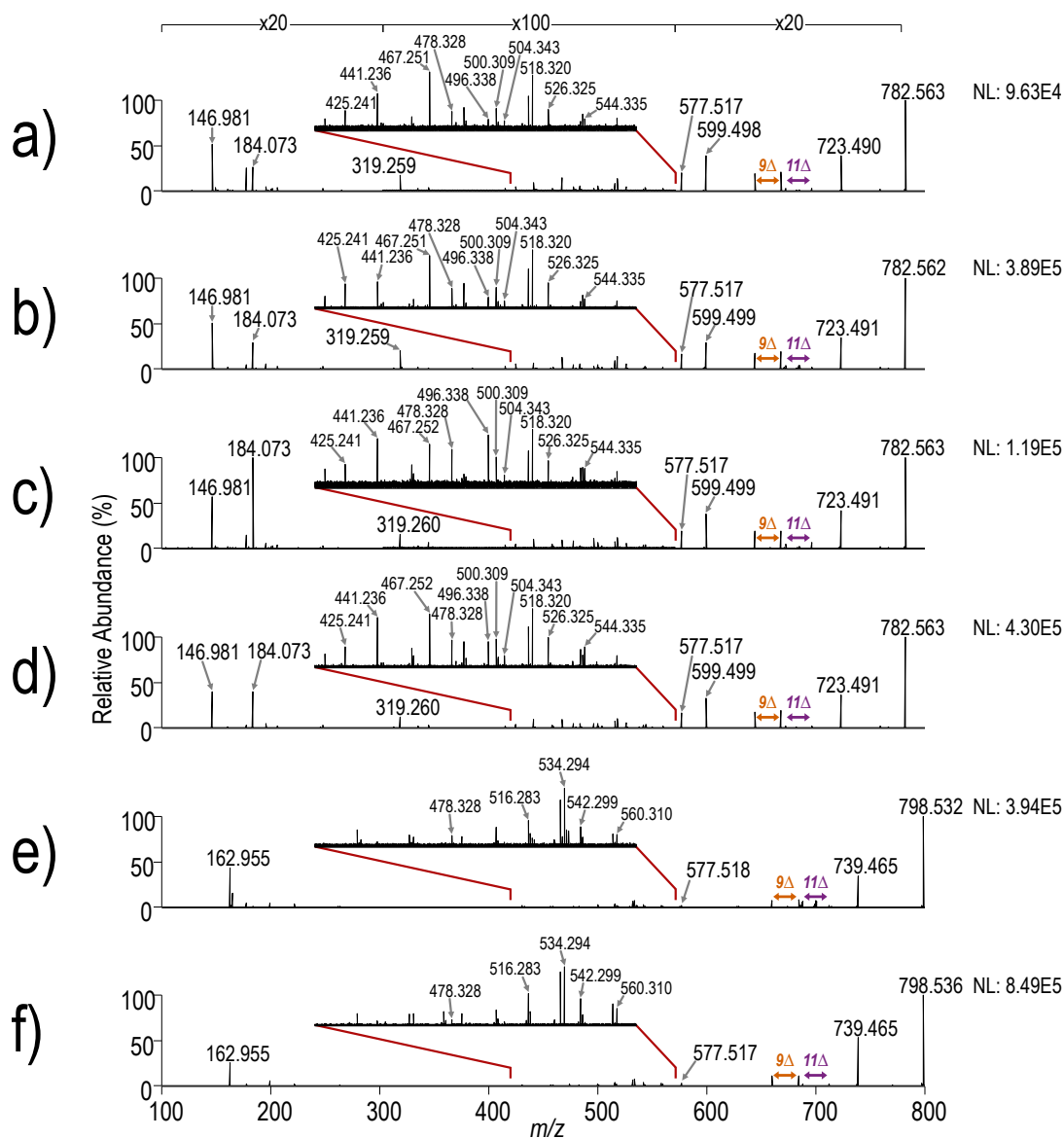


Figure 4.11 UVPD (20 pulses, 6 mJ) mass spectra from DESI profiling of a) endometrial tissue (m/z 782), b) kidney tissue (m/z 782), c) lymph node tissue (m/z 782), d) ovarian tissue (m/z 782), e) pancreas tissue (m/z 798), and f) brain tissue (m/z 798). All tissues were human. Magnification indicated at the top of the spectra applies to all spectra.

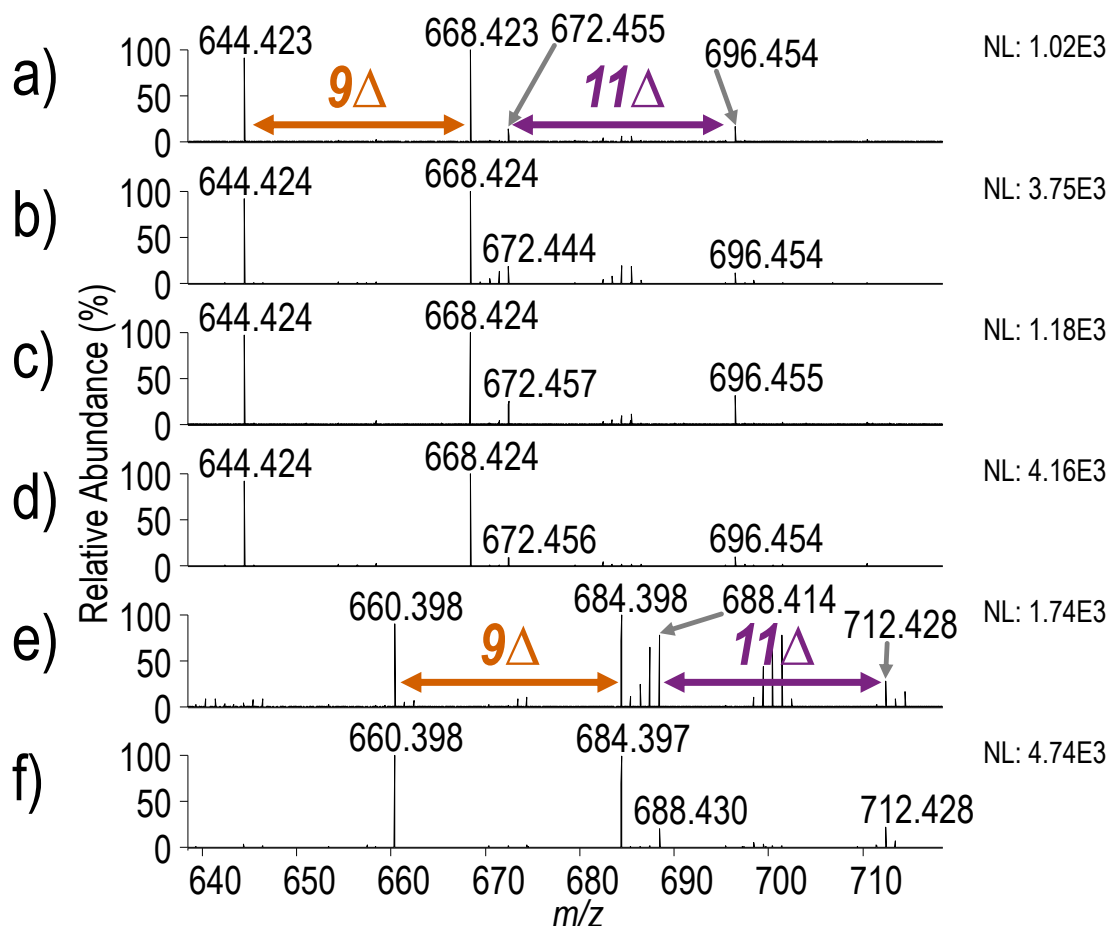


Figure 4.12 Expansions of UVPD (20 pulses, 6 mJ) mass spectra from DESI profiling of a) endometrial tissue (m/z 782), b) kidney tissue (m/z 782), c) lymph node tissue (m/z 782), d) ovarian tissue (m/z 782), e) pancreas tissue (m/z 798), and f) brain tissue (m/z 798), showcasing the key diagnostic ions that differentiate two isomeric lipids [PC 16:0_18:1(9 Δ), PC 16:0_18:1(11 Δ)]. All tissues were human. The full m/z range HCD and UVPD mass spectra are shown in Supporting Information **Figures 4.10** and **4.11**.

Figure 4.12 shows expanded regions of the UVPD mass spectra for sodium-adducted and potassium-adducted ions of m/z 782 or m/z 798, respectively, collected for each tissue type, focusing on the diagnostic fragment ions used to identify double bond isomers. While the PC 16:0_18:1(9 Δ) isomer is consistently more dominant across the tissue types

based on the greater abundance of the m/z 644/668 or m/z 660/684 ion pair (corresponding to the 9 Δ isomer) relative to the m/z 672/696 or m/z 688/712 ion pair (11 Δ isomer), respectively, there is a notable change in the relative abundances of PC 16:0_18:1(9 Δ) and PC 16:0_18:1(11 Δ) across all five tissue types. In some of the mass spectra, most notably Figure 2e, additional product ions are present corresponding to fragment ions from lipid species that are isobaric to the lipid of interest. The high resolving power and mass accuracy of the Orbitrap mass analyzer allows these product ions from isobaric species to be differentiated from specific diagnostic ions. Integration of the UVPD method on an imaging mass spectrometer also equipped with ion mobility separation capabilities is an intriguing idea that may enable acquisition of MS/MS spectra free from extraneous ion peaks.

The profiling mode experiments described above confirmed the successful differentiation of isomeric lipids by UVPD, thus motivating the exploration of UVPD for tissue imaging experiments. To determine the ability of UVPD to discern spatially resolved differences in the relative abundances of phospholipid isomers during DESI-MSI, a set of phospholipid isomer standards, PC 18:1(6Z)/18:1(6Z) and PC 18:1(9Z)/18:1(9Z), in varying concentration ratios and with a summed concentration of 10 μ M, were spotted onto a glass slide and imaged (**Figure 4.13**). UVPD mass spectra of m/z 808, corresponding to a sodium-adducted ion, shown in **Figure 4.14**, provide structural confirmation of the isomers, with UVPD mass spectra containing diagnostic sets of ions of m/z 628 and m/z 652 for PC 18:1(6Z)/18:1(6Z), and m/z 670 and m/z 694 for PC 18:1(9Z)/18:1(9Z). Changes in ion intensities in the DESI-UVPD images of each diagnostic ion correlate with variations in the lipid concentration ratios (**Figure 4.13**, **Figure 4.15**). Excellent agreement ($R^2 = 0.999$) between the concentration ratio of PC 18:1(6Z)/18:1(6Z) to PC 18:1(9Z)/18:1(9Z) ($C_{PC\ 18:1(6Z)/18:1(6Z)}/C_{PC\ 18:1(9Z)/18:1(9Z)}$) and the

ratio of summed diagnostic ion intensities ($I_{m/z\ 628 + 652}/I_{m/z\ 670 + 694}$) was achieved (**Figure 4.13b**). The lowest concentration detectable based on the UVPD-MS method was estimated to be ~500 nM.

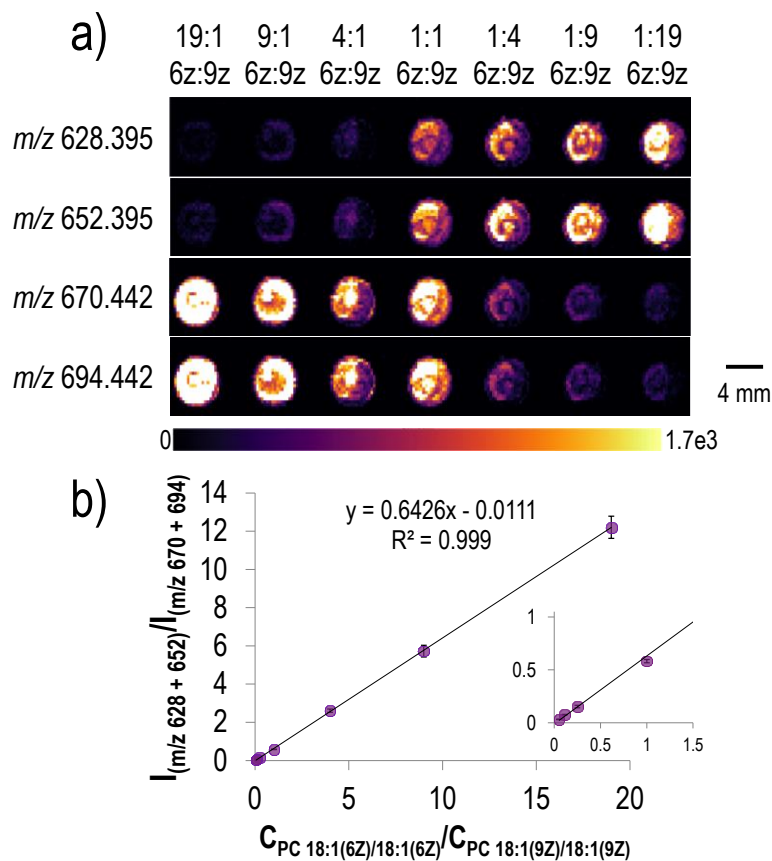


Figure 4.13 a) DESI-UVPD ion images of two isomeric phospholipid standards, PC 18:1(6Z)/18:1(6Z) and PC 18:1(9Z)/18:1(9Z), in varying concentration ratios. Each pair of product ions diagnostic for the double bond position are tracked. b) Plot of concentration ratio of PC 18:1(6Z)/18:1(6Z) to PC 18:1(9Z)/18:1(9Z) ($C_{PC\ 18:1(6Z)/18:1(6Z)}/C_{PC\ 18:1(9Z)/18:1(9Z)}$) versus the ratio of the summed intensities of the diagnostic ions ($I_{(m/z\ 628 + 652)}/I_{(m/z\ 670 + 694)}$) containing an expanded inset.

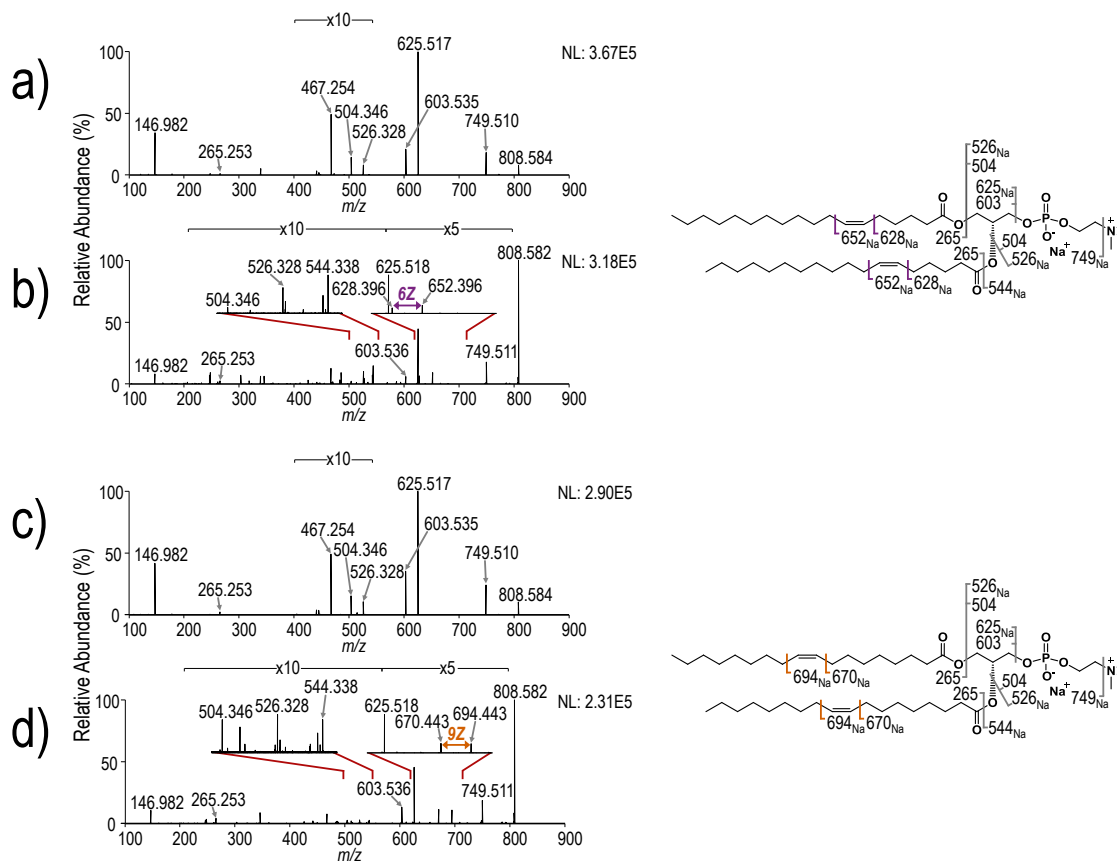


Figure 4.14 a) HCD (NCE 30) and b) UVPD (20 pulses, 6 mJ) mass spectra from DESI profiling of PC 18:1(6Z)/18:1(6Z). c) HCD (NCE 30) and d) UVPD (20 pulses, 6 mJ) mass spectra from DESI profiling of PC 18:1(9Z)/18:1(9Z). Subscripts indicate the presence of a sodium (Na) adduct.

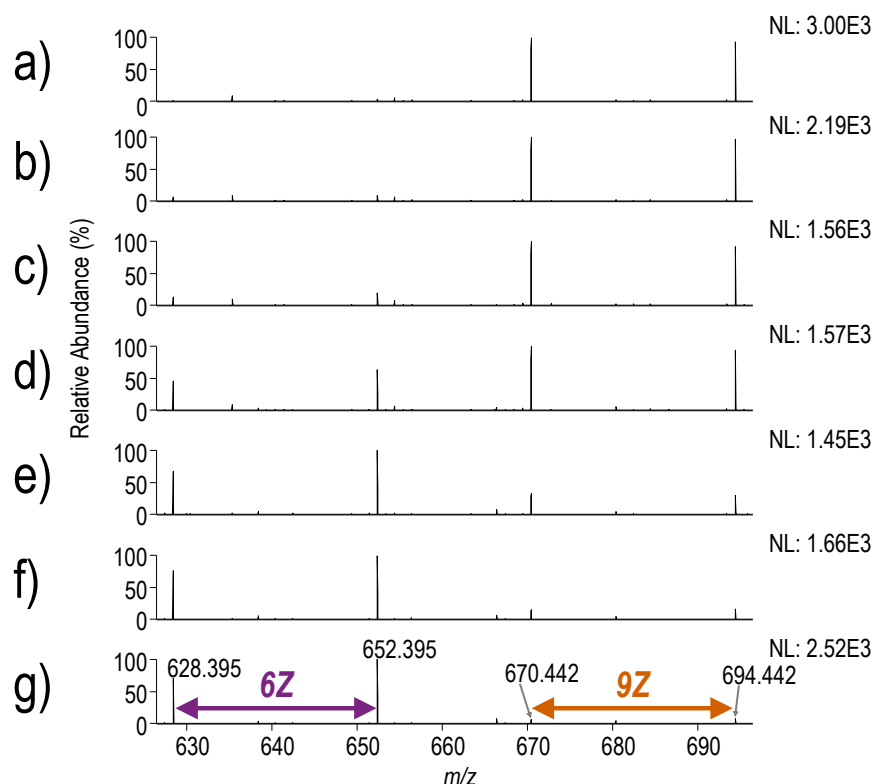


Figure 4.15 Representative expanded regions of UVPD (20 pulses, 6 mJ) mass spectra of isomeric phospholipid standards, PC 18:1(6Z)/18:1(6Z) and PC 18:1(9Z)/18:1(9Z), in varying concentration ratios from DESI-UVPD ion imaging experiments. Mass spectra correspond to the following ratios of PC 18:1(6Z)/18:1(6Z) to PC 18:1(9Z)/18:1(9Z): a) 1:19, b) 1:9, c) 1:4, d) 1:1, e) 4:1, f) 9:1 and g) 19:1.

These results confirm that the developed DESI-UVPD-MSI method can successfully detect changes in the relative abundances of phospholipid isomers in two dimensions indicating that differences detected in tissue should directly result from changes in isomer concentrations.

DESI-UVPD-MSI experiments were performed in triplicate for coronal mouse brain tissue sections (**Figure 4.16**). H&E optical images for all tissues were collected after collection of DESI data.

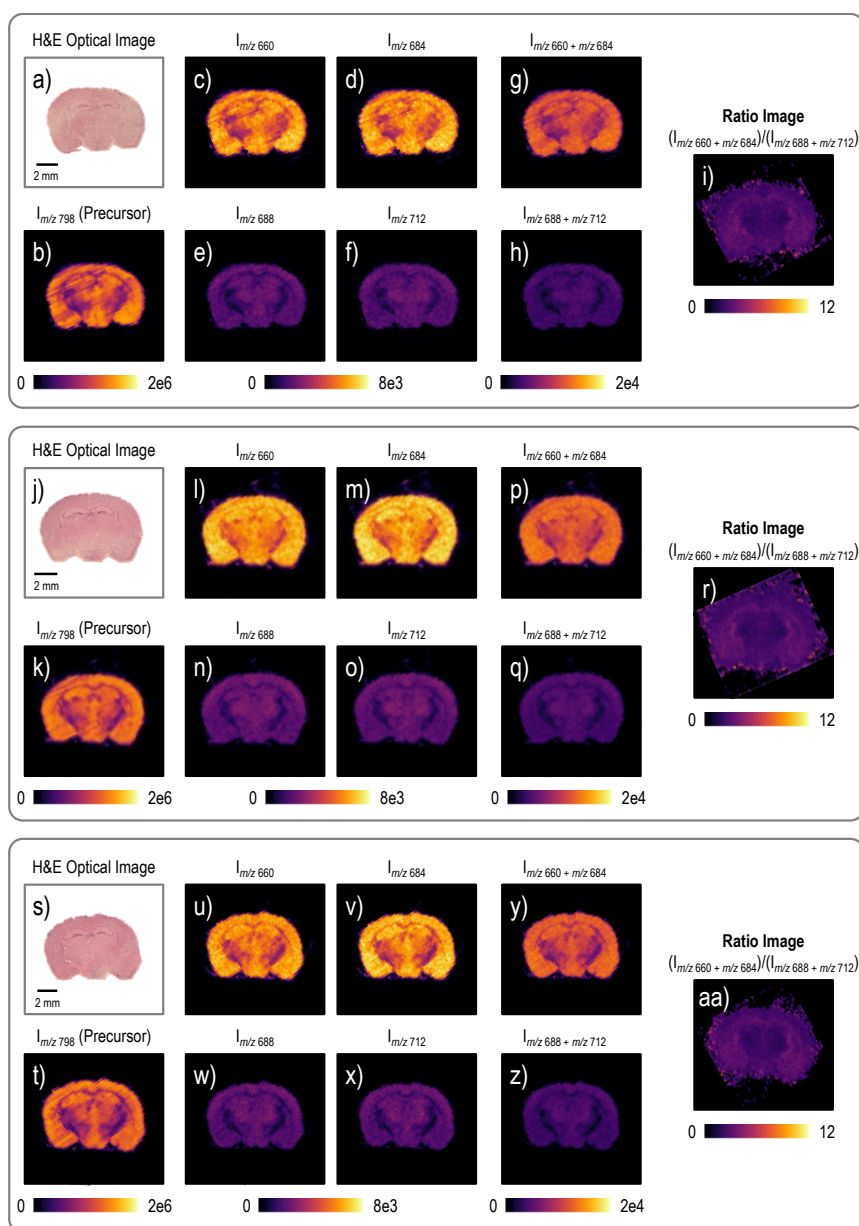


Figure 4.16 DESI-UPVD ion imaging of a mouse brain tissue section. a, j, s) H&E image of a mouse brain tissue section; b, k, t) DESI-MS ion image of m/z 798; c, l, u) DESI-UPVD ion image of m/z 660; d, m, v) DESI-UPVD ion image of m/z 684; e, n, w) DESI-UPVD ion image of m/z 688; f, o, x) DESI-UPVD ion image of m/z 712; g, p, y) DESI-UPVD ion image of the summed intensity of m/z 660 and m/z 684 ($I_{m/z\ 660 + m/z\ 684}$); h, q, z) DESI-UPVD ion image of the summed intensity of m/z 660 and m/z 684 ($I_{m/z\ 688 + m/z\ 712}$); i, r, aa) DESI-UPVD ratio image of the ratio of the summed intensities of the UVPD double bond diagnostic ions ($I_{m/z\ 660 + m/z\ 684} / (I_{m/z\ 688 + m/z\ 712})$).

The DESI ion image (**Figure 4.16b, k, t**) reveals a lower abundance of the lipid ion of m/z 798 (corresponding to PC 16:0_18:1) in the white matter compared to the gray matter. DESI-UPVD ion images for each of the diagnostic ions previously detected during DESI-UPVD profiling experiments are shown for each replicate ($I_{m/z\ 660}$: **Figure 4.16c, l, u**; $I_{m/z\ 684}$: **Figure 4.16d, m, v**; $I_{m/z\ 688}$: **Figure 4.16e, n, w**; $I_{m/z\ 712}$: **Figure 4.16f, o, x**), along with images of the summed intensities of the diagnostic ions ($I_{m/z\ 660 + 684}$: **Figure 4.16g, p, y**; $I_{m/z\ 688 + 712}$: **Figure 4.16h, q, z**). Ratio images of the ratio of the summed intensities of the diagnostic ions ($I_{m/z\ 660 + 684}/I_{m/z\ 688 + 712}$) demonstrate that there are, in fact, notable changes in the relative abundances of PC 16:0_18:1(9 Δ) and PC 16:0_18:1(11 Δ) throughout the tissue corresponding to areas of gray matter and white matter (**Figure 4.16i, r, aa**). Key expanded regions of the representative UVPD mass spectra of gray and white matter are shown in **Figure 4.17**.

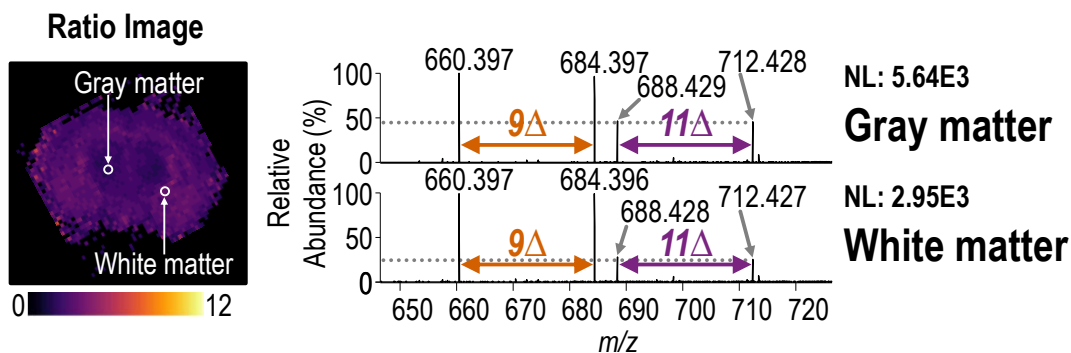


Figure 4.17 Expanded regions of UVPD mass spectra of the white and gray matter of a mouse brain tissue section. The DESI-UPVD ratio image presented here is the same as that presented in **Figure 4.16aa**.

While the overall abundance of m/z 798 appears to decrease in the white matter based on DESI-MSI data, the ratio of PC 16:0_18:1(9 Δ) to PC 16:0_18:1(11 Δ) increases in the white matter relative to the gray matter. A similar observation is drawn for human brain

tissue (**Figure 4.18**) with branches of white matter in the human brain section observed in both the optical and DESI images.

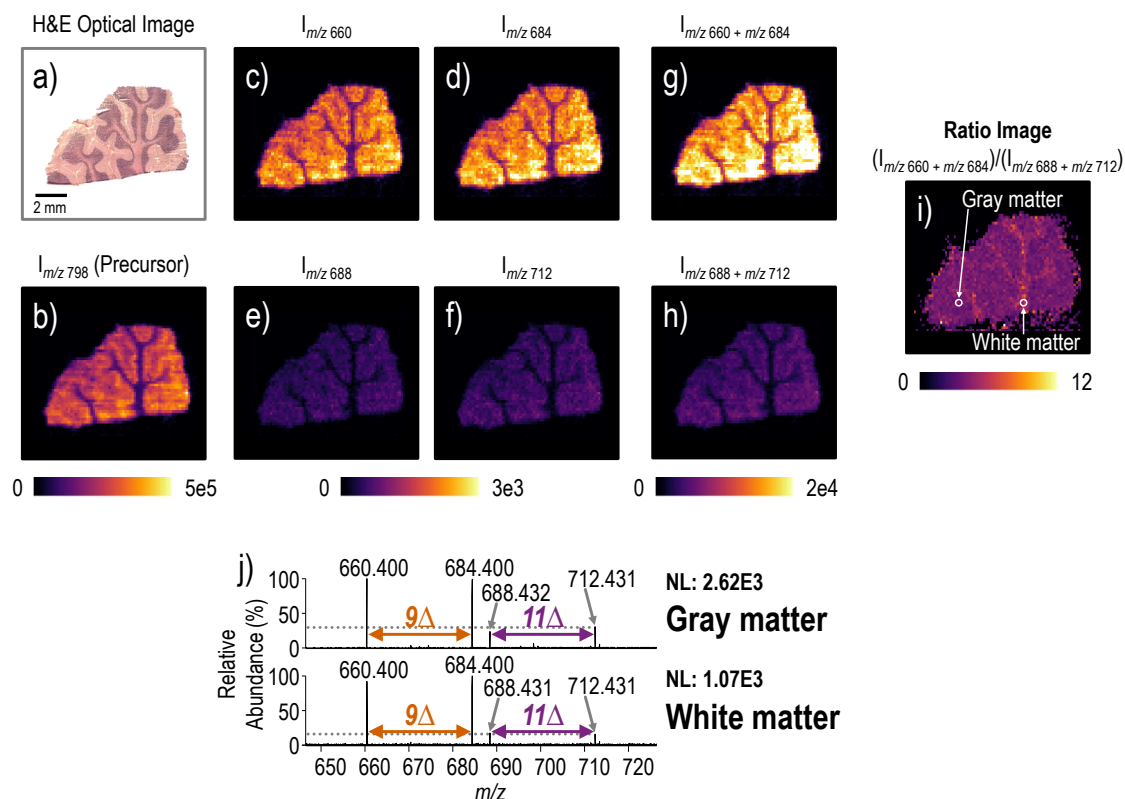


Figure 4.18 DESI-UPVD ion imaging of a human brain tissue section. a) H&E image of a mouse brain tissue section, b) DESI-MS ion image of m/z 798, c) DESI-UPVD ion image of m/z 660, d) DESI-UPVD ion image of m/z 684, e) DESI-UPVD ion image of m/z 688, f) DESI-UPVD ion image of m/z 712, g) DESI-UPVD ion image of the summed intensity of m/z 660 and m/z 684 ($I_{m/z\ 660 + 684}$), h) DESI-UPVD ion image of the summed intensity of m/z 660 and m/z 684 ($I_{m/z\ 688 + 712}$), i) DESI-UPVD ratio image of the ratio of the summed intensities of the UVPD double bond diagnostic ions ($I_{m/z\ 660 + 684} / I_{m/z\ 688 + 712}$), and j) expanded regions of UVPD mass spectra of the white and gray matter.

DESI-UVPD-MSI also offers the unique opportunity to investigate differences in the abundance of lipid isomers between normal and cancerous regions of tissue sections. DESI-UVPD-MSI was performed on a section of human lymph node tissue containing thyroid cancer metastasis based on monitoring the ion of m/z 798 (**Figure 4.19**).⁴⁴

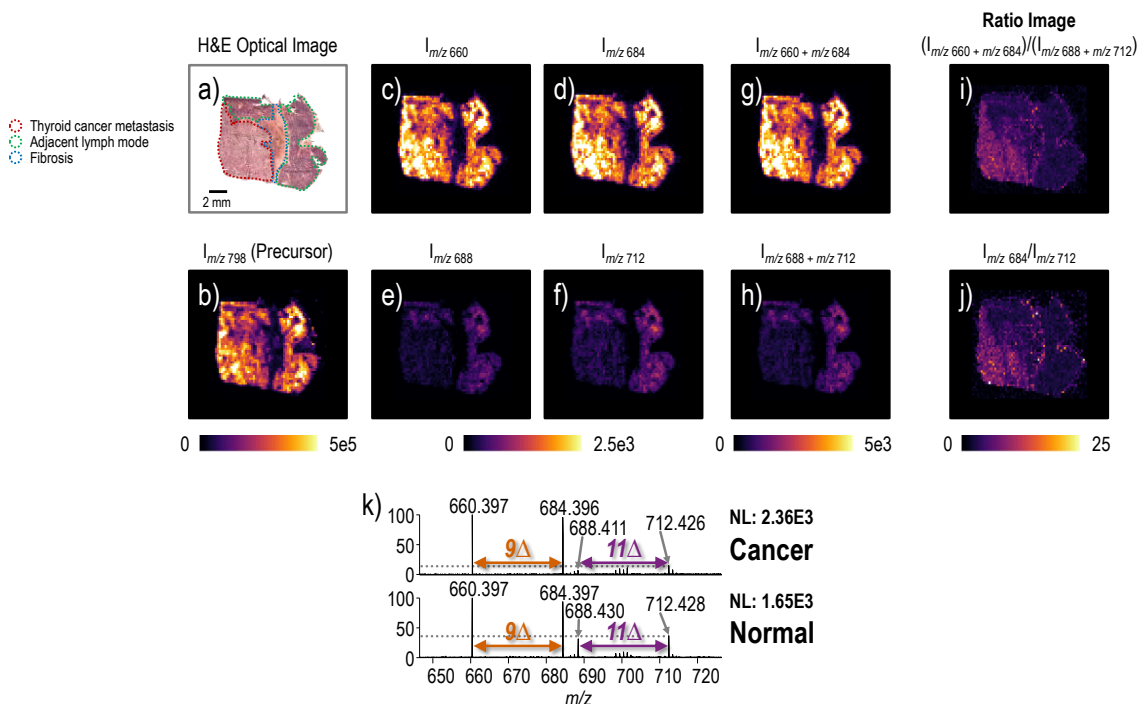


Figure 4.19 DESI-UVPD ion imaging of a lymph node tissue section with thyroid cancer metastasis. a) H&E image of a lymph node tissue section with thyroid cancer metastasis, b) DESI-MS ion image of m/z 798, c) DESI-UVPD ion image of m/z 660, d) DESI-UVPD ion image of m/z 684, e) DESI-UVPD ion image of m/z 688, f) DESI-UVPD ion image of m/z 712, g) DESI-UVPD ion image of the summed intensity of m/z 660 and m/z 684 ($I_{m/z\ 660 + 684}$), h) DESI-UVPD ion image of the summed intensity of m/z 660 and m/z 684 ($I_{m/z\ 660 + 684}$), i) DESI-UVPD ratio image of the ratio of the summed intensities of the UVPD double bond diagnostic ions ($I_{m/z\ 660 + 684}/(I_{m/z\ 688 + 712})$), j) DESI-UVPD ratio image of m/z 684 to m/z 712, and k) expanded regions of UVPD mass spectra of the cancerous and normal regions of tissue.

The presence of both PC 16:0_18:1(9 Δ) and PC 16:0_18:1(11 Δ) were confirmed by UVPD-MS based on the paired fragment ions. (**Figure 4.20**). One selected ion from each pair of diagnostic ions was used to create a ratio image that revealed a distinctive change in the relative abundance of the two lipid isomers between normal and diseased tissue (**Figure 4.21**). Although there appears to be a notable change in the relative abundances of the two isomers between the normal and cancerous portions of tissue, a larger sample set is required to establish the generality of this finding.

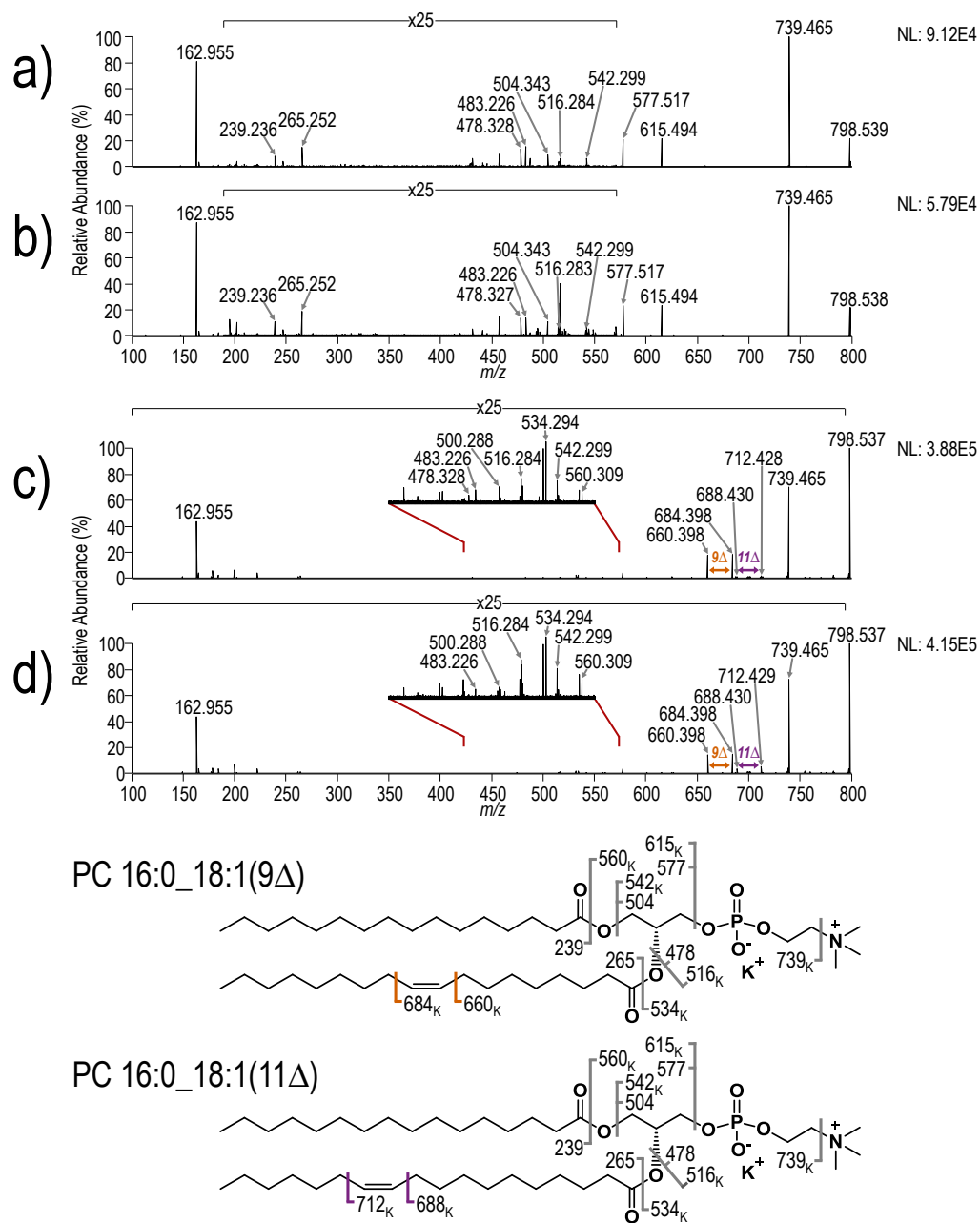


Figure 4.20 HCD profiling spectra of regions of a) cancerous and b) normal tissue from the lymph node tissue section with thyroid cancer metastasis and UVPD profiling spectra of regions of c) cancerous and d) normal tissue from the lymph node tissue section with thyroid cancer metastasis with corresponding fragment ion maps.

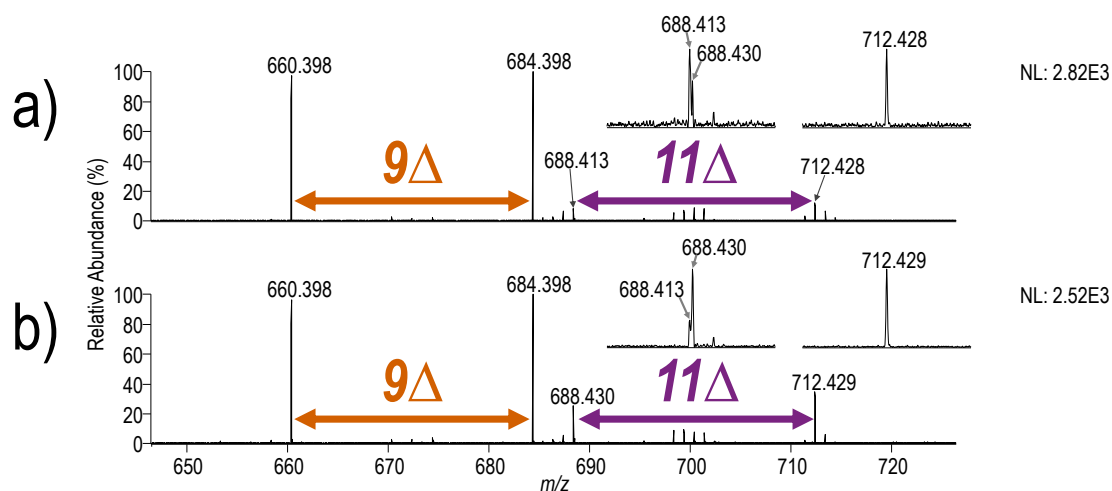


Figure 4.21 Expanded UVPD spectra from regions of a) cancerous and b) normal tissue from Figure 4.20 showing an obstructing ion at m/z 688.411. The DESI-UVPD ratio image was therefore made from division of m/z 688.430 and m/z 712.43 for avoid contributing signal form m/z 688.4.

4.5 CONCLUSIONS

This study represents the first coupling of ambient MSI with an ion activation technique capable of determining double bond positions in phospholipid acyl chains. DESI-UVPD not only differentiates phospholipid isomers but also unveils spatial changes in their relative abundances that are otherwise undetected during DESI-MSI experiments. The short activation period of UVPD enables fast acquisition of diagnostic MS/MS information. Considering the informative spectra generated by UVPD, application of this method to other types of lipids offers the potential to provide insights into the processes that result in altered lipid metabolism.

4.6 REFERENCES

- (1) Amstalden van Hove, E. R.; Smith, D. F.; Heeren, R. M. A. A Concise Review of Mass Spectrometry Imaging. *J. Chromatogr. A* **2010**, *1217*, 3946–3954.
- (2) Gode, D.; A. Volmer, D. Lipid Imaging by Mass Spectrometry – a Review. *Analyst* **2013**, *138*, 1289–1315.
- (3) Vaysse, P.; A. Heeren, R. M.; Porta, T.; Balluff, B. Mass Spectrometry Imaging for Clinical Research – Latest Developments, Applications, and Current Limitations. *Analyst* **2017**, *142*, 2690–2712.
- (4) Sans, M.; Gharpure, K.; Tibshirani, R.; Zhang, J.; Liang, L.; Liu, J.; Young, J. H.; Dood, R. L.; Sood, A. K.; Eberlin, L. S. Metabolic Markers and Statistical Prediction of Serous Ovarian Cancer Aggressiveness by Ambient Ionization Mass Spectrometry Imaging. *Cancer Res.* **2017**, *77*, 2903–2913.
- (5) Norris, J. L.; Caprioli, R. M. Analysis of Tissue Specimens by Matrix-Assisted Laser Desorption/Ionization Imaging Mass Spectrometry in Biological and Clinical Research. *Chem. Rev.* **2013**, *113*, 2309–2342.
- (6) Gessel, M. M.; Norris, J. L.; Caprioli, R. M. MALDI Imaging Mass Spectrometry: Spatial Molecular Analysis to Enable a New Age of Discovery. *J. Proteomics* **2014**, *107*, 71–82.
- (7) Wiseman, J. M.; Ifa, D. R.; Song, Q.; Cooks, R. G. Tissue Imaging at Atmospheric Pressure Using Desorption Electrospray Ionization (DESI) Mass Spectrometry. *Angew. Chem. Int. Ed.* **2006**, *45*, 7188–7192.
- (8) Ifa, D. R.; Wu, C.; Ouyang, Z.; Cooks, R. G. Desorption Electrospray Ionization and Other Ambient Ionization Methods: Current Progress and Preview. *Analyst* **2010**, *135*, 669–681.
- (9) Eberlin, L. S.; Ferreira, C. R.; Dill, A. L.; Ifa, D. R.; Cooks, R. G. Desorption Electrospray Ionization Mass Spectrometry for Lipid Characterization and Biological Tissue Imaging. *Biochim. Biophys. Acta BBA - Mol. Cell Biol. Lipids* **2011**, *1811*, 946–960.
- (10) Bereman, M. S.; Nyadong, L.; Fernandez, F. M.; Muddiman, D. C. Direct High-resolution Peptide and Protein Analysis by Desorption Electrospray Ionization Fourier Transform Ion Cyclotron Resonance Mass Spectrometry. *Rapid Commun. Mass Spectrom.* **2006**, *20*, 3409–3411.
- (11) Pól, J.; Vidová, V.; Kruppa, G.; Kobliha, V.; Novák, P.; Lemr, K.; Kotiaho, T.; Kostianen, R.; Havlíček, V.; Volný, M. Automated Ambient Desorption–Ionization Platform for Surface Imaging Integrated with a Commercial Fourier Transform Ion Cyclotron Resonance Mass Spectrometer. *Anal. Chem.* **2009**, *81*, 8479–8487.

- (12) Manicke, N. E.; Dill, A. L.; Ifa, D. R.; Cooks, R. G. High-resolution Tissue Imaging on an Orbitrap Mass Spectrometer by Desorption Electrospray Ionization Mass Spectrometry. *J. Mass Spectrom.* **2010**, *45*, 223–226.
- (13) Römpp, A.; Spengler, B. Mass Spectrometry Imaging with High Resolution in Mass and Space. *Histochem. Cell Biol.* **2013**, *139*, 759–783.
- (14) Lietz, C. B.; Gemperline, E.; Li, L. Qualitative and Quantitative Mass Spectrometry Imaging of Drugs and Metabolites. *Adv. Drug Deliv. Rev.* **2013**, *65*, 1074–1085.
- (15) Prideaux, B.; Dartois, V.; Staab, D.; Weiner, D. M.; Goh, A.; Via, L. E.; Barry, C. E.; Stoeckli, M. High-Sensitivity MALDI-MRM-MS Imaging of Moxifloxacin Distribution in Tuberculosis-Infected Rabbit Lungs and Granulomatous Lesions. *Anal. Chem.* **2011**, *83*, 2112–2118.
- (16) Pulfer, M.; Murphy, R. C. Electrospray Mass Spectrometry of Phospholipids. *Mass Spectrom. Rev.* **2003**, *22*, 332–364.
- (17) Harayama, T.; Riezman, H. Understanding the Diversity of Membrane Lipid Composition. *Nat. Rev. Mol. Cell Biol.* **2018**, 1–16.
- (18) Martinez-Seara, H.; Róg, T.; Pasenkiewicz-Gierula, M.; Vattulainen, I.; Karttunen, M.; Reigada, R. Effect of Double Bond Position on Lipid Bilayer Properties: Insight through Atomistic Simulations. *J. Phys. Chem. B* **2007**, *111*, 11162–11168.
- (19) Shinzawa-Itoh, K.; Aoyama, H.; Muramoto, K.; Terada, H.; Kurauchi, T.; Tadehara, Y.; Yamasaki, A.; Sugimura, T.; Kurono, S.; Tsujimoto, K.; Mizushima, T.; Yamashita, E.; Tsukihara, T.; Yoshikawa, S. Structures and Physiological Roles of 13 Integral Lipids of Bovine Heart Cytochrome c Oxidase. *EMBO J.* **2007**, *26*, 1713–1725.
- (20) Ma, X.; Chong, L.; Tian, R.; Shi, R.; Hu, T. Y.; Ouyang, Z.; Xia, Y. Identification and Quantitation of Lipid C=C Location Isomers: A Shotgun Lipidomics Approach Enabled by Photochemical Reaction. *Proc. Natl. Acad. Sci.* **2016**, *113*, 2573–2578.
- (21) Ma, X.; Xia, Y. Pinpointing Double Bonds in Lipids by Paternò-Büchi Reactions and Mass Spectrometry. *Angew. Chem.* **2014**, *126*, 2630–2634.
- (22) Tang, F.; Guo, C.; Ma, X.; Zhang, J.; Su, Y.; Tian, R.; Shi, R.; Xia, Y.; Wang, X.; Ouyang, Z. Rapid In Situ Profiling of Lipid C=C Location Isomers in Tissue Using Ambient Mass Spectrometry with Photochemical Reactions. *Anal. Chem.* **2018**, *90*, 5612–5619.
- (23) Shimma, S.; Kubo, A.; Satoh, T.; Toyoda, M. Detailed Structural Analysis of Lipids Directly on Tissue Specimens Using a MALDI-SpiralTOF-Reflectron TOF Mass Spectrometer. *PLOS ONE* **2012**, *7*, e37107.

- (24) Toyoda, M. Development of Multi-Turn Time-of-Flight Mass Spectrometers and Their Applications. *Eur. J. Mass Spectrom.* **2010**, *16*, 397–406.
- (25) Pham, H. T.; Ly, T.; Trevitt, A. J.; Mitchell, T. W.; Blanksby, S. J. Differentiation of Complex Lipid Isomers by Radical-Directed Dissociation Mass Spectrometry. *Anal. Chem.* **2012**, *84*, 7525–7532.
- (26) Pham, H. T.; Trevitt, A. J.; Mitchell, T. W.; Blanksby, S. J. Rapid Differentiation of Isomeric Lipids by Photodissociation Mass Spectrometry of Fatty Acid Derivatives. *Rapid Commun. Mass Spectrom.* **2013**, *27*, 805–815.
- (27) Yoo, H. J.; Håkansson, K. Determination of Double Bond Location in Fatty Acids by Manganese Addition and Electron Induced Dissociation. *Anal. Chem.* **2010**, *82*, 6940–6946.
- (28) Jones, J. W.; Thompson, C. J.; Carter, C. L.; Kane, M. A. Electron-induced Dissociation (EID) for Structure Characterization of Glycerophosphatidylcholine: Determination of Double-bond Positions and Localization of Acyl Chains. *J. Mass Spectrom.* **2015**, *50*, 1327–1339.
- (29) Campbell, J. L.; Baba, T. Near-Complete Structural Characterization of Phosphatidylcholines Using Electron Impact Excitation of Ions from Organics. *Anal. Chem.* **2015**, *87*, 5837–5845.
- (30) Baba, T.; Campbell, J. L.; Yves Le Blanc, J. C.; Baker, P. R. S. In-Depth Sphingomyelin Characterization Using Electron Impact Excitation of Ions from Organics and Mass Spectrometry. *J. Lipid Res.* **2016**, *57*, 858–867.
- (31) Pham, H. T.; Maccarone, A. T.; Thomas, M. C.; Campbell, J. L.; Mitchell, T. W.; Blanksby, S. J. Structural Characterization of Glycerophospholipids by Combinations of Ozone- and Collision-Induced Dissociation Mass Spectrometry: The next Step towards “Top-down” Lipidomics. *Analyst* **2014**, *139*, 204–214.
- (32) Kozłowski, R. L.; Mitchell, T. W.; Blanksby, S. J. A Rapid Ambient Ionization-Mass Spectrometry Approach to Monitoring the Relative Abundance of Isomeric Glycerophospholipids. *Sci. Rep.* **2015**, *5*, 9243.
- (33) Poad, B. L. J.; Green, M. R.; Kirk, J. M.; Tomczyk, N.; Mitchell, T. W.; Blanksby, S. J. High-Pressure Ozone-Induced Dissociation for Lipid Structure Elucidation on Fast Chromatographic Timescales. *Anal. Chem.* **2017**, *89*, 4223–4229.
- (34) Poad, B. L. J.; Zheng, X.; Mitchell, T. W.; Smith, R. D.; Baker, E. S.; Blanksby, S. J. Online Ozonolysis Combined with Ion Mobility-Mass Spectrometry Provides a New Platform for Lipid Isomer Analyses. *Anal. Chem.* **2018**, *90*, 1292–1300.

- (35) Paine, M. R. L.; Poad, B. L. J.; Eijkel, G. B.; Marshall, D. L.; Blanksby, S. J.; Heeren, R. M. A.; Ellis, S. R. Mass Spectrometry Imaging with Isomeric Resolution Enabled by Ozone-Induced Dissociation. *Angew. Chem. Int. Ed.* **2018**.
- (36) Deimler, R. E.; Sander, M.; Jackson, G. P. Radical-Induced Fragmentation of Phospholipid Cations Using Metastable Atom-Activated Dissociation Mass Spectrometry (MAD-MS). *Int. J. Mass Spectrom.* **2015**, *390*, 178–186.
- (37) Li, P.; Hoffmann, W. D.; Jackson, G. P. Multistage Mass Spectrometry of Phospholipids Using Collision-Induced Dissociation (CID) and Metastable Atom-Activated Dissociation (MAD). *Int. J. Mass Spectrom.* **2016**, *403*, 1–7.
- (38) Brodbelt, J. S. Photodissociation Mass Spectrometry: New Tools for Characterization of Biological Molecules. *Chem. Soc. Rev.* **2014**, *43*, 2757–2783.
- (39) Klein, D. R.; Brodbelt, J. S. Structural Characterization of Phosphatidylcholines Using 193 nm Ultraviolet Photodissociation Mass Spectrometry. *Anal. Chem.* **2017**, *89*, 1516–1522.
- (40) Williams, P. E.; Klein, D. R.; Greer, S. M.; Brodbelt, J. S. Pinpointing Double Bond and Sn-Positions in Glycerophospholipids via Hybrid 193 nm Ultraviolet Photodissociation (UVPD) Mass Spectrometry. *J. Am. Chem. Soc.* **2017**, *139*, 15681–15690.
- (41) Ryan, E.; Nguyen, C. Q. N.; Shiea, C.; Reid, G. E. Detailed Structural Characterization of Sphingolipids via 193 nm Ultraviolet Photodissociation and Ultra High Resolution Tandem Mass Spectrometry. *J. Am. Soc. Mass Spectrom.* **2017**, *28*, 1406–1419.
- (42) Klein, D. R.; Holden, D. D.; Brodbelt, J. S. Shotgun Analysis of Rough-Type Lipopolysaccharides Using Ultraviolet Photodissociation Mass Spectrometry. *Anal. Chem.* **2016**, *88*, 1044–1051.
- (43) Kessner, D.; Chambers, M.; Burke, R.; Agus, D.; Mallick, P. ProteoWizard: Open Source Software for Rapid Proteomics Tools Development. *Bioinformatics* **2008**, *24*, 2534–2536.
- (44) Liebisch, G.; Vizcaíno, J. A.; Köfeler, H.; Trötz Müller, M.; Griffiths, W. J.; Schmitz, G.; Spener, F.; Wakelam, M. J. O. Shorthand Notation for Lipid Structures Derived from Mass Spectrometry. *J. Lipid Res.* **2013**, *54*, 1523–1530.
- (45) Škrášková, K.; Claude, E.; Jones, E. A.; Towers, M.; Ellis, S. R.; Heeren, R. M. A. Enhanced Capabilities for Imaging Gangliosides in Murine Brain with Matrix-Assisted Laser Desorption/Ionization and Desorption Electrospray Ionization Mass Spectrometry Coupled to Ion Mobility Separation. *Methods* **2016**, *104*, 69–78.

Chapter 5: Shotgun Analysis of Rough-Type Lipopolysaccharides Using Ultraviolet Photodissociation*

5.1 OVERVIEW

Detailed structural characterization of intact rough-type lipopolysaccharides (R-LPS) was accomplished using an MS³ strategy consisting of low-energy collision-induced dissociation (CID) followed by 193 nm ultraviolet photodissociation (UVPD) implemented on an Orbitrap Fusion mass spectrometer. Complex mixtures of R-LPS from either *E. coli* or *S. enterica* were directly infused into the mass spectrometer using static source nanoESI. An initial CID event performed on an R-LPS precursor produced spectra with abundant ions corresponding to the lipid A and core oligosaccharide (OS) substructures. Comparison of CID spectra of R-LPS ions with varying lipid A and core OS structures verify that lipid A and core OS ions are consistently produced in high abundance. The resulting lipid A and core OS ions were subsequently activated by CID, higher-energy collision-induced dissociation (HCD), or UVPD. For both the lipid A and core OS substructures, HCD and UVPD produced highly informative complementary spectra, with UVPD of the core OS producing an extensive array of cross-ring cleavage fragments. Successful discernment of *E. coli* R-LPS structures with isomeric core structures confirmed the degree to which subtle structural differences could be determined using this method.

*Klein, D. R.; Holden, D. D.; Brodbelt, J. S. Shotgun Analysis of Rough-Type Lipopolysaccharides Using Ultraviolet Photodissociation Mass Spectrometry. *Anal. Chem.* **2016**, 88, 1044–1051.

DDH largely contributed to the implementation of UVPD on the Orbitrap Fusion. JSB provided mentorship and reviewed the manuscript prior to publication.

5.2 INTRODUCTION

Lipopolysaccharides (LPS), the main component of the outer membrane of most Gram-negative bacteria, are complex biomolecules responsible for immune system response to pathogen invasion.¹ The generic structure of LPS includes three regions: lipid A, core oligosaccharide (OS) and O-antigen. LPS molecules with and without the O-antigen are termed smooth-type (S-LPS) and rough-type (R-LPS) or lipooligosaccharides (LOS), respectively. Although there exist R-LPS mutant strains of bacteria that normally produce an O-antigen, some bacteria, including *Neisseria* and *Haemophilus*, have naturally evolved to produce R-LPS.² Lipid A, the hydrophobic anchor that activates the Toll-like receptor 4 (TLR4), and the core OS, largely responsible for outer membrane stability, are essential for the viability of all Gram-negative bacteria.³⁻⁷ Variations in the acyl chain distribution, phosphorylation, and sugar orientation and distribution in both lipid A and the core oligosaccharide greatly impact the virulence of bacteria.⁸⁻¹² For example, diphosphoryl hexa-acylated lipid A induces the strongest inflammatory response of the TLR4. Alteration of the acylation pattern or phosphorylation status can reduce the activity of lipid A by more than two orders of magnitude.¹³ Manipulation of lipid A structure to reduce toxicity, yet still initiate an immune response, is the basis for detoxified lipid A as a vaccine adjuvant.¹⁴⁻¹⁷ Additionally, phosphorylation of the core oligosaccharide has been shown to significantly contribute to outer membrane stability. Mutant strains of *Escherichia coli* (*E. coli*) modified to lack phosphorylations in the core region of the have shown increased susceptibility to antibiotics and detergents.⁴ Considering the impact of subtle modifications to LPS, detailed structural characterization of LPS is necessary to further investigate the role of LPS in bacteria viability and to understand how LPS structure influences immune stimulation to facilitate development of bacterial vaccines.

Mass spectrometry has emerged as a powerful tool for characterization of LPS substructures. The amphiphilic nature of LPS causes micelle formation which can complicate mass spectrometric analysis. Consequently, a common approach for characterization of LPS involves hydrolysis of the glycosidic bond between lipid A and the core OS, and subsequent analysis of each substructure.^{10,18,19} Additionally, lipid A acyl chains can be removed by hydrolysis prior to analysis of the intact carbohydrate chain. Low-energy collisional induced dissociation (CID) is commonly used to obtain fragmentation patterns for the hydrolyzed lipid A^{20–25} and saccharide²⁶ substructures. However, CID does not always provide adequate fragmentation for elucidation of subtle structural differences. Limitations of CID have been the impetus for the development of alternative activation methods including infrared multiphoton photodissociation (IRMPD), negative-electron transfer dissociation (NETD), ultraviolet photodissociation (UVPD) and activated-electron photodetachment (a-EPD) which have been employed to produce either complementary or more informative fragmentation spectra.^{27–29} 193 nm UVPD, a fast and high energy activation method that entails irradiation of ions with 193 nm (6.4 eV) photons, has previously been shown to produce highly informative spectra for many biomolecules.²⁹ When biological molecules are deliberately truncated or degraded prior to analysis (as is the case with “bottom up” approaches), some structural features or integrated patterns of features may be lost. This is also the case with LPS analysis, for which attention has primarily focused on characterization of the lipid A substructure rather than the core OS or O-antigen. With approaches that evaluate hydrolyzed LPS substructures, not only are labile modifications potentially lost, but combinations of modifications occurring between lipid A and the core oligosaccharide are also not adequately reflected. Therefore, analysis of intact LPS molecules via a top-down

approach offers many advantages, albeit with concomitant challenges associated with the amphiphilic characteristics of LPS.

Although there have been a few studies reported on the analysis of intact LPS, most have measured molecular weights and MS/MS spectra have not been commonly evaluated.^{26,30,31} Recently, we examined the fragmentation patterns of intact R-LPS using a hybrid UVPD/HCD method.³² UVPD and hybrid UVPD/HCD produced very rich fragmentation patterns arising from a diverse array of C-O, C-N, and C-C cleavages from both the lipid and oligosaccharide portions of the LPS, as illustrated for endotoxin structures from *E. coli*.³² The structural complexity of LPS makes interpretation of the resulting MS/MS spectra challenging. Previous studies have shown that the glycosidic bond between the 3-deoxy-D-*manno*-octulosonic acid (Kdo) of the core OS and the glucosamine of lipid A is particularly weak and can be easily cleaved in the gas phase.³³ Considering the successful implementation of 193 nm UVPD to analyze lipid A^{27,28,34–36} and saccharide³⁷ structures and the ease with which this glycosidic bond can be cleaved, multi-stage tandem mass spectrometry can be implemented to interrogate intact LPS structures while at the same time simplifying data interpretation. The present study uses MS³ to cleave the glycosidic bonds between lipid A and the core OS of intact LPS transferred to the gas-phase by nano-electrospray ionization (nanoESI), and subsequent UVPD of each substructure to gain detailed structural characterization of intact R-LPS with complete core.

5.3 EXPERIMENTAL

All R-LPS *E. coli* and *Salmonella enterica* sv. *Minnesota* (*S. enterica*) LPS samples were purchased from Glycobiotech (Research Center Borstel, Germany) and used without further purification. As an example, the structure of *S. enterica* is shown in

Figure 5.1, along with a legend displaying a key to the color coded sub-units and common neutral losses observed in the MS/MS spectra.

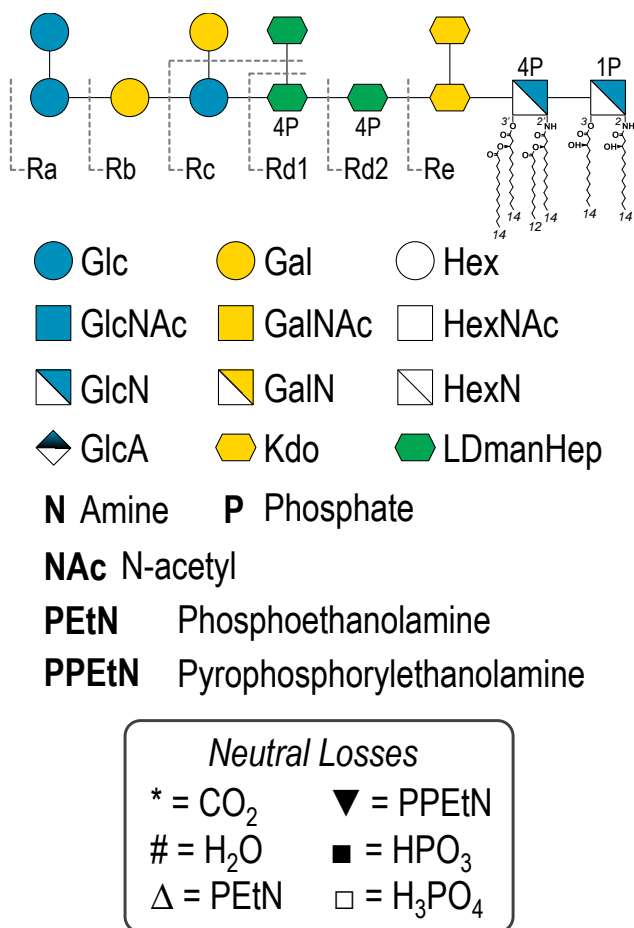


Figure 5.1 Structures of rough-type mutant strains of *S. enterica* (Ra-Re), saccharides symbols using the official Symbol Nomenclature for Glycans (SNFG), and key of symbols used to depict neutral losses observed in the MS/MS spectra.³⁸

Methanol (MeOH) and water (H₂O) were purchased from EMD Millipore (Billerica, MA) and chloroform (CHCl₃) was purchase from Sigma Aldrich (St. Louis, MO). All samples were diluted in 62:36:2 MeOH:H₂O:CHCl₃ to 100 µg/mL. Approximately 10 µL of sample were loaded into a silver-coated pulled tip capillary (1.2 mm OD) and sprayed

using a Proxeon offline nano-electrospray set-up (Thermo Scientific, San Jose, CA). The spray voltage was set to 1.1 kV. All spectra were collected in negative mode on a Thermo Scientific Orbitrap Fusion mass spectrometer (San Jose, CA) modified with a 193 nm Coherent Existar excimer laser (Santa Cruz, CA) to perform UVPD in the high pressure linear ion trap (**Figure 5.2**).³⁹

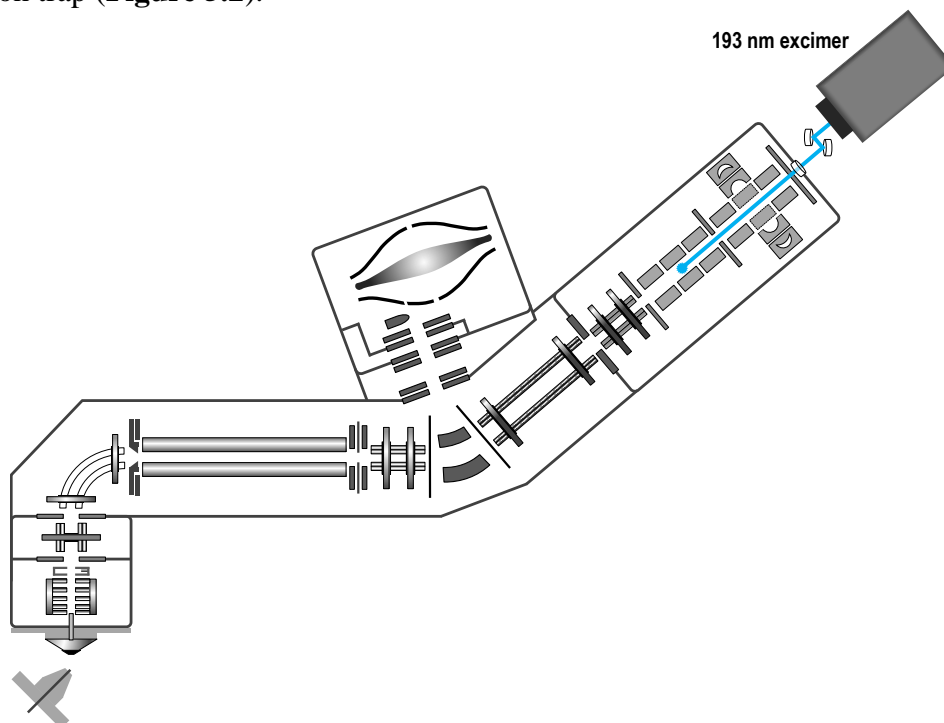


Figure 5.2 Schematic of a Thermo Orbitrap Fusion modified with a 193 nm excimer laser

UVPD was implemented by modifying the back end of the dual linear ion trap with a fused silica window to allow entrance of the laser beam into the high pressure trap of the instrument. A periscope and appropriate mirrors were used to guide the laser beam to the center of the high pressure ion trap, and a pulse generator and customized instrument code were used to pulse the laser during the time of ion trapping. Data were collected with an AGC target between 5e4 and 2e5 at a resolution of 120,000. For CID and HCD

25 scans were averaged and for UVPD 100-200 scans were averaged with 2-3 μ scans per scan. For CID activation at the MS² level the NCE was set to 18. At the MS³ level CID, HCD and UVPD activation parameters were set to NCE 30, NCE 35 and five 2 mJ pulses, respectively. Default activation times were used CID and HCD. All data were analyzed in XCalibur Qual Browser and manually interpreted. For spectra that were deconvoluted to neutral forms, Xtract was used with a signal to noise threshold of 3.

5.4 RESULTS AND DISCUSSION

Due to the complex amphipathic nature of intact LPS, a universal workflow was developed to facilitate a streamlined approach for individual characterization of the two main sub-structures: the lipid A sub-structure and the core Kdo/oligosaccharide sub-structure. As shown below, conventional CID provided the optimal means to cleave LPS into the two constituent sub-structures, and then the capabilities of CID, HCD and UVPD were compared for the subsequent characterization of the two sub-structures. The first step of the workflow required a robust means to transfer intact LPS into the mass spectrometer. The most common mass spectrometry approaches to LPS structural analysis generally involve deliberate degradation of LPS prior to analysis, via hydrolysis of the glycosidic bond between Kdo and glucosamine, or partial or complete removal of acyl chains. To approach analysis of intact LPS, conditions that allow dissolution of the LPS for direct analysis by nanoESI were developed. Raetz *et al.* identified chromatographic conditions that allowed successful chromatographic separation and ionization of Kdo2-lipid A.⁴⁰ Building on this earlier work, the starting gradient conditions employed in the Raetz study were used to successfully dissolve heterogeneous samples of R-LPS in the present study. LPS samples were dissolved in 62:36:2 MeOH:H₂O:CHCl₃ to attain a concentration of approximately 100 μ g/mL and sprayed

without chromatographic separation via a “shotgun” approach using a static nanoESI source. Due to the large number of lipids in each sample and the production of multiple charge states upon ESI, the resulting mass spectra were quite complex for three *S. enterica* and two *E. coli* samples (**Figure 5.3, Figure 5.4a**).

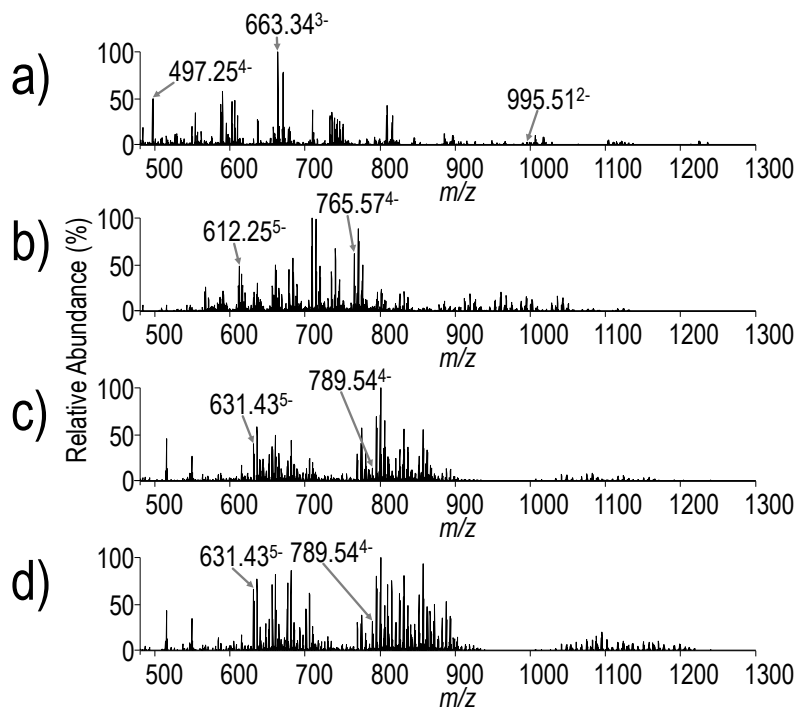


Figure 5.3 a) nanoESI mass spectra (100 µg/mL) of a) *S. enterica* Rd1, b) *S. enterica* Rb, c) *E. coli* R2 and d) *E. coli* R3 infused without chromatographic separation into the mass spectrometer via static emitters.

The charge-deconvoluted spectra confirm the high degree of heterogeneity in the samples (as exemplified in **Figure 5.4b** for *S. Enterica* Rc). Although some of this heterogeneity is likely a result of the method used to isolate the LPS, the resulting array of LPS species present in each sample was advantageous for the more elaborate comparisons done in this study.

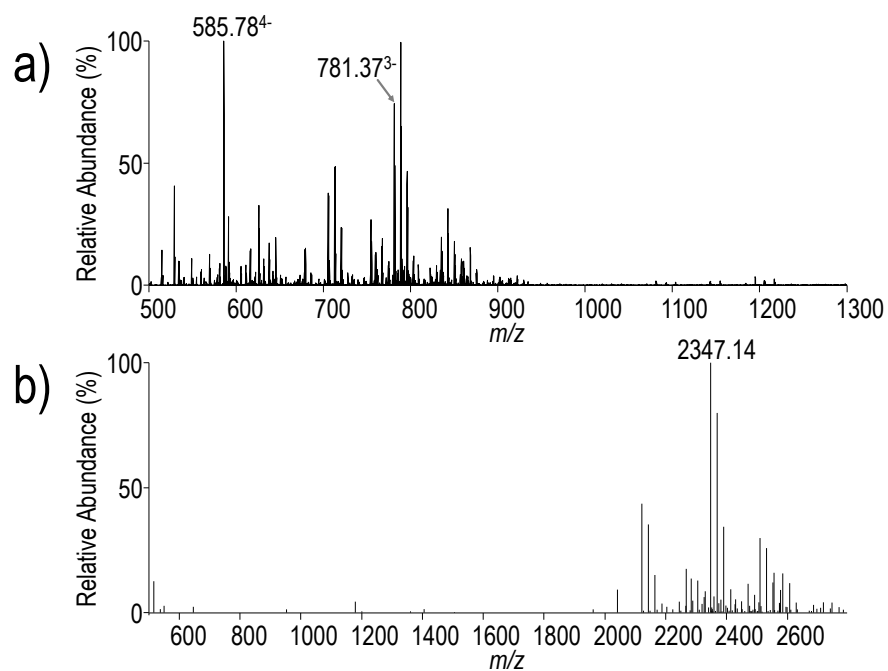


Figure 5.4 a) nanoESI mass spectrum of *S. enterica* Rc (100 ug/mL) infused without chromatographic separation into the mass spectrometer via a static emitter, and b) deconvolved spectrum.

Interpretation, assignment and labelling of the MS³ spectra of LPS poses its own set of challenges, especially in the context of displaying the results in a meaningful way to others. For the MS/MS spectra presented, LPS structures are depicted using the official Symbol Nomenclature for Glycans (SNFG).³⁸ The complex MS/MS spectra shown in the present study are conveyed schematically as fragmentation maps, in which saccharide fragments are labeled using the nomenclature of Domon and Costello (**Figure 5.5**)⁴¹ and acyl chain cleavages are numbered. This same system is used to label the ions in the MS/MS spectra, and for products where acyl chains are cleaved, the numbers corresponding to those particular acyl chain are shown as losses from the LPS (which is designated as “M”). For instance, **Figure 5.6a** shows the CID mass spectrum of penta-acylated *S. enterica* Rd1 (4-) and corresponding fragment ion map.

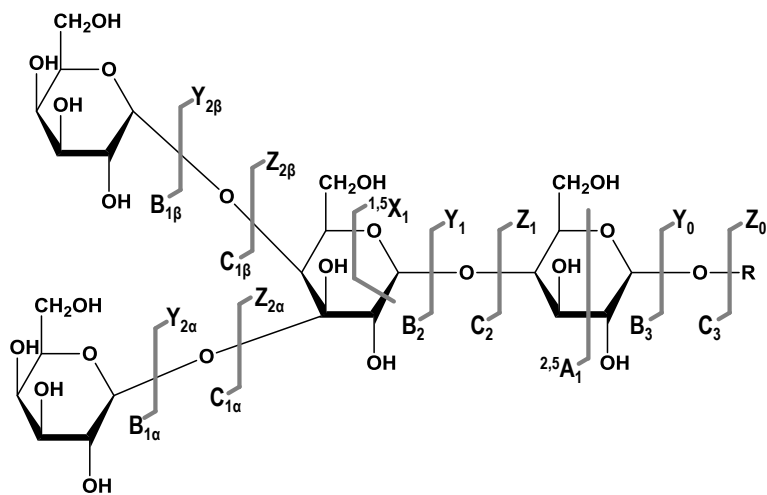


Figure 5.5 Domon and Costello carbohydrate fragmentation nomenclature⁴¹

The ion of m/z 587.32 labeled as $[Y_2 - 2]^{2-}$ corresponds to the lipid A substructure generated upon cleavage of the Kdo-GlcN bond along with loss of the secondary 12-carbon acyl chain (laurate) which is labeled as acyl chain 2. For products corresponding to the cleaved acyl chains, the number corresponding to the cleaved bond is used. For example, in **Figure 5.6a**, the ion of m/z 199.17 corresponds to the laurate moiety and is labeled as 2.

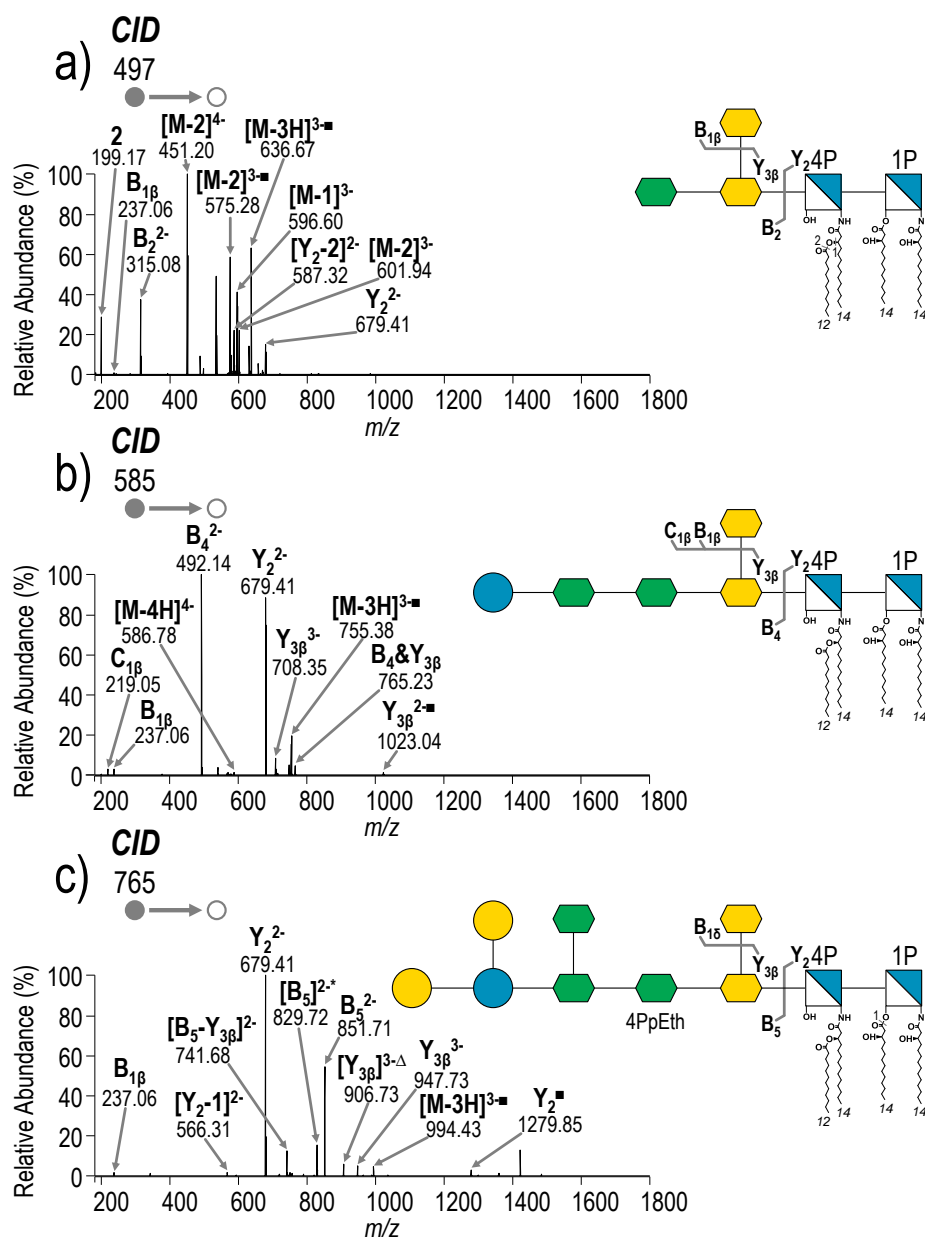


Figure 5.6 CID (NCE 18) of the 4- charge state of a) tetra-acylated *S. enterica* Rd1 (m/z 497.25) b) tetra-acylated *S. enterica* Rc (m/z 585.78) and c) tetra-acylated *S. enterica* Rb (m/z 765.56) (25 spectra averaged, LPS concentration 100 $\mu\text{g/mL}$ in 62:36:2 MeOH:H₂O CHCl₃). The acyl chains are numbered, and the loss of a particular acyl chain is denoted as M – N where M represents the LPS and N represents the acyl chain that is lost.

Examples of the CID mass spectra obtained for three mutant glycoforms of tetraacylated *S. enterica* LPS and three lipofoms of *S. enterica* Rc are shown in **Figures 5.6** and **5.7**, respectively. (**Figure 5.1** shows the naming convention and structures for the different mutants of *S. enterica*.) In all cases, glycosidic bond cleavages lead to the most prominent products for each LPS. For example, isolation and collisional activation of the tetra-acylated species from *S. enterica* Rc (MW = 2347.12 Da) shows predominant cleavage of the glycosidic bond between Kdo and glucosamine leading to product ions of m/z 679.41 (Y_2^{2-}) and m/z 492.14 (B_4^{2-}) corresponding to the lipid A and saccharide substructures, respectively (**Figure 5.6b**). The highly acidic nature of this glycosidic bond provides an explanation for its facile cleavage. This specific glycosidic cleavage is consistent with previous work from our group³¹ and is generally observed in matrix-assisted laser desorption ionization (MALDI) spectra as well.^{18,42} Preferential cleavage of this glycosidic bond is particularly advantageous for two reasons. First, it allows general localization of structural modifications of LPS to either the lipid A or core OS substructures based on the masses of the two products relative to the intact LPS, especially for comparisons of series of LPS like the three shown in **Figure 5.6** that possess the same lipid A sub-structure but with different oligosaccharides. Second, the preferential glycosidic cleavage results in two well-defined and abundant products that can be interrogated individually via MS³ to allow characterization of the two sub-units (e.g. lipid A and oligosaccharide). In essence, subsequent activation of each of these products reveals more detailed structural information.

To optimize the formation of the two key sub-structure products in the initial MS/MS step, the collisional energy was varied over a range of values. One of the resulting energy-variable diagrams for penta-acylated *S. enterica* Rc was constructed to determine the optimal normalized collision energy (NCE) to achieve maximum signal abundance for the lipid A and saccharide substructures (**Figure 5.8**). An NCE of 18 proved to be the optimal collisional activation condition and was used throughout this study.

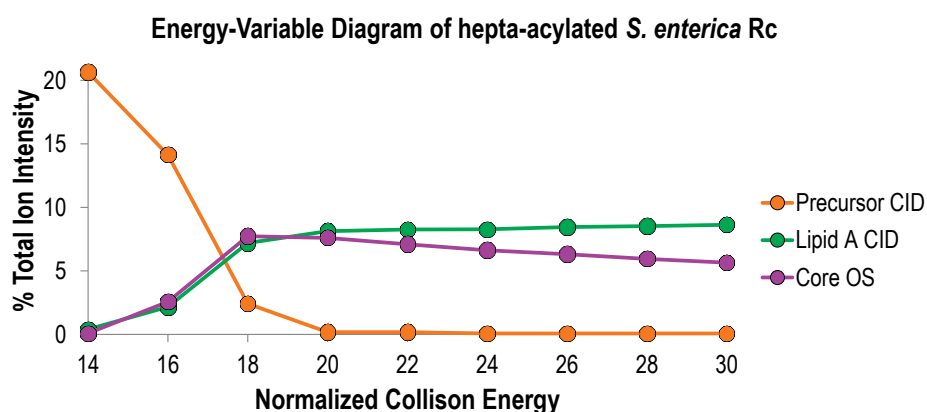


Figure 5.8 CID energy-variable diagram of penta-acylated *S. enterica* Rc monitoring the precursor ion (m/z 642.57) and products ions corresponding to the saccharide substructure (m/z 492.14) and lipid A substructure (m/z 792.5)

To verify that the lipid A and core OS ions would be consistently formed for an array of LPS, various R-LPS structures from mutant *S. enterica* were subjected to CID. The effect of core OS chain length was evaluated by comparing the CID patterns of tetra-acylated *S. enterica* Rd1, tetra-acylated *S. enterica* Rc, and tetra-acylated *S. enterica* Rb, all with the same lipid A substructure but with variations in the core OS (**Figure 5.6**). Despite changes in the relative abundances of the lipid A and OS ions, these products are readily identified. Additionally, significantly larger number of acyl chains fragments (i.e. products labelled as [M - N]) are observed upon collisional activation of *S. enterica* Rd1

(**Figure 5.6a**) than for *S. enterica* Rc or *S. enterica* Rb. Similar to changes in fragmentation that occur in glycopeptides as a function of glycan structure and peptide length, the observed changes reflect changes in the size and complexity of the core OS, suggesting that acyl chain cleavages are less prominent when there are more opportunities for energetically favorable glycosidic cleavages.⁴³ Regardless of this change in the distribution of products, the two key substructure ions are readily identified for all of the mutants. Similarly, the effect of lipid A structure was evaluated by comparing the fragmentation patterns of tetra-acylated *S. enterica* Rc, penta-acylated *S. enterica* Rc and hexa-acylated *S. enterica* Rc (**Figure 5.7**), three lipofoms which vary in the number of acyl chains of lipid A but all with the same OS substructure. In the CID spectrum of hexa-acylated *S. enterica* Rc (**Figure 5.7c**), although the lipid A and core OS substructure ions are readily identified (Y_2^{2-} and B_4), the predominant product is an ion of m/z 850.76 that corresponds to loss of the distal myristate secondary acyl chain (e.g. $[M-4]^{3-}$). Previous reports have shown this acyl chain linkage at the 3' position to be particularly labile.²⁸ Although this alternative cleavage site diminishes the abundance of the targeted products corresponding to the full lipid A and core OS substructures, this ion can be used to confirm the presence of a secondary acyl chain at the 3' position.

After optimization of the conditions to enhance the formation of the two substructure products by CID, the products were subsequently isolated and subjected to CID, HCD, and UVPD (MS^3) to complete the characterization of LPS. Examples of the resulting MS^3 spectra are shown in **Figure 5.9** for tetra-acylated *S. enterica* Rb that contains a pyrophosphorylethanolamine modification with the spectra for the OS (m/z 851.82, 2- charge state) on the left and the complementary spectra for the lipid A substructure (m/z 679.41, 2- charge state) on the right.

All identified ions in the spectra in **Figure 5.9** are listed in **Table 5.1** (Chapter 5, Supporting Information). CID/CID of the core OS substructure results in predominant losses of Kdo ($Y_{3\beta}$ and $Z_{3\beta}$) and Kdo₂ ($B_{1\alpha}$ and $C_{1\alpha}$), in addition to neutral losses of CO₂ and H₂O (**Figure 5.9a**, **Figure 5.10**).

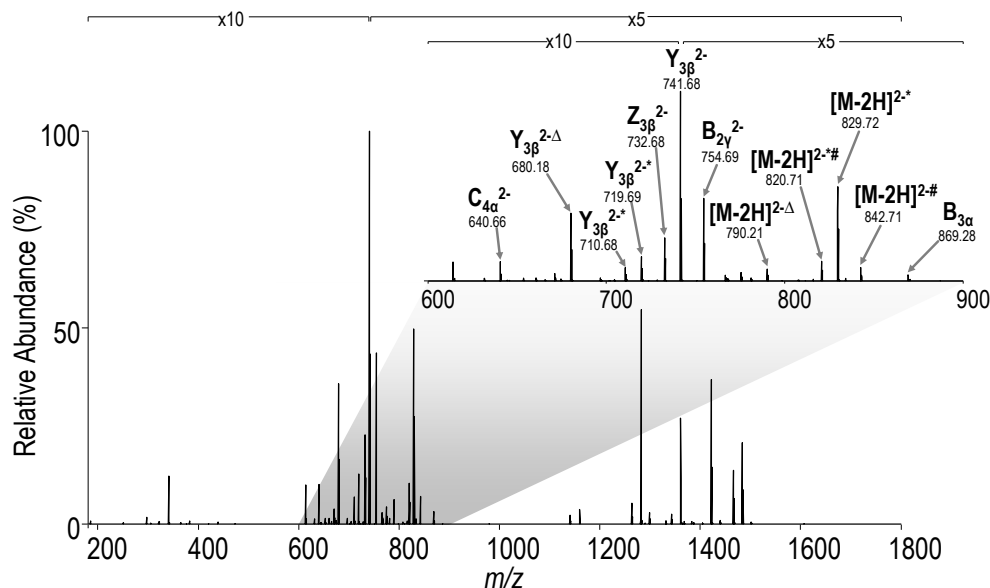


Figure 5.10 CID/CID mass spectrum (NCE 18/NCE 30) of the core OS substructure of tetra-acylated *S. enterica* Rb containing a pyrophosphorylethanolamine modification (m/z 851.81). (Data also present in **Figure 5.9a**) The inset shows expansion of the range from m/z 600 to 900. Δ = loss of phosphoethanolamine; * = loss of CO₂; # = loss of H₂O

CID/HCD of the same OS (**Figure 5.9b**) yields a spectrum similar to the CID/CID spectrum. A notable ion of m/z 219.98 (labeled as ▼ in **Figure 5.9b**) confirms the presence of the pyrophosphorylethanolamine modification on the core OS. The high resolution and high mass accuracy capabilities of the Orbitrap mass spectrometer allow this ion to be distinguished from the ion of m/z 219.05, which corresponds to the $B_{1\beta}$ ion. Additionally, fragment ions of m/z 967.25 and m/z 869.28 labeled as $[C_{4\alpha}-Y_{5\gamma}]^{\Delta}$ and $B_{3\alpha}$,

respectively, that appear exclusively in the CID/HCD spectrum provide information regarding the saccharide branching pattern and localize the position of the pyrophosphoethanolamine modification. CID/VPD of the ion of m/z 851.81 yields the richest mass spectrum with numerous fragments corresponding to cross-ring cleavages (X-type ions) that give saccharide linkage information (**Figure 5.9c**). For example, the $^{0,4}X_{4\alpha}$ ion (m/z 1422.37) confirms the linkage pattern of L-glycero-D-manno-heptose (heptose) (II) and glucose to heptose (I). By combining the information from the CID/HCD spectrum and the CID/VPD spectrum, cleavages are observed between every glycosidic bond in the core OS. This level of structural characterization is unprecedented.

The MS³ spectra for the companion lipid A substructure (m/z 679.41, charge state 2-) of *S. enterica* Rb are shown on the right side of **Figure 4**. CID/CID and CID/HCD yield similar spectra (**Figure 5.9d** and **5.9e**) that confirm the presence of laurate and myristate chains on the lipid A substructure based on m/z 199.19 and m/z 243.20, respectively, but do not localize their positions on the lipid A substructure. The CID/HCD spectrum displays an additional ion of m/z 242.21 that corresponds to cleavage of the proximal N-linked acyl chain. Again, high resolution and high mass accuracy allowed this ion to be distinguished from the ion of m/z 243.20 corresponding to the proximal O-linked acyl chain. CID/VPD (**Figure 5.9f**) produces a richer array of fragment ions that assist in discerning the more subtle structural features of the lipid A substructure. For example the $^{1,5}X_1$ cross-ring cleavage (m/z 738.42) allows the distribution of acyl chains on the distal (containing 3',2' positions) and proximal (containing 3,2 positions) sides of the lipid A substructure to be determined.^{27,28} Additional cross-ring and acyl chain cleavages allow acyl chain connectivity to be determined and hydroxyl modifications to be localized, respectively. For example, the

product assigned as $^{0,2}X_1$, in concert with $^{1,5}X_1$, confirms that the secondary laurate acyl chain is connected to the distal N-linked myristate acyl chain. For characterization of the lipid A substructure, integration of the information from CID/HCD and CID/VPD together offer the most comprehensive elucidation of the lipid A moiety.

Comparison of VPD and CID/VPD spectra of penta-acylated *E. coli* lipid A and penta-acylated *S. enterica* Rc, respectively, confirms that the integrity of the MS³ spectra collected for the lipid A substructure is maintained after the initial CID activation event (**Figure 5.11**). All identified ions in the spectra in **Figure 5.11** are listed in **Table 5.2** (Chapter 5, Supporting Information). The complexity of the resulting spectra reinforces the rationale for “separating” the characterization of the lipid A and core OS substructures based on the MS³ strategy. By first performing a CID event to cleave the bond between lipid A and core OS, the spectral complexity that acyl chain fragmentation would otherwise add to identification of glycosidic cleavages in core OS is eliminated, and manual interpretation of spectra becomes practical.

Within *E. coli* LPS there are five naturally occurring core types: R1-R4 and K12. These core types are very similar, all containing heptose and Kdo in their inner core (various other non-stoichiometric modifications can occur in the inner core depending on the core type) and a series of hexose carbohydrates in the outer core.⁴⁴ The nature, position and linkage of the hexoses in the outer core are dependent on the core type, with some of the variation being as subtle as a difference in the kind of linkage. To further confirm the detail to which core OS structures can be determined using this multi-stage mass spectrometry method, MS³ spectra were acquired for two isomeric R-LPS structures from *E. coli* R2 and *E. coli* R3. CID of was performed on the main LPS ion (MW = 3162.16 Da, m/z 631.43, charge state 5-) in each of the *E. coli* R2 and *E. coli* R3 samples (**Figure 5.12**).

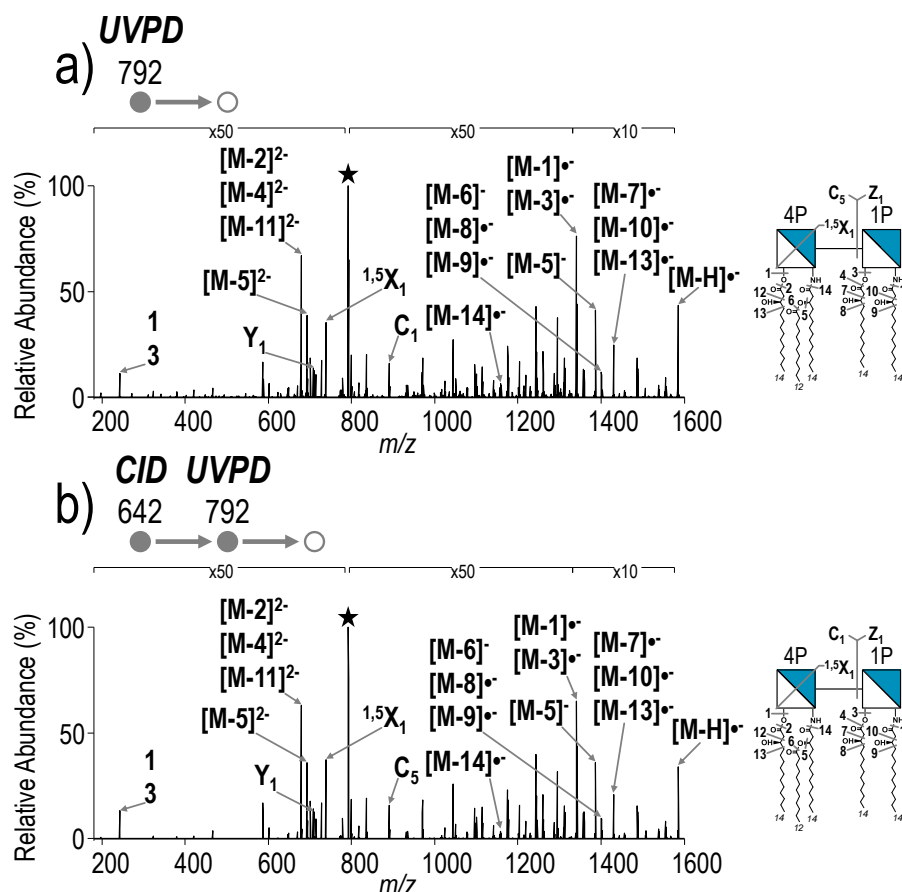


Figure 5.11 a) UVPD (5 pulses, 2 mJ) of penta-acylated from *E. coli* lipid A and b) CID/UVPD (NCE of the penta-acylated lipid A substructure from *S. enterica* Rc. ■ = neutral loss of HPO_3 ; A black star is used to indicate the precursor. The acyl chains are numbered, and the loss of a particular acyl chain is denoted as M – N where M represents the LPS and N represents the acyl chain that is lost.

Other than small differences in ion abundances, the spectra are identical. The Y_2^{2-} (lipid substructure, m/z 566.31) and B_7^{3-} (OS substructure, m/z 674.84) are the two most prominent product ions in the CID spectra. The CID/HCD and CID/UVPD spectra of the lipid A substructures (Y_2^{2-} , m/z 566.31) also look the same for *E. coli* R2 and *E. coli* R3

(**Figure 5.13**), confirming that the variation in the LPS structure must be a result of core OS structure and not lipid A structure.

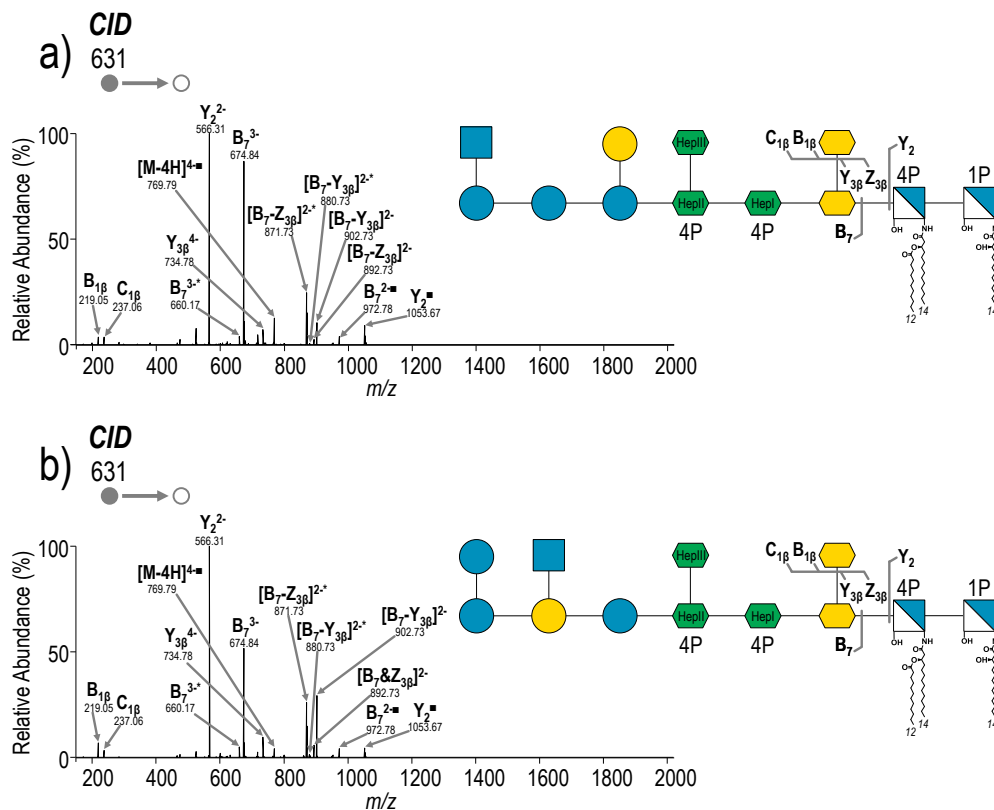


Figure 5.12 a) CID (NCE 18) of *E. coli* R2 (MW = 3162.16 Da, precursor m/z 631.43, charge state 5-) b) CID (NCE 18) of *E. coli* R3 (MW = 3162.16 Da, precursor m/z 631.43, charge state 5-); ■ = neutral loss of HPO_3

CID/HCD and CID/VPD spectra of the core OS substructures (m/z 674.84, **Figure 5.14**) are very similar; however, there exist fragment ions that allow the two isomeric structures to be distinguished from one another. All identified ions in the spectra in **Figure 5.14** are listed in **Table 5.3** (Chapter 5, Supporting Information). In the CID/HCD spectra, the $B_{3\alpha}$ product in **Figure 5.14a** and $B_{2\alpha}$ and $C_{2\alpha}$ products in **Figure 5.14b** correspond to glycosidic cleavages unique to the *E. coli* R2 and *E. coli* R3 cores, respectively.

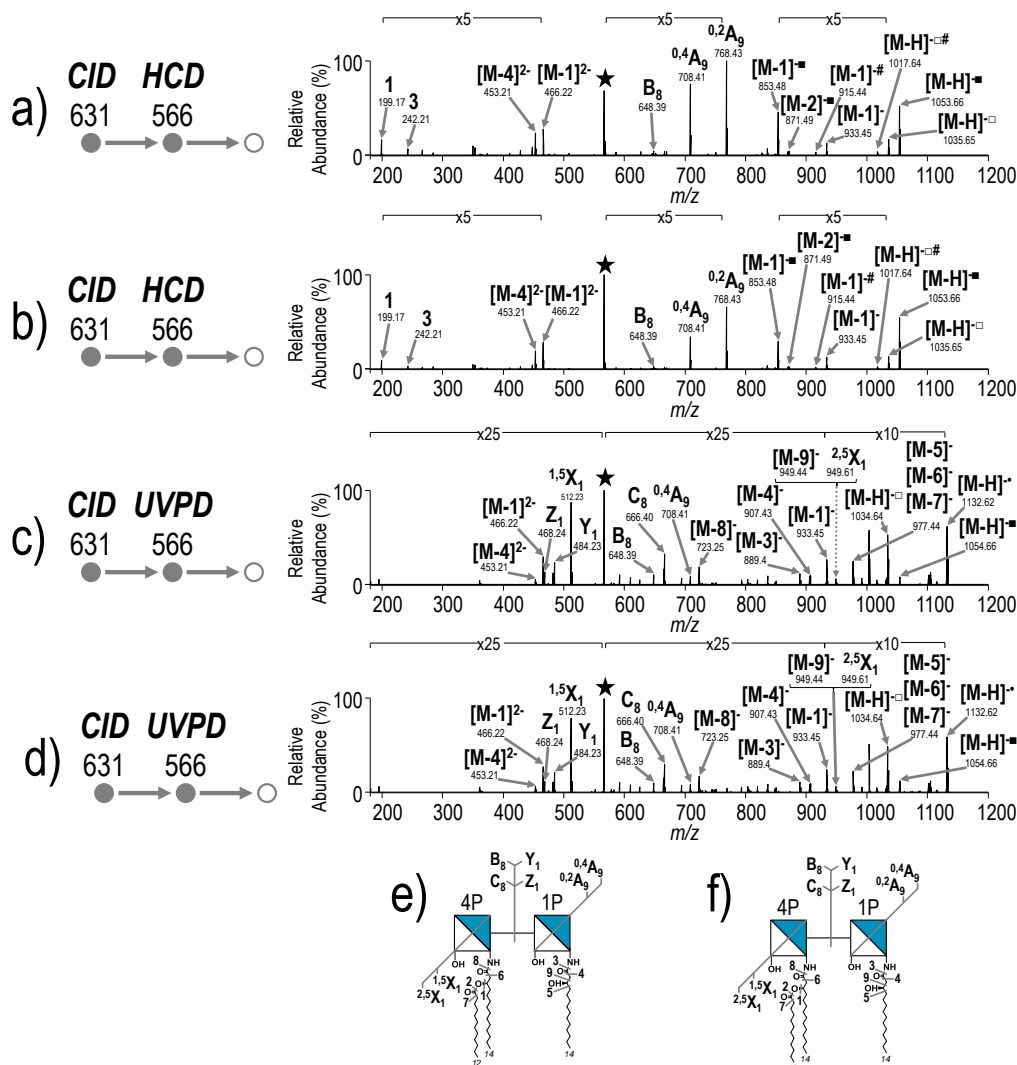


Figure 5.13 a) CID/HCD (NCE 18/NCE 30) of the lipid A substructure of *E. coli* R2 (m/z 566.31, charge state 2-) b) CID/HCD (NCE 18/NCE 30) of the lipid A substructure of *E. coli* R3 (m/z 566.31, charge state 2-), c) CID/VPD (NCE 18/5 pulses, 2 mJ) of the lipid A substructure of *E. coli* R2 (m/z 566.31, charge state 2-) and d) CID/VPD (NCE 18/5 pulses, 2 mJ) of the lipid A substructure of *E. coli* R3 (m/z 566.31, charge state 2-). ■ = neutral loss of HPO_3 , □ = neutral loss of H_3PO_4 . A bracket under a pair of ions indicates the presence of two resolved ions, but the mass difference is too small to allow inclusion of separate arrows. The acyl chains are numbered, and the loss of a particular acyl chain is denoted as M – N where M represents the LPS and N represents the acyl chain that is lost.

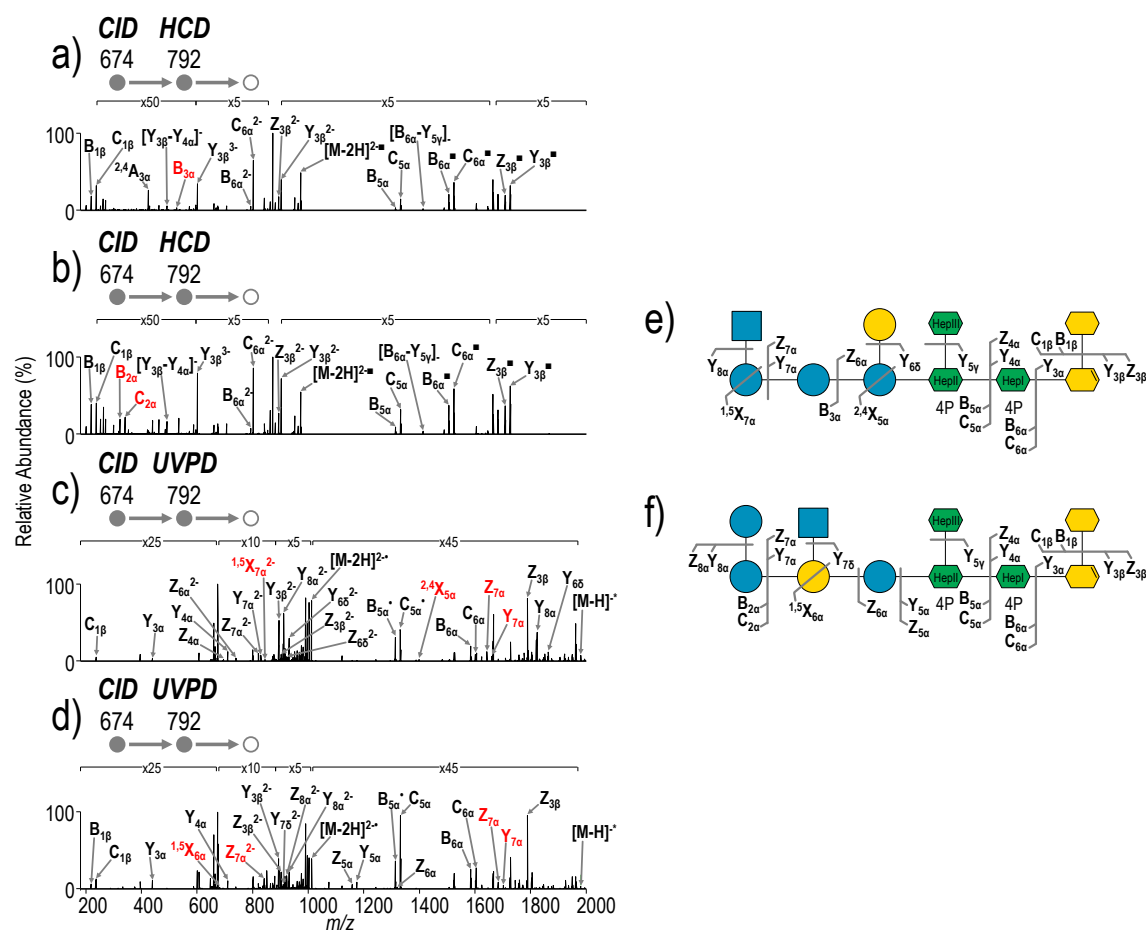


Figure 5.14 a) CID/HCD (NCE 18/NCE 30) of the core oligosaccharide substructure of *E. coli* R2 (m/z 674.84, charge state 3-) b) CID/HCD (NCE 18/NCE 30) of the core OS substructure of *E. coli* R3 (m/z 674.84, charge state 3-), c) CID/VPD (NCE 18/5 pulses, 2 mJ) of the core OS substructure of *E. coli* R2 (m/z 674.84, charge state 3-) and d) CID/VPD (NCE 18/5 pulses, 2 mJ) of the core oligosaccharide substructure of *E. coli* R3 (m/z 674.84, charge state, 3-). Unique ions that can be used to identify each isomer appear in red. ■ = neutral loss of HPO_3 ; the black star indicates the precursor ion in the spectrum.

Similarly, in the CID/VPD spectra, Y_{7a} , Z_{7a} , $^{2,4}X_{5a}$ and $^{1,5}X_{7a}^{2-}$ ions in **Figure 5.14c** and Y_{7a} , Z_{7a} , Z_{7a}^{2-} and $^{1,5}X_{6a}$ ions in **Figure 5.14d** correspond to glycosidic and cross-ring cleavages that uniquely identify the *E. coli* R2 and *E. coli* R3 cores, respectively. CID/HCD and CID/VPD yield complementary fragmentation patterns that enable

almost complete structural elucidation of core OS structures as reflected in the comprehensive fragmentation maps shown in **Figure 5.14e** and **Figure 5.14f**.

5.5 CONCLUSION

An MS³ strategy utilizing UVPD has been developed to enable the detailed structural characterization of intact R-LPS. An initial CID event produced lipid A and core OS ions that were subsequently activated in a second stage using CID, HCD or UVPD. Subsequent HCD produced ions from glycosidic cleavages that provide saccharide branching information, while UVPD produced ions from cross ring cleavages that revealed saccharide connectivity. The complementary spectra produced by HCD and UVPD enabled confident re-construction of R-LPS structures. The high resolution and high mass accuracy of the Orbitrap analyzer allowed facile differentiation of informative but nearly isobaric fragment ions. Despite the unprecedented characterization achieved in this study, the “shotgun” approach used here produces congested ESI mass spectra that can make isolation of a single LPS species challenging. Although mass isolation of a single R-LPS species was feasible in this study, smooth-type LPS has a significantly higher degree of heterogeneity as a result of the varying number of saccharide repeat units; isolation of single species is increasingly challenging. To address this concern, we are developing appropriate offline and online separation methods to facilitate analysis of smooth-type LPS in a higher throughput manner. Additionally, both online and offline separations will alleviate signal suppression associated with direct infusion of a complex mixture and potentially allow sample consumption to be further diminished.

5.6 SUPPORTING INFORMATION

Table 5.1 List of identified ions in **Figure 5.9**

Figure 5.9a		Figure 5.9b		Figure 5.9c		Figure 5.9d		Figure 5.9e		Figure 5.9f	
m/z	Fragment	m/z	Fragment	m/z	Fragment	m/z	Fragment	m/z	Fragment	m/z	Fragment
1484.37	Y _{3β}	1501.45	[M-▼] ⁻	1703.42	[M-H] ⁻	1279.85	[M-H] [■]	1279.85	[M-H] [■]	1358.81	[M-H] ⁻
1466.36	Z _{3β}	1484.37	Y _{3β}	1685.41	[M-H] [†] #	1261.84	[M-H] [□]	1261.84	[M-H] [□]	1298.79	^{0.4} X ₁
1440.38	Y _{3α} [*]	1466.36	Z _{3β}	1673.41	[M-CH ₂ O] [†] #	1159.64	[M-3] ⁻	1159.64	[M-3] ⁻	1203.63	[M-7] ⁻ , [M-9] ⁻
1422.37	Z _{3β} [*]	1440.38	Y _{3α} [*]	1661.39	[M-C ₂ H ₆ N] ⁻	1115.61	[M-1] ⁻	1115.61	[M-1] ⁻	1175.80	^{2.5} X ₁
1361.36	Y _{3β} ^Δ	1422.37	Z _{3β} [*]	1630.39	^{3.5} X _{6α} , ^{3.5} X _{6β}	1095.67	[M-4] [■]	1095.67	[M-4] [■]	1174.63	[M-6] ⁻ , [M-8] ⁻
1343.35	Z _{3β} ^Δ	1361.36	Y _{3β} ^Δ	1601.39	^{2.5} X _{6α} , ^{2.5} X _{6β}	1079.67	[M-3] [■]	1079.67	[M-3] [■]	1159.81	^{0.2} X ₁
1282.32	C _{4α}	1343.35	Z _{3β} ^Δ	1570.37	^{1.5} X _{6α} , ^{1.5} X _{6β}	1035.65	[M-1] [■] , [M-2] [□] , [M-5] [□]	1035.65	[M-1] [■] , [M-2] [□] , [M-5] [□]	1159.64	[M-3] ⁻
1264.31	B _{4α}	1282.32	C _{4α}	1540.36	Y _{6α} , Y _{6β}	994.62	^{1.3} A ₇	994.62	^{1.3} A ₇	949.44	[M-11] ⁻
1159.32	C _{4α} ^Δ	1264.31	B _{4α}	1525.37	Z _{6α} , Z _{6β}	915.44	[M-1-3] ⁻	915.44	[M-1-3] ⁻	920.42	^{1.2} X ₁
1141.31	Z _{4α} ^Δ	1159.32	C _{4α} ^Δ	1512.37	Y _{5γ}	708.41	Y ₁	708.41	Y ₁	892.42	^{1.3} X ₁
869.28	B _{3α}	1141.31	B _{4α} ^Δ	1467.37	Z _{3β}	670.40	Z ₂ ²⁻	664.38	C ₆	874.41	[M-1-10] ⁻
842.71	[M-2H] ^{2-#}	1123.29	B _{4α} [#]	1422.37	Z _{3β} [*]	587.31	[M-4] ²⁻	587.31	[M-4] ²⁻	817.38	^{1.4} A ₇
829.72	[M-2H] ^{2-*}	967.25	[C _{4α} &Y _{5γ}] ^Δ	1282.32	C _{4β}	579.32	[M-3] ²⁻	579.32	[M-3] ²⁻	738.42	^{1.5} X ₁
820.71	[M-2H] ^{2-#*}	869.28	B _{3α}	1263.31	B _{4β}	566.31	[M-2] ²⁻ , [M-5] ²⁻	566.31	[M-2] ²⁻ , [M-5] ²⁻	710.42	Y ₁
790.21	[M-2H] ^{2-Δ}	851.71	B _{3α}	1246.27	^{1.5} X _{5α}	557.30	[M-1] ²⁻	557.30	[M-1] ²⁻	692.41	Z ₁
754.69	B _{2γ} ²⁻	842.71	[M-2H] ^{2-#}	1218.27	Y _{5α}	466.22	[M-2-3] ²⁻ , [M-1-4] ²⁻	466.22	[M-2-3] ²⁻ , [M-1-4] ²⁻	664.38	C ₆
741.68	Y _{3β} ²⁻	829.72	[M-2H] ^{2-*}	1200.26	Z _{5α}	457.21	[M-1-3] ²⁻	457.21	[M-1-3] ²⁻	587.31	[M-4] ²⁻
732.68	Z _{3β} ²⁻	820.71	[M-2H] ^{2-#*}	862.15	^{1.5} X _{4α}	444.21	[M-1-5] ²⁻	448.21	[M-1-3] ^{2-#}	579.32	[M-3] ²⁻
719.69	Y _{3β} ^{2-*}	790.21	[M-2H] ^{2-Δ}	851.71	B ₅	243.20	1	444.21	[M-1-5] ²⁻	566.31	[M-2] ⁻ , [M-5] ⁻
710.68	Z _{3β} ^{2-*}	754.69	B _{2γ} ²⁻	842.20	[M-2H] ^{2-#*}	199.19	3	243.20	1	474.22	[M-2-4] ²⁻
680.18	Y _{3β} ^{2-Δ}	741.68	Y _{3β} ²⁻	829.21	[M-C ₂ H ₆ N] ²⁻			242.21	10	466.22	[M-2-3] ²⁻ , [M-1-4] ²⁻
640.66	C _{4α} ²⁻	732.68	Z _{3β} ²⁻	799.69	^{2.5} X _{6α} ²⁻ , ^{2.5} X _{6β} ²⁻			199.19	3	243.20	1
421.10	Y _{3α} [*]	719.69	Y _{3β} ^{2-*}	770.68	Y _{6α} ²⁻ , Y _{6β} ²⁻						
377.11	Z _{3α} [*]	710.68	Z _{3β} ^{2-*}	762.18	Z _{6α} ²⁻ , Z _{6β} ²⁻						
		680.18	Y _{3β} ^{2-Δ}	755.68	Y _{5γ} ²⁻						
		640.66	C _{4α} ²⁻	741.68	Y _{3β} ²⁻						
		439.11	Y _{3α} [*]	733.68	Z _{3β} ²⁻						
		421.10	Y _{3α} [*]	640.66	C _{4α} ²⁻						
		377.11	Z _{3α} [*]								
		237.06	C _{1β}								
		219.98	▼								
		219.05	B _{4β}								
		201.04	B _{4β} [#]								

Table 5.2 List of identified ions in **Figure 5.11**

Figure 5.11a		Figure 5.11b	
<i>m/z</i>	Fragment	<i>m/z</i>	Fragment
1585.00	[M-H] ⁻	1585.00	[M-H] ⁻
1506.05	[M-H] ^{•-}	1506.05	[M-H] ^{•-}
1487.03	[M-H] ^{+□-}	1487.03	[M-H] ^{+□-}
1429.82	[M-7] ⁻ , [M-10] ⁻ , [M-13] ⁻	1429.82	[M-7] ⁻ , [M-10] ⁻ , [M-13] ⁻
1400.82	[M-6] ⁻ , [M-8] ⁻ , [M-9] ⁻	1400.82	[M-6] ⁻ , [M-8] ⁻ , [M-9] ⁻
1385.83	[M-5] ⁻	1385.83	[M-5] ⁻
1340.80	[M-1] ⁻ , [M-3] ⁻	1340.80	[M-1] ⁻ , [M-3] ⁻
1158.64	[M-14] ⁻	1158.64	[M-14] ⁻
890.58	C ₁	890.58	C ₁
738.42	^{1,5} X ₁	738.42	^{1,5} X ₁
710.43	Y ₁	710.43	Y ₁
692.42	[M-5] ²⁻	692.42	[M-5] ²⁻
679.41	[M-2] ²⁻ , [M-4] ²⁻ , [M-11] ²⁻	679.41	[M-2] ²⁻ , [M-4] ²⁻ , [M-11] ²⁻
243.20	1,3	243.20	1,3

Table 5.3 List of identified ions in Figure 5.11

Figure 5.14a		Figure 5.14a		Figure 5.14a		Figure 5.14a	
<i>m/z</i>	Fragment	<i>m/z</i>	Fragment	<i>m/z</i>	Fragment	<i>m/z</i>	Fragment
1726.50	$Y_{3\beta}^{\bullet}$	1726.50	$Y_{3\beta}^{\bullet}$	1980.51	$[M-H]^+$	1980.51	$[M-H]^+$
1708.49	$Z_{3\beta}^{\bullet}$	1708.49	$Z_{3\beta}^{\bullet}$	1863.46	$Y_{6\delta}$	1788.45	$Z_{3\beta}$
1524.45	C_{6a}^{\bullet}	1524.45	C_{6a}^{\bullet}	1823.44	Y_{8a}	1702.42	Y_{7a}
1506.44	B_{6a}^{\bullet}	1506.44	B_{6a}^{\bullet}	1788.45	$Z_{3\beta}$	1684.41	Z_{7a}
1412.35	$[B_{6a}-Y_{5\gamma}]^{\bullet}$	1412.35	$[B_{6a}-Y_{5\gamma}]^{\bullet}$	1661.39	Y_{7a}	1604.42	C_{6a}
1332.38	C_{5a}	1332.38	C_{5a}	1643.48	Z_{7a}	1585.39	B_{6a}
1314.37	B_{5a}	1314.37	B_{5a}	1604.42	C_{6a}	1332.39	C_{5a}
972.77	$[M-2H]^{2-\bullet}$	972.77	$[M-2H]^{2-\bullet}$	1585.39	B_{6a}	1321.29	Z_{6a}
902.73	$Y_{3\beta}^{2-}$	902.73	$Y_{3\beta}^{2-}$	1399.32	$^{2,4}X_{5a}$	1313.37	B_{5a}^{\bullet}
893.72	$Z_{3\beta}^{2-}$	893.72	$Z_{3\beta}^{2-}$	1330.37	C_{5a}^{\bullet}	1175.23	Y_{5a}
801.70	C_{6a}^{2-}	801.70	C_{6a}^{2-}	1313.37	B_{5a}^{\bullet}	1159.24	Z_{5a}
792.70	B_{6a}^{2-}	792.70	B_{6a}^{2-}	1012.25	$[M-2H]^{2+}$	1012.25	$[M-2H]^{2+}$
601.48	$Y_{3\beta}^{3-}$	601.48	$Y_{3\beta}^{3-}$	931.73	$Y_{6\delta}^{2-}$	931.73	Y_{8a}^{2-}
526.18	B_{3a}	491.08	$[Y_{3\beta}-Y_{4a}]^{\bullet}$	922.72	$Z_{6\delta}^{2-}$	922.72	Z_{8a}^{2-}
491.08	$[Y_{3\beta}-Y_{4a}]^{\bullet}$	341.11	C_{2a}	911.22	Y_{8a}^{2-}	910.22	$Y_{7\delta}^{2-}$
424.15	$^{2,4}A_{3a}$	323.10	B_{2a}	902.73	$Z_{3\beta}^{2-}$	902.73	$Z_{3\beta}^{2-}$
237.06	$C_{1\beta}$	237.06	$C_{1\beta}$	894.23	$Y_{3\beta}^{2-}$	894.23	$Y_{3\beta}^{2-}$
219.05	$B_{1\beta}$	219.05	$B_{1\beta}$	844.19	$^{1,5}X_{7a}^{2-}$	841.7	Z_{7a}^{2-}
				830.19	Y_{7a}^{2-}	711.14	Y_{4a}
				821.19	Z_{7a}^{2-}	682.14	$^{1,5}X_{6a}$
				740.16	Z_{6a}^{2-}	439.11	Y_{3a}
				711.14	Y_{4a}	237.06	$C_{1\beta}$
				695.15	Z_{4a}	219.05	$B_{1\beta}$
				439.11	Y_{3a}		
				237.06	$C_{1\beta}$		

5.7 REFERENCES

- (1) Beutler, B.; Rietschel, E. T. Innate Immune Sensing and Its Roots: The Story of Endotoxin. *Nat. Rev. Immunol.* **2003**, *3*, 169–176.
- (2) Preston, Andrew; Mandrell, Robert E.; Gibson, Bradford W.; Apicella, Michael A. The Lipooligosaccharides of Pathogenic Gram-Negative Bacteria. *Crit. Rev. Microbiol.* **1996**, *22*, 139–180.
- (3) Raetz, C. R. H.; Whitfield, C. Lipopolysaccharide Endotoxins. *Annu. Rev. Biochem.* **2002**, *71*, 635–700.
- (4) Yethon, J. A.; Heinrichs, D. E.; Monteiro, M. A.; Perry, M. B.; Whitfield, C. Involvement of WaaY, WaaQ, AndwaaP in the Modification of Escherichia Coli Lipopolysaccharide and Their Role in the Formation of a Stable Outer Membrane. *J. Biol. Chem.* **1998**, *273*, 26310–26316.
- (5) Heinrichs, D. E.; Yethon, J. A.; Whitfield, C. Molecular Basis for Structural Diversity in the Core Regions of the Lipopolysaccharides of Escherichia Coli and Salmonella Enterica. *Mol. Microbiol.* **1998**, *30*, 221–232.
- (6) Delcour, A. H. Outer Membrane Permeability and Antibiotic Resistance. *Biochim. Biophys. Acta* **2009**, *1794*, 808–816.
- (7) Silipo, A.; Molinaro, A. The Diversity of the Core Oligosaccharide in Lipopolysaccharides. In *Endotoxins: Structure, Function and Recognition*; Wang, X., Quinn, P. J., Eds.; Subcellular Biochemistry; Springer Netherlands, 2010; pp 69–99.
- (8) Yethon, J. A.; Vinogradov, E.; Perry, M. B.; Whitfield, C. Mutation of the Lipopolysaccharide Core Glycosyltransferase Encoded by WaaG Destabilizes the Outer Membrane of Escherichia Coli by Interfering with Core Phosphorylation. *J. Bacteriol.* **2000**, *182*, 5620–5623.
- (9) Needham, B. D.; Carroll, S. M.; Giles, D. K.; Georgiou, G.; Whiteley, M.; Trent, M. S. Modulating the Innate Immune Response by Combinatorial Engineering of Endotoxin. *Proc. Natl. Acad. Sci.* **2013**, *110*, 1464–1469.
- (10) Molinaro, A.; Holst, O.; Di Lorenzo, F.; Callaghan, M.; Nurisso, A.; D’Errico, G.; Zamyatina, A.; Peri, F.; Berisio, R.; Jerala, R.; Jiménez-Barbero, J.; Silipo, A.; Martín-Santamaría, S. Chemistry of Lipid A: At the Heart of Innate Immunity. *Chem. – Eur. J.* **2015**, *21*, 500–519.
- (11) Li, Y.; Powell, D. A.; Shaffer, S. A.; Rasko, D. A.; Pelletier, M. R.; Leszyk, J. D.; Scott, A. J.; Masoudi, A.; Goodlett, D. R.; Wang, X.; Raetz, C. R. H.; Ernst, R. K. LPS Remodeling Is an Evolved Survival Strategy for Bacteria. *Proc. Natl. Acad. Sci.* **2012**, *109*, 8716–8721.
- (12) Boll, J. M.; Tucker, A. T.; Klein, D. R.; Beltran, A. M.; Brodbelt, J. S.; Davies, B. W.; Trent, M. S. Reinforcing Lipid A Acylation on the Cell Surface of

- Acinetobacter Baumannii Promotes Cationic Antimicrobial Peptide Resistance and Desiccation Survival. *mBio* **2015**, *6*, e00478-15.
- (13) Park, B. S.; Song, D. H.; Kim, H. M.; Choi, B.-S.; Lee, H.; Lee, J.-O. The Structural Basis of Lipopolysaccharide Recognition by the TLR4–MD-2 Complex. *Nature* **2009**, *458*, 1191–1195.
 - (14) Zariri, A.; van der Ley, P. Biosynthetically Engineered Lipopolysaccharide as Vaccine Adjuvant. *Expert Rev. Vaccines* **2015**, *14*, 861–876.
 - (15) Casella, C. R.; Mitchell, T. C. Putting Endotoxin to Work for Us: Monophosphoryl Lipid A as a Safe and Effective Vaccine Adjuvant. *Cell. Mol. Life Sci.* **2008**, *65*, 3231–3240.
 - (16) Needham, B. D.; Trent, M. S. Fortifying the Barrier: The Impact of Lipid A Remodelling on Bacterial Pathogenesis. *Nat. Rev. Microbiol.* **2013**, *11*, 467–481.
 - (17) Raetz, C. R. H.; Reynolds, C. M.; Trent, M. S.; Bishop, R. E. Lipid A Modification Systems in Gram-Negative Bacteria. *Annu. Rev. Biochem.* **2007**, *76*, 295–329.
 - (18) Kilár, A.; Dörnyei, Á.; Kocsis, B. Structural Characterization of Bacterial Lipopolysaccharides with Mass Spectrometry and On- and off-Line Separation Techniques. *Mass Spectrom. Rev.* **2013**, *32*, 90–117.
 - (19) Weinbaum, G.; Kadis, S.; Ajl, S. J. *Bacterial Endotoxins: A Comprehensive Treatise*; Elsevier, 2013.
 - (20) Jones, J. W.; Cohen, I. E.; Tureček, F.; Goodlett, D. R.; Ernst, R. K. Comprehensive Structure Characterization of Lipid A Extracted from *Yersinia Pestis* for Determination of Its Phosphorylation Configuration. *J. Am. Soc. Mass Spectrom.* **2010**, *21*, 785–799.
 - (21) Silipo, A.; De Castro, C.; Lanzetta, R.; Molinaro, A.; Parrilli, M.; Vago, G.; Sturiale, L.; Messina, A.; Garozzo, D. Structural Characterizations of Lipids A by MS/MS of Doubly Charged Ions on a Hybrid Linear Ion Trap/Orbitrap Mass Spectrometer. *J. Mass Spectrom.* **2008**, *43*, 478–484.
 - (22) Jones, J. W.; Shaffer, S. A.; Ernst, R. K.; Goodlett, D. R.; Tureček, F. Determination of Pyrophosphorylated Forms of Lipid A in Gram-Negative Bacteria Using a Multivaried Mass Spectrometric Approach. *Proc. Natl. Acad. Sci.* **2008**, *105*, 12742–12747.
 - (23) Madalinski, G.; Fournier, F.; Wind, F.-L.; Afonso, C.; Tabet, J.-C. Gram-Negative Bacterial Lipid A Analysis by Negative Electrospray Ion Trap Mass Spectrometry: Stepwise Dissociations of Deprotonated Species under Low Energy CID Conditions. *Int. J. Mass Spectrom.* **2006**, *249–250*, 77–92.

- (24) Kussak, A.; Weintraub, A. Quadrupole Ion-Trap Mass Spectrometry to Locate Fatty Acids on Lipid A from Gram-Negative Bacteria. *Anal. Biochem.* **2002**, *307*, 131–137.
- (25) Chan, S.; Reinhold, V. N. Detailed Structural Characterization of Lipid A: Electrospray Ionization Coupled with Tandem Mass-Spectrometry. *Anal. Biochem.* **1994**, *218*, 63–73.
- (26) Kojima, H.; Inagaki, M.; Tomita, T.; Watanabe, T. Diversity of Non-Stoichiometric Substitutions on the Lipopolysaccharide of E. Coli C Demonstrated by Electrospray Ionization Single Quadrupole Mass Spectrometry. *Rapid Commun. Mass Spectrom.* **2010**, *24*, 43–48.
- (27) Madsen, J. A.; Cullen, T. W.; Trent, M. S.; Brodbelt, J. S. IR and UV Photodissociation as Analytical Tools for Characterizing Lipid A Structures. *Anal. Chem.* **2011**, *83*, 5107–5113.
- (28) O'Brien, J. P.; Needham, B. D.; Henderson, J. C.; Nowicki, E. M.; Trent, M. S.; Brodbelt, J. S. 193 nm Ultraviolet Photodissociation Mass Spectrometry for the Structural Elucidation of Lipid A Compounds in Complex Mixtures. *Anal. Chem.* **2014**, *86*, 2138–2145.
- (29) Brodbelt, J. S. Photodissociation Mass Spectrometry: New Tools for Characterization of Biological Molecules. *Chem. Soc. Rev.* **2014**, *43*, 2757–2783.
- (30) Silipo, A.; Leone, S.; Molinaro, A.; Sturiale, L.; Garozzo, D.; Nazarenko, E. L.; Gorshkova, R. P.; Ivanova, E. P.; Lanzetta, R.; Parrilli, M. Complete Structural Elucidation of a Novel Lipooligosaccharide from the Outer Membrane of the Marine Bacterium Shewanella Pacifica. *Eur. J. Org. Chem.* **2005**, *2005*, 2281–2291.
- (31) Banoub, J. H.; Aneed, A. E.; Cohen, A. M.; Joly, N. Structural Investigation of Bacterial Lipopolysaccharides by Mass Spectrometry and Tandem Mass Spectrometry. *Mass Spectrom. Rev.* **2010**, *29*, 606–650.
- (32) O'Brien, J. P.; Needham, B. D.; Brown, D. B.; Trent, M. S.; Brodbelt, J. S. Top-down Strategies for the Structural Elucidation of Intact Gram-Negative Bacterial Endotoxins. *Chem. Sci.* **2014**, *5*, 4291–4301.
- (33) Sturiale, L.; Garozzo, D.; Silipo, A.; Lanzetta, R.; Parrilli, M.; Molinaro, A. New Conditions for Matrix-Assisted Laser Desorption/Ionization Mass Spectrometry of Native Bacterial R-Type Lipopolysaccharides. *Rapid Commun. Mass Spectrom.* **2005**, *19*, 1829–1834.
- (34) Hankins, J. V.; Madsen, J. A.; Giles, D. K.; Childers, B. M.; Klose, K. E.; Brodbelt, J. S.; Trent, M. S. Elucidation of a Novel Vibrio Cholerae Lipid A Secondary Hydroxy-Acyltransferase and Its Role in Innate Immune Recognition. *Mol. Microbiol.* **2011**, *81*, 1313–1329.

- (35) Hankins, J. V.; Madsen, J. A.; Giles, D. K.; Brodbelt, J. S.; Trent, M. S. Amino Acid Addition to *Vibrio Cholerae* LPS Establishes a Link between Surface Remodeling in Gram-Positive and Gram-Negative Bacteria. *Proc. Natl. Acad. Sci.* **2012**, *109*, 8722–8727.
- (36) Nowicki, E. M.; O'Brien, J. P.; Brodbelt, J. S.; Trent, M. S. Extracellular Zinc Induces Phosphoethanolamine Addition to *Pseudomonas Aeruginosa* Lipid A via the ColRS Two-Component System. *Mol. Microbiol.* **2015**, *97*, 166–178.
- (37) Ko, B. J.; Brodbelt, J. S. 193 nm Ultraviolet Photodissociation of Deprotonated Sialylated Oligosaccharides. *Anal. Chem.* **2011**, *83*, 8192–8200.
- (38) Varki, A.; Cummings, R. D.; Aebi, M.; Packer, N. H.; Seeberger, P. H.; Esko, J. D.; Stanley, P.; Hart, G.; Darvill, A.; Kinoshita, T.; Prestegard, J. J.; Schnaar, R. L.; Freeze, H. H.; Marth, J. D.; Bertozzi, C. R.; Etzler, M. E.; Frank, M.; Vliegenthart, J. F.; Lütke, T.; Perez, S.; Bolton, E.; Rudd, P.; Paulson, J.; Kanehisa, M.; Toukach, P.; Aoki-Kinoshita, K. F.; Dell, A.; Narimatsu, H.; York, W.; Taniguchi, N.; Kornfeld, S. Symbol Nomenclature for Graphical Representations of Glycans. *Glycobiology* **2015**, *25*, 1323–1324.
- (39) Holden, Dustin; Canterbury, Jesse; Zhuk, Eugene; Izgarian, Nick; Schwartz, Jae; Brodbelt, Jennifer S. Top Down Protein Analysis by Ultraviolet Photodissociation (UVPD) in an Orbitrap Tribrid Mass Spectrometer. In *62nd American Society for Mass Spectrometry and Allied Topics*; Baltimore, MD, 2014.
- (40) Raetz, C. R. H.; Garrett, T. A.; Reynolds, C. M.; Shaw, W. A.; Moore, J. D.; Smith, D. C.; Ribeiro, A. A.; Murphy, R. C.; Ulevitch, R. J.; Fearn, C.; Reichart, D.; Glass, C. K.; Benner, C.; Subramaniam, S.; Harkewicz, R.; Bowers-Gentry, R. C.; Buczynski, M. W.; Cooper, J. A.; Deems, R. A.; Dennis, E. A. Kdo2-Lipid A of *Escherichia Coli*, a Defined Endotoxin That Activates Macrophages via TLR-4. *J. Lipid Res.* **2006**, *47*, 1097–1111.
- (41) Domon, B.; Costello, C. E. A Systematic Nomenclature for Carbohydrate Fragmentations in FAB-MS/MS Spectra of Glycoconjugates. *Glycoconj. J.* **1988**, *5*, 397–409.
- (42) Pupo, E.; Lindner, B.; Brade, H.; Schromm, A. B. Intact Rough- and Smooth-Form Lipopolysaccharides from *Escherichia Coli* Separated by Preparative Gel Electrophoresis Exhibit Differential Biologic Activity in Human Macrophages. *FEBS J.* **2013**, *280*, 1095–1111.
- (43) Nishikaze, T.; Kawabata, S.; Tanaka, K. Fragmentation Characteristics of Deprotonated N-Linked Glycopeptides: Influences of Amino Acid Composition and Sequence. *J. Am. Soc. Mass Spectrom.* **2014**, *25*, 988–998.
- (44) Amor, K.; Heinrichs, D. E.; Fridrich, E.; Ziebell, K.; Johnson, R. P.; Whitfield, C. Distribution of Core Oligosaccharide Types in Lipopolysaccharides from *Escherichia Coli*. *Infect. Immun.* **2000**, *68*, 1116–1124.

Chapter 6: Top-Down Characterization of Lipooligosaccharides from Antibiotic-Resistance Bacteria

6.1 OVERVIEW

Modification of lipopolysaccharide (LPS) and lipooligosaccharide (LOS) structures represents one prevalent mechanism by which Gram-negative bacteria can become resistant to key antibiotics. While the structural characterization of LPS has largely focused on elucidation of lipid A substructures, analysis of intact LPS/LOS enables detection of core oligosaccharide modifications and gives insight into the heterogeneity that results from combinations of lipid A and oligosaccharide substructures. Top-down analysis of intact LPS/LOS also provides the opportunity to determine unknown oligosaccharide structures which is particularly advantageous in the context of glycoconjugate vaccine development. Advances in mass spectrometry technologies, including the development of MSⁿ capabilities and alternative ion activation techniques, have made it an indispensable tool for structural characterization of complex biomolecules. Here we combine a chromatographic method that uses a three-part mobile phase with MS³ utilizing ultraviolet photodissociation (UVPD). This integrated approach was used to characterize LOS from *Acinetobacter baumannii* 5075 and *A. baumannii* 1205. Notably, MS³ spectra for *A. baumannii* 1205, an antibiotic resistant strain, confirmed phosphoethanolamine and hexosamine modification of the lipid A substructure and further enabled derivation of a core oligosaccharide structure.

6.2 INTRODUCTION

Multidrug- and pan-resistant bacteria pose one of the most serious public health threats to date.¹⁻⁵ Gram-negative bacteria are intrinsically resistant to many antibiotics effective against Gram-positive bacteria owing to their unique dual membrane architecture, of which the outer leaflet of the outer membrane is comprised predominantly of lipopolysaccharides (LPS) that form a protective barrier.⁵⁻⁸ LPS is composed of three covalently linked regions: (1) lipid A, the most highly conserved portion of LPS responsible for immune system stimulation, (2) core oligosaccharide (OS), which serves to stabilize the membrane structure and (3) O-antigen, a key bacterial virulence factor.⁹⁻¹¹ Various species of Gram-negative bacteria, including *Campylobacter jejuni*, *Neisseria meningitis*, *Bordetella pertussis*, and *Acinetobacter baumannii* naturally produce lipooligosaccharides (LOS), a rough-type LPS devoid of O-antigen.¹² A growing global threat is the development of resistance acquired from genomic changes in a manner that defeats antibiotics previously effective against Gram-negative bacteria. One mechanism of acquired resistance involves modification of the antibiotic target.⁵⁻⁷ In the context of Gram-negative bacteria, alterations in the structure of LPS/LOS, including non-stoichiometric addition of phosphoethanolamine (pEtN), aminoarabinose (Ara4N), and galactosamine (GalN) to the lipid A and core OS, have been shown to promote immune system evasion and influence susceptibility to cationic antimicrobial peptides (CAMPs).¹³⁻²⁰ The aforementioned modifications confer resistance by neutralizing anionic surface charge that promote CAMP affinity to the cell surface. An increasing number of Gram-negative species have been found to contain LPS/LOS modifications.²¹⁻²⁸ For example, several strains of multi-drug resistant *A. baumannii*, a pathogen that causes nosocomial infections commonly treated with the CAMP colistin, a “last-resort”

antibiotic, have developed colistin-resistance through modification of lipid A with pEtN and GalN.^{27–29}

Comprehensive structural characterization of LPS/LOS is crucial considering the critical relationship between LPS/LOS structure and antibiotic resistance³ as well as the important role of LPS/LOS in the development of new therapeutics and vaccines.^{30,31} Glycoconjugate vaccines that couple antigenic surface carbohydrates to immune-system-stimulating carrier proteins have been successful for a number of bacterial species.^{32,33} While bacterial surface carbohydrates appear to be ideal candidates for vaccine development, they cause a T-cell independent immune response which results in poor protective immunity.³² Conjugation of carbohydrate structures to proteins that elicit a T-cell dependent response and impart protective immunity is the cornerstone of glycoconjugate vaccines. Development of new glycoconjugate vaccines relies on identification of surface targets, including LPS/LOS.³⁴ Structural characterization of surface antigens that show promise for glycoconjugate construction is pivotal, especially in the context of antibiotic-resistant bacteria for which effective vaccines are critical.³⁵

Mass spectrometry (MS) has become a primary method for analysis of LPS/LOS.³⁶ Challenges associated with LPS solubility and heterogeneity have led to the development of methods that decompose LPS/LOS and analyze its constituent lipid A and polysaccharide portions, often in conjunction with separation by liquid chromatography (LC) or capillary electrophoresis (CE).^{36–44} Decomposition of LPS/LOS simplifies its analysis but likely underrepresents the true heterogeneity that results from combinations of structures and modifications occurring on the lipid A and polysaccharide portions. Additionally, decomposition has the potential to remove biologically relevant labile modifications.⁴⁴ Intact LPS/LOS analysis is therefore a more desirable analytical goal. Of the studies that have investigated intact LPS/LOS, most directly analyze

complex mixtures in a shotgun-type approach without separation.^{44–54} The shotgun mode can lead to signal suppression as well as generation of tandem mass spectra that are challenging to interpret owing to co-isolation of isobaric and isomeric species (the chimera spectra problem). Only a few studies have reported online electrophoretic or chromatographic separations of intact LPS/LOS.^{45,46,55} From these past reports, CE separations resulted in reduced sensitivity and peak broadening owing to the deleterious mixing of the make-up liquid with background electrolyte,⁴⁶ and LC separations suffered from sub-par efficiency for intact LPS/LOS.⁴⁵

For structural characterization of intact LPS/LOS or its decomposition products (e.g., lipid A and oligosaccharides), tandem mass spectrometry (MS^2 , MS^3 , MS^n) is employed.³⁷ Low-energy collision-induced dissociation (CID), the most widely available ion activation method, has been utilized to disassemble LPS/LOS into lipid A and oligosaccharide sections that can be correlated to intact LPS/LOS structures.^{52,53} However, owing to its low energy deposition that results in preferential cleavage of the most labile bonds, CID often produces tandem mass spectra lacking fragments necessary to determine subtle yet important structural features including saccharide branching patterns and the locations of non-stoichiometric modifications.⁴¹ Ultraviolet photodissociation (UVPD) at 193 nm, an alternative activation method that uses high energy photons to energize ions, has been shown to provide additional acyl chain, glycosidic, and cross-ring cleavages for both lipid A and intact LOS.^{41–43,45,52,56} Implementation of UVPD on high resolution mass spectrometers has enabled acquisition of rich tandem mass spectra generated from a variety of complex biomolecules.^{52,57} A number of the UVPD methods developed for lipid A and LPS/LOS characterization use MS^n methods that are advantageous from the standpoint of spectral interpretation.^{29,43,52} One such method entails collisional activation for bisection of intact LOS and subsequent

UVPD on the resulting lipid A and oligosaccharide portions.⁵² To further advance the characterization of LPS/LOS in increasingly complex samples, coupling MSⁿ methods that enable detailed structural characterization with online chromatography for separation of mixtures presents an attractive means to acquire high quality data in a high throughput manner, as detailed here.

The present method provides unprecedented chromatographic separation of intact LOS and enables acquisition of high resolution MS³ data on an LC timescale. For each sample a data-dependent CID analysis is first performed to identify the lipid A and core OS portions of chromatographically-separated LOS. A second MS³ analysis targeting the identified lipid A and core OS portions allows detailed structural characterization. This strategy is highlighted for analysis of LOS isolated from various strains of *A. baumannii*, including a clinically relevant antibiotic-resistant strain. LOS structures are identified, and new oligosaccharide structures are deciphered.

6.3 EXPERIMENTAL

6.3.1 Materials and Reagents

Escherichia coli R3 LOS was purchased from Glycobiotech (Research Center Borstel, Germany) and used without further purification. All *A. baumannii* LOS were isolated using a hot-phenol extraction described below.⁵⁸ HPLC-grade methanol (MeOH) and water (H₂O) were obtained from EMD Millipore (Billerica, MA), and chloroform (CHCl₃) was obtained from Sigma-Aldrich (St. Louis, MO). LC/MS grade ammonium acetate was purchased from Fisher Scientific (Fairlawn, NJ).

6.3.2 LOS Isolation

250 mL cultures of each strain were grown at 37°C to an OD ~ 1.0. Cells were pelleted at 5000xg, frozen, and lyophilized. Dried bacteria were resuspended in ddH₂O to a concentration of 20 mg/mL and transferred to a 250 mL Teflon centrifuge tube. An equal volume of 80% w/v phenol was added to the sample, and incubated with shaking at 65°C for 1 hour.⁵⁸ The mixture was cooled on ice and centrifuged at 5000xg for 30 min at room temperature. The upper aqueous layer was transferred to a glass flask. The extraction was repeated once more via the addition of an equal volume of ddH₂O to the residual organic phase. The combined aqueous phases were dialyzed against ddH₂O for 24 hours with a MWCO of 3500, with a minimum of 6 exchanges. To remove any insoluble material, the aqueous solution was centrifuged at 17k x g for 20 minutes at RT and the supernatant was lyophilized. The dried LPS sample was resuspended in 10 mL of 10 mM Tris, pH 7.8 and transferred to a 50 mL Teflon centrifuge tube. RNase and DNase I were added to a final concentration of 25 µg/mL and 100 µg/mL respectively and incubated for 2 hours at 37°C. Proteinase K was added to a concentration of 100 µg/mL and incubated at 37 °C for 2 hours. The proteinase treatment was repeated once. After enzymatic treatments, 5 mL of water saturated phenol was added to the sample, vortexed, and the phases were separated via centrifugation at 5000 x g for 30 mins at RT. The upper aqueous phase was removed and dialyzed for 12 hours against ddH₂O at 4°C with a MWCO of 3500 with a total of 5 exchanges. Dialyzed solution was centrifuged at 17k x g for 20 mins at RT to remove insoluble material prior to lyophilization. Final lyophilized product was resuspended to a concentration of ~ 10 mg/mL in endotoxin free ddH₂O.

6.3.3 Liquid Chromatography and Mass Spectrometry

Separations were performed using a Dionex Ultimate 3000 microflow liquid chromatography system (Sunnyvale, CA) equipped with a Dikma Bio-Bond C8 column (2.1 mm X 150 mm, 3 μ m particle size) (Lake Forest, CA) heated to 65°C. Mobile phase A consisted of 62:36:2 MeOH:H₂O:CHCl₃, mobile phase B consisted of 80:20:2 CHCl₃:MeOH:H₂O, and mobile phase C consisted of 62:36:2 MeOH:H₂O:CHCl₃ with 100 mM ammonium acetate.⁵⁵ Chromatographic runs were performed at flow rate of 400 μ L/min. From 0 to 2 minutes the solvent composition was held at 15% B, followed by a linear gradient over the next 18 minutes to a final composition of 30% B. The mobile phase composition was then held at 30% B for 10 minutes and then returned to 15% B for a 10 minute re-equilibration period. Mobile phase C was held at 2% during the entire chromatographic run to ensure a constant ammonium acetate concentration of 2 mM. Samples were diluted such that their final solvent composition was 62:36:2 MeOH:H₂O:CHCl₃. For *E. coli* R3, 1 μ g of sample was injected. For all *A. baumannii* samples, 20 μ L of solution was injected. Chromatographic separations were coupled online to a Thermo Scientific Orbitrap Fusion Lumos mass spectrometer (San Jose, CA) modified with a 193 nm Coherent Existar excimer laser (Santa Clara, CA) via electrospray ionization as previously described.⁵² All experiments were performed in negative ion mode using Orbitrap detection with an electrospray voltage of 4.5 kV. The sheath gas and auxiliary gases were set to 50 and 25 arbitrary units, respectively, and the ion transfer tube temperature was set to 300°C. For each sample, three chromatographic runs were performed: (1) a data-dependent CID survey analysis, (2) a targeted MS³ CID/HCD analysis and (3) a targeted MS³ CID/UVPD analysis. For the data-dependent CID survey analysis, MS¹ spectra were collected at a resolving power of 30,000 at m/z 200 with a mass range of m/z 450-2000, and CID spectra were collected at a resolving

power of 15,000 with a normalized collision energy (NCE) of 25. For CID, precursor ions were accumulated in the ion trap using quadrupole isolation with an isolation width of m/z 3. For MS¹ and CID spectra, AGC targets were set to 5E5 and 2E5, respectively. From the data-dependent CID survey analysis, a list of specific MS³ transitions was manually generated. Two MS³ transitions, a lipid A fragment ion and a core OS fragment ion, were targeted for each intact LOS ion, with transitions targeted at specific times during the chromatographic run. All MS³ data was collected at resolving power of 15,000 at m/z 200. For CID/HCD spectra, HCD was performed with an NCE of 30. For CID/UVPD, UVPD was performed with 10 laser pulses at 2-4 mJ per pulse, corresponding to a 20 ms ion activation time. All spectra were collected with a maximum ion injection time of 300 ms and 2 μ scans per scan.

6.3.4 Data Analysis

LOS structures are depicted using the official Symbol Nomenclature for Glycans (SNFG) (**Figure 6.1**).⁵⁹ All spectra were manually interpreted. Identified fragment ions corresponding to glycosidic and cross-ring saccharide cleavages are mapped on to LOS structures using Domon and Costello nomenclature.⁶⁰ Acyl cleavages are numbered on the lipid A substructure. Acyl chain neutral losses are labeled as [M-X]⁻ where X represents the numbered cleavages. Acyl chain fragment ions are just listed as numbers. In MS² spectra, fragment ions with multiple cleavages are labeled with “-” between different cleavages. For example, [B₆-Y_{3 β}]⁻ indicates a fragment ion with two cleavage points. For MS³ spectra, fragment ions are labeled as though they originate from the intact LOS structure. It is implied that all MS³ fragment ions are generated from either a B or Y MS² fragment ion; the MS² cleavage is therefore not included in the labels of all MS³ fragment ions. Presented MS² and MS³ spectra are averages of multiple scans and

are labeled with either m/z values or according to previously mentioned fragment ion nomenclature.

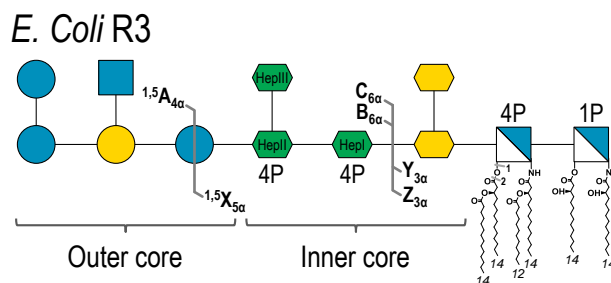
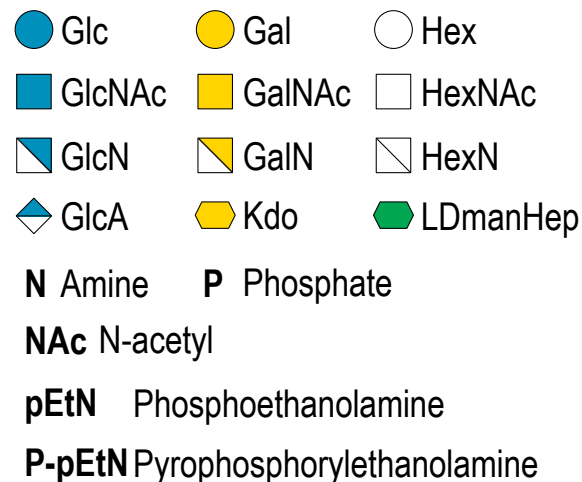


Figure 6.1 Key of saccharide symbols used in the official Symbol Nomenclature for Glycans (SNFG). Hexa-acylated *E. coli* R3 LOS is provided as an example to show how LOS structures are depicted. Fragments are labeled on LOS structures using Domon and Costello nomenclature.^{59,60}

6.4 RESULTS AND DISCUSSION

Analysis of intact LPS/LOS by tandem mass spectrometry gives insight into the structural heterogeneity that can result from combinations of lipid A and oligosaccharides structures. With such complexity, it is essential to perform chromatographic separations to alleviate the suppression of low abundance species that is inevitable during ESI of complex mixtures and to mitigate the production of chimeric tandem mass spectra which

confounds interpretation and thwarts assignment of structures. However, few methods have been developed that provide high quality separations given the limited solubility of LPS/LOS. The chromatographic method used throughout this work is an adaptation of the method developed by Raetz and co-workers for the evaluation of 3-deoxyl-D-mannooctulosonic acid (Kdo)₂-lipid A, the simplest LOS structure.⁵⁵ This prior protocol used a two-part mobile phase; mobile phase A consisted of 62:36:2 MeOH:H₂O:CHCl₃ with 20 mM ammonium acetate and mobile phase B consisted of 80:20:2 CHCl₃:MeOH:H₂O with 50 mM ammonium acetate.⁵⁵ As detailed in the present work, the ammonium acetate was removed from mobile phases A and B, and a third mobile phase was added which consisted of 62:36:2 MeOH:H₂O:CHCl₃ with 100 mM ammonium acetate. Addition of mobile phase C enabled tunability of the ammonium acetate concentration to alleviate ESI signal suppression caused by excess salts.⁶¹ Mobile phase C was held at 2% of the mobile phase composition, thus maintaining a constant 2 mM concentration of ammonium acetate throughout the separation. The use of this three-part mobile phase afforded unparalleled separation efficiency.

LOS from *E. coli* R3, an O-antigen-deficient mutant strain of *E. coli* containing the R3 core type, served as a benchmark mixture to allow assessment of the performance metrics of both the chromatographic and MSⁿ methods. **Figure 6.2** shows the base peak chromatogram of a data-dependent CID analysis of *E. coli* R3 with a series of extracted ion chromatograms. CID was previously determined as an effective means to bisect LOS, releasing lipid A and core oligosaccharide products which provide mass information about the lipid A and core oligosaccharide substructures and also allowed subsequent MS³ analysis.⁵² The masses of the CID fragment ions give insight into the degree of acylation and phosphorylation of the lipid A portion as well as the extent of modification of the core oligosaccharide portion.

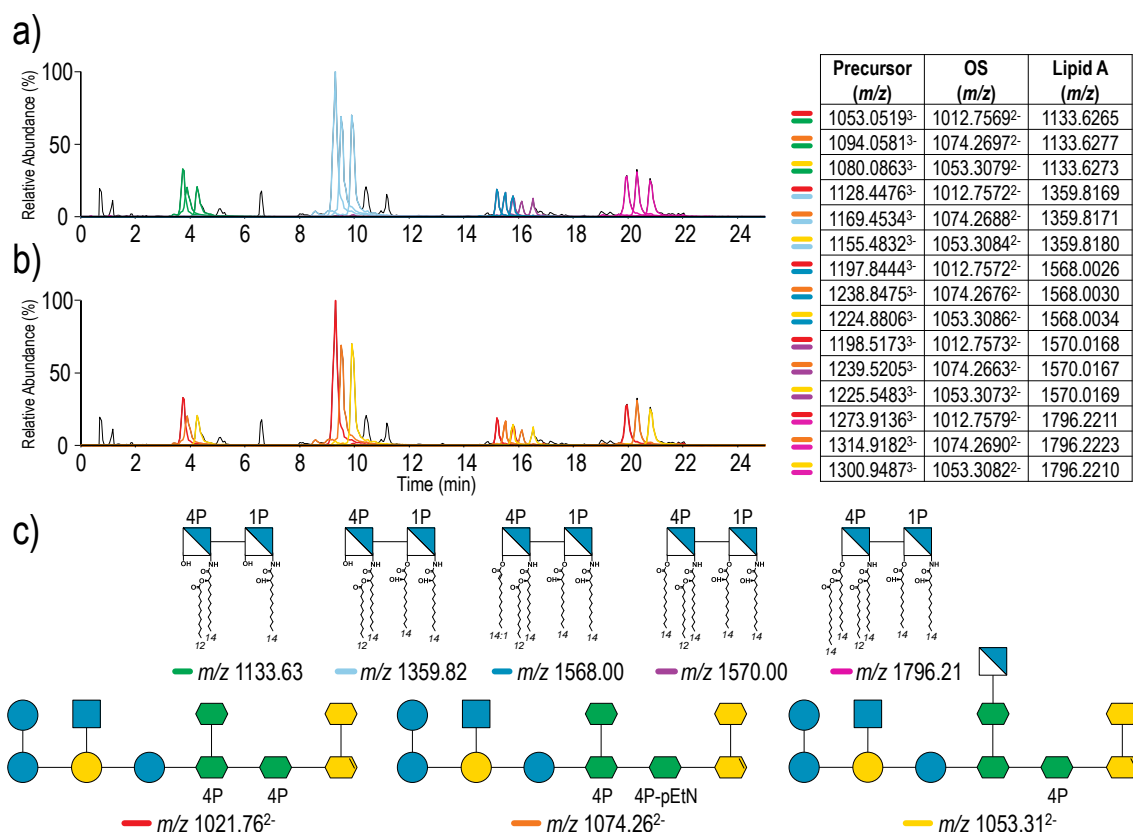


Figure 6.2 Base peak chromatograms of LOS from *E. coli* R3 with intact mass extracted ion chromatograms colored according to a) the lipid A substructure and b) the core oligosaccharide substructure. The table to the right of the extracted ion chromatograms lists the intact LOS m/z detected from MS¹ spectra and the m/z of each substructure detected from CID spectra. c) A color-coded key containing each lipid A and core oligosaccharide substructure with m/z . MS¹ and MS² spectra appear in **Figure 6.3**.

Previously published lipid A and core OS substructures of *E. coli* provide a guide for structural characterization of intact LOS of the R3 strain.^{55,62} Extracted ion chromatograms of each identified intact LOS species are color-coded in **Figure 6.2a** and **Figure 6.2b** according to the directory of lipid A and core oligosaccharide substructures in **Figure 6.2c**, respectively, and provide a visual representation of combinations of lipid A and core oligosaccharide substructures present in the intact LOS. The m/z values of

fragment ions from the LOS are summarized in the companion table (to the right of **Figure 6.2a, b**) with each species uniquely represented by two colored markers associated with the lipid A and core oligosaccharide structures in **Figure 6.2c**. MS¹ and CID spectra for all identified species are shown in **Figure 6.3**. Extracted ion chromatograms in **Figure 6.2a** occur in clusters and confirm a primary separation based on the lipid A substructure, with dramatic differences in retention times for increasingly acylated lipid A, in addition to separation based on more subtle lipid A structural features including degree of unsaturation. For example, CID of ions of m/z 1197.84, m/z 1238.85, m/z 1224.88, m/z 1198.52, m/z 1239.52, and m/z 1225.55 in the MS¹ spectra result in production of fragment ions indicative of a penta-acylated lipid A substructure (**Figure 6.3**). However, the product ion characteristic of the lipid A portion originating from LOS precursors of m/z 1197.85, m/z 1238.85, and m/z 1224.88 occurs at m/z 1568.00, whereas the lipid A portion evolving from CID of LOS precursors of m/z 1198.85, m/z 1239.52, and m/z 1225.55 appears at m/z 1570.01. The observed mass difference (~2 Da) between the lipid A substructure for each penta-acylated LOS corresponds to a single acyl chain unsaturation. The LOS structures with one unsaturated acyl chain elute earlier as a result of the overall decrease in hydrophobicity. This subtle structural feature that otherwise may be obscured using a shotgun method is resolved in the LC separation. **Figure 6.2b** confirms a secondary level of separation based on the variations in the core oligosaccharide structures. For example, structures with two core oligosaccharide phosphate modifications elute earlier than species with one phosphate modification and one pyrophosphorylethanolamine (P-pEtN) modification. As expected, a P-pEtN modification slightly increases the overall hydrophobicity and results in a longer retention time.

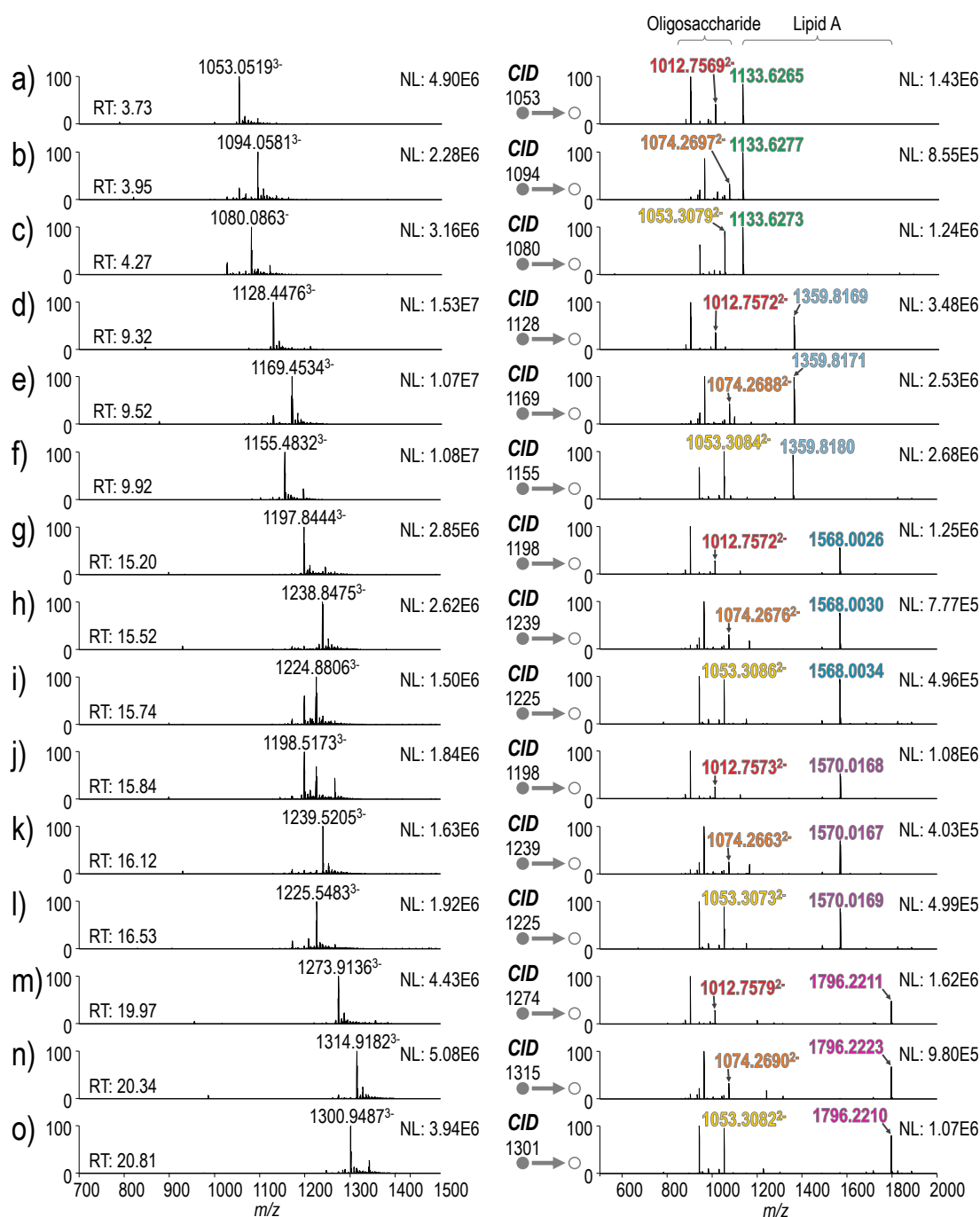


Figure 6.3 MS¹ and corresponding CID spectra for species detected in *E. coli* R3 LOS at the following chromatographic retention times in seconds: a) 3.73, b) 3.95, c) 4.27, d) 9.32, e) 9.52, f) 9.92, g) 15.20, h) 15.52, i) 15.74, j) 15.84, k) 16.12, l) 16.53, m) 19.97, n) 20.34, and o) 20.81.

For detailed structural characterization, the lipid A and core oligosaccharide substructures created by CID are subsequently activated using either higher-energy collisional dissociation (HCD) or UVPD. These two stage MS³ methods are designated as CID/HCD or CID/UVPD. These two stage MS³ methods are designated as CID/HCD or CID/UVPD. As an example, analysis of an intact LOS species (m/z 1155.48) composed of penta-acylated lipid A and a mono-phosphorylated core OS provides an opportunity to showcase the critical impact of using the MS³ method for characterization of each substructure and localization of specific structural features (**Figure 6.4**). Core OS and lipid A fragment ions identified during the data-dependent CID survey analysis of LOS were targeted for specific MS³ transitions. CID/HCD (**Figure 6.4d, f**) and CID/UVPD (**Figure 6.4c, e**) spectra were collected for the ions of m/z 1053.31 and 1359.81, corresponding to the lipid A and core OS moieties, respectively. HCD generally provides information on the presence of labile modifications via neutral loss fragments in addition to the saccharide linkage arrangement, whereas UVPD gives more detailed insight about saccharide branching and the positions of non-stoichiometric modifications. While acyl chain fragment ions in the spectra of the lipid A substructure (m/z 1359.81) confirm the acyl chain lengths (C₁₂ and C₁₄), other glycosidic and cross-ring cleavages confirm the acyl chain orientation, namely the presence of an O-linked acyl chain on the reducing end GlcN (**Figure 6.4e, f**). For the core oligosaccharide portion, both the intact mass of the core oligosaccharide ion in the CID spectrum (**Figure 6.4b**) and the resulting fragment ions in the companion CID/HCD (**Figure 6.4d**) and CID/UVPD (**Figure 6.4c**) spectra confirm that the ion of m/z 1053.31 corresponds to a core oligosaccharide containing a single phosphate modification and a GlcN modification. The fragment ion map in **Figure 2g** depicts the MS³ fragment ions from both the lipid A and core oligosaccharide substructures.

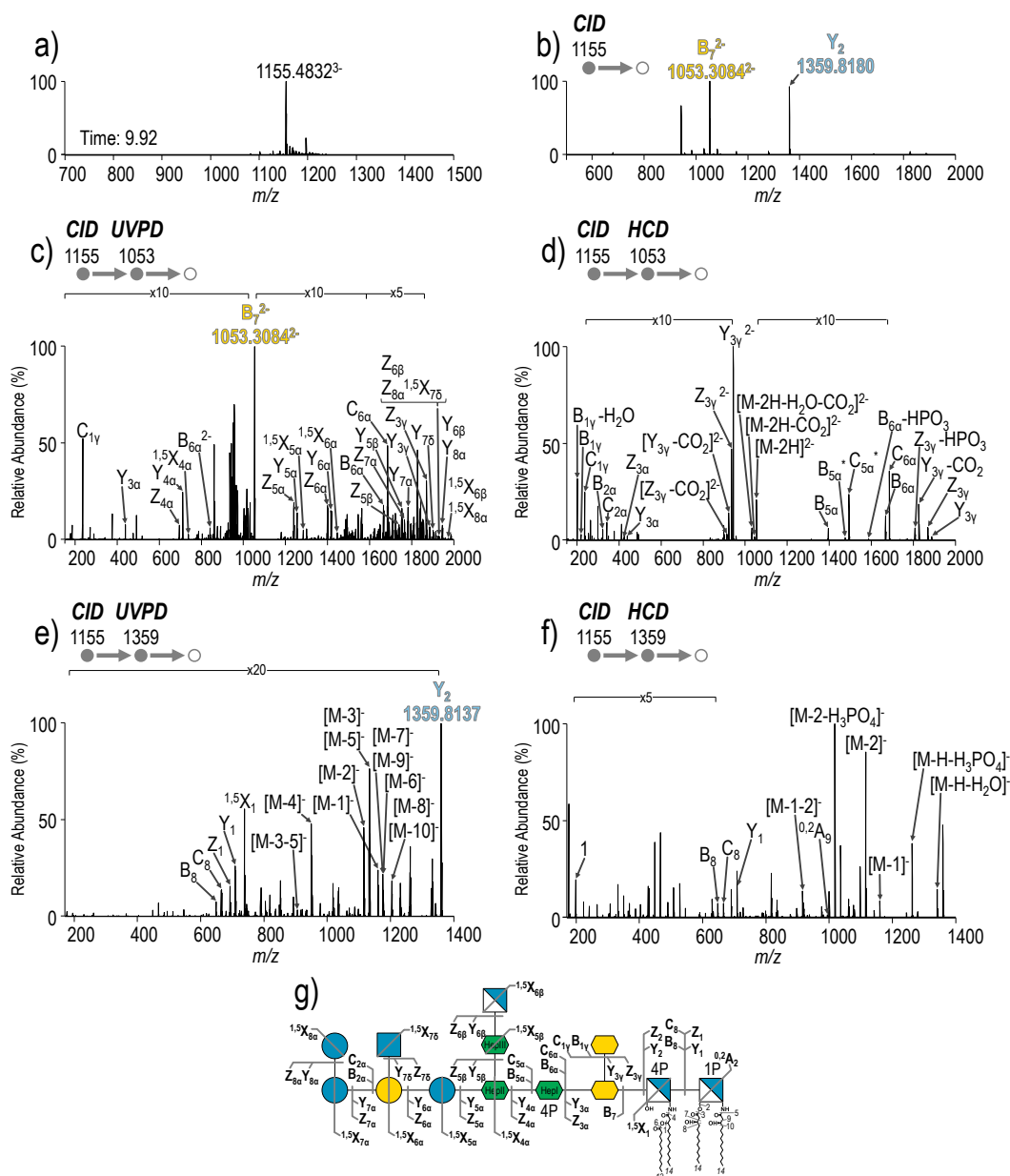


Figure 6.4 a) MS^1 spectrum of m/z 1155.48 $^{3-}$ from chromatographic separation of LOS from *E. coli* R3; b) CID spectrum of m/z 1155.48 $^{3-}$; c) targeted MS^3 CID/VPD and d) CID/HCD spectra of m/z 1053.31 $^{2-}$ corresponding to a core oligosaccharide substructure with a single phosphorylation and a GlcN modification; e) targeted MS^3 CID/VPD and f) CID/HCD spectra of m/z 1359.81 corresponding to a tetra-acylated lipid A substructure; g) Fragment ion map of the intact LOS structure mapping both CID/HCD and CID/VPD data. Fragment ion lists appear in **Table 6.1**.

There has been some debate as to whether HepIII is modified with GlcN or GlcNAc.¹³ While a previous study of *E. coli* R3 reported modification of HepIII with GlcN, a deacylation method was used to treat lipid A, which consequently also removed acetyl groups on the core oligosaccharide.⁶³ MS³ data of untreated intact LOS presented here unequivocally confirm modification of HepIII with GlcN. While non-stoichiometric modification of HepIII with GlcNAc may also occur, it happens at much lower non-stoichiometric abundance. Regarding the phosphate modification, in the CID/HCD spectrum (**Figure 6.4d**) fragment ions of m/z 1475.46 and m/z 1493.46 corresponding to B₅^{*} and C₅^{*} ions, respectively, indicate phosphorylation of HepII. Alternatively, fragment ions of m/z 739.14, m/z 711.14 and m/z 695.14 produced exclusively in the CID/UVPD spectrum (**Figure 6.4c**) correspond to ^{1,5}X₄, Y₄, and Z₄ ions, respectively, indicating phosphorylation of HepI. Previous studies reported that phosphorylation of the core oligosaccharide occurred exclusively at HepI when HepIII was modified with GlcN, suggesting that CID/UVPD can more confidently localize phosphate modifications on LOS structures.¹³

Figure 6.5 provides another example of the high level of structural characterization that is achieved with a targeted MS³ method. CID/HCD (**Figure 6.5c**) and CID/UVPD (**Figure 6.5d**) spectra of the ion of m/z 1796.21 are consistent with prior MS² data acquired for hexa-acylated lipid A from *E. coli*.⁴¹ Both the intact mass of the core oligosaccharide fragment ion in the CID spectrum (**Figure 6.3m**) and fragment ions in the CID/HCD (**Figure 6.5a**) and CID/UVPD (**Figure 6.5b**) spectra confirm that m/z 1012.76 corresponds to a core OS containing two phosphate modifications. Fragment ions in both CID/HCD and CID/UVPD spectra of m/z 1314.38 and m/z 1332.38 correspond to B₅ and C₅ ions with a single phosphorylation of HepII.

Y_5 , Z_5 , $^{1,5}X_4$, Y_4 , Z_4 and $^{1,5}X_3$ ions that occur exclusively in the CID/UVPD mass spectrum (**Figure 6.5b**) confirm phosphorylation of HepI and HepII. In conclusion, while CID/HCD provides complementary information to CID/UVPD regarding the saccharide composition, CID/UVPD provides fragmentation that uniquely allows confident localization of modifications.

A. baumannii is an opportunistic pathogen that exclusively produces LOS and is among the list of “ESKAPE” pathogens that pose the greatest threat to public health.⁶⁴ *A. baumannii* has developed antibiotic resistance via a number of mechanisms including LOS modification; infections caused by *A. baumannii* are therefore increasingly challenging to treat.⁶⁵ *A. baumannii* 19606 is a strain for which the deacylated LOS structures, but not intact LOS, have been determined previously.⁶⁶ **Figure 6.6** shows a base peak chromatogram for LOS isolated from *A. baumannii* 19606. Four of the predominant intact LOS structures identified herein, shown through a series of extracted ion chromatograms (**Figure 6.6a**), are consistent with combinations of two oligosaccharide structures determined for *A. baumannii* 19606, and two hexa-acylated and hepta-acylated lipid A structures previously determined for *A. baumannii* 17978.^{67,68} The m/z values of the intact LOS and CID product ions for all identified LOS species are shown in **Figure 6.6** (right side). MS¹ and CID spectra are shown in **Figure 6.7**. **Figure 6.6b** shows fragment ion maps combining CID/HCD and CID/UVPD data for two intact LOS structures, ones corresponding to m/z 1191.23 (identified in **Figure 6.7a** and characterized in **Figures 6.8a, e** and **6.9a, e**) and m/z 1049.89 (identified in **Figure 6.7l** and characterized in **Figure 6.8d, h** and **6.8d, h**) that represent two combinations containing all four lipid A and core OS substructures. CID/HCD and CID/UVPD spectra confirmed that the lipid A and core OS substructures are consistent with the previous findings obtained for truncated species.^{66–68}

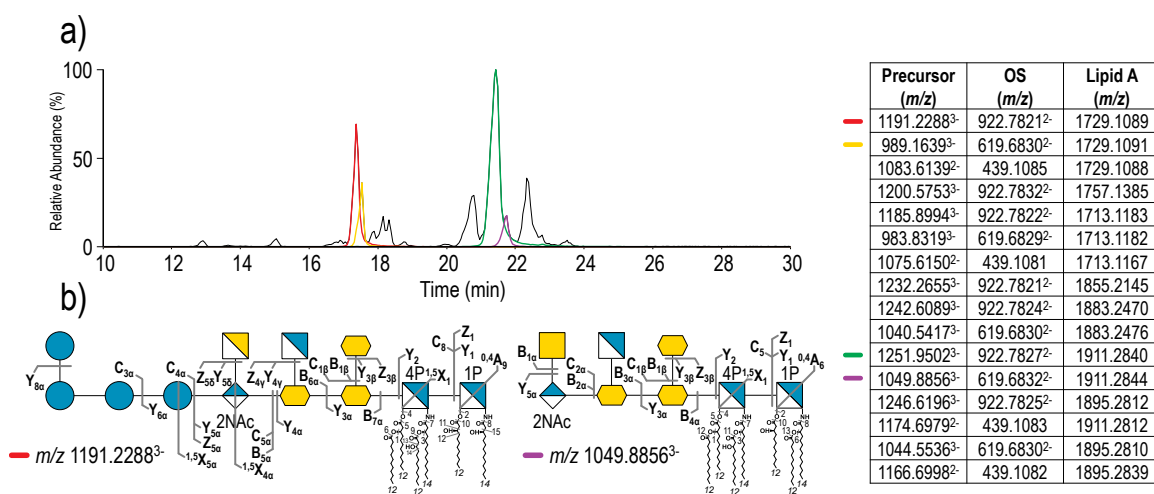


Figure 6.6 Structural characterization of LOS from *A. baumannii* 19606. a) Base peak chromatogram of *A. baumannii* 19606 LOS with intact mass extracted ion chromatograms. The table to the right of the extracted ion chromatogram lists the intact LOS m/z detected from MS¹ spectra and the m/z of each substructure detected from CID spectra. b) Fragment ion maps for intact LOS structures mapping both CID/HCD and CID/VPD (10 pulses, 4 mJ) data: decasaccharide core with hexa-acylated lipid A (left) and truncated core hexasaccharide core with hepta-acylated lipid A (right). MS³ spectra appear in **Figure 6.8** and **Figure 6.9**. Fragment ion lists appear in **Table 6.3** and **Table 6.4** (Supporting Information, Chapter 6). Colored markers in the table represent m/z values of intact LOS species and correspond to the colored extracted ion chromatograms in part a).

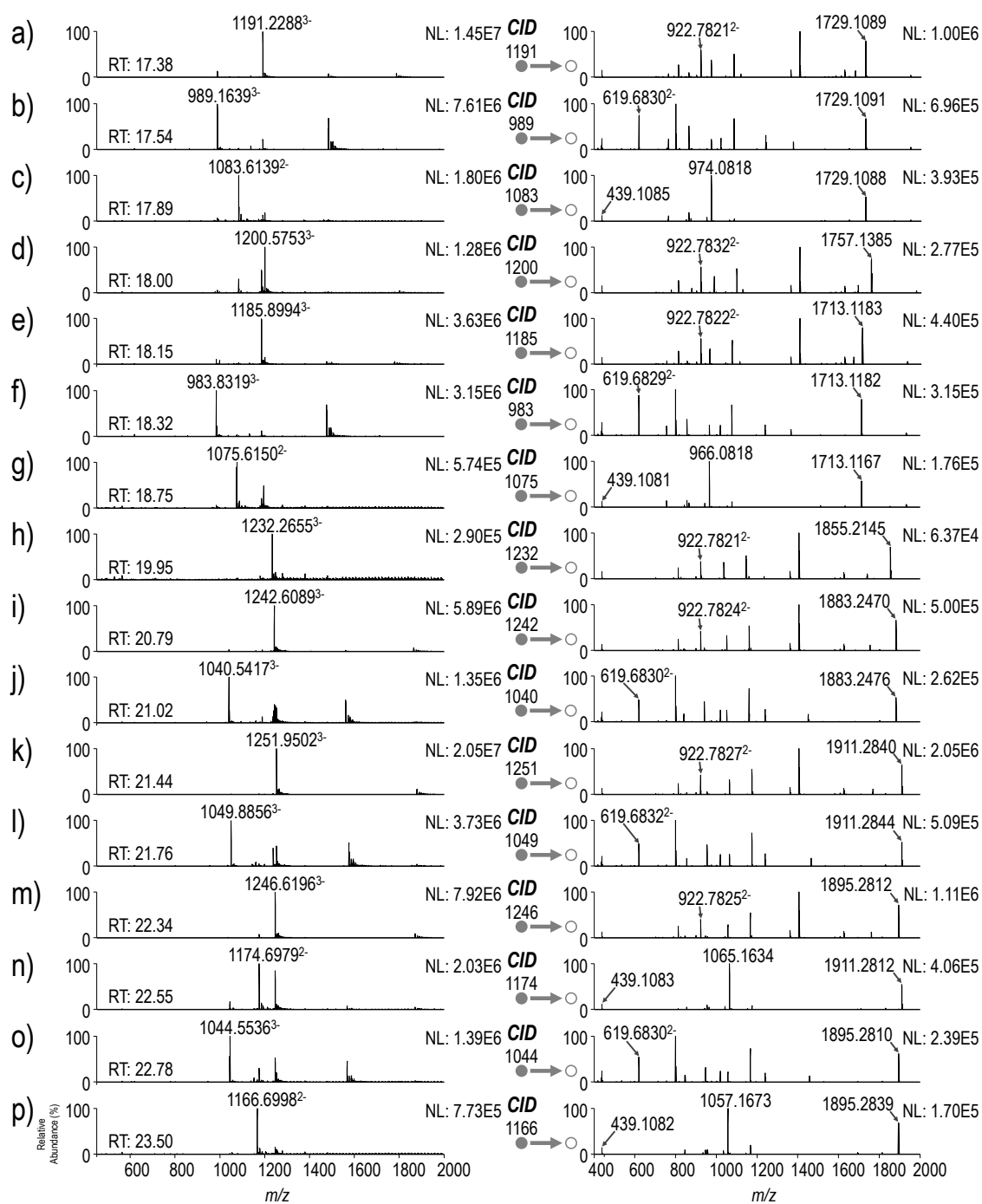


Figure 6.7 MS¹ and corresponding CID spectra for species detected in *A. baumannii* 19606 LOS.

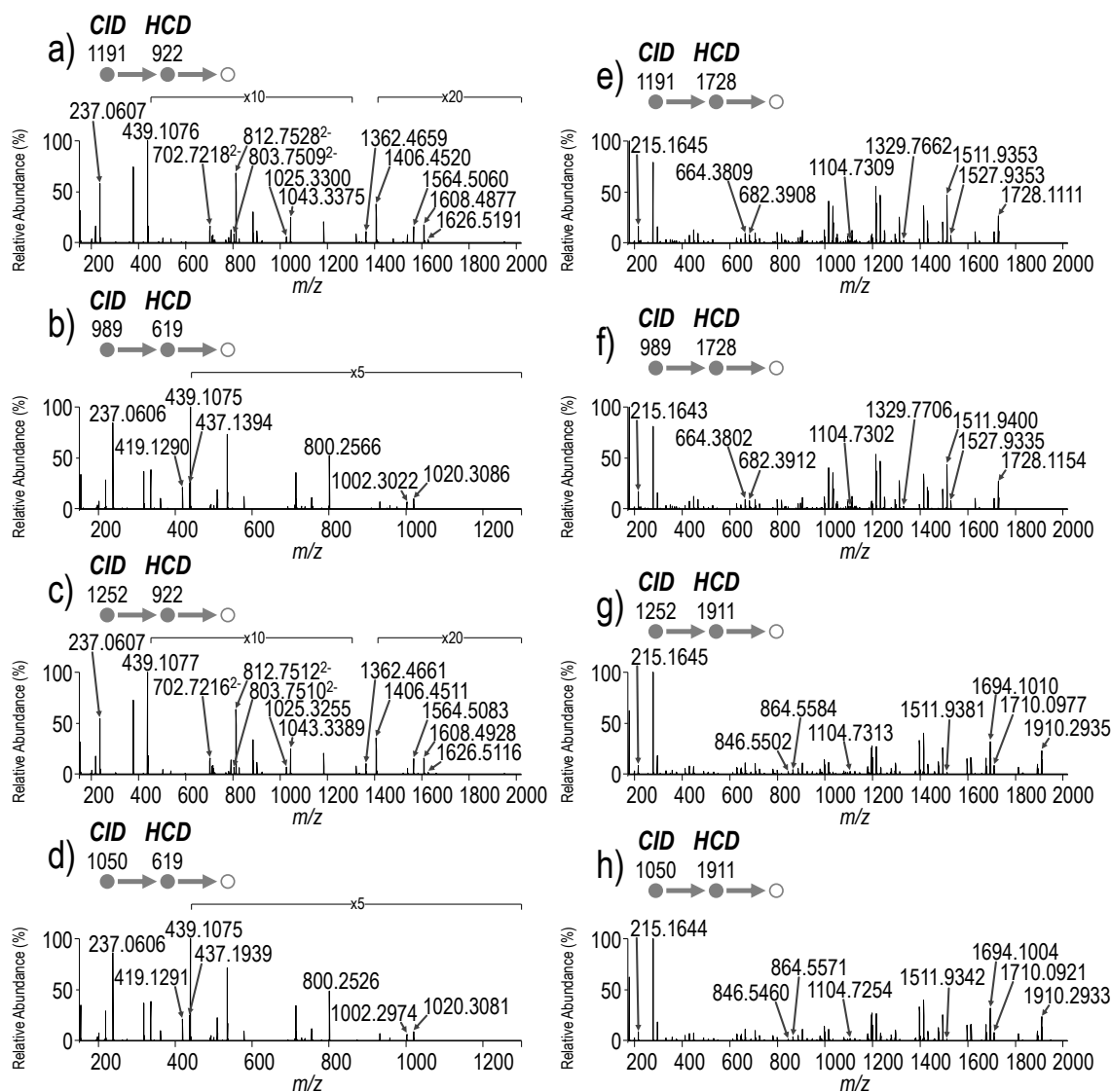


Figure 6.8 Targeted MS³ CID/HCD spectra of the core OS and lipid A substructure of four LOS structure from *A. baumannii* 19606. Fragment ion lists appear in **Table 6.3** (Supporting Information, Chapter 6).

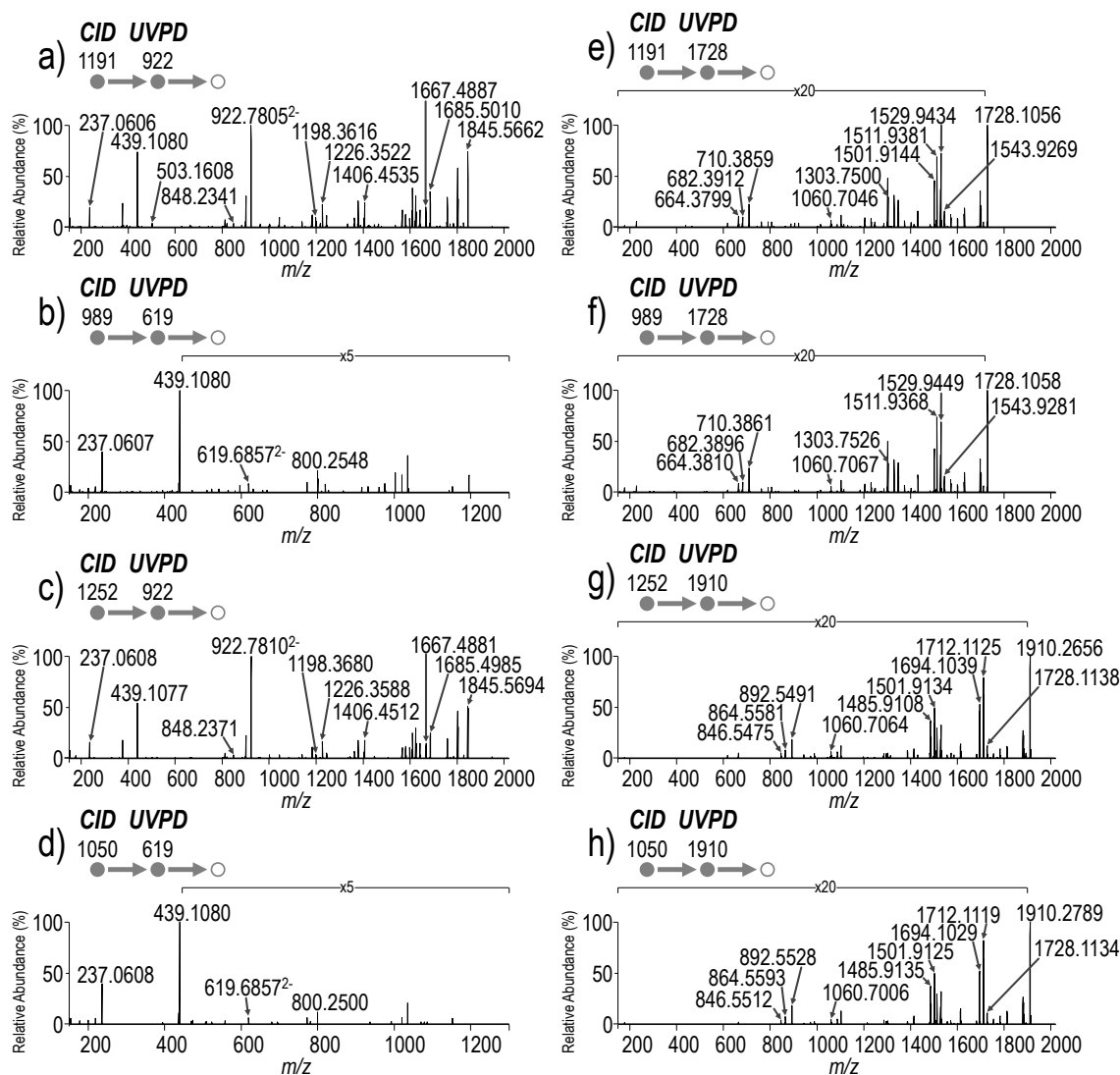


Figure 6.9 Targeted MS³ CID/UPVD (10 pulses, 4 mJ) spectra of the core OS and lipid A substructure of four LOS structure from *A. baumannii* 19606. Fragment ion lists appear in **Table 6.4** (Supporting Information, Chapter 6).

MS³ spectra obtained for all four LOS structures are shown in **Figure 6.8** (CID/HCD) and **Figure 6.9** (CID/UPVD). Most importantly, this analysis of MS³ spectra makes obvious that information regarding the combinations of lipid A and core oligosaccharide substructures is incomplete or even lost when traditional structural characterization

methods that rely on separation of LOS and analysis of extracted lipid A and oligosaccharide sections are used.

The newly developed MS³ method also provides the opportunity to investigate *A. baumannii* strains for which the core OS structures are unknown. Understanding the core OS structure of species that deviate from the most studied *E. coli* and *S. enterica* opens up doors for forward genetics to identify enzymes that help assemble the core OS. This knowledge assists in the development of potential new antibiotic targets and glycoconjugate vaccine platforms. To showcase the compelling analytical impact of the MS³ strategy, structural characterization of *A. baumannii* 5075 was undertaken. The LC trace obtained for *A. baumannii* 5075 is shown in **Figure 6.10**. For the initial data-dependent CID survey analysis, many of the m/z values of the lipid A substructures match ions found in *A. baumannii* 19606, qualitatively suggesting a similar lipid A composition for *A. baumannii* 5075. Based on the m/z values observed in the MS¹ spectra (**Figure 6.10**) and the corresponding lipid A fragment ions observed in the CID spectra (**Figure 6.10**), m/z values for the intact core OS fragment ion were determined. For example, the intact LOS species of m/z 1164.56 in the 3- charge state eluting at 17.66 min produces a CID spectrum with a lipid A fragment ion of m/z 1728.11 (**Figure 6.10b**). Therefore, the theoretical m/z of the core OS ion in the 2- charge state is calculated to be m/z 882.79 (corresponding to a net mass of 1767.59 Da). This theoretical m/z value matches the detected fragment ion of m/z 882.78 (**Figure 6.10b**). This core OS fragment ion was common in many of the CID mass spectra (**Figure 6.10**) and was selected as a target for MS³ analysis.

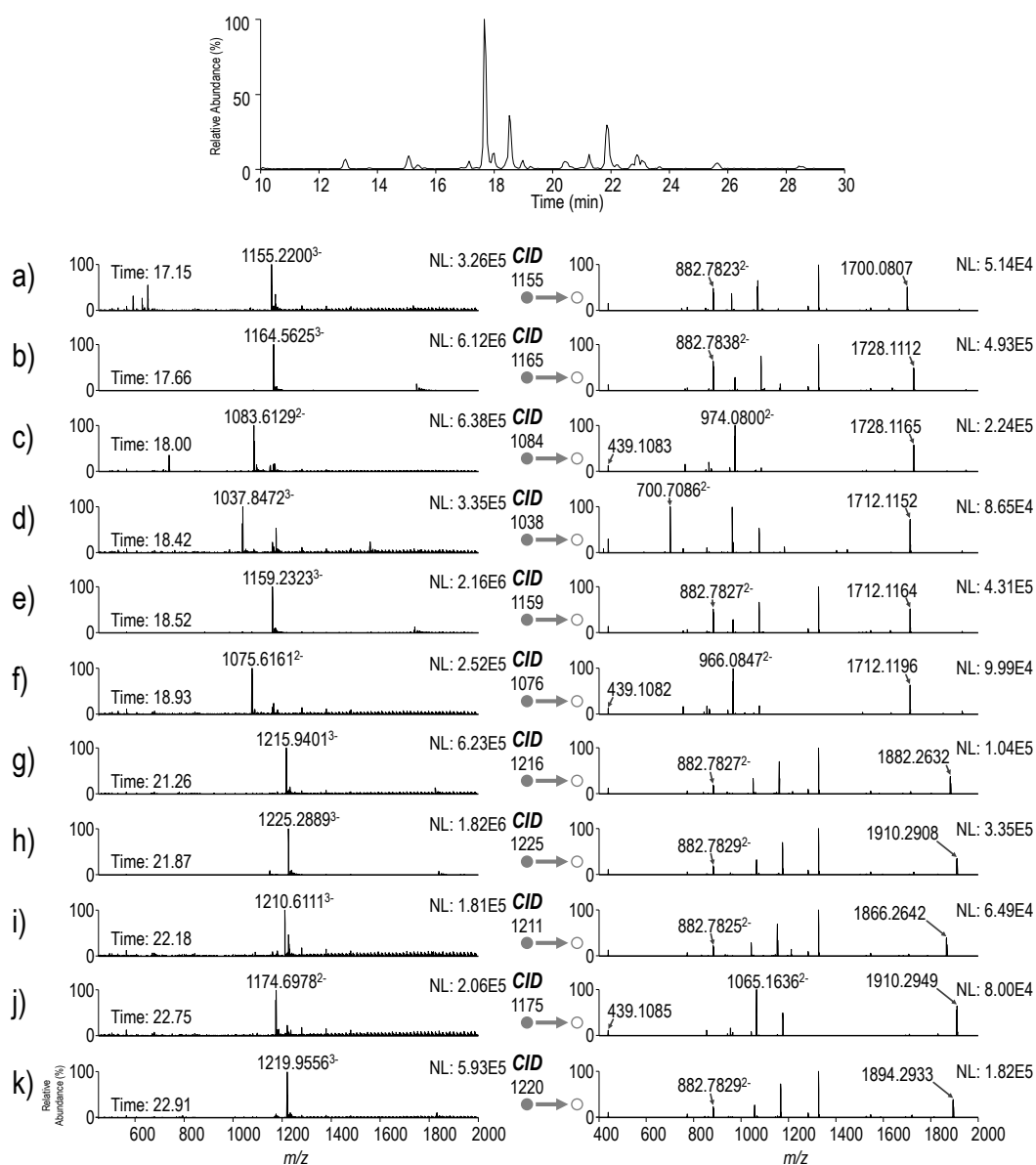
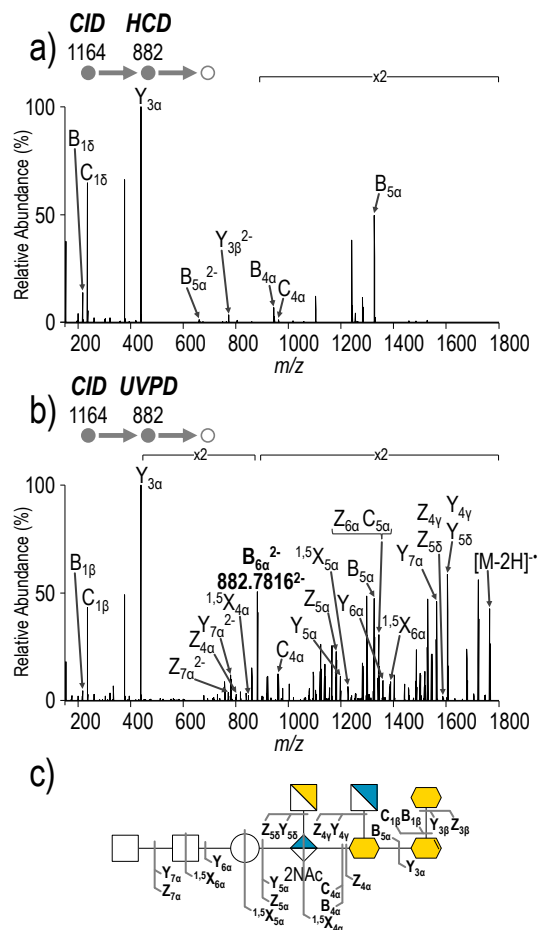


Figure 6.10 Base peak chromatogram, and MS¹ and corresponding CID spectra for species detected in *A. baumannii* 5075 LOS at the following chromatographic retention times in seconds: a) 17.15, b) 17.66, c) 18.00, d) 18.42, e) 18.52, f) 18.93, g) 21.26, h) 21.87, i) 22.18, j) 22.75, and k) 22.91.

Based on the intact mass of the core OS fragment ion and manual *de novo* saccharide analysis of the CID/HCD (**Figure 6.11a**) and CID/UVPD (**Figure 6.11b**) spectra, a core OS structure is derived for *A. baumannii* 5075 in **Figure 6.11c**. The CID/UVPD spectrum

(**Figure 6.11b**) is dense with informative fragments including both glycosidic and cross-ring cleavages that enable confident assignment of the saccharide arrangement. These results suggest a conserved inner core structure terminating with GlcANac, and different outer core structures for each strain.



In contrast to the *A. baumannii* 19606 outer core structure which is composed of four linearly linked Glc saccharides, the *A. baumannii* 5075 outer core structure is composed of one Hex and two HexNAc saccharides. In addition, the CID spectra (**Figure 6.10c, d, f, j**) suggest that *A. baumannii* 5075 also produces LOS structures with truncated core oligosaccharides. Three of the identified species produce a core OS ion of m/z 439.11 (**Figure 6.10c, f, j**), which corresponds to two Kdo saccharides, and one species produced a yet unidentified core OS ion of m/z 700.71 (**Figure 6.10d**).

Structural characterization was performed in a similar manner for *A. baumannii* 1205, an antibiotic-resistant strain containing modified lipid A (**Figure 6.12**). Based on CID (**Figure 6.13**), CID/HCD and CID/UVPD (**Figures 6.14-6.19**, Supporting Information, Chapter 6) spectra, all of the lipid A substructures were hexa- or hepta-acylated and were found to contain either phosphoethanolamine or galactosamine modifications, as previously described for this strain.²⁷ While intact core OS ions of m/z 1725.54 and m/z 862.26 were detected, their abundances were not optimal for detailed MS³ analysis. Therefore, an ion of m/z 1285.43, corresponding to the core OS ion lacking two Kdo saccharides was selected for targeted MS³ analysis (**Figure 6.12b, c**). Again, the inner core structure is consistent with *A. baumannii* 19606, and the outer core structure is composed of two Hex and one HexNAc saccharides arranged linearly. While the MS³ spectra for both *A. baumannii* 5075 and *A. baumannii* 1205 confirm linear connectivity of the outer core saccharides, the specific linkage positions or the types of hexoses could not be confirmed. For this reason, the outer core saccharides are not colored in the fragment ion maps in **Figure 6.11c** and **Figure 6.12c**.

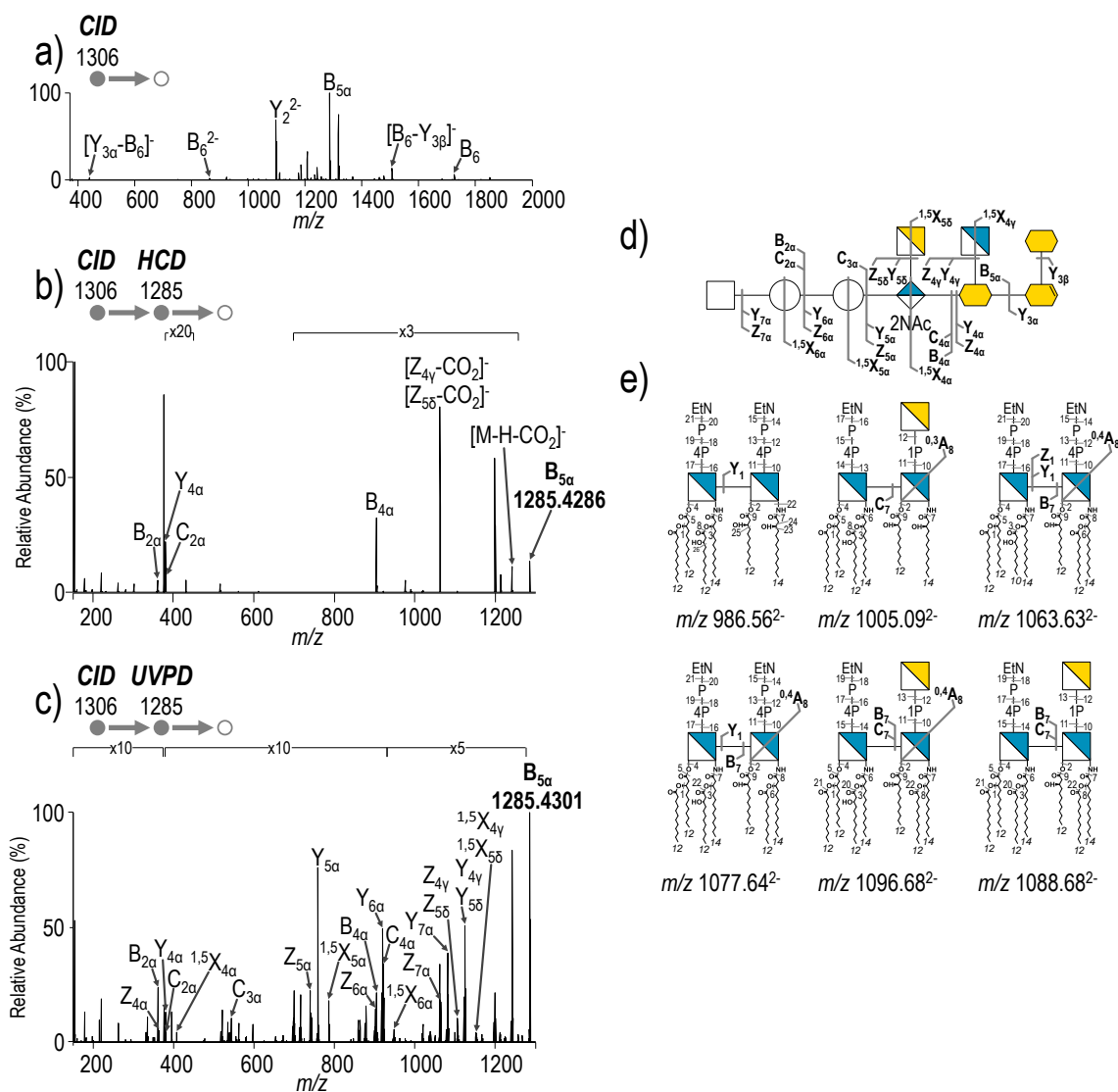


Figure 6.12 Structural characterization of *A. baumannii* 1205 LOS. a) CID spectrum of m/z 1306.30³⁻, b) targeted MS³ CID/HCD and c) targeted MS³ CID/UPVD (10 pulses, 2 mJ) data of m/z 1285.43 corresponding to a core OS substructure of *A. baumannii* 1205, d) fragment ion map of the core OS substructure mapping both CID/HCD and CID/UPVD data, and e) fragment ion maps lipid A substructures mapping both CID/HCD and CID/UPVD data. Fragment ion lists for part a) and b) appear in **Table 6.6** (Supporting Information, Chapter 6). MS³ spectra and fragment ion lists for all lipid A substructures can be found in **Figure 6.14-Figure 6.19** and **Table 6.7-Table 6.12**, respectively.

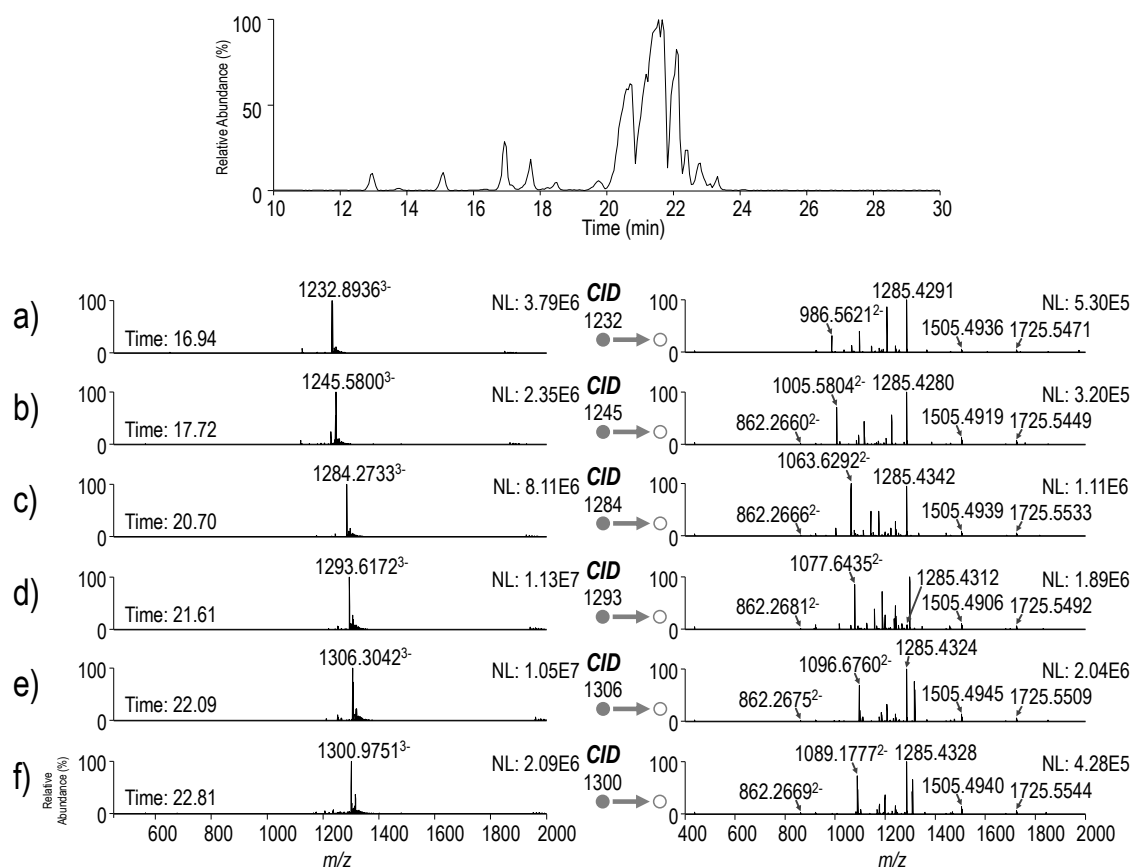


Figure 6.13 Base peak chromatogram MS¹ and corresponding CID spectra for species detected in *A. baumannii* 1205 LOS at the following chromatographic retention times in seconds: a) 16.94, b) 17.72, c) 20.70, d) 21.61, e) 22.09, f) 18.93, and g) 22.81.

6.5 CONCLUSION

The present method couples impressive chromatographic separations with MS³ analysis to achieve structural characterization of intact LOS structures from complex mixtures. CID/HCD and CID/VPD provided complementary information, thus facilitating confident structure assignment and localization of non-stoichiometric modifications. In particular, CID/HCD afforded more non-reducing end saccharide fragment ions, whereas CID/VPD provided an extensive array of reducing end

fragments, including cross-ring cleavages, that enabled modification localization. The results obtained for *E. coli* R3 and *A. baumannii* 19606 are consistent with previously determined structures pieced together based on analysis of separate lipid A and core OS substructures and showcase the level of detail that is possible using top-down analysis of intact LOS. In addition, MS³ analysis of *A. baumannii* 5075 and *A. baumannii* 1205 allow core OS structures to be derived. The present workflow addresses a number of the challenges associated with structural characterization of complex mixtures of LOS and is broadly applicable to any LOS-producing Gram-negative bacteria. In light of the global health threat that antibiotic-resistant Gram-negative bacteria pose, this method provides an unparalleled strategy to investigate LOS structures and has the potential to aid vaccine and therapeutic development.

6.6 SUPPORTING INFORMATION

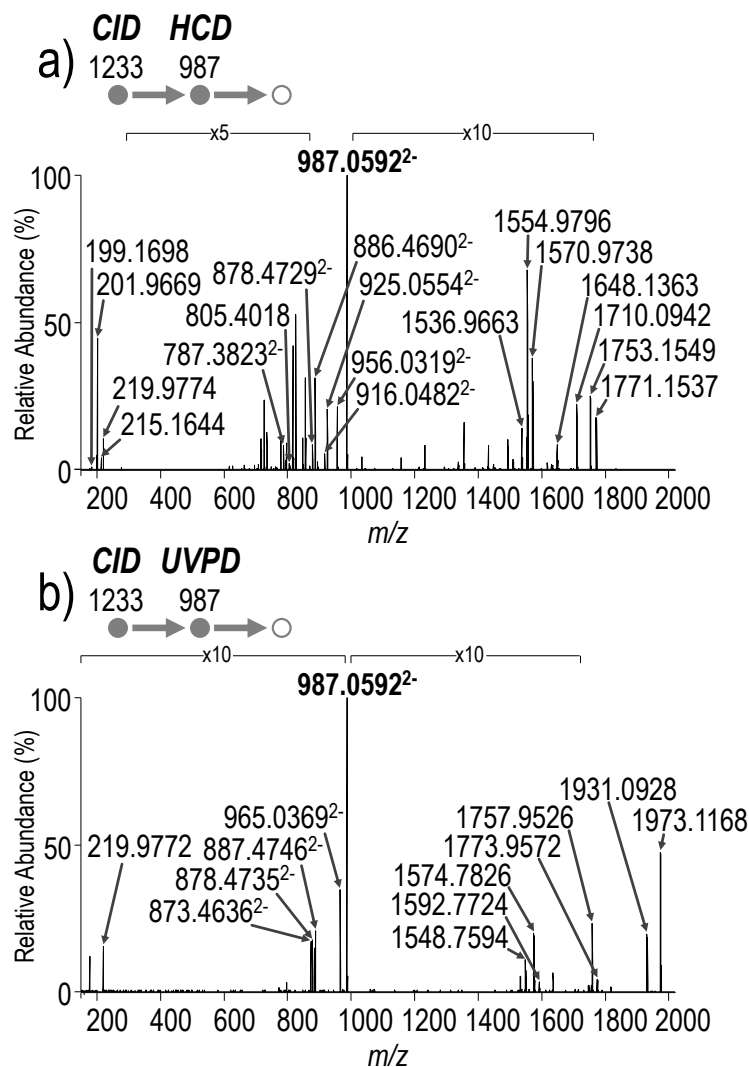


Figure 6.14 a) Targeted MS³ CID/HCD and b) targeted MS³ CID/UVPD (10 pulses, 2 mJ) spectra of m/z 987.06²⁻ from *A. baumannii* 1205 corresponding to a hexa-acylated phosphoethanolamine-modified lipid A substructure. Fragment ion lists appear in **Table 6.7**.

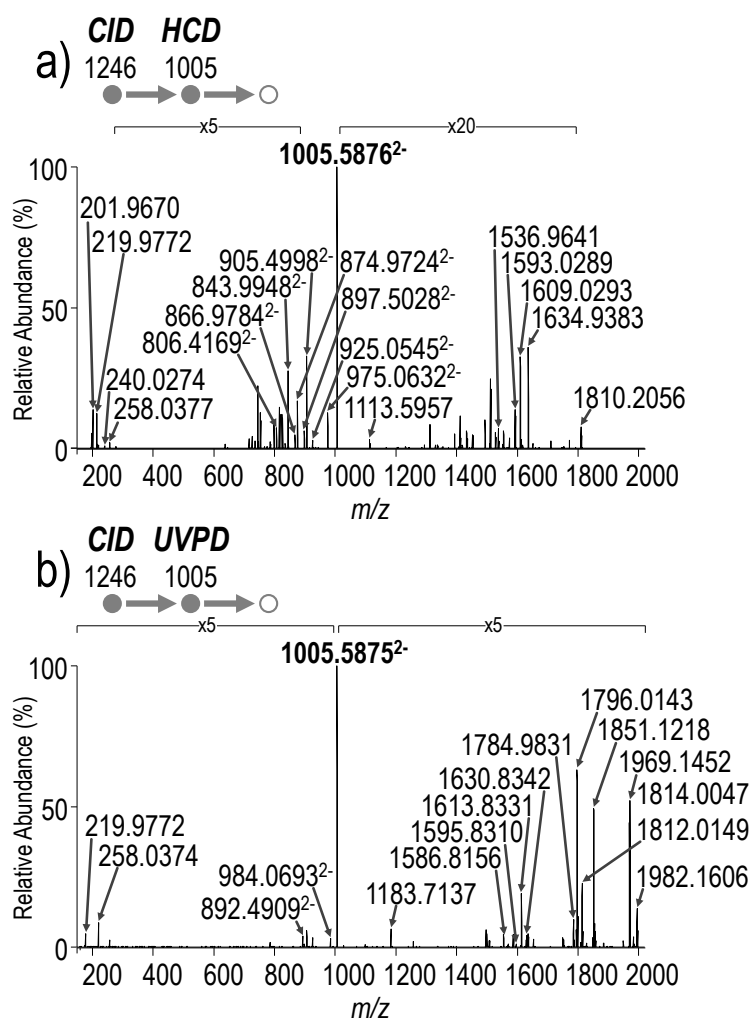


Figure 6.15 a) Targeted MS³ CID/HCD and b) targeted MS³ CID/UVPD (10 pulses, 2 mJ) spectra of m/z 1005.59²⁻ from *A. baumannii* 1205 corresponding to a hexa-acylated phosphoethanolamine and hexosamine-modified lipid A substructure. Fragment ion lists appear in **Table 6.8**.

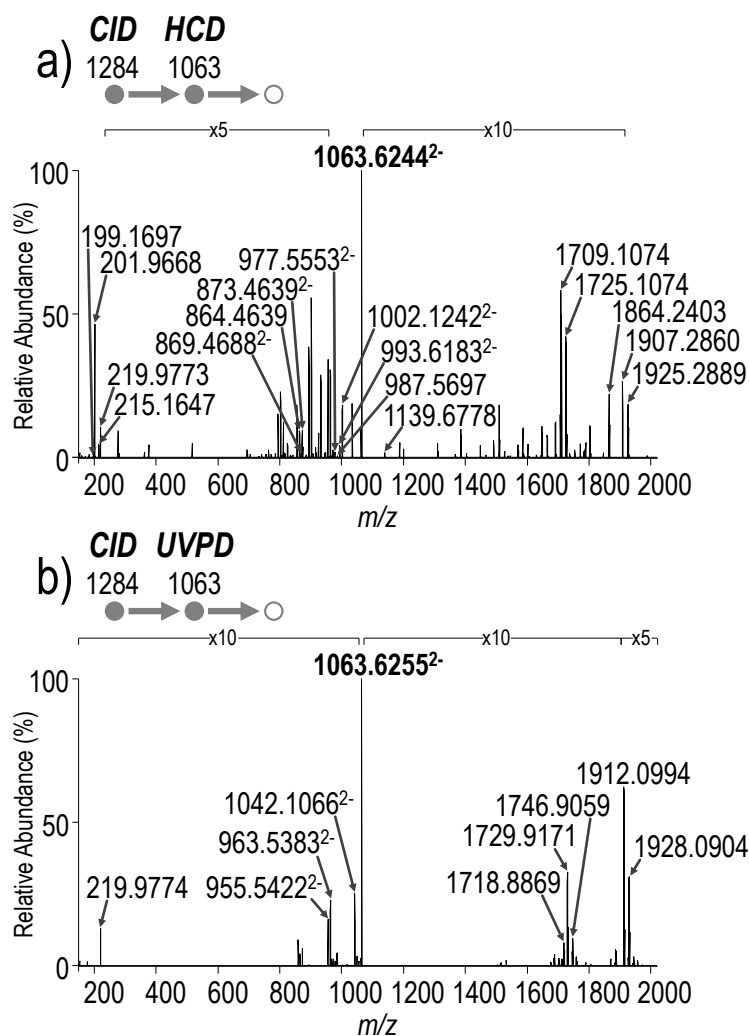


Figure 6.16 a) Targeted MS³ CID/HCD and b) targeted MS³ CID/UVPD (10 pulses, 2 mJ) spectra of *m/z* 1063.63²⁻ from *A. baumannii* 1205 corresponding to a hepta-acylated phosphoethanolamine-modified lipid A substructure. Fragment ion lists appear in **Table 6.9**.

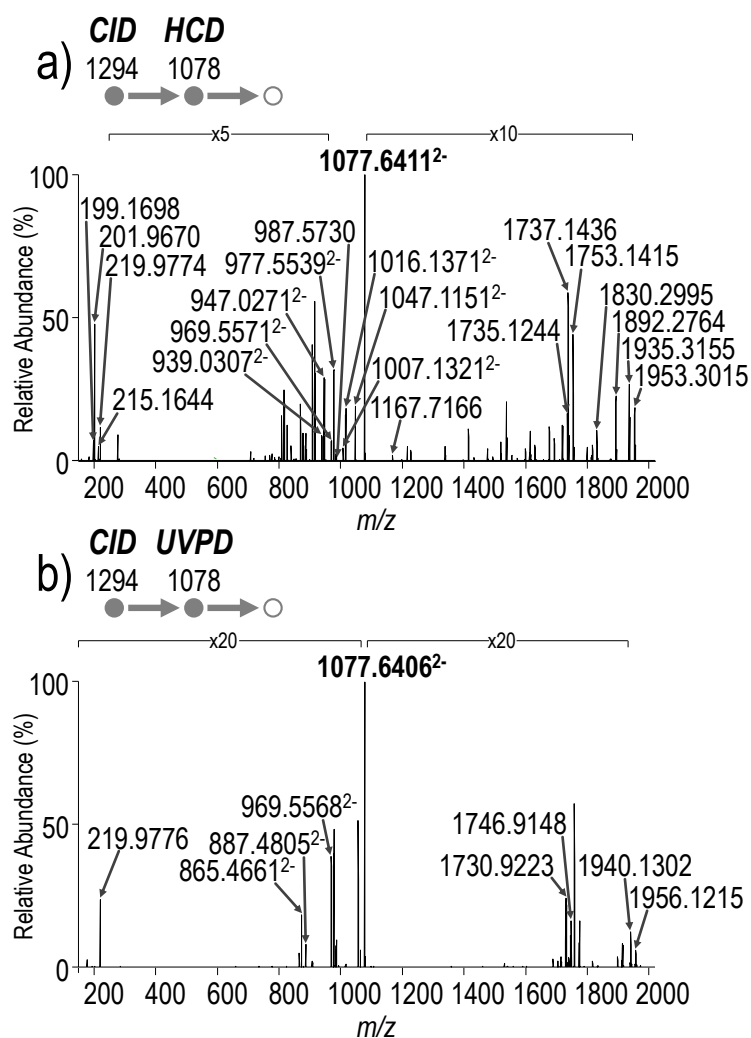


Figure 6.17 a) Targeted MS³ CID/HCD and b) targeted MS³ CID (NCE 25)/UVPD (10 pulses, 2 mJ) spectra of m/z 1077.64²⁻ from *A. baumannii* 1205 corresponding to a hepta-acylated phosphoethanolamine-modified lipid A substructure. Fragment ion lists appear in **Table 6.10**.

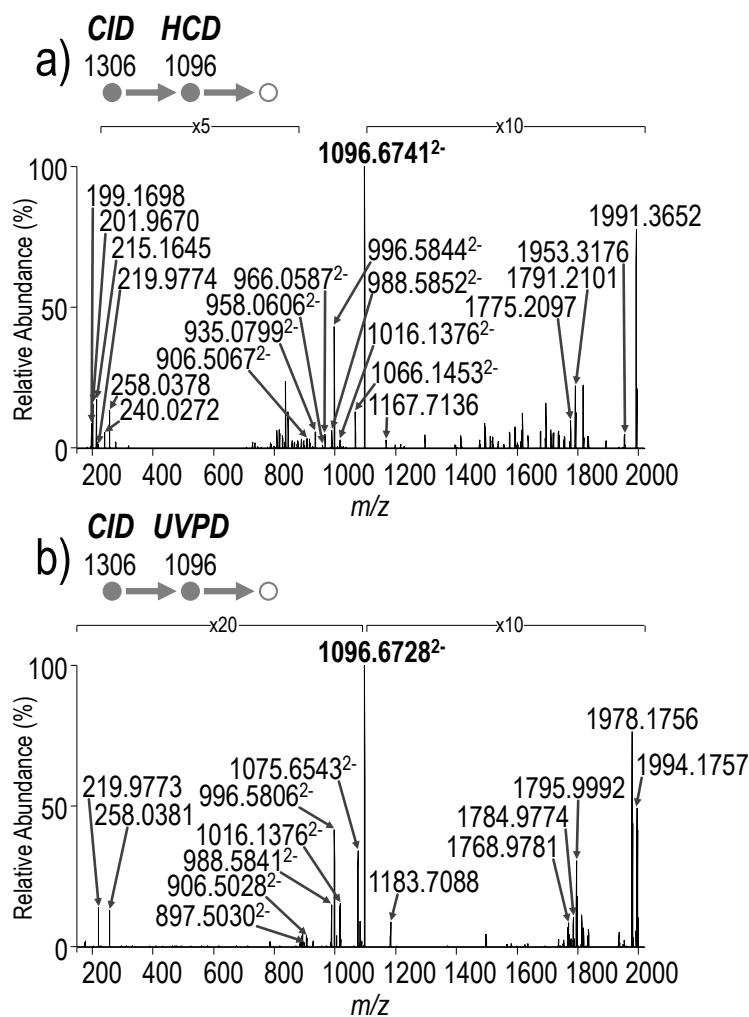


Figure 6.18 a) Targeted MS³ CID/HCD and b) targeted MS³ CID/UVPD (10 pulses, 2 mJ) spectra of m/z 1096.67²⁻ from *A. baumannii* 1205 corresponding to a hepta-acylated phosphoethanolamine and hexosamine-modified lipid A substructure. Fragment ion lists appear in **Table 6.11**.

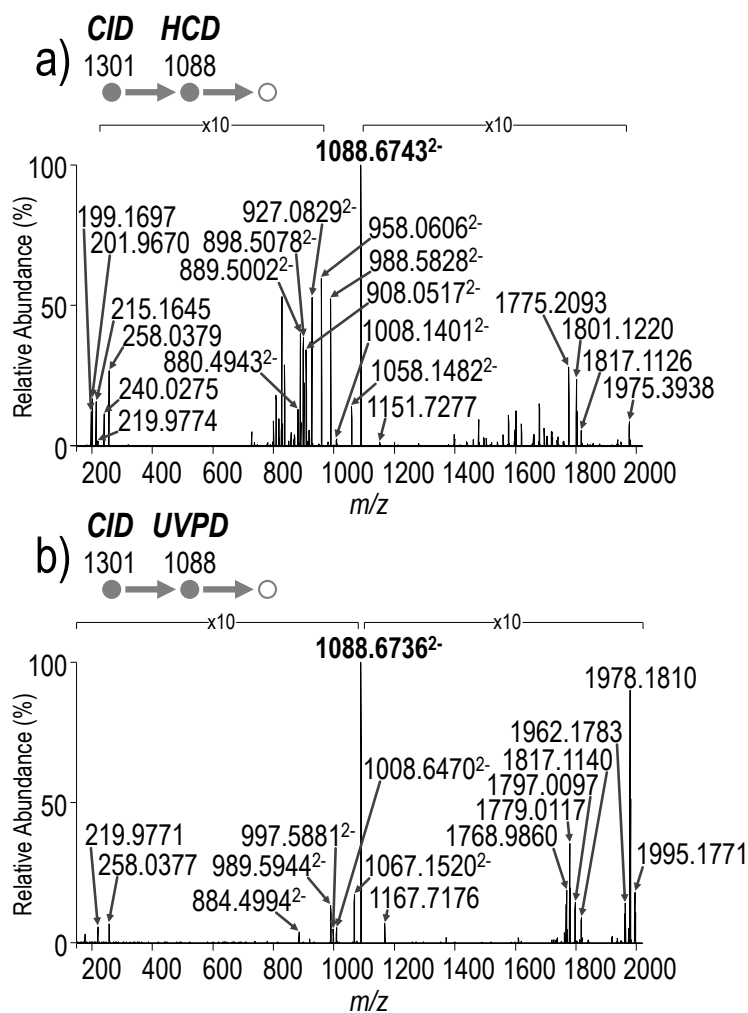


Figure 6.19 a) Targeted MS³ CID/HCD and b) targeted MS³ CID/UVPD (10 pulses, 2 mJ) data of m/z 1088.67²⁻ from *A. baumannii* 1205 corresponding to a hepta-acylated phosphoethanolamine and hexosamine-modified lipid A substructure. Fragment ion lists appear in **Table 6.12**.

Table 6.1 List of identified fragment ions for a) targeted MS³ CID/HCD of m/z 1053.31²⁻, b) targeted MS³ CID/UPVD (10 pulses, 4 mJ) of 1053.31²⁻, c) targeted MS³ CID/HCD of m/z 1359.81 and d) targeted MS³ CID/UPVD (10 pulses, 4 mJ) of m/z 1359.81.

a) CID HCD 1155 1053		b) CID UVPD 1155 1053		c) CID HCD 1155 1359		d) CID UVPD 1155 1359	
m/z	Fragment	m/z	Fragment	m/z	Fragment	m/z	Fragment
1887.5780	Y _{3y}	1974.5668	^{1,5} X _{6β}	1341.8075	[M-H-H ₂ O] ⁻	1341.8070	Z ₂
1869.5645	Z _{3y}	1973.5686	^{1,5} X _{8α}	1279.8504	[M-H-HPO ₃] ⁻	1261.8372	[M-H-H ₃ PO ₄] ⁻
1825.5726	[Y _{3y} -CO ₂] ⁻	1946.5546	Y _{6β}	1261.8409	[M-H-H ₃ PO ₄] ⁻	1203.6258	[M-8] ⁻ , [M-10] ⁻
1807.6067	[Z _{3y} -HPO ₃] ⁻	1945.5618	Y _{8α}	1243.8309	[M-H-H ₃ PO ₄ -H ₂ O] ⁻	1177.6415	[M-6] ⁻
1685.5171	C _{6α}	1932.5464	^{1,5} X _{7β}	1159.6405	[M-1] ⁻	1175.6222	[M-7] ⁻ , [M-9] ⁻
1667.5034	B _{6α}	1928.5463	Z _{6β}	1141.6275	[M-1-H ₂ O] ⁻	1159.6066	[M-1] ⁻
1587.5235	[B _{6α} -HPO ₃] ⁻	1927.5499	Z _{8α}	1115.6130	[M-2] ⁻	1133.6226	[M-3] ⁻ , [M-5] ⁻
1493.4562	C _{5α}	1902.5339	Y _{7β}	1097.6022	[M-2-H ₂ O] ⁻	1115.6114	[M-2] ⁻
1475.4596	B _{5α}	1886.5377	Y _{3y}	1079.6479	[M-1-HPO ₃] ⁻	1097.6044	[M-2-H ₂ O] ⁻
1395.4714	[B _{5α} -HPO ₃] ⁻	1870.5582	Z _{3y}	1061.6644	[M-1-H ₃ PO ₄] ⁻	1061.6673	[M-1-H ₃ PO ₄] ⁻
1053.3070 ²⁻	[M-2H] ²⁻	1783.5200	Y _{7α}	1035.6477	[M-2-HPO ₃] ⁻ , [M-3-H ₃ PO ₄] ⁻	1035.6452	[M-2-HPO ₃] ⁻ , [M-3-H ₃ PO ₄] ⁻
1044.8021 ²⁻	[M-2H-H ₂ O] ²⁻	1765.5105	Z _{7α}	1017.6368	[M-2-H ₃ PO ₄] ⁻	1017.6354	[M-2-H ₃ PO ₄] ⁻
1031.3119 ²⁻	[M-2H-CO ₂] ²⁻	1754.4954	Y _{5β}	999.6260	[M-2-H ₃ PO ₄ -H ₂ O] ⁻	949.4406	[M-4] ⁻
1022.3144 ²⁻	[M-2H-H ₂ O-CO ₂] ²⁻	1736.4941	Z _{5β}	994.6222	^{0,2} A ₃	915.4384	[M-1-2] ⁻
943.2790 ²⁻	Y _{3y} ²⁻	1685.5099	C _{6α}	981.6173	[M-1-H ₃ PO ₄ -HPO ₃] ⁻	905.4192	[M-3-5] ⁻
934.2737 ²⁻	Z _{3y} ²⁻	1666.4816	B _{6α}	937.6712	[M-2-H ₃ PO ₄ -HPO ₃] ⁻	738.4175	^{1,5} X ₁
921.2809 ²⁻	[Y _{3y} -CO ₂] ²⁻	1446.3971	^{1,5} X _{6α}	919.6601	[M-2-H ₃ PO ₄ -H ₃ PO ₄] ⁻	710.4244	Y ₁
912.2776 ²⁻	[Z _{3y} -CO ₂] ²⁻	1418.3870	Y _{6α}	915.4377	[M-1-2] ⁻	692.4130	Z ₁
439.1083	Y ₃	1402.3850	Z _{6α}	710.4244	Y ₁	666.3954	C ₈
421.1446	Z _{3α}	1285.3355	^{1,5} X _{5α}	666.3970	C ₈	648.3857	B ₈
341.1094	C _{2α}	1256.3335	Y _{5α}	648.3874	B ₈		
323.0985	B _{2α}	1238.3206	Z _{5α}	199.0009	1		
237.0609	C _{1y}	957.2735 ²⁻	[Z _{6β} -CH ₂] ²⁻				
219.0507	B _{1y}	951.7625 ²⁻	Y _{7β} ²⁻				
201.0399	B _{1y} -H ₂ O	943.2671 ²⁻	Y _{3y} ²⁻				
		935.2786 ²⁻	Z _{3y} ²⁻				
		861.2416 ²⁻	[Z _{5β} -CH ₂] ²⁻				
		842.2522 ²⁻	B _{6α} ²⁻				
		739.1355	^{1,5} X _{4α}				
		711.1386	Y _{4α}				
		695.1426	Z _{4α}				
		439.1083	Y _{3α}				
		237.0611	C _{1y}				

Table 6.2 *E. coli* R3 LOS fragment ion lists. List of identified fragment ions for a) targeted MS³ CID/HCD of m/z 1012.76²⁻, b) targeted MS³ CID/VPD (10 pulses, 4 mJ) of m/z 1012.76²⁻, c) targeted MS³ CID/HCD (NCE 30) of m/z 1796.21 and d) targeted MS³ CID/VPD (10 pulses, 4 mJ) of m/z 1796.21.

a) CID HCD 1273 1012		b) CID VPD 1273 1012		c) CID HCD 1273 1796		d) CID VPD 1273 1796	
m/z	Fragment	m/z	Fragment	m/z	Fragment	m/z	Fragment
1928.5371	[M-H-H ₂ PO ₄] ⁻	1892.4622	^{1,5} X _{8a}	1796.2179	[M-H] ⁻	1796.2179	[M-H] ⁻
1726.4940	[Y ₃₈ -HPO ₃] ⁻	1864.4595	Y _{8a}	1778.2052	[M-H-H ₂ O] ⁻	1766.1925	[M-H-CO] ⁻
1708.4860	[Y ₃₈ -H ₃ PO ₄] ⁻ , [Z ₃₈ -HPO ₃] ⁻	1862.4575	^{1,5} X ₅₅	1716.2450	[M-H-HPO ₃] ⁻	1698.2286	[M-H-H ₃ PO ₄] ⁻
1682.5015	[Y ₃₈ -HPO ₃ -CO ₂] ⁻	1851.4414	^{1,5} X _{7y}	1698.2299	[M-H-H ₃ PO ₄] ⁻	1640.0305	[M-8] ⁻ , [M-10] ⁻
1664.4912	[Y ₃₈ -H ₃ PO ₄ -CO ₂] ⁻ , [Z ₃₈ -HPO ₃ -CO ₂] ⁻	1834.4534	Z ₅₅	1596.0344	[M-2] ⁻	1612.0206	[M-7] ⁻ , [M-9] ⁻
1604.4142	C _{6a}	1806.4511	Y ₃₈	1569.9994	[M-3] ⁻	1596.0287	[M-2] ⁻
1586.4061	B _{6a}	1788.4489	Z ₃₈	1568.0004	[M-1] ⁻	1570.0099	[M-3] ⁻ , [M-12] ⁻
1524.4570	[C _{6a} -HPO ₃] ⁻	1730.4122	^{1,5} X _{7a}	1552.0092	[M-4] ⁻	1568.0031	[M-1] ⁻
1506.4370	[B _{6a} -HPO ₃] ⁻	1702.4179	Y _{7a}	1549.9902	[M-1-H ₂ O] ⁻	1552.0006	[M-4] ⁻
1488.4282	[B _{6a} -HPO ₃ -H ₂ O] ⁻	1684.4217	Z _{7a}	1533.9985	[M-4-H ₂ O] ⁻	1471.0231	[M-4-HPO ₃] ⁻
1332.3814	C _{5a}	1604.4031	C _{6a}	1516.0302	[M-2-HPO ₃] ⁻	1385.8356	[M-11] ⁻
1314.3757	B _{5a}	1586.3863	B _{6a}	1454.0289	[M-4-H ₃ PO ₄] ⁻	1370.8254	[M-14] ⁻
1004.2515 ²⁻	[M-2H-H ₂ O] ²⁻	1337.2820	Y _{6a}	1359.8156	[M-6] ⁻	1359.8198	[M-6] ⁻
990.7602 ²⁻	[M-2H-CO ₂] ²⁻	1332.3804	C _{5a}	1341.8092	[M-5] ⁻	1341.8045	[M-5] ⁻
968.7633 ²⁻	[M-2H-CO ₂ -CO ₂] ²⁻	1319.2685	Z _{6a}	1323.7960	[M-1-4] ⁻	1100.7688	C ₈
963.7701 ²⁻	[M-2H-H ₃ PO ₄] ²⁻	1314.3611	B _{6a}	1305.7855	[M-1-4-H ₂ O] ⁻	738.4193	^{1,5} X ₁
902.7265 ²⁻	Y ₃₈ ²⁻	1203.2289	^{1,5} X _{5a}	1261.8403	[M-5-HPO ₃] ⁻ , [M-6-H ₃ PO ₄] ⁻	710.4239	Y ₁
893.7209 ²⁻	Z ₃₈ ²⁻	1175.2295	Y _{5a}	1243.8301	[M-5-H ₃ PO ₄] ⁻	692.4154	Z ₁
880.7322 ²⁻	[Y ₃₈ -CO ₂] ²⁻	1159.2355	Z _{5a}	1225.8167	[M-1-4-H ₃ PO ₄] ⁻		
871.7257 ²⁻	[Z ₃₈ -CO ₂] ²⁻	1131.2390	[Y _{5a} -CO ₂] ⁻	1144.8020	^{0,4} A ₉		
853.7378 ²⁻	[Y ₃₈ -H ₃ PO ₄] ²⁻ , [Z ₃₈ -HPO ₃] ²⁻	991.2466 ²⁻	[M-2H-CO ₂] ²⁻	999.6272	[M-4-5-H ₃ PO ₄] ⁻		
844.7228 ²⁻	[Z ₃₈ -H ₃ PO ₄] ²⁻	911.2084 ²⁻	Y _{7y} ²⁻	874.5789	C ₈ -1		
801.7036 ²⁻	C _{6a} ²⁻	902.7213 ²⁻	Y ₃₈ ²⁻	856.5682	B ₈ -1		
792.6991 ²⁻	B _{6a} ²⁻	894.7204 ²⁻	Z ₃₈ ²⁻	710.4349	Y ₁		
439.1079	Y _{3a}	801.6967 ²⁻	C _{6a} ²⁻	242.2124	13		
237.0610	C ₁₈	792.6866 ²⁻	B _{6a} ²⁻	227.2013	1		
219.0493	B ₁₈	739.1433	^{1,5} X _{4a}	199.1701	2		
201.0400	[B ₁₈ -H ₂ O] ⁻	711.1383	Y _{4a}				
		237.0607	C ₁₈				

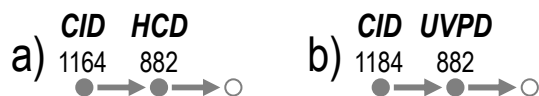
Table 6.3 A. *baumannii* 19606 LOS fragment ion lists. List of identified fragment ions for a) targeted MS³ CID/HCD of m/z 922.78²⁻, b) targeted MS³ CID/VPD (10 pulses, 4 mJ) of m/z 922.78²⁻, c) targeted MS³ CID/HCD of m/z 1728.11 and d) targeted MS³ CID/VPD (10 pulses, 4 mJ) of m/z 1728.11.

a) CID HCD 1191 922		b) CID VUPD 1191 922		c) CID HCD 1191 1728		d) CID VUPD 1191 1728	
m/z	Fragment	m/z	Fragment	m/z	Fragment	m/z	Fragment
1626.5191	Y ₃₈	1845.5662	[M-2H] ⁺	1698.0882	[M-H-CO ₂] ⁻	1728.1111	[M-H] ⁻
1608.4877	Z ₃₈	1827.5471	[M-2H-H ₂ O] ⁺	1630.1281	[M-H-H ₃ PO ₄] ⁻	1710.0968	[M-H-H ₂ O] ⁻
1564.5060	[Z ₃₈ -CO ₂] ⁻	1802.5427	[M-2H-C ₂ H ₂ O] ⁺	1600.0207	[M-12] ⁻ , [M-14] ⁻	1648.1407	[M-H-HPO ₃] ⁻
1406.4520	B _{6a}	1758.5498	[M-2H-C ₂ H ₂ O-CO ₂] ⁺	1571.9346	[M-11] ⁻ , [M-13] ⁻	1630.1311	[M-H-H ₃ PO ₃] ⁻
1362.4659	[B _{6a} -CO ₂] ⁻	1685.5010	Y ₄₄ , Y ₅₈	1543.9269	[M-6] ⁻ , [M-15] ⁻	1527.9340	[M-1] ⁻
1320.4521	[B _{6a} -CO ₂ -C ₂ H ₂ O] ⁻	1684.5043	Y _{8a}	1529.9434	[M-9] ⁻ , [M-10] ⁻	1511.9353	[M-2] ⁻ , [M-3] ⁻
1183.3876	[B _{6a} -Z ₄₄ -CO ₂] ⁻ , [B _{6a} -Z ₅₈ -CO ₂] ⁻	1667.4887	Z ₄₄ , Z ₅₈	1527.9389	[M-1] ⁻	1493.9253	[M-2-H ₂ O] ⁻ , [M-3-H ₂ O] ⁻
1043.3375	C _{5a}	1465.4258	[Y ₃₈ -Y ₄₄] ⁻ , [Y ₃₈ -Y ₅₈] ⁻	1511.9381	[M-2] ⁻ , [M-3] ⁻	1475.9162	[M-2-2H ₂ O] ⁻ , [M-3-2H ₂ O] ⁻
1025.3300	B _{5a}	1406.4535	B _{6a}	1501.9144	[M-8] ⁻	1431.9670	[M-2-HPO ₃] ⁻ , [M-3-HPO ₃] ⁻
900.7865 ²⁻	[M-2H-CO ₂] ²⁻	1362.4659	[B _{6a} -CO ₂] ⁻	1347.7777	[M-5] ⁻	1429.9527	[M-1-H ₃ PO ₄] ⁻
812.7528 ²⁻	Y ₃₈ ²⁻	1360.4305	Y _{6a}	1329.7634	[M-4] ⁻	1413.9569	[M-2-H ₃ PO ₄] ⁻ , [M-3-H ₃ PO ₄] ⁻
803.7509 ²⁻	Z ₃₈ ²⁻	1245.3873	[C _{6a} -Y ₄₄] ⁻ , [C _{6a} -Y ₅₈] ⁻	1303.7500	[M-7] ⁻	1395.9499	[M-2-H ₂ PO ₄ -H ₂ O] ⁻ , [M-3-H ₂ PO ₄ -H ₂ O] ⁻
790.7583 ²⁻	[Y ₃₈ -CO ₂] ²⁻	1226.3522	^{1,5} X _{5a}	1060.7046	C ₈	1347.7817	[M-5] ⁻
781.7551 ²⁻	[Z ₃₈ -CO ₂] ²⁻	1198.3616	Y _{5a}	710.3859	^{1,5} X ₁	1329.7662	[M-4] ⁻
723.2149 ²⁻	[Y ₃₈ -Z ₄₄] ²⁻ , [Y ₃₈ -Z ₄₈] ²⁻ , [Z ₃₈ -Y ₄₄] ²⁻ , [Z ₃₈ -Y ₄₈] ²⁻	1180.3469	Z _{5a}	682.3912	Y ₁	1311.7599	[M-1-3] ⁻ , [M-1-2] ⁻
711.7289 ²⁻	C _{5a} ²⁻	901.2731	[M-2H-C ₂ H ₂ O] ²⁻	664.3799	Z ₁	1295.7584	[M-2-3] ⁻
702.7218 ²⁻	B _{6a} ²⁻	848.2341	^{1,5} X _{4a}			1249.7978	[M-4-HPO ₃] ⁻
503.1588	C _{3a}	820.2386	Y _{4a}			1231.7898	[M-1-3-HPO ₃] ⁻ , [M-1-2-HPO ₃] ⁻
439.1076	Y _{3a}	812.2365	[Y ₃₈ -1] ²⁻			1213.7802	[M-1-3-H ₃ PO ₄] ⁻ , [M-1-2-H ₃ PO ₄] ⁻
237.0607	C ₁₈	665.2168	C _{4a}			1113.5971	[M-2-4] ⁻
219.0503	B ₁₈	503.1608	C _{3a}			1104.7309	^{0,4} A ₉
201.0396	B ₁₈ -H ₂ O	439.1080	Y _{3a}			682.3908	Y ₁
		237.0606	C ₁₈			664.3809	Z ₁

Table 6.4 A. *baumannii* 19606 LOS fragment ion lists. List of identified fragment ions for a) targeted MS³ CID/HCD of m/z 619.69²⁻, b) targeted MS³ CID/VPD (10 pulses, 2 mJ) of m/z 619.69²⁻, c) targeted MS³ CID/HCD (NCE 30) of m/z 1910.29 and d) targeted MS³ CID/VPD (10 pulses, 2 mJ) of m/z 1910.29.

a) CID HCD		b) CID VVPD		c) CID HCD		d) CID VVPD	
989 → 619 → ○		989 → 619 → ○		989 → 1910 → ○		989 → 1910 → ○	
m/z	Fragment	m/z	Fragment	m/z	Fragment	m/z	Fragment
1020.3081	Y _{3b}	800.2500	B _{3a}	1892.2800	[M-H-H ₂ O] ⁻	1880.2588	[M-H-CO ₂] ⁻
1002.2974	Z _{3b}	439.1080	Y _{3a}	1830.3169	[M-H-HPO ₃] ⁻	1812.3011	[M-H-H ₃ PO ₄] ⁻
958.3122	[Z _{3b} -CO ₂] ⁻	437.1414	C _{2a}	1812.3156	[M-H-H ₃ PO ₄] ⁻	1728.1134	[M-12] ⁻ , [M-13] ⁻
800.2526	B _{3a}	237.0608	C _{1b}	1710.0921	[M-1] ⁻ , [M-6] ⁻	1712.1119	[M-10] ⁻ , [M-11] ⁻
756.2564	[B _{3a} -CO ₂] ⁻	219.0498	B _{1b}	1694.1004	[M-2] ⁻ , [M-3] ⁻	1710.1017	[M-1] ⁻ , [M-6] ⁻
714.2549	[B _{3a} -CO ₂ -CH ₃ CHO] ⁻	202.0716	B _{1a}	1676.0886	[M-2-H ₂ O] ⁻ , [M-3-H ₂ O] ⁻	1694.1029	[M-2] ⁻ , [M-3] ⁻
579.1653	[B _{3a} -Y _{5a}] ⁻	201.0394	B _{1b} -H ₂ O	1614.1235	[M-10-H ₃ PO ₄] ⁻ , [M-11-H ₃ PO ₄] ⁻	1529.9437	[M-5] ⁻ , [M-10-12] ⁻ , [M-10-13] ⁻ , [M-11-12] ⁻ , [M-11-13] ⁻
535.1770	[B _{3a} -Y _{5a} -CO ₂] ⁻			1612.1233	[M-1-H ₃ PO ₄] ⁻ , [M-6-H ₃ PO ₄] ⁻	1511.9362	[M-4] ⁻ , [M-1-10] ⁻ , [M-1-11] ⁻ , [M-6-10] ⁻ , [M-6-11] ⁻
509.6525 ²⁻	Y _{3b} ²⁻			1596.1260	[M-2-H ₃ PO ₄] ⁻ , [M-3-H ₃ PO ₄] ⁻	1501.9125	[M-8] ⁻
439.1075	Y _{3a}			1511.9342	[M-4] ⁻ , [M-1-10] ⁻ , [M-1-11] ⁻ , [M-6-10] ⁻ , [M-6-11] ⁻	1485.9135	[M-7] ⁻
437.1393	C _{2a}			1493.9243	[M-1-2] ⁻ , [M-1-3] ⁻ , [M-2-6] ⁻ , [M-3-6] ⁻	1061.7144	C ₅
419.1291	B _{2a}			1104.7254	^{0.4} A ₇	892.5528	^{1.5} X ₁
237.0606	C _{1b}			864.5337	Y ₁	864.5593	Y ₁
219.0502	B _{1b}			846.5460	Z ₁	846.5512	Z ₁
202.0712	B _{1a}			215.1644	2, 3		
201.0396	B _{1b} -H ₂ O			199.1694	1, 6		

Table 6.5 A. *baumannii* 5075 LOS fragment ion lists Lists of identified fragment ions for a) targeted MS³ CID/HCD and targeted MS³ CID/UVPD (10 pulses, 2 mJ) of *m/z* 882.78²⁻.



<i>m/z</i>	Fragment
1326.4541	B _{5a}
1282.4659	[B _{5a} -CO ₂] ⁻
1240.4524	[B _{5a} -CO ₂ -CH ₃ CHO] ⁻
963.3365	C _{4a}
945.3262	B _{4a}
772.7522 ²⁻	Y _{3b} ²⁻
763.7517 ²⁻	Z _{3b} ²⁻
750.7610 ²⁻	[Y _{3b} -CO ₂] ²⁻
662.7230 ²⁻	B _{5a} ²⁻
439.1078	Y _{3a}
237.0607	C _{1b}
219.0503	B _{1b}

<i>m/z</i>	Fragment
1765.5592	[M-2H] ⁺
1722.5527	[M-2H-CO ₂] ⁺
1678.5530	[M-2H-CO ₂ -CH ₃ CHO] ⁺
1605.5031	Y _{4y} , Y _{5b}
1587.4886	Z _{4y} , Z _{5b}
1563.4918	Y _{7a}
1545.4917	Z _{7a}
1528.5104	Y _{3b}
1388.4168	^{1,5} X _{6a}
1360.4151	Y _{6a}
1344.4252	C _{5a}
1342.4211	Z _{6a}
1326.4484	B _{5a}
1298.4563	[Z _{6a} -CO ₂] ⁻
1226.3633	^{1,5} X _{6a}
1198.3579	Y _{5a}
1182.3653	Z _{5a}
1165.3820	[B _{5a} -Y _{4y}] ⁻ , [B _{5a} -Y _{5b}] ⁻
963.3225	C _{4a}
861.2731 ²⁻	[M-2H-CH ₃ CO] ²⁻
781.2419 ²⁻	Y _{7a} ²⁻
772.2366 ²⁻	Z _{7a} ²⁻
848.2314	^{1,5} X _{5a}
802.2452	Z _{4a}
439.1078	Y _{3a}
237.0606	C _{1b}
219.0498	B _{1b}

Table 6.6 A. *baumannii* 1205 LOS fragment ion lists. Lists of identified fragment ions for a) targeted MS³ CID/HCD and b) targeted MS³ CID/VPD (10 pulses, 2 mJ) of *m/z* 1285.43.

a) CID HCD

b) CID VVPD


<i>m/z</i>	Fragment
1285.4286	[M-H] ⁻
1241.4379	[M-H-CO ₂] ⁻
1199.4261	[M-H-CO ₂ -CH ₃ CO] ⁻
1062.3600	[Z _{4y} -CO ₂] ⁻ , [Z _{5δ} -CO ₂] ⁻
904.3012	B _{4α}
382.1342	C _{2α}
380.1191	Y _{4α}
362.1083	B _{2α}

<i>m/z</i>	Fragment
1285.4301	[M-H] ⁻
1242.4146	[M-H-CH ₃ CO] ⁻
1152.3647	^{1,5} X _{4y} ⁻ , ^{1,5} X _{5δ} ⁻
1124.3628	Y _{4y} ⁻ , Y _{5δ} ⁻
1106.3532	Z _{4y} ⁻ , Z _{5δ} ⁻
1082.3505	Y _{7α}
1064.3480	Z _{7α}
948.2978	^{1,5} X _{6α}
922.3088	C _{4α}
920.2964	Y _{6α}
904.3012	B _{4α}
902.2872	Z _{6α}
786.2386	^{1,5} X _{5α}
758.2350	Y _{5α}
740.2336	Z _{5α}
544.1854	C _{3α}
408.1146	^{1,5} X _{4α}
382.1336	C _{2α}
380.1183	Y _{4α}
364.1228	B _{2α}
362.1081	Z _{4α}

Table 6.7 A. *baumannii* 1205 LOS fragment ion lists. List of identified fragment ions for a) targeted MS³ CID/HCD and targeted MS³ CID/VPD (10 pulses, 2 mJ) of m/z 987.05²⁻.

a) **CID HCD**


m/z	Fragment
1771.1537	[M-11] ⁻ , [M-17] ⁻
1753.1549	[M-10] ⁻ , [M-16] ⁻
1710.0942	[M-10-21] ⁻ , [M-11-20] ⁻ , [M-14-17] ⁻ , [M-15-16] ⁻
1648.1363	[M-11-19] ⁻ , [M-13-17] ⁻
1570.9738	[M-1-11] ⁻ , [M-1-17] ⁻
1554.9796	[M-2-11] ⁻ , [M-3-11] ⁻ , [M-2-17] ⁻ , [M-3-17] ⁻
1552.9676	[M-1-10] ⁻ , [M-1-16] ⁻
1536.9663	[M-2-10] ⁻ , [M-3-10] ⁻ , [M-2-16] ⁻ , [M-3-16] ⁻
956.0319 ²⁻	[M-14] ²⁻ , [M-20] ²⁻
925.0554 ²⁻	[M-13] ²⁻ , [M-19] ²⁻
916.0482 ²⁻	[M-12] ²⁻ , [M-18] ²⁻
886.4690 ²⁻	[M-1] ²⁻
805.4018	Y ₁
878.4729 ²⁻	[M-2] ²⁻ , [M-3] ²⁻
787.3823 ²⁻	[M-4] ²⁻ , [M-1-8] ²⁻ , [M-1-9] ²⁻
219.9774	10, 16
215.1644	2, 3
201.9669	11, 17
199.1698	1

b) **CID VVPD**


m/z	Fragment
1973.1168	[M-2H] ⁺
1931.0928	[M-15] ⁻ , [M-21] ⁻
1845.9717	[M-25] ⁻ , [M-26] ⁻
1817.9618	[M-23] ⁻
1788.9387	[M-24] ⁻
1773.9572	[M-1] ⁻
1757.9226	[M-2] ⁻ , [M-3] ⁻
1747.9307	[M-7] ⁻
1732.9225	[M-22] ⁻
1592.7724	[M-5] ⁻
1574.7826	[M-4] ⁻ , [M-1-8] ⁻ , [M-1-9] ⁻
1548.7594	[M-6] ⁻
965.0369 ²⁻	[M-15] ²⁻ , [M-21] ²⁻
887.4746 ²⁻	[M-8] ²⁻ , [M-9] ²⁻
886.4699 ²⁻	[M-1] ²⁻
878.4735 ²⁻	[M-2] ²⁻ , [M-3] ²⁻
873.4636 ²⁻	[M-7] ²⁻
219.9772	10, 16

Table 6.8 A. *baumannii* 1205 LOS fragment ion lists. List of identified fragment ions for a) targeted MS³ CID/HCD and targeted MS³ CID/UVPD (10 pulses, 2 mJ) of *m/z* 1005.59²⁻.

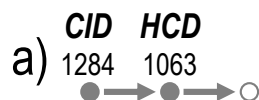
a) CID HCD

b) CID UVPD

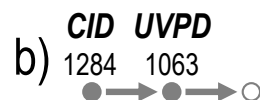
<i>m/z</i>	Fragment
1809.2212	[M-14] ⁻
1634.9383	[M-2-12] ⁻ , [M-3-12] ⁻
1609.0293	[M-1-14] ⁻
1593.0289	[M-2-14] ⁻ , [M-3-14] ⁻
1536.9641	[M-2-10] ⁻ , [M-3-10] ⁻
975.0632 ²⁻	[M-16] ²⁻
925.0545 ²⁻	[M-12] ²⁻
905.4998 ²⁻	[M-1] ²⁻
897.5028 ²⁻	[M-2] ²⁻ , [M-3] ²⁻
866.9784 ²⁻	[M-2-16] ²⁻ , [M-3-1]
843.9948 ²⁻	[M-1-15] ²⁻
806.4169 ²⁻	[M-4] ²⁻ , [M-1-8] ²⁻ , [M-1-9] ²⁻
258.0377	10
219.9775	13
215.1645	2
201.967	11

<i>m/z</i>	Fragment
1994.1525	[M-H-H ₂ O] ⁻
1982.1606	[M-H-CO ₂] ⁻
1969.1452	[M-17] ⁻
1851.1218	[M-12] ⁻
1814.0047	[M-8] ⁻ , [M-9] ⁻
1812.0149	[M-1] ⁻
1796.0143	[M-2] ⁻ , [M-3] ⁻
1784.9831	[M-7] ⁻
1630.8342	[M-5] ⁻
1613.8331	[M-4] ⁻ , [M-1-8] ⁻ , [M-1-9] ⁻
1595.8310	[M-1-2] ⁻ , [M-1-3] ⁻
1586.8156	[M-6] ⁻
1256.7479	^{0,3} A ₈
1183.7137	C ₇
984.0693	[M-17] ²⁻
892.4909	[M-7] ²⁻
258.0374	10
219.9772	14

Table 6.9 A. *baumannii* 1205 LOS fragment ion lists. List of identified fragment ions for a) targeted MS³ CID/HCD and targeted MS³ CID/UVPD (10 pulses, 2 mJ) of *m/z* 1063.62²⁻.




<i>m/z</i>	Fragment
1925.2889	[M-11] ⁻ , [M-17] ⁻
1907.2860	[M-10] ⁻ , [M-16] ⁻
1864.2403	[M-10-21] ⁻ , [M-11-20] ⁻ , [M-14-17] ⁻ , [M-14-17] ⁻
1725.1074	[M-1-11] ⁻ , [M-11-17] ⁻ , [M-6-11] ⁻ , [M-6-17] ⁻
1709.1125	[M-2-11] ⁻ , [M-2-17] ⁻
1139.6778	B ₇
1002.1242 ²⁻	[M-13] ²⁻ , [M-19] ²⁻
993.1184 ²⁻	[M-12] ²⁻ , [M-18] ²⁻
987.5697	Y ₁
977.5553 ²⁻	[M-3] ²⁻
955.5421 ²⁻	[M-2] ²⁻
873.4631 ²⁻	[M-5] ²⁻
869.4688 ²⁻	[M-1-3] ²⁻ , [M-3-6] ²⁻
864.4639 ²⁻	[M-4] ²⁻ , [M-1-9] ²⁻ , [M-6-9] ²⁻
219.9773	10, 16
215.1647	2
201.9668	11, 17
199.1697	1, 6




<i>m/z</i>	Fragment
1928.0904	[M-1] ⁻ , [M-6] ⁻
1912.0994	[M-2] ⁻ , [M-3] ⁻
1746.9059	[M-5] ⁻
1729.9171	[M-4] ⁻ , [M-7] ⁻ , [M-1-9] ⁻ , [M-6-9] ⁻
1718.8869	[M-8] ⁻
1042.1066 ²⁻	[M-15] ²⁻ , [M-21] ²⁻
987.567	Y ₁
969.5562	Z ₁
963.5383 ²⁻	[M-1] ²⁻ , [M-6] ²⁻
955.5422 ²⁻	[M-2] ²⁻
219.9774	10, 16

Table 6.10 A. *baumannii* 1205 LOS fragment ion lists. List of identified fragment ions for a) targeted MS³ CID/HCD and targeted MS³ CID/UVPD (10 pulses, 2 mJ) of *m/z* 1077.64²⁻.

a) **CID HCD**


<i>m/z</i>	Fragment
1953.3015	[M-11] ⁻ , [M-17] ⁻
1935.3155	[M-10] ⁻ , [M-16] ⁻
1892.2764	[M-11-20] ⁻ , [M-14-17] ⁻
1830.2995	[M-11-19] ⁻ , [M-13-17] ⁻
1753.1415	[M-1-11] ⁻ , [M-1-17] ⁻ , [M-6-11] ⁻ , [M-6-17] ⁻
1737.1436	[M-2-11] ⁻ , [M-2-17] ⁻ , [M-3-11] ⁻ , [M-3-17] ⁻
1735.1244	[M-1-10] ⁻ , [M-1-16] ⁻ , [M-6-10] ⁻ , [M-6-16] ⁻
1227.7371	^{0,4} A ₇
1167.7166	B ₇
1047.1151 ²⁻	[M-14] ²⁻ , [M-20] ²⁻
1016.1371 ²⁻	[M-13] ²⁻ , [M-19] ²⁻
1007.1321 ²⁻	[M-12] ²⁻ , [M-18] ²⁻
987.573	Y ₁
977.5539 ²⁻	[M-1] ²⁻ , [M-6] ²⁻
969.5571 ²⁻	[M-2] ²⁻ , [M-3] ²⁻
947.0271 ²⁻	[M-1-14] ²⁻ , [M-1-20] ²⁻ , [M-6-14] ²⁻ , [M-6-20] ²⁻
939.0307 ²⁻	[M-2-14] ²⁻ , [M-2-20] ²⁻ , [M-3-14] ²⁻ , [M-3-20] ²⁻
878.4794 ²⁻	[M-4] ²⁻ , [M-1-9] ²⁻ , [M-1-22] ²⁻ , [M-6-9] ²⁻ , [M-6-22] ²⁻
219.9774	10, 16
215.1644	2, 3
201.967	11, 17
199.1698	1, 6

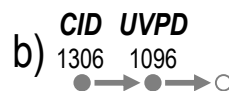
b) **CID UVPD**


<i>m/z</i>	Fragment
1956.1215	[M-1] ⁻ , [M-6] ⁻
1940.1302	[M-2] ⁻ , [M-3] ⁻
1746.9148	[M-8] ⁻
1730.9223	[M-7] ⁻
1056.1219 ²⁻	[M-15] ²⁻ , [M-21] ²⁻
977.5544 ²⁻	[M-1] ²⁻ , [M-6] ²⁻
969.5568 ²⁻	[M-2] ²⁻ , [M-3] ²⁻
887.4805 ²⁻	[M-5] ²⁻
872.4569 ²⁻	[M-8] ²⁻
865.4661 ²⁻	[M-7] ²⁻
219.9775	10, 16

Table 6.11 *A. baumannii* 1205 LOS fragment ion lists. List of identified fragment ions for a) targeted MS³ CID/HCD and targeted MS³ CID/UVPD (10 pulses, 2 mJ) of m/z 1096.67²⁻.



m/z	Fragment
1991.3652	[M-15] ⁻
1953.3176	[M-11] ⁻
1791.2101	[M-1-15] ⁻ , [M-8-15] ⁻
1775.2097	[M-2-15] ⁻ , [M-3-15] ⁻
1227.7257	^{0,4} A ₈
1167.7136	B ₇
1066.1453 ²⁻	[M-18] ²⁻
1035.1696 ²⁻	[M-17] ²⁻
1026.1613 ²⁻	[M-16] ²⁻
1016.1376 ²⁻	[M-13] ²⁻
1007.1282 ²⁻	[M-12] ²⁻
996.5844 ²⁻	[M-1] ²⁻ , [M-8] ²⁻
988.5852 ²⁻	[M-2] ²⁻ , [M-3] ²⁻
966.0587 ²⁻	[M-1-18] ²⁻ , [M-8-18] ²⁻
958.0606 ²⁻	[M-2-18] ²⁻ , [M-3-18] ²⁻
935.0799 ²⁻	[M-1-17] ²⁻ , [M-8-17] ²⁻
906.5067 ²⁻	[M-5] ²⁻
897.5014 ²⁻	[M-4] ²⁻ , [M-1-9] ²⁻ , [M-1-20] ²⁻ , [M-6-9] ²⁻ , [M-6-20] ²⁻
258.0378	10
240.0272	11
215.1645	2, 3
201.9670	15
199.1698	1, 6

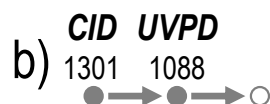


m/z	Fragment
1994.1757	[M-1] ⁻ , [M-8] ⁻
1978.1756	[M-2] ⁻ , [M-3] ⁻
1795.9992	[M-4] ⁻ , [M-1-9] ⁻ , [M-1-20] ⁻ , [M-6-9] ⁻ , [M-6-20] ⁻
1784.9774	[M-7] ⁻
1768.9781	[M-6] ⁻
1183.7088	C ₇
1075.1548 ²⁻	[M-19] ²⁻
1016.1376 ²⁻	[M-13] ²⁻
1005.5917 ²⁻	[M-21] ²⁻ , [M-22] ²⁻
997.5864 ²⁻	[M-20] ²⁻
996.5806 ²⁻	[M-1] ²⁻ , [M-8] ²⁻
988.5841 ²⁻	[M-2] ²⁻ , [M-3] ²⁻
906.5028 ²⁻	[M-5] ²⁻
897.5030 ²⁻	[M-4] ²⁻ , [M-1-9] ²⁻ , [M-1-20] ²⁻ , [M-6-9] ²⁻ , [M-6-20] ²⁻
892.4899 ²⁻	[M-7] ²⁻
258.0381	10
219.9773	14

Table 6.12 A. *baumannii* 1205 LOS fragment ion lists. List of identified fragment ions for a) targeted MS³ CID/HCD and targeted MS³ CID/UVPD (10 pulses, 2 mJ) of *m/z* 1088.67²⁻.



<i>m/z</i>	Fragment
1975.3938	[M-15] ⁺
1817.1126	[M-1-13] ⁺ , [M-3-13] ⁺ , [M-8-13] ⁺
1801.1220	[M-2-13] ⁺
1775.2093	[M-1-15] ⁺ , [M-3-15] ⁺ , [M-8-15] ⁺
1151.7277	B ₇
1058.1482 ²⁻	[M-18] ²⁻
1008.1401 ²⁻	[M-13] ²⁻
999.1340 ²⁻	[M-12] ²⁻
988.5828 ²⁻	[M-1] ²⁻ , [M-3] ²⁻ , [M-8] ²⁻
958.0606 ²⁻	[M-1-18] ²⁻ , [M-3-18] ²⁻ , [M-8-18] ²⁻
927.0829 ²⁻	[M-1-17] ²⁻ , [M-3-17] ²⁻ , [M-8-17] ²⁻
918.0775 ²⁻	[M-1-16] ²⁻ , [M-3-16] ²⁻ , [M-8-16] ²⁻
908.0517 ²⁻	[M-1-13] ²⁻ , [M-3-13] ²⁻ , [M-8-13] ²⁻
898.5078 ²⁻	[M-5] ²⁻
889.5002 ²⁻	[M-4] ²⁻ , [M-1-9] ²⁻ , [M-3-9] ²⁻ , [M-8-9] ²⁻
888.4916 ²⁻	[M-1-3] ²⁻ , [M-1-8] ²⁻ , [M-3-8] ²⁻
880.4943 ²⁻	[M-1-2] ²⁻ , [M-2-3] ²⁻ , [M-2-8] ²⁻
258.0379	10
240.0275	11
219.9774	14
215.1645	2
201.9670	15
199.1697	1, 3, 8



<i>m/z</i>	Fragment
1995.1771	[M-20] ⁺ , [M-21] ⁺ , [M-22] ⁺
1978.1810	[M-1] ⁺ , [M-3] ⁺ , [M-8] ⁺
1962.1783	[M-2] ⁺
1817.1140	[M-1-13] ⁺ , [M-3-13] ⁺ , [M-8-13] ⁺
1797.0097	[M-5] ⁺
1779.0117	[M-4] ⁺ , [M-1-9] ⁺ , [M-3-9] ⁺ , [M-8-9] ⁺
1768.9860	[M-6] ⁺ , [M-7] ⁺
1167.7176	C ₇
1067.1520 ²⁻	[M-19] ²⁻
1008.6470 ²⁻	[M-13] ²⁻
997.5881 ²⁻	[M-20] ²⁻ , [M-21] ²⁻ , [M-22] ²⁻
989.5944 ²⁻	[M-9] ²⁻
988.5882 ²⁻	[M-1] ²⁻ , [M-3] ²⁻ , [M-8] ²⁻
884.4994 ²⁻	[M-6] ²⁻ , [M-7] ²⁻
258.0377	10
219.9771	14

6.6 REFERENCES

- (1) Michael, C. A.; Dominey-Howes, D.; Labbate, M. The Antimicrobial Resistance Crisis: Causes, Consequences, and Management. *Front. Public Health* **2014**, *2*.
- (2) Ventola, C. L. The Antibiotic Resistance Crisis. *Pharm. Ther.* **2015**, *40*, 277–283.
- (3) Ventola, C. L. The Antibiotic Resistance Crisis. *Pharm. Ther.* **2015**, *40*, 344–352.
- (4) Martens, E.; Demain, A. L. The Antibiotic Resistance Crisis, with a Focus on the United States. *J. Antibiot. (Tokyo)* **2017**, *70*, 520–526.
- (5) Miller, S. I. Antibiotic Resistance and Regulation of the Gram-Negative Bacterial Outer Membrane Barrier by Host Innate Immune Molecules. *mBio* **2016**, *7*, e01541-16.
- (6) Delcour, A. H. Outer Membrane Permeability and Antibiotic Resistance. *Biochim. Biophys. Acta BBA - Proteins Proteomics* **2009**, *1794*, 808–816.
- (7) Blair, J. M. A.; Webber, M. A.; Baylay, A. J.; Ogbolu, D. O.; Piddock, L. J. V. Molecular Mechanisms of Antibiotic Resistance. *Nat. Rev. Microbiol.* **2015**, *13*, 42–51.
- (8) Exner, M.; Bhattacharya, S.; Christiansen, B.; Gebel, J.; Goroncy-Bermes, P.; Hartemann, P.; Heeg, P.; Ilchner, C.; Kramer, A.; Larson, E.; Merkens, W.; Mielke, M.; Oltmanns, P.; Ross, B.; Rotter, M.; Schmithausen, R. M.; Sonntag, H.-G.; Trautmann, M. Antibiotic Resistance: What Is so Special about Multidrug-Resistant Gram-Negative Bacteria? *GMS Hyg. Infect. Control* **2017**, *12*.
- (9) Molinaro, A.; Holst, O.; Di Lorenzo, F.; Callaghan, M.; Nurisso, A.; D’Errico, G.; Zamyatina, A.; Peri, F.; Berisio, R.; Jerala, R.; Jiménez-Barbero, J.; Silipo, A.; Martín-Santamaría, S. Chemistry of Lipid A: At the Heart of Innate Immunity. *Chem. – Eur. J.* **2015**, *21*, 500–519.
- (10) Silipo, A.; Molinaro, A. The Diversity of the Core Oligosaccharide in Lipopolysaccharides. In *Endotoxins: Structure, Function and Recognition*; Wang, X., Quinn, P. J., Eds.; Subcellular Biochemistry; Springer Netherlands, 2010; pp 69–99.
- (11) Lerouge, I.; Vanderleyden, J. O-Antigen Structural Variation: Mechanisms and Possible Roles in Animal/Plant–Microbe Interactions. *FEMS Microbiol. Rev.* **2002**, *26*, 17–47.
- (12) Preston, Andrew; Mandrell, Robert E.; Gibson, Bradford W.; Apicella, Michael A. The Lipooligosaccharides of Pathogenic Gram-Negative Bacteria. *Crit. Rev. Microbiol.* **1996**, *22*, 139–180.
- (13) Fridrich, E.; Whitfield, C. Lipopolysaccharide Inner Core Oligosaccharide Structure and Outer Membrane Stability in Human Pathogens Belonging to the Enterobacteriaceae. *J. Endotoxin Res.* **2005**, *11*, 133–144.

- (14) Needham, B. D.; Trent, M. S. Fortifying the Barrier: The Impact of Lipid A Remodelling on Bacterial Pathogenesis. *Nat. Rev. Microbiol.* **2013**, *11*, 467–481.
- (15) Whitfield, C.; Trent, M. S. Biosynthesis and Export of Bacterial Lipopolysaccharides. *Annu. Rev. Biochem.* **2014**, *83*, 99–128.
- (16) Maldonado, R. F.; Sá-Correia, I.; Valvano, M. A. Lipopolysaccharide Modification in Gram-Negative Bacteria during Chronic Infection. *FEMS Microbiol. Rev.* **2016**, *40*, 480–493.
- (17) Nuri, R.; Shprung, T.; Shai, Y. Defensive Remodeling: How Bacterial Surface Properties and Biofilm Formation Promote Resistance to Antimicrobial Peptides. *Biochim. Biophys. Acta BBA - Biomembr.* **2015**, *1848*, 3089–3100.
- (18) Salazar, J.; Alarcón, M.; Huerta, J.; Navarro, B.; Aguayo, D. Phosphoethanolamine Addition to the Heptose I of the Lipopolysaccharide Modifies the Inner Core Structure and Has an Impact on the Binding of Polymyxin B to the Escherichia Coli Outer Membrane. *Arch. Biochem. Biophys.* **2017**, *620*, 28–34.
- (19) Agrawal, A.; Weisshaar, J. C. Effects of Alterations of the E. Coli Lipopolysaccharide Layer on Membrane Permeabilization Events Induced by Cecropin A. *Biochim. Biophys. Acta BBA - Biomembr.* **2018**, *1860*, 1470–1479.
- (20) Wang, Z.; Wang, J.; Ren, G.; Li, Y.; Wang, X. Influence of Core Oligosaccharide of Lipopolysaccharide to Outer Membrane Behavior of Escherichia Coli. *Mar. Drugs* **2015**, *13*, 3325–3339.
- (21) Marr, N.; Tirsoaga, A.; Blanot, D.; Fernandez, R.; Caroff, M. Glucosamine Found as a Substituent of Both Phosphate Groups in Bordetella Lipid A Backbones: Role of a BvgAS-Activated ArnT Ortholog. *J. Bacteriol.* **2008**, *190*, 4281–4290.
- (22) Shah, N. R.; Hancock, R. E. W.; Fernandez, R. C. Bordetella Pertussis Lipid A Glucosamine Modification Confers Resistance to Cationic Antimicrobial Peptides and Increases Resistance to Outer Membrane Perturbation. *Antimicrob. Agents Chemother.* **2014**, *58*, 4931–4934.
- (23) Tzeng, Y.-L.; Stephens, D. S. Antimicrobial Peptide Resistance in Neisseria Meningitidis. *Biochim. Biophys. Acta BBA - Biomembr.* **2015**, *1848*, 3026–3031.
- (24) Cullen, T. W.; Giles, D. K.; Wolf, L. N.; Ecobichon, C.; Boneca, I. G.; Trent, M. S. Helicobacter Pylori versus the Host: Remodeling of the Bacterial Outer Membrane Is Required for Survival in the Gastric Mucosa. *PLOS Pathog.* **2011**, *7*, e1002454.
- (25) Leung, L. M.; Cooper, V. S.; Rasko, D. A.; Guo, Q.; Pacey, M. P.; McElheny, C. L.; Mettus, R. T.; Yoon, S. H.; Goodlett, D. R.; Ernst, R. K.; Doi, Y. Structural Modification of LPS in Colistin-Resistant, KPC-Producing Klebsiella Pneumoniae. *J. Antimicrob. Chemother.* **2017**, *72*, 3035–3042.

- (26) Liu, Y.-Y.; Chandler, C. E.; Leung, L. M.; McElheny, C. L.; Mettus, R. T.; Shanks, R. M. Q.; Liu, J.-H.; Goodlett, D. R.; Ernst, R. K.; Doi, Y. Structural Modification of Lipopolysaccharide Conferred by Mcr-1 in Gram-Negative ESKAPE Pathogens. *Antimicrob. Agents Chemother.* **2017**, *61*, e00580-17.
- (27) Adams, M. D.; Nickel, G. C.; Bajaksouzian, S.; Lavender, H.; Murthy, A. R.; Jacobs, M. R.; Bonomo, R. A. Resistance to Colistin in *Acinetobacter Baumannii* Associated with Mutations in the PmrAB Two-Component System. *Antimicrob. Agents Chemother.* **2009**, *53*, 3628–3634.
- (28) Qureshi, Z. A.; Hittle, L. E.; O’Hara, J. A.; Rivera, J. I.; Syed, A.; Shields, R. K.; Pasculle, A. W.; Ernst, R. K.; Doi, Y. Colistin-Resistant *Acinetobacter Baumannii*: Beyond Carbapenem Resistance. *Clin. Infect. Dis.* **2015**, civ048.
- (29) M. Crittenden, C.; M. Herrera, C.; E. Williams, P.; P. Ricci, D.; R. Swem, L.; Stephen Trent, M.; S. Brodbelt, J. Mapping Phosphate Modifications of Substituted Lipid A via a Targeted MS 3 CID/UVPD Strategy. *Analyst* **2018**.
- (30) Zhao, Y.; Arce-Gorvel, V.; Conde-Álvarez, R.; Moriyon, I.; Gorvel, J.-P. Vaccine Development Targeting Lipopolysaccharide Structure Modification. *Microbes Infect.* **2017**.
- (31) Micoli, F.; Costantino, P.; Adamo, R. Potential Targets for next Generation Antimicrobial Glycoconjugate Vaccines. *FEMS Microbiol. Rev.* **2018**, *42*, 388–423.
- (32) Astronomo, R. D.; Burton, D. R. Carbohydrate Vaccines: Developing Sweet Solutions to Sticky Situations? *Nat. Rev. Drug Discov.* **2010**, *9*, 308–324.
- (33) Rappuoli, R. Glycoconjugate Vaccines: Principles and Mechanisms. *Sci. Transl. Med.* **2018**, *10*, eaat4615.
- (34) Chen, W. Current Advances and Challenges in the Development of *Acinetobacter* Vaccines. *Hum. Vaccines Immunother.* **2015**, *11*, 2495–2500.
- (35) Berti, F.; Adamo, R. Antimicrobial Glycoconjugate Vaccines: An Overview of Classic and Modern Approaches for Protein Modification. *Chem. Soc. Rev.* **2018**.
- (36) Kilár, A.; Dörnyei, Á.; Kocsis, B. Structural Characterization of Bacterial Lipopolysaccharides with Mass Spectrometry and On- and off-Line Separation Techniques. *Mass Spectrom. Rev.* **2013**, *32*, 90–117.
- (37) Banoub, J. H.; Aneed, A. E.; Cohen, A. M.; Joly, N. Structural Investigation of Bacterial Lipopolysaccharides by Mass Spectrometry and Tandem Mass Spectrometry. *Mass Spectrom. Rev.* **2010**, *29*, 606–650.
- (38) Sándor, V.; Dörnyei, Á.; Makszin, L.; Kilár, F.; Péterfi, Z.; Kocsis, B.; Kilár, A. Characterization of Complex, Heterogeneous Lipid A Samples Using HPLC–MS/MS Technique I. Overall Analysis with Respect to Acylation,

- Phosphorylation and Isobaric Distribution. *J. Mass Spectrom.* **2016**, *51*, 1043–1063.
- (39) Sándor, V.; Kilár, A.; Kilár, F.; Kocsis, B.; Dörnyei, Á. Characterization of Complex, Heterogeneous Lipid A Samples Using HPLC–MS/MS Technique II. Structural Elucidation of Non-Phosphorylated Lipid A by Negative-Ion Mode Tandem Mass Spectrometry. *J. Mass Spectrom.* **51**, 615–628.
 - (40) Sándor, V.; Kilár, A.; Kilár, F.; Kocsis, B.; Dörnyei, Á. Characterization of Complex, Heterogeneous Lipid A Samples Using HPLC–MS/MS Technique III. Positive-Ion Mode Tandem Mass Spectrometry to Reveal Phosphorylation and Acylation Patterns of Lipid A. *J. Mass Spectrom.* **2018**, *53*, 146–161.
 - (41) Madsen, J. A.; Cullen, T. W.; Trent, M. S.; Brodbelt, J. S. IR and UV Photodissociation as Analytical Tools for Characterizing Lipid A Structures. *Anal. Chem.* **2011**, *83*, 5107–5113.
 - (42) O’Brien, J. P.; Needham, B. D.; Henderson, J. C.; Nowicki, E. M.; Trent, M. S.; Brodbelt, J. S. 193 nm Ultraviolet Photodissociation Mass Spectrometry for the Structural Elucidation of Lipid A Compounds in Complex Mixtures. *Anal. Chem.* **2014**, *86*, 2138–2145.
 - (43) Morrison, L. J.; Parker, W. R.; Holden, D. D.; Henderson, J. C.; Boll, J. M.; Trent, M. S.; Brodbelt, J. S. UVLiPiD: A UVPD-Based Hierarchical Approach for De Novo Characterization of Lipid A Structures. *Anal. Chem.* **2016**, *88*, 1812–1820.
 - (44) Kondakov, A.; Lindner, B. Structural Characterization of Complex Bacterial Glycolipids by Fourier Transform Mass Spectrometry. *Eur. J. Mass Spectrom.* **2005**, *11*, 535–546.
 - (45) O’Brien, J. P.; Needham, B. D.; Brown, D. B.; Trent, M. S.; Brodbelt, J. S. Top-down Strategies for the Structural Elucidation of Intact Gram-Negative Bacterial Endotoxins. *Chem. Sci.* **2014**, *5*, 4291–4301.
 - (46) Hübner, G.; Lindner, B. Separation of R-Form Lipopolysaccharide and Lipid A by CE–Fourier-Transform Ion Cyclotron Resonance MS. *Electrophoresis* **2009**, *30*, 1808–1816.
 - (47) Sturiale, L.; Garozzo, D.; Silipo, A.; Lanzetta, R.; Parrilli, M.; Molinaro, A. New Conditions for Matrix-Assisted Laser Desorption/Ionization Mass Spectrometry of Native Bacterial R-Type Lipopolysaccharides. *Rapid Commun. Mass Spectrom.* **2005**, *19*, 1829–1834.
 - (48) John, C. M.; Liu, M.; Jarvis, G. A. Profiles of Structural Heterogeneity in Native Lipooligosaccharides of Neisseria and Cytokine Induction. *J. Lipid Res.* **2009**, *50*, 424–438.

- (49) John, C. M.; Liu, M.; Phillips, N. J.; Yang, Z.; Funk, C. R.; Zimmerman, L. I.; Griffiss, J. M.; Stein, D. C.; Jarvis, G. A. Lack of Lipid A Pyrophosphorylation and Functional LptA Reduces Inflammation by *Neisseria* Commensals. *Infect. Immun.* **2012**, *80*, 4014–4026.
- (50) Stephenson, H. N.; John, C. M.; Naz, N.; Gundogdu, O.; Dorrell, N.; Wren, B. W.; Jarvis, G. A.; Bajaj-Elliott, M. *Campylobacter* Jejuni Lipooligosaccharide Sialylation, Phosphorylation, and Amide/Ester Linkage Modifications Fine-Tune Human Toll-like Receptor 4 Activation. *J. Biol. Chem.* **2013**, *288*, 19661–19672.
- (51) Sturiale, L.; Palmigiano, A.; Silipo, A.; Knirel, Y. A.; Anisimov, A. P.; Lanzetta, R.; Parrilli, M.; Molinaro, A.; Garozzo, D. Reflectron MALDI TOF and MALDI TOF/TOF Mass Spectrometry Reveal Novel Structural Details of Native Lipooligosaccharides. *J. Mass Spectrom.* **2011**, *46*, 1135–1142.
- (52) Klein, D. R.; Holden, D. D.; Brodbelt, J. S. Shotgun Analysis of Rough-Type Lipopolysaccharides Using Ultraviolet Photodissociation Mass Spectrometry. *Anal. Chem.* **2016**, *88*, 1044–1051.
- (53) Phillips, N. J.; John, C. M.; Jarvis, G. A. Analysis of Bacterial Lipooligosaccharides by MALDI-TOF MS with Traveling Wave Ion Mobility. *J. Am. Soc. Mass Spectrom.* **2016**, *27*, 1263–1276.
- (54) Oyler, B. L.; Khan, M. M.; Smith, D. F.; Harberts, E. M.; Kilgour, D. P. A.; Ernst, R. K.; Cross, A. S.; Goodlett, D. R. Top Down Tandem Mass Spectrometric Analysis of a Chemically Modified Rough-Type Lipopolysaccharide Vaccine Candidate. *J. Am. Soc. Mass Spectrom.* **2018**, 1–9.
- (55) Raetz, C. R. H.; Garrett, T. A.; Reynolds, C. M.; Shaw, W. A.; Moore, J. D.; Smith, D. C.; Ribeiro, A. A.; Murphy, R. C.; Ulevitch, R. J.; Fearn, C.; Reichart, D.; Glass, C. K.; Benner, C.; Subramaniam, S.; Harkewicz, R.; Bowers-Gentry, R. C.; Buczynski, M. W.; Cooper, J. A.; Deems, R. A.; Dennis, E. A. Kdo2-Lipid A of *Escherichia Coli*, a Defined Endotoxin That Activates Macrophages via TLR-4. *J. Lipid Res.* **2006**, *47*, 1097–1111.
- (56) Brodbelt, J. S. Photodissociation Mass Spectrometry: New Tools for Characterization of Biological Molecules. *Chem. Soc. Rev.* **2014**, *43*, 2757–2783.
- (57) Shaw, J. B.; Li, W.; Holden, D. D.; Zhang, Y.; Griep-Raming, J.; Fellers, R. T.; Early, B. P.; Thomas, P. M.; Kelleher, N. L.; Brodbelt, J. S. Complete Protein Characterization Using Top-Down Mass Spectrometry and Ultraviolet Photodissociation. *J. Am. Chem. Soc.* **2013**, *135*, 12646–12651.
- (58) Westphal, O.; Jann, K. Bacterial Lipopolysaccharides: Extraction with Phenol-Water and Further Applications of the Procedure. In *Methods in Carbohydrate Chemistry*; Whistler, R. L., Ed.; Academic Press, Inc.: New York, 1965; Vol. 5, pp 83–91.

- (59) Varki, A.; Cummings, R. D.; Aebi, M.; Packer, N. H.; Seeberger, P. H.; Esko, J. D.; Stanley, P.; Hart, G.; Darvill, A.; Kinoshita, T.; Prestegard, J. J.; Schnaar, R. L.; Freeze, H. H.; Marth, J. D.; Bertozzi, C. R.; Etzler, M. E.; Frank, M.; Vliegthart, J. F.; Lütke, T.; Perez, S.; Bolton, E.; Rudd, P.; Paulson, J.; Kanehisa, M.; Toukach, P.; Aoki-Kinoshita, K. F.; Dell, A.; Narimatsu, H.; York, W.; Taniguchi, N.; Kornfeld, S. Symbol Nomenclature for Graphical Representations of Glycans. *Glycobiology* **2015**, *25*, 1323–1324.
- (60) Domon, B.; Costello, C. E. A Systematic Nomenclature for Carbohydrate Fragmentations in FAB-MS/MS Spectra of Glycoconjugates. *Glycoconj. J.* **1988**, *5*, 397–409.
- (61) Furey, A.; Moriarty, M.; Bane, V.; Kinsella, B.; Lehane, M. Ion Suppression; A Critical Review on Causes, Evaluation, Prevention and Applications. *Talanta* **2013**, *115*, 104–122.
- (62) Heinrichs, D. E.; Yethon, J. A.; Whitfield, C. Molecular Basis for Structural Diversity in the Core Regions of the Lipopolysaccharides of Escherichia Coli and Salmonella Enterica. *Mol. Microbiol.* **1998**, *30*, 221–232.
- (63) Müller-Loennies, S.; Lindner, B.; Brade, H. Structural Analysis of Deacylated Lipopolysaccharide of Escherichia Coli Strains 2513 (R4 Core-Type) and F653 (R3 Core-Type). *Eur. J. Biochem.* **2002**, *269*, 5982–5991.
- (64) Pogue, J. M.; Cohen, D. A.; Marchaim, D. Polymyxin-Resistant Acinetobacter Baumannii: Urgent Action Needed. *Clin. Infect. Dis.* **2015**.
- (65) Michalopoulos, A.; Falagas, M. E. Treatment of Acinetobacter Infections. *Expert Opin. Pharmacother.* **2010**, *11*, 779–788.
- (66) Vinogradov, E. V.; Duus, J. Ø.; Brade, H.; Holst, O. The Structure of the Carbohydrate Backbone of the Lipopolysaccharide from Acinetobacter Baumannii Strain ATCC 19606. *Eur. J. Biochem.* **2002**, *269*, 422–430.
- (67) Pelletier, M. R.; Casella, L. G.; Jones, J. W.; Adams, M. D.; Zurawski, D. V.; Hazlett, K. R. O.; Doi, Y.; Ernst, R. K. Unique Structural Modifications Are Present in the Lipopolysaccharide from Colistin-Resistant Strains of Acinetobacter Baumannii. *Antimicrob. Agents Chemother.* **2013**, *57*, 4831–4840.
- (68) Boll, J. M.; Tucker, A. T.; Klein, D. R.; Beltran, A. M.; Brodbelt, J. S.; Davies, B. W.; Trent, M. S. Reinforcing Lipid A Acylation on the Cell Surface of Acinetobacter Baumannii Promotes Cationic Antimicrobial Peptide Resistance and Desiccation Survival. *mBio* **2015**, *6*, e00478-15.

Chapter 7: Structural Characterization of Glycosaminoglycan Carbohydrates Using Ultraviolet Photodissociation*

7.1 OVERVIEW

Structural characterization of sulfated glycosaminoglycans (GAGs) by mass spectrometry has long been a formidable analytical challenge owing to their high structural variability and the propensity for sulfate decomposition upon activation with low-energy ion activation methods. While derivatization and complexation workflows have aimed to generate informative spectra using low-energy ion activation methods, alternative ion activation methods present the opportunity to obtain informative spectra from native GAG structures. Both electron- and photon-based activation methods, including electron detachment dissociation (EDD), negative electron transfer dissociation (NETD) and extreme ultraviolet photon activation, have been explored previously to overcome the limitations associated with low-energy activation methods for GAGs and other sulfated oligosaccharides. Further, implementation of such methods on high resolution mass spectrometers has aided the interpretation of the complex spectra generated. Here, we explore ultraviolet photodissociation (UVPD) implemented on an Orbitrap mass spectrometer as another option for structural characterization of GAGs. UVPD spectra for both dermatan and heparan sulfate structures display extensive fragmentation including both glycosidic and cross-ring cleavages with the extent of sulfate retention comparable to that observed by EDD and NETD. In addition, the

*Klein, D. R.; Leach III, F. E.; Amster, I. J.; Brodbelt, J. S. Structural Characterization of Glycosaminoglycans using Ultraviolet Photodissociation. *Anal. Chem.* **2019**, ASAP.

FEL assisted in making figures. FEL, IJA, and JSB provided mentorship and reviewed the manuscript prior to publication.

relatively short activation time of UVPD makes it promising for higher throughput analysis of GAGs in complex mixtures.

7.2 INTRODUCTION

Glycosaminoglycans (GAGs), linear polysaccharides composed of repeating hexosamine and uronic acid disaccharides, are complex molecules that participate in a number of biological processes ranging from tissue development to inflammation.¹⁻³ GAG structural complexity arises from variations in their degree of polymerization, the extent of saccharide sulfation, and uronic acid stereochemistry. Such modifications are responsible for the specific interactions GAGs have with proteins, with misregulation of modifications implicated in a number of genetic diseases, including Alzheimer's and cancer.⁴⁻⁷ Development and quality control of GAG therapeutics also relies on a detailed knowledge of GAG structures.^{1,8} In 2008, heparin, an anticoagulant drug, contaminated with oversulfated chondroitin sulfate resulted in 81 deaths.⁸ Detailed structural characterization of GAGs is therefore essential yet still impeded by a number of technical challenges. Advances in modern mass spectrometry, including the development of high resolution/high mass accuracy mass analyzers and hybrid instrumentation, have made it an indispensable tool for the structural characterization of GAGs.⁹⁻¹³ Owing to their acidic nature, GAGs are most frequently analyzed in the negative ion mode, and deprotonation of the sulfate half-ester leads to stabilization of this labile modification. If these moieties remain protonated, sequencing attempts with low-energy tandem mass spectrometry methods, including collision-induced dissociation (CID) and infrared multiphoton dissociation (IRMPD), or by using improper tuning conditions in high pressure regions of the mass spectrometer can result in preferential sulfate decomposition, especially for highly modified heparin and heparan sulfate. The

prevalence of sulfate decomposition impedes complete saccharide sequencing and sulfate localization.^{14,15} Previous studies have shown that informative CID spectra can be obtained after deprotonation of all sites of sulfation.^{16,17} Metal adduction using sodium or calcium ions effectively allows deprotonation of acidic sites that would otherwise lead to SO₃ loss and enables informative spectra to be obtained from low-energy collisional activated dissociation.^{14,18–20} Derivatization strategies, while requiring more sample preparation, have similarly been beneficial for obtaining information spectra upon low-energy collisional activated dissociation.^{21,22} High-energy collisional activation has also been found to produce informative MS/MS spectra with some fragments resulting from electron detachment.²³

As a result of the limitations of low-energy activation methods a number of alternative ion activation methods have successfully been applied to analyze GAGs. Electron-based activation methods include electron detachment dissociation (EDD)^{24–33}, negative electron transfer dissociation (NETD)^{33–37} and electron-induced dissociation (EID)³⁸. EDD produces an extensive array of fragment ions, including sulfate-retaining glycosidic and cross-ring cleavage products for both free acid and sodium-proton exchanged species with observed fragments resulting from both direct dissociation and electron detachment.^{24–27} Both EDD and NETD has also shown promise for distinguishing hexuronic acid epimers based on both the presence of unique fragments and fragment ion abundances.^{28–31} While long activation times and low abundance product ions have prevented coupling of EDD with online separations, successful interfacing of field asymmetric-waveform ion mobility spectrometry (FAIMS) with an EDD-equipped FTICR instrument has enabled gas-phase separation and detection of GAG epimers.³² NETD has also shown great promise as an alternative activation method for negative ions, exhibiting similar fragmentation to EDD and the potential to be

performed on any mass spectrometer capable of gas phase ion-ion reactions.^{33,35,36} The recent application of NETD to GAG analysis on an Orbitrap platform confirmed that NETD can produce highly informative spectra with activation times amenable to a chromatographic or electrophoretic timescale.³⁶

Ultraviolet photon-based activation methods have also been considered as alternatives to low energy methods for the analysis of GAGs anions.³⁹⁻⁴⁶ The use of UV photons for oligosaccharide fragmentation was first reported by Reilly.⁴⁷ In their work, both underivatized and derivatized oligosaccharides were fragmented on a home-build MALDI TOF/TOF equipped with a 157 nm excimer laser.⁴⁷⁻⁴⁹ Since then, others have investigated a range of wavelengths to activate oligosaccharides on a number of platforms. Racaud *et al.* performed ultraviolet photodissociation (UVPD) in the 220-290 nm range in an ion trap mass spectrometer on a set of heparin-derived disaccharides and observed informative cross-ring cleavage fragments.⁴⁰ UVPD favored a large number of cross ring cleavages in addition to unique electron-photodetachment ions with corresponding charge-reduced neutral loss products. Racaud *et al.* also investigated the influence of charge on the preference for fragmentation versus electron-photodetachment using UVPD.⁴¹ Similar to low-energy and electron-based activation methods, deprotonation of sulfate modification greatly influenced the fragmentation patterns with full deprotonation achieved through sodium adduction.^{40,41} Extreme UVPD (X-UVPD) at a photon energy of 18 eV was performed with synchrotron radiation on an ion trap mass spectrometer and provided detailed structure characterization of highly sulfated oligosaccharides.⁴³⁻⁴⁵ While synchrotrons provide a high-energy and tunable source of radiation, their limited accessibility make them less feasible for routine usage and broad applications. Moreover, while UVPD produces rich fragmentation patterns, it is apparent with increasingly large and complex biomolecules that interpretation of UVPD spectra

becomes challenging, if not impossible, when using low resolution ion trap mass spectrometers.

Excimer lasers have been successfully interfaced to a number of mass spectrometers and likewise provide access to high energy photons.⁵⁰ Integration of 193 nm excimer lasers with high accuracy Orbitrap mass analyzers has greatly expanded the utility of UVPD as an activation method for larger biomolecules, enabling successful interpretation of complex fragmentation patterns.⁵⁰⁻⁵² The successful structural characterization of acidic saccharides⁵³ and localization of sulfate modifications on peptides⁵⁴ using 193 nm UVPD, suggest it as a viable tool for GAG analysis. Additionally, the recent commercialization of UVPD with a 213 nm Nd:YAG laser has further increased its accessibility.^{55,56} The present study evaluates the use of UVPD for the structural characterization of GAGs. UVPD was found to perform comparably to collision-based activation methods for heparan and dermatan sulfate GAGs with low degrees of sulfation. More significantly, UVPD produced an extensive array of cross-ring cleavage fragments for fondaparinux, a highly sulfated heparin-like anticoagulant drug, enabling more detailed characterization than collision-based methods and comparable fragmentation to electron-based methods such as NETD.

7.3 EXPERIMENTAL

7.3.1 Materials and Reagents

HPLC grade methanol (MeOH) and water (H₂O) were acquired from EMD Millipore (Billerica, MA). Fondaparinux sodium was purchased from Sigma (St. Louis, MO). For data collection of fondaparinux with salt adduction, fondaparinux sodium was desalted on a PD MiniTrap G-10 column (GE Healthcare, Buckinghamshire, UK). Heparan sulfate tetrasaccharide standards were prepared by chemical synthesis using a

modular approach.⁵⁷ Dermatan sulfate oligosaccharides were prepared by partial enzymatic depolymerization of porcine intestinal mucosa dermatan sulfate (Celsus Laboratories, Cincinnati, OH, USA). A detailed protocol can be found in prior reports.³⁰ The structures of all the GAGs analyzed in the present study are shown in **Table 7.1**.

Table 7.1 Structure and molecular weights of all GAGs analyzed

GAG name	Molecular weight (Da)	Structure
GlcA-GlcNAc-GlcA-GlcNAc-(CH ₂) ₅ NH ₂	861.32	
IdoA-GlcNAc6S-GlcA-GlcNAc6S-(CH ₂) ₅ NH ₂	1021.24	
Dermatan sulfate dp4 (DS dp4)	918.14	
Dermatan sulfate dp 10 (DS dp10)	2263.35	
Fondaparinux	1506.95	

7.3.2 Mass Spectrometry

Higher-energy collisional dissociation (HCD) and UVPD spectra for all samples were collected on a Thermo Fisher Orbitrap Fusion Lumos mass spectrometer (San Jose, CA) equipped with a Coherent Excistar 193 nm excimer laser (Santa Clara, CA).⁵² Samples were diluted in 50:50 MeOH:H₂O to 50 µg/mL and sprayed from a nano-electrospray ionization (nanoESI) static source with a spray voltage of 0.8-1.2kV. The spray voltage and distance between the nanoESI source and the mass spectrometer inlet were adjusted to manipulate the observed charge state distribution. Spectra were collected in the negative ion mode at a resolving power of 120,000 at *m/z* 200 with the instrument in full-profile mode. The ion funnel RF was set to 10% to minimize sulfate decomposition in MS¹ spectra. Precursor ions were isolated in the ion trap with an

isolation width of 3 m/z . HCD was performed with a normalized collision energy (NCE) of 15-25, and UVPD was performed with 8 pulses at 4 mJ per pulse resulting in a 16 ms activation time. All presented HCD and UVPD spectra are an average of 50 transients. EDD and NETD spectra of IdoA-GlcNAc6S-GlcA-GlcNAc6S-(CH₂)₅NH₂ were collected on a 9.4 T Bruker Apex Ultra Qe FTMS mass spectrometer (Billerica, MA) and a Thermo Scientific Instruments Orbitrap Elite mass spectrometer (Bremen, Germany), respectively. EDD was performed on quadrupole mass selected precursor ions by irradiation with 19 eV electrons for a pulse duration of 1 s. Twenty-four spectra were averaged and internally calibrated. NETD was enabled by software modifications and performed on mass-selected precursors by ion-ion reaction with radical fluoranthene cations for 150 ms. Thirty-six spectra were summed with a specified resolution of 120,000. Fragment ions are labeled using Domon and Costello nomenclature (**Figure 7.1**).⁵⁸ Spectra were interpreted in a semi-automated fashion through the use of GlycoWorkbench.⁵⁹ Fragment ions maps are depicted using dashed lines drawn through chemical structures with hash marks at the ends of dashed lines to indicate the presence of a fragment ion. An open circle at the end of a hash mark indicates a fragment ion with loss of a single SO₃. A filled circle at the end of a hash mark indicates a fragment ion with loss of more than one SO₃. Donut plots represent percentages of the summed ion abundances for each ion type (glycosidic, cross-ring, glycosidic-SO₃, cross-ring-SO₃) relative to summed abundances of all ion types. Precursor neutral losses and ions resulting from electron-photodetachment are reported as percentages of the total ion current.

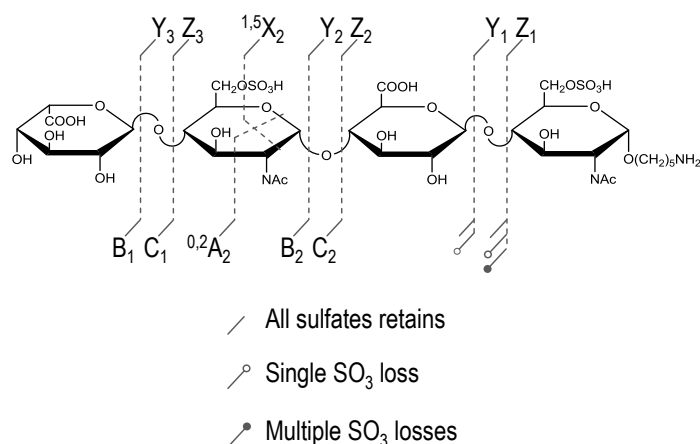


Figure 7.1 Domon and Costello nomenclature with key indicating the symbols used to denote sulfate retention and decomposition.⁵⁸

7.4 RESULTS AND DISCUSSION

Both synthetic and enzymatically-depolymerized GAG standards were analyzed to evaluate the capabilities of 193 nm UVPD for structural characterization, along with comparisons to HCD, EDD, and NETD spectra. **Figure 7.2** shows the UVPD and HCD spectra of the $[M-2H]^{2-}$ precursor ion of the unsulfated tetrasaccharide GlcA-GlcNAc-GlcA-GlcNAc-(CH₂)₅NH₂. The UVPD spectrum displays cleavage of every glycosidic bond in addition to many cross-ring cleavages distributed across the four monosaccharide residues.

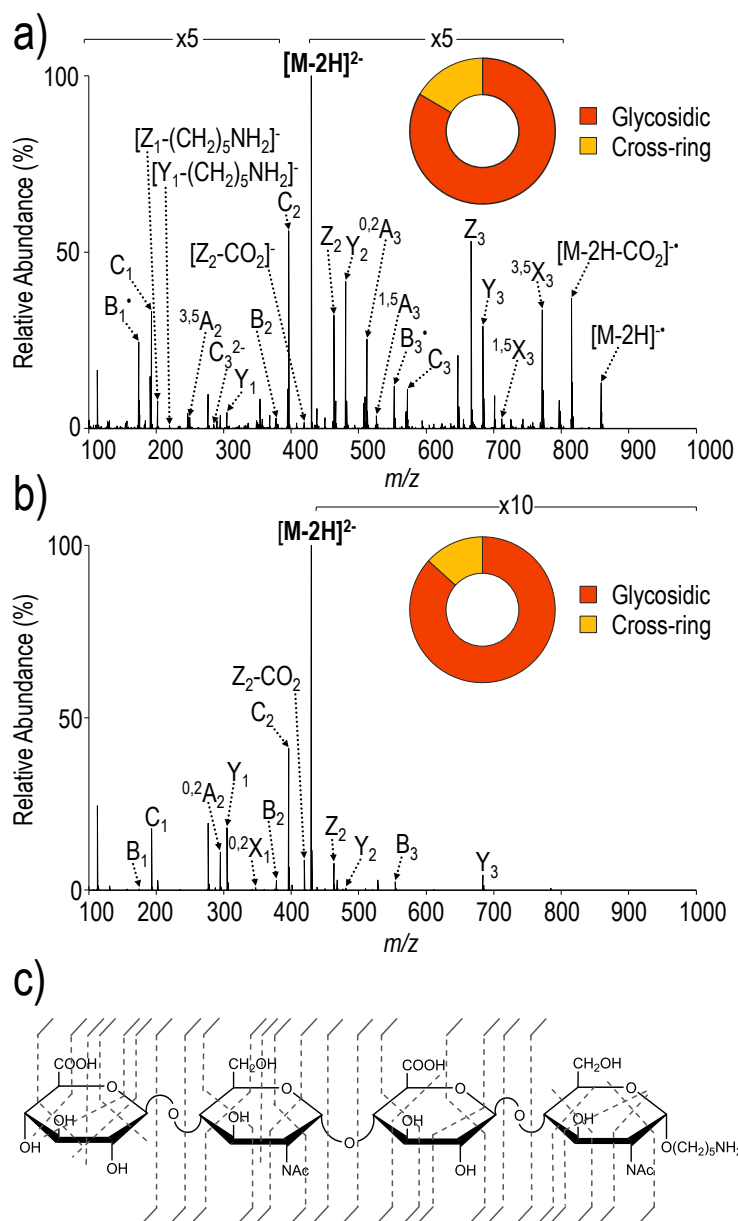


Figure 7.2 a) UVPD (8 pulses, 4 mJ) and b) HCD (NCE 20) spectrum of $[M-2H]^{2-}$ (m/z 429) of GlcA-GlcNAc-GlcA-GlcNAc- $(CH_2)_5NH_2$ and c) 193 nm UVPD fragment ion map. The UVPD spectrum contains an inset donut plot depicting the fragment ion composition (based on summed abundances of products from glycosidic versus cross-ring cleavages). **Table 7.2** and **Table 7.3** contain lists of identified fragment ions for UVPD and HCD, respectively (Chapter 7, Supporting Information).

The UVPD spectrum also contains a characteristic charge-reduced, electron-photodetachment product at m/z 859.31, which accounts for 2.6% of the total ion current, in addition the loss of CO₂ from that species (m/z 815.32) which accounts for 7.6% of the total ion current. HCD of the same tetrasaccharide primarily yielded glycosidic cleavages in addition to a few low abundance cross-ring cleavages. The distribution of glycosidic and cross-ring fragments between HCD (glycosidic = 86.7%; cross-ring = 13.2%) and UVPD (glycosidic = 83.5%; cross-ring = 16.5%), as depicted in the donut plots of **Figure 7.2**, is quite similar owing to the lack of labile sulfate modifications and ionization of both carboxylates. Comparison of fragment ions that are observed in both the UVPD and HCD spectra reveals that although B/Y and C/Z are prominent in both spectra, additional odd-electron species are generated exclusively upon UVPD. For example, in the HCD spectrum the even-electron B₃ ion of m/z 554.14 is observed, while both even- and odd-electron B₃ and B₃[•] ions appear (m/z 554.14 and m/z 553.13) in the UVPD spectrum (**Figure 7.3**, **Table 7.2**, **Table 7.3**). These results are analogous to prior findings reported for the electron-based activation method EDD and suggest radical-based fragmentation as one of the contributing pathways of UVPD.^{24,25} Moreover, the broad array of cross-ring cleavages observed upon UVPD, including fragmentation across residues without ionizable sites, suggests that radical migration may play an active role in the fragmentation processes akin to prior observations for EDD and NETD of GAGs.²⁵

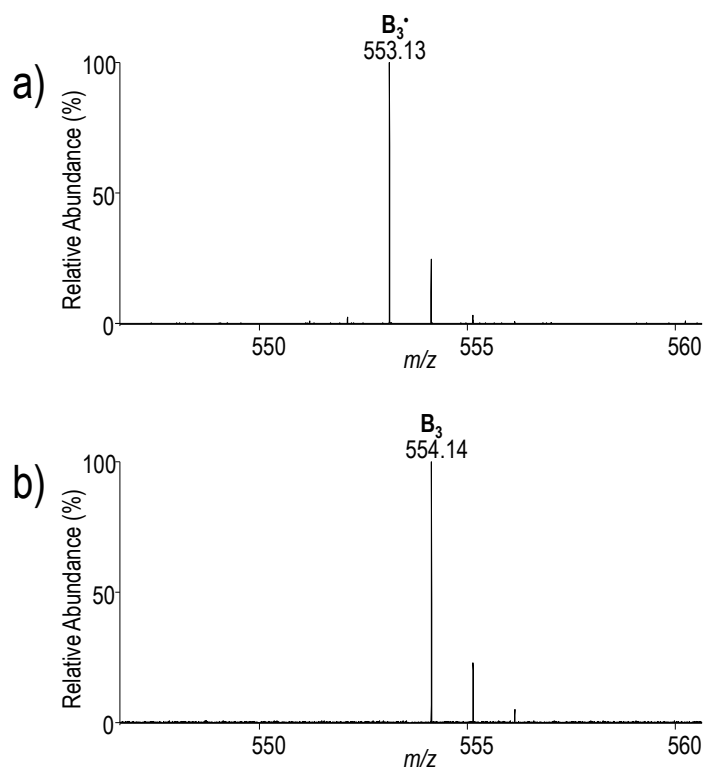


Figure 7.3 Expanded a) UVPD (8 pulses, 4 mJ) and b) HCD (NCE 20) spectra $[M-2H]^{2-}$ (m/z 429) of GlcA-GlcNAc-GlcA-GlcNAc- $(CH_2)_5NH_2$.

Figure 7.4 shows the UVPD and HCD spectra of the $[M-2H]^{2-}$ precursor ion of the tetrasaccharide IdoA-GlcNAc6S-GlcA-GlcNAc6S- $(CH_2)_5NH_2$, a synthetic heparan sulfate with a low degree of sulfation. While the HCD spectrum does contain informative glycosidic fragments (primarily B, C, Y and Z ions), sulfate decomposition is a predominant fragmentation pathway. Sulfate decomposition is possible when these sites are protonated, a process that can result from either protonation during ionization or possible proton migration in the gas phase.^{24,60} With increasingly sulfated heparan sulfate species that have more than more than one sulfate per disaccharide, complete deprotonation is unlikely owing to charge repulsion, and incomplete deprotonation contributes to excessive sulfate decomposition upon collisional activation.

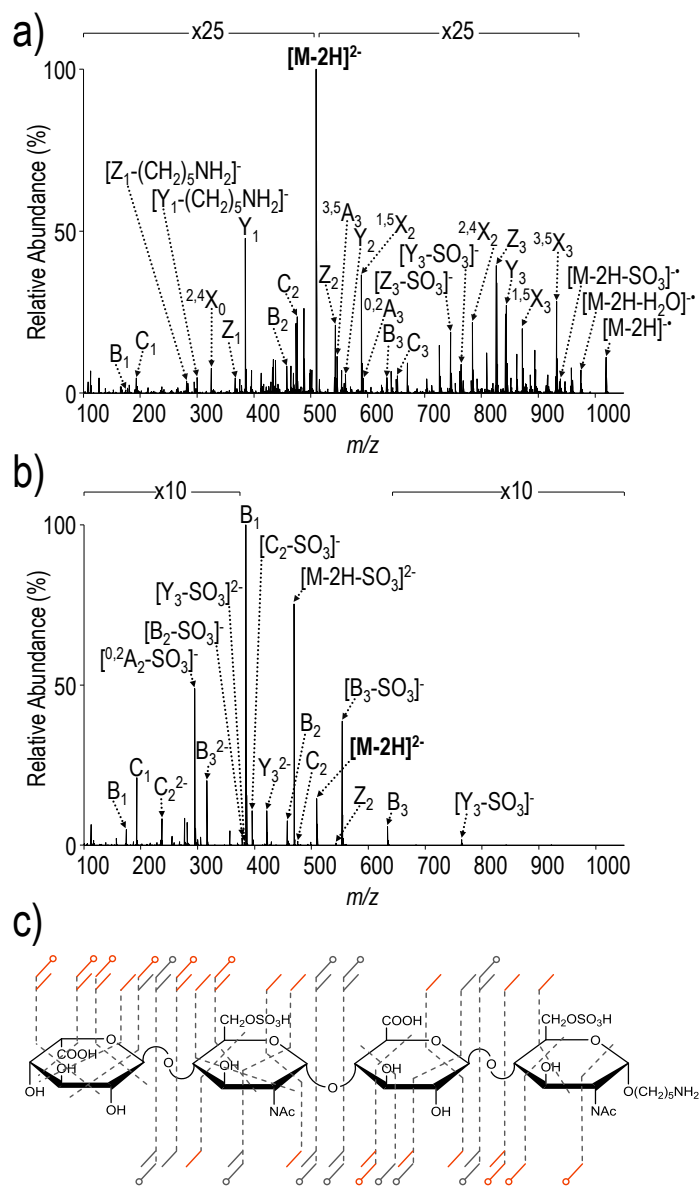


Figure 7.4 a) UVPD and b) HCD (NCE 25) spectra of $[M-2H]^{2-}$ (m/z 509) of IdoA-GlcNAc6S-GlcA-GlcNAc6S- $(CH_2)_5NH_2$. c) Fragment ion map contain fragment ions for both UVPD and HCD. Fragment ions only produced exclusively by UVPD are in red. **Table 7.4** and **Table 7.5** contain lists of identified fragment ions for UVPD and HCD, respectively (Chapter 7, Supporting Information).

In contrast, the UVPD spectrum exhibits cleavage of every glycosidic bond in addition to cross-ring cleavages with considerably less sulfate loss. Cross-ring cleavages

allow determination of the saccharide linkage pattern and enable localization of 6-*O* sulfation to the glucosamine residues. Similar to GlcA-GlcNAc-GlcA-GlcNAc-(CH₂)₅NH₂, UVPD of IdoA-GlcNAc6S-GlcA-GlcNAc6S-(CH₂)₅NH₂ (2-) generates an electron-photodetachment fragment of m/z 1019.22, in addition to a series of secondary electron-photodetachment products (m/z 975.23 and m/z 939.26) originating from neutral losses of CO₂ and SO₃, respectively. A comparative summary of fragmentation pathways for this compound in EDD, NETD, and UVPD is visualized in the donut plots in **Figure 7.5**. The predominant ion of m/z 469.63 corresponding to sulfate decomposition from the precursor (**Figure 7.4b**) accounts for 18.1% of the total ion current. Based on the summed abundances of glycosidic and cross-ring fragments in the HCD spectrum, 28.2% and 2.7% of the glycosidic and cross-ring fragments, respectively, undergo sulfate decomposition. For EDD, NETD, and UVPD, 5.4%, 0.0% and 10.3% of glycosidic, and 1.3%, 4.7% and 5.2% of cross-ring fragments, respectively, undergo sulfate decomposition relative to the total summed abundances of glycosidic and cross-ring fragments. EDD, NETD, and UVPD all exhibit less sulfate decomposition than HCD and generally produce spectra that are more structurally informative. While the distribution of glycosidic and cross-ring cleavages is quite comparable between NETD and UVPD, EDD appears to favor production of glycosidic cleavages. Based on the summed abundances of all cross-ring fragment ions, 33.2% and 38.6% are sulfate-retaining cross-ring fragments for NETD and UVPD, respectively, while only 4.9% are sulfate-retaining cross-ring fragments for EDD.

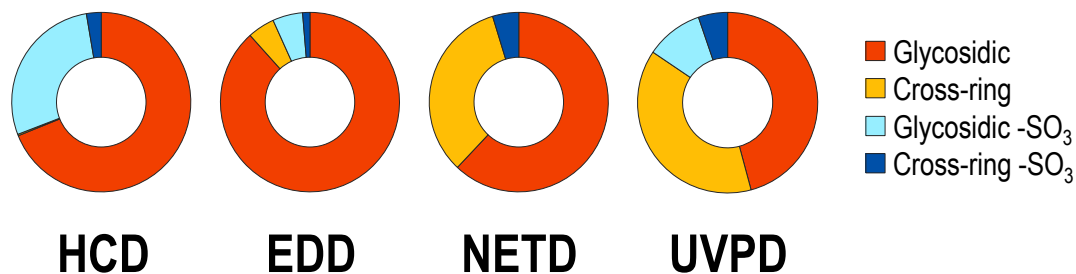


Figure 7.5 Donut plots depicting fragment ion compositions for HCD, EDD, NETD and UVPD for $[M-2H]^{2-}$ of IdoA-GlcNAc6S-GlcA-GlcNAc6S-(CH₂)₅NH₂ based on summed abundances of fragment types. **Table 7.6** and **Table 7.7** contain lists of identified fragment ions for EDD and NETD, respectively (Chapter 7, Supporting Information).

Dermatan sulfate (DS) is a sulfated GAG composed of repeating β -1,4 linked disaccharide units each comprised of β 1,3-linked iduronic acid and 4-O-sulfated N-acetyl galactosamine (GalNAc) residues. **Figure 7.6** shows the UVPD spectrum for a doubly sulfated DS tetrasaccharide. Although similar in length and sulfation extent, it contains a different linkage pattern and therefore different sulfate positions, and differing uronic acid stereochemistry than IdoA-GlcNAc6S-GlcA-GlcNAc6S-(CH₂)₅NH₂.

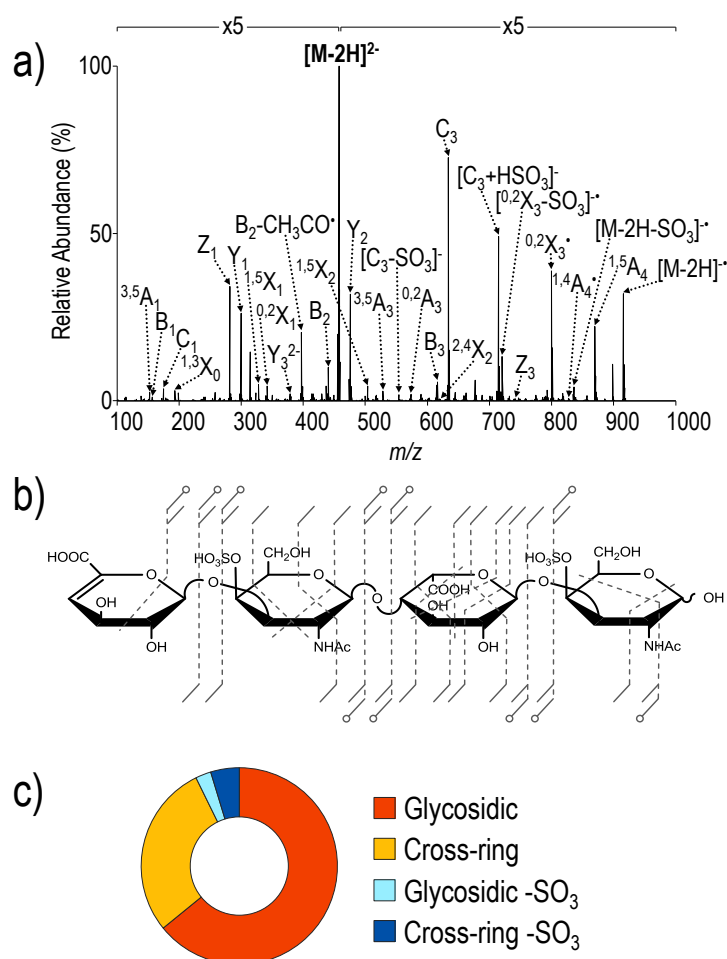


Figure 7.6 a) UVPD spectrum of $[M-2H]^{2-}$ (m/z 458) of DS dp4, b) UVPD fragment ion map, and c) UVPD donut plot depicting the fragment ion composition based on summed abundances of fragment types. **Table 7.8** contains a list of identified fragment ions (Chapter 7, Supporting Information).

These subtle structural differences have resulted in challenges to determine sequence and epimer content of chondroitin sulfate (CS)/DS GAGs *de novo*.^{25,30} The UVPD spectrum of $[M-2H]^{2-}$ contains a complete series of glycosidic cleavages in addition to cross-ring cleavages that again enable localization of sulfate modifications. For example, pairs of fragment ions, Z_3 and $^{2,4}X_2$, and C_3 and $^{1,4}A_4$, confirm 4-*O* sulfation of each GalNAc. These cross-ring cleavages do not arise during EDD or NETD of the same precursor ion.

The symmetry of this GAG precludes differentiation of C_2/Z_2 ions as these fragment ions are isobaric with the precursor ion. UVPD again causes a relatively low degree of sulfate decomposition, thus minimizing the congestion of the spectrum with uninformative ions. In general, a larger number of cross-ring fragments were identified for UVPD of DS dp4 compared to EDD and NETD, which is perhaps related in part to the increased signal-to-noise of the UVPD spectrum.^{25,34} We estimate that approximately 20-30% of ions in the UVPD spectra are currently unassigned, whereas this value is 10-20% in EDD/NETD spectra. Interestingly, there is a prominent fragment ion of m/z 715.05 (1-). Further interrogation of this ion via MS^3 results in a predominant neutral loss of 80.96 Da (HSO_3^{\cdot}) to form an abundant C_3 ion of m/z 634.09 (**Figure 7.7**). We speculate that this product arises during MS^2 from a gas-phase rearrangement that entails loss of GalNAc by glycosidic bond cleavage in conjunction with the transfer of the sulfate modification to the reducing end of the incipient product. This fragment ion occurs in the 1- charge state and contains all sites of ionization; therefore this fragment is likely an odd-electron ion resulting from electron-photodetachment. The MS^3 spectrum also shows an ion of m/z 272.99, corresponding to a sulfate-containing uronic acid, further suggesting retention of the reducing end 4-*O* GalNAc sulfate group on uronic acid. This unusual ion of m/z 715.05 has also been observed in EDD and NETD spectra of $[M-2H]^{2-}$ of DS dp4, but has not been previously assigned.^{25,30} UVPD of $[M-3H]^{3-}$ does not generate the ion at m/z 715.05, indicating that number and sites of deprotonation influence gas-phase rearrangement processes (**Figure 7.8**). As expected, $[M-3H]^{3-}$ yields lower percentages of sulfate decomposition in relation to the summed abundances of the glycosidic and cross-ring fragments; $[M-3H]^{3-}$ has 0.7% and 0.02% sulfate decomposition for glycosidic and cross-ring fragments, respectively, whereas $[M-2H]^{2-}$ displays 2.6% and 4.7% sulfate decomposition for glycosidic and cross-ring fragment, respectively.

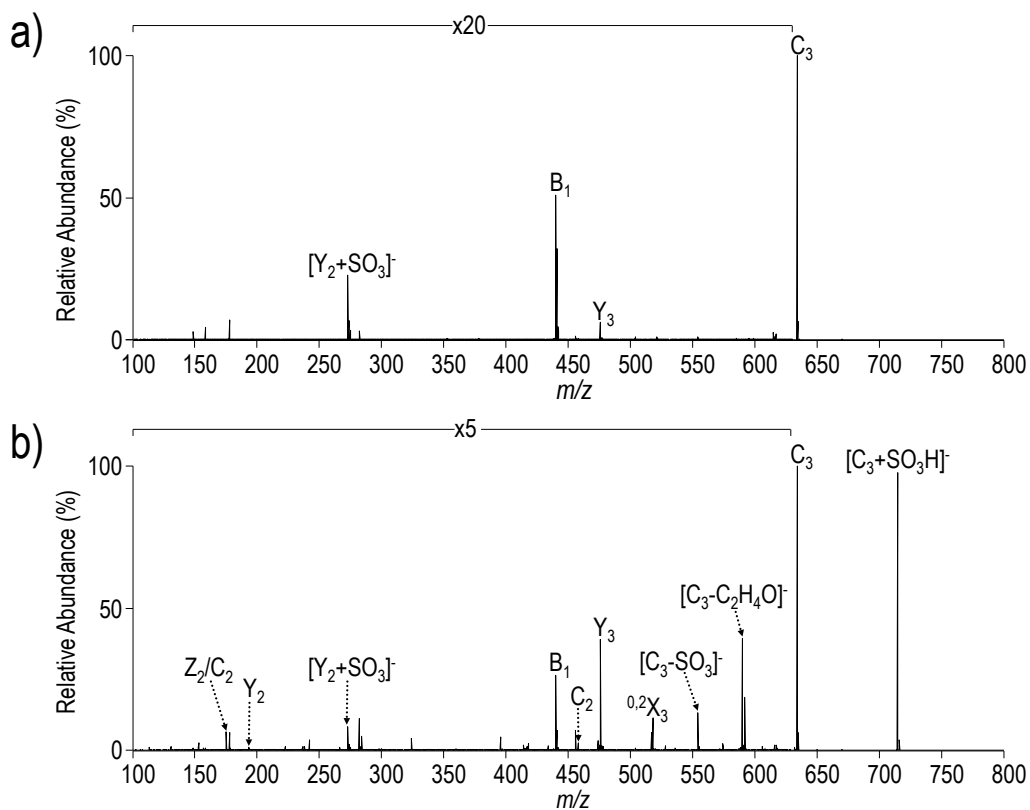
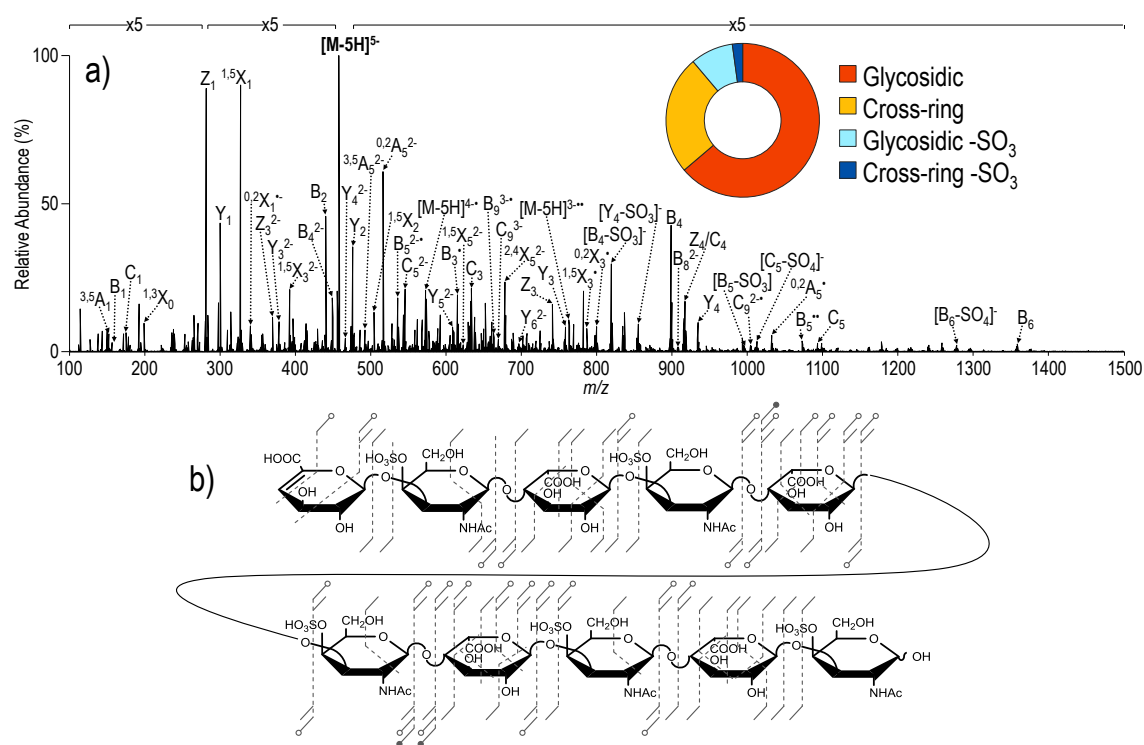


Figure 7.7 MS^3 activation of the fragment ion m/z 715.05 from DS dp4 by a) UVPD (8 pulses, 4 mJ)/HCD (NCE 20) and b) UVPD (8 pulses, 4 mJ)/UVPD (8 pulses, 4 mJ). **Tables 7.9** and **7.10** contain lists of identified fragment ions for UVPD/HCD and UVPD/UVPD, respectively (Chapter 7, Supporting Information).

degree of sulfate decomposition. In addition, ions originating from sequential photodetachment events, analogous to multiple electron transfer events that are possible with NETD, are observed.⁶¹ For example, ions of m/z 763.43 and m/z 1145.15 correspond to $[M-5H]^{3-}$ and $[M-5H]^{2-}$, representing doubly and triply charge-reduced species. The observed UVPD fragmentation pattern for DS dp10 is quite similar to that of EDD, with UVPD affording more identified cross-ring fragments.²⁵



observed from EDD^{25,30} and NETD,^{30,34} including abundant uronic acid cross-ring cleavages, albeit production of more abundant fragment ions by UVPD than EDD with a significantly shorter ion activation period.

The prior examples have demonstrated the utility of UVPD in analytes with varied sulfation density (0-1 per dp2) and oligomer length yet were all homopolymers. Fondaparinux (trade name Arixtra) is a synthetic, highly-sulfated pentasaccharide with anticoagulant activity.⁶² The sulfation pattern of fondaparinux is based on a naturally occurring pentasaccharide motif in heparin that binds antithrombin III, and is therefore representative of the complex GAG structures that occur naturally in heteropolymers. Fondaparinux has therefore served as a benchmark for appraisal of new GAG ion activation methods. As stated previously, with increasingly sulfated GAGs, charge repulsion limits the number of ionized sites during ESI and promotes sulfate decomposition via residual protons. Assessing the impact of precursor charge state in conjunction with the use of sodium adduction to achieve a higher degree of deprotonation is a key milestone in the evaluation of performance metrics of MS/MS methods. While deprotonation of highly-sulfated GAGs via sodium adduction increases the effectiveness of collisional activation, benefits are only observed when all sites of ionization are deprotonated.¹⁴ The limited utility of collisional activation for highly-sulfated GAGs has led to exploration of other ion activation methods, including NETD. For comparison to previously reported collisional activation and NETD data, UVPD was used to characterize two ionization states of sodiated fondaparinux ($[M-8H+3Na]^{5-}$ and $[M-10H+5Na]^{5-}$).^{14,36} **Figure 7.10** shows the UVPD mass spectrum acquired for the $[M-8H+3Na]^{5-}$. This charge state represents one in which the number of ionized sites matches the number of sulfate groups in an attempt to minimize sulfate decomposition. The fragment ion map in **Figure 7.10b** reflects cleavage between all saccharides while the

donut plot in **Figure 7.10a** confirms a relatively low degree of SO₃ loss (glycosidic-SO₃ = 7.3%; cross-ring-SO₃ = 0.3%).

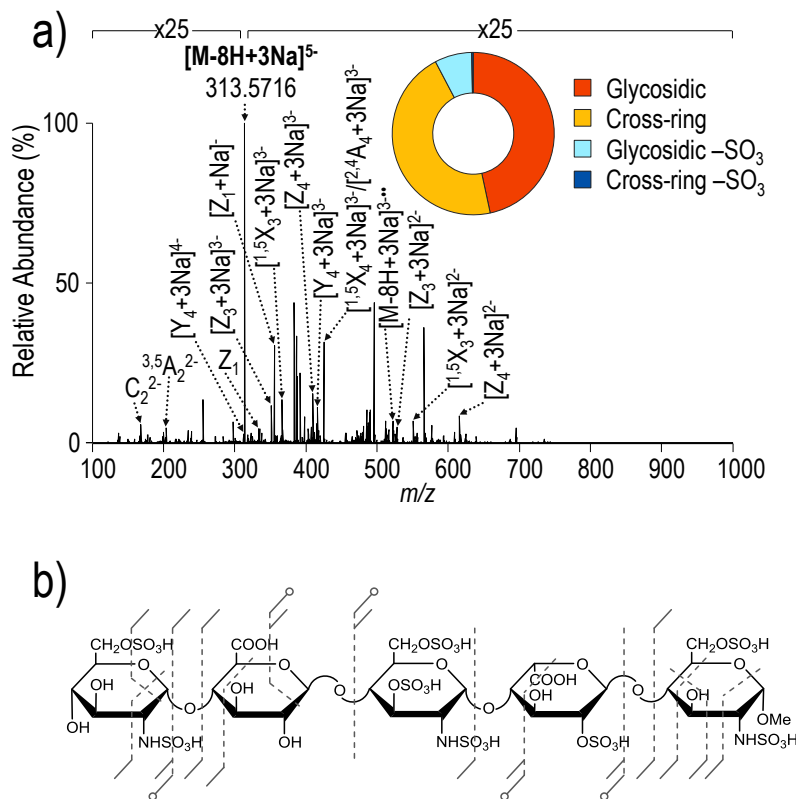


Figure 7.10 a) UVPD spectrum of [M-8H+3Na]⁵⁻ (*m/z* 313) of fondaparinux with donut plot depicting the fragment ion composition based on summed abundances of fragment types, and b) UVPD fragment ion map. **Table 7.13** contains a list of identified fragment ions (Chapter 7, Supporting Information).

Figure 7.11 shows the UVPD fragmentation spectrum for [M-10H+5Na]⁵⁻ and corresponding fragment ion map and donut plot. This charge state exhibits an even lower degree of SO₃ loss (glycosidic-SO₃ = 5.8%; cross-ring-SO₃ = 0.0%) than [M-8H+3Na]⁵⁻, but overall produces fewer informative fragments. This observation is consistent with EDD results for GAGs in which SO₃ loss is minimized when the number of ionized sites is greater than the number of sulfate groups.^{26,36} However, less overall fragmentation is

observed when all ionizable sites are deprotonated, as sites that remain protonated are hypothesized to facilitate radical-based reactions that provide informative fragment ions.

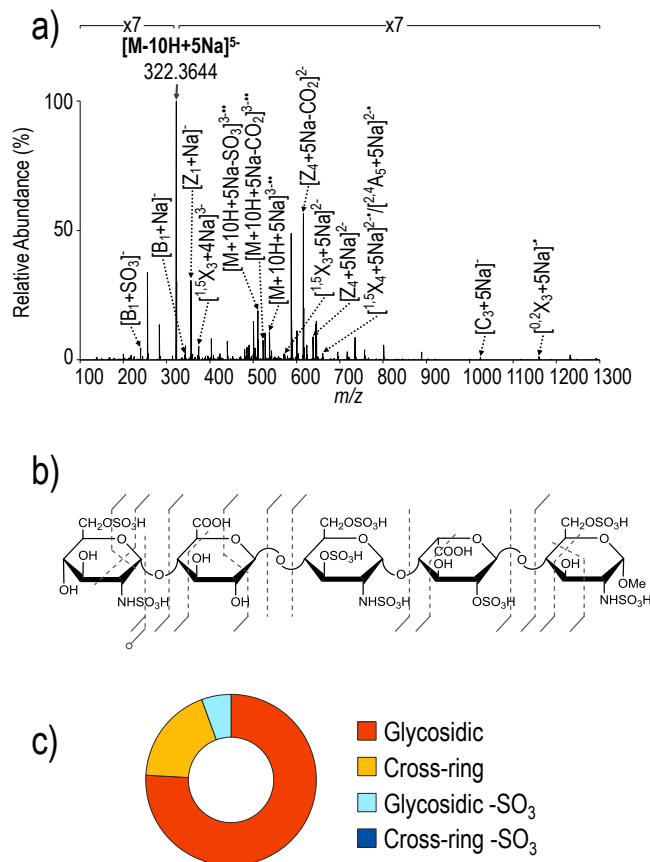


Figure 7.11 a) UVPD spectrum of $[M-10H-5Na]^{5-}$ (m/z 322) of fondaparinux, b) UVPD fragment ion map, and c) UVPD donut plot depicting the fragment ion composition based on summed abundances of fragment types. **Table 7.14** contains a list of identified fragment ions (Chapter 7, Supporting Information).

While deprotonation via sodium adduction represents one strategy to sequence highly sulfated GAGs, sodium adduction increases the number of possible ion types through generation of ions both with and without sodium adducts, which has the potential to increase spectral complexity, convolute interpretation, and increase the likelihood of false identifications. In addition, fragment ion signals can be split across various

adduction states and can lead to reduced ion intensities. Conversely, highly-sulfated GAG ions without salt adducts often contain protonated sulfate moieties, which are particularly problematic during collisional activation as they promote sulfate decomposition and preclude modification localization. NETD has previously shown success for activation of fondaparinux with protonated sulfate groups, generating spectra that contain informative fragment ions with minimal sulfate loss.³³ The UVPD mass spectrum of the $[M-4H]^4$ ion of fondaparinux is displayed in **Figure 7.12**. In contrast to collisional activation (**Table 7.15** Supporting Information, Chapter 7), UVPD generates a complete series of glycosidic fragments that retain sulfate modifications to a much larger extent (glycosidic- $SO_3 = 12.2\%$; cross-ring- $SO_3 = 9.2\%$). The informative spectrum re-confirms that sulfate decomposition is further minimized with UVPD even when sulfate groups are likely protonated, consistent with the prevailing understanding of the different mechanism of UVPD compared to collisional activation.⁶³

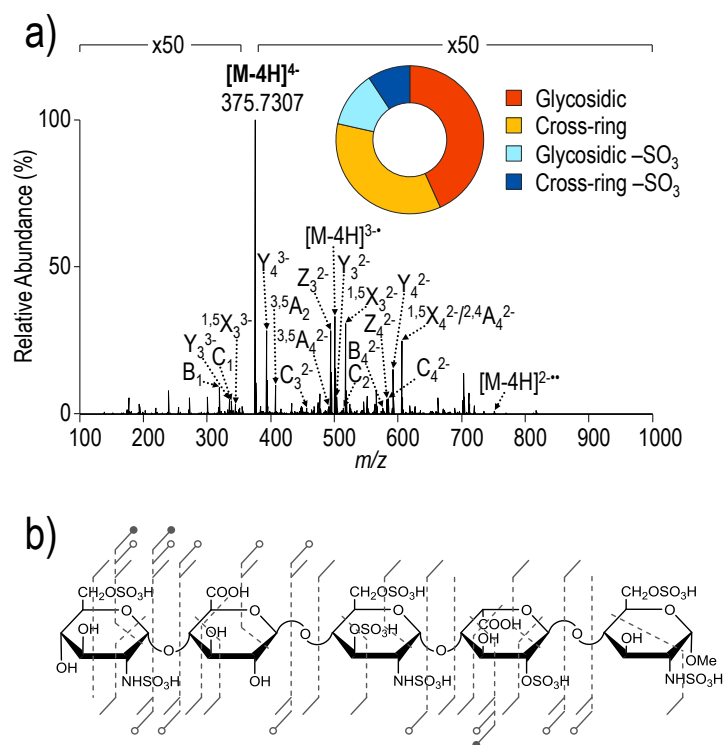


Figure 7.12 a) UVPD spectrum of [M-4H]⁴⁻ (*m/z* 375) of fondaparinux with donut plot depicting the fragment ion composition based on summed abundances of fragment types, and b) UVPD fragment ion map. **Table 7.15** contains a list of identified fragment ions (Chapter 7, Supporting Information).

While the advantages of alternative ion activation methods for GAG analysis are apparent, many methods have limited accessibility and require instrument hardware modifications. Addition of a 213 nm solid state laser to an Orbitrap mass spectrometer was commercialized in 2017, thus making UVPD a more widely available technique.^{55,56} We assessed the capabilities of 213 nm UVPD for GAG structural characterization, and one example is illustrated in **Figure 7.13** for DS dp4, [M-3H]³⁻. While the 213 nm Nd:YAG laser is considerably less powerful than the 193 nm excimer laser, comparison of the UVPD fragment ion maps in **Figure 7.8b** and **Figure 7.13b** suggests that 213 nm UVPD results in fragmentation that is similar to that obtained by 193 nm UVPD.

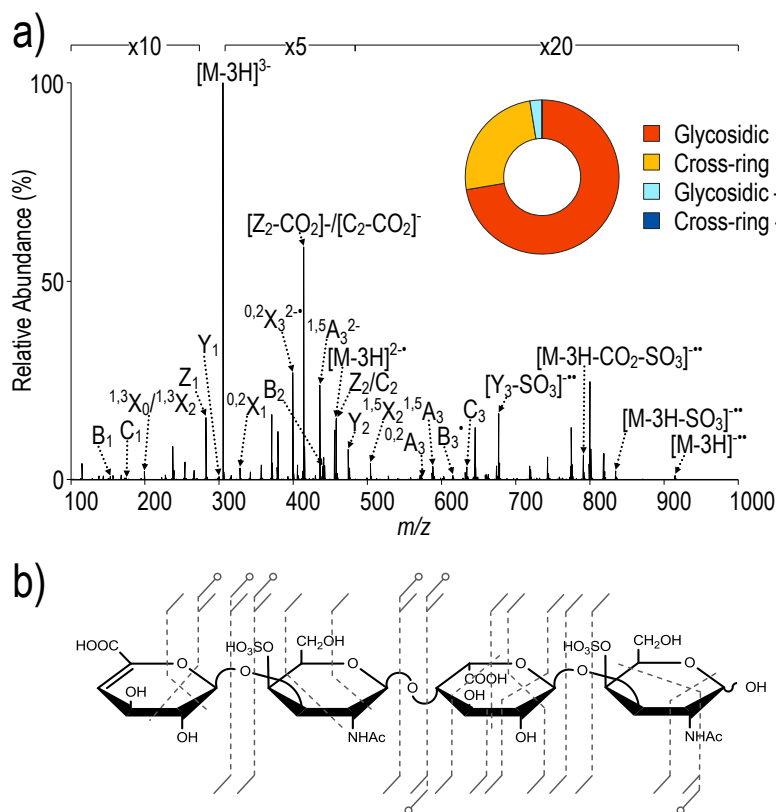


Figure 7.13. a) 213 nm UVPD (500 pulses, 3 $\mu\text{J}/\text{pulse}$; 200 ms activation time) spectrum of $[\text{M}-3\text{H}]^{3-}$ (m/z 305) of DS dp4 with donut plot depicting the fragment ion composition based on summed abundances of fragment types, and b) 213 nm UVPD fragment ion map. The 213 nm UVPD spectrum was collected on the same Thermo Fisher Orbitrap Fusion Lumos mass spectrometer used for 193 nm UVPD with a 213 nm laser (2.5 kHz rep. rate) in place of the 193 nm excimer laser. For 213 nm UVPD, photoirradiation occurred in the lower pressure linear ion trap. **Table 7.17** contains a list of identified fragment ions for 213 nm UVPD.

However, the activation period for 213 nm UVPD (200 ms) is substantially greater than that used for 193 nm UVPD (16 ms). Future improvements to 213 nm UVPD are anticipated to decrease the required activation period. Variations between the 193 nm and 213 nm UVPD spectra in **Figure S5** are attributed to differences in the laser powers (which influence the distribution of multiphoton absorption events and accumulation of

energy) and the different wavelengths which may access different excited electronic states. The fast, high-energy deposition of UVPD enhances cleavage of C-C and C-O bonds while minimizing loss of labile modifications. Moreover, UV photoabsorption can cause electron detachment, particularly for multiply-charged negative ions, potentially leading to both radical and hydrogen migration in the course of fragmentation. Considering the informative spectra that can be generated with short activation times, UVPD appears to be a natural fit for coupling to online or gas-phase separations of GAGs.^{64,65} Recent coupling of NETD with trapped ion mobility spectrometry demonstrates the advantage of coupling alternative ion activation methods with separation techniques for GAG analysis.⁶⁵ For GAGs with a higher degree of sulfation, it is worthwhile to investigate separation techniques that can accommodate sodium cationization of GAGs for increased sulfate retention with spectra collected on high resolution mass spectrometers to alleviate concerns regarding spectral interpretation. These spectra are also amenable to automatic spectral interpretation which further enables the incorporation of this sequencing method for increased throughput.⁶⁶

7.5 CONCLUSION

The work presented here confirms that 193 nm UVPD demonstrates great promise for sequencing of GAGs by tandem mass spectrometry. Similar to electron-based activation methods, UVPD produces sulfate-retaining glycosidic and cross-ring fragment ions, with activation times comparable to NETD and much shorter than EDD. In general, the high resolution capabilities of the Orbitrap mass analyzer enabled confident assignment of fragment ions and permitted interpretation of the complex tandem mass spectra typical of GAGs. While informative fragment ions were generated for all charge states, the degree of sulfate decomposition and extent of fragmentation showed some

dependence on the ionization state, reiterating the important impact of both ionization conditions and precursor ion selection. In addition, the ability to modulate fragmentation patterns based on the particular ionization state of the precursor provides another strategic option when developing a workflow for high throughput analysis of GAGs in mixtures.

7.6 SUPPORTING INFORMATION

Table 7.2 Fragment ion list for UVPD (8 pulses, 4 mJ) of $[M-2H]^{2-}$ of GlcA-GlcNAc-GlcA-GlcNAc- $(CH_2)_5NH_2$.

Measured m/z	Intensity	Relative intensity	Ion	ppm error	Theoretical m/z
174.0164	9.29E+05	4.81	B_1^+	0.22	174.0164
193.0347	1.25E+06	6.49	C_1	3.50	193.0354
202.0716	2.89E+05	1.50	$[Z_1-(CH_2)_5NH_2]^+$	-0.26	202.0715
220.0820	3.17E+04	0.16	$[Y_1-(CH_2)_5NH_2]^+$	0.51	220.0821
235.0452	2.90E+04	0.15	$^{2,4}A_2$	3.15	235.0459
249.0610	1.18E+05	0.61	$^{3,5}A_2$	2.37	249.0616
285.5686	4.36E+04	0.23	C_3^{2-}	4.13	285.5698
295.0662	1.43E+05	0.74	$^{0,2}A_2$	2.95	295.0671
305.1710	1.70E+05	0.88	Y_1	2.82	305.1719
306.0824	6.93E+03	0.04	$^{1,4}A_2$	2.14	306.0831
349.1009	8.65E+04	0.45	$^{1,5}A_2^+$	-0.01	349.1009
378.1038	1.16E+05	0.60	B_2	1.02	378.1042
396.1138	1.06E+07	54.64	C_2	2.40	396.1147
421.1826	2.13E+04	0.11	$^{2,4}X_1$	0.52	421.1828
429.6534	1.93E+07	100.00	$[M-2H]^{2-}$	1.55	429.6541
438.1244	2.19E+05	1.13	$^{2,4}A_3$	2.08	438.1253
463.1924	1.23E+06	6.39	Z_2	2.12	463.1934
466.1192	2.88E+05	1.49	$^{3,5}A_3$	2.21	466.1202
481.2028	1.54E+06	7.95	Y_2	2.39	481.2039
482.1146	1.98E+04	0.10	$^{0,3}A_3$	1.13	482.1151
509.1977	3.31E+05	1.71	$^{1,5}X_2$	2.28	509.1989
512.1245	9.38E+05	4.86	$^{0,2}A_3$	2.36	512.1257
526.1403	1.34E+05	0.70	$^{1,5}A_3$	2.01	526.1414
553.1273	4.62E+05	2.39	B_3^+	1.08	553.1279
564.2399	2.47E+04	0.13	$^{0,2}X_2$	2.06	564.2411
572.1457	4.31E+05	2.23	C_3	1.99	572.1468
579.2271	2.09E+04	0.11	$^{2,5}X_2^+$	0.78	579.2276
623.2529	5.19E+04	0.27	$^{2,4}X_2^+$	1.39	623.2538
628.1722	2.64E+04	0.14	$^{3,5}A_4$	1.36	628.1731
666.2714	2.04E+06	10.57	Z_3	2.04	666.2728
674.1777	5.45E+03	0.03	$^{0,2}A_4$	1.23	674.1785
684.2819	1.07E+06	5.56	Y_3	2.08	684.2833
712.2769	1.03E+05	0.53	$^{1,5}X_3$	1.88	712.2782
725.2845	9.85E+04	0.51	$^{0,2}X_3^+$	1.33	725.2855
729.2202	1.56E+04	0.08	$^{1,5}A_4$	0.73	729.2207
742.2854	6.58E+03	0.03	$^{2,5}X_3$	4.58	742.2888
755.2939	2.41E+04	0.12	$^{0,3}X_3^+$	2.82	755.2960
770.2819	9.13E+03	0.05	$^{1,4}X_3$	2.36	770.2837
772.2978	1.24E+06	6.43	$^{3,5}X_3$	2.03	772.2994
800.2928	3.30E+04	0.17	$^{2,4}X_3/^{1,3}X_3$	1.85	800.2943
815.3163	6.92E+06	35.86	$[M-2H-CO_2]^+$	1.05	815.3172
859.3059	2.38E+06	12.33	$[M-2H]^+$	1.26	859.3070

Table 7.3 Fragment ion list for HCD (NCE 20) of $[M-2H]^{2-}$ of GlcA-GlcNAc-GlcA-GlcNAc-(CH₂)₅NH₂.

Measured m/z	Intensity	Relative intensity	Ion	ppm error	Theoretical m/z
133.0143	1.44E+04	0.01	$^{0,2}A_1$	-0.40	133.0142
175.0246	3.51E+05	0.32	B_1	1.21	175.0248
193.0350	1.99E+07	18.31	C_1	1.95	193.0354
218.5587	4.18E+04	0.04	$^{2,4}A_3^{2-}$	1.46	218.5590
235.0458	2.15E+05	0.20	$^{2,4}A_2$	0.60	235.0459
276.5641	3.91E+05	0.36	B_3^{2-}	1.44	276.5645
285.5691	6.24E+04	0.06	C_3^{2-}	2.38	285.5698
287.1610	7.38E+05	0.68	Z_1	1.03	287.1613
295.0668	1.23E+07	11.36	$^{0,2}A_2$	0.92	295.0671
305.1716	1.93E+07	17.79	Y_1	0.85	305.1719
341.6379	1.83E+05	0.17	Y_3^{2-}	0.36	341.6380
347.1824	8.21E+05	0.76	$^{0,2}X_1$	0.07	347.1824
378.1042	3.08E+06	2.83	B_2	-0.04	378.1042
396.1149	4.49E+07	41.30	C_2	-0.38	396.1147
399.6442	3.49E+04	0.03	$^{2,4}X_3/^{1,3}X_3$	-1.75	399.6435
429.6554	1.09E+08	100.00	$[M-2H]^{2-}$	-3.10	429.6541
438.1256	9.26E+04	0.09	$^{2,4}A_3$	-0.65	438.1253
463.1935	8.58E+05	0.79	Z_2	-0.25	463.1934
468.1360	3.18E+05	0.29	$^{1,4}A_3$	-0.26	468.1359
481.2043	5.91E+04	0.05	Y_2	-0.73	481.2039
510.1475	4.54E+04	0.04	$[B_3-CO_2]^-$	-2.08	510.1464
554.1367	2.64E+05	0.24	B_3	-0.77	554.1363
666.2747	9.48E+03	0.01	Z_3	-2.92	666.2728
684.2840	4.80E+05	0.44	Y_3	-0.99	684.2833

Table 7.4 Fragment ion list for UVPD (8 pulses, 4 mJ) of $[M-2H]^{2-}$ IdoA-GlcNAcS6-GlcA-GlcNAcS6-(CH₂)₅NH₂.

Measured <i>m/z</i>	Intensity	Relative intensity	Ion	ppm error	Theoretical <i>m/z</i>
138.9704	1.24E+04	0.06	^{0.4} A ₂ / ^{0.4} A ₄	1.92	138.9707
175.0245	8.73E+03	0.04	B ₁	1.78	175.0248
193.0351	3.89E+04	0.18	C ₁	1.43	193.0354
282.0286	3.27E+04	0.15	[Z ₁ -(CH ₂) ₅ NH ₂] ⁻	-0.84	282.0284
295.0667	2.89E+04	0.13	[^{0.2} A ₂ -SO ₃] ⁻	1.25	295.0671
300.0389	4.05E+04	0.18	[Y ₁ -(CH ₂) ₅ NH ₂] ⁻	0.09	300.0389
316.5423	4.76E+03	0.02	B ₃ ²⁻	1.91	316.5429
325.1071	6.43E+04	0.29	^{2.4} X ₀	1.06	325.1074
329.0179	9.38E+03	0.04	^{3.5} A ₂	1.54	329.0184
367.1176	3.95E+04	0.18	Z ₁	1.12	367.1180
375.0234	3.63E+04	0.16	^{0.2} A ₂	1.29	375.0239
378.1035	2.10E+04	0.09	[B ₂ -SO ₃] ⁻	1.81	378.1042
385.1281	4.07E+05	1.84	Y ₁	1.23	385.1286
396.1141	5.86E+04	0.27	[C ₂ -SO ₃] ⁻	1.64	396.1147
413.1229	5.18E+04	0.23	^{1.5} X ₁	1.43	413.1235
421.5943	1.71E+04	0.08	Y ₃ ²⁻	1.16	421.5948
426.1305	1.84E+04	0.08	^{0.2} X ₁ [•]	0.74	426.1308
430.0657	2.96E+04	0.13	^{1.5} A ₂	0.89	430.0661
435.5918	1.93E+04	0.09	^{1.5} X ₃ ²⁻	1.02	435.5922
458.0606	7.04E+04	0.32	B ₂	0.87	458.0610
466.1193	1.62E+04	0.07	[^{3.5} A ₃ -SO ₃] ⁻	1.99	466.1202
469.6316	5.50E+04	0.25	[M-2H-SO ₃] ²⁻	1.75	469.6324
476.0709	2.02E+05	0.91	C ₂	1.39	476.0716
481.2035	1.10E+04	0.05	[Y ₂ -SO ₃] ⁻	0.72	481.2038
488.1010	2.21E+05	1.00	[M-2H-C ₂ H ₂ O] ²⁻	0.23	488.1011
509.6099	2.21E+07	100.00	[M-2H] ²⁻	1.83	509.6108
543.1494	1.80E+05	0.82	Z ₂	1.29	543.1501
546.0762	9.66E+04	0.44	^{3.5} A ₃	1.54	546.0770
554.1358	6.17E+04	0.28	[B ₃ -SO ₃] ⁻	0.85	554.1363
561.1597	4.83E+04	0.22	Y ₂	1.72	561.1607
572.1475	9.99E+03	0.05	[C ₃ -SO ₃] ⁻	-1.16	572.1468
589.1548	3.13E+05	1.42	^{1.5} X ₂	1.32	589.1556
592.0818	3.88E+04	0.18	^{0.2} A ₃	1.22	592.0825
606.0974	1.58E+04	0.07	^{1.5} A ₃	1.27	606.0982
634.0923	4.01E+04	0.18	B ₃	1.24	634.0931
644.1971	1.51E+04	0.07	^{0.2} X ₂	1.05	644.1978
652.1030	4.61E+04	0.21	C ₃	1.00	652.1037
704.2184	3.75E+04	0.17	[^{2.4} X ₂ -SO ₃] ⁻	0.72	704.2189
708.1288	6.28E+03	0.03	[^{3.5} A ₄ -SO ₃] ⁻	1.51	708.1299
713.1381	1.99E+04	0.09	^{1.4} X ₂	0.71	713.1386
746.2288	1.57E+05	0.71	[Z ₃ -SO ₃] ⁻	0.90	746.2295
754.1343	2.51E+04	0.11	[^{0.2} A ₄ -SO ₃] ⁻	1.39	754.1353
764.2393	7.61E+04	0.34	[Y ₃ -SO ₃] ⁻	0.96	764.2400
784.1747	1.88E+05	0.85	^{2.4} X ₂	1.30	784.1757
792.2341	3.70E+04	0.17	[^{1.5} X ₃ -SO ₃] ⁻	1.07	792.2350
806.2493	1.08E+04	0.05	[^{0.2} X ₃ -SO ₃] ⁻	1.61	806.2506
826.1853	3.46E+05	1.57	Z ₃	1.19	826.1863
844.1957	2.34E+05	1.06	Y ₃	1.36	844.1969
852.2548	4.07E+04	0.18	[^{3.5} X ₃ -SO ₃] ⁻	1.50	852.2561
866.2704	4.93E+03	0.02	[^{0.4} X ₃ -SO ₃] ⁻	1.54	866.2717
872.1906	1.67E+05	0.76	^{1.5} X ₃	1.34	872.1918
879.2416	2.26E+04	0.10	[^{2.4} X ₃ -SO ₃] ⁻ /[^{1.3} X ₃ -SO ₃] ⁻	1.22	879.2427
886.2062	4.73E+04	0.21	^{0.2} X ₃	1.37	886.2074
916.2169	3.87E+04	0.18	^{0.3} X ₃	1.18	916.2180
932.2115	2.35E+05	1.07	^{3.5} X ₃	1.50	932.2129
939.2618	3.73E+04	0.17	[M-2H-SO ₃] [•]	2.13	939.2638
960.2062	3.48E+04	0.16	^{2.4} X ₃ / ^{1.3} X ₃	1.68	960.2078
975.2291	1.47E+06	6.67	[M-2H-CO ₂] [•]	1.17	975.2302
1019.2188	2.33E+06	10.56	[M-2H] [•]	1.24	1019.2201

Table 7.5 Fragment ion list for HCD (NCE 25) of $[M-2H]^{2-}$ of IdoA-GlcNAcS6-GlcA-GlcNAcS6-(CH₂)₅NH₂.

Measured m/z	Intensity	Relative Intensity	Ion	ppm error	Theoretical m/z
138.9705	6.35E+03	0.03	$^{0.4}A_2/^{0.4}A_4$	1.21	138.9707
175.0247	1.24E+05	0.50	B ₁	0.64	175.0248
187.0081	2.86E+04	0.12	$^{0.2}A_2^{2-}$	1.09	187.0083
193.0352	5.50E+05	2.22	C ₁	0.91	193.0354
228.5267	2.01E+04	0.08	B ₂ ²⁻	0.70	228.5269
235.0458	4.36E+04	0.18	$^{2.4}A_2$	0.60	235.0459
237.532	2.14E+05	0.87	C ₂ ²⁻	0.60	237.5321
271.0713	4.38E+03	0.02	Z ₂ ²⁻	0.41	271.0714
276.5646	4.43E+03	0.02	[B ₃ -SO ₃] ²⁻	-0.37	276.5645
280.0767	1.17E+04	0.05	Y ₂ ²⁻	-0.02	280.0767
295.0669	1.23E+06	4.96	[$^{0.2}A_2$ -SO ₃] ⁻	0.58	295.0671
305.1717	6.63E+04	0.27	[Y ₁ -SO ₃] ⁻	0.20	305.1718
316.5427	5.31E+05	2.14	B ₃ ²⁻	0.65	316.5429
378.1042	5.60E+05	2.26	[B ₂ -SO ₃] ⁻	-0.04	378.1042
381.6166	2.56E+05	1.03	[Y ₃ -SO ₃] ²⁻	-0.58	381.6164
385.1283	2.48E+07	100.00	Y ₁	0.71	385.1286
396.1144	2.67E+06	10.78	[C ₂ -SO ₃] ⁻	0.88	396.1147
421.5946	2.74E+06	11.04	Y ₃ ²⁻	0.44	421.5948
427.1392	3.53E+04	0.14	$^{0.2}X_1$	-0.14	427.1391
429.6537	2.92E+05	1.18	[M-2H-2SO ₃] ²⁻	0.74	429.6540
438.1248	3.49E+04	0.14	[$^{2.4}A_3$ -SO ₃] ⁻	1.17	438.1253
442.5992	1.00E+04	0.04	$^{0.2}X_3^{2-}$	1.96	442.6001
458.0609	1.96E+06	7.91	B ₂	0.22	458.0610
463.1929	2.37E+04	0.10	[Z ₂ -SO ₃] ⁻	0.83	463.1933
469.6321	1.88E+07	76.00	[M-2H-SO ₃] ²⁻	0.69	469.6324
476.0711	2.92E+05	1.18	C ₂	0.97	476.0716
481.2035	5.41E+04	0.22	[Y ₂ -SO ₃] ⁻	0.72	481.2038
509.6107	3.62E+06	14.61	[M-2H] ²⁻	0.26	509.6108
512.1244	8.93E+03	0.04	[$^{0.2}A_3$ -SO ₃] ⁻	2.55	512.1257
543.1501	1.95E+05	0.79	Z ₂	0.00	543.1501
554.1358	9.79E+06	39.52	[B ₃ -SO ₃] ⁻	0.85	554.1363
561.1605	7.94E+04	0.32	Y ₂	0.29	561.1607
634.0928	1.46E+06	5.88	B ₃	0.45	634.0931
684.2818	3.73E+03	0.02	[Y ₃ -2SO ₃] ⁻	2.08	684.2832
764.2397	4.57E+04	0.18	[Y ₃ -SO ₃] ⁻	0.44	764.2400

Table 7.6 Fragment ion list for EDD of $[M-2H]^{2-}$ (m/z 509) of IdoA-GlcNAcS6-GlcA-GlcNAcS6-(CH₂)₅NH₂.

Measured m/z	Intensity	Relative Intensity	Ion	ppm error	Theoretical m/z
175.0248	1.52E+05	0.02	B ₁	0.07	175.0248
193.0354	8.90E+05	0.10	C ₁	-0.12	193.0354
235.0457	6.80E+04	0.01	^{2,4} A ₂	1.03	235.0459
255.5586	4.23E+04	0.00	$[^{0,2}A_3-SO_3]^{2-}$	2.41	255.5592
295.0669	6.05E+05	0.07	$[^{0,2}A_7-SO_3]^-$	0.58	295.0671
316.5427	1.61E+05	0.02	B ₃ ²⁻	0.65	316.5429
325.1071	1.58E+05	0.02	^{2,4} X ₀	1.06	325.1074
325.5481	3.23E+04	0.00	C ₃ ²⁻	0.27	325.5482
329.0184	5.92E+04	0.01	^{3,5} A ₂	0.02	329.0184
367.1181	5.05E+05	0.06	Z ₁	-0.24	367.1180
375.0238	1.50E+05	0.02	^{0,2} A ₂	0.23	375.0239
378.1040	4.98E+05	0.05	$[B_2-SO_3]^-$	0.49	378.1042
385.1286	1.10E+07	1.22	Y ₁	-0.06	385.1286
396.1147	8.47E+05	0.09	$[C_2-SO_3]^-$	0.12	396.1147
413.1236	4.09E+05	0.05	^{1,5} X ₁	-0.27	413.1235
421.5948	1.51E+06	0.17	Y ₃ ²⁻	-0.03	421.5948
427.1388	6.45E+04	0.01	^{0,2} X ₁	0.80	427.1391
430.0660	3.96E+05	0.04	^{1,5} A ₂	0.20	430.0661
435.5922	1.42E+05	0.02	^{1,5} X ₃ ²⁻	0.10	435.5922
458.0610	2.40E+06	0.27	B ₂	0.00	458.0610
466.1206	8.53E+04	0.01	$[^{3,5}A_7-SO_3]^-$	-0.80	466.1202
469.6325	2.90E+06	0.32	$[M-2H-SO_3]^{2-}$	-0.16	469.6324
476.0715	1.97E+06	0.22	C ₂	0.13	476.0716
509.1980	1.44E+05	0.02	$[^{1,5}X_2-SO_3]^-$	1.50	509.1988
509.6094	9.05E+08	100.00	$[M-2H]^{2-}$	2.81	509.6108
526.1417	8.83E+04	0.01	$[^{1,5}A_5-SO_3]^-$	-0.65	526.1414
543.1499	7.53E+05	0.08	Z ₂	0.37	543.1501
546.0769	1.44E+06	0.16	^{3,5} A ₃	0.26	546.0770
548.0947	7.56E+04	0.01	^{1,4} A ₃	-3.66	548.0927
554.1365	2.70E+06	0.30	$[B_3-SO_3]^-$	-0.41	554.1363
561.1605	2.10E+05	0.02	Y ₂	0.29	561.1607
562.0722	3.36E+04	0.00	^{0,3} A ₃	-0.43	562.0720
572.1483	3.87E+04	0.00	$[C_3-SO_3]^-$	-2.56	572.1468
576.0917	3.13E+04	0.00	^{2,5} A ₃	-7.10	576.0876
589.1556	1.38E+06	0.15	^{1,5} X ₂	-0.04	589.1556
592.0821	4.63E+05	0.05	^{0,2} A ₃	0.71	592.0825
606.0980	5.24E+05	0.06	^{1,5} A ₃	0.28	606.0982
634.0933	4.09E+06	0.45	B ₃	-0.34	634.0931
652.1039	7.93E+05	0.09	C ₃	-0.38	652.1037
694.1122	3.30E+04	0.00	^{2,4} A ₄	2.90	694.1142
708.1274	3.21E+04	0.00	$[^{3,5}A_7-SO_3]^-$	3.48	708.1299
713.1380	3.65E+05	0.04	^{1,4} X ₂	0.85	713.1386
729.2269	1.08E+05	0.01	$[^{1,5}A_7-SO_3]^-$	-8.46	729.2207
746.2295	4.23E+05	0.05	$[Z_3-SO_3]^-$	-0.04	746.2295
754.1353	2.04E+05	0.02	$[^{0,2}A_4-SO_3]^-$	0.06	754.1353
764.2403	1.43E+05	0.02	$[Y_3-SO_3]^-$	-0.35	764.2400
784.1724	5.28E+05	0.06	^{2,4} X ₃	4.24	784.1757
792.2370	1.26E+05	0.01	$[^{1,5}X_3-SO_3]^-$	-2.59	792.2350
809.1834	9.01E+05	0.10	$[^{1,5}A_4-SO_3]^-$	-7.24	809.1775
826.1866	6.06E+06	0.67	Z ₃	-0.38	826.1863
834.0937	8.31E+04	0.01	^{0,2} A ₄	-1.85	834.0922
836.2620	8.21E+04	0.01	$[^{0,3}X_3-SO_3]^-$	-1.00	836.2612
844.1962	3.20E+06	0.35	Y ₃	0.77	844.1969
872.1925	1.74E+06	0.19	^{1,5} X ₃	-0.84	872.1918
880.2466	4.88E+04	0.01	$[^{2,4}X_3-SO_3]^-$	4.99	880.2510
880.2466	4.88E+04	0.01	$[^{1,3}X_3-SO_3]^-$	4.99	880.2510
886.2080	6.31E+05	0.07	^{0,2} X ₃	-0.66	886.2074
916.2186	6.41E+05	0.07	^{0,3} X ₃	-0.68	916.2180
932.2078	6.91E+04	0.01	^{3,5} X ₃	5.46	932.2129
940.2720	6.81E+04	0.01	$[M-H-SO_3]^-$	0.13	940.2721
946.2298	5.58E+04	0.01	^{0,4} X ₃	-1.33	946.2285
960.2074	5.63E+05	0.06	^{2,4} X ₃	0.43	960.2078
960.2074	5.63E+05	0.06	^{1,3} X ₃	0.43	960.2078
1020.2264	1.37E+06	0.15	$[M-H]^-$	2.49	1020.2289

Table 7.7 Fragment ion list for NETD of $[M-2H]^{2-}$ (m/z 509) of IdoA-GlcNAcS6-GlcA-GlcNAcS6-(CH₂)₅NH₂.

Measured m/z	Intensity	Relative Intensity	Ion	ppm error	Theoretical m/z
430.0662	1.96E+01	0.03	^{1,5} A ₂	-0.27	430.0661
458.0611	3.54E+02	0.57	B ₂	-0.22	458.0610
476.0707	1.23E+03	1.98	C ₁	1.81	476.0716
509.6107	6.22E+04	100.00	$[M-2H]^{2-}$	0.26	509.6108
546.0764	1.37E+02	0.22	^{3,5} A ₃	1.18	546.0770
592.0824	3.77E+01	0.06	^{0,2} A ₃	0.21	592.0825
606.0953	3.94E+01	0.06	^{1,5} A ₃	4.74	606.0982
634.0881	1.04E+03	1.67	B ₃	7.86	634.0931
652.0997	1.52E+03	2.45	C ₃	6.06	652.1037
713.1360	3.97E+02	0.64	^{1,4} X ₂	3.66	713.1386
784.1726	3.98E+02	0.64	^{2,4} X ₂	3.98	784.1757
809.1797	1.50E+03	2.41	$[^{1,5}A_4-SO_3]^-$	-2.66	809.1775
826.1825	1.18E+04	19.01	Z ₃	4.58	826.1863
844.1909	3.76E+03	6.05	Y ₃	7.05	844.1969
872.1873	4.53E+03	7.28	^{1,5} X ₃	5.12	872.1918
886.2027	2.69E+02	0.43	^{0,2} X ₃	5.32	886.2074
916.2133	1.84E+03	2.95	^{0,3} X ₃	5.11	916.2180
932.2052	3.26E+01	0.05	^{3,5} X ₃	8.25	932.2129
940.2632	3.84E+01	0.06	$[M-H-SO_3]^-$	9.49	940.2721
960.2031	1.44E+03	2.32	^{1,3} X ₃	4.90	960.2078
960.2031	1.44E+03	2.32	^{2,4} X ₃	4.90	960.2078
1020.2197	3.38E+04	54.34	$[M-H]^-$	9.06	1020.2289

Table 7.8 Fragment ion list for UVPD (8 pulses, 4 mJ) of $[M-2H]^{2-}$ of DS dp4.

Measured m/z	Intensity	Relative intensity	Ion	ppm error	Theoretical m/z
152.9863	2.38E+04	0.47	$^{3,5}A_2/^{3,5}A_4$	0.11	152.9863
157.0141	1.18E+04	0.23	B_1	0.94	157.0142
175.0248	3.47E+04	0.69	C_1	0.07	175.0248
198.9917	2.20E+04	0.44	$^{1,3}X_0/^{1,3}X_2$	0.49	198.9918
202.0720	1.76E+03	0.03	$[Z_1-SO_3]^-$	0.48	202.0721
237.5319	7.23E+02	0.01	Y_2^{2-}	1.02	237.5321
282.0285	3.44E+05	6.82	Z_1	1.46	282.0289
300.0392	2.57E+05	5.10	Y_1	0.92	300.0395
328.0343	4.72E+04	0.94	$^{1,5}X_1$	0.27	328.0344
342.0501	4.34E+04	0.86	$^{0,2}X_1$	-0.18	342.0500
357.0371	5.27E+03	0.10	$^{2,5}X_1^+$	-0.08	357.0371
360.0939	4.32E+03	0.09	$[B_2-SO_3]^-$	-0.78	360.0936
372.0609	4.31E+03	0.09	$^{0,3}X_1$	-0.79	372.0606
378.1041	5.95E+03	0.12	$[Z_2-SO_3]^-/[C_2-SO_3]^-$	0.22	378.1042
379.0501	2.14E+04	0.43	Y_3^{2-}	0.36	379.0502
396.1147	2.11E+04	0.42	$[Y_2-SO_3]^-$	0.12	396.1147
397.0319	1.96E+05	3.89	$[B_2-CH_3CO]^-$	-1.02	397.0315
412.0554	4.05E+03	0.08	$^{1,5}A_2$	0.29	412.0555
416.0503	2.13E+04	0.42	$^{2,4}X_1$	0.32	416.0504
440.0504	1.01E+05	2.00	B_2	0.08	440.0504
458.0610	5.04E+06	100.00	$Z_2/C_2/[M-2H]^{2-}$	0.00	458.0610
476.0713	3.04E+05	6.03	Y_2	0.55	476.0716
500.0717	1.46E+04	0.29	$^{2,4}A_3$	-0.27	500.0716
504.0662	4.33E+04	0.86	$^{1,5}X_2$	0.55	504.0665
528.0663	2.83E+04	0.56	$^{3,5}A_3$	0.34	528.0665
536.1262	3.49E+03	0.07	$[B_3-SO_3]^-$	-0.92	536.1257
554.1360	1.78E+04	0.35	$[C_3-SO_3]^-$	0.49	554.1363
559.1078	3.54E+03	0.07	$^{0,2}X_2$	1.57	559.1087
574.0717	1.89E+04	0.38	$^{0,2}A_3$	0.45	574.0720
588.0869	4.51E+03	0.09	$^{1,5}A_3$	1.20	588.0876
616.0822	5.53E+04	1.10	B_3	0.52	616.0825
619.1297	5.80E+03	0.12	$^{2,4}X_2$	0.17	619.1298
634.0928	7.12E+05	14.12	C_3	0.45	634.0931
662.1478	2.27E+04	0.45	$[Z_3-SO_3]^+$	-0.23	662.1476
679.1503	4.70E+03	0.09	$[Y_3-SO_3]^+$	0.94	679.1509
720.1534	1.26E+05	2.51	$[^{0,2}X_3-SO_3]^+$	-0.38	720.1531
740.0887	5.62E+03	0.11	Z_3^+	0.15	740.0888
747.1400	7.92E+03	0.16	$[^{1,4}A_4-SO_3]^-$	1.02	747.1408
758.0990	5.74E+03	0.11	Y_3^+	0.50	758.0994
777.1499	3.00E+03	0.06	$[^{1,3}X_4-SO_3]^-$	1.84	777.1513
791.1669	1.31E+04	0.26	$[^{1,5}A_4-SO_3]^-$	0.10	791.1670
800.1102	3.85E+05	7.63	$^{0,2}X_3^+$	-0.32	800.1099
816.0816	4.42E+03	0.09	$^{0,2}A_4$	-0.01	816.0816
818.1538	2.19E+04	0.44	$[M-2H-H_2SO_4]^+$	-0.34	818.1535
828.1043	7.23E+03	0.14	$^{1,4}A_4^+$	0.67	828.1049
836.1641	4.14E+04	0.82	$[M-2H-SO_3]^+$	-0.02	836.1641
857.1077	1.48E+04	0.29	$^{1,3}X_3$	0.52	857.1081
870.1158	2.12E+05	4.20	$^{1,5}A_4$	-1.07	870.1149
898.1108	1.06E+05	2.09	$[M-2H-H_2O]^+$	-0.52	898.1103
916.1213	3.04E+05	6.03	$[M-2H]^+$	-0.44	916.1209

Table 7.9 Fragment ion list for MS³ activation of the fragment ion m/z 715.05 from DS dp4 by UVPD (8 pulses, 4 mJ)/HCD (NCE 20).

Measured m/z	Intensity	Relative intensity	Ion	ppm error	Theoretical m/z
272.9922	2.19E+05	1.07	$[Y_2+SO_3]^-$	0.00	272.9922
440.0503	4.90E+05	2.40	B_2	0.30	440.0504
476.0714	6.08E+04	0.30	Y_3	0.34	476.0716
634.0930	2.04E+07	100.00	C_3	0.14	634.0931

Table 7.10 Fragment ion list for MS³ activation of the fragment ion m/z 715.05 from DS dp4 by UVPD (8 pulses, 4 mJ)/ UVPD (8 pulses, 4 mJ).

Measured m/z	Intensity	Relative intensity	Ion	ppm error	Theoretical m/z
272.9920	1.01E+05	1.73	$[Y_2+SO_3]^-$	0.73	272.9922
440.0499	3.23E+05	5.49	B_2	1.21	440.0504
458.0603	3.11E+04	0.53	C_2	1.53	458.0610
476.0710	4.56E+05	7.76	Y_3	1.18	476.0716
518.0816	1.34E+05	2.28	$^{0.2}X_3$	0.97	518.0821
554.1356	1.58E+05	2.69	$[C_3-SO_3]^-$	1.21	554.1363
590.0663	4.59E+05	7.81	$[C_3-C_2H_4O]^-$	1.02	590.0669
634.0924	5.88E+06	100.00	C_3	1.08	634.0931
715.0571	5.78E+06	98.23	$[C_3+HSO_3]^-$	0.84	715.0577

Table 7.11 Fragment ion list for UVPD (8 pulses, 4 mJ) of $[M-3H]^{3-}$ of DS dp4.

Measured m/z	Intensity	Relative intensity	Ion	ppm error	Theoretical m/z
152.9862	4.01E+05	0.43	$^{3,5}A_2/^{3,5}A_4$	0.77	152.9863
157.0141	1.98E+05	0.21	B_1	0.94	157.0142
175.0246	2.71E+05	0.29	C_1	1.21	175.0248
198.9918	7.80E+05	0.85	$^{1,3}X_0/^{1,3}X_2$	-0.02	198.9918
202.0719	1.67E+04	0.02	$[Z_1-SO_3]^-$	-0.99	202.0721
237.5322	3.40E+05	0.37	Y_2^{2-}	-0.24	237.5321
282.0287	9.23E+07	100.00	Z_1	0.75	282.0289
300.0392	4.66E+06	5.05	Y_1	0.92	300.0395
305.0382	6.44E+07	69.81	$[M-3H]^{3-}$	0.13	305.0382
316.5428	1.00E+05	0.11	C_3^{2-}	0.33	316.5429
328.0345	2.64E+06	2.86	$^{1,5}X_1$	-0.34	328.0344
342.0502	3.18E+06	3.44	$^{0,2}X_1$	-0.47	342.0500
357.0374	1.95E+06	2.11	$^{2,5}X_1^+$	0.76	357.0371
370.0452	2.22E+05	0.24	Z_3^{2-}	-0.66	370.0450
378.1042	2.39E+04	0.03	$[Z_2-SO_3]^-/[C_2-SO_3]^-$	-0.04	378.1042
379.0504	1.16E+06	1.25	Y_3^{2-}	-0.43	379.0502
393.0479	7.31E+04	0.08	$^{1,5}X_3^{2-}$	-0.52	393.0477
396.1149	8.37E+04	0.09	$[Y_2-SO_3]^-$	-0.38	396.1147
399.5516	3.50E+06	3.79	$^{0,2}X_3^{2-}$	-1.36	399.5511
407.5367	3.55E+04	0.04	$^{0,2}A_4^{2-}$	1.13	407.5372
414.0713	3.82E+07	41.45	$[Z_2-CO_2]^-$	-1.64	414.0706
435.0583	2.75E+05	0.30	$^{1,5}A_3^{2-}$	-0.09	435.0583
440.0507	1.50E+06	1.63	B_2	-0.60	440.0504
457.5572	2.97E+06	3.22	$[M-3H]^{2-}$	-1.45	457.5565
458.0609	6.82E+06	7.39	Z_2/C_2	0.22	458.0610
476.0717	9.98E+05	1.08	Y_2	-0.29	476.0716
499.0638	5.61E+04	0.06	$^{2,4}A_3^+$	-0.12	499.0637
504.0667	6.25E+05	0.68	$^{1,5}X_2$	-0.44	504.0665
528.0666	3.49E+05	0.38	$^{3,5}A_3$	-0.23	528.0665
574.0725	8.54E+04	0.09	$^{0,2}A_3$	-0.95	574.0720
588.0879	6.84E+05	0.74	$^{1,5}A_3$	-0.50	588.0876
615.0751	7.34E+04	0.08	B_3^+	-1.55	615.0741
619.1301	6.62E+04	0.07	$^{2,4}X_2$	-0.47	619.1298
634.0934	4.50E+05	0.49	C_3	-0.49	634.0931
661.1409	1.70E+05	0.18	$[Z_3-SO_3]^-$	-0.80	661.1404
677.1357	6.79E+05	0.74	$[Y_3-SO_3]^{--}$	-1.42	677.1347
741.0975	3.33E+04	0.04	Z_3	-0.42	741.0972
747.1414	2.81E+04	0.03	$[^{1,4}A_4-SO_3]^-$	-0.85	747.1408
758.1007	5.82E+04	0.06	Y_3^+	-1.74	758.0994
719.1464	8.05E+05	0.87	$[^{0,2}X_3-SO_3]^{--}$	0.76	719.1459
791.1675	2.16E+06	2.34	$[M-3H-CO_2-SO_3]^{--}$	-0.66	791.1670
800.1110	3.08E+05	0.33	$^{0,2}X_3^+$	-1.32	800.1099
835.1575	1.02E+06	1.11	$[M-3H-SO_3]^{--}$	-1.48	835.1563
871.1244	1.35E+05	0.15	$[M-3H-CO_2]^{--}$	-0.70	871.1238
915.1144	1.07E+05	0.12	$[M-3H]^{--}$	-1.45	915.1131

Table 7.12 Fragment ion list for UVPD (8 pulses, 4 mJ) of $[M-5H]^{5-}$ of DS dp10.

Measured m/z	Intensity	Relative intensity	Ion	ppm error	Theoretical m/z	Measured m/z	Intensity	Relative intensity	Ion	ppm error	Theoretical m/z
152.9863	3.69E+03	1.22	$^{3.5}A_0/^{3.5}A_4$	0.11	152.9863	589.1069	4.79E+03	1.58	$[^{1.5}X_0-SO_3]^{2-}$	-0.19	589.1068
157.0140	1.94E+03	0.64	B_1	1.57	157.0142	599.5781	1.53E+03	0.51	Z_2^{2-}	1.65	599.5791
175.0248	4.08E+03	1.35	C_1	0.07	175.0248	604.7438	6.28E+02	0.21	B_3^{3-}	-0.09	604.7437
198.9917	5.73E+03	1.89	$^{1.3}X_0$	0.49	198.9918	607.7653	9.92E+02	0.33	$[^{3.5}A_0-SO_3]^{3-}$	2.21	607.7666
282.0285	2.78E+05	91.74	Z_1	1.46	282.0289	608.5839	5.02E+03	1.66	Y_5^{2-}	0.78	608.5844
300.0392	2.68E+04	8.84	Y_1	0.92	300.0395	611.0811	3.68E+03	1.21	Z_3^{3-}/C_6^{3-}	4.35	611.0838
328.0342	5.38E+04	17.76	$^{1.5}X_1$	0.58	328.0344	615.0743	1.16E+04	3.84	B_1^+	-0.25	615.0741
341.0423	5.39E+03	1.78	$^{0.5}X_1^+$	-1.86	341.0417	622.5813	1.43E+03	0.47	$^{1.5}X_0^{2-}$	0.85	622.5818
357.0372	3.68E+03	1.21	$^{2.5}X_1^+$	0.19	357.0371	626.4183	6.84E+02	0.23	$^{1.5}X_8^{3-}$	0.98	626.4189
360.0935	1.51E+03	0.50	$[B_2-SO_3]^-$	0.33	360.0936	629.0856	6.15E+03	2.03	$^{0.5}X_5^{2-}$	-0.64	629.0852
370.0448	7.02E+03	2.32	Z_2^{2-}	0.42	370.0450	634.0928	1.28E+04	4.23	C_3	0.45	634.0931
378.1042	5.67E+03	1.87	$[Z_2-SO_3]/[C_2-SO_3]$	-0.04	378.1042	634.4182	1.76E+03	0.58	$^{3.5}A_3^{3-}$	1.13	634.4189
379.0501	6.35E+03	2.10	Y_2^{2-}	0.36	379.0502	638.6108	7.30E+03	2.41	$[B_2-SO_3]^{2-}$	1.01	638.6114
386.0396	8.62E+02	0.28	$^{1.4}X_1^{2-}$	0.70	386.0399	647.6162	2.25E+03	0.74	$[Z_2-SO_3]^{3-}/[C_2-SO_3]^{3-}$	0.82	647.6167
393.0475	1.28E+04	4.15	$^{1.5}X_3^{2-}$	0.49	393.0477	654.4242	1.03E+03	0.34	$^{1.5}A_9^{3-}$	2.69	654.4240
396.1145	2.11E+03	0.70	$[Y_7-SO_3]^-$	0.63	396.1147	656.6216	2.04E+03	0.67	$[Y_6-SO_3]^{2-}$	0.63	656.6220
399.5514	2.97E+03	0.98	$^{0.2}X_1^{2-}$	-0.85	399.5511	661.1401	6.13E+03	2.02	$[Z_3-SO_3]^-$	0.41	661.1404
407.5490	1.75E+03	0.58	$^{2.5}X_3^{2-}$	-1.19	407.5485	663.4213	3.73E+03	1.23	B_3^{3-}	-0.29	663.4211
412.0555	2.38E+03	0.78	$^{1.5}A_2$	0.05	412.0555	666.5893	9.64E+02	0.32	$^{2.4}X_5^{2-}$	0.83	666.5899
414.7184	3.02E+03	1.00	$^{1.5}X_5^{3-}$	0.95	414.7188	669.7596	2.48E+03	0.82	C_5^{2-}	2.27	669.7611
416.0504	4.61E+03	1.52	$^{2.4}X_1$	0.08	416.0504	678.5893	1.47E+04	4.84	$^{2.5}X_2^{2-}$	0.82	678.5899
425.5539	2.06E+03	0.68	$^{1.5}X_7^{4-}$	1.05	425.5543	679.1507	4.00E+03	1.32	$[Y_3-SO_3]^-$	0.35	679.1509
437.0551	1.13E+03	0.37	$^{2.4}X_3^{2-}$	1.41	437.0557	687.5950	1.80E+03	0.59	Z_6^{2-}/C_6^{2-}	0.20	687.5951
440.0503	2.87E+04	9.49	B_2	0.30	440.0504	696.5999	1.66E+03	0.55	Y_6^{2-}	0.74	696.6004
449.0554	7.08E+03	2.34	B_4^{2-}	0.70	449.0557	698.4457	1.04E+03	0.34	$[^{0.5}X_0-SO_3]^{3-}$	2.48	698.4474
452.0568	7.30E+02	0.24	B_5^{3-}	1.50	452.0575	702.1425	3.29E+03	1.09	$[^{0.5}X_0-H_2SO_4]^-$	0.09	702.1426
458.0607	3.03E+05	100.00	$Z_2/Z_3/Z_4^{3-}/Z_6^{4-}/C_2/C_3/C_4^{4-}/[M-5H]^{5-}$	0.65	458.0610	707.1455	3.68E+03	1.21	$[^{1.5}X_3-SO_3-H_2O]^-$	0.50	707.1459
464.0644	1.58E+03	0.52	Y_6^{3-}	0.26	464.0645	710.1289	1812.7	0.60	$[M-5H-2SO_3]^{3-}$	0.90	710.1295
467.0659	1.36E+04	4.50	Y_4^{2-}	0.82	467.0663	720.1530	2.17E+03	0.72	$[^{0.2}X_3-SO_3]^-$	0.18	720.1531
476.0712	1.07E+05	35.28	Y_2	0.76	476.0716	725.0984	4.30E+03	1.42	$^{0.5}X_3^{3-}$	1.80	725.0997
481.0634	9.93E+02	0.33	$^{1.5}X_2^{2-}$	0.70	481.0637	726.6254	6.95E+02	0.23	$[B_1-SO_3]^{2-}$	2.88	726.6275
481.3963	1.11E+03	0.37	$^{3.5}A_2^{2-}$	-0.29	481.3962	736.7816	2126.9	0.70	$[M-5H-SO_3]^{3-}$	0.29	736.7818
493.0632	4.63E+03	1.53	$^{3.5}A_2^{2-}$	1.09	493.0637	741.0968	9.68E+03	3.19	Z_3	0.52	741.0972
496.7307	2.28E+03	0.75	$^{0.2}A_3^{3-}$	1.24	496.7313	759.1074	5.28E+03	1.74	Y_3	0.46	759.1078
502.0687	1.24E+03	0.41	C_5^{4-}	0.64	502.0690	763.4336	6.61E+03	2.18	$[M-5H]^{3-}$	0.63	763.4341
504.0661	8.18E+03	2.70	$^{1.5}X_2$	0.75	504.0665	766.6038	1.21E+03	0.40	B_7	2.74	766.6059
510.3982	1.77E+03	0.58	B_7^{3+}	0.29	510.3983	775.6097	1.83E+03	0.60	C_7^{2-}	1.91	775.6112
516.0661	3.77E+04	12.46	$^{0.2}A_5^{2-}$	0.73	516.0665	777.1511	1.24E+03	0.41	$^{1.5}A_8^{2-}$	0.30	777.1513
516.7382	8.12E+02	0.27	C_7^{3-}	0.31	516.7384	787.1021	4.69E+03	1.55	$^{1.5}X_3$	0.72	787.1027
523.5834	1.24E+03	0.41	$[^{0.5}X_0-SO_3]^{4-}$	0.42	523.5836	795.1622	8.67E+02	0.29	$[^{2.4}X_3-SO_3]^-$	-0.38	795.1619
528.0660	5.73E+03	1.89	$^{3.5}A_3$	0.91	528.0665	800.1104	5.34E+03	1.76	$^{0.2}X_3^+$	-0.57	800.1099
530.0827	2.67E+03	0.88	$^{1.4}A_3$	-1.08	530.0821	819.1613	1.81E+04	5.96	$[B_4-SO_3]^-$	0.73	819.1619
531.7568	2.46E+03	0.81	$[Y_7-SO_3]^{3-}$	1.59	531.7576	837.1725	8.01E+03	2.64	$[Z_4-SO_3]/[C_4-SO_3]^-$	-0.05	837.1725
533.3192	6.97E+02	0.23	Y_5^{4-}	6.54	533.3227	855.1827	5.63E+03	1.86	$[Y_4-SO_3]^-$	0.38	855.1830
536.5674	1.14E+04	3.78	B_2^{2-}	-0.19	536.5673	899.1183	2.69E+04	8.88	B_4	0.45	899.1187
541.0887	8.26E+02	0.27	$^{1.5}X_3^{3-}$	1.08	541.0893	907.1780	9.66E+02	0.32	$[^{3.5}A_0-SO_3]^-$	-0.07	907.1779
543.5729	7.88E+03	2.60	$^{0.2}X_9^{4+}$	-0.14	543.5728	908.1213	9.60E+02	0.32	B_2^{2-}	2.96	908.1240
546.0768	1.35E+04	4.44	C_5^{2-}	0.44	546.0770	917.1287	1.03E+04	3.40	Z_4/C_4	0.63	917.1293
552.4055	9.81E+02	0.32	Z_7^{3-}	1.62	552.4064	935.1396	5.89E+03	1.94	Y_4	0.25	935.1398
552.8364	9.23E+02	0.30	$[M-5H-SO_3]^{4+}$	4.46	552.8389	953.1829	8.91E+02	0.29	$[^{0.2}A_0-SO_3]^-$	0.54	953.1834
558.4092	4.55E+03	1.50	Y_3^{3-}	1.28	558.4099	963.1348	7.12E+02	0.23	$^{1.5}X_4$	-0.05	963.1348
559.6006	1.36E+03	0.45	$[Z_2-SO_3]^{2-}$	0.15	559.6007	987.1334	7.31E+02	0.24	$^{3.5}A_5$	1.37	987.1348
567.7407	2.13E+03	0.70	$^{1.5}X_3^{3-}$	1.50	567.7416	995.1918	1.17E+03	0.39	$[B_2-SO_3]^-$	2.19	995.1940
568.6055	6.56E+03	2.16	$[Y_2-SO_3]^{2-}$	0.82	568.6060	1004.6394	1.26E+03	0.42	C_5^{2-}	1.45	1004.6409
572.0770	2.42E+03	0.80	$^{0.2}X_3^{3+}$	-0.09	572.0769	1013.2045	2.10E+03	0.69	$[C_2-SO_3]^-$	0.05	1013.2045
572.5754	1.28E+04	4.23	$[M-5H]^{4+}$	0.28	572.5756	1032.1318	3.46E+03	1.14	$^{0.2}A_5$	0.06	1032.1319
574.0715	1.09E+04	3.60	$^{0.2}A_3$	0.80	574.0720	1073.1349	2.28E+03	0.75	B_2^{++}	-0.28	1073.1346
577.4086	4.40E+03	1.45	$^{2.5}X_3^{3-}$	-0.02	577.4086	1093.1608	1.74E+03	0.57	C_5	0.51	1093.1614
578.4267	6.78E+02	0.22	$[B_2-SO_3]^{3-}$	2.19	578.4280	1145.1505	4.56E+02	0.16	$[M-5H]^{++}$	-1.27	1145.1520
582.6032	2.20E+03	0.73	$[^{1.5}X_0-SO_3]^{2-}$	0.39	582.6034	1198.2717	7.01E+02	0.23	$[B_2-2SO_3]^-$	1.38	1198.2734
588.0863	1.47E+03	0.48	$^{1.5}A_3$	2.22	588.0876	1216.2826	5.89E+02	0.19	$[C_2-2SO_3]/[Z_2-2SO_3]$	1.09	1216.2839
						1278.2295	1.39E+03	0.46	$[B_2-SO_3]^-$	0.52	1278.2302
						1296.2401	7.11E+02	0.23	$[C_2-SO_3]/[Z_2-SO_3]$	0.49	1296.2407
						1358.1857	1.60E+03	0.53	B_6	0.95	1358.1870

Table 7.13 Fragment ion list for UVPD (8 pulses, 4 mJ) of $[M-8H+3Na]^{5-}$ of fondaparinux.

Measured m/z	Intensity	Relative intensity	Ion	ppm error	Theoretical m/z
138.9702	3.30E+02	0.08	$^{1,3}A_1/^{0,4}A_1/^{0,4}A_3/^{0,4}A_5$	3.36	138.9707
159.4835	2.23E+02	0.05	B_1^{2-}	2.77	159.4839
168.4888	1.01E+03	0.23	C_1^{2-}	2.52	168.4892
198.9913	3.40E+02	0.08	$^{0,2}A_1$	2.50	198.9918
203.4915	8.20E+02	0.19	$^{3,5}A_2^{2-}$	2.28	203.4920
240.0178	6.62E+02	0.15	$[B_1-SO_3]^-$	2.27	240.0183
297.5798	1.16E+03	0.27	$[M-8H+3Na-SO_3]^{5-}$	3.34	297.5808
311.9709	4.61E+03	1.06	$[Y_4+3Na]^{4-}$	1.62	311.9714
313.4745	1.32E+04	3.05	$[^{1,5}X_4+2Na]^{2-}/[^{2,4}A_4+2Na]^{2-}$	0.47	313.4746
313.5716	4.33E+05	100.00	$[M-8H+3Na]^{5-}$	1.77	313.5722
333.9900	7.92E+02	0.18	Z_1	2.43	333.9908
337.9848	5.74E+02	0.13	C_1	2.74	337.9857
351.6160	2.12E+03	0.49	$[Z_3+3Na]^{3-}$	2.13	351.6167
355.9719	5.29E+03	1.22	$[Z_1+Na]^-$	2.40	355.9728
357.6198	4.14E+02	0.10	$[Y_3+3Na]^{3-}$	1.31	357.6203
359.6236	3.88E+02	0.09	$[1,5X_3+2Na]^{3-}$	2.76	359.6246
366.9511	2.39E+03	0.55	$[1,5X_3+3Na]^{3-}$	2.20	366.9519
387.4616	5.80E+03	1.34	$[M-8H+3Na-H_2O]^{4-}$	1.10	387.4628
391.9642	3.77E+03	0.87	$[M-8H+3Na]^{4-}$	2.71	391.9655
398.2939	1.42E+03	0.33	$[B_4+2Na]^{3-}$	2.54	398.2949
402.9660	7.43E+02	0.17	$[Z_4+2Na]^{3-}$	1.98	402.9668
404.2978	4.77E+02	0.11	$[C_4+2Na]^{3-}$	1.57	404.2984
405.6212	2.12E+02	0.05	$[B_4+3Na]^{3-}$	2.53	405.6222
410.2932	2.76E+03	0.64	$[Z_4+3Na]^{3-}$	2.22	410.2941
411.6252	5.99E+02	0.14	$[C_4+3Na]^{3-}$	1.33	411.6257
416.2970	2.01E+03	0.46	$[Y_4+3Na]^{3-}$	1.52	416.2976
418.3008	3.60E+02	0.08	$[^{1,5}X_4+2Na]^{3-}/[^{2,4}X_4+2Na]^{3-}$	2.76	418.3020
425.6284	5.59E+03	1.29	$[^{1,5}X_4+3Na]^{3-}/[2,4A_4+3Na]^{3-}$	2.05	425.6293
456.9524	5.76E+02	0.13	$[^{3,5}A_5+3Na]^{3-}$	2.25	456.9534
472.2874	6.58E+02	0.15	$[^{0,2}A_5+3Na]^{3-}$	2.51	472.2886
476.9580	4.03E+02	0.09	$[Z_3+2Na-SO_3]^{2-}$	2.90	476.9594
485.9631	1.85E+03	0.43	$[Y_3+2Na-SO_3]^{3-}$	3.22	485.9647
487.9492	1.15E+03	0.26	$[Z_3+3Na-SO_3]^{2-}$	2.36	487.9504
495.9667	7.77E+03	1.79	$[M-8H+3Na-SO_3]^{3-}$	2.79	495.9682
499.9610	1.82E+02	0.04	$[^{1,5}X_3+2Na-SO_3]^{2-}/[^{2,4}A_4+2Na]^{2-}$	2.24	499.9621
510.9518	2.37E+02	0.05	$[^{1,5}X_3+3Na-SO_3]^{2-}/[2,4A_4+3Na]^{2-}$	2.53	510.9531
513.9584	4.48E+02	0.10	$[^{3,5}A_4+2Na]^{2-}$	2.29	513.9596
516.6152	7.29E+02	0.17	$[M-8H+3Na-H_2O]^{3-}$	2.60	516.6169
522.6187	1.19E+03	0.27	$[M-8H+3Na]^{3-}$	0.89	522.6204
527.9277	8.91E+02	0.21	$[Z_3+3Na]^{2-}$	2.01	527.9288
536.9330	2.88E+02	0.07	$[Y_3+3Na]^{2-}$	1.94	536.9340
550.9305	1.25E+03	0.29	$[^{1,5}X_3+3Na]^{2-}$	1.82	550.9315
568.9586	3.01E+02	0.07	$[B_4+3Na-SO_3]^{2-}$	-0.05	568.9586
608.9356	5.93E+02	0.14	$[B_4+3Na]^{2-}$	2.27	608.9370
615.9433	1.54E+03	0.36	$[Z_4+3Na]^{2-}$	2.44	615.9448
617.9420	4.57E+02	0.11	$[C_4+3Na]^{2-}$	0.42	617.9423
624.9497	4.70E+02	0.11	$[Y_4+3Na]^{2-}$	0.62	624.9501
638.9462	3.31E+02	0.08	$[^{1,5}X_4+3Na]^{2-}/[^{2,4}A_5+3Na]^{2-}$	2.10	638.9475

Table 7.14 Fragment ion list for UVPD (8 pulses, 4 mJ) of $[M-10H+5Na]^{5-}$ of fondaparinux.

Measured m/z	Intensity	Relative intensity	Ion	ppm error	Theoretical m/z
138.9704	7.46E+03	0.15	$^{0.4}A_1/^{0.4}A_3/^{0.4}A_5$	1.92	138.9707
203.4916	4.31E+03	0.08	$^{3.5}A_2^{2-}$	1.79	203.492
240.0179	3.34E+04	0.65	$[B_1-SO_3]^-$	1.86	240.0183
244.4931	8.69E+03	0.17	$[^{1.5}A_2+Na]^{2-}/[^{2.4}X_1+Na-SO_3]^{2-}$	1.64	244.4935
322.3644	5.12E+06	100.00	$[M-10H+5Na]^{5-}$	1.66	322.3649
341.9564	9.71E+03	0.19	$[B_1+Na]^-$	2.06	341.9571
355.9721	2.13E+05	4.16	$[Z_1+Na]^-$	1.84	355.9728
359.9671	1.46E+04	0.28	$[C_1+Na]^-$	1.58	359.9677
374.2784	3.58E+04	0.70	$[1.5X_3+4Na]^{3-}$	2.20	374.2792
402.9552	5.77E+04	1.13	$[M-10H+5Na]^{4-}$	0.70	402.9555
412.9485	2.06E+03	0.04	$[B_4+4Na]^{3-}$	2.53	412.9495
418.9523	7.64E+03	0.15	$[C_4+4Na]^{3-}$	1.82	418.9531
426.2796	5.72E+03	0.11	$[C_4+5Na]^{3-}$	1.83	426.2804
471.6072	5.98E+03	0.12	$[^{3.5}A_5+5Na]^{3-}$	1.81	471.6081
495.9582	7.08E+03	0.14	$[M-10H+5Na-SO_3-CO_2]^{3-}$	-1.57	495.9574
500.6178	1.03E+05	2.02	$[M-10H+5Na-CH_2O-SO_3]^{3-}$	0.77	500.6182
500.9378	1.04E+05	2.03	$[C_3+4Na]^{2-}$	1.96	500.9388
510.6213	1.30E+05	2.54	$[M-10H+5Na-SO_3]^{3-}$	0.79	510.6217
522.6103	5.27E+04	1.03	$[M-10H+5Na-CO_2]^{3-}$	0.77	522.6107
527.2700	7.17E+04	1.40	$[M-10H+5Na-CH_2O]^{3-}$	2.76	527.2715
535.9402	3.54E+03	0.07	$[^{3.5}A_4+4Na]^{2-}$	2.47	535.9415
537.2736	7.48E+04	1.46	$[M-10H+5Na]^{3-}$	0.70	537.274
538.9189	9.82E+03	0.19	$[Z_3+4Na]^{2-}$	1.55	538.9197
547.9240	2.61E+03	0.05	$[Y_3+4Na]^{2-}$	1.85	547.925
549.9097	8.40E+03	0.16	$[Z_3+5Na]^{2-}$	1.83	549.9107
561.9214	4.21E+03	0.08	$[^{1.5}X_3+4Na]^{2-}$	1.91	561.9225
572.9124	1.38E+04	0.27	$[^{1.5}X_3+5Na]^{2-}$	1.82	572.9134
615.9307	3.91E+05	7.64	$[Z_4+5Na-CO_2]^{2-}$	0.95	615.9313
637.9256	6.10E+04	1.19	$[Z_4+5Na]^{2-}$	1.80	637.9267
639.9232	7.26E+03	0.14	$[C_4+5Na]^{2-}$	1.57	639.9242
660.9284	1.75E+04	0.34	$[^{1.5}X_4+5Na]^{2-}/[^{2.4}X_5+5Na]^{2-}$	1.65	660.9295
1024.8645	7.60E+03	0.15	$[C_3+5Na]^-$	2.23	1024.867
1159.8390	9.36E+03	0.18	$[^{0.2}X_3+5Na]^+$	2.11	1159.841

Table 7.15 Fragment ion list for UVPD (8 pulses, 4 mJ) of $[M-4H]^{4-}$ of fondaparinux.

Measured m/z	Intensity	Relative intensity	Ion	ppm error	Theoretical m/z
198.9916	2.41E+03	0.01	$^{0,2}A_1$	0.99	198.9918
240.0181	3.01E+04	0.16	$[B_1-SO_3]^-$	1.02	240.0183
258.0287	2.91E+03	0.02	$[C_1-SO_3]^-$	0.82	258.0289
315.7623	2.06E+03	0.01	$[M-4H-3SO_3]^{4-}$	2.04	315.7629
319.9749	3.39E+04	0.18	B_1	0.81	319.9752
335.6379	1.87E+04	0.10	Y_{3-3-}	1.27	335.6383
335.7516	7.91E+03	0.04	$[M-4H-2SO_3]^{4-}$	1.64	335.7521
337.9853	1.75E+04	0.09	C_1	1.26	337.9857
341.0098	4.47E+03	0.02	$[Y_4-2SO_3]^{3-}$	3.94	341.0111
344.9692	1.37E+04	0.07	$^{1,5}X_3^{3-}$	2.21	344.9700
352.0018	7.86E+03	0.04	Y_1	-1.21	352.0014
355.7409	4.67E+05	2.50	$[M-4H-SO_3]^{4-}$	1.27	355.7414
367.6641	3.28E+03	0.02	$[Y_4-SO_3]^{3-}$	-1.86	367.6634
375.7307	1.86E+07	100.00	$[M-4H]^{4-}$	-0.38	375.7306
376.9936	9.61E+03	0.05	$[^{1,5}X_4-SO_3]^{3-}/[^{2,4}A_5-SO_3]^{3-}$	3.86	376.9951
379.9969	6.94E+03	0.04	$^{1,5}X_{1/2,4}A_2$	-1.61	379.9963
388.3119	3.59E+03	0.02	Z_4^{3-}	0.69	388.3122
394.3153	1.10E+05	0.59	Y_4^{3-}	0.98	394.3157
407.9909	3.68E+04	0.20	$^{3,5}A_2$	0.75	407.9912
416.0510	6.59E+03	0.04	$[B_2-SO_3]^-$	-1.36	416.0504
456.9747	7.86E+03	0.04	C_3^{2-}	0.42	456.9749
463.9823	5.58E+03	0.03	$[Y_3-SO_3]^{2-}$	0.90	463.9827
474.3213	1.50E+04	0.08	$[M-4H-SO_3]^{3-}$	0.70	474.3216
477.9798	2.65E+04	0.14	$[^{1,5}X_3-SO_3]^{2-}/^{2,4}A_4^{2-}$	0.79	477.9802
491.9771	9.70E+03	0.05	$^{3,5}A_4^{2-}$	1.08	491.9776
494.9561	1.26E+04	0.07	Z_3^{2-}	-0.52	494.9558
496.0070	9.65E+03	0.05	B_2	0.50	496.0072
500.9736	1.25E+05	0.67	$[M-4H]^{3-}$	0.60	500.9739
503.9606	2.20E+04	0.12	Y_3^{2-}	1.04	503.9611
510.0227	2.80E+03	0.02	$[Z_2-SO_3]^-$	0.39	510.0229
512.0197	3.35E+03	0.02	$[Y_4-SO_3]^{2-}$	1.28	512.0204
514.0178	7.49E+03	0.04	C_2	0.03	514.0178
514.9797	1.34E+03	0.01	$^{0,2}A_4$	1.31	514.9804
517.9581	1.17E+05	0.63	$^{1,5}X_3^{2-}$	0.93	517.9586
526.0175	8.22E+03	0.04	$[^{1,5}X_4-2SO_3]^{2-}/[^{2,4}A_4-2SO_3]^{2-}$	0.60	526.0178
535.9843	3.44E+03	0.02	$[B_4-SO_3]^{2-}$	2.53	535.9857
542.9929	4.54E+03	0.02	$[Z_4-SO_3]^{2-}$	1.07	542.9935
544.9905	5.05E+03	0.03	$[C_4-SO_3]^{2-}$	0.80	544.9909
551.9984	2.41E+04	0.13	$[Y_4-SO_3]^{2-}$	0.66	551.9988
565.9957	3.18E+04	0.17	$[^{1,5}X_4-SO_3]^{2-}/[^{2,4}A_5-SO_3]^{2-}$	0.92	565.9962
575.9633	7.38E+03	0.04	B_4^{2-}	1.32	575.9641
582.9707	1.43E+04	0.08	Z_4^{2-}	2.04	582.9719
584.9691	1.96E+04	0.11	C_4^{2-}	0.42	584.9693
591.9769	5.64E+04	0.30	Y_4^{2-}	0.46	591.9772
605.9742	9.33E+04	0.50	$^{1,5}X_4^{2-}/^{2,4}A_4^{2-}$	0.71	605.9746
607.9895	6.19E+03	0.03	Y_2	1.28	607.9903
635.9849	4.42E+03	0.02	$^{1,5}X_{2/2,4}A_3$	0.46	635.9852
660.4659	3.22E+03	0.02	$^{2,5}X_4^{2-}/^{1,4}A_5^{2-}$	0.62	660.4663
711.4818	2.72E+04	0.15	$[M-4H-SO_3]^{2-}$	0.35	711.4822
816.9885	4.08E+03	0.02	$[B_3-SO_3]^{2-}$	1.45	816.9897

Table 7.16 Fragment ion list for HCD (NCE 15) of $[M-4H]^{4-}$ of fondaparinux.

Measured m/z	Intensity	Relative intensity	Ion	ppm error	Theoretical m/z
159.4837	4.12E+03	0.12	B_1^{2-}	1.52	159.4839
168.4890	2.51E+03	0.07	C_1^{2-}	1.33	168.4892
175.4968	5.33E+04	1.51	Y_1^{2-}	1.42	175.4970
207.5213	2.21E+03	0.06	$[B_2-SO_3]^{2-}$	1.34	207.5216
223.5344	2.98E+03	0.08	$[Y_2-2SO_3]^{2-}$	1.28	223.5347
240.0181	5.27E+05	14.97	$[B_1-SO_3]^{2-}$	1.02	240.0183
245.0058	9.76E+03	0.28	$[B_3-2SO_3]^{3-}$	1.25	245.0061
247.4997	5.10E+04	1.45	B_2^{2-}	1.16	247.5000
255.6812	7.38E+04	2.09	$[Y_3-3SO_3]^{3-}$	1.22	255.6815
256.5050	1.17E+04	0.33	C_2^{2-}	1.05	256.5053
258.0286	5.77E+03	0.16	$[C_1-SO_3]^{2-}$	1.20	258.0289
263.5128	4.79E+04	1.36	$[Y_2-SO_3]^{2-}$	1.11	263.5131
271.6581	1.78E+04	0.51	$[B_2-SO_3]^{3-}$	1.02	271.6584
272.0443	3.32E+04	0.94	$[Y_1-SO_3]^{2-}$	0.96	272.0446
275.7841	1.83E+03	0.05	$[M-4H-5SO_3]^{4-}$	1.59	275.7845
282.3335	1.96E+05	5.57	$[Y_3-2SO_3]^{3-}$	1.00	282.3338
287.4781	5.33E+03	0.15	B_4^{4-}	1.02	287.4784
295.7734	1.39E+06	39.59	$[M-4H-4SO_3]^{4-}$	1.16	295.7737
298.3102	3.85E+03	0.11	B_3^{3-}	1.51	298.3106
303.4912	1.36E+04	0.39	Y_2^{2-}	0.99	303.4915
303.6831	7.28E+04	2.07	$[B_4-3SO_3]^{3-}$	1.21	303.6835
308.9857	5.81E+04	1.65	$[Y_3-SO_3]^{3-}$	1.15	308.9861
309.6866	7.16E+04	2.03	$[C_4-3SO_3]^{3-}$	1.26	309.6870
314.3588	3.80E+05	10.80	$[Y_4-3SO_3]^{3-}$	0.23	314.3589
315.7627	3.52E+06	100.00	$[M-4H-3SO_3]^{4-}$	0.78	315.7629
319.9747	3.63E+04	1.03	B_1	1.44	319.9752
321.0038	6.38E+02	0.02	$[^{24}X_3-2SO_3]^{3-}/[^{15}A_4-2SO_3]^{3-}$	0.94	321.0041
323.6903	1.36E+03	0.04	$[^{15}X_4-3SO_3]^{3-}/[^{12}A_6-3SO_3]^{3-}$	0.65	323.6905
328.0340	3.52E+04	1.00	$[B_3-3SO_3]^{2-}$	1.19	328.0344
330.3353	1.09E+05	3.11	$[B_4-2SO_3]^{3-}$	1.33	330.3357
333.9906	1.47E+03	0.04	Z_1	0.63	333.9908
335.0068	1.17E+03	0.03	$[Z_4-2SO_3]^{3-}$	2.46	335.0076
335.0419	1.18E+04	0.33	$[Z_3-4SO_3]^{2-}$	0.94	335.0422
335.7518	5.59E+05	15.88	$[M-4H-2SO_3]^{4-}$	1.04	335.7521
336.0934	2.89E+03	0.08	$[B_2-2SO_3]^{2-}$	0.65	336.0936
336.3389	5.17E+04	1.47	$[C_4-2SO_3]^{3-}$	1.08	336.3393
337.0393	4.32E+03	0.12	$[C_3-3SO_3]^{2-}$	1.10	337.0397
341.0107	8.25E+05	23.44	$[Y_4-2SO_3]^{3-}$	1.31	341.0111
342.9839	2.15E+03	0.06	$^{62}A_4^{3-}$	1.72	342.9845
344.0470	1.78E+04	0.51	$[Y_3-4SO_3]^{2-}$	1.45	344.0475
347.6559	1.60E+03	0.05	$[^{24}X_3-SO_3]^{3-}/[^{15}A_6-SO_3]^{3-}$	1.36	347.6564
352.0009	6.84E+03	0.19	Y_1	1.35	352.0014
355.7410	5.87E+03	0.17	$[M-4H-SO_3]^{4-}$	0.99	355.7414
356.9876	9.97E+03	0.28	$[B_4-SO_3]^{3-}$	1.15	356.9880
362.9910	3.37E+03	0.10	$[C_4-SO_3]^{3-}$	1.47	362.9915
367.6630	1.09E+05	3.11	$[Y_4-SO_3]^{3-}$	1.13	367.6634
368.0123	2.12E+04	0.60	$[B_3-2SO_3]^{2-}$	1.35	368.0128
368.1193	1.53E+03	0.04	$[Y_2-3SO_3]^{2-}$	1.45	368.1198
375.0203	8.80E+04	2.50	$[Z_3-3SO_3]^{2-}$	0.86	375.0206
376.0717	1.17E+04	0.33	$[B_4-5SO_3]^{2-}$	0.87	376.0720
377.0176	1.95E+03	0.06	$[C_3-2SO_3]^{2-}$	1.27	377.0181
392.0849	1.37E+03	0.04	$[Y_4-5SO_3]^{2-}$	0.60	392.0851
407.9908	2.21E+03	0.06	$[B_2-SO_3]^{2-}$	0.99	407.9912
414.9987	1.81E+04	0.51	$[Z_3-2SO_3]^{2-}$	0.79	414.9990
416.0500	2.88E+05	8.17	$[B_2-SO_3]/[B_4-4SO_3]^{2-}$	1.04	416.0504
423.0579	2.94E+03	0.08	$[Z_4-4SO_3]^{2-}$	0.85	423.0583
424.0040	3.03E+03	0.09	$[Y_3-2SO_3]^{2-}$	0.74	424.0043
425.0553	1.69E+04	0.48	$[C_4-4SO_3]^{2-}$	0.98	425.0557
430.0658	1.47E+03	0.04	$[Z_2-2SO_3]^{2-}$	0.66	430.0661
432.0631	1.52E+04	0.43	$[Y_4-4SO_3]^{2-}$	1.02	432.0635
434.0605	1.20E+04	0.34	$[C_2-SO_3]^{2-}$	1.15	434.0610
442.0309	7.59E+02	0.02	$[^{24}X_3-3SO_3]^{2-}/[^{15}A_4-3SO_3]^{2-}$	1.09	442.0314
448.0763	1.19E+04	0.34	$[Y_2-2SO_3]^{2-}$	0.78	448.0766
456.0284	4.50E+04	1.28	$[B_4-3SO_3]^{2-}$	0.97	456.0288
463.0362	4.64E+04	1.32	$[Z_4-3SO_3]^{2-}$	1.01	463.0367
465.0336	2.20E+04	0.63	$[C_4-3SO_3]^{2-}$	1.13	465.0341
472.0416	6.48E+03	0.18	$[Y_4-3SO_3]^{2-}$	0.74	472.0419
496.0069	1.20E+04	0.34	$B_2/[B_4-2SO_3]^{2-}$	0.70	496.0072
503.0147	1.05E+04	0.30	$[Z_4-2SO_3]^{2-}$	0.74	503.0151
505.0122	1.80E+03	0.05	$[C_4-2SO_3]^{2-}$	0.66	505.0125
510.0227	1.46E+03	0.04	$[Z_2-SO_3]^{2-}$	0.39	510.0229
514.0174	3.60E+03	0.10	C_2	0.80	514.0178
577.1193	1.39E+03	0.04	$[B_3-4SO_3]^{2-}$	-0.10	577.1192
671.0916	2.25E+03	0.06	$[Z_3-4SO_3]^{2-}$	0.16	671.0917

Table 17. Fragment ion list for 213 nm UVPD of $[M-3H]^{3-}$ of DS dp4.

Measured m/z	Intensity	Relative intensity	Ion	ppm error	Theoretical m/z
152.9863	1.82E+04	0.08	$^{3.5}A_2/^{3.5}A_4$	0.11	152.9863
157.0143	2.39E+04	0.10	B_1	-0.34	157.0142
175.0249	1.18E+04	0.05	C_1	-0.51	175.0248
198.9919	4.76E+04	0.21	$^{1.3}X_0/^{1.3}X_2$	-0.52	198.9918
228.5270	1.04E+04	0.04	Z_2^2-/C_2^2-	-0.61	228.5269
237.5322	2.00E+05	0.87	Y_2^2-	-0.24	237.5321
252.3645	1.06E+04	0.05	Y_3^3-	-0.40	252.3644
282.0290	3.59E+06	15.49	Z_1	-0.32	282.0289
300.0397	1.90E+05	0.82	Y_1	-0.75	300.0395
305.0384	2.31E+07	100.00	$[M-3H]^{3-}$	-0.52	305.0382
316.5429	5.14E+04	0.22	C_3^2-	0.02	316.5429
328.0345	1.38E+05	0.59	$^{1.5}X_1$	-0.34	328.0344
342.0501	8.79E+04	0.38	$^{0.2}X_1$	-0.18	342.0500
357.0372	1.70E+05	0.73	$^{2.5}X_1^+$	0.19	357.0371
370.0453	1.79E+04	0.08	Z_3^2-	-0.93	370.0450
378.1046	1.48E+03	0.01	$[Z_2-SO_3]/[C_2-SO_3]^-$	-1.10	378.1042
379.0503	5.67E+05	2.45	Y_3^2-	-0.17	379.0502
393.0478	3.59E+04	0.16	$^{1.5}X_3^2-$	-0.27	393.0477
399.5517	1.24E+06	5.35	$^{0.2}X_3^2+$	-1.61	399.5511
407.5372	1.19E+04	0.05	$^{0.2}A_4^2-$	-0.10	407.5372
435.0584	1.59E+04	0.07	$^{1.5}A_3^2-$	-0.32	435.0583
440.0507	1.62E+05	0.70	B_2	-0.60	440.0504
457.5572	6.77E+05	2.92	$[M-3H]^{2+}$	-1.45	457.5565
458.0607	7.17E+05	3.10	Z_2/C_2	0.65	458.0610
476.0717	1.34E+05	0.58	Y_2	-0.29	476.0716
499.0642	5.67E+03	0.02	$^{2.4}A_3^+$	-0.92	499.0637
504.0667	4.70E+04	0.20	$^{1.5}X_2$	-0.44	504.0665
528.0667	1.10E+04	0.05	$^{3.5}A_3$	-0.42	528.0665
558.1009	6.90E+03	0.03	$^{0.2}X_2^+$	-0.09	558.1009
574.0725	4.50E+03	0.02	$^{0.2}A_3$	-0.95	574.0720
588.0879	3.94E+04	0.17	$^{1.5}A_3$	-0.50	588.0876
615.0751	1.27E+04	0.05	B_3^+	-1.55	615.0741
634.0936	3.72E+04	0.16	C_3	-0.81	634.0931
661.1403	8.17E+03	0.04	Z_3-SO_3	0.11	661.1404
677.1357	1.92E+05	0.83	$[Y_3-SO_3]^{++}$	-1.42	677.1347
719.1464	3.98E+04	0.17	$[^{0.2}X_3-SO_3]^{++}$	0.69	719.1459
741.0974	2.68E+03	0.01	Z_3	-0.29	741.0972
747.1422	1.96E+03	0.01	$[^{1.4}A_4-SO_3]^-$	-1.92	747.1408
759.1083	7.67E+03	0.03	Y_3	-0.72	759.1078
791.1675	7.29E+04	0.31	$[M-3H-CO_2-SO_3]^{++}$	-0.66	791.1670
800.1110	2.82E+05	1.22	$^{0.2}X_3^+$	-1.32	800.1099
835.1575	2.52E+04	0.11	$[M-3H-SO_3]^{++}$	-1.48	835.1563
871.1234	2.99E+03	0.01	$[M-3H-CO_2]^{++}$	0.45	871.1238
915.1133	1.17E+04	0.05	$[M-3H]^{++}$	-0.25	915.1131

7.7 REFERENCES

- (1) Lever, R.; Page, C. P. Novel Drug Development Opportunities for Heparin. *Nat. Rev. Drug Discov.* **2002**, *1*, 140–148.
- (2) Häcker, U.; Nybakken, K.; Perrimon, N. Developmental Cell Biology: Heparan Sulphate Proteoglycans: The Sweet Side of Development. *Nat. Rev. Mol. Cell Biol.* **2005**, *6*, nrm1681.
- (3) Parish, C. R. The Role of Heparan Sulphate in Inflammation. *Nat. Rev. Immunol.* **2006**, *6*, 633–643.
- (4) Sasisekharan, R.; Shriver, Z.; Venkataraman, G.; Narayanasami, U. Roles of Heparan-Sulphate Glycosaminoglycans in Cancer. *Nat. Rev. Cancer* **2002**, *2*, nrc842.
- (5) da Costa, D. S.; Reis, R. L.; Pashkuleva, I. Sulfation of Glycosaminoglycans and Its Implications in Human Health and Disorders. *Annu. Rev. Biomed. Eng.* **2017**, *19*, 1–26.
- (6) Turnbull, J. E.; Linhardt, R. J. Synthetic Sugars Enhance the Functional Glycomics Toolkit. *Nat. Chem. Biol.* **2006**, *2*, 449–450.
- (7) Afratis, N.; Gialeli, C.; Nikitovic, D.; Tsegenidis, T.; Karousou, E.; Theocharis, A. D.; Pavão, M. S.; Tzanakakis, G. N.; Karamanos, N. K. Glycosaminoglycans: Key Players in Cancer Cell Biology and Treatment. *FEBS J.* **2012**, *279*, 1177–1197.
- (8) Liu, H.; Zhang, Z.; Linhardt, R. J. Lessons Learned from the Contamination of Heparin. *Nat. Prod. Rep.* **2009**, *26*, 313–321.
- (9) Mormann, M.; Zamfir, A. D.; Seidler, D. G.; Kresse, H.; Peter-Katalinić, J. Analysis of Oversulfation in a Chondroitin Sulfate Oligosaccharide Fraction from Bovine Aorta by Nanoelectrospray Ionization Quadrupole Time-of-Flight and Fourier-Transform Ion Cyclotron Resonance Mass Spectrometry. *J. Am. Soc. Mass Spectrom.* **2007**, *18*, 179–187.
- (10) Laremore, T. N.; Zhang, F.; Dordick, J. S.; Liu, J.; Linhardt, R. J. Recent Progress and Applications in Glycosaminoglycan and Heparin Research. *Curr. Opin. Chem. Biol.* **2009**, *13*, 633–640.
- (11) Laremore, T. N.; Leach III, F. E.; Solakyildirim, K.; Amster, I. J.; Linhardt, R. J. Glycosaminoglycan Characterization by Electrospray Ionization Mass Spectrometry Including Fourier Transform Mass Spectrometry. In *Methods in Enzymology*; Abelson, J. N., Simon, M. I., Eds.; Glycomics; Academic Press, 2010; Vol. 478, pp 79–108.
- (12) Chi, L.; Wolff, J. J.; Laremore, T. N.; Restaino, O. F.; Xie, J.; Schiraldi, C.; Toida, T.; Amster, I. J.; Linhardt, R. J. Structural Analysis of Bikunin Glycosaminoglycan. *J. Am. Chem. Soc.* **2008**, *130*, 2617–2625.

- (13) Ly, M.; Leach III, F. E.; Laremore, T. N.; Toida, T.; Amster, I. J.; Linhardt, R. J. The Proteoglycan Bikunin Has a Defined Sequence. *Nat. Chem. Biol.* **2011**, *7*, 827–833.
- (14) Kailemia, M. J.; Li, L.; Ly, M.; Linhardt, R. J.; Amster, I. J. Complete Mass Spectral Characterization of a Synthetic Ultralow-Molecular-Weight Heparin Using Collision-Induced Dissociation. *Anal. Chem.* **2012**, *84*, 5475–5478.
- (15) Wolff, J. J.; Laremore, T. N.; Leach III, F. E.; Linhardt, R. J.; Amster, I. J. Electron Capture Dissociation, Electron Detachment Dissociation and Infrared Multiphoton Dissociation of Sucrose Octasulfate. *Eur. J. Mass Spectrom.* **2008**, *15*, 275–281.
- (16) Zaia, J.; McClellan, J. E.; Costello, C. E. Tandem Mass Spectrometric Determination of the 4S/6S Sulfation Sequence in Chondroitin Sulfate Oligosaccharides. *Anal. Chem.* **2001**, *73*, 6030–6039.
- (17) Zaia, J.; Costello, C. E. Compositional Analysis of Glycosaminoglycans by Electrospray Mass Spectrometry. *Anal. Chem.* **2001**, *73*, 233–239.
- (18) Zaia, J.; Costello, C. E. Tandem Mass Spectrometry of Sulfated Heparin-Like Glycosaminoglycan Oligosaccharides. *Anal. Chem.* **2003**, *75*, 2445–2455.
- (19) Naggar, E. F.; Costello, C. E.; Zaia, J. Competing Fragmentation Processes in Tandem Mass Spectra of Heparin-like Glycosaminoglycans. *J. Am. Soc. Mass Spectrom.* **2004**, *15*, 1534–1544.
- (20) Kailemia, M. J.; Li, L.; Xu, Y.; Liu, J.; Linhardt, R. J.; Amster, I. J. Structurally Informative Tandem Mass Spectrometry of Highly Sulfated Natural and Chemoenzymatically Synthesized Heparin and Heparan Sulfate Glycosaminoglycans. *Mol. Cell. Proteomics* **2013**, *12*, 979–990.
- (21) Huang, R.; Pomin, V. H.; Sharp, J. S. LC-MSn Analysis of Isomeric Chondroitin Sulfate Oligosaccharides Using a Chemical Derivatization Strategy. *J. Am. Soc. Mass Spectrom.* **2011**, *22*, 1577.
- (22) Huang, R.; Liu, J.; Sharp, J. S. An Approach for Separation and Complete Structural Sequencing of Heparin/Heparan Sulfate-like Oligosaccharides. *Anal. Chem.* **2013**, *85*, 5787–5795.
- (23) Taylor, C. J.; Burke, R. M.; Wu, B.; Panja, S.; Nielsen, S. B.; Dessent, C. E. H. Structural Characterization of Negatively Charged Glycosaminoglycans Using High-Energy (50–150keV) Collisional Activation. *Int. J. Mass Spectrom.* **2009**, *285*, 70–77.
- (24) Wolff, J. J.; Amster, I. J.; Chi, L.; Linhardt, R. J. Electron Detachment Dissociation of Glycosaminoglycan Tetrasaccharides. *J. Am. Soc. Mass Spectrom.* **2007**, *18*, 234–244.

- (25) Wolff, J. J.; Laremore, T. N.; Busch, A. M.; Linhardt, R. J.; Amster, I. J. Electron Detachment Dissociation of Dermatan Sulfate Oligosaccharides. *J. Am. Soc. Mass Spectrom.* **2008**, *19*, 294–304.
- (26) Wolff, J. J.; Laremore, T. N.; Busch, A. M.; Linhardt, R. J.; Amster, I. J. Influence of Charge State and Sodium Cationization on the Electron Detachment Dissociation and Infrared Multiphoton Dissociation of Glycosaminoglycan Oligosaccharides. *J. Am. Soc. Mass Spectrom.* **2008**, *19*, 790–798.
- (27) Leach III, F. E.; Wolff, J. J.; Laremore, T. N.; Linhardt, R. J.; Amster, I. J. Evaluation of the Experimental Parameters Which Control Electron Detachment Dissociation, and Their Effect on the Fragmentation Efficiency of Glycosaminoglycan Carbohydrates. *Int. J. Mass Spectrom.* **2008**, *276*, 110–115.
- (28) Wolff, J. J.; Chi, L.; Linhardt, R. J.; Amster, I. J. Distinguishing Glucuronic from Iduronic Acid in Glycosaminoglycan Tetrasaccharides by Using Electron Detachment Dissociation. *Anal. Chem.* **2007**, *79*, 2015–2022.
- (29) Oh, H. B.; Leach III, F. E.; Arungundram, S.; Al-Mafraji, K.; Venot, A.; Boons, G. J.; Amster, I. J. Multivariate Analysis of Electron Detachment Dissociation and Infrared Multiphoton Dissociation Mass Spectra of Heparan Sulfate Tetrasaccharides Differing Only in Hexuronic Acid Stereochemistry. *J. Am. Soc. Mass Spectrom.* **2011**, *22*, 582–590.
- (30) Leach III, F. E.; Ly, M.; Laremore, T. N.; Wolff, J. J.; Perlow, J.; Linhardt, R. J.; Amster, I. J. Hexuronic Acid Stereochemistry Determination in Chondroitin Sulfate Glycosaminoglycan Oligosaccharides by Electron Detachment Dissociation. *J. Am. Soc. Mass Spectrom.* **2012**, *23*, 1488–1497.
- (31) Agyekum, I.; Zong, C.; Boons, G. J.; Amster, I. J. Single Stage Tandem Mass Spectrometry Assignment of the C-5 Uronic Acid Stereochemistry in Heparan Sulfate Tetrasaccharides Using Electron Detachment Dissociation. *J. Am. Soc. Mass Spectrom.* **2017**, 1–10.
- (32) Kailemia, M. J.; Park, M.; Kaplan, D. A.; Venot, A.; Boons, G. J.; Li, L.; Linhardt, R. J.; Amster, I. J. High-Field Asymmetric-Waveform Ion Mobility Spectrometry and Electron Detachment Dissociation of Isobaric Mixtures of Glycosaminoglycans. *J. Am. Soc. Mass Spectrom.* **2014**, *25*, 258–268.
- (33) Huang, Y.; Yu, X.; Mao, Y.; Costello, C. E.; Zaia, J.; Lin, C. De Novo Sequencing of Heparan Sulfate Oligosaccharides by Electron-Activated Dissociation. *Anal. Chem.* **2013**, *85*, 11979–11986.
- (34) Wolff, J. J.; Leach III, F. E.; Laremore, T. N.; Kaplan, D. A.; Easterling, M. L.; Linhardt, R. J.; Amster, I. J. Negative Electron Transfer Dissociation of Glycosaminoglycans. *Anal. Chem.* **2010**, *82*, 3460–3466.
- (35) Leach III, F. E.; Wolff, J. J.; Xiao, Z.; Ly, M.; Laremore, T. N.; Arungundram, S.; Al-Mafraji, K.; Venot, A.; Boons, G. J.; Linhardt, R. J.; Amster, I. J. Negative

- Electron Transfer Dissociation Fourier Transform Mass Spectrometry of Glycosaminoglycan Carbohydrates. *Eur. J. Mass Spectrom.* **2011**, *17*, 167–176.
- (36) Leach III, F. E.; Riley, N. M.; Westphall, M. S.; Coon, J. J.; Amster, I. J. Negative Electron Transfer Dissociation Sequencing of Increasingly Sulfated Glycosaminoglycan Oligosaccharides on an Orbitrap Mass Spectrometer. *J. Am. Soc. Mass Spectrom.* **2017**, *28*, 1844–1854.
 - (37) Wu, J.; Wei, J.; Hogan, J. D.; Chopra, P.; Joshi, A.; Lu, W.; Klein, J.; Boons, G. J.; Lin, C.; Zaia, J. Negative Electron Transfer Dissociation Sequencing of 3-O-Sulfation-Containing Heparan Sulfate Oligosaccharides. *J. Am. Soc. Mass Spectrom.* **2018**, *29*, 1262–1272.
 - (38) Wolff, J. J.; Laremore, T. N.; Aslam, H.; Linhardt, R. J.; Amster, I. J. Electron-Induced Dissociation of Glycosaminoglycan Tetrasaccharides. *J. Am. Soc. Mass Spectrom.* **2008**, *19*, 1449–1458.
 - (39) Ropartz, D.; Li, P.; Fanuel, M.; Giuliani, A.; Rogniaux, H.; Jackson, G. P. Charge Transfer Dissociation of Complex Oligosaccharides: Comparison with Collision-Induced Dissociation and Extreme Ultraviolet Dissociative Photoionization. *J. Am. Soc. Mass Spectrom.* **2016**, *27*, 1614–1619.
 - (40) Racaud, A.; Antoine, R.; Joly, L.; Mesplet, N.; Dugourd, P.; Lemoine, J. Wavelength-Tunable Ultraviolet Photodissociation (UVPD) of Heparin-Derived Disaccharides in a Linear Ion Trap. *J. Am. Soc. Mass Spectrom.* **2009**, *20*, 1645–1651.
 - (41) Racaud, A.; Antoine, R.; Dugourd, P.; Lemoine, J. Photoinduced Dissociation of Heparin-Derived Oligosaccharides Controlled by Charge Location. *J. Am. Soc. Mass Spectrom.* **2010**, *21*, 2077–2084.
 - (42) Ortiz, D.; Enjalbert, Q.; MacAleese, L.; Dugourd, P.; Salpin, J.-Y. Effects of Calcium Complexation on Heparin-like Disaccharides. A Combined Theoretical, Tandem Mass Spectrometry and Ultraviolet Experiment. *Rapid Commun. Mass Spectrom.* **2015**, *29*, 1135–1144.
 - (43) Ropartz, D.; Lemoine, J.; Giuliani, A.; Bittebière, Y.; Enjalbert, Q.; Antoine, R.; Dugourd, P.; Ralet, M.-C.; Rogniaux, H. Deciphering the Structure of Isomeric Oligosaccharides in a Complex Mixture by Tandem Mass Spectrometry: Photon Activation with Vacuum Ultra-Violet Brings Unique Information and Enables Definitive Structure Assignment. *Anal. Chim. Acta* **2014**, *807*, 84–95.
 - (44) Ropartz, D.; Giuliani, A.; Hervé, C.; Geairon, A.; Jam, M.; Czjzek, M.; Rogniaux, H. High-Energy Photon Activation Tandem Mass Spectrometry Provides Unprecedented Insights into the Structure of Highly Sulfated Oligosaccharides Extracted from Macroalgal Cell Walls. *Anal. Chem.* **2015**, *87*, 1042–1049.
 - (45) Ropartz, D.; Giuliani, A.; Fanuel, M.; Hervé, C.; Czjzek, M.; Rogniaux, H. Online Coupling of High-Resolution Chromatography with Extreme UV Photon

- Activation Tandem Mass Spectrometry: Application to the Structural Investigation of Complex Glycans by Dissociative Photoionization. *Anal. Chim. Acta* **2016**, 933, 1–9.
- (46) Compagnon, I.; Schindler, B.; Renois-Predelus, G.; Daniel, R. Lasers and Ion Mobility: New Additions to the Glycosaminoglycanomics Toolkit. *Curr. Opin. Struct. Biol.* **2018**, 50, 171–180.
- (47) Devakumar, A.; Thompson, M. S.; Reilly, J. P. Fragmentation of Oligosaccharide Ions with 157 Nm Vacuum Ultraviolet Light. *Rapid Commun. Mass Spectrom.* **2005**, 19, 2313–2320.
- (48) Cui, W.; Thompson, M. S.; Reilly, J. P. Pathways of Peptide Ion Fragmentation Induced by Vacuum Ultraviolet Light. *J. Am. Soc. Mass Spectrom.* **2005**, 16, 1384–1398.
- (49) Reilly, J. P. Ultraviolet Photofragmentation of Biomolecular Ions. *Mass Spectrom. Rev.* **2009**, 28, 425–447.
- (50) Brodbelt, J. S. Photodissociation Mass Spectrometry: New Tools for Characterization of Biological Molecules. *Chem. Soc. Rev.* **2014**, 43, 2757–2783.
- (51) Shaw, J. B.; Li, W.; Holden, D. D.; Zhang, Y.; Griep-Raming, J.; Fellers, R. T.; Early, B. P.; Thomas, P. M.; Kelleher, N. L.; Brodbelt, J. S. Complete Protein Characterization Using Top-Down Mass Spectrometry and Ultraviolet Photodissociation. *J. Am. Chem. Soc.* **2013**, 135, 12646–12651.
- (52) Klein, D. R.; Holden, D. D.; Brodbelt, J. S. Shotgun Analysis of Rough-Type Lipopolysaccharides Using Ultraviolet Photodissociation Mass Spectrometry. *Anal. Chem.* **2016**, 88, 1044–1051.
- (53) Ko, B. J.; Brodbelt, J. S. 193 Nm Ultraviolet Photodissociation of Deprotonated Sialylated Oligosaccharides. *Anal. Chem.* **2011**, 83, 8192–8200.
- (54) Robinson, M. R.; Moore, K. L.; Brodbelt, J. S. Direct Identification of Tyrosine Sulfation by Using Ultraviolet Photodissociation Mass Spectrometry. *J. Am. Soc. Mass Spectrom.* **2014**, 25, 1461–1471.
- (55) Fornelli, L.; Srzentić, K.; Huguet, R.; Mullen, C.; Sharma, S.; Zabrouskov, V.; Fellers, R. T.; Durbin, K. R.; Compton, P. D.; Kelleher, N. L. Accurate Sequence Analysis of a Monoclonal Antibody by Top-Down and Middle-Down Orbitrap Mass Spectrometry Applying Multiple Ion Activation Techniques. *Anal. Chem.* **2018**, 90, 8421–8429.
- (56) Brodie, N. I.; Huguet, R.; Zhang, T.; Viner, R.; Zabrouskov, V.; Pan, J.; Petrotchenko, E. V.; Borchers, C. H. Top-Down Hydrogen–Deuterium Exchange Analysis of Protein Structures Using Ultraviolet Photodissociation. *Anal. Chem.* **2018**, 90, 3079–3082.

- (57) Arungundram, S.; Al-Mafraji, K.; Asong, J.; Leach III, F. E.; Amster, I. J.; Venot, A.; Turnbull, J. E.; Boons, G. J. Modular Synthesis of Heparan Sulfate Oligosaccharides for Structure–Activity Relationship Studies. *J. Am. Chem. Soc.* **2009**, *131*, 17394–17405.
- (58) Domon, B.; Costello, C. E. A Systematic Nomenclature for Carbohydrate Fragmentations in FAB-MS/MS Spectra of Glycoconjugates. *Glycoconj. J.* **1988**, *5*, 397–409.
- (59) Ceroni, A.; Maass, K.; Geyer, H.; Geyer, R.; Dell, A.; Haslam, S. M. GlycoWorkbench: A Tool for the Computer-Assisted Annotation of Mass Spectra of Glycans. *J. Proteome Res.* **2008**, *7*, 1650–1659.
- (60) Shi, X.; Huang, Y.; Mao, Y.; Naimy, H.; Zaia, J. Tandem Mass Spectrometry of Heparan Sulfate Negative Ions: Sulfate Loss Patterns and Chemical Modification Methods for Improvement of Product Ion Profiles. *J. Am. Soc. Mass Spectrom.* **2012**, *23*, 1498–1511.
- (61) Brunet, C.; Antoine, R.; Dugourd, P.; Canon, F.; Giuliani, A.; Nahon, L. Photo-Induced Electron Detachment of Protein Polyanions in the VUV Range. *J. Chem. Phys.* **2013**, *138*, 064301.
- (62) Walenga, J. M.; Jeske, W. P.; Frapaise, F. X.; Bick, R. L.; Fareed, J.; Samama, M. M. Fondaparinux: A Synthetic Heparin Pentasaccharide as a New Antithrombotic Agent. *Expert Opin. Investig. Drugs* **2002**, *11*, 397–407.
- (63) Julian, R. R. The Mechanism Behind Top-Down UVPD Experiments: Making Sense of Apparent Contradictions. *J. Am. Soc. Mass Spectrom.* **2017**, *28*, 1823–1826.
- (64) Sanderson, P.; Stickney, M.; Leach, F. E.; Xia, Q.; Yu, Y.; Zhang, F.; Linhardt, R. J.; Amster, I. J. Heparin/Heparan Sulfate Analysis by Covalently Modified Reverse Polarity Capillary Zone Electrophoresis-Mass Spectrometry. *J. Chromatogr. A* **2018**, *1545*, 75–83.
- (65) Wei, J.; Wu, J.; Tang, Y.; Ridgeway, M. E.; Park, M. A.; Costello, C. E.; Zaia, J.; Lin, C. Characterization and Quantification of Highly Sulfated Glycosaminoglycan Isomers by Gated-Trapped Ion Mobility Spectrometry Negative Electron Transfer Dissociation MS/MS. *Anal. Chem.* **2019**, *91*, 2994–3001.
- (66) Duan, J.; Jonathan Amster, I. An Automated, High-Throughput Method for Interpreting the Tandem Mass Spectra of Glycosaminoglycans. *J. Am. Soc. Mass Spectrom.* **2018**, *29*, 1802–1811.

Chapter 8: Conclusions

8.1 SUMMARY OF CHAPTERS

The rapid growth of the field of lipidomics can largely be attributed to innovations in mass spectrometry instrumentation. However, conventional tandem mass spectrometry methods often prevent determination of subtle structural features and provide limited information on targets that are structurally complex. Implementation of alternative ion activation methods, in particular UVPD, on high resolution mass spectrometers has significantly contributed to the ultimate goal of obtaining complete lipid structural characterization.¹ The work presented in the dissertation both reaffirms 193 nm UVPD as an effective means to obtain additional structural information and confirms that it can be successfully coupled to shotgun, chromatographic and imaging workflows.

193 nm UVPD of phosphatidylcholine cations produced diagnostic pairs of ions that permitted localization of unsaturations within acyl chains. The number of double bonds appears to both influence the extent of fragmentation and the production of even- and odd- electron fragment ions. This result is not surprising considering the UV absorption properties of unsaturations in which molar attenuation coefficient increases with the number of double bonds.² Application of 193 nm UVPD to a shotgun lipidomic workflow confirmed that double bond positional isomers could be detected in a complex lipid extract and that relative quantitation could be performed based on diagnostic ion intensities. Coupling of the developed UVPD method with DESI allowed double bond positional isomers to be detected *in situ*. Further, changes in the relative abundance of double bond positional isomers were localized to specific tissue features.

Lipopolysaccharides (LOS) represent an even more structurally complex lipid target than phospholipids. In Chapter 5, a shotgun electrospray infusion method was developed in which collisional activation was used to bisect intact LOS ions to produce lipid A and oligosaccharide substructures. Subsequent activation of lipid A and oligosaccharide fragment ions by UVPD generated rich spectra that provided an unprecedented level of structural characterization for intact LOS. The developed MS³ method was then coupled, in a targeted fashion, with online chromatographic separations in Chapter 6. The chromatographic method revealed the true heterogeneity of LOS samples and facilitated detection subtle structural features that of otherwise may have gone unnoticed during a shotgun infusion method. For example, intact LOS structures that differed only by the presence of a single unsaturation in one acyl chain were baseline separated; the isotope pattern of these species would have overlapped during shotgun infusion. Using the developed LC-MS³ method, the structures of LOS from strains of *Acinetobacter baumannii*, for which the structures were unknown, were determined.

8.2 FUTURE DIRECTIONS

The work presented in this dissertation establishes a versatile framework for characterization of phospholipids and lipopolysaccharides. There remain many avenues for continuation of the methods development aspects and new applications that exploit the UVPD strategies.

8.2.1 Glycerophospholipids

To date, all methods utilizing UVPD for localization of double bonds within lipid acyl chains, including the work presented in Chapters 3 and 4, have been performed in positive mode.^{3,4} Positive mode analysis was the natural choice for PC and

sphingomyelin characterization, owing to the fixed positive charge on the head groups.⁴ Williams *et al.* showed that sodium adduction using infusion of a sodium salt via a tee can be used to determine acyl chain and double bond positions in positive mode for a variety of glycerophospholipids via UVPD.³ However, introduction of a non-volatile salt is not practical for all workflows. Extension of the UVPD method to negative mode would allow a higher level of structural characterization for glycerophospholipids that preferentially ionize in negative mode.^{5,6} Preliminary data for a phosphatidylglycerol anion in **Figure 8.1** confirm that UVPD can be used in the negative mode to determine the glycerophospholipids subclass, acyl chain composition and double bond positions in a single MS/MS event. This data further establishes UVPD as a promising method that can be used in either polarity.

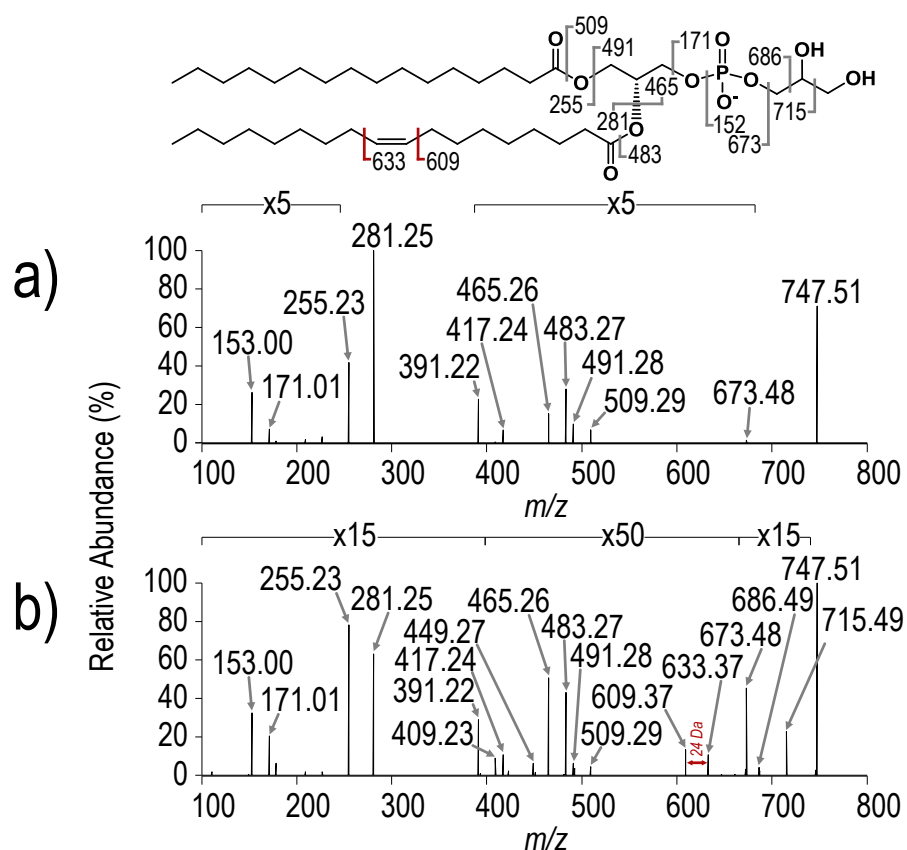


Figure 8.1 a) HCD (NCE 25) and b) UVPD (20 pulses, 4mJ) spectra of deprotonated phosphatidylglycerol 16:0/18:1 ($[M-H]^-$, m/z 747.51)

8.2.2 LPS/LOS

For the work presented in Chapters 5 and 6, LOS served as good starting point for top-down structural characterization. However, LOS represents a relatively simple structure compared to LPS structures that contain O-antigen. Bacterial serotyping, which allows classification beyond the species level, is done based on bacterial surface antigens, including O-antigen. Classification by serotype not only assists in identifying the source of the bacteria but also allows the potential severity of disease to be determined.^{7,8} O-antigen also represents a target for the development of vaccine therapeutics.⁹ Traditional

agglutination-based serotyping methods require a large number of O-antigen specific antibodies be maintained and can lead to false-positives as results are based on visual detection of agglutination.¹⁰ The development of mass spectrometry-based serotyping methods built on O-antigen characterization would allow accurate classification of bacteria, and allow more subtle structural features, including non-stoichiometric modifications, to be investigated. The next natural step with this work is to evaluate the compatibility of the developed methods with intact analysis of LPS.

8.3 REFERENCES

- (1) Brodbelt, J. S. Photodissociation Mass Spectrometry: New Tools for Characterization of Biological Molecules. *Chem. Soc. Rev.* **2014**, *43*, 2757–2783.
- (2) McHowat, J.; Jones, J. H.; Creer, M. H. Quantitation of Individual Phospholipid Molecular Species by UV Absorption Measurements. *J. Lipid Res.* **1996**, *37*, 2450–2460.
- (3) Williams, P. E.; Klein, D. R.; Greer, S. M.; Brodbelt, J. S. Pinpointing Double Bond and Sn-Positions in Glycerophospholipids via Hybrid 193 nm Ultraviolet Photodissociation (UVPD) Mass Spectrometry. *J. Am. Chem. Soc.* **2017**, *139*, 15681–15690.
- (4) Ryan, E.; Nguyen, C. Q. N.; Shiea, C.; Reid, G. E. Detailed Structural Characterization of Sphingolipids via 193 nm Ultraviolet Photodissociation and Ultra High Resolution Tandem Mass Spectrometry. *J. Am. Soc. Mass Spectrom.* **2017**, *28*, 1406–1419.
- (5) Pulfer, M.; Murphy, R. C. Electrospray Mass Spectrometry of Phospholipids. *Mass Spectrom. Rev.* **2003**, *22*, 332–364.
- (6) Ivanova, P. T.; Milne, S. B.; Byrne, M. O.; Xiang, Y.; Brown, H. A. Glycerophospholipid Identification and Quantitation by Electrospray Ionization Mass Spectrometry. In *Methods in Enzymology; Lipidomics and Bioactive Lipids: Mass-Spectrometry–Based Lipid Analysis*; Academic Press, 2007; Vol. 432, pp 21–57.
- (7) Ranieri, M. L.; Shi, C.; Switt, A. I. M.; Bakker, H. C. den; Wiedmann, M. Comparison of Typing Methods with a New Procedure Based on Sequence Characterization for Salmonella Serovar Prediction. *J. Clin. Microbiol.* **2013**, *51*, 1786–1797.

- (8) Liu, B.; Knirel, Y. A.; Feng, L.; Perepelov, A. V.; Senchenkova, S. N.; Reeves, P. R.; Wang, L. Structural Diversity in Salmonella O-Antigens and Its Genetic Basis. *FEMS Microbiol. Rev.* **2014**, *38*, 56–89.
- (9) Chen, L.; Valentine, J. L.; Huang, C.-J.; Endicott, C. E.; Moeller, T. D.; Rasmussen, J. A.; Fletcher, J. R.; Boll, J. M.; Rosenthal, J. A.; Dobruchowska, J.; Wang, Z.; Heiss, C.; Azadi, P.; Putnam, D.; Trent, M. S.; Jones, B. D.; DeLisa, M. P. Outer Membrane Vesicles Displaying Engineered Glycotopes Elicit Protective Antibodies. *Proc. Natl. Acad. Sci.* **2016**, *113*, E3609–E3618.
- (10) Wattiau, P.; Boland, C.; Bertrand, S. Methodologies for Salmonella Enterica Subsp. Enterica Subtyping: Gold Standards and Alternatives. *Appl. Environ. Microbiol.* **2011**, *77*, 7877–7885.

References

CHAPTER 1

- (1) Dennis, E. A. Lipidomics Joins the Omics Evolution. *Proc. Natl. Acad. Sci.* **2009**, *106*, 2089–2090.
- (2) van Meer, G.; Voelker, D. R.; Feigenson, G. W. Membrane Lipids: Where They Are and How They Behave. *Nat. Rev. Mol. Cell Biol.* **2008**, *9*, 112–124.
- (3) Holthuis, J. C. M.; Levine, T. P. Lipid Traffic: Floppy Drives and a Superhighway. *Nat. Rev. Mol. Cell Biol.* **2005**, *6*, 209–220.
- (4) Sezgin, E.; Levental, I.; Mayor, S.; Eggeling, C. The Mystery of Membrane Organization: Composition, Regulation and Roles of Lipid Rafts. *Nat. Rev. Mol. Cell Biol.* **2017**, *18*, 361–374.
- (5) Janmey, P. A.; Kinnunen, P. K. J. Biophysical Properties of Lipids and Dynamic Membranes. *Trends Cell Biol.* **2006**, *16*, 538–546.
- (6) Zhang, Y.-M.; Rock, C. O. Membrane Lipid Homeostasis in Bacteria. *Nat. Rev. Microbiol.* **2008**, *6*, 222–233.
- (7) Raetz, C. R. H.; Reynolds, C. M.; Trent, M. S.; Bishop, R. E. Lipid A Modification Systems in Gram-Negative Bacteria. *Annu. Rev. Biochem.* **2007**, *76*, 295–329.
- (8) Harayama, T.; Riezman, H. Understanding the Diversity of Membrane Lipid Composition. *Nat. Rev. Mol. Cell Biol.* **2018**, 1–16.
- (9) Wenk, M. R. The Emerging Field of Lipidomics. *Nat. Rev. Drug Discov.* **2005**, *4*, 594–610.
- (10) Shevchenko, A.; Simons, K. Lipidomics: Coming to Grips with Lipid Diversity. *Nat. Rev. Mol. Cell Biol.* **2010**, *11*, 593–598.
- (11) Hu, T.; Zhang, J.-L. Mass-Spectrometry-Based Lipidomics. *J. Sep. Sci.* **2018**, *41*, 351–372.
- (12) Han, X. Lipidomics for Studying Metabolism. *Nat. Rev. Endocrinol.* **2016**, *12*, 668–679.
- (13) Gross, R. W. The Evolution of Lipidomics through Space and Time. *Biochim. Biophys. Acta BBA - Mol. Cell Biol. Lipids* **2017**, *1862*, 731–739.
- (14) Köfeler, H. C.; Fauland, A.; Rechberger, G. N.; Trötzmüller, M. Mass Spectrometry Based Lipidomics: An Overview of Technological Platforms. *Metabolites* **2012**, *2*, 19–38.

- (15) Rolim, A. E. H.; Henrique-Araújo, R.; Ferraz, E. G.; de Araújo Alves Dultra, F. K.; Fernandez, L. G. Lipidomics in the Study of Lipid Metabolism: Current Perspectives in the Omic Sciences. *Gene* **2015**, *554*, 131–139.
- (16) Harkewicz, R.; Dennis, E. A. Applications of Mass Spectrometry to Lipids and Membranes. *Annu. Rev. Biochem.* **2011**, *80*, 301–325.
- (17) Wenk, M. R. Lipidomics: New Tools and Applications. *Cell* **2010**, *143*, 888–895.
- (18) Holčápek, M.; Liebisch, G.; Ekroos, K. Lipidomic Analysis. *Anal. Chem.* **2018**, *90*, 4249–4257.
- (19) Hsu, F.-F. Mass Spectrometry-Based Shotgun Lipidomics – a Critical Review from the Technical Point of View. *Anal. Bioanal. Chem.* **2018**, *410*, 6387–6409.
- (20) Rustam, Y. H.; Reid, G. E. Analytical Challenges and Recent Advances in Mass Spectrometry Based Lipidomics. *Anal. Chem.* **2018**, *90*, 374–397.
- (21) Han, X.; Gross, R. W. Shotgun Lipidomics: Electrospray Ionization Mass Spectrometric Analysis and Quantitation of Cellular Lipidomes Directly from Crude Extracts of Biological Samples. *Mass Spectrom. Rev.* **2005**, *24*, 367–412.
- (22) Yang, K.; Han, X. Lipidomics: Techniques, Applications, and Outcomes Related to Biomedical Sciences. *Trends Biochem. Sci.* **2016**, *41*, 954–969.
- (23) Wang, M.; Wang, C.; Han, R. H.; Han, X. Novel Advances in Shotgun Lipidomics for Biology and Medicine. *Prog. Lipid Res.* **2016**, *61*, 83–108.
- (24) Damen, C. W. N.; Isaac, G.; Langridge, J.; Hankemeier, T.; Vreeken, R. J. Enhanced Lipid Isomer Separation in Human Plasma Using Reversed-Phase UPLC with Ion-Mobility/High-Resolution MS Detection. *J. Lipid Res.* **2014**, *55*, 1772–1783.
- (25) Cajka, T.; Fiehn, O. Comprehensive Analysis of Lipids in Biological Systems by Liquid Chromatography-Mass Spectrometry. *TrAC Trends Anal. Chem.* **2014**, *61*, 192–206.
- (26) Gode, D.; A. Volmer, D. Lipid Imaging by Mass Spectrometry – a Review. *Analyst* **2013**, *138*, 1289–1315.
- (27) Paglia, G.; Kliman, M.; Claude, E.; Geromanos, S.; Astarita, G. Applications of Ion-Mobility Mass Spectrometry for Lipid Analysis. *Anal. Bioanal. Chem.* **2015**, *407*, 4995–5007.
- (28) Sans, M.; Feider, C. L.; Eberlin, L. S. Advances in Mass Spectrometry Imaging Coupled to Ion Mobility Spectrometry for Enhanced Imaging of Biological Tissues. *Curr. Opin. Chem. Biol.* **2018**, *42*, 138–146.
- (29) Brown, S. H. J.; Mitchell, T. W.; Oakley, A. J.; Pham, H. T.; Blanksby, S. J. Time to Face the Fats: What Can Mass Spectrometry Reveal about the Structure of

- Lipids and Their Interactions with Proteins? *J. Am. Soc. Mass Spectrom.* **2012**, *23*, 1441–1449.
- (30) Schwudke, D.; Schuhmann, K.; Herzog, R.; Bornstein, S. R.; Shevchenko, A. Shotgun Lipidomics on High Resolution Mass Spectrometers. *Cold Spring Harb. Perspect. Biol.* **2011**, *3*, a004614.
 - (31) Pulfer, M.; Murphy, R. C. Electrospray Mass Spectrometry of Phospholipids. *Mass Spectrom. Rev.* **2003**, *22*, 332–364.
 - (32) Antonny, B.; Vanni, S.; Shindou, H.; Ferreira, T. From Zero to Six Double Bonds: Phospholipid Unsaturation and Organelle Function. *Trends Cell Biol.* **2015**, *25*, 427–436.
 - (33) Martinez-Seara, H.; Róg, T.; Pasenkiewicz-Gierula, M.; Vattulainen, I.; Karttunen, M.; Reigada, R. Interplay of Unsaturated Phospholipids and Cholesterol in Membranes: Effect of the Double-Bond Position. *Biophys. J.* **2008**, *95*, 3295–3305.
 - (34) Hishikawa, D.; Hashidate, T.; Shimizu, T.; Shindou, H. Diversity and Function of Membrane Glycerophospholipids Generated by the Remodeling Pathway in Mammalian Cells. *J. Lipid Res.* **2014**, *55*, 799–807.
 - (35) Canez, C. R.; Shields, S. W. J.; Bugno, M.; Wasslen, K. V.; Weinert, H. P.; Willmore, W. G.; Manthorpe, J. M.; Smith, J. C. Trimethylation Enhancement Using ¹³C-Diazomethane (¹³C-TrEnDi): Increased Sensitivity and Selectivity of Phosphatidylethanolamine, Phosphatidylcholine, and Phosphatidylserine Lipids Derived from Complex Biological Samples. *Anal. Chem.* **2016**, *88*, 6996–7004.
 - (36) Stutzman, J. R.; Blanksby, S. J.; McLuckey, S. A. Gas-Phase Transformation of Phosphatidylcholine Cations to Structurally Informative Anions via Ion/Ion Chemistry. *Anal. Chem.* **2013**, *85*, 3752–3757.
 - (37) Rojas-Betancourt, S.; Stutzman, J. R.; Londry, F. A.; Blanksby, S. J.; McLuckey, S. A. Gas-Phase Chemical Separation of Phosphatidylcholine and Phosphatidylethanolamine Cations via Charge Inversion Ion/Ion Chemistry. *Anal. Chem.* **2015**, *87*, 11255–11262.
 - (38) Betancourt, S. K.; Canez, C. R.; Shields, S. W. J.; Manthorpe, J. M.; Smith, J. C.; McLuckey, S. A. Trimethylation Enhancement Using ¹³C-Diazomethane: Gas-Phase Charge Inversion of Modified Phospholipid Cations for Enhanced Structural Characterization. *Anal. Chem.* **2017**, *89*, 9452–9458.
 - (39) Junot, C.; Fenaille, F.; Colsch, B.; Bécher, F. High Resolution Mass Spectrometry Based Techniques at the Crossroads of Metabolic Pathways. *Mass Spectrom. Rev.* **2014**, *33*, 471–500.

- (40) Ghaste, M.; Mistrik, R.; Shulaev, V. Applications of Fourier Transform Ion Cyclotron Resonance (FT-ICR) and Orbitrap Based High Resolution Mass Spectrometry in Metabolomics and Lipidomics. *Int. J. Mol. Sci.* **2016**, *17*, 816.
- (41) *Lipidomics: Technologies and Applications*; Ekroos, K., Ed.; Wiley-VCH: Weinheim, Germany, 2012.
- (42) Zheng, X.; Smith, R. D.; Baker, E. S. Recent Advances in Lipid Separations and Structural Elucidation Using Mass Spectrometry Combined with Ion Mobility Spectrometry, Ion-Molecule Reactions and Fragmentation Approaches. *Curr. Opin. Chem. Biol.* **2018**, *42*, 111–118.
- (43) Hsu, F.-F.; Turk, J. Electrospray Ionization with Low-Energy Collisionally Activated Dissociation Tandem Mass Spectrometry of Glycerophospholipids: Mechanisms of Fragmentation and Structural Characterization. *J. Chromatogr. B* **2009**, *877*, 2673–2695.
- (44) Blanksby, S. J.; Mitchell, T. W. Advances in Mass Spectrometry for Lipidomics. *Annu. Rev. Anal. Chem.* **2010**, *3*, 433–465.
- (45) Yoo, H. J.; Håkansson, K. Determination of Phospholipid Regiochemistry by Ag(I) Adduction and Tandem Mass Spectrometry. *Anal. Chem.* **2011**, *83*, 1275–1283.
- (46) Yang, K.; Cheng, H.; Gross, R. W.; Han, X. Automated Lipid Identification and Quantification by Multidimensional Mass Spectrometry-Based Shotgun Lipidomics. *Anal. Chem.* **2009**, *81*, 4356–4368.
- (47) Schuhmann, K.; Herzog, R.; Schwudke, D.; Metelmann-Strupat, W.; Bornstein, S. R.; Shevchenko, A. Bottom-Up Shotgun Lipidomics by Higher Energy Collisional Dissociation on LTQ Orbitrap Mass Spectrometers. *Anal. Chem.* **2011**, *83*, 5480–5487.
- (48) Han, X.; Yang, K.; Gross, R. W. Multi-Dimensional Mass Spectrometry-Based Shotgun Lipidomics and Novel Strategies for Lipidomic Analyses. *Mass Spectrom. Rev.* **2012**, *31*, 134–178.
- (49) Svane, S.; Gorshkov, V.; Kjeldsen, F. Charge Inversion of Phospholipids by Dimetal Complexes for Positive Ion-Mode Electrospray Ionization Mass Spectrometry Analysis. *Anal. Chem.* **2015**, *87*, 8732–8739.
- (50) Hsu, F.-F.; Bohrer, A.; Turk, J. Formation of Lithiated Adducts of Glycerophosphocholine Lipids Facilitates Their Identification by Electrospray Ionization Tandem Mass Spectrometry. *J. Am. Soc. Mass Spectrom.* **1998**, *9*, 516–526.
- (51) Hsu, F.-F.; Turk, J. Structural Characterization of Unsaturated Glycerophospholipids by Multiple-Stage Linear Ion-Trap Mass Spectrometry with Electrospray Ionization. *J. Am. Soc. Mass Spectrom.* **2008**, *19*, 1681–1691.

- (52) Ho, Y.-P.; Huang, P.-C.; Deng, K.-H. Metal Ion Complexes in the Structural Analysis of Phospholipids by Electrospray Ionization Tandem Mass Spectrometry. *Rapid Commun. Mass Spectrom.* **2003**, *17*, 114–121.
- (53) Ma, X.; Chong, L.; Tian, R.; Shi, R.; Hu, T. Y.; Ouyang, Z.; Xia, Y. Identification and Quantitation of Lipid C=C Location Isomers: A Shotgun Lipidomics Approach Enabled by Photochemical Reaction. *Proc. Natl. Acad. Sci.* **2016**, *113*, 2573–2578.
- (54) Ma, X.; Xia, Y. Pinpointing Double Bonds in Lipids by Paternò-Büchi Reactions and Mass Spectrometry. *Angew. Chem.* **2014**, *126*, 2630–2634.
- (55) Stinson, C. A.; Xia, Y. A Method of Coupling the Paternò-Büchi Reaction with Direct Infusion ESI-MS/MS for Locating the C=C Bond in Glycerophospholipids. *Analyst* **2016**, 3696–3704.
- (56) Tang, F.; Guo, C.; Ma, X.; Zhang, J.; Su, Y.; Tian, R.; Shi, R.; Xia, Y.; Wang, X.; Ouyang, Z. Rapid In Situ Profiling of Lipid C=C Location Isomers in Tissue Using Ambient Mass Spectrometry with Photochemical Reactions. *Anal. Chem.* **2018**, *90*, 5612–5619.
- (57) Wäldchen, F.; Becher, S.; Esch, P.; Kompauer, M.; Heiles, S. Selective Phosphatidylcholine Double Bond Fragmentation and Localisation Using Paternò-Büchi Reactions and Ultraviolet Photodissociation. *Analyst* **2017**, *142*, 4744–4755.
- (58) Jeck, V.; Korf, A.; Vosse, C.; Hayen, H. Localization of double-bond positions in lipids by tandem mass spectrometry succeeding high-performance liquid chromatography with post-column derivatization. *Rapid Commun. Mass Spectrom.* **2018**, 1–9.
- (59) Zhang, W.; Zhang, D.; Chen, Q.; Wu, J.; Ouyang, Z.; Xia, Y. Online Photochemical Derivatization Enables Comprehensive Mass Spectrometric Analysis of Unsaturated Phospholipid Isomers. *Nat. Commun.* **2019**, *10*, 79.
- (60) Zhao, Y.; Zhao, H.; Zhao, X.; Jia, J.; Ma, Q.; Zhang, S.; Zhang, X.; Chiba, H.; Hui, S.-P.; Ma, X. Identification and Quantitation of C=C Location Isomers of Unsaturated Fatty Acids by Epoxidation Reaction and Tandem Mass Spectrometry. *Anal. Chem.* **2017**, *89*, 10270–10278.
- (61) Cao, W.; Ma, X.; Li, Z.; Zhou, X.; Ouyang, Z. Locating Carbon–Carbon Double Bonds in Unsaturated Phospholipids by Epoxidation Reaction and Tandem Mass Spectrometry. *Anal. Chem.* **2018**, *90*, 10286–10292.
- (62) Feng, Y.; Chen, B.; Yu, Q.; Li, L. Identification of Double Bond Position Isomers in Unsaturated Lipids by M-CPBA Epoxidation and Mass Spectrometry Fragmentation. *Anal. Chem.* **2019**.

- (63) Moe, M. K.; Strøm, M. B.; Jensen, E.; Claeys, M. Negative Electrospray Ionization Low-Energy Tandem Mass Spectrometry of Hydroxylated Fatty Acids: A Mechanistic Study. *Rapid Commun. Mass Spectrom.* **2004**, *18*, 1731–1740.
- (64) Stinson, C. A.; Zhang, W.; Xia, Y. UV Lamp as a Facile Ozone Source for Structural Analysis of Unsaturated Lipids Via Electrospray Ionization-Mass Spectrometry. *J. Am. Soc. Mass Spectrom.* **2017**, 1–9.
- (65) Harris, R. A.; May, J. C.; Stinson, C. A.; Xia, Y.; McLean, J. A. Determining Double Bond Position in Lipids Using Online Ozonolysis Coupled to Liquid Chromatography and Ion Mobility-Mass Spectrometry. *Anal. Chem.* **2018**, *90*, 1915–1924.
- (66) Yang, K.; Diltthey, B. G.; Gross, R. W. Identification and Quantitation of Fatty Acid Double Bond Positional Isomers: A Shotgun Lipidomics Approach Using Charge-Switch Derivatization. *Anal. Chem.* **2013**, *85*, 9742–9750.
- (67) Xu, Y.; Brenna, J. T. Atmospheric Pressure Covalent Adduct Chemical Ionization Tandem Mass Spectrometry for Double Bond Localization in Monoene- and Diene-Containing Triacylglycerols. *Anal. Chem.* **2007**, *79*, 2525–2536.
- (68) Stroobant, Vincent; de Hoffmann, E. *Mass Spectrometry: Principles and Applications*, 3rd ed.; Jon Wiley & Sons, Ltd: Hoboken, NJ, 2007.
- (69) Sleno, L.; Volmer, D. A. Ion Activation Methods for Tandem Mass Spectrometry. *J. Mass Spectrom.* **2004**, *39*, 1091–1112.
- (70) Brouwers, J. F. H. M.; Versluis, C.; Golde, L. M. G. van; Tielens, A. G. M. 5-Octadecenoic Acid: Evidence for a Novel Type of Fatty Acid Modification in Schistosomes. *Biochem. J.* **1998**, *334*, 315–319.
- (71) Vestal, M. L.; Campbell, J. M. Tandem Time-of-Flight Mass Spectrometry. In *Methods in Enzymology*; Biological Mass Spectrometry; Academic Press, 2005; Vol. 402, pp 79–108.
- (72) Pittenauer, E.; Allmaier, G. High-Energy Collision Induced Dissociation of Biomolecules: MALDITOF/ RTOF Mass Spectrometry in Comparison to Tandem Sector Mass Spectrometry. *Comb. Chem. High Throughput Screen.* **2009**, *12*, 137–155.
- (73) Pittenauer, E.; Allmaier, G. The Renaissance of High-Energy CID for Structural Elucidation of Complex Lipids: MALDI-TOF/RTOF-MS of Alkali Cationized Triacylglycerols. *J. Am. Soc. Mass Spectrom.* **2009**, *20*, 1037–1047.
- (74) Pittenauer, E.; Allmaier, G. A Universal Product Ion Nomenclature for $[M-H]^-$, $[M+H]^+$ and $[M+nNa-(N-1)H]^+$ ($N=1-3$) Glycerophospholipid Precursor Ions Based on High-Energy CID by MALDI-TOF/RTOF Mass Spectrometry. *Int. J. Mass Spectrom.* **2011**, *301*, 90–101.

- (75) Shimma, S.; Kubo, A.; Satoh, T.; Toyoda, M. Detailed Structural Analysis of Lipids Directly on Tissue Specimens Using a MALDI-SpiralTOF-Reflectron TOF Mass Spectrometer. *PLOS ONE* **2012**, *7*, e37107.
- (76) Thomas, M. C.; Mitchell, T. W.; Harman, D. G.; Deeley, J. M.; Nealon, J. R.; Blanksby, S. J. Ozone-Induced Dissociation: Elucidation of Double Bond Position within Mass-Selected Lipid Ions. *Anal. Chem.* **2008**, *80*, 303–311.
- (77) Poad, B. L. J.; Pham, H. T.; Thomas, M. C.; Nealon, J. R.; Campbell, J. L.; Mitchell, T. W.; Blanksby, S. J. Ozone-Induced Dissociation on a Modified Tandem Linear Ion-Trap: Observations of Different Reactivity for Isomeric Lipids. *J. Am. Soc. Mass Spectrom.* **2010**, *21*, 1989–1999.
- (78) Pham, H. T.; Maccarone, A. T.; Thomas, M. C.; Campbell, J. L.; Mitchell, T. W.; Blanksby, S. J. Structural Characterization of Glycerophospholipids by Combinations of Ozone- and Collision-Induced Dissociation Mass Spectrometry: The next Step towards “Top-down” Lipidomics. *Analyst* **2014**, *139*, 204–214.
- (79) Kozłowski, R.; Mitchell, T.; Blanksby, S. Separation and Identification of Phosphatidylcholine Regioisomers by Combining Liquid Chromatography with a Fusion of Collision-and Ozone-Induced Dissociation. *Eur. J. Mass Spectrom.* **2015**, *21*, 191–200.
- (80) Kozłowski, R. L.; Mitchell, T. W.; Blanksby, S. J. A Rapid Ambient Ionization-Mass Spectrometry Approach to Monitoring the Relative Abundance of Isomeric Glycerophospholipids. *Sci. Rep.* **2015**, *5*, 9243.
- (81) Kozłowski, R. L.; Campbell, J. L.; Mitchell, T. W.; Blanksby, S. J. Combining Liquid Chromatography with Ozone-Induced Dissociation for the Separation and Identification of Phosphatidylcholine Double Bond Isomers. *Anal. Bioanal. Chem.* **2015**, *407*, 5053–5064.
- (82) Paine, M. R. L.; Poad, B. L. J.; Eijkel, G. B.; Marshall, D. L.; Blanksby, S. J.; Heeren, R. M. A.; Ellis, S. R. Mass Spectrometry Imaging with Isomeric Resolution Enabled by Ozone-Induced Dissociation. *Angew. Chem.* **2018**, *130*, 10690–10694.
- (83) Poad, B. L. J.; Green, M. R.; Kirk, J. M.; Tomczyk, N.; Mitchell, T. W.; Blanksby, S. J. High-Pressure Ozone-Induced Dissociation for Lipid Structure Elucidation on Fast Chromatographic Timescales. *Anal. Chem.* **2017**, *89*, 4223–4229.
- (84) Poad, B. L. J.; Zheng, X.; Mitchell, T. W.; Smith, R. D.; Baker, E. S.; Blanksby, S. J. Online Ozonolysis Combined with Ion Mobility-Mass Spectrometry Provides a New Platform for Lipid Isomer Analyses. *Anal. Chem.* **2018**, *90*, 1292–1300.

- (85) Liang, X.; Liu, J.; LeBlanc, Y.; Covey, T.; Ptak, A. C.; Brenna, J. T.; McLuckey, S. A. Electron Transfer Dissociation of Doubly Sodiated Glycerophosphocholine Lipids. *J. Am. Soc. Mass Spectrom.* **2007**, *18*, 1783–1788.
- (86) James, P. F.; Perugini, M. A.; O’Hair, R. A. J. Electron Capture Dissociation of Complexes of Diacylglycerophosphocholine and Divalent Metal Ions: Competition between Charge Reduction and Radical Induced Phospholipid Fragmentation. *J. Am. Soc. Mass Spectrom.* **2008**, *19*, 978–986.
- (87) Jones, J. W.; Thompson, C. J.; Carter, C. L.; Kane, M. A. Electron-Induced Dissociation (EID) for Structure Characterization of Glycerophosphatidylcholine: Determination of Double-Bond Positions and Localization of Acyl Chains. *J. Mass Spectrom.* **2015**, *50*, 1327–1339.
- (88) Campbell, J. L.; Baba, T. Near-Complete Structural Characterization of Phosphatidylcholines Using Electron Impact Excitation of Ions from Organics. *Anal. Chem.* **2015**, *87*, 5837–5845.
- (89) Baba, T.; Campbell, J. L.; Blanc, J. C. Y. L.; Baker, P. R. S.; Ikeda, K. Quantitative Structural Multi-Class Lipidomics Using Differential Mobility-Electron Impact Excitation of Ions from Organics (EIEIO) Mass Spectrometry. *J. Lipid Res.* **2018**, jlr.D083261.
- (90) Baba, T.; Campbell, J. L.; Le Blanc, J. C. Y.; Baker, P. R. S. Distinguishing Cis and Trans Isomers in Intact Complex Lipids Using Electron Impact Excitation of Ions from Organics Mass Spectrometry. *Anal. Chem.* **2017**, *89*, 7307–7315.
- (91) Li, P.; Jackson, G. P. Charge Transfer Dissociation of Phosphocholines: Gas-Phase Ion/Ion Reactions between Helium Cations and Phospholipid Cations. *J. Mass Spectrom.* **2017**, *52*, 271–282.
- (92) Deimler, R. E.; Sander, M.; Jackson, G. P. Radical-Induced Fragmentation of Phospholipid Cations Using Metastable Atom-Activated Dissociation Mass Spectrometry (MAD-MS). *Int. J. Mass Spectrom.* **2015**, *390*, 178–186.
- (93) Li, P.; Hoffmann, W. D.; Jackson, G. P. Multistage Mass Spectrometry of Phospholipids Using Collision-Induced Dissociation (CID) and Metastable Atom-Activated Dissociation (MAD). *Int. J. Mass Spectrom.* **2016**, *403*, 1–7.
- (94) Brodbelt, J. S. Photodissociation Mass Spectrometry: New Tools for Characterization of Biological Molecules. *Chem. Soc. Rev.* **2014**, *43*, 2757–2783.
- (95) Pham, H. T.; Julian, R. R. Re-Print of “Radical Delivery and Fragmentation for Structural Analysis of Glycerophospholipids.” *Int. J. Mass Spectrom.* **2015**, *378*, 225–231.
- (96) Pham, H. T.; Ly, T.; Trevitt, A. J.; Mitchell, T. W.; Blanksby, S. J. Differentiation of Complex Lipid Isomers by Radical-Directed Dissociation Mass Spectrometry. *Anal. Chem.* **2012**, *84*, 7525–7532.

- (97) Pham, H. T.; Trevitt, A. J.; Mitchell, T. W.; Blanksby, S. J. Rapid Differentiation of Isomeric Lipids by Photodissociation Mass Spectrometry of Fatty Acid Derivatives. *Rapid Commun. Mass Spectrom.* **2013**, *27*, 805–815.
- (98) Becher, S.; Spengler, B.; Heiles, S. Effects of Wavelength, Fluence, and Dose on Fragmentation Pathways and Photoproduct Ion Yield in 213 Nm and 266 Nm Ultraviolet Photodissociation Experiments. *Eur. J. Mass Spectrom.* **2018**, *24*, 54–65.
- (99) Becher, S.; Esch, P.; Heiles, S. Relative Quantification of Phosphatidylcholine Sn-Isomers Using Positive Doubly Charged Lipid–Metal Ion Complexes. *Anal. Chem.* **2018**, *90*, 11486–11494.
- (100) Madsen, J. A.; Cullen, T. W.; Trent, M. S.; Brodbelt, J. S. IR and UV Photodissociation as Analytical Tools for Characterizing Lipid A Structures. *Anal. Chem.* **2011**, *83*, 5107–5113.
- (101) O’Brien, J. P.; Brodbelt, J. S. Structural Characterization of Gangliosides and Glycolipids via Ultraviolet Photodissociation Mass Spectrometry. *Anal. Chem.* **2013**, *85*, 10399–10407.
- (102) Klein, D. R.; Brodbelt, J. S. Structural Characterization of Phosphatidylcholines Using 193 nm Ultraviolet Photodissociation Mass Spectrometry. *Anal. Chem.* **2017**, *89*, 1516–1522.
- (103) Klein, D. R.; Feider, C. L.; Garza, K. Y.; Lin, J. Q.; Eberlin, L. S.; Brodbelt, J. S. Desorption Electrospray Ionization Coupled with Ultraviolet Photodissociation for Characterization of Phospholipid Isomers in Tissue Sections. *Anal. Chem.* **2018**, *90*, 10100–10104.
- (104) Ryan, E.; Nguyen, C. Q. N.; Shiea, C.; Reid, G. E. Detailed Structural Characterization of Sphingolipids via 193 nm Ultraviolet Photodissociation and Ultra High Resolution Tandem Mass Spectrometry. *J. Am. Soc. Mass Spectrom.* **2017**, *28*, 1406–1419.
- (105) Williams, P. E.; Klein, D. R.; Greer, S. M.; Brodbelt, J. S. Pinpointing Double Bond and Sn-Positions in Glycerophospholipids via Hybrid 193 nm Ultraviolet Photodissociation (UVPD) Mass Spectrometry. *J. Am. Chem. Soc.* **2017**, *139*, 15681–15690.
- (106) Raetz, C. R. H.; Whitfield, C. Lipopolysaccharide Endotoxins. *Annu. Rev. Biochem.* **2002**, *71*, 635–700.
- (107) Kawai, T.; Akira, S. The Role of Pattern-Recognition Receptors in Innate Immunity: Update on Toll-like Receptors. *Nat. Immunol.* **2010**, *11*, 373–384.
- (108) Park, B. S.; Song, D. H.; Kim, H. M.; Choi, B.-S.; Lee, H.; Lee, J.-O. The Structural Basis of Lipopolysaccharide Recognition by the TLR4–MD-2 Complex. *Nature* **2009**, *458*, 1191–1195.

- (109) Park, B. S.; Lee, J.-O. Recognition of Lipopolysaccharide Pattern by TLR4 Complexes. *Exp. Mol. Med.* **2013**, *45*, e66.
- (110) Molinaro, A.; Holst, O.; Di Lorenzo, F.; Callaghan, M.; Nurisso, A.; D'Errico, G.; Zamyatina, A.; Peri, F.; Berisio, R.; Jerala, R.; Jiménez-Barbero, J.; Silipo, A.; Martín-Santamaría, S. Chemistry of Lipid A: At the Heart of Innate Immunity. *Chem. – Eur. J.* **2015**, *21*, 500–519.
- (111) Needham, B. D.; Trent, M. S. Fortifying the Barrier: The Impact of Lipid A Remodelling on Bacterial Pathogenesis. *Nat. Rev. Microbiol.* **2013**, *11*, 467–481.
- (112) Cullen, T. W.; Giles, D. K.; Wolf, L. N.; Ecobichon, C.; Boneca, I. G.; Trent, M. S. Helicobacter Pylori versus the Host: Remodeling of the Bacterial Outer Membrane Is Required for Survival in the Gastric Mucosa. *PLOS Pathog.* **2011**, *7*, e1002454.
- (113) Suarez, G.; Peek, R. M. Helicobacter Pylori: Expect the Unexpected. *Mol. Microbiol.* **2014**, *91*, 858–861.
- (114) Silipo, A.; Molinaro, A. The Diversity of the Core Oligosaccharide in Lipopolysaccharides. In *Endotoxins: Structure, Function and Recognition*; Wang, X., Quinn, P. J., Eds.; Subcellular Biochemistry; Springer Netherlands, 2010; pp 69–99.
- (115) Fridrich, E.; Whitfield, C. Lipopolysaccharide Inner Core Oligosaccharide Structure and Outer Membrane Stability in Human Pathogens Belonging to the Enterobacteriaceae. *J. Endotoxin Res.* **2005**, *11*, 133–144.
- (116) Agrawal, A.; Weisshaar, J. C. Effects of Alterations of the E. Coli Lipopolysaccharide Layer on Membrane Permeabilization Events Induced by Cecropin A. *Biochim. Biophys. Acta BBA - Biomembr.* **2018**, *1860*, 1470–1479.
- (117) Wang, L.; Wang, Q.; Reeves, P. R. The Variation of O Antigens in Gram-Negative Bacteria. In *Endotoxins: Structure, Function and Recognition*; Wang, X., Quinn, P. J., Eds.; Subcellular Biochemistry; Springer Netherlands, 2010; pp 123–152.
- (118) Preston, Andrew; Mandrell, Robert E.; Gibson, Bradford W.; Apicella, Michael A. The Lipooligosaccharides of Pathogenic Gram-Negative Bacteria. *Crit. Rev. Microbiol.* **1996**, *22*, 139–180.
- (119) Lerouge, I.; Vanderleyden, J. O-Antigen Structural Variation: Mechanisms and Possible Roles in Animal/Plant–Microbe Interactions. *FEMS Microbiol. Rev.* **2002**, *26*, 17–47.
- (120) Li, H.; Liao, T.; Debowski, A. W.; Tang, H.; Nilsson, H.-O.; Stubbs, K. A.; Marshall, B. J.; Benghezal, M. Lipopolysaccharide Structure and Biosynthesis in Helicobacter Pylori. *Helicobacter* **2016**, *21*, 445–461.

- (121) Kilár, A.; Dörnyei, Á.; Kocsis, B. Structural Characterization of Bacterial Lipopolysaccharides with Mass Spectrometry and On- and off-Line Separation Techniques. *Mass Spectrom. Rev.* **2013**, *32*, 90–117.
- (122) Banoub, J. H.; Aneed, A. E.; Cohen, A. M.; Joly, N. Structural Investigation of Bacterial Lipopolysaccharides by Mass Spectrometry and Tandem Mass Spectrometry. *Mass Spectrom. Rev.* **2010**, *29*, 606–650.
- (123) Sándor, V.; Dörnyei, Á.; Makszin, L.; Kilár, F.; Péterfi, Z.; Kocsis, B.; Kilár, A. Characterization of Complex, Heterogeneous Lipid A Samples Using HPLC–MS/MS Technique I. Overall Analysis with Respect to Acylation, Phosphorylation and Isobaric Distribution. *J. Mass Spectrom.* **2016**, *51*, 1043–1063.
- (124) Sándor, V.; Kilár, A.; Kilár, F.; Kocsis, B.; Dörnyei, Á. Characterization of Complex, Heterogeneous Lipid A Samples Using HPLC–MS/MS Technique II. Structural Elucidation of Non-Phosphorylated Lipid A by Negative-Ion Mode Tandem Mass Spectrometry. *J. Mass Spectrom.* *51*, 615–628.
- (125) Sándor, V.; Kilár, A.; Kilár, F.; Kocsis, B.; Dörnyei, Á. Characterization of Complex, Heterogeneous Lipid A Samples Using HPLC–MS/MS Technique III. Positive-Ion Mode Tandem Mass Spectrometry to Reveal Phosphorylation and Acylation Patterns of Lipid A. *J. Mass Spectrom.* **2018**, *53*, 146–161.
- (126) Kondakov, A.; Lindner, B. Structural Characterization of Complex Bacterial Glycolipids by Fourier Transform Mass Spectrometry. *Eur. J. Mass Spectrom.* **2005**, *11*, 535–546.
- (127) O'Brien, J. P.; Needham, B. D.; Henderson, J. C.; Nowicki, E. M.; Trent, M. S.; Brodbelt, J. S. 193 nm Ultraviolet Photodissociation Mass Spectrometry for the Structural Elucidation of Lipid A Compounds in Complex Mixtures. *Anal. Chem.* **2014**, *86*, 2138–2145.
- (128) Morrison, L. J.; Parker, W. R.; Holden, D. D.; Henderson, J. C.; Boll, J. M.; Trent, M. S.; Brodbelt, J. S. UVliPiD: A UVPD-Based Hierarchical Approach for De Novo Characterization of Lipid A Structures. *Anal. Chem.* **2016**, *88*, 1812–1820.
- (129) Li, J.; Purves, R. W.; Richards, J. C. Coupling Capillary Electrophoresis and High-Field Asymmetric Waveform Ion Mobility Spectrometry Mass Spectrometry for the Analysis of Complex Lipopolysaccharides. *Anal. Chem.* **2004**, *76*, 4676–4683.
- (130) Leung, L. M.; Fondrie, W. E.; Doi, Y.; Johnson, J. K.; Strickland, D. K.; Ernst, R. K.; Goodlett, D. R. Identification of the ESKAPE Pathogens by Mass Spectrometric Analysis of Microbial Membrane Glycolipids. *Sci. Rep.* **2017**, *7*, 6403.

- (131) Rütters, H.; Möhring, T.; Rullkötter, J.; Griep-Raming, J.; Metzger, J. O. The Persistent Memory Effect of Triethylamine in the Analysis of Phospholipids by Liquid Chromatography/Mass Spectrometry. *Rapid Commun. Mass Spectrom.* **14**, 122–123.
- (132) Jones, J. W.; Shaffer, S. A.; Ernst, R. K.; Goodlett, D. R.; Tureček, F. Determination of Pyrophosphorylated Forms of Lipid A in Gram-Negative Bacteria Using a Multivaried Mass Spectrometric Approach. *Proc. Natl. Acad. Sci.* **2008**, *105*, 12742–12747.
- (133) M. Crittenden, C.; M. Herrera, C.; E. Williams, P.; P. Ricci, D.; R. Swem, L.; Stephen Trent, M.; S. Brodbelt, J. Mapping Phosphate Modifications of Substituted Lipid A via a Targeted MS 3 CID/UVPD Strategy. *Analyst* **2018**, *143*, 3091–3099.
- (134) Madalinski, G.; Fournier, F.; Wind, F.-L.; Afonso, C.; Tabet, J.-C. Gram-Negative Bacterial Lipid A Analysis by Negative Electrospray Ion Trap Mass Spectrometry: Stepwise Dissociations of Deprotonated Species under Low Energy CID Conditions. *Int. J. Mass Spectrom.* **2006**, *249–250*, 77–92.
- (135) Ting, Y. S.; Shaffer, S. A.; Jones, J. W.; Ng, W. V.; Ernst, R. K.; Goodlett, D. R. Automated Lipid A Structure Assignment from Hierarchical Tandem Mass Spectrometry Data. *J. Am. Soc. Mass Spectrom.* **2011**, *22*, 856–866.
- (136) Sturiale, L.; Garozzo, D.; Silipo, A.; Lanzetta, R.; Parrilli, M.; Molinaro, A. New Conditions for Matrix-Assisted Laser Desorption/Ionization Mass Spectrometry of Native Bacterial R-Type Lipopolysaccharides. *Rapid Commun. Mass Spectrom.* **2005**, *19*, 1829–1834.
- (137) Sturiale, L.; Palmigiano, A.; Silipo, A.; Knirel, Y. A.; Anisimov, A. P.; Lanzetta, R.; Parrilli, M.; Molinaro, A.; Garozzo, D. Reflectron MALDI TOF and MALDI TOF/TOF Mass Spectrometry Reveal Novel Structural Details of Native Lipooligosaccharides. *J. Mass Spectrom.* **2011**, *46*, 1135–1142.
- (138) Kanie, Y.; Yamaguchi, Y.; Hayashi, A.; Uzawa, J.; Hatakeyama, M.; Hidaka, Y.; Toda, N.; Nakamura, S.; Kanie, O. Structural Analysis of a Novel Lipooligosaccharide (LOS) from Rhodobacter Azotoformans. *Carbohydr. Res.* **2019**, *473*, 104–114.
- (139) Phillips, N. J.; John, C. M.; Jarvis, G. A. Analysis of Bacterial Lipooligosaccharides by MALDI-TOF MS with Traveling Wave Ion Mobility. *J. Am. Soc. Mass Spectrom.* **2016**, *27*, 1263–1276.
- (140) Oyler, B. L.; Khan, M. M.; Smith, D. F.; Harberts, E. M.; Kilgour, D. P. A.; Ernst, R. K.; Cross, A. S.; Goodlett, D. R. Top Down Tandem Mass Spectrometric Analysis of a Chemically Modified Rough-Type Lipopolysaccharide Vaccine Candidate. *J. Am. Soc. Mass Spectrom.* **2018**, 1–9.

- (141) O'Brien, J. P.; Needham, B. D.; Brown, D. B.; Trent, M. S.; Brodbelt, J. S. Top-down Strategies for the Structural Elucidation of Intact Gram-Negative Bacterial Endotoxins. *Chem. Sci.* **2014**, *5*, 4291–4301.
- (142) Hübner, G.; Lindner, B. Separation of R-Form Lipopolysaccharide and Lipid A by CE–Fourier-Transform Ion Cyclotron Resonance MS. *Electrophoresis* **2009**, *30*, 1808–1816.

CHAPTER 2

- (1) Fenn, J. B.; Mann, M.; Meng, C. K.; Wong, S. F.; Whitehouse, C. M. Electrospray Ionization for Mass Spectrometry of Large Biomolecules. *Science* **1989**, *246*, 64–71.
- (2) Konermann, L.; Ahadi, E.; Rodriguez, A. D.; Vahidi, S. Unraveling the Mechanism of Electrospray Ionization. *Anal. Chem.* **2013**, *85*, 2–9.
- (3) Wilm, M. S.; Mann, M. Electrospray and Taylor-Cone Theory, Dole's Beam of Macromolecules at Last? *Int. J. Mass Spectrom. Ion Process.* **1994**, *136*, 167–180.
- (4) Takáts, Z.; Wiseman, J. M.; Gologan, B.; Cooks, R. G. Mass Spectrometry Sampling Under Ambient Conditions with Desorption Electrospray Ionization. *Science* **2004**, *306*, 471–473.
- (5) Eberlin, L. S.; Ferreira, C. R.; Dill, A. L.; Ifa, D. R.; Cooks, R. G. Desorption Electrospray Ionization Mass Spectrometry for Lipid Characterization and Biological Tissue Imaging. *Biochim. Biophys. Acta BBA - Mol. Cell Biol. Lipids* **2011**, *1811*, 946–960.
- (6) Schwartz, J. C.; Senko, M. W.; Syka, J. E. P. A Two-Dimensional Quadrupole Ion Trap Mass Spectrometer. *J. Am. Soc. Mass Spectrom.* **2002**, *13*, 659–669.
- (7) Hu, Q.; Noll, R. J.; Li, H.; Makarov, A.; Hardman, M.; Cooks, R. G. The Orbitrap: A New Mass Spectrometer. *J. Mass Spectrom.* **2005**, *40*, 430–443.

CHAPTER 3

- (1) Brown, S. H. J.; Mitchell, T. W.; Oakley, A. J.; Pham, H. T.; Blanksby, S. J. Time to Face the Fats: What Can Mass Spectrometry Reveal about the Structure of Lipids and Their Interactions with Proteins? *J. Am. Soc. Mass Spectrom.* **2012**, *23*, 1441–1449.
- (2) *Bacterial Membranes: Structural and Molecular Biology*; Remaut, H., Fronzes, R., Eds.; Horizon Scientific Press, 2014.
- (3) Zhang, Y.-M.; Rock, C. O. Membrane Lipid Homeostasis in Bacteria. *Nat. Rev. Microbiol.* **2008**, *6*, 222–233.

- (4) Hussain, N. F.; Siegel, A. P.; Ge, Y.; Jordan, R.; Naumann, C. A. Bilayer Asymmetry Influences Integrin Sequestering in Raft-Mimicking Lipid Mixtures. *Biophys. J.* **2013**, *104*, 2212–2221.
- (5) van Meer, G.; Voelker, D. R.; Feigenson, G. W. Membrane Lipids: Where They Are and How They Behave. *Nat. Rev. Mol. Cell Biol.* **2008**, *9*, 112–124.
- (6) Shevchenko, A.; Simons, K. Lipidomics: Coming to Grips with Lipid Diversity. *Nat. Rev. Mol. Cell Biol.* **2010**, *11*, 593–598.
- (7) Blanksby, S. J.; Mitchell, T. W. Advances in Mass Spectrometry for Lipidomics. *Annu. Rev. Anal. Chem.* **2010**, *3*, 433–465.
- (8) Wenk, M. R. The Emerging Field of Lipidomics. *Nat. Rev. Drug Discov.* **2005**, *4*, 594–610.
- (9) Janmey, P. A.; Kinnunen, P. K. J. Biophysical Properties of Lipids and Dynamic Membranes. *Trends Cell Biol.* **2006**, *16*, 538–546.
- (10) Sandra, K.; Sandra, P. Lipidomics from an Analytical Perspective. *Curr. Opin. Chem. Biol.* **2013**, *17*, 847–853.
- (11) Holthuis, J. C. M.; Levine, T. P. Lipid Traffic: Floppy Drives and a Superhighway. *Nat. Rev. Mol. Cell Biol.* **2005**, *6*, 209–220.
- (12) Martinez-Seara, H.; Róg, T.; Pasenkiewicz-Gierula, M.; Vattulainen, I.; Karttunen, M.; Reigada, R. Interplay of Unsaturated Phospholipids and Cholesterol in Membranes: Effect of the Double-Bond Position. *Biophys. J.* **2008**, *95*, 3295–3305.
- (13) Brouwers, J. F. Liquid Chromatographic–Mass Spectrometric Analysis of Phospholipids. Chromatography, Ionization and Quantification. *Biochim Biophys Acta Mol Cell Biol Lipids* **2011**, *1811*, 763–775.
- (14) Damen, C. W. N.; Isaac, G.; Langridge, J.; Hankemeier, T.; Vreeken, R. J. Enhanced Lipid Isomer Separation in Human Plasma Using Reversed-Phase UPLC with Ion-Mobility/High-Resolution MS Detection. *J. Lipid Res.* **2014**, *55*, 1772–1783.
- (15) Maccarone, A. T.; Duldig, J.; Mitchell, T. W.; Blanksby, S. J.; Duchoslav, E.; Campbell, J. L. Characterization of Acyl Chain Position in Unsaturated Phosphatidylcholines Using Differential Mobility-Mass Spectrometry. *J. Lipid Res.* **2014**, *55*, 1668–1677.
- (16) Lintonen, T. P. I.; Baker, P. R. S.; Suoniemi, M.; Ubhi, B. K.; Koistinen, K. M.; Duchoslav, E.; Campbell, J. L.; Ekroos, K. Differential Mobility Spectrometry-Driven Shotgun Lipidomics. *Anal. Chem.* **2014**, *86*, 9662–9669.
- (17) Pulfer, M.; Murphy, R. C. Electrospray Mass Spectrometry of Phospholipids. *Mass Spectrom. Rev.* **2003**, *22*, 332–364.

- (18) Wenk, M. R. Lipidomics: New Tools and Applications. *Cell* **2010**, *143*, 888–895.
- (19) Brügger, B. Lipidomics: Analysis of the Lipid Composition of Cells and Subcellular Organelles by Electrospray Ionization Mass Spectrometry. *Annu. Rev. Biochem.* **2014**, *83*, 79–98.
- (20) Han, X.; Yang, K.; Gross, R. W. Multi-Dimensional Mass Spectrometry-Based Shotgun Lipidomics and Novel Strategies for Lipidomic Analyses. *Mass Spectrom. Rev.* **2012**, *31*, 134–178.
- (21) Han, X.; Gross, R. W. Shotgun Lipidomics: Electrospray Ionization Mass Spectrometric Analysis and Quantitation of Cellular Lipidomes Directly from Crude Extracts of Biological Samples. *Mass Spectrom. Rev.* **2005**, *24*, 367–412.
- (22) Schuhmann, K.; Almeida, R.; Baumert, M.; Herzog, R.; Bornstein, S. R.; Shevchenko, A. Shotgun Lipidomics on a LTQ Orbitrap Mass Spectrometer by Successive Switching between Acquisition Polarity Modes. *J. Mass Spectrom.* **2012**, *47*, 96–104.
- (23) Schuhmann, K.; Herzog, R.; Schwudke, D.; Metelmann-Strupat, W.; Bornstein, S. R.; Shevchenko, A. Bottom-Up Shotgun Lipidomics by Higher Energy Collisional Dissociation on LTQ Orbitrap Mass Spectrometers. *Anal. Chem.* **2011**, *83*, 5480–5487.
- (24) Hsu, F.-F.; Turk, J. Electrospray Ionization with Low-Energy Collisionally Activated Dissociation Tandem Mass Spectrometry of Glycerophospholipids: Mechanisms of Fragmentation and Structural Characterization. *J. Chromatogr. B* **2009**, *877*, 2673–2695.
- (25) Wasslen, K. V.; Canez, C. R.; Lee, H.; Manthorpe, J. M.; Smith, J. C. Trimethylation Enhancement Using Diazomethane (TrEnDi) II: Rapid In-Solution Concomitant Quaternization of Glycerophospholipid Amino Groups and Methylation of Phosphate Groups via Reaction with Diazomethane Significantly Enhances Sensitivity in Mass Spectrometry Analyses via a Fixed, Permanent Positive Charge. *Anal. Chem.* **2014**, *86*, 9523–9532.
- (26) Canez, C. R.; Shields, S. W. J.; Bugno, M.; Wasslen, K. V.; Weinert, H. P.; Willmore, W. G.; Manthorpe, J. M.; Smith, J. C. Trimethylation Enhancement Using ¹³C-Diazomethane (¹³C-TrEnDi): Increased Sensitivity and Selectivity of Phosphatidylethanolamine, Phosphatidylcholine, and Phosphatidylserine Lipids Derived from Complex Biological Samples. *Anal. Chem.* **2016**, *88*, 6996–7004.
- (27) Stutzman, J. R.; Blanksby, S. J.; McLuckey, S. A. Gas-Phase Transformation of Phosphatidylcholine Cations to Structurally Informative Anions via Ion/Ion Chemistry. *Anal. Chem.* **2013**, *85*, 3752–3757.
- (28) Rojas-Betancourt, S.; Stutzman, J. R.; Londry, F. A.; Blanksby, S. J.; McLuckey, S. A. Gas-Phase Chemical Separation of Phosphatidylcholine and

- Phosphatidylethanolamine Cations via Charge Inversion Ion/Ion Chemistry. *Anal. Chem.* **2015**, *87*, 11255–11262.
- (29) Ho, Y.-P.; Huang, P.-C.; Deng, K.-H. Metal Ion Complexes in the Structural Analysis of Phospholipids by Electrospray Ionization Tandem Mass Spectrometry. *Rapid Commun. Mass Spectrom.* **2003**, *17*, 114–121.
 - (30) Hsu, F.-F.; Turk, J. Structural Characterization of Unsaturated Glycerophospholipids by Multiple-Stage Linear Ion-Trap Mass Spectrometry with Electrospray Ionization. *J. Am. Soc. Mass Spectrom.* **2008**, *19*, 1681–1691.
 - (31) Ma, X.; Xia, Y. Pinpointing Double Bonds in Lipids by Paternò-Büchi Reactions and Mass Spectrometry. *Angew. Chem.* **2014**, *126*, 2630–2634.
 - (32) Stinson, C. A.; Xia, Y. A Method of Coupling the Paternò-Büchi Reaction with Direct Infusion ESI-MS/MS for Locating the C=C Bond in Glycerophospholipids. *Analyst* **2016**, 3696–3704.
 - (33) Ma, X.; Chong, L.; Tian, R.; Shi, R.; Hu, T. Y.; Ouyang, Z.; Xia, Y. Identification and Quantitation of Lipid C=C Location Isomers: A Shotgun Lipidomics Approach Enabled by Photochemical Reaction. *Proc. Natl. Acad. Sci.* **2016**, *113*, 2573–2578.
 - (34) Yang, K.; Zhao, Z.; Gross, R. W.; Han, X. Identification and Quantitation of Unsaturated Fatty Acid Isomers by Electrospray Ionization Tandem Mass Spectrometry: A Shotgun Lipidomics Approach. *Anal. Chem.* **2011**, *83*, 4243–4250.
 - (35) Pham, H. T.; Ly, T.; Trevitt, A. J.; Mitchell, T. W.; Blanksby, S. J. Differentiation of Complex Lipid Isomers by Radical-Directed Dissociation Mass Spectrometry. *Anal. Chem.* **2012**, *84*, 7525–7532.
 - (36) Pham, H. T.; Trevitt, A. J.; Mitchell, T. W.; Blanksby, S. J. Rapid Differentiation of Isomeric Lipids by Photodissociation Mass Spectrometry of Fatty Acid Derivatives. *Rapid Commun. Mass Spectrom.* **2013**, *27*, 805–815.
 - (37) Pham, H. T.; Julian, R. R. Re-Print of “Radical Delivery and Fragmentation for Structural Analysis of Glycerophospholipids.” *Int. J. Mass Spectrom.* **2015**, *378*, 225–231.
 - (38) Kozłowski, R.; Mitchell, T.; Blanksby, S. Separation and Identification of Phosphatidylcholine Regioisomers by Combining Liquid Chromatography with a Fusion of Collision-and Ozone-Induced Dissociation. *Eur. J. Mass Spectrom.* **2015**, *21*, 191–200.
 - (39) Brown, S. H. J.; Mitchell, T. W.; Blanksby, S. J. Analysis of Unsaturated Lipids by Ozone-Induced Dissociation. *Biochim. Biophys. Acta BBA - Mol. Cell Biol. Lipids* **2011**, *1811*, 807–817.

- (40) Pham, H. T.; Maccarone, A. T.; Thomas, M. C.; Campbell, J. L.; Mitchell, T. W.; Blanksby, S. J. Structural Characterization of Glycerophospholipids by Combinations of Ozone- and Collision-Induced Dissociation Mass Spectrometry: The next Step towards “Top-down” Lipidomics. *Analyst* **2014**, *139*, 204–214.
- (41) Campbell, J. L.; Baba, T. Near-Complete Structural Characterization of Phosphatidylcholines Using Electron Impact Excitation of Ions from Organics. *Anal. Chem.* **2015**, *87*, 5837–5845.
- (42) Deimler, R. E.; Sander, M.; Jackson, G. P. Radical-Induced Fragmentation of Phospholipid Cations Using Metastable Atom-Activated Dissociation Mass Spectrometry (MAD-MS). *Int. J. Mass Spectrom.* **2015**, *390*, 178–186.
- (43) Li, P.; Hoffmann, W. D.; Jackson, G. P. Multistage Mass Spectrometry of Phospholipids Using Collision-Induced Dissociation (CID) and Metastable Atom-Activated Dissociation (MAD). *Int. J. Mass Spectrom.* **2016**, *403*, 1–7.
- (44) Liang, X.; Liu, J.; LeBlanc, Y.; Covey, T.; Ptak, A. C.; Brenna, J. T.; McLuckey, S. A. Electron Transfer Dissociation of Doubly Sodiated Glycerophosphocholine Lipids. *J. Am. Soc. Mass Spectrom.* **2007**, *18*, 1783–1788.
- (45) Brodbelt, J. S. Photodissociation Mass Spectrometry: New Tools for Characterization of Biological Molecules. *Chem. Soc. Rev.* **2014**, *43*, 2757–2783.
- (46) Madsen, J. A.; Cullen, T. W.; Trent, M. S.; Brodbelt, J. S. IR and UV Photodissociation as Analytical Tools for Characterizing Lipid A Structures. *Anal. Chem.* **2011**, *83*, 5107–5113.
- (47) O’Brien, J. P.; Brodbelt, J. S. Structural Characterization of Gangliosides and Glycolipids via Ultraviolet Photodissociation Mass Spectrometry. *Anal. Chem.* **2013**, *85*, 10399–10407.
- (48) O’Brien, J. P.; Needham, B. D.; Henderson, J. C.; Nowicki, E. M.; Trent, M. S.; Brodbelt, J. S. 193 nm Ultraviolet Photodissociation Mass Spectrometry for the Structural Elucidation of Lipid A Compounds in Complex Mixtures. *Anal. Chem.* **2014**, *86*, 2138–2145.
- (49) O’Brien, J. P.; Needham, B. D.; Brown, D. B.; Trent, M. S.; Brodbelt, J. S. Top-down Strategies for the Structural Elucidation of Intact Gram-Negative Bacterial Endotoxins. *Chem. Sci.* **2014**, *5*, 4291–4301.
- (50) Hankins, J. V.; Madsen, J. A.; Giles, D. K.; Brodbelt, J. S.; Trent, M. S. Amino Acid Addition to *Vibrio Cholerae* LPS Establishes a Link between Surface Remodeling in Gram-Positive and Gram-Negative Bacteria. *Proc. Natl. Acad. Sci.* **2012**, *109*, 8722–8727.
- (51) Shaw, J. B.; Li, W.; Holden, D. D.; Zhang, Y.; Griep-Raming, J.; Fellers, R. T.; Early, B. P.; Thomas, P. M.; Kelleher, N. L.; Brodbelt, J. S. Complete Protein

- Characterization Using Top-Down Mass Spectrometry and Ultraviolet Photodissociation. *J. Am. Chem. Soc.* **2013**, *135*, 12646–12651.
- (52) Klein, D. R.; Holden, D. D.; Brodbelt, J. S. Shotgun Analysis of Rough-Type Lipopolysaccharides Using Ultraviolet Photodissociation Mass Spectrometry. *Anal. Chem.* **2016**, *88*, 1044–1051.
- (53) Liebisch, G.; Vizcaíno, J. A.; Köfeler, H.; Trötz Müller, M.; Griffiths, W. J.; Schmitz, G.; Spener, F.; Wakelam, M. J. O. Shorthand Notation for Lipid Structures Derived from Mass Spectrometry. *J. Lipid Res.* **2013**, *54*, 1523–1530.

CHAPTER 4

- (1) Amstalden van Hove, E. R.; Smith, D. F.; Heeren, R. M. A. A Concise Review of Mass Spectrometry Imaging. *J. Chromatogr. A* **2010**, *1217*, 3946–3954.
- (2) Gode, D.; A. Volmer, D. Lipid Imaging by Mass Spectrometry – a Review. *Analyst* **2013**, *138*, 1289–1315.
- (3) Vaysse, P.; A. Heeren, R. M.; Porta, T.; Balluff, B. Mass Spectrometry Imaging for Clinical Research – Latest Developments, Applications, and Current Limitations. *Analyst* **2017**, *142*, 2690–2712.
- (4) Sans, M.; Gharpure, K.; Tibshirani, R.; Zhang, J.; Liang, L.; Liu, J.; Young, J. H.; Dood, R. L.; Sood, A. K.; Eberlin, L. S. Metabolic Markers and Statistical Prediction of Serous Ovarian Cancer Aggressiveness by Ambient Ionization Mass Spectrometry Imaging. *Cancer Res.* **2017**, *77*, 2903–2913.
- (5) Norris, J. L.; Caprioli, R. M. Analysis of Tissue Specimens by Matrix-Assisted Laser Desorption/Ionization Imaging Mass Spectrometry in Biological and Clinical Research. *Chem. Rev.* **2013**, *113*, 2309–2342.
- (6) Gessel, M. M.; Norris, J. L.; Caprioli, R. M. MALDI Imaging Mass Spectrometry: Spatial Molecular Analysis to Enable a New Age of Discovery. *J. Proteomics* **2014**, *107*, 71–82.
- (7) Wiseman, J. M.; Ifa, D. R.; Song, Q.; Cooks, R. G. Tissue Imaging at Atmospheric Pressure Using Desorption Electrospray Ionization (DESI) Mass Spectrometry. *Angew. Chem. Int. Ed.* **2006**, *45*, 7188–7192.
- (8) Ifa, D. R.; Wu, C.; Ouyang, Z.; Cooks, R. G. Desorption Electrospray Ionization and Other Ambient Ionization Methods: Current Progress and Preview. *Analyst* **2010**, *135*, 669–681.
- (9) Eberlin, L. S.; Ferreira, C. R.; Dill, A. L.; Ifa, D. R.; Cooks, R. G. Desorption Electrospray Ionization Mass Spectrometry for Lipid Characterization and Biological Tissue Imaging. *Biochim. Biophys. Acta BBA - Mol. Cell Biol. Lipids* **2011**, *1811*, 946–960.

- (10) Bereman, M. S.; Nyadong, L.; Fernandez, F. M.; Muddiman, D. C. Direct High-resolution Peptide and Protein Analysis by Desorption Electrospray Ionization Fourier Transform Ion Cyclotron Resonance Mass Spectrometry. *Rapid Commun. Mass Spectrom.* **2006**, *20*, 3409–3411.
- (11) Pól, J.; Vidová, V.; Kruppa, G.; Kobliha, V.; Novák, P.; Lemr, K.; Kotiaho, T.; Kostianen, R.; Havlíček, V.; Volný, M. Automated Ambient Desorption–Ionization Platform for Surface Imaging Integrated with a Commercial Fourier Transform Ion Cyclotron Resonance Mass Spectrometer. *Anal. Chem.* **2009**, *81*, 8479–8487.
- (12) Manicke, N. E.; Dill, A. L.; Ifa, D. R.; Cooks, R. G. High-resolution Tissue Imaging on an Orbitrap Mass Spectrometer by Desorption Electrospray Ionization Mass Spectrometry. *J. Mass Spectrom.* **2010**, *45*, 223–226.
- (13) Römpp, A.; Spengler, B. Mass Spectrometry Imaging with High Resolution in Mass and Space. *Histochem. Cell Biol.* **2013**, *139*, 759–783.
- (14) Lietz, C. B.; Gemperline, E.; Li, L. Qualitative and Quantitative Mass Spectrometry Imaging of Drugs and Metabolites. *Adv. Drug Deliv. Rev.* **2013**, *65*, 1074–1085.
- (15) Prideaux, B.; Dartois, V.; Staab, D.; Weiner, D. M.; Goh, A.; Via, L. E.; Barry, C. E.; Stoeckli, M. High-Sensitivity MALDI-MRM-MS Imaging of Moxifloxacin Distribution in Tuberculosis-Infected Rabbit Lungs and Granulomatous Lesions. *Anal. Chem.* **2011**, *83*, 2112–2118.
- (16) Pulfer, M.; Murphy, R. C. Electrospray Mass Spectrometry of Phospholipids. *Mass Spectrom. Rev.* **2003**, *22*, 332–364.
- (17) Harayama, T.; Riezman, H. Understanding the Diversity of Membrane Lipid Composition. *Nat. Rev. Mol. Cell Biol.* **2018**, 1–16.
- (18) Martinez-Seara, H.; Róg, T.; Pasenkiewicz-Gierula, M.; Vattulainen, I.; Karttunen, M.; Reigada, R. Effect of Double Bond Position on Lipid Bilayer Properties: Insight through Atomistic Simulations. *J. Phys. Chem. B* **2007**, *111*, 11162–11168.
- (19) Shinzawa-Itoh, K.; Aoyama, H.; Muramoto, K.; Terada, H.; Kurauchi, T.; Tadehara, Y.; Yamasaki, A.; Sugimura, T.; Kurono, S.; Tsujimoto, K.; Mizushima, T.; Yamashita, E.; Tsukihara, T.; Yoshikawa, S. Structures and Physiological Roles of 13 Integral Lipids of Bovine Heart Cytochrome c Oxidase. *EMBO J.* **2007**, *26*, 1713–1725.
- (20) Ma, X.; Chong, L.; Tian, R.; Shi, R.; Hu, T. Y.; Ouyang, Z.; Xia, Y. Identification and Quantitation of Lipid C=C Location Isomers: A Shotgun Lipidomics Approach Enabled by Photochemical Reaction. *Proc. Natl. Acad. Sci.* **2016**, *113*, 2573–2578.

- (21) Ma, X.; Xia, Y. Pinpointing Double Bonds in Lipids by Paternò-Büchi Reactions and Mass Spectrometry. *Angew. Chem.* **2014**, *126*, 2630–2634.
- (22) Tang, F.; Guo, C.; Ma, X.; Zhang, J.; Su, Y.; Tian, R.; Shi, R.; Xia, Y.; Wang, X.; Ouyang, Z. Rapid In Situ Profiling of Lipid C=C Location Isomers in Tissue Using Ambient Mass Spectrometry with Photochemical Reactions. *Anal. Chem.* **2018**, *90*, 5612–5619.
- (23) Shimma, S.; Kubo, A.; Satoh, T.; Toyoda, M. Detailed Structural Analysis of Lipids Directly on Tissue Specimens Using a MALDI-SpiralTOF-Reflectron TOF Mass Spectrometer. *PLOS ONE* **2012**, *7*, e37107.
- (24) Toyoda, M. Development of Multi-Turn Time-of-Flight Mass Spectrometers and Their Applications. *Eur. J. Mass Spectrom.* **2010**, *16*, 397–406.
- (25) Pham, H. T.; Ly, T.; Trevitt, A. J.; Mitchell, T. W.; Blanksby, S. J. Differentiation of Complex Lipid Isomers by Radical-Directed Dissociation Mass Spectrometry. *Anal. Chem.* **2012**, *84*, 7525–7532.
- (26) Pham, H. T.; Trevitt, A. J.; Mitchell, T. W.; Blanksby, S. J. Rapid Differentiation of Isomeric Lipids by Photodissociation Mass Spectrometry of Fatty Acid Derivatives. *Rapid Commun. Mass Spectrom.* **2013**, *27*, 805–815.
- (27) Yoo, H. J.; Håkansson, K. Determination of Double Bond Location in Fatty Acids by Manganese Addition and Electron Induced Dissociation. *Anal. Chem.* **2010**, *82*, 6940–6946.
- (28) Jones, J. W.; Thompson, C. J.; Carter, C. L.; Kane, M. A. Electron-induced Dissociation (EID) for Structure Characterization of Glycerophosphatidylcholine: Determination of Double-bond Positions and Localization of Acyl Chains. *J. Mass Spectrom.* **2015**, *50*, 1327–1339.
- (29) Campbell, J. L.; Baba, T. Near-Complete Structural Characterization of Phosphatidylcholines Using Electron Impact Excitation of Ions from Organics. *Anal. Chem.* **2015**, *87*, 5837–5845.
- (30) Baba, T.; Campbell, J. L.; Yves Le Blanc, J. C.; Baker, P. R. S. In-Depth Sphingomyelin Characterization Using Electron Impact Excitation of Ions from Organics and Mass Spectrometry. *J. Lipid Res.* **2016**, *57*, 858–867.
- (31) Pham, H. T.; Maccarone, A. T.; Thomas, M. C.; Campbell, J. L.; Mitchell, T. W.; Blanksby, S. J. Structural Characterization of Glycerophospholipids by Combinations of Ozone- and Collision-Induced Dissociation Mass Spectrometry: The next Step towards “Top-down” Lipidomics. *Analyst* **2014**, *139*, 204–214.
- (32) Kozłowski, R. L.; Mitchell, T. W.; Blanksby, S. J. A Rapid Ambient Ionization-Mass Spectrometry Approach to Monitoring the Relative Abundance of Isomeric Glycerophospholipids. *Sci. Rep.* **2015**, *5*, 9243.

- (33) Poad, B. L. J.; Green, M. R.; Kirk, J. M.; Tomczyk, N.; Mitchell, T. W.; Blanksby, S. J. High-Pressure Ozone-Induced Dissociation for Lipid Structure Elucidation on Fast Chromatographic Timescales. *Anal. Chem.* **2017**, *89*, 4223–4229.
- (34) Poad, B. L. J.; Zheng, X.; Mitchell, T. W.; Smith, R. D.; Baker, E. S.; Blanksby, S. J. Online Ozonolysis Combined with Ion Mobility-Mass Spectrometry Provides a New Platform for Lipid Isomer Analyses. *Anal. Chem.* **2018**, *90*, 1292–1300.
- (35) Paine, M. R. L.; Poad, B. L. J.; Eijkel, G. B.; Marshall, D. L.; Blanksby, S. J.; Heeren, R. M. A.; Ellis, S. R. Mass Spectrometry Imaging with Isomeric Resolution Enabled by Ozone-Induced Dissociation. *Angew. Chem. Int. Ed.* **2018**.
- (36) Deimler, R. E.; Sander, M.; Jackson, G. P. Radical-Induced Fragmentation of Phospholipid Cations Using Metastable Atom-Activated Dissociation Mass Spectrometry (MAD-MS). *Int. J. Mass Spectrom.* **2015**, *390*, 178–186.
- (37) Li, P.; Hoffmann, W. D.; Jackson, G. P. Multistage Mass Spectrometry of Phospholipids Using Collision-Induced Dissociation (CID) and Metastable Atom-Activated Dissociation (MAD). *Int. J. Mass Spectrom.* **2016**, *403*, 1–7.
- (38) Brodbelt, J. S. Photodissociation Mass Spectrometry: New Tools for Characterization of Biological Molecules. *Chem. Soc. Rev.* **2014**, *43*, 2757–2783.
- (39) Klein, D. R.; Brodbelt, J. S. Structural Characterization of Phosphatidylcholines Using 193 nm Ultraviolet Photodissociation Mass Spectrometry. *Anal. Chem.* **2017**, *89*, 1516–1522.
- (40) Williams, P. E.; Klein, D. R.; Greer, S. M.; Brodbelt, J. S. Pinpointing Double Bond and Sn-Positions in Glycerophospholipids via Hybrid 193 nm Ultraviolet Photodissociation (UVPD) Mass Spectrometry. *J. Am. Chem. Soc.* **2017**, *139*, 15681–15690.
- (41) Ryan, E.; Nguyen, C. Q. N.; Shiea, C.; Reid, G. E. Detailed Structural Characterization of Sphingolipids via 193 nm Ultraviolet Photodissociation and Ultra High Resolution Tandem Mass Spectrometry. *J. Am. Soc. Mass Spectrom.* **2017**, *28*, 1406–1419.
- (42) Klein, D. R.; Holden, D. D.; Brodbelt, J. S. Shotgun Analysis of Rough-Type Lipopolysaccharides Using Ultraviolet Photodissociation Mass Spectrometry. *Anal. Chem.* **2016**, *88*, 1044–1051.
- (43) Kessner, D.; Chambers, M.; Burke, R.; Agus, D.; Mallick, P. ProteoWizard: Open Source Software for Rapid Proteomics Tools Development. *Bioinformatics* **2008**, *24*, 2534–2536.

- (44) Liebisch, G.; Vizcaíno, J. A.; Köfeler, H.; Trötz Müller, M.; Griffiths, W. J.; Schmitz, G.; Spener, F.; Wakelam, M. J. O. Shorthand Notation for Lipid Structures Derived from Mass Spectrometry. *J. Lipid Res.* **2013**, *54*, 1523–1530.
- (45) Škrášková, K.; Claude, E.; Jones, E. A.; Towers, M.; Ellis, S. R.; Heeren, R. M. A. Enhanced Capabilities for Imaging Gangliosides in Murine Brain with Matrix-Assisted Laser Desorption/Ionization and Desorption Electrospray Ionization Mass Spectrometry Coupled to Ion Mobility Separation. *Methods* **2016**, *104*, 69–78.

CHAPTER 5

- (1) Beutler, B.; Rietschel, E. T. Innate Immune Sensing and Its Roots: The Story of Endotoxin. *Nat. Rev. Immunol.* **2003**, *3*, 169–176.
- (2) Preston, Andrew; Mandrell, Robert E.; Gibson, Bradford W.; Apicella, Michael A. The Lipooligosaccharides of Pathogenic Gram-Negative Bacteria. *Crit. Rev. Microbiol.* **1996**, *22*, 139–180.
- (3) Raetz, C. R. H.; Whitfield, C. Lipopolysaccharide Endotoxins. *Annu. Rev. Biochem.* **2002**, *71*, 635–700.
- (4) Yethon, J. A.; Heinrichs, D. E.; Monteiro, M. A.; Perry, M. B.; Whitfield, C. Involvement of WaaY, WaaQ, AndwaaP in the Modification of Escherichia Coli Lipopolysaccharide and Their Role in the Formation of a Stable Outer Membrane. *J. Biol. Chem.* **1998**, *273*, 26310–26316.
- (5) Heinrichs, D. E.; Yethon, J. A.; Whitfield, C. Molecular Basis for Structural Diversity in the Core Regions of the Lipopolysaccharides of Escherichia Coli and Salmonella Enterica. *Mol. Microbiol.* **1998**, *30*, 221–232.
- (6) Delcour, A. H. Outer Membrane Permeability and Antibiotic Resistance. *Biochim. Biophys. Acta* **2009**, *1794*, 808–816.
- (7) Silipo, A.; Molinaro, A. The Diversity of the Core Oligosaccharide in Lipopolysaccharides. In *Endotoxins: Structure, Function and Recognition*; Wang, X., Quinn, P. J., Eds.; Subcellular Biochemistry; Springer Netherlands, 2010; pp 69–99.
- (8) Yethon, J. A.; Vinogradov, E.; Perry, M. B.; Whitfield, C. Mutation of the Lipopolysaccharide Core Glycosyltransferase Encoded by WaaG Destabilizes the Outer Membrane of Escherichia Coli by Interfering with Core Phosphorylation. *J. Bacteriol.* **2000**, *182*, 5620–5623.
- (9) Needham, B. D.; Carroll, S. M.; Giles, D. K.; Georgiou, G.; Whiteley, M.; Trent, M. S. Modulating the Innate Immune Response by Combinatorial Engineering of Endotoxin. *Proc. Natl. Acad. Sci.* **2013**, *110*, 1464–1469.

- (10) Molinaro, A.; Holst, O.; Di Lorenzo, F.; Callaghan, M.; Nurisso, A.; D'Errico, G.; Zamyatina, A.; Peri, F.; Berisio, R.; Jerala, R.; Jiménez-Barbero, J.; Silipo, A.; Martín-Santamaría, S. Chemistry of Lipid A: At the Heart of Innate Immunity. *Chem. – Eur. J.* **2015**, *21*, 500–519.
- (11) Li, Y.; Powell, D. A.; Shaffer, S. A.; Rasko, D. A.; Pelletier, M. R.; Leszyk, J. D.; Scott, A. J.; Masoudi, A.; Goodlett, D. R.; Wang, X.; Raetz, C. R. H.; Ernst, R. K. LPS Remodeling Is an Evolved Survival Strategy for Bacteria. *Proc. Natl. Acad. Sci.* **2012**, *109*, 8716–8721.
- (12) Boll, J. M.; Tucker, A. T.; Klein, D. R.; Beltran, A. M.; Brodbelt, J. S.; Davies, B. W.; Trent, M. S. Reinforcing Lipid A Acylation on the Cell Surface of *Acinetobacter Baumannii* Promotes Cationic Antimicrobial Peptide Resistance and Desiccation Survival. *mBio* **2015**, *6*, e00478-15.
- (13) Park, B. S.; Song, D. H.; Kim, H. M.; Choi, B.-S.; Lee, H.; Lee, J.-O. The Structural Basis of Lipopolysaccharide Recognition by the TLR4–MD-2 Complex. *Nature* **2009**, *458*, 1191–1195.
- (14) Zariri, A.; van der Ley, P. Biosynthetically Engineered Lipopolysaccharide as Vaccine Adjuvant. *Expert Rev. Vaccines* **2015**, *14*, 861–876.
- (15) Casella, C. R.; Mitchell, T. C. Putting Endotoxin to Work for Us: Monophosphoryl Lipid A as a Safe and Effective Vaccine Adjuvant. *Cell. Mol. Life Sci.* **2008**, *65*, 3231–3240.
- (16) Needham, B. D.; Trent, M. S. Fortifying the Barrier: The Impact of Lipid A Remodelling on Bacterial Pathogenesis. *Nat. Rev. Microbiol.* **2013**, *11*, 467–481.
- (17) Raetz, C. R. H.; Reynolds, C. M.; Trent, M. S.; Bishop, R. E. Lipid A Modification Systems in Gram-Negative Bacteria. *Annu. Rev. Biochem.* **2007**, *76*, 295–329.
- (18) Kilár, A.; Dörnyei, Á.; Kocsis, B. Structural Characterization of Bacterial Lipopolysaccharides with Mass Spectrometry and On- and off-Line Separation Techniques. *Mass Spectrom. Rev.* **2013**, *32*, 90–117.
- (19) Weinbaum, G.; Kadis, S.; Ajl, S. J. *Bacterial Endotoxins: A Comprehensive Treatise*; Elsevier, 2013.
- (20) Jones, J. W.; Cohen, I. E.; Tureček, F.; Goodlett, D. R.; Ernst, R. K. Comprehensive Structure Characterization of Lipid A Extracted from *Yersinia Pestis* for Determination of Its Phosphorylation Configuration. *J. Am. Soc. Mass Spectrom.* **2010**, *21*, 785–799.
- (21) Silipo, A.; De Castro, C.; Lanzetta, R.; Molinaro, A.; Parrilli, M.; Vago, G.; Sturiale, L.; Messina, A.; Garozzo, D. Structural Characterizations of Lipids A by MS/MS of Doubly Charged Ions on a Hybrid Linear Ion Trap/Orbitrap Mass Spectrometer. *J. Mass Spectrom.* **2008**, *43*, 478–484.

- (22) Jones, J. W.; Shaffer, S. A.; Ernst, R. K.; Goodlett, D. R.; Tureček, F. Determination of Pyrophosphorylated Forms of Lipid A in Gram-Negative Bacteria Using a Multivaried Mass Spectrometric Approach. *Proc. Natl. Acad. Sci.* **2008**, *105*, 12742–12747.
- (23) Madalinski, G.; Fournier, F.; Wind, F.-L.; Afonso, C.; Tabet, J.-C. Gram-Negative Bacterial Lipid A Analysis by Negative Electrospray Ion Trap Mass Spectrometry: Stepwise Dissociations of Deprotonated Species under Low Energy CID Conditions. *Int. J. Mass Spectrom.* **2006**, *249–250*, 77–92.
- (24) Kussak, A.; Weintraub, A. Quadrupole Ion-Trap Mass Spectrometry to Locate Fatty Acids on Lipid A from Gram-Negative Bacteria. *Anal. Biochem.* **2002**, *307*, 131–137.
- (25) Chan, S.; Reinhold, V. N. Detailed Structural Characterization of Lipid A: Electrospray Ionization Coupled with Tandem Mass-Spectrometry. *Anal. Biochem.* **1994**, *218*, 63–73.
- (26) Kojima, H.; Inagaki, M.; Tomita, T.; Watanabe, T. Diversity of Non-Stoichiometric Substitutions on the Lipopolysaccharide of *E. Coli* C Demonstrated by Electrospray Ionization Single Quadrupole Mass Spectrometry. *Rapid Commun. Mass Spectrom.* **2010**, *24*, 43–48.
- (27) Madsen, J. A.; Cullen, T. W.; Trent, M. S.; Brodbelt, J. S. IR and UV Photodissociation as Analytical Tools for Characterizing Lipid A Structures. *Anal. Chem.* **2011**, *83*, 5107–5113.
- (28) O'Brien, J. P.; Needham, B. D.; Henderson, J. C.; Nowicki, E. M.; Trent, M. S.; Brodbelt, J. S. 193 nm Ultraviolet Photodissociation Mass Spectrometry for the Structural Elucidation of Lipid A Compounds in Complex Mixtures. *Anal. Chem.* **2014**, *86*, 2138–2145.
- (29) Brodbelt, J. S. Photodissociation Mass Spectrometry: New Tools for Characterization of Biological Molecules. *Chem. Soc. Rev.* **2014**, *43*, 2757–2783.
- (30) Silipo, A.; Leone, S.; Molinaro, A.; Sturiale, L.; Garozzo, D.; Nazarenko, E. L.; Gorshkova, R. P.; Ivanova, E. P.; Lanzetta, R.; Parrilli, M. Complete Structural Elucidation of a Novel Lipooligosaccharide from the Outer Membrane of the Marine Bacterium *Shewanella Pacifica*. *Eur. J. Org. Chem.* **2005**, *2005*, 2281–2291.
- (31) Banoub, J. H.; Aneed, A. E.; Cohen, A. M.; Joly, N. Structural Investigation of Bacterial Lipopolysaccharides by Mass Spectrometry and Tandem Mass Spectrometry. *Mass Spectrom. Rev.* **2010**, *29*, 606–650.
- (32) O'Brien, J. P.; Needham, B. D.; Brown, D. B.; Trent, M. S.; Brodbelt, J. S. Top-down Strategies for the Structural Elucidation of Intact Gram-Negative Bacterial Endotoxins. *Chem. Sci.* **2014**, *5*, 4291–4301.

- (33) Sturiale, L.; Garozzo, D.; Silipo, A.; Lanzetta, R.; Parrilli, M.; Molinaro, A. New Conditions for Matrix-Assisted Laser Desorption/Ionization Mass Spectrometry of Native Bacterial R-Type Lipopolysaccharides. *Rapid Commun. Mass Spectrom.* **2005**, *19*, 1829–1834.
- (34) Hankins, J. V.; Madsen, J. A.; Giles, D. K.; Childers, B. M.; Klose, K. E.; Brodbelt, J. S.; Trent, M. S. Elucidation of a Novel *Vibrio Cholerae* Lipid A Secondary Hydroxy-Acyltransferase and Its Role in Innate Immune Recognition. *Mol. Microbiol.* **2011**, *81*, 1313–1329.
- (35) Hankins, J. V.; Madsen, J. A.; Giles, D. K.; Brodbelt, J. S.; Trent, M. S. Amino Acid Addition to *Vibrio Cholerae* LPS Establishes a Link between Surface Remodeling in Gram-Positive and Gram-Negative Bacteria. *Proc. Natl. Acad. Sci.* **2012**, *109*, 8722–8727.
- (36) Nowicki, E. M.; O'Brien, J. P.; Brodbelt, J. S.; Trent, M. S. Extracellular Zinc Induces Phosphoethanolamine Addition to *Pseudomonas Aeruginosa* Lipid A via the ColRS Two-Component System. *Mol. Microbiol.* **2015**, *97*, 166–178.
- (37) Ko, B. J.; Brodbelt, J. S. 193 nm Ultraviolet Photodissociation of Deprotonated Sialylated Oligosaccharides. *Anal. Chem.* **2011**, *83*, 8192–8200.
- (38) Varki, A.; Cummings, R. D.; Aebi, M.; Packer, N. H.; Seeberger, P. H.; Esko, J. D.; Stanley, P.; Hart, G.; Darvill, A.; Kinoshita, T.; Prestegard, J. J.; Schnaar, R. L.; Freeze, H. H.; Marth, J. D.; Bertozzi, C. R.; Etzler, M. E.; Frank, M.; Vliegenthart, J. F.; Lütkeke, T.; Perez, S.; Bolton, E.; Rudd, P.; Paulson, J.; Kanehisa, M.; Toukach, P.; Aoki-Kinoshita, K. F.; Dell, A.; Narimatsu, H.; York, W.; Taniguchi, N.; Kornfeld, S. Symbol Nomenclature for Graphical Representations of Glycans. *Glycobiology* **2015**, *25*, 1323–1324.
- (39) Holden, Dustin; Canterbury, Jesse; Zhuk, Eugene; Izgarian, Nick; Schwartz, Jae; Brodbelt, Jennifer S. Top Down Protein Analysis by Ultraviolet Photodissociation (UVPD) in an Orbitrap Tribrid Mass Spectrometer. In *62nd American Society for Mass Spectrometry and Allied Topics*; Baltimore, MD, 2014.
- (40) Raetz, C. R. H.; Garrett, T. A.; Reynolds, C. M.; Shaw, W. A.; Moore, J. D.; Smith, D. C.; Ribeiro, A. A.; Murphy, R. C.; Ulevitch, R. J.; Fearn, C.; Reichart, D.; Glass, C. K.; Benner, C.; Subramaniam, S.; Harkewicz, R.; Bowers-Gentry, R. C.; Buczynski, M. W.; Cooper, J. A.; Deems, R. A.; Dennis, E. A. Kdo2-Lipid A of *Escherichia Coli*, a Defined Endotoxin That Activates Macrophages via TLR-4. *J. Lipid Res.* **2006**, *47*, 1097–1111.
- (41) Domon, B.; Costello, C. E. A Systematic Nomenclature for Carbohydrate Fragmentations in FAB-MS/MS Spectra of Glycoconjugates. *Glycoconj. J.* **1988**, *5*, 397–409.
- (42) Pupo, E.; Lindner, B.; Brade, H.; Schromm, A. B. Intact Rough- and Smooth-Form Lipopolysaccharides from *Escherichia Coli* Separated by Preparative Gel

- Electrophoresis Exhibit Differential Biologic Activity in Human Macrophages. *FEBS J.* **2013**, *280*, 1095–1111.
- (43) Nishikaze, T.; Kawabata, S.; Tanaka, K. Fragmentation Characteristics of Deprotonated N-Linked Glycopeptides: Influences of Amino Acid Composition and Sequence. *J. Am. Soc. Mass Spectrom.* **2014**, *25*, 988–998.
- (44) Amor, K.; Heinrichs, D. E.; Fridrich, E.; Ziebell, K.; Johnson, R. P.; Whitfield, C. Distribution of Core Oligosaccharide Types in Lipopolysaccharides from *Escherichia Coli*. *Infect. Immun.* **2000**, *68*, 1116–1124.

CHAPTER 6

- (1) Michael, C. A.; Dominey-Howes, D.; Labbate, M. The Antimicrobial Resistance Crisis: Causes, Consequences, and Management. *Front. Public Health* **2014**, *2*.
- (2) Ventola, C. L. The Antibiotic Resistance Crisis. *Pharm. Ther.* **2015**, *40*, 277–283.
- (3) Ventola, C. L. The Antibiotic Resistance Crisis. *Pharm. Ther.* **2015**, *40*, 344–352.
- (4) Martens, E.; Demain, A. L. The Antibiotic Resistance Crisis, with a Focus on the United States. *J. Antibiot. (Tokyo)* **2017**, *70*, 520–526.
- (5) Miller, S. I. Antibiotic Resistance and Regulation of the Gram-Negative Bacterial Outer Membrane Barrier by Host Innate Immune Molecules. *mBio* **2016**, *7*, e01541-16.
- (6) Delcour, A. H. Outer Membrane Permeability and Antibiotic Resistance. *Biochim. Biophys. Acta BBA - Proteins Proteomics* **2009**, *1794*, 808–816.
- (7) Blair, J. M. A.; Webber, M. A.; Baylay, A. J.; Ogbolu, D. O.; Piddock, L. J. V. Molecular Mechanisms of Antibiotic Resistance. *Nat. Rev. Microbiol.* **2015**, *13*, 42–51.
- (8) Exner, M.; Bhattacharya, S.; Christiansen, B.; Gebel, J.; Goroncy-Bermes, P.; Hartemann, P.; Heeg, P.; Ilschner, C.; Kramer, A.; Larson, E.; Merckens, W.; Mielke, M.; Oltmanns, P.; Ross, B.; Rotter, M.; Schmuthausen, R. M.; Sonntag, H.-G.; Trautmann, M. Antibiotic Resistance: What Is so Special about Multidrug-Resistant Gram-Negative Bacteria? *GMS Hyg. Infect. Control* **2017**, *12*.
- (9) Molinaro, A.; Holst, O.; Di Lorenzo, F.; Callaghan, M.; Nurisso, A.; D’Errico, G.; Zamyatina, A.; Peri, F.; Berisio, R.; Jerala, R.; Jiménez-Barbero, J.; Silipo, A.; Martín-Santamaría, S. Chemistry of Lipid A: At the Heart of Innate Immunity. *Chem. – Eur. J.* **2015**, *21*, 500–519.
- (10) Silipo, A.; Molinaro, A. The Diversity of the Core Oligosaccharide in Lipopolysaccharides. In *Endotoxins: Structure, Function and Recognition*; Wang, X., Quinn, P. J., Eds.; Subcellular Biochemistry; Springer Netherlands, 2010; pp 69–99.

- (11) Lerouge, I.; Vanderleyden, J. O-Antigen Structural Variation: Mechanisms and Possible Roles in Animal/Plant–Microbe Interactions. *FEMS Microbiol. Rev.* **2002**, *26*, 17–47.
- (12) Preston, Andrew; Mandrell, Robert E.; Gibson, Bradford W.; Apicella, Michael A. The Lipooligosaccharides of Pathogenic Gram-Negative Bacteria. *Crit. Rev. Microbiol.* **1996**, *22*, 139–180.
- (13) Frirdich, E.; Whitfield, C. Lipopolysaccharide Inner Core Oligosaccharide Structure and Outer Membrane Stability in Human Pathogens Belonging to the Enterobacteriaceae. *J. Endotoxin Res.* **2005**, *11*, 133–144.
- (14) Needham, B. D.; Trent, M. S. Fortifying the Barrier: The Impact of Lipid A Remodelling on Bacterial Pathogenesis. *Nat. Rev. Microbiol.* **2013**, *11*, 467–481.
- (15) Whitfield, C.; Trent, M. S. Biosynthesis and Export of Bacterial Lipopolysaccharides. *Annu. Rev. Biochem.* **2014**, *83*, 99–128.
- (16) Maldonado, R. F.; Sá-Correia, I.; Valvano, M. A. Lipopolysaccharide Modification in Gram-Negative Bacteria during Chronic Infection. *FEMS Microbiol. Rev.* **2016**, *40*, 480–493.
- (17) Nuri, R.; Shprung, T.; Shai, Y. Defensive Remodeling: How Bacterial Surface Properties and Biofilm Formation Promote Resistance to Antimicrobial Peptides. *Biochim. Biophys. Acta BBA - Biomembr.* **2015**, *1848*, 3089–3100.
- (18) Salazar, J.; Alarcón, M.; Huerta, J.; Navarro, B.; Aguayo, D. Phosphoethanolamine Addition to the Heptose I of the Lipopolysaccharide Modifies the Inner Core Structure and Has an Impact on the Binding of Polymyxin B to the Escherichia Coli Outer Membrane. *Arch. Biochem. Biophys.* **2017**, *620*, 28–34.
- (19) Agrawal, A.; Weisshaar, J. C. Effects of Alterations of the E. Coli Lipopolysaccharide Layer on Membrane Permeabilization Events Induced by Cecropin A. *Biochim. Biophys. Acta BBA - Biomembr.* **2018**, *1860*, 1470–1479.
- (20) Wang, Z.; Wang, J.; Ren, G.; Li, Y.; Wang, X. Influence of Core Oligosaccharide of Lipopolysaccharide to Outer Membrane Behavior of Escherichia Coli. *Mar. Drugs* **2015**, *13*, 3325–3339.
- (21) Marr, N.; Tirsoaga, A.; Blanot, D.; Fernandez, R.; Caroff, M. Glucosamine Found as a Substituent of Both Phosphate Groups in Bordetella Lipid A Backbones: Role of a BvgAS-Activated ArnT Ortholog. *J. Bacteriol.* **2008**, *190*, 4281–4290.
- (22) Shah, N. R.; Hancock, R. E. W.; Fernandez, R. C. Bordetella Pertussis Lipid A Glucosamine Modification Confers Resistance to Cationic Antimicrobial Peptides and Increases Resistance to Outer Membrane Perturbation. *Antimicrob. Agents Chemother.* **2014**, *58*, 4931–4934.

- (23) Tzeng, Y.-L.; Stephens, D. S. Antimicrobial Peptide Resistance in *Neisseria Meningitidis*. *Biochim. Biophys. Acta BBA - Biomembr.* **2015**, *1848*, 3026–3031.
- (24) Cullen, T. W.; Giles, D. K.; Wolf, L. N.; Ecobichon, C.; Boneca, I. G.; Trent, M. S. *Helicobacter Pylori* versus the Host: Remodeling of the Bacterial Outer Membrane Is Required for Survival in the Gastric Mucosa. *PLOS Pathog.* **2011**, *7*, e1002454.
- (25) Leung, L. M.; Cooper, V. S.; Rasko, D. A.; Guo, Q.; Pacey, M. P.; McElheny, C. L.; Mettus, R. T.; Yoon, S. H.; Goodlett, D. R.; Ernst, R. K.; Doi, Y. Structural Modification of LPS in Colistin-Resistant, KPC-Producing *Klebsiella Pneumoniae*. *J. Antimicrob. Chemother.* **2017**, *72*, 3035–3042.
- (26) Liu, Y.-Y.; Chandler, C. E.; Leung, L. M.; McElheny, C. L.; Mettus, R. T.; Shanks, R. M. Q.; Liu, J.-H.; Goodlett, D. R.; Ernst, R. K.; Doi, Y. Structural Modification of Lipopolysaccharide Conferred by Mcr-1 in Gram-Negative ESKAPE Pathogens. *Antimicrob. Agents Chemother.* **2017**, *61*, e00580-17.
- (27) Adams, M. D.; Nickel, G. C.; Bajaksouzian, S.; Lavender, H.; Murthy, A. R.; Jacobs, M. R.; Bonomo, R. A. Resistance to Colistin in *Acinetobacter Baumannii* Associated with Mutations in the PmrAB Two-Component System. *Antimicrob. Agents Chemother.* **2009**, *53*, 3628–3634.
- (28) Qureshi, Z. A.; Hittle, L. E.; O'Hara, J. A.; Rivera, J. I.; Syed, A.; Shields, R. K.; Pasculle, A. W.; Ernst, R. K.; Doi, Y. Colistin-Resistant *Acinetobacter Baumannii*: Beyond Carbapenem Resistance. *Clin. Infect. Dis.* **2015**, civ048.
- (29) M. Crittenden, C.; M. Herrera, C.; E. Williams, P.; P. Ricci, D.; R. Swem, L.; Stephen Trent, M.; S. Brodbelt, J. Mapping Phosphate Modifications of Substituted Lipid A via a Targeted MS 3 CID/UVPD Strategy. *Analyst* **2018**.
- (30) Zhao, Y.; Arce-Gorvel, V.; Conde-Álvarez, R.; Moriyon, I.; Gorvel, J.-P. Vaccine Development Targeting Lipopolysaccharide Structure Modification. *Microbes Infect.* **2017**.
- (31) Micoli, F.; Costantino, P.; Adamo, R. Potential Targets for next Generation Antimicrobial Glycoconjugate Vaccines. *FEMS Microbiol. Rev.* **2018**, *42*, 388–423.
- (32) Astronomo, R. D.; Burton, D. R. Carbohydrate Vaccines: Developing Sweet Solutions to Sticky Situations? *Nat. Rev. Drug Discov.* **2010**, *9*, 308–324.
- (33) Rappuoli, R. Glycoconjugate Vaccines: Principles and Mechanisms. *Sci. Transl. Med.* **2018**, *10*, eaat4615.
- (34) Chen, W. Current Advances and Challenges in the Development of *Acinetobacter* Vaccines. *Hum. Vaccines Immunother.* **2015**, *11*, 2495–2500.
- (35) Berti, F.; Adamo, R. Antimicrobial Glycoconjugate Vaccines: An Overview of Classic and Modern Approaches for Protein Modification. *Chem. Soc. Rev.* **2018**.

- (36) Kilár, A.; Dörnyei, Á.; Kocsis, B. Structural Characterization of Bacterial Lipopolysaccharides with Mass Spectrometry and On- and off-Line Separation Techniques. *Mass Spectrom. Rev.* **2013**, *32*, 90–117.
- (37) Banoub, J. H.; Aneed, A. E.; Cohen, A. M.; Joly, N. Structural Investigation of Bacterial Lipopolysaccharides by Mass Spectrometry and Tandem Mass Spectrometry. *Mass Spectrom. Rev.* **2010**, *29*, 606–650.
- (38) Sándor, V.; Dörnyei, Á.; Makszin, L.; Kilár, F.; Péterfi, Z.; Kocsis, B.; Kilár, A. Characterization of Complex, Heterogeneous Lipid A Samples Using HPLC–MS/MS Technique I. Overall Analysis with Respect to Acylation, Phosphorylation and Isobaric Distribution. *J. Mass Spectrom.* **2016**, *51*, 1043–1063.
- (39) Sándor, V.; Kilár, A.; Kilár, F.; Kocsis, B.; Dörnyei, Á. Characterization of Complex, Heterogeneous Lipid A Samples Using HPLC–MS/MS Technique II. Structural Elucidation of Non-Phosphorylated Lipid A by Negative-Ion Mode Tandem Mass Spectrometry. *J. Mass Spectrom.* *51*, 615–628.
- (40) Sándor, V.; Kilár, A.; Kilár, F.; Kocsis, B.; Dörnyei, Á. Characterization of Complex, Heterogeneous Lipid A Samples Using HPLC–MS/MS Technique III. Positive-Ion Mode Tandem Mass Spectrometry to Reveal Phosphorylation and Acylation Patterns of Lipid A. *J. Mass Spectrom.* **2018**, *53*, 146–161.
- (41) Madsen, J. A.; Cullen, T. W.; Trent, M. S.; Brodbelt, J. S. IR and UV Photodissociation as Analytical Tools for Characterizing Lipid A Structures. *Anal. Chem.* **2011**, *83*, 5107–5113.
- (42) O’Brien, J. P.; Needham, B. D.; Henderson, J. C.; Nowicki, E. M.; Trent, M. S.; Brodbelt, J. S. 193 nm Ultraviolet Photodissociation Mass Spectrometry for the Structural Elucidation of Lipid A Compounds in Complex Mixtures. *Anal. Chem.* **2014**, *86*, 2138–2145.
- (43) Morrison, L. J.; Parker, W. R.; Holden, D. D.; Henderson, J. C.; Boll, J. M.; Trent, M. S.; Brodbelt, J. S. UVliPiD: A UVPD-Based Hierarchical Approach for De Novo Characterization of Lipid A Structures. *Anal. Chem.* **2016**, *88*, 1812–1820.
- (44) Kondakov, A.; Lindner, B. Structural Characterization of Complex Bacterial Glycolipids by Fourier Transform Mass Spectrometry. *Eur. J. Mass Spectrom.* **2005**, *11*, 535–546.
- (45) O’Brien, J. P.; Needham, B. D.; Brown, D. B.; Trent, M. S.; Brodbelt, J. S. Top-down Strategies for the Structural Elucidation of Intact Gram-Negative Bacterial Endotoxins. *Chem. Sci.* **2014**, *5*, 4291–4301.
- (46) Hübner, G.; Lindner, B. Separation of R-Form Lipopolysaccharide and Lipid A by CE–Fourier-Transform Ion Cyclotron Resonance MS. *Electrophoresis* **2009**, *30*, 1808–1816.

- (47) Sturiale, L.; Garozzo, D.; Silipo, A.; Lanzetta, R.; Parrilli, M.; Molinaro, A. New Conditions for Matrix-Assisted Laser Desorption/Ionization Mass Spectrometry of Native Bacterial R-Type Lipopolysaccharides. *Rapid Commun. Mass Spectrom.* **2005**, *19*, 1829–1834.
- (48) John, C. M.; Liu, M.; Jarvis, G. A. Profiles of Structural Heterogeneity in Native Lipooligosaccharides of Neisseria and Cytokine Induction. *J. Lipid Res.* **2009**, *50*, 424–438.
- (49) John, C. M.; Liu, M.; Phillips, N. J.; Yang, Z.; Funk, C. R.; Zimmerman, L. I.; Griffiss, J. M.; Stein, D. C.; Jarvis, G. A. Lack of Lipid A Pyrophosphorylation and Functional LptA Reduces Inflammation by Neisseria Commensals. *Infect. Immun.* **2012**, *80*, 4014–4026.
- (50) Stephenson, H. N.; John, C. M.; Naz, N.; Gundogdu, O.; Dorrell, N.; Wren, B. W.; Jarvis, G. A.; Bajaj-Elliott, M. Campylobacter Jejuni Lipooligosaccharide Sialylation, Phosphorylation, and Amide/Ester Linkage Modifications Fine-Tune Human Toll-like Receptor 4 Activation. *J. Biol. Chem.* **2013**, *288*, 19661–19672.
- (51) Sturiale, L.; Palmigiano, A.; Silipo, A.; Knirel, Y. A.; Anisimov, A. P.; Lanzetta, R.; Parrilli, M.; Molinaro, A.; Garozzo, D. Reflectron MALDI TOF and MALDI TOF/TOF Mass Spectrometry Reveal Novel Structural Details of Native Lipooligosaccharides. *J. Mass Spectrom.* **2011**, *46*, 1135–1142.
- (52) Klein, D. R.; Holden, D. D.; Brodbelt, J. S. Shotgun Analysis of Rough-Type Lipopolysaccharides Using Ultraviolet Photodissociation Mass Spectrometry. *Anal. Chem.* **2016**, *88*, 1044–1051.
- (53) Phillips, N. J.; John, C. M.; Jarvis, G. A. Analysis of Bacterial Lipooligosaccharides by MALDI-TOF MS with Traveling Wave Ion Mobility. *J. Am. Soc. Mass Spectrom.* **2016**, *27*, 1263–1276.
- (54) Oyler, B. L.; Khan, M. M.; Smith, D. F.; Harberts, E. M.; Kilgour, D. P. A.; Ernst, R. K.; Cross, A. S.; Goodlett, D. R. Top Down Tandem Mass Spectrometric Analysis of a Chemically Modified Rough-Type Lipopolysaccharide Vaccine Candidate. *J. Am. Soc. Mass Spectrom.* **2018**, 1–9.
- (55) Raetz, C. R. H.; Garrett, T. A.; Reynolds, C. M.; Shaw, W. A.; Moore, J. D.; Smith, D. C.; Ribeiro, A. A.; Murphy, R. C.; Ulevitch, R. J.; Fearn, C.; Reichart, D.; Glass, C. K.; Benner, C.; Subramaniam, S.; Harkewicz, R.; Bowers-Gentry, R. C.; Buczynski, M. W.; Cooper, J. A.; Deems, R. A.; Dennis, E. A. Kdo2-Lipid A of Escherichia Coli, a Defined Endotoxin That Activates Macrophages via TLR-4. *J. Lipid Res.* **2006**, *47*, 1097–1111.
- (56) Brodbelt, J. S. Photodissociation Mass Spectrometry: New Tools for Characterization of Biological Molecules. *Chem. Soc. Rev.* **2014**, *43*, 2757–2783.
- (57) Shaw, J. B.; Li, W.; Holden, D. D.; Zhang, Y.; Griep-Raming, J.; Fellers, R. T.; Early, B. P.; Thomas, P. M.; Kelleher, N. L.; Brodbelt, J. S. Complete Protein

- Characterization Using Top-Down Mass Spectrometry and Ultraviolet Photodissociation. *J. Am. Chem. Soc.* **2013**, *135*, 12646–12651.
- (58) Westphal, O.; Jann, K. Bacterial Lippolysaccharides: Extraction with Phenol-Water and Further Applications of the Procedure. In *Methods in Carbohydrate Chemistry*; Whistler, R. L., Ed.; Academic Press, Inc.: New York, 1965; Vol. 5, pp 83–91.
 - (59) Varki, A.; Cummings, R. D.; Aebi, M.; Packer, N. H.; Seeberger, P. H.; Esko, J. D.; Stanley, P.; Hart, G.; Darvill, A.; Kinoshita, T.; Prestegard, J. J.; Schnaar, R. L.; Freeze, H. H.; Marth, J. D.; Bertozzi, C. R.; Etzler, M. E.; Frank, M.; Vliegenthart, J. F.; Lütke, T.; Perez, S.; Bolton, E.; Rudd, P.; Paulson, J.; Kanehisa, M.; Toukach, P.; Aoki-Kinoshita, K. F.; Dell, A.; Narimatsu, H.; York, W.; Taniguchi, N.; Kornfeld, S. Symbol Nomenclature for Graphical Representations of Glycans. *Glycobiology* **2015**, *25*, 1323–1324.
 - (60) Domon, B.; Costello, C. E. A Systematic Nomenclature for Carbohydrate Fragmentations in FAB-MS/MS Spectra of Glycoconjugates. *Glycoconj. J.* **1988**, *5*, 397–409.
 - (61) Furey, A.; Moriarty, M.; Bane, V.; Kinsella, B.; Lehane, M. Ion Suppression; A Critical Review on Causes, Evaluation, Prevention and Applications. *Talanta* **2013**, *115*, 104–122.
 - (62) Heinrichs, D. E.; Yethon, J. A.; Whitfield, C. Molecular Basis for Structural Diversity in the Core Regions of the Lipopolysaccharides of Escherichia Coli and Salmonella Enterica. *Mol. Microbiol.* **1998**, *30*, 221–232.
 - (63) Müller-Loennies, S.; Lindner, B.; Brade, H. Structural Analysis of Deacylated Lipopolysaccharide of Escherichia Coli Strains 2513 (R4 Core-Type) and F653 (R3 Core-Type). *Eur. J. Biochem.* **2002**, *269*, 5982–5991.
 - (64) Pogue, J. M.; Cohen, D. A.; Marchaim, D. Polymyxin-Resistant Acinetobacter Baumannii: Urgent Action Needed. *Clin. Infect. Dis.* **2015**.
 - (65) Michalopoulos, A.; Falagas, M. E. Treatment of Acinetobacter Infections. *Expert Opin. Pharmacother.* **2010**, *11*, 779–788.
 - (66) Vinogradov, E. V.; Duus, J. Ø.; Brade, H.; Holst, O. The Structure of the Carbohydrate Backbone of the Lipopolysaccharide from Acinetobacter Baumannii Strain ATCC 19606. *Eur. J. Biochem.* **2002**, *269*, 422–430.
 - (67) Pelletier, M. R.; Casella, L. G.; Jones, J. W.; Adams, M. D.; Zurawski, D. V.; Hazlett, K. R. O.; Doi, Y.; Ernst, R. K. Unique Structural Modifications Are Present in the Lipopolysaccharide from Colistin-Resistant Strains of Acinetobacter Baumannii. *Antimicrob. Agents Chemother.* **2013**, *57*, 4831–4840.
 - (68) Boll, J. M.; Tucker, A. T.; Klein, D. R.; Beltran, A. M.; Brodbelt, J. S.; Davies, B. W.; Trent, M. S. Reinforcing Lipid A Acylation on the Cell Surface of

Acinetobacter Baumannii Promotes Cationic Antimicrobial Peptide Resistance and Desiccation Survival. *mBio* **2015**, 6, e00478-15.

CHAPTER 7

- (1) Lever, R.; Page, C. P. Novel Drug Development Opportunities for Heparin. *Nat. Rev. Drug Discov.* **2002**, 1, 140–148.
- (2) Häcker, U.; Nybakken, K.; Perrimon, N. Developmental Cell Biology: Heparan Sulphate Proteoglycans: The Sweet Side of Development. *Nat. Rev. Mol. Cell Biol.* **2005**, 6, nrm1681.
- (3) Parish, C. R. The Role of Heparan Sulphate in Inflammation. *Nat. Rev. Immunol.* **2006**, 6, 633–643.
- (4) Sasisekharan, R.; Shriver, Z.; Venkataraman, G.; Narayanasami, U. Roles of Heparan-Sulphate Glycosaminoglycans in Cancer. *Nat. Rev. Cancer* **2002**, 2, nrc842.
- (5) da Costa, D. S.; Reis, R. L.; Pashkuleva, I. Sulfation of Glycosaminoglycans and Its Implications in Human Health and Disorders. *Annu. Rev. Biomed. Eng.* **2017**, 19, 1–26.
- (6) Turnbull, J. E.; Linhardt, R. J. Synthetic Sugars Enhance the Functional Glycomics Toolkit. *Nat. Chem. Biol.* **2006**, 2, 449–450.
- (7) Afratis, N.; Gialeli, C.; Nikitovic, D.; Tsegenidis, T.; Karousou, E.; Theocharis, A. D.; Pavão, M. S.; Tzanakakis, G. N.; Karamanos, N. K. Glycosaminoglycans: Key Players in Cancer Cell Biology and Treatment. *FEBS J.* **2012**, 279, 1177–1197.
- (8) Liu, H.; Zhang, Z.; Linhardt, R. J. Lessons Learned from the Contamination of Heparin. *Nat. Prod. Rep.* **2009**, 26, 313–321.
- (9) Mormann, M.; Zamfir, A. D.; Seidler, D. G.; Kresse, H.; Peter-Katalinić, J. Analysis of Oversulfation in a Chondroitin Sulfate Oligosaccharide Fraction from Bovine Aorta by Nanoelectrospray Ionization Quadrupole Time-of-Flight and Fourier-Transform Ion Cyclotron Resonance Mass Spectrometry. *J. Am. Soc. Mass Spectrom.* **2007**, 18, 179–187.
- (10) Laremore, T. N.; Zhang, F.; Dordick, J. S.; Liu, J.; Linhardt, R. J. Recent Progress and Applications in Glycosaminoglycan and Heparin Research. *Curr. Opin. Chem. Biol.* **2009**, 13, 633–640.
- (11) Laremore, T. N.; Leach III, F. E.; Solakyildirim, K.; Amster, I. J.; Linhardt, R. J. Glycosaminoglycan Characterization by Electrospray Ionization Mass Spectrometry Including Fourier Transform Mass Spectrometry. In *Methods in Enzymology*; Abelson, J. N., Simon, M. I., Eds.; Glycomics; Academic Press, 2010; Vol. 478, pp 79–108.

- (12) Chi, L.; Wolff, J. J.; Laremore, T. N.; Restaino, O. F.; Xie, J.; Schiraldi, C.; Toida, T.; Amster, I. J.; Linhardt, R. J. Structural Analysis of Bikunin Glycosaminoglycan. *J. Am. Chem. Soc.* **2008**, *130*, 2617–2625.
- (13) Ly, M.; Leach III, F. E.; Laremore, T. N.; Toida, T.; Amster, I. J.; Linhardt, R. J. The Proteoglycan Bikunin Has a Defined Sequence. *Nat. Chem. Biol.* **2011**, *7*, 827–833.
- (14) Kailemia, M. J.; Li, L.; Ly, M.; Linhardt, R. J.; Amster, I. J. Complete Mass Spectral Characterization of a Synthetic Ultralow-Molecular-Weight Heparin Using Collision-Induced Dissociation. *Anal. Chem.* **2012**, *84*, 5475–5478.
- (15) Wolff, J. J.; Laremore, T. N.; Leach III, F. E.; Linhardt, R. J.; Amster, I. J. Electron Capture Dissociation, Electron Detachment Dissociation and Infrared Multiphoton Dissociation of Sucrose Octasulfate. *Eur. J. Mass Spectrom.* **2008**, *15*, 275–281.
- (16) Zaia, J.; McClellan, J. E.; Costello, C. E. Tandem Mass Spectrometric Determination of the 4S/6S Sulfation Sequence in Chondroitin Sulfate Oligosaccharides. *Anal. Chem.* **2001**, *73*, 6030–6039.
- (17) Zaia, J.; Costello, C. E. Compositional Analysis of Glycosaminoglycans by Electrospray Mass Spectrometry. *Anal. Chem.* **2001**, *73*, 233–239.
- (18) Zaia, J.; Costello, C. E. Tandem Mass Spectrometry of Sulfated Heparin-Like Glycosaminoglycan Oligosaccharides. *Anal. Chem.* **2003**, *75*, 2445–2455.
- (19) Naggar, E. F.; Costello, C. E.; Zaia, J. Competing Fragmentation Processes in Tandem Mass Spectra of Heparin-like Glycosaminoglycans. *J. Am. Soc. Mass Spectrom.* **2004**, *15*, 1534–1544.
- (20) Kailemia, M. J.; Li, L.; Xu, Y.; Liu, J.; Linhardt, R. J.; Amster, I. J. Structurally Informative Tandem Mass Spectrometry of Highly Sulfated Natural and Chemoenzymatically Synthesized Heparin and Heparan Sulfate Glycosaminoglycans. *Mol. Cell. Proteomics* **2013**, *12*, 979–990.
- (21) Huang, R.; Pomin, V. H.; Sharp, J. S. LC-MSn Analysis of Isomeric Chondroitin Sulfate Oligosaccharides Using a Chemical Derivatization Strategy. *J. Am. Soc. Mass Spectrom.* **2011**, *22*, 1577.
- (22) Huang, R.; Liu, J.; Sharp, J. S. An Approach for Separation and Complete Structural Sequencing of Heparin/Heparan Sulfate-like Oligosaccharides. *Anal. Chem.* **2013**, *85*, 5787–5795.
- (23) Taylor, C. J.; Burke, R. M.; Wu, B.; Panja, S.; Nielsen, S. B.; Dessent, C. E. H. Structural Characterization of Negatively Charged Glycosaminoglycans Using High-Energy (50–150keV) Collisional Activation. *Int. J. Mass Spectrom.* **2009**, *285*, 70–77.

- (24) Wolff, J. J.; Amster, I. J.; Chi, L.; Linhardt, R. J. Electron Detachment Dissociation of Glycosaminoglycan Tetrasaccharides. *J. Am. Soc. Mass Spectrom.* **2007**, *18*, 234–244.
- (25) Wolff, J. J.; Laremore, T. N.; Busch, A. M.; Linhardt, R. J.; Amster, I. J. Electron Detachment Dissociation of Dermatan Sulfate Oligosaccharides. *J. Am. Soc. Mass Spectrom.* **2008**, *19*, 294–304.
- (26) Wolff, J. J.; Laremore, T. N.; Busch, A. M.; Linhardt, R. J.; Amster, I. J. Influence of Charge State and Sodium Cationization on the Electron Detachment Dissociation and Infrared Multiphoton Dissociation of Glycosaminoglycan Oligosaccharides. *J. Am. Soc. Mass Spectrom.* **2008**, *19*, 790–798.
- (27) Leach III, F. E.; Wolff, J. J.; Laremore, T. N.; Linhardt, R. J.; Amster, I. J. Evaluation of the Experimental Parameters Which Control Electron Detachment Dissociation, and Their Effect on the Fragmentation Efficiency of Glycosaminoglycan Carbohydrates. *Int. J. Mass Spectrom.* **2008**, *276*, 110–115.
- (28) Wolff, J. J.; Chi, L.; Linhardt, R. J.; Amster, I. J. Distinguishing Glucuronic from Iduronic Acid in Glycosaminoglycan Tetrasaccharides by Using Electron Detachment Dissociation. *Anal. Chem.* **2007**, *79*, 2015–2022.
- (29) Oh, H. B.; Leach III, F. E.; Arungundram, S.; Al-Mafraji, K.; Venot, A.; Boons, G. J.; Amster, I. J. Multivariate Analysis of Electron Detachment Dissociation and Infrared Multiphoton Dissociation Mass Spectra of Heparan Sulfate Tetrasaccharides Differing Only in Hexuronic Acid Stereochemistry. *J. Am. Soc. Mass Spectrom.* **2011**, *22*, 582–590.
- (30) Leach III, F. E.; Ly, M.; Laremore, T. N.; Wolff, J. J.; Perlow, J.; Linhardt, R. J.; Amster, I. J. Hexuronic Acid Stereochemistry Determination in Chondroitin Sulfate Glycosaminoglycan Oligosaccharides by Electron Detachment Dissociation. *J. Am. Soc. Mass Spectrom.* **2012**, *23*, 1488–1497.
- (31) Agyekum, I.; Zong, C.; Boons, G. J.; Amster, I. J. Single Stage Tandem Mass Spectrometry Assignment of the C-5 Uronic Acid Stereochemistry in Heparan Sulfate Tetrasaccharides Using Electron Detachment Dissociation. *J. Am. Soc. Mass Spectrom.* **2017**, 1–10.
- (32) Kailemia, M. J.; Park, M.; Kaplan, D. A.; Venot, A.; Boons, G. J.; Li, L.; Linhardt, R. J.; Amster, I. J. High-Field Asymmetric-Waveform Ion Mobility Spectrometry and Electron Detachment Dissociation of Isobaric Mixtures of Glycosaminoglycans. *J. Am. Soc. Mass Spectrom.* **2014**, *25*, 258–268.
- (33) Huang, Y.; Yu, X.; Mao, Y.; Costello, C. E.; Zaia, J.; Lin, C. De Novo Sequencing of Heparan Sulfate Oligosaccharides by Electron-Activated Dissociation. *Anal. Chem.* **2013**, *85*, 11979–11986.

- (34) Wolff, J. J.; Leach III, F. E.; Laremore, T. N.; Kaplan, D. A.; Easterling, M. L.; Linhardt, R. J.; Amster, I. J. Negative Electron Transfer Dissociation of Glycosaminoglycans. *Anal. Chem.* **2010**, *82*, 3460–3466.
- (35) Leach III, F. E.; Wolff, J. J.; Xiao, Z.; Ly, M.; Laremore, T. N.; Arungundram, S.; Al-Mafraji, K.; Venot, A.; Boons, G. J.; Linhardt, R. J.; Amster, I. J. Negative Electron Transfer Dissociation Fourier Transform Mass Spectrometry of Glycosaminoglycan Carbohydrates. *Eur. J. Mass Spectrom.* **2011**, *17*, 167–176.
- (36) Leach III, F. E.; Riley, N. M.; Westphall, M. S.; Coon, J. J.; Amster, I. J. Negative Electron Transfer Dissociation Sequencing of Increasingly Sulfated Glycosaminoglycan Oligosaccharides on an Orbitrap Mass Spectrometer. *J. Am. Soc. Mass Spectrom.* **2017**, *28*, 1844–1854.
- (37) Wu, J.; Wei, J.; Hogan, J. D.; Chopra, P.; Joshi, A.; Lu, W.; Klein, J.; Boons, G. J.; Lin, C.; Zaia, J. Negative Electron Transfer Dissociation Sequencing of 3-O-Sulfation-Containing Heparan Sulfate Oligosaccharides. *J. Am. Soc. Mass Spectrom.* **2018**, *29*, 1262–1272.
- (38) Wolff, J. J.; Laremore, T. N.; Aslam, H.; Linhardt, R. J.; Amster, I. J. Electron-Induced Dissociation of Glycosaminoglycan Tetrasaccharides. *J. Am. Soc. Mass Spectrom.* **2008**, *19*, 1449–1458.
- (39) Ropartz, D.; Li, P.; Fanuel, M.; Giuliani, A.; Rogniaux, H.; Jackson, G. P. Charge Transfer Dissociation of Complex Oligosaccharides: Comparison with Collision-Induced Dissociation and Extreme Ultraviolet Dissociative Photoionization. *J. Am. Soc. Mass Spectrom.* **2016**, *27*, 1614–1619.
- (40) Racaud, A.; Antoine, R.; Joly, L.; Mesplet, N.; Dugourd, P.; Lemoine, J. Wavelength-Tunable Ultraviolet Photodissociation (UVPD) of Heparin-Derived Disaccharides in a Linear Ion Trap. *J. Am. Soc. Mass Spectrom.* **2009**, *20*, 1645–1651.
- (41) Racaud, A.; Antoine, R.; Dugourd, P.; Lemoine, J. Photoinduced Dissociation of Heparin-Derived Oligosaccharides Controlled by Charge Location. *J. Am. Soc. Mass Spectrom.* **2010**, *21*, 2077–2084.
- (42) Ortiz, D.; Enjalbert, Q.; MacAleese, L.; Dugourd, P.; Salpin, J.-Y. Effects of Calcium Complexation on Heparin-like Disaccharides. A Combined Theoretical, Tandem Mass Spectrometry and Ultraviolet Experiment. *Rapid Commun. Mass Spectrom.* **2015**, *29*, 1135–1144.
- (43) Ropartz, D.; Lemoine, J.; Giuliani, A.; Bittebière, Y.; Enjalbert, Q.; Antoine, R.; Dugourd, P.; Ralet, M.-C.; Rogniaux, H. Deciphering the Structure of Isomeric Oligosaccharides in a Complex Mixture by Tandem Mass Spectrometry: Photon Activation with Vacuum Ultra-Violet Brings Unique Information and Enables Definitive Structure Assignment. *Anal. Chim. Acta* **2014**, *807*, 84–95.

- (44) Ropartz, D.; Giuliani, A.; Hervé, C.; Geairon, A.; Jam, M.; Czjzek, M.; Rogniaux, H. High-Energy Photon Activation Tandem Mass Spectrometry Provides Unprecedented Insights into the Structure of Highly Sulfated Oligosaccharides Extracted from Macroalgal Cell Walls. *Anal. Chem.* **2015**, *87*, 1042–1049.
- (45) Ropartz, D.; Giuliani, A.; Fanuel, M.; Hervé, C.; Czjzek, M.; Rogniaux, H. Online Coupling of High-Resolution Chromatography with Extreme UV Photon Activation Tandem Mass Spectrometry: Application to the Structural Investigation of Complex Glycans by Dissociative Photoionization. *Anal. Chim. Acta* **2016**, *933*, 1–9.
- (46) Compagnon, I.; Schindler, B.; Renois-Predelus, G.; Daniel, R. Lasers and Ion Mobility: New Additions to the Glycosaminoglycanomics Toolkit. *Curr. Opin. Struct. Biol.* **2018**, *50*, 171–180.
- (47) Devakumar, A.; Thompson, M. S.; Reilly, J. P. Fragmentation of Oligosaccharide Ions with 157 Nm Vacuum Ultraviolet Light. *Rapid Commun. Mass Spectrom.* **2005**, *19*, 2313–2320.
- (48) Cui, W.; Thompson, M. S.; Reilly, J. P. Pathways of Peptide Ion Fragmentation Induced by Vacuum Ultraviolet Light. *J. Am. Soc. Mass Spectrom.* **2005**, *16*, 1384–1398.
- (49) Reilly, J. P. Ultraviolet Photofragmentation of Biomolecular Ions. *Mass Spectrom. Rev.* **2009**, *28*, 425–447.
- (50) Brodbelt, J. S. Photodissociation Mass Spectrometry: New Tools for Characterization of Biological Molecules. *Chem. Soc. Rev.* **2014**, *43*, 2757–2783.
- (51) Shaw, J. B.; Li, W.; Holden, D. D.; Zhang, Y.; Griep-Raming, J.; Fellers, R. T.; Early, B. P.; Thomas, P. M.; Kelleher, N. L.; Brodbelt, J. S. Complete Protein Characterization Using Top-Down Mass Spectrometry and Ultraviolet Photodissociation. *J. Am. Chem. Soc.* **2013**, *135*, 12646–12651.
- (52) Klein, D. R.; Holden, D. D.; Brodbelt, J. S. Shotgun Analysis of Rough-Type Lipopolysaccharides Using Ultraviolet Photodissociation Mass Spectrometry. *Anal. Chem.* **2016**, *88*, 1044–1051.
- (53) Ko, B. J.; Brodbelt, J. S. 193 Nm Ultraviolet Photodissociation of Deprotonated Sialylated Oligosaccharides. *Anal. Chem.* **2011**, *83*, 8192–8200.
- (54) Robinson, M. R.; Moore, K. L.; Brodbelt, J. S. Direct Identification of Tyrosine Sulfation by Using Ultraviolet Photodissociation Mass Spectrometry. *J. Am. Soc. Mass Spectrom.* **2014**, *25*, 1461–1471.
- (55) Fornelli, L.; Srzentić, K.; Huguet, R.; Mullen, C.; Sharma, S.; Zabrouskov, V.; Fellers, R. T.; Durbin, K. R.; Compton, P. D.; Kelleher, N. L. Accurate Sequence Analysis of a Monoclonal Antibody by Top-Down and Middle-Down Orbitrap

- Mass Spectrometry Applying Multiple Ion Activation Techniques. *Anal. Chem.* **2018**, *90*, 8421–8429.
- (56) Brodie, N. I.; Huguet, R.; Zhang, T.; Viner, R.; Zabrouskov, V.; Pan, J.; Petrotchenko, E. V.; Borchers, C. H. Top-Down Hydrogen–Deuterium Exchange Analysis of Protein Structures Using Ultraviolet Photodissociation. *Anal. Chem.* **2018**, *90*, 3079–3082.
- (57) Arungundram, S.; Al-Mafraji, K.; Asong, J.; Leach III, F. E.; Amster, I. J.; Venot, A.; Turnbull, J. E.; Boons, G. J. Modular Synthesis of Heparan Sulfate Oligosaccharides for Structure–Activity Relationship Studies. *J. Am. Chem. Soc.* **2009**, *131*, 17394–17405.
- (58) Domon, B.; Costello, C. E. A Systematic Nomenclature for Carbohydrate Fragmentations in FAB-MS/MS Spectra of Glycoconjugates. *Glycoconj. J.* **1988**, *5*, 397–409.
- (59) Ceroni, A.; Maass, K.; Geyer, H.; Geyer, R.; Dell, A.; Haslam, S. M. GlycoWorkbench: A Tool for the Computer-Assisted Annotation of Mass Spectra of Glycans. *J. Proteome Res.* **2008**, *7*, 1650–1659.
- (60) Shi, X.; Huang, Y.; Mao, Y.; Naimy, H.; Zaia, J. Tandem Mass Spectrometry of Heparan Sulfate Negative Ions: Sulfate Loss Patterns and Chemical Modification Methods for Improvement of Product Ion Profiles. *J. Am. Soc. Mass Spectrom.* **2012**, *23*, 1498–1511.
- (61) Brunet, C.; Antoine, R.; Dugourd, P.; Canon, F.; Giuliani, A.; Nahon, L. Photo-Induced Electron Detachment of Protein Polyanions in the VUV Range. *J. Chem. Phys.* **2013**, *138*, 064301.
- (62) Walenga, J. M.; Jeske, W. P.; Frapaise, F. X.; Bick, R. L.; Fareed, J.; Samama, M. M. Fondaparinux: A Synthetic Heparin Pentasaccharide as a New Antithrombotic Agent. *Expert Opin. Investig. Drugs* **2002**, *11*, 397–407.
- (63) Julian, R. R. The Mechanism Behind Top-Down UVPD Experiments: Making Sense of Apparent Contradictions. *J. Am. Soc. Mass Spectrom.* **2017**, *28*, 1823–1826.
- (64) Sanderson, P.; Stickney, M.; Leach, F. E.; Xia, Q.; Yu, Y.; Zhang, F.; Linhardt, R. J.; Amster, I. J. Heparin/Heparan Sulfate Analysis by Covalently Modified Reverse Polarity Capillary Zone Electrophoresis-Mass Spectrometry. *J. Chromatogr. A* **2018**, *1545*, 75–83.
- (65) Wei, J.; Wu, J.; Tang, Y.; Ridgeway, M. E.; Park, M. A.; Costello, C. E.; Zaia, J.; Lin, C. Characterization and Quantification of Highly Sulfated Glycosaminoglycan Isomers by Gated-Trapped Ion Mobility Spectrometry Negative Electron Transfer Dissociation MS/MS. *Anal. Chem.* **2019**, *91*, 2994–3001.

- (66) Duan, J.; Jonathan Amster, I. An Automated, High-Throughput Method for Interpreting the Tandem Mass Spectra of Glycosaminoglycans. *J. Am. Soc. Mass Spectrom.* **2018**, *29*, 1802–1811.

CHAPTER 8

- (1) Brodbelt, J. S. Photodissociation Mass Spectrometry: New Tools for Characterization of Biological Molecules. *Chem. Soc. Rev.* **2014**, *43*, 2757–2783.
- (2) McHowat, J.; Jones, J. H.; Creer, M. H. Quantitation of Individual Phospholipid Molecular Species by UV Absorption Measurements. *J. Lipid Res.* **1996**, *37*, 2450–2460.
- (3) Williams, P. E.; Klein, D. R.; Greer, S. M.; Brodbelt, J. S. Pinpointing Double Bond and Sn-Positions in Glycerophospholipids via Hybrid 193 nm Ultraviolet Photodissociation (UVPD) Mass Spectrometry. *J. Am. Chem. Soc.* **2017**, *139*, 15681–15690.
- (4) Ryan, E.; Nguyen, C. Q. N.; Shiea, C.; Reid, G. E. Detailed Structural Characterization of Sphingolipids via 193 nm Ultraviolet Photodissociation and Ultra High Resolution Tandem Mass Spectrometry. *J. Am. Soc. Mass Spectrom.* **2017**, *28*, 1406–1419.
- (5) Pulfer, M.; Murphy, R. C. Electrospray Mass Spectrometry of Phospholipids. *Mass Spectrom. Rev.* **2003**, *22*, 332–364.
- (6) Ivanova, P. T.; Milne, S. B.; Byrne, M. O.; Xiang, Y.; Brown, H. A. Glycerophospholipid Identification and Quantitation by Electrospray Ionization Mass Spectrometry. In *Methods in Enzymology; Lipidomics and Bioactive Lipids: Mass-Spectrometry-Based Lipid Analysis*; Academic Press, 2007; Vol. 432, pp 21–57.
- (7) Ranieri, M. L.; Shi, C.; Switt, A. I. M.; Bakker, H. C. den; Wiedmann, M. Comparison of Typing Methods with a New Procedure Based on Sequence Characterization for Salmonella Serovar Prediction. *J. Clin. Microbiol.* **2013**, *51*, 1786–1797.
- (8) Liu, B.; Knirel, Y. A.; Feng, L.; Perepelov, A. V.; Senchenkova, S. N.; Reeves, P. R.; Wang, L. Structural Diversity in Salmonella O-Antigens and Its Genetic Basis. *FEMS Microbiol. Rev.* **2014**, *38*, 56–89.
- (9) Chen, L.; Valentine, J. L.; Huang, C.-J.; Endicott, C. E.; Moeller, T. D.; Rasmussen, J. A.; Fletcher, J. R.; Boll, J. M.; Rosenthal, J. A.; Dobruchowska, J.; Wang, Z.; Heiss, C.; Azadi, P.; Putnam, D.; Trent, M. S.; Jones, B. D.; DeLisa, M. P. Outer Membrane Vesicles Displaying Engineered Glycotopes Elicit Protective Antibodies. *Proc. Natl. Acad. Sci.* **2016**, *113*, E3609–E3618.

- (10) Wattiau, P.; Boland, C.; Bertrand, S. Methodologies for Salmonella Enterica Subsp. Enterica Subtyping: Gold Standards and Alternatives. *Appl. Environ. Microbiol.* **2011**, *77*, 7877–7885.